UNIVERSITY OF SOUTHAMPTON

BLENDS OF BITUMEN AND POLYPROPYLENE:

THEIR PHYSICO-CHEMICAL PROPERTIES

A Thesis submitted to the
University of Southampton
in support of candidature for
the degree of
Master of Philosophy

by

Maureen June Hanney, BSc (Hons) , CChem, MRSC

Department of Chemistry, June 2000

UNIVERSITY OF SOUTHAMPTON

ABSTRACT

FACULTY OF SCIENCE

CHEMISTRY

MASTER OF PHILOSOPHY

BLENDS OF BITUMEN AND POLYPROPYLENE: THEIR PHYSICO-CHEMICAL PROPERTIES

by Maureen June Hanney

The project was designed to study 'atactic polypropylenes,' bitumens, and their blends, as used in commercial waterproof roofing membranes. Low temperature DSC was used to investigate the lowering of the glass transition (T_g) of the blends by 'atactic polypropylene' ('APP'), in order to find the optimum, and therefore most cost-effective, proportion of this additive. This value, about 17 % 'APP,' beyond which further addition made negligible difference, was about the same as the known inversion point between APP-in-bitumen and bitumen-in-APP behaviour, so this relationship probably applies to all such blends. This relationship is of value to the industry, and any technique for finding the inversion point would suffice, such as the two much simpler methods that were devised - by melting and by degradation of a series of blends – and another using addition of DSC plots.

Information was also gathered on other behaviour of the materials that was relevant to their use, *i.e.* all aspects of weathering. TMA of 'APPs' under static load showed the creep behaviour of 'APPs,' gave linear coefficient of expansion, and revealed stress-induced crystallization. Dynamic load TMA results led to the proposal of critical load and critical sample depth, beyond which this occurs. Novel treatment of other dynamic load data, and of DSC data, indicated two new methods that could be used to find T_g. High temperature DSC work, particularly with linked methods, measured 'APP' crystallinity, showed the effects of repeated annealing and quenching upon it, showed that atactic PP oxidized faster than isotactic PP, and analyzed oxidation in air and decomposition in nitrogen. Thin layer chromatography with flame ionization detection (TLC-FID) achieved good separation of the four main components of five bitumens. Long-term thermal degradation, monitored by percentage mass change under controlled conditions in light and dark, on the supplied materials and on 'APPs' prepared in three ways, showed that bitumen and 'APP' protected each other and showed how crystallinity, light level and temperature affected degradation. A mechanism for oxidative degradation was proposed that accounted for all the features of the percentage mass change graphs, and an Excel spreadsheet was used to show how this model could give rise to those features. Other techniques used during the work were FT-Raman, FT-IR, UV, MS and a density gradient column.

CONTENTS

Chapter 1	Introduction	1-14
Chapter 2	Experimental	1-16
Chapter 3	Creep in 'Atactic Polypropylenes'	1-13
Chapter 4	Crystallinity in 'Atactic Polypropylenes'	1-14
Chapter 5	Glass Transitions in Bitumens, Polymers & Their Blends	1-18
Chapter 6	Thermo-Oxidative Degradation of Bitumens, 'Atactic Polypropylenes' & Their Blends	1-28
Chapter 7	Extra Experiments	1-16
Chapter 8	Conclusions	1-4

Excel Spreadsheets

T_g by Dynamic Load TMA (5 pp)

Summation of DSC Plots of Blends (2 pp)

Modelling of Degradation (9 pp)

Diagrams Chapter 1 (2 p), Chapter 2 (7 pp), Chapter 3 (8 pp), Chapter 4 (8 pp), Chapter 5 (11 pp), Chapter 6 (18 pp), Chapter 7 (5 pp).

Appendix : Excel Spreadsheets on Degradation Data

Pelleted 'APPs' and Series of 'APP'/Bitumen Blends in Light (9 pp)

Pelleted 'APPs' and Series of 'APP'/Bitumen Blends in Darkness (7 pp)

Pre-treated 'APPs' in Light (10 pp)

Pre-treated 'APPs' in Darkness (12 pp)

DIAGRAMS

CHAPTER 1 (Introduction)
Fig.1.1. Simplified Manufacture of Bitumen in a Refinery
Fig.1.2. Industrial Uses of Bitumen
Fig.1.3. Computer-Controlled Bending System for Roofing Sheets
Fig.1.4. Relationship Between Rate of Crystallization, T_g and T_m of a Polymer
Fig.1.5. S-Curve of Polymers: Variation of Young's Modulus with Temperature
Fig.1.6. Features in a DSC Heat Flow Plot
Fig.1.7. Phase Inversion in 'APP'/Bitumens

CHAPTER 2 (Experimental)
Fig.2.1. Mass Spectrum of 'APPs' 1C, MF80 and Background Air
Fig.2.2. Reference FT-Raman Spectra of APP and IPP
Fig.2.3. Overlaid FT-Raman and FT-IR Spectra of 'APP' 1C
Fig.2.4. FT-Raman Spectra of 'APPs' 32C and 43C, and IPP
Fig.2.5. Potential Energy of a Molecular Vibration
Fig.2.6. Energy Level Transitions arising from Rayleigh, Stokes and Anti-Stokes Scattering
Fig.2.7. The Michelson Interferometer
Fig.2.8. Basics of an FT-IR Spectrometer
Fig.2.9. Basics of an FT-Raman Spectrometer
Fig.2.10. Thermomechanical Analysis (TMA)
Fig.2.11. Differential Scanning Calorimetry (DSC)
Fig.2.12. The Iatroscan® TH-10 Mark IV and Chromarod® Development

CHAPTER 3 (Creep in 'Atactic Polypropylenes')
Fig.3.1. TMA Chart of L vs T, and $\delta L/\delta T$ vs T, for 'APP' 1C (3.0 mm)
Fig.3.2. TMA Chart of L vs T, and $\delta L/\delta T$ vs T, for (a) 1st Run, (b) 2nd Run, and (c) 3rd Run of 'APP' 1C (2.1 mm) to 130°C
Fig.3.3. Overlaid Plots of Stress vs T for 1st, 2nd and 3rd Runs of 'APP' 1C (2.1 mm) to 130°C
Fig.3.4. TMA Chart of L vs T, and $\delta L/\delta T$ vs T, for (a) 1st Run, (b) 2nd Run of 'APP' 43C to 130°C
Fig.3.5. TMA Chart of L vs T, and $\delta L/\delta T$ vs T, for (a) 1st Run, (b) 2nd Run of 'APP' 32C to 130°C
Fig.3.6. Overlaid Plots of Stress vs T for 6 Runs of 'APP' 1C to 130°C
Fig.3.7. Creep Curves of Separate 'APP' 1C Samples Held for an Hour at Different Temperatures under 0.02 N Load
Fig.3.8. Expected Variation of Creep of Separate 'APP' Samples at Different Temperatures ($T_3 > T_2 > T_1$) under the Same Load
Fig.3.9. Observed Variation of Creep of One 'APP' Sample at Different Temperatures ($T_3 > T_2 > T_1$) under the Same Load (0.02 N)
Fig.3.10. TMA Charts of L vs T for 'APP'1C under 0.2N Load at (a) 20°C, (b) 50°C
Fig.3.11. Expected Variation of Creep of Separate 'APP' Samples under Different Forces ($F_3 > F_2 > F_1$) at the Same Temperature

Diagrams

Fig.3.12. Creep Curve of 'APP' 1C Sample (a) under Increasing Loads, (b) after 10 and 20 min at Each Load
Fig.3.13. Creep Curve of 'APP' 32C Sample with Stepwise Increase and then Decrease in Load
Fig.3.14. Stress per Newton of Load *vs* Time for 'APP' 32C
Fig.3.15. Effect of Stepping-up Loads on 'APP' 32C: Optimized Sample Length *vs* Time
Fig.3.16. Effect of Stepping-down Loads on 'APP' 32C: Optimized Sample Length *vs* Time
Fig.3.17. Surface Depression of 'APP' 1C under Oscillating Load 0.06N (Samples 9 & 10)
Fig.3.18. Surface Depression of 'APP' 1C under Oscillating Load 0.06N with Different Lower Loads (Samples 7, 10, 11, 12)
Fig.3.19. Typical On-line and Evaluation TMA Charts of 'APP' 1C under Dynamic Load
Fig.3.20. Surface Depression of 'APP' 1C under Oscillating Loads (a) (1) 0.40, (2) 0.30, (3) 0.24 N, and (4) 0.16, (5) 0.14 and (6) 0.12 N, Showing "Bites"
Fig.3.21. Surface Depression of 'APP' 1C under Oscillating Loads (a) (7) 0.10, (8) 0.08, (10) 0.06 N and (b) (0) 0.5, (1) 0.4, (2) 0.3 N
Fig.3.22. Surface Depression *vs* Temperature T for 'APP' Samples of Length L_A Subjected to Different Dynamic Forces F
Fig.3.23. Surface Depression *vs* Dynamic Force for 'APP' Samples of Length L_A at Temperature T_1
Fig.3.24. Surface Depression *vs* Dynamic Force for 'APP' Samples of Length L_A at Different Temperatures ($T_3 > T_2 > T_1$)
Fig.3.25. Relationship between Critical Dynamic Force and Critical Depth for an 'APP' at Different Temperatures ($T_3 > T_2 > T_1$)
Fig.3.26. Surface Depression *vs* Temperature T for 'APP' Samples of Length L_A Under Different Dynamic Forces
Fig.3.27. Temperature vs Dynamic Force for 'APP' Samples of Length L_A at Different Depressions ($D_3 > D_2 > D_1$)
Fig.3.28. Relationship between Critical Dynamic Force and Temperature for an 'APP' at Different Depressions ($D_3 > D_2 > D_1$)
Fig.3.29. Action of Dynamic Load on an 'APP' at 50°C
Fig.3.30. Variation of Young's Modulus with Temperature for an 'APP,' Found by Dynamic TMA

CHAPTER 4 (Crystallinity in 'Atactic Polypropylenes')

Fig.4.1. DSC Curve of 'APP' 32C on (a) 1st Run, (b) 2nd Run after Medium Cooling and (c) 4th Run after Slow Cooling
Fig.4.2. DSC Curve of 'APP' MF80 on (a) 1st Run, (b) 2nd Run after Slow Cooling
Fig.4.3. DSC Curve of 'APP' MF80 after 90 min at 200°C
Fig.4.4. Specific Heat vs Temperature, and Heat Flow vs Temperature, for APP Extracted from 1C
Fig.4.5. Heat Flow after Slow Cooling of 'APP' 1C, Showing Shoulder for Crystals Deposited by Phase Separation
Fig.4.6. Heat Intake by 'APP' 32C in Phase Separation Crystallization at 130°C
Fig.4.7. Heat Flow in 'APP' 32C after (a) 60 min at 120°C and (b) 10 min at 130°C
Fig.4.8. Heat Flow in 'APP' 32C after 60 min at 100°C and 60 min at 70°C

Diagrams

Fig.4.9. Predicted Crystallinity of 'APPs' 32C and 43C Over Several Years when Maximum Temperature <65°C
Fig.4.10. Predicted Crystallinity of 'APPs' 32C and 43C Over Several Years when Maximum Temperature >65°C
Fig.4.11a. Predicted Crystallinity of 'APPs' 1C, 32C, 43C, MF80 Over a Year when Maximum Temperature <65°C
Fig.4.11b. Predicted Crystallinity of 'APPs' 1C, 32C, 43C and MF80 Over a Year when Maximum Temperature >65° but <107°C
Fig.4.11c. Predicted Crystallinity of 'APPs' 1C, 32C, 43C and MF80 up to 120°C, when Maximum Temperature Exceeds T_m of Lowest Melting Component (107°C)
Fig.4.11d. Predicted Total Crystallinity of 'APPs' 1C, 32C, 43C and MF80 up to 130°C, when Maximum Temperature Exceeds T_m of Both Lower Melting Components (107°, 122°C)
Fig.4.12. DSC Thermo-oxidation of Crystalline and Amorphous Polymers (without Air Flow)
Fig.4.13. DSC Thermo-oxidation of 1C and its Constituent APP and IPP (without Air Flow)
Fig.4.14. DSC Thermo-oxidation of IPP from Different Sources (without Air Flow)
Fig.4.15. Use of Straight Base-Line to Evaluate DSC Peak Position for Decomposition
Fig.4.16. DSC Curves of (a) Atactic PP and (b) Isotactic PP in 'APP' 1C (without Air Flow)
Fig.4.17. DSC Curves of Commercial Isotactic PP (without Air Flow)
Fig.4.18. DSC Curve of Ethylene-Propylene (EP) Copolymer (without Air Flow)
Fig.4.19. DSC Curve of 200 Pen Bitumen (without Air Flow)
Fig.4.20. Melting Endotherms of 'APP' 32C on one 2nd Run to 210°C (without Air Flow), after 1st Run to 180°C
Fig.4.21. Heat Flow Curve of 'APP' 32C in Pierced Pan (in 100 ml/min Dry Air)
Fig.4.22. Heat Flow Curve of 'APP' 32C in Open Pan (in 200 ml/min Dry Air)
Fig.4.23. Temperatures at (a) Onset of Melting, and –1 mW Threshold, and (b) Onset of Oxidation, and +1 mW Threshold
Fig.4.24. Heat Flow Curve of 'APP' 32C (in 50 ml/min Nitrogen)
Fig.4.25. Automatic Marking of Onset of Rapid Oxidation of 'APP' 1C (in 200 ml/min of Nitrogen)
Fig.4.26. Decomposition Endotherm of 'APP' 1C (in 200 ml/min of Nitrogen)
Fig.4.27. Energy Changes in (a) Exothermic and (b) Endothermic Reactions
Fig.4.28. Kinetic Data and Alpha vs Time Plot for Oxidation of 'APP' 32C
Fig.4.29. Kinetic Data and Alpha vs Time Plot for Decomposition of 'APP' 1C

CHAPTER 5 (Glass Transitions)

Fig.5.1. Distortion of Weak T_g Curve by Nearby Weak Melting Endotherm of Ice after Slow Cooling: (A) T_m of Ice, (B) T_g of 'APP,' (C) Resultant of A + B
Fig.5.2. T_g Curves for Two Materials Not Fully Miscible, Showing Bend Between Adjacent T_gs
Fig.5.3. Clear Separation of Strong T_g Curve and Weak Melting Endotherm of Ice after Rapid Quenching: (A) T_m of Ice, (B) T_g of 'APP,' (C) Resultant of A + B
Fig.5.4. Sharp Ice-melting Endotherm for Blend 98
Fig.5.5. Predicted Effect of Water Intake on the T_g of Bitumen Modified with (a) an 'APP,' (b) a Polymer of Lower T_g than an 'APP'

Diagrams

Fig.5.6. Small Melting Endotherm, Onset about RT, in 1st but not 2nd Heating Scan of Stored 'APP' 32C
Fig.5.7. Small Melting Endotherms, Onset about RT and 90°C, for Blend 97 after Reaching 90°C and then a Hold at 20°C
Fig.5.8. Cold Crystallization and Immediate Melting at Temperature of Pause (20°C) in Previous Quench of Blend 98
Fig.5.9. Heat Flow Charts of Blend 96: (a) 1st Scan: Cold Crystallization, (b) 2nd Scan: No Cold Crystallization
Fig.5.10. DSC Curve of SBS/Bitumen 55: (a) 1st Scan, (b) later 2nd Scan
Fig.5.11. DSC Curve of 'APP' 43C after Quench to –80°C, (a) with hold at 20°C, (b) with no hold at 20°C
Fig.5.12. Graph of Variation of T_g with 'APP' 32C Content in 100 Pen Bitumen (from Scans of Melts Quenched to –120°C)
Fig.5.13. Crystallinity from Content Program on DSC Curve of 'APP' 32C
Fig.5.14. DSC Curve of 'APP' 43C after Cooling of the Melt at Different Rates: (a) Rapid Quench, (b) 50°C/min
Fig.5.15. Decreasing Background Oscillations with Decreasing Cooling Rate: (a) 50°C/min, (b) 40°C/min, (c) 30°C/min, (e) 10°C/min
Fig.5.16. Heating and Cooling Cycles for Linked Method Experiments
Fig.5.17. Heating Scans for 'APP' 32C to 180°C after Quench to Timed Pause at 20°C: (a) initial scan from storage, (b) 0 min, (c) 3 min, (d) 4 min, (e) 6 min, (f) 8 min, (g) 10 min, (h) 20 h at 20°C
Fig.5.18. New Melting Endotherms in 'APP' 43C with Onset at Temperature of the 10 min Hold During the Previous Quench
Fig.5.19. Chart of Heat Input to 'APP' 43C in 10 min Hold at Different Temperatures During the Quench of the Melt (Day 2)
Fig.5.20. Chart of Heat Output from 'APP' 43C in 10 min Hold at Different Temperatures During the Quench of the Melt (Day 3)
Fig.5.21. Graph of Heat Change in 'APP' 43C in 10 min Hold at Different Temperatures During Quench from 180°C on Different Days
Fig.5.22. Chart of Heat Change in 'APP' 43C During a 10 min Hold in the Quench from 180°C: Change From Endothermic to Exothermic Crystallization
Fig.5.23. Scan Cycle for Crystallizing and Melting 'APP' 43C at Progressively Higher Temperatures
Fig.5.24. DSC Chart of 'APP' 43C Heated on Successive Scans to (a) 0°C, (b) 25°C, (c) 50°C, (d) 75°C, (e) 100°C, (f) 125°C, (g) 150°C, and Held There for 5 min
Fig.5.25. Predicted Removal of Successive Melting Endotherms in the DSC Chart of a Semi-Crystalline Polymer:
Fig.5.26. T_g of 'APP' 32C from Linked Scans from –120° to 180°C
Fig.5.27. Graph of Variation in Glass Transition of Blends of an 'APP'/Bitumen with 'APP' Content
Fig.5.28. Glass Transitions (T_g) (a) 200 Pen Bitumen (b) SBS (c) 9% SBS in 200 Pen (d) PFSD (6% IB in 100 Pen)
Fig.5.29. Glass Transitions (T_g) (a) Oxidized Bitumen (b) SIS (c) LDPE (d) HDPE (e) 'APP' V808 (f) 'APP' C80 (g) 'APP' T1180 (h) 'APP' 95-X-06

Diagrams

CHAPTER 6 (Thermo-Oxidative Degradation)

Fig.6.1. Degradation of 4 Pelleted 'APPs' at *c.*120°C on Alternating Light and Dark Days
Fig.6.2. Degradation of 4 Pelleted 'APPs' at *c.*120°C in Near Darkness
(a) to 100 h and (b) to 1500 h
Fig.6.3. Degradation of 4 Pelleted 'APPs' at *c.*120°C in Daylight
(a) to 100 h and (b) to 500 h
Fig.6.4. Degradation of 4 Pelleted 'APPs' at 110°C in Daylight
Fig.6.5. Degradation of 4 Pelleted 'APPs' at 120°C in Daylight -
Behind Extra Soda Glass - with 14 Week Gap in Measurements
Fig.6.6. Comparison of Initial Degradation of 4 Pelleted 'APPs' in Daylight Under
Different Conditions: (a) 1C, (b) 32C, (c) 43C and (d) MF80
Fig.6.7. Degradation of (a) 4 'APPs' and a Bitumen Blend, and (b) 2 'APPs,'
4 Other Polymers and Oxidized Bitumen, at 120°C in Daylight
Fig.6.8. Degradation of 'APPs' at 120°C in Daylight - Effect of Sample Size
for (a) Supplied 95-X-06 and (b) Heat-treated V808 and V891
Fig.6.9. UV Spectra of (a) Soda Glass and (b) Pyrex
Fig.6.10. Degradation of 4 Pelleted 'APPs' at 120°C in 5 Lux (a) to 100 h and (b) to 716 h
Fig.6.11. Degradation of SBS, SIS, PFSD and 9%/13% SBS in 200 Pen Bitumen
at 120°C in 4 Lux
Fig.6.12. Degradation of Four 'APPs' (1C, 32C, 43C and MF80) at 120°C in 4 Lux
Fig.6.13. Degradation of Four 'APPs' (MF500, C80, T1180 and 95-X-06) at 120°C in 4 Lux
Fig.6.14. Degradation of Different Size Samples of Two 'APPs' at 120°C in 4 Lux:
(a) 95-X-06 and (b) T1180
Fig.6.16. Degradation of Blends of 'APP' 32C in 100 Pen Bitumen at 120°C in 4 Lux
Fig.6.17. Variation of Degradation at 120°C with % 32C Content for Blends of 'APP' 32C
in 100 Pen Bitumen, after Different Times – (a) in 4 Lux,
(b) in Darkness, with Exposure to about 4 Lux During Cooling
Fig.6.18. Degradation of Blends of 'APP' 32C in 100 Pen Bitumen at 120°C in Darkness,
with Exposure to About 4 Lux During Cooling
Fig.6.19. Degradation of 8 Pelleted 'APPs' in Duplicate at 120°C in Darkness,
with Exposure to 4 Lux During Cooling: (a) 1C, 32C, 43C, MF80,
(b) MF500, C80, T1180, 95-X-06
Fig.6.20. Degradation of 4 Pelleted 'APPs' in Duplicate at 120°C in Darkness,
with Exposure to <<1 Lux During Cooling: (a) 1C, 32C, 43C, MF80,
(b) MF500, C80, T1180, 95-X-06
Fig.6.15. Degradation at 120°C in 4 Lux of 'APPs' 95-X-06 (360 mg in 8 Pieces) & T1180
(250 mg in 12 Pieces)
Fig.6.21. Dependance of Degradation of 2 'APPs' Upon Prior Light Exposure Conditions
Fig.6.22. Degradation of 4 'APPs' at 120°C in a Sealed Tin –
(a) 'APPs' Affected in the Opposite Way to Oxidized Bitumen,
(b) 'APPs' Affected in the Same Way as Oxidized Bitumen
Fig.6.23. Degradation of 4 'APPs' – 1C, 32C, 43C and MF80 –
at 120°C in 4 Lux after Preparations A, B and C
Fig.6.24. Degradation of 4 'APPs' – MF500, C80, T1180 and 95-X-06 –
at 120°C in 4 Lux after Preparations A, B and C

Fig.6.25. Degradation at 120°C of 'APPs' (a) V808 and (b)V891 in 4 Lux, and (c,d) 1C in Darkness, after Preparations A, B and C
Fig.6.26. Degradation at 120°C of 'APPs' (a) 32C, (b) 43C, (c) MF80, (d) T1180 in Darkness, after Preparations A, B and C
Fig.6.27. Degradation at 120°C of 'APPs' (a,b) MF500, (c,d) C80 in Darkness, after Preparations A, B and C
Fig.6.28. Degradation at 120°C of 'APPs' (a,b) MF500, (c,d) C80 in Darkness, after Preparations A, B and C
Fig.6.29. Predicted Attainment of Steady State in O_2 Links Between Amorphous APP Molecules During PSC/Degradation
Fig.6.30. Predicted Point of Change from Mainly A-O-O-X to Mainly A-O-O-A Links During Degradation of an 'APP' undergoing (a) Fast PSC and (b) Medium PSC, and No Change-over for (c) Slow PSC

CHAPTER 7 (Extra Experiments)

Fig.7.1. FT-Raman Spectra of 'APP' 32C (A) Before and (E) After Heating at 120°C in Darkness and Daylight
Fig.7.2. FT-Raman Spectra of Supplied 'APP' 32C (B) Before and (A) After 716 h at 120°C in 5 Lux
Fig.7.3a,b. Monitoring of one FT-Raman Peak During Degradation of 'APP' 32C at 120°C in 5 Lux: (a) Area and (b) Height
Fig.7.4. Monitoring of Degradation of 'APP' 32C at 120°C in 5 Lux: % Mass Loss
Fig.7.5a. Trial Chromatograms of Bitumen 200E on Iatroscan Mark II, after Development in Decreasing Polarity Solvents
Fig.7.5b. Trial Chromatograms of Bitumen 200E on Iatroscan Mark II, after Development in Increasing Polarity Solvents
Fig.7.6. Trial Chromatograms of Bitumens 200E and X2 on Iatroscan Mark IV
Fig.7.7a. Chromatogram of Bitumen X1 on Iatroscan Mark IV
Fig.7.7b. Chromatogram of Bitumen 200 on Iatroscan Mark IV
Fig.7.7c. Chromatogram of Bitumen 200E on Iatroscan Mark IV
Fig.7.7d. Chromatogram of Bitumen X2 on Iatroscan Mark IV
Fig.7.7e. Chromatogram of Bitumen 100 on Iatroscan Mark IV
Fig.7.8. Chromatogram of Bitumen X2 in 2nd Analysis on Iatroscan Mark IV
Fig.7.9. SARA Analysis of Bitumens: Saturates, Aromatics, Resins and Asphaltenes
Fig.7.10. Photocopied Melts of Series of 'APP' 32C in 100 Pen Bitumen (71% original size)
Fig.7.11. Inversion Point for Blends of 'APP' 32C in 100 Pen Bitumen from Mass of Melt Area
Fig.7.12. Crystals on the Surface of 5% 'APP' 32C in 100 Pen Bitumen after Degradation at 120°C in the Dark for 125 h. Magnification × 9 (It had only a few seconds exposure to << 1 lux during cooling).

ACKNOWLEDGEMENTS

This thesis is dedicated to all my family, for their support in their many different ways.

This thesis came about through Professor Patrick Hendra's faith and good sense in taking on a "Returner" on a New Horizons IT course. This opened the door to a great challenge and very rapid re-learning and learning curves!

My gratitude goes to:

Professor Patrick Hendra for his support and encouragement in returning to chemistry;

my sponsor companies Vulcanite (in Wakefield) and Callenders (in Basildon) for their financial support;

their representatives, John Roberts and Norman Heath, for their help with background to the project and regular discussions;

my fellow postgraduate students in the polymer group for their company, help and friendly acceptance of a more mature 'mature student;'

Dr Rod Bottom of Mettler-Toledo, for running repairs to the DSC equipment;

Les Brown of Analytical & Environmental Consultancy & Services, Bridgend, for supplying useful background information on TLC-FID;

Dr Mark Varney of the Southampton Oceanography Department, for the use of TLC-FID facilities;

the Chemistry Department technical staff for their help and cheerful provision of equipment and materials.

Chapter 1 BACKGROUND AND AIMS 1

1.1 Bitumens 1

1.1.1 Composition of Bitumens 1

1.1.2 Standard Tests on Bitumens 1

1.1.3 Industrial Applications of Bitumens 2

1.1.4 Improved Roofing Products and Systems: Polymer-Modified Bitumens 3

1.2 Built-Up Roofing Systems (BURs) 4

1.2.1 Other Components of BUR Systems 4

1.2.2 Performance Tests on BUR Systems 6

1.3 Bitumen Modification By Thermoplastic Rubbers (TRs) 7

1.4 Bitumen Modification by 'Atactic Polypropylenes' ('APPs') 8

1.4.1 Production of 'APP'/Bitumen Blends 8

1.4.2 'Atactic Polypropylenes' 8

1.4.3 Glass Transition Temperatures (T_g) of Blends 9

1.4.4 'Inversion Point' in 'APP'/Bitumen Blends 10

1.4.5 Weathering of 'APP'/Bitumen Blends 10

1.5 Information from Literature 11

1.6 Questions Requiring Answers 12

1.7 Sponsorship 12

1.8 Tables 13

1.9 References 13

Chapter 1 BACKGROUND AND AIMS

1.1 Bitumens

1.1.1 Composition of Bitumens

Bitumens, which are obtained mainly as residues from distillation of crude oil (Fig.1.1), are very complex mixtures of molecular species: they can be divided by an alkane solvent such as n-heptane into asphaltenes (precipitated) and maltenes (soluble), which can be divided further by chromatography into saturates, aromatics and resins (Scott; Blanken and van Gooswilligen). Saturates - colourless, greasy materials - may contain structures based on naphthenes and paraffins and long straight chains that can crystallize to form wax. The saturates and aromatics (dark brown viscous oils) fractions, with molecular weights of only 300-2000, form the solvent medium or carrier for the polar aromatics, the resins/asphaltenes system. The aromatics contain condensed ring systems – which associate with the resins/asphaltenes system at low temperatures - and some heteroatoms and sulphur. The resins, with molecular weights of about 500 to 50 000, are brown-black semi-solids, which melt on heating and have a H/C ratio of 1.3. It is thought that the resins peptise the asphaltenes, keeping them in colloidal solution in the bitumen. Asphaltenes are dark solids, made up of polycyclic condensed ring systems containing heteroatoms and aliphatic side chains, and they have molecular weights from about 500 to over 100 000, and a H/C ratio of 1.1. Hydrogen bonding between polar groups and structure-building interactions between the sheets of condensed rings produce associative forces in the bitumen, even leading to three-dimensional networks. Since dissociation occurs at higher temperatures, these interactions are reversible, which leads to the viscoelastic properties of the bitumen. The rheological properties (gel or more spread-out sol behaviour) of the bitumen depend on the strength and extent of the associative interactions between the larger molecules. The important viscoelastic properties of the bitumen depend on the concentration, molecular weight distribution and polarity of the asphaltenes, and upon the nature and amount of the solvent medium. Thus bitumen properties can vary with the crude origin.

1.1.2 Standard Tests on Bitumens

Bitumen from different sources can be compared by two basic specifications, needle penetration (in 0.1 mm) at a specified temperature (usually 25°C) and the softening point,

measured by the ring and ball (R&B) method. Sensitivity to temperature change, as given by the penetration index (PI) – determined from the penetration values at two temperatures - is important. 'Straight run' or primary bitumens have PI values from –2 to +1, low values indicating high sensitivity to temperature change. Other standard tests on bitumens measure flow pass/fail temperatures, critical fracture temperature, cold bending temperature (5°C higher), Fraass breaking point, % elongation at break, % permanent set and stiffness modulus. The proportions of saturates, aromatics, resins and asphaltenes (SARA analysis) can be measured by thin layer chromatography with flame ionization detection (TLC with FID).

1.1.3 Industrial Applications of Bitumens

Bitumens are very versatile as they are waterproof, thermoplastic, durable, adhesive, resistant to most chemicals and relatively cheap. 70% are used in civil engineering (mainly roads) but the roofing industry accounts for over 50% of the many industrial uses (Fig.1.2). Bituminous waterproofing membranes have been in use for 100 years. Nowadays most flat and low-slope roofs in Europe and the USA are built-up roofing (BUR) systems comprising several roofing sheet layers held together by a bituminous 'mopping adhesive.' This work was confined to the roofing industry, to bitumens that, together with additives, fillers, carriers and granules, make up the BUR systems.

'Straight run' bitumens from oil distillation had limited use in roofing because they have low flow temperatures and they are hard and brittle at low temperatures. Modern designs of lighter, insulated roof structures, subject to more frequent and greater movement, required that BUR coating compounds should exhibit greater pliability and resistance to flow over a wider temperature range than straight run bitumens. In order to modify their properties to reduce their temperature susceptibility, air was blown through them at high temperature (250-300°C), producing more rubbery bitumens, termed R-grades.

There were two main effects: (a) condensation reactions increased the concentration and molecular weight of the asphaltenes; (b) chemical incorporation of oxygen increased the polarity of the asphaltenes. (Concentration of saturates remained about the same, while that of aromatics and resins fell). This combination increased the number and intensity of associative interactions, and the resultant stronger structural network dissociated less readily

with increasing temperature, so it had a higher softening point (85 to 110°C rather than 35 to 55°C), lower temperature susceptibility, and higher PI. Hence grades could be produced with required mechanical and rheological properties, and blown bitumens extended the application of BURs to a wider range of roof structures and of climate. However, improving properties by air blowing had its limits – if applied too long, the asphaltene network could precipitate from the softer, demixed, lower-molecular-weight phase. The limited cold flexibility at low ambient temperatures for sheets based on blown bitumen can cause problems with application - the cold bending temperature should be 20-25°C below the lowest application temperature. Nevertheless blown bitumens are still widely used as coating grades and adhesives.

1.1.4 Improved Roofing Products and Systems: Polymer-Modified Bitumens

With wider ranges of use, durability became a concern, particularly stability to chemical attack by air, UV and moisture, but a covering layer of mineral granules was found to almost eliminate exposure to UV and reduce that to air. Slow oxidation was reduced further by the use of light-coloured granules or chippings, which kept the bitumen coating cooler. Problems with moisture arose from two causes, from use of rag-felt or carrier materials based on cellulose, and from condensation processes in various roofing structures. The first cause was overcome by use of glass fleece or polymeric carriers, and the second cause by better design detail, and such BURs can give 20 years' service.

Two developments created problems for these BUR systems – the trend towards lightweight structures (rather than concrete) and the growing use of an insulating lower layer. Movement in a lightweight roof could cause excessive strain, rupturing the carriers and coatings. Insulation aggravated this problem by inducing more frequent and greater temperature changes (thermal shock), causing excessive repetitive strain. This was particularly true with synthetic insulation materials with high thermal expansion coefficients. With insulation, hot summers could raise the temperature of the bitumen coating to above the softening point and flow threshold. Thirdly, the use of synthetics (thermoplastics) in roofing accessories, such as ventilation pipes and rain-water drains, affected the roofing felt layers. Fourthly, labour costs affected the quality of roofing materials: costs could be reduced by the use of fewer layers or 'plies,' but then the remaining ones still needed to meet the demands for resistance to deformation at high temperatures and flexibility at low ambient temperatures. The latter

was even more important when the lack of plies was made up for by a thicker bitumen coating. Overall costs could be kept low by employing the labour force all-year-round. All these four factors influenced the need for further modifications to BUR materials, so as to resist flow, allow higher strains and prolong fatigue life. Use of plasticizers in the coating compounds did not increase flexibility sufficiently.

The logical progression was to incorporate synthetic polymers, with their tensile/elastic properties, into bitumens, while maintaining manufacturing and application methods. 100% polymer-based membranes (e.g. PVC, butylrubber) were impractical as they were too expensive and would not employ common practice. Viscosity, and impregnation and coating of the carrier, had to remain acceptable and the product had to have improved low temperature properties and resistance to high-temperature flow and mechanical damage. The choice of polymer depended on three criteria: physical stability and homogeneity on hot storage or at service temperatures, good performance over a long time/temperature/stress history, negligible effect on hot-melt viscosity (so that existing equipment and methods could be used). Two types of polymer - thermoplastic rubbers (TRs) and atactic polypropylenes (APPs) - were found to be successful.

1.2 Built-Up Roofing Systems (BURs)

1.2.1 Other Components of BUR Systems

Mineral fillers are important in bitumen coatings, as they extend and stiffen them, improving mechanical strength and flow resistance. The BUR industry uses a range of fillers of different chemical composition, powder morphology and specific gravity. The choice is usually based on initial cost and short-term apparent effectiveness, and is often limestone (calcium carbonate). The properties of the coating go through a maximum as filler content is increased, so optimum concentration is determined by experiment.

Carriers or felts for the bitumen coatings were formerly organic felts, but are now glass fleece and non-woven polymeric materials such as polyesters, some including an aluminium foil inlay. Heavyweight carriers, but not lightweight ones, need to be impregnated before coating, so that they are saturated properly first, preferably with the same coating bitumen. Where this is not possible, because of viscosity/temperature limitations, there may be problems due to the extra interface involved, and hence a lower quality product.

A typical waterproof membrane is based on a non-woven polyester carrier weighing 180 gm^{-2}, about 0.85 mm thick, with upper and lower polymer/bitumen coatings of 1.2 mm and 1.8 mm thickness respectively. Membranes are dressed with sand, talcum powder, slate particles or aluminium flakes. Granules of natural or synthetic minerals, used to protect the cap sheets from exposure to the elements, are available in various colours (for aesthetic reasons or heat/light reflection), shapes and textures. The granules should be well embedded and stuck to the coating, especially on sloping or wet, flat roofs.

Plant design and processing procedures depend upon the nature of the materials. In-line high shear mixers are commonly used as these can handle supplied polymer granules efficiently, with short blending times, operating a continuous production line over several days. Thus these mixers avoid deleterious prolonged stirring at high temperatures in air. Use of antioxidants or of a nitrogen blanket during blending also help. The bitumen/polymer blend is best not stored but mixed with filler straight away and then used. If stored, it should be stirred and kept at the lowest possible temperature. The more compatible the choice of components, the less chance there is of their separation. When granules are added to the cap-sheet felts they must adhere and embed well, but viscosity increases rapidly with cooling, so timing is important.

Felt application usually involves an adhesive bitumen or a torching technique. The adhesive bitumen can be a blown bitumen with softening point and penetration similar to those of the coating. R-grades with low softening points are often used on flat roofs, but those with higher softening points on sloping roofs. In practice, there are few problems with using conventional roofing adhesives for bitumen/polymer premium coatings. With torching it is important to avoid heating the felt more than necessary.

Certain carrier materials may improve crack bridging capacity, deformation/puncture resistance ('walking resistance') and long-term performance if they act as 'crack arrestors,' preventing spread of a lower layer crack to upper layers. High-modulus, high-tensile-strength carriers, such as heavy polyester fleeces or cloths may act in this way. Performance is also improved if a felt with rubber-elastic bitumen coating compound is combined with a similar rubber-elastic bitumen adhesive rather than a blown bitumen adhesive, or if it is applied by torching.

1.2.2 Performance Tests on BUR Systems

Roofing sheets comprising carrier and bitumen binder undergo laboratory tests at the plant in order to predict their likely service lifetime.

a) Zero crack test: this test measures the crack bridging capacity of a sheet, a sample (5 cm by 20 cm) of which is stuck down to a pair of touching steel plates with a 2-component epoxy resin adhesive. After conditioning at the test temperature, the plates, in a tensile tester, are pulled apart so that the gap increases by 0.1 mm/min up to 5 mm, to simulate typical roof movement. Gap width/stresses are determined at the break of carrier and coating.

b) Fatigue test: this test oscillates the gap from 1 mm to 2 mm at set rates, and sheets are inspected for cracks, wrinkles and loss of adhesion (loss of 'tack').

c) Other routine tests (tensile strength, elongation at break, cold bending temperature, flow temperature) are carried out on fresh (unaged) sheets. A computer-controlled bending system was constructed (Fig.1.3, Fawcett and Lor) about 10 years ago to characterize bending properties – bending elasticity, yield point and stress relaxation after distortion.

   Ageing tests: (a), (b) and (c) are also carried out on aged sheets. There are also practical outdoor tests and accelerated ageing tests at 60-80°C.

Many compatible bitumen/polymer blends show good resistance to ageing, and have higher flow temperatures, lower cold bending temperatures, greater ability to absorb strains, better elongation at break and permanent set than R-grade bitumens. Polymer-modified bitumens have been proved to provide good mechanical performance and durability. Sheets for non-insulated roofs may pass the high temperature flow resistance test at 60°C, but they should be tested at 80°C if destined for insulated roofs. Changes in mechanical properties and in rubber content/molecular weight led to claims of useful lifetimes of up to 30 years, particularly with a top layer of mineral granules to reduce the action of UV and air. Bitumens modified by thermoplastic rubbers are flexible even at –40°C, so felts can be laid in cold weather, and they resist puncture and tear at 60-70°C, so they can be walked on during construction.

1.3 Bitumen Modification By Thermoplastic Rubbers (TRs)

In 1965 Shell introduced block copolymers of TRs of the type $(SB)_n$ or $(SI)_n$, where S, B and I stand for polystyrene, polybutadiene and polyisoprene. TRs consist of two incompatible polymers, one (plastic) with a glass transition temperature (see section 1.4.3) higher than ambient and the other (rubber) much lower than ambient. Uniquely, they are non-cross-linked (therefore plastic) at high mixing temperatures (160°C) but cross-linked (therefore rubbery) at lower service temperatures. In $(SB)_n$ the polymer blocks of polybutadiene confer rubber elasticity while those of polystyrene provide thermally reversible physical vulcanisation (*i.e.* networking) by associating into domains via Van der Waals forces. At processing temperatures or in solvents, these domains dissociate but they reform on cooling or solvent evaporation.

The components of TR/bitumen blends must be carefully matched to give a 'compatible' blend. The TR should be able to make a continuous network when dispersed in the bitumen, but this 'vulcanisation' can be less effective if (a) the polystyrene is too soluble in the bitumen, or (b) high molecular weight asphaltene concentrations are very high, causing phase separation.

TR constitution affects blending and blend properties. (i) Blending time is reduced if molecular weight is low, extender oil is added, polystyrene content is low, or TR powder is used. (ii) Flow resistance is increased if molecular weight is high, or polystyrene content is high, but extender oil reduces it slightly. (iii) Cold flexibility becomes poorer when polystyrene content is high. (iv) Rubber elasticity is poor if molecular weight is low or polystyrene content is high. (v) Hot-melt viscosity increases with increasing molecular weight, for linear or star shaped TRs. (vi) Softening point increases with overall molecular weight and with polystyrene content, but it is not a reliable indicator of high temperature performance. A TR with star-shaped structure needs to have a much higher molecular weight than a linear one with the same polystyrene content, so the final blend will have much higher viscosity. Viscosity affects blend workability in the factory because it affects power consumption and production rates. In general, high rubber concentration increases softening point, viscosity, flow temperature and elasticity, and reduces penetration, cold bending temperature and elongation at break (after passing through a maximum). Thus final properties depend on a compromise of content factors.

1.4 Bitumen Modification by 'Atactic Polypropylenes' ('APPs')

1.4.1 Production of 'APP'/Bitumen Blends

Bitumen/olefin blends such as those with APP show different characteristic properties from those with TR. The amorphous nature and weak rubbery character of the additive lead to high softening points and excellent flow resistance. APP is used to improve the high-temperature properties of coating grades for roofing felt in hot climates. Cold bending results are adequate to good, and elongations in tensile testing are slightly larger than in the R-grade, but permanent set is considerable (Table 1.1). Since the polymer is relatively weak, higher concentrations of APP (about 30%) than of TR are generally needed to achieve required property modifications. This causes few blending problems, but care must be taken to avoid phase separation on prolonged storage. The product has only very limited elasticity and low temperature flexibility. When torched, blends with APP begin to flow at about 155°C, the melting point of their minor fraction of crystalline material, whereas blends with SBS begin to flow when the polystyrene domains disperse.

Table 1.1 Comparison of Some Properties of Blown Bitumens and APP- or SBS-Modified Bitumens

Product	Blown bitumen	30%w APP in straight run bitumen	14%w linear SBS in 200 pen bitumen
Elongation at break / %	140	400	2200
Permanent set / %	>100	>300	9
Cold bend temperature /°C pass	0	-5	-35
fail	-5	-10	-40
Fatigue resistance: no. of cycles till hole in coating	1	700	>10,000

1.4.2 'Atactic Polypropylenes'

Polypropylene (PP) and polyethylene (PE) are two of the four major thermoplastics, plastics that can be melted and processed by moulding or extrusion. The parent homopolymers PP and PE can be mixed in each chain to form different types of EP copolymers. PP molecules can be isotactic – with the pendant CH_3 groups on the $-(CH_2\text{-}CH.CH_3)-$ repeat units all on the same 'side' of the chain – or they can be atactic – with the pendant CH_3 groups arranged randomly. The tacticity or stereoregularity of the material greatly affects its mechanical properties because it affects packing and forces between molecules. Polymers can possess a

high or low degree of crystallinity, so they can range from amorphous to highly crystalline. The higher the tacticity the greater the chance of high crystallinity under suitable conditions. These polymers have low relative densities – EP 0.86, PP 0.90, PE 0.91-0.97 - and density rises with crystallinity. Some crystallinity is needed to impart required characteristics to the bitumen blends - good torching properties, high temperature behaviour and tensile strength (Dussek Campbell pamphlets 1 & 2).

Partially crystalline 'APPs' undergo phase separation crystallization – that is, when held at one temperature, the crystalline and amorphous phases separate out progressively. The optimum temperature for phase separation of a polymer (i.e. giving the highest rate of crystallization) is about mid-way between the glass transition (T_g) and melting point (T_m) (Fig.1.4). The degree of crystallinity in the 'atactic' materials can be investigated by high temperature DSC (> 20°C).

'APPs' experience displacement under load, *i.e.* they 'creep.' This behaviour can be studied by thermomechanical analysis (TMA), employing both static and dynamic loads. 'APPs' readily undergo thermo-oxidative degradation, and there are many literature papers on the subject, which is covered in depth in Section 1.5.

1.4.3 Glass Transition Temperatures (T_g) of Blends

On cooling, materials change from rubbery to brittle at the glass transition temperature T_g (Fig.1.5) and if cooled very rapidly from the melt to below the T_g they form a glass, because they do not have time to crystallize. A T_g appears as a step or inflexion in a DSC heat flow plot (Fig.1.6), corresponding to a change in specific heat C_p, but in practice the plot is not always horizontal before and after the T_g. By convention, plots are labelled not by just T_g but by T_{g1}, T_{g2} and T_{g3} for onset, middle and end of a glass transition. When bitumens are modified by polymers such as 'APP,' which have lower T_gs, the bitumen T_gs are lowered, and the higher the proportion of 'APP' added to a bitumen, the lower is the T_g. It was important to find out the optimum amount of 'APP' required to lower the T_g sufficiently for the material to be workable in cold weather and to have a reasonable lifetime through British winters – too little would produce a poor product, too much would be unnecessarily expensive. The lowering of the cold crack temperature by addition of the polymer should in theory increase with proportion of polymer.

A mixture of two compatible, fully miscible materials A and B (of different T_gs) has only one T_g, somewhere between the two values, for (A+B), the new homogeneous material. Where low T_g material A (e.g. an 'APP') is added to higher T_g material B (e.g. a bitumen), it can be seen from the relevant equation (Equation 1.1), that the effect of A is greater for higher mole fraction x_A or for a larger difference between A and B.

Eqn. 1.1 $\quad 1/Tg_{mix} = x_A/Tg_A + x_B/Tg_B \quad etc$

However, if the two materials are not fully miscible, *i.e.* some of B will not dissolve in A, then two T_gs are seen, one for (A+B), and one for the remaining B. Heat flow into and out of a material, and hence T_g values, can be measured by differential scanning calorimetry (DSC), at low temperatures (below 20°C) for polymers and bitumens and their blends. This technique may also illustrate the phenomenon of cold crystallisation, whereby, on warming, the constituents of a glass become able to move and crystallization (that could not happen when cooling was too rapid) is initiated, giving out heat.

1.4.4 'Inversion Point' in 'APP'/Bitumen Blends

According to a technical information pamphlet (Dussek Campbell 2), the 'cold crack' temperature of bitumens is lowered by addition of PP. However, bitumen with a low percentage of PP behaves as bitumen with PP as the minor dispersed phase, whereas bitumen with a high percentage of PP behaves as if PP is the major continuous phase. The 'inversion point' is at about 20-25% 'APP,' above which properties - softening point, cold crack and hardness - are those of the polymer (Fig.1.7). To quote, 'once such a system is allowed to solidify, the resulting membrane is essentially a sheet of APP containing dispersed regions of asphaltenes and resins acting as a filler.'

1.4.5 Weathering of 'APP'/Bitumen Blends

Several processes could happen concurrently at the surface of a bitumen blend on a roof. When mixed into a much larger volume of bitumen, itself covered with mineral granules, most of the added 'APPs' are well-protected from daylight. However, bitumens contain volatile substances (Zenkevich and Ventura, 1992), steam-volatile substances (Brons and Siskin, 1994; Adewusi, 1991) and basic nitrogen compounds (Yamamoto *et al*, 1991), and can form emulsions in water (Yan *et al*, 1992; Marcano *et al*, 1991). So heat would gradually drive off the more

volatile constituents of bitumen; neutral hot rainwater might remove some of the surface bitumen; acidic hot rainwater might remove even more bitumen.

Bitumen-mineral adhesion also depends upon chemical properties of both materials (Nowell and Powell, 1991; Evans *et al*, 1993): 'bitumen-quartz bonding is promoted by the presence of basic species in the bitumen.' So gradual leaching away of slightly basic, slightly water-miscible bitumen by acidic rainwater would possibly reduce mineral adhesion and also expose fresh 'APP' chains to daylight and degradation.

Gradual loss of more volatile constituents of bitumen would leave a higher proportion of 'APP.' 'APP' crystallinity would also be rising because of phase separation crystallization and degradation losses of amorphous PP, PE and EPR. These factors would probably eventually affect adhesion at the mineral surface. It was known that adhesion deteriorated with time but there is no standard method of relating crystallinity and adhesion.

Only a few papers were found on polymer-modified bitumens - Bahl *et al*, 1993; Fawcett and Lor, 1992; Jovanovic *et al*, 1993; Peltonen, 1991 - and none of these covered the same ground as this sponsored project. One paper described an effective treatment for bitumen burns (Juma, 1994).

1.5 Information from Literature

Coupled Methods are often used to obtain more information about thermal degradation, *e.g.* by combinations of thermogravimetric analysis (TGA), DSC, MS or FTIR. As part of a presentation to the Royal Society of Chemistry Thermal Methods Group on 15/11/95, Bauer reported that combined stacked FTIR scans and TGA from 20° to 400°C showed that thermo-oxidative oxidation of IPP produces (at different stages) water, carbon monoxide, carbon dioxide, aldehydes and ketones. Another group (Rotival *et al*, 1994) studied the degradation of PP film by TGA and determination of the emitted gases, fixed chemically: the main products were CO_2, CO, formaldehyde, acetaldehyde and propanal. A group used FTIR to study the thermo-oxidative degradation of ethylene-propylene copolymers (Singh *et al*, 1993) and showed that it occurred mainly in the crystalline PP phase – ethylene decreased oxidation rate and the onset of degradation. Other workers studied, by IR, carboxylic acids formed by PP photo-oxidation (Wilhelm and Gardette, 1994).

1.6 Questions Requiring Answers

Compromises between property requirements, service lifetime and the costs involved lead to a series of questions (1-4) and also some secondary questions (5-8):

1. How does T_g depend on composition in the 'APP'/bitumen system?
2. Previous work suggested that the relationship between T_g and composition was not linear. No researched explanation is available. Is there a method to find the optimum, most cost-effective, amount of polymer additive for lowering the bitumen T_g?
3. An important consideration in the use of a bitumen-polymer blend system is the creep resistance. What is the relationship between content and performance?
4. These materials are exposed to high levels of light and UV in use for very extended periods in air. Thus their oxidative deterioration is crucial. How does the deterioration rate depend on composition of the bitumen blends?
5. Can the progress of thermo-oxidative degradation of 'APPs' be followed by spectroscopic measurements on the residue rather than the products, as usually done?
6. Compatibility between polymer and bitumen is important. How do various bitumens differ in their SARA analysis?
7. Can the inversion point of an 'APP'/bitumen be found by other means not mentioned in the literature?
8. How does (a) the deterioration rate and (b) the relative crystallinity of 'APPs' differ with pre-treatment before degradation, and is there a connection between the two factors?

1.7 Sponsorship

The work described in this thesis was funded jointly by two linked companies that make waterproof roofing membranes: Callenders Ltd, Harvey Road, Basildon, Essex, SS13 1EJ, and Vulcanite Ltd, Crigglestone, Wakefield, W Yorkshire, WF4 3HT. They generously supplied ten commercial polypropylenes, five bitumens (100 and 200 pen, 200E, X1 and X2), and two series of polymer/bitumen blends. They also supplied three Shell technical reports as background information on polymer-modified bitumens (Scott; Bull and Vonk; Blanken and van Gooswilligen) and a roof design manual.

Regular meetings and reports kept the sponsors up-to-date with progress. For their purposes, it was unnecessary to go into the details of polymer morphology, the inner levels of structural organisation. There are papers (*e.g.* by Mandelkern) on the subject and many comprehensive textbooks on polymers, including those written or edited by the following: Brandrup and Immergut; Hall, Chap.5, 121-152; Kaufman and Falcetta; Mark et al; a Polymer Chemistry Symposium; Rodriguez; Strobl; Tadokoro; Urban and Craver, and Ward.

1.8 Tables

Table 1.1 Comparison of Some Properties of Blown Bitumens and APP- or SBS-Modified Bitumens 8

1.9 References

8

Adewusi V A, Enhanced Recovery of Bitumen by Steam with Chemical Additives. *Energy Sources*, 1991, 13, 2, 121-135. 10

Atactic Polypropylene Systems for Bitumen Roofing Membranes, APP Polymers Division, Dussek Campbell Ltd., Market Drayton, Shropshire, pamphlet bmodroof22.7.94 10

Bahl J S, Atheya N and Singh H, Bitumen Properties Modification using Organic Polymers. A Review. *Erdol und Kohle*, 1993, 46, 1, 22-25. 11

Blanken T C and van Gooswilligen G, Bitumen/polymer blends for premium-quality roofing products and systems. Koninklijke/Shell-Laboratorium, Amsterdam. Shell Reprographics, London, 62089. 1, 12

Brons G and Siskin M, Bitumen Chemical Changes During Aquathermolytic Treatments of Cold Lake Tar Sands. *Fuel*, 1994, 73, 2, 183-191. 10

Bull A L and Vonk W C, Shell Elastomers Report: Thermoplastic rubber/bitumen blends for roof and road. *Thermoplastic Rubbers Technical Manual*, TR 8.15. 12

Dussek-Campbell pamphlet 2: *Atactic Polypropylene Systems for Bitumen Roofing Membranes,* APP Polymers Division, Dussek Campbell Ltd., Market Drayton, Shropshire, pamphlet bmodroof22.7.94 9

Evans M B, Nowell D V and Powell M W, Determination of Adhesion in Bitumen-Mineral Systems by Heat-of-Immersion Calorimetry. 2. Correlation of Chemical Properties with Adhesion. *J Thermal Analysis*, 1993, 40, 1, 121-131. 11

Fawcett A H and Lor S-K, Studies on membranes composed of polymer-bitumen blends. Polymer, 1992, 33, 9, 2003-2006. 6, 11

Jovanovic J, Sokic M, Smiljanic M, Pap I, Neumann H-J and Rahimian I, The Production of Stable Bitumen-Polymer Blends. *Erdol und Kohle*, 46, 1, 18-21. 11

Juma A, Bitumen burns and the use of baby oil. *Burns*, 20, (4), 1994, 363-364. 11

Mandelkern L, The Structure of Crystalline Polymers. *Acc Chem Res*, (Amer Chem Soc), 1990, 23, 11, 380-386. 13

Marcano The Combustion of Bitumen-in-water Emulsions. *Fuel*, 1991, 70, 8, 917-923. 10

Mark J E, Eisenberg A, Graessley W W, Mandelkern L and Koenig J L, *Physical Properties of Polymers*, Amer Chem Soc, 1984. 13

Nowell D V and Powell M W, Determination of Adhesion in Bitumen-Mineral Systems by Heat-of-Immersion Calorimetry. 1. The Effect of Crude-Oil Source on Adhesive Performance. *J Thermal Analysis*, 1991, 37, 9, 2109-2124. 11

Peltonen P V, Characterization and testing of the fibre-modified bitumen composites. *J Mat Sci*, 1991, 26, 5618-5622. 11

Rodriguez F, *Principles of Polymer Systems*, 2nd Edition, McGraw-Hill, Washington/New York/London, Year?, Chap.3, 33-58. 13

Rotival C, Renacco E, Arfi C, Pauli A M and Pastor J, Gases Emitted During Thermal Decomposition of a Polypropylene Film and a Polyurethane Adhesive. *J of Thermal Analysis*, 1994, 41, 1519-1527. 11

Scott J A N, Shell Elastomers Report: A discussion of the component materials in bitumen and polymer-modified-bitumen built-up roofing systems. *Thermoplastic Rubbers Technical Manual*, TR 8.14. 1, 12

Singh R P, Mani R and Sivaram S, Thermo-oxidative Degradation of Heterophasic Ethylene-Propylene Copolymers and their Fractions. *Poly Internat*, 1993, 32, 189-196. 11

Strobl G, *The Physics of Polymers: Concepts for Understanding their Structures and Behavior*, Springer, Berlin , 1996. 13

Structure and Properties of Oriented Polymers, Editor: Ward I M, Applied Science Publishers, London, 1975. 13

Structure-Property Relations in Polymers, Advances in Chemistry Series No. 236, Editors: Urban M W and Craver C D,, Amer Chem Soc, Washington DC, 1993. 13

Symposium on State of the Art for Chemical Educators III: Polymer Chemistry. *J Chem Educ* 13

Tadokoro H, *Structure of Crystalline Polymers*, John Wiley & Sons, A Wiley-Interscience publication, 1979. 13

Wilhelm C and Gardette J-L, Infrared Identification of Carboxylic Acids Formed in Polymer Photooxidation. *J Appl Poly Sci*, 1994, 51, 1411-1420. 11

Yamamoto M, Taguchi M and Sasaki K, Basic Nitrogen Compounds in Bitumen and Crude Oils. *Chemical Geology*, 1991, 93, 1-2, 193-206. 10

Yan Y H, Pal R and Masliyah J, Rheological Properties of Bitumen in Water Emulsions with Added Solids. *Can J Chem Eng*, 1992, 70, 1, 13-19. 10

Zenkevich I G and Ventura K, Gas-Chromatographic Identification of Volatile Products from Thermal Processing of Bitumen. Translated from *Zhurnal Prikladnoi Khimii*, 1992, 64, 9, 1974-1979. 10

Chapter 2 EXPERIMENTAL 1

2.1 Materials Studied 1

2.2 Basic Properties of the 'Atactic Polypropylenes' 3

2.3 Outline of Methods 4

2.4 Vibrational Spectroscopy 6

2.4.1 IR and Raman Activity 6

2.4.2 The Michelson Interferometer 7

2.4.3 FT-IR Spectroscopy 7

2.4.4 FT-Raman Spectroscopy 7

2.5 Thermomechanical Analysis (TMA) 8

2.5.1 Under Static Loads 8

2.5.2 Under Dynamic Loads 8

2.6 Differential Scanning Calorimetry (DSC) 10

2.6.1 The Mettler DSC-30 10

2.6.2 Kinetic Analysis 11

2.6.3 Low Temperature Work 12

2.6.4 Linked Scan Methods 12

2.7 SARA Analysis of Bitumens By Thin-Layer Chromatography (TLC) With Flame Ionisation Detection (FID) 12

2.8 Density Gradient Column 13

2.9 Tables 14

2.10 References 15

Chapter 2 EXPERIMENTAL

2.1 Materials Studied

The bitumen-modifying 'atactic polypropylenes' studied in this work were always referred to as 'APPs' for brevity, as in the industry, even though they were all partially crystalline and some were copolymers. Four 'APPs' were studied alone initially (Table 2.1). Data were provided on the approximate contents of the polymers (and related ones, Table 2.2), which were mainly homo- or co-polymers of PP, or SBS, and mainly in pellet form. Some recent successive samples from production lines were studied too, for quality control testing (Table 2.3). Later another six 'APPs' were included (Table 2.4). The T_gs of most of the polymers are available in the literature (Table 2.5). Two series of bitumen blends were also studied: 9 and 13% SBS in 200 Pen bitumen, and 5, 10, 15, 20 and 30% 'APP' in 100 Pen bitumen. The original supply codes of the 10 'APPs' were retained in this thesis because they were more distinctive and easier to relate to, like names of people, rather than just numbers PP1-PP10. This labelling, which was also put into bold font for clarity (just like normal compound numbering), would also be more useful to a reader in the industry.

Table 2.1 Four 'Atactic Polypropylenes' Investigated Initially

Sample No.	Supply Code	Approximate Content	Suppliers	Ref.
PP1	1C	IPP:APP = 4:7 (homopolymer)	APP Polymers Division of Dussek Campbell	DSM data sheet
PP2	MF80	IPP:APP = 4:7 (homopolymer)	APP Polymers Division of Dussek Campbell	DSM data sheet
PP3	32C	IPP:APP:EPR:PE = 3:8:5:5 (co-polymer)	Dutch State Mines, DSM	DSM data sheet
PP4	43C	IPP:APP:EPR:PE = 3:8:5:5 (co-polymer)	Dutch State Mines, DSM	DSM data sheet

Table 2.2 Approximate Proportions of Related Polymer Blends

	IPP	APP	EPR	PE	PS	PI	PB	Ref.
Isotactic Homopolymer PP	7	4						DSM data sheet
Isotactic Copolymer PP	8	3	5	5				DSM data sheet
Copolymer SBS (Cariflex TR1184)					3		7	Shell Chemicals data sheet
Copolymer IB (in PFSD only)						1	5	Shell Chemicals data sheet

IPP = isotactic polypropylene, APP = atactic polypropylene, EPR = ethylene-propylene rubber, PE = propylene-ethylene co-polymer, PS = polystyrene, PI = polyisobutylene, PB = polybutadiene

Table 2.3 Production Line Samples for Quality Control Testing

Sample Code	Polymer	Bitumen	Pen	SP / °C	Sample Code	Polymer	Bitumen	Pen	SP / °C
55	2% SBS	105/35 Oxidized	28	119	97	27% 'APP'	100 Pen	-	-
56	.. ..	.. .. ..	31	119	98	.. ..	.. ..	-	-
822	9% SBS	200 Pen	55	116	392	30% P4	200 Pen	53	149
823	.. ..	.. ..	55	116	393	.. ..	.. ..	49	152
96	27% 'APP'	100 Pen	-	-	PFSD	6% IB	100 Pen	-	95

Table 2.4 Further 'Atactic Polypropylenes' for Investigation

Sample No.	Supply Code	Supplier	Approx Contents	Sample No.	Supply Code	Supplier	Approx Contents
PP5	MF500	?	?	PP8	95-X-06	?	?
PP6	C80	Corapren	?	PP9	V808	Vestoplast	?
PP7	T1180	Corapren	?	PP10	V891	Vestoplast	?

Table 2.5 Glass Transition Temperatures of Relevant Polymers and Copolymers

Polymer	T_g / °C	Ref	T_g / °C	Ref
Atactic PP [APP]	-30	DSM Stamyroid data sheets; Hoechst data sheet	-18	Kaufman and Falcetta, Table 6.3, 239-300
Isotactic PP [IPP]	-10	Kaufman and Falcetta, Table 6.3, 239-300; Hall, Table 2.3; Shell Data Sheet		
Ethylene [PE] LDPE	-125	Kaufman and Falcetta, Table 6.3, 239-300; Brandrup and Immergut, VI, p.44	-120 to -70	Netzsch Annual 1
Butadiene [PB] 1,4-trans	-102 to -83	Brandrup and Immergut, VI, p.53	-107 to -83	Netzsch Annual 1
Isoprene (unvulcanised) [PI] 1,4-cis	-72	Brandrup and Immergut, VI, p.58	-74 to -60	Netzsch Annual 1
Butadiene-co-styrene [SBS] (23%) PS	-64 to -59	Brandrup and Immergut, VI, p.61	-55 to -35	Netzsch Annual 1
Styrene [PS]	-80 to -90	Brandrup and Immergut, VI, p.75	-80 to 105	Netzsch Annual 1
LDPE	-120 to -70	Netzsch Annual 2		
HDPE	-130 to -80	Netzsch Annual 2		

2.2 Basic Properties of the 'Atactic Polypropylenes'

Before the major investigations of the 'APPs,' their physical properties were checked, in terms of 'volatile' loss and crystallinity. In the APP Data Sheet from Dutch State Mines, volatile loss was given as <2% in 1 h at 160°C. So, to compare the four polymers, three pellets of each (weighing 175-345 mg) were heated at 120°C for four days on glass slides in the dark. Mass losses were in the order **MF80>1C>43C>>32C**, *i.e.* 3.22, 2.88, 2.34, 1.61 %, so the two homopolymers lost more mass than the two copolymers. Anti-oxidants were not included in these 'APPs.' Would this non-negligible 'volatile' loss level off or was it the start of thermal degradation, even under these conditions? This was investigated later.

In an attempt to identify the 'volatiles,' mass spectra were recorded (Fig.2.1) on the gaseous product(s) of heating 4 pellets (of about the same size, mass and surface area) of **1C** and **MF80** separately in sealed, nitrogen-filled flasks at 120°C for 48 h. Peaks for water were present at 41% and 28% respectively (relative to 100% for air in the instrument), compared to 17.5% for background laboratory air. A Shell PP Data Sheet gives water absorption as only 0.01% in 24 h, so both batches had retained a little water after the manufacturing process. Only negligible amounts of contaminants were present, but no other volatiles were detected.

The 'APP' pellets were known to contain both amorphous and crystalline material, to give the best properties for specific applications, as explained in manufacturers' data sheets. For simplicity, they were called 'APPs,' the term used commercially. Their crystalline content was not known, so it was checked by solvent extraction. Samples of each 'APP' (*c.*220 mg), cut into tiny pieces, and some commercial crystalline IPP were extracted with several portions of petroleum ether (bp 40°-60°C), kept at room temperature for several days (because dissolution is extremely slow), and the dried residues were weighed (Table 2.6). Only non-crystalline material was removed, confirmed later by DSC. Later *c.*1 g samples of extra 'APPs' were treated likewise (Table 2.7).

Table 2.6 Percentage Crystalline Content of Four 'APPs' and IPP

PP Blend	1C	MF80	32C	43C	IPP
% Crystalline IPP	43.7	43.5	43.1	39.7	100
% Amorphous APP(+EP)	56.3	56.5	56.9	60.3	0

Table 2.7 Percentage Crystalline Content of Extra 'Atactic Polypropylenes'

'APP'	MF500	C80	T1180	95-X-06	V808	V891
% Crystalline IPP	28.4	38.1	30.6	-	36.5	26.6
% Amorphous APP(+EP)	71.6	61.9	69.4	-	63.5	73.4

Raman spectra were compared with reference spectra (Fig.2.2) (Hendra and Agbenyega, 1993). FT-IR and FT-Raman spectra of **1C** and **32C** were overlaid to show their relationship (Fig.2.3), and the Raman spectra of the four 'APPs' and of some commercial 56% crystalline IPP were compared (Fig.2.4). These spectra differed only slightly, most noticeably at the 809/842 cm^{-1} twin peaks for adjacent aromatic C-H stretch (Williams and Fleming, 1989; Colthup et al, 1975). Peak heights were 1:1 for **1C**, **32C** and **43C** but 3:2 for IPP, so FT-Raman could be used to compare crystallinities. [The poor spectrum of dark grey **MF80** could not be improved because the 'APP' began to lose material if the laser beam was more intense].

For IPP, a dense crystalline powder that could be well compressed, all bands were stronger and sharper, so weak bands stood out better from the background noise. Some bands were assigned to vibrations. Raman spectra of all four 'APPs' resembled that of IPP rather than APP, suggesting a very high proportion of IPP; however, crystalline materials give much stronger, sharper peaks than amorphous ones, so *c.*56% crystalline 'APP' should resemble IPP.

2.3 Outline of Methods

FT-IR and FT-Raman spectra were used to show the high degree of crystallinity in the 'atactic' materials (Chapter 2). The creep behaviour (displacement under load) of the first four 'APPs' (**1C**, **32C**, **43C**, **MF80**) was monitored by thermomechanical analysis (TMA), with both static and dynamic loads (Chapter 3). Linear coefficients of expansion were also measured. Crystallinity was investigated by high temperature (above 20°C) differential scanning calorimetry (DSC, Chapter 4), which also illustrated other phenomena such as phase separation crystallization, cold crystallisation, oxidation and decomposition.

T_g studies were carried out on 'APPs,' bitumens and blends using low temperature DSC (below 20°C) on the Mettler DSC-30 (Chapter 5). The method was sensitive enough to show up the water content, which was also shown by mass spectroscopy. T_g features observed were not fully explicable initially but became so with time, experience and more data. DSC heat flow

plots of production line samples of blends were compared. Then two series of blends were studied, *i.e.* 9 and 13% SBS in 200 Pen bitumen, and 5, 10, 15, 20 and 30% **32C** in 100 Pen bitumen. The ultimate aim was to relate T_g to polymer content, and hence deduce the optimum percentage needed to reduce the T_g of bitumens to -25°C or below.

As the relative ease of thermo-oxidative degradation of the 'APPs' was expected to have some effect on blends, four pelleted 'APPs' were initially heated in different temperatures (usually 120°C) and light conditions (Chapter 6), without any prior heat treatment to replace their different thermal histories with the same one. UV spectroscopy was used to study two types of glass, known to cut out UV, which was known to enhance degradation. Repeat heating tests were run for 1500 h in darkness and 800 h in daylight, on these and six other 'APPs' supplied for this purpose, and some polymers from stock (SBS, SIS, LDPE, HDPE). The long-term degradation results for the **32C**/100 Pen bitumen were analysed to see whether (a) one protected the other, (b) they protected each other, and (c) degradation behaviour showed an inversion point. Next, samples were standardized - annealed and quenched in three different ways – for very long term heating experiments in light and in darkness.

Several extra experiments were run alongside the main ones, to investigate related phenomena, which seemed relevant to the project (Chapter 7). 'APP' crystallinity changed with degradation, and FT-Raman spectra changed with crystallinity, so spectra were run throughout the thermal degradation, to see whether progress could be followed in this way.

Another line of investigation was the content of the bitumen from five different sources, as the sponsor companies needed to know the ratio of saturates/aromatics/resins/asphaltenes (SARA). Therefore samples were analysed by thin layer chromatography with flame ionization detection (TLC-FID) on Iatroscan TH-10's.

The inversion point of an 'APP'/bitumen was fundamental to its behaviour. It seemed likely that the inversion point at about 20% 'APP' might determine another property of the blends not reported previously: *i.e.* the melting behaviour, so this was checked.

Since 'APP' density increased with crystallinity, values were compared for the supplied pellets, for discs prepared by three different heat treatments, and then after degradation, using a density gradient column and an alternative method.

2.4 Vibrational Spectroscopy

2.4.1 IR and Raman Activity

Molecular motion can be translational, rotational or vibrational. IR and Raman spectroscopy are based upon the interaction of electromagnetic radiation with molecular vibrations. A non-linear molecule has 3N-6 fundamental modes of vibration and a linear molecule has 3N-5 modes, where N is the number of atoms in the molecule. For small oscillations, following simple harmonic motion, a plot of potential energy *vs* displacement (from equilibrium position) is a parabola, but larger oscillations are anharmonic, and the plot follows a Morse function (Fig.2.5). Vibrational energy levels are quantized, and each has a quantum number (0, 1, 2, etc), and energy changes involve absorption or emission of a quantum of energy equivalent to the difference in energy between the levels or states, represented by horizontal lines in the plot, converging as V increases.

A vibration is IR active if it involves a change in molecular dipole moment (μ). This selection rule is expressed as an equation (Eqn.2.1), in which q_0 is the equilibrium position of the vibration.

Eqn.2.1. $\delta\mu / \delta q_0 \neq 0$

Basically Raman spectral bands (or peaks) arise from scatter of incident light by a material at characteristic symmetric displacements above and below the frequency of the incident beam. The Raman spectrometer monitors the stronger set of bands on the lower frequency side. If a molecule vibrating at frequency ν_{vib} is irradiated with radiation of frequency ν_o, the dipole has oscillation frequencies at ν_0, $(\nu_0+\nu_{vib})$ and $(\nu_0-\nu_{vib})$, so it emits radiation at ν_0 [Rayleigh radiation], $(\nu_0+\nu_{vib})$ [Anti-Stokes radiation] and $(\nu_0-\nu_{vib})$ [Stokes radiation]. The relative intensities of Stokes and Anti-Stokes elastic scattering, both much weaker than Rayleigh inelastic scattering, depend upon the relative populations of the ground and first excited vibrational energy levels (Fig.2.6). Raman spectroscopy measures the more intense Stokes scattering. A vibration is Raman active if it involves a change in polarisability (α) (Eqn.2.2).

Eqn.2.2. $\delta\alpha / \delta q_0 \neq 0$

The basics of Raman spectroscopy can be found in papers (Hendra 1; Hendra 2, 1989) and textbooks (e.g. Banwell, 1972; Gilson and Hendra, 1970; Tobin, 1971). In a centro-

symmetric molecule some vibrations are active in only the Raman spectrum, while others are active in only the IR spectrum, but never in both, so the two methods are complementary.

2.4.2 The Michelson Interferometer

Most modern IR and Raman spectroscopy uses Fourier transform (FT) instrumentation based upon the Michelson interferometer (Fig.2.7). In this, the beamsplitter partly transmits and partly reflects the incoming light, so it divides it into two beams, one to a fixed mirror and one to a moving mirror. The mirrors fully reflect the beams back to the beamsplitter, which again partly transmits and partly reflects them. They recombine but interfere because of their path difference, and the detector samples the interference pattern, called an interferogram, at a series of data points. The interferogram is the sum of all the wavelengths of light involved, so the spectrum is time-based rather than frequency-based, and has to be converted to a conventional spectrum by a Fourier transformation.

2.4.3 FT-IR Spectroscopy

In an FT-IR spectrometer (Fig.2.8), the IR source is often an electrically-heated ceramic, the mirrors are aluminium, and the beamsplitter a thin layer of germanium on potassium bromide. The detector is either a thermal detector (e.g. deuterated triglycine sulphate DTGS) or a quantum detector (e.g. mercury cadnium telluride, MCT). Registration of each point in the interferogram is triggered by a low power helium-neon (HeNe) laser beam that travels along exactly the same path as the measured radiation.

IR spectra normally show the % transmittance of incident light by a material at characteristic frequencies, though spectra can be displayed as absorbance. [Uses of IR and other spectroscopy on polymers are described by Haslam (Haslam *et al*, 1972)]. IR spectra were recorded on a Perkin Elmer PE-2000, with 10 scans at 4 cm^{-1} resolution, on 30 micron (for **1C**) and 65 micron (for **32C**) films. The Perkin Elmer Infrared Data Manager (IRDM) software system was used to process data. Even the 30 micron film was too thick for the highest wavenumber peak to be clear, but the hot press broke down so no more films could be made.

2.4.4 FT-Raman Spectroscopy

An FT-Raman spectrometer (Fig.2.9) is generally a modified FT-IR instrument, except that there is no direct radiation source. A laser illuminates the sample, and it is the Raman scattered light that is collected by the optics. The laser, usually a neodymium yttrium

aluminium garnet (NdYAG) laser, excites in the near IR at 1064 nm (9400 cm^{-1}). The beamsplitter is usually quartz or calcium fluoride, which transmit the scattered light better in the 9400-5400 cm^{-1} range, and the mirrors are usually gold, which are more reflective in this range. The detector is usually an indium gallium arsenide (InGaAs) semi-conductor or a germanium photodiode. Filters are placed between the Raman collection optics and the beamsplitter, and between the beamsplitter and the detector, to remove the Rayleigh scattering signal, which is about a million times stronger than the Raman scattering.

Raman spectra were recorded on a Perkin Elmer PE-1700 using 100 scans at 4 cm^{-1} resolution and 300 mW laser power. Resolution was correct if set to the width (or less) of the narrowest peak at half its height, found by optimizing this peak to fill the screen. The IRDM software system was used again to process data, and the Galactic Industries GRAMS software package was used to overlay FT-IR and FT-Raman spectra and to analyse peak areas.

2.5 Thermomechanical Analysis (TMA)

2.5.1 Under Static Loads

TMA measures the deformation of a sample under load during linear heating inside a furnace (Fig.2.10). The Mettler TMA-40 was used, controlled by the TC-10A processor. 'Chart' was used for TMA print-outs, and 'plot' for graphs plotted from them. TMA charts followed Length (sample thickness, L) *vs* Temperature (T), or Length *vs* Time (t). The Length axis was always optimized to fit the chartpaper width, so for comparisons on the same scale axes, δL values were measured in mm from each chart and normalised, *i.e.* divided by the starting length L to convert to stress, $L'=\delta L/L$. On charts of Length *vs* Temperature, δL was taken as zero at 30°C, to allow for the instrument adjustment time of 1 min. These charts also gave the change in the derivative $\delta L/\delta T$ *vs* T. For repeated runs on the same sample, comparison of normalised change in length ($L' = \delta L/L$) required that the start length L for each run was calculated from L and final δL of the previous run. For normal slow cooling the TMA was left alone to cool; for rapid cooling, the furnace was lifted and swung away from the base.

2.5.2 Under Dynamic Loads

For testing of the capabilities of the TMA instrument in dynamic load mode, several charts were recorded under different conditions. 2-3 mm samples were cut with a craft knife from

the interior of supplied pellets of homopolymer **1C**. Each fresh sample was subjected to a different dynamic load as it was heated at 10 K/min up to 130°C. For almost all scans the lower limit of the dynamic load was 0.02 N; the probe tip area was 1 mm^2. The melting point was known to be 149°C from Step Analysis of the static load TMA chart run at the same speed. Loads oscillated between 0.02-0.08N and 0.02-0.42 N, so the dynamic load or mini-hammering force was 0.06-0.40 N (Table 2.8). The 1 mm^2 probe oscillated up and down (Fig.2.10), and therefore the recording pen did so too. The effect upon the pen position at the lower limit load, as loads increased, was studied first.

Table 2.8 Sample Thickness and Dynamic Loads Studied for Homopolymer 1C

Chart	Dynamic Load / N	Thickness /mm	Curve	Dynamic Load / N	Thickness / mm
0	0.50 = 0.52-0.02	1.81	7	0.10 = 0.12-0.02	1.86
1	0.40 = 0.42-0.02	2.20	8	0.08 = 0.10-0.02	2.31
2	0.30 = 0.32-0.02	1.85	9	0.06 = 0.08-0.02	3.21
3	0.24 = 0.26-0.02	1.54	10	0.06 = 0.08-0.02	2.14
4	0.16 = 0.18-0.02	2.21	11	0.06 = 0.09-0.03	2.01
5	0.14 = 0.16-0.02	2.65	12	0.10 = 0.11-0.01	3.40
6	0.12 = 0.14-0.02	2.31			

Another feature of the dynamic load TMA plots for **1C** seemed worth a brief study - the depth of the pen oscillations on the chartpaper, related to oscillations of the 1 mm^2 probe, were deduced to be a measure of the compressibility under those conditions. Conventionally Young's Modulus of Compressibility (C) is measured by applying a range of loads at a fixed temperature (Eqns.2.1 and 2.2), where force (F) is in N, area (A) in m^2, length change (c) in m, and start length (L) in m.

Eqn. 2.1 Young's Modulus = stress / strain = (force / area) / (length change / start length)

Eqn. 2.2 $C = (F / A) / (c / L)$

However measurements of oscillation depth taken at regular temperature intervals from charts recorded at different dynamic loads should give the same information. Although the experiment was not planned, a graph of data for stress and strain were plotted for each temperature, and the Modulus was obtained from the gradient. That is, graphs of c/L *vs* F gave C = (1 / A) * (1 / gradient). A was 1 mm^2 and the lower load was always 0.02 N.

2.6 Differential Scanning Calorimetry (DSC)

2.6.1 The Mettler DSC-30

The instrument used was the Mettler DSC-30, controlled by the TC-10A processor. An empty aluminium reference pan R (about 50 mg) and a similar sample pan S containing about 10 mg of sample are heated electrically inside a furnace (Fig.2.11). The temperature of R is set to rise linearly, and any temperature difference between them is automatically scanned and corrected by adjustment of the current to the sample pan S. When crystalline material melts it takes in extra heat of fusion, so S requires more heat to stay at the same temperature as R: heat flow to S is endothermal. An endotherm also accompanies decomposition. When material crystallizes or reacts with another material (*e.g.* oxidizes) it gives out heat, so S requires less heat than R: heat flow from S is exothermal (Fig.1.6). Reactions can be followed as high as 600°C. Polymers and bitumens pass from a brittle state to a leathery state at the lowest glass transition temperature (T_g), which appears as a step in the DSC plot, corresponding to a change in specific heat. Using liquid nitrogen, the DSC can detect T_gs down to about -150°C.

The instrument calculates the heat of fusion on melting (ΔH) from the area enclosed by the curve using one of several base-lines, the best being usually the curved one because it allows for the step due to change in specific heat (C_p) with change in structure. Where the step is very large, curvature of the base-line can affect T_m, the temperature at the maximum difference between peak height and base-line. Then T_m is best found using a straight base-line. For quantitative work, the onset of melting is a better thermal property to compare, particularly for polymers, which melt over a wide range of temperature. With Auto-limit off, evaluations are made between the temperatures keyed in (T_1 and T_2) but, with Auto-limit on, the DSC-30 selects the best limits within that range. C_p can be evaluated from a Screen run of heat flow *vs* T, whether or not preceded by a blank run for an empty pan of known weight; without the blank, the values are approximate. Evaluation involving the blank, and the mass of the sample pan, allows for C_p of the sample pan.

Data are printed out as a plot of heat flow (mW) *vs* temperature (°C). According to the Icta Convention for signs of inputs and results, heat flow of an endothermal effect has a negative sign. Plots are mainly given here as 50% reduced photocopies of the print-out. Presentation of DSC data usually has temperature T (°C), along the horizontal axis and heat flow (mW) on the vertical axis. T for a feature can vary slightly with scan speed (K/min), which should be quoted.

Recording time was short but total time per sample was governed by evaluation time. Each peak (of sometimes several) had to be evaluated separately, using the same processor. Running another sample erased the previous data from memory, so data could not be processed later. The heat flow scale was different on every chart because it was optimised to fit the paper, so overlaying of plots afterwards required re-scaling to a common scale. Without computerised data storage and handling, which would have helped tremendously, this treatment took a long time. Quantitative interpretation of DSC results has been described (Richardson, 1976).

2.6.2 Kinetic Analysis

Kinetic analysis can be carried out automatically on the stored DSC data for a full oxidation exotherm or full decomposition endotherm. Analysis determines activation energy, the energy input needed to make a reaction start - endothermic and exothermic reactions both have an energy 'hill' to be climbed before they will start. Analysis also determines reaction order, which refers to the total number of molecules involved in the rate-determining stage, *e.g.* 1 molecule of species A (1st order), or 1 of A and 1 of B (2nd order), or 1 of A and 2 of B (3rd order). So, using [ ] to denote concentration, rate would depend on $[A]^1$ or on $[A]^1[B]^1$ or on $[A]^1[B]^2$. k is the rate constant that links rate and concentration of each species (Eqn.2.1).

Eqn. 2.3 $rate = k * [A]^x[B]^y[C]^z$, *where the reaction order is* $x+y+z$

On the DSC charts, the steepness of the plot of Alpha *vs* Time is an indicator of the speed of the reaction, since Alpha (α) represents the degree of completion of a reaction from 0 at the start to 1 at the end. Temperature (T) and heat output (P) are the quantities that are actually measured; Time (t) is calculated to attain a chosen degree of conversion $Alpha_{end}$, which was set at α=0.9 for 90% conversion. Each evaluation gave (a) the plot of the whole peak if required, and (b) a table of reaction order, activation energy E_a (kJ/mol) and ln k_o (reaction rate constant), together with their respective confidence limits (for 95% probability). [Confidence limits should be <10% of the corresponding kinetic data]. Then was printed either (c) a table of values, at chosen temperatures, of ln k, heat output P (W/kg), reaction time t (min), or (d) a graph of Alpha *vs* Time at any three isothermal temperatures.

2.6.3 Low Temperature Work

Before low temperature work (below room temperature) on the Mettler DSC-30, the time constant (Tau Lag) for temperature equilibration between the furnace and sensor was checked from measurements of the melting point of a pure substance (indium) at three different heating rates. Then the temperature calibration was carried out from -80° to 600°C using three pure metals of exactly-known melting point. The base-line deviation for only this calibration programme was large, but the deviation on a Blank run with empty pans was negligible. Settling time before scans was 2 min, and the start-up deflection took about 1 min for both increasing and decreasing temperature. At the recommended scan speed below RT of 5°C/min, the trace was very noisy, and the noise affected evaluation, so faster scan speeds were tried and 20°C/min was judged to be the best: this was also the usual value given in literature. It was important to use dry air purge gas and the 11 mm thick lid on the cell, to minimize air space above the samples, and hence minimize ice formation.

2.6.4 Linked Scan Methods

On the DSC-30, scanning methods – temperature limits, direction (cooler or hotter) and scan rate - could be linked and stored in memory by number, and later used from any point in the sequence. The print-out gave the on-line plot and one evaluation plot per method. Thus repeated runs, without stopping in between (except for the 2 min settling time for each scan), were possible, as well as cycling between chosen temperatures, with variation of just one factor in each cycle. That factor could be rate of heating or cooling, or hold time or hold temperature at any point. Liquid nitrogen was used for cooling, giving rapid quenching at an uncontrolled rate between the controlled heating runs.

2.7 SARA Analysis of Bitumens By Thin-Layer Chromatography (TLC) With Flame Ionisation Detection (FID)

Bitumens consist of a mixture of Saturates (saturated hydrocarbons), Aromatics, Resins and Asphaltenes, SARA for short (Blanken and van Gooswilligen). They can be analysed by a technique that combines the separation achievable by TLC with the quantitative analysis possible with FID. Separation is achieved over about 10 cm on 1-mm diameter silica-gel-coated quartz rods called Chromarods®, and the rods travel in turn upwards past a hydrogen flame. The greater the ionisation in burning off each component of the mixture, the greater the

voltage produced. Plots of response (in mV) *vs* time (in min) give retention times for each component of a mixture, and relative peak areas give the approximate percentage composition. Several rods of one sample should agree within about 4%. The Trivector processor on the Mark IV analyzer was inoperative, so measurements were made in the Oceanography department on a Mark II analyzer, whose FID was attached via a Perkin Elmer-Nelson 760 series interface to a PC with Turbochrom 3 data acquisition software. The components of bitumens were expected to burn off in the order SARA, giving four peaks, with the 3rd and 4th peaks close together. Five bitumens were supplied by the project sponsors for analysis: 100 Pen, 200 Pen, 200E, and two unknowns, which were therefore labelled X1 and X2. They were looking for bitumens with a particular peak distribution, which would suit their manufacturing needs.

A Mark IV analyzer instruction manual was obtained from AECS (Manual 1), which covered general principles, system overview, Chromarods®, the Iatroscan® scanner, installation and pre-operation, operation, maintenance, accessories and scientific references (Fig.2.12). A review of industrial applications of TLC/FID to high- and non-boiling mineral oil fractions was obtained from AECS (Review 1). The method had been used before by others to analyse heavy distillates (Barman, 1994), asphalts (Wolever *et al*, 1992; BenXian *et al*, 1994), petroleum fractions (Karlsen and Larter, 1991), heavy petroleum residues and oils (Leazar, 1986).

SIII Chromarods® (from Iatron Laboratories Inc., Japan) were stored in a constant humidity chamber containing a saturated solution of calcium chloride to give about 65% humidity. Immediately before use they were activated by passage twice through the FID. They were extremely delicate and were handled with great care. The transfer, at the beginning and end of a working session, between the storage rack and the Mark II rack was particularly tricky. Care also needed to be taken over rod numbering when they were transferred to and fro.

Half-way through the investigation, the Mark II analyzer was replaced by the much more sensitive Mark IV analyzer. It was operated with a hydrogen pressure of 3 kg/cm^2, flow rate 160 ml/min, an air flow of 2000 ml/min and a scan speed of about 4 mm/sec (approx 30 sec/scan).

2.8 Density Gradient Column

The density gradient column in the polymer laboratory was set up with ethanol-water according to the British Standard 2782: Methods Of Testing Plastics, Part 6. Dimensional

Properties. Methods 620A to 620D. Determination of density and relative density of non-cellular plastics. Method D: Density Gradient Column. Connected flasks A and B at the head of the 1-metre 500-ml column were each filled with 250 cm^3 of solvent(s), with the less dense mixture in the flask A nearer to the column. The relative densities of water and ethanol are 1.000 and 0.7893 respectively. With the A-to-B tap and outlet tap open, the increasingly dense mixture flowed down the inner capillary tube and slowly filled the outer column from the bottom, pushing up the less dense liquid above it. When the column was full, the liquid density went from that of flask B (at the bottom of the column) to that of flask A (at the top). The range can be as small as 0.1000 g cm^{-3} over 100 cm, so it is a very sensitive measuring device.

Several extra actions were taken: all glassware was washed with acetone; joints were sealed with high vacuum grease (but not too much, so as to avoid a blockage); the large tube was securely fixed with strong parcel tape so as to rest on the base of the thermostat tank; liquids were de-gassed by gentle stirring overnight; the delivery capillary tube was wired on to the outflow tap; to avoid dropping the samples from several centimetres above the liquid, they were released from a narrow glass tube very close to the surface.

Each time the column was set up, coloured beads of known densities were first added as reference markers, and a graph was plotted for their density *vs* height in the column. If the graph was linear over most of the column, then it was satisfactory, 'APP' samples were introduced, and the equation (or Trendline in Excel) for the line was used to calculate the densities of samples from their heights. Most measurements were made in triplicate and an average was taken of the positions at 2 min. For some samples, which did not settle but sank slowly to the bottom of the tube over several hours, pieces were coded for tracking down the tank by pen markings on the outside.

2.9 Tables

Table 2.1 Four 'Atactic Polypropylenes' Investigated Initially 1

Table 2.2 Approximate Proportions of Related Polymer Blends 1

Table 2.3 Production Line Samples for Quality Control Testing 2

Table 2.4 Further 'Atactic Polypropylenes' for Investigation 2

Table 2.5 Glass Transition Temperatures of Relevant Polymers and Copolymers 2

Table 2.6 Percentage Crystalline Content of Four 'APPs' and IPP 3

Table 2.7 Percentage Crystalline Content of Extra 'Atactic Polypropylenes' 4

Table 2.8 Sample Thickness and Dynamic Loads Studied for Homopolymer 1C 9

2.10 References

8

Banwell C N, *Fundamentals of Molecular Spectroscopy*, 2nd Edition, McGraw-Hill, 1972, 121-156. 7

Barman B N, Comparison of TLC/FID and ASTM D 2007 Methods for the Hydrocarbon Type Analysis of Heavy Distillates. *APACS*, 1994, 207, 2, 48-PETR. 13

BenXian S, LiMing Z and FuYing L, TLC/FID Group Compositional Analytical Method of Micro-amounts of Asphalts and its Application. *Fuel Sci and Tech Internat*, 1994, 12 (5), 665-673. 13

Brandrup J and Immergut E H, Editors, *Polymer Handbook*, Wiley-Interscience, New York, 1975. 2

Colthup N B, Daly N H and Wiberley S E, *Introduction to Infrared and Raman Spectroscopy*, 2nd Edition, Academic Press Inc., London, 1975. 4

DSM Data Sheet: on content ratios in isotactic and atactic homo- and copolymers 1

DSM Stamyroid data sheets for 32C and 43C 2

Gilson T R and Hendra P J, *Laser Raman Spectroscopy*, John Wiley, 1970. 7

Hall C, *Polymer Materials: An Introduction for Technologists and Scientists*, 2nd Edition, Macmillan Education, Basingstoke and London, 1989. 2

Haslam J, Willis and Squirrell D C M, *Identification and Analysis of Plastics*. Iliffe Books, London, 1972. 7

Hendra P J and Agbenyega J K, *The Raman Spectra of Polymers*, John Wiley and Sons, Chichester, 1993. 4

Hendra P J, *Fourier Transform Raman Spectroscopy. Laboratory Practice*, 39, 10, 61-69. 7

Hendra P J, *Fourier Transform Raman Spectroscopy. Naval Research Reviews*, 1989, 4, 18-25. 7

Hoechst data sheet 2

Karlsen D A and Larter S R, Analysis of petroleum fractions by TLC-FID: application to petroleum reservoir description. *Org Geochem*, 1991, 17, 5, 603-617. 13

Kaufman H S and Falcetta J J, *Introduction to Polymer Science and Technology: An SPE Textbook*, (Society of Plastics Engineers), John Wiley & Sons Ltd, a Wiley-Interscience Publication, New York, 1977. 2

Leazar L L, Quantitative Analysis of Petroleum Residues and Heavy Oils by TLC/FID. *J Chromatographic Sci*, 1986, 24, 340-343. 13

Manual 1: *Instruction Manual for Iatroscan® TH-10 TLC+FID Chromatographic Analyzer Mark IV Series*, Publisher: Iatron Laboratories, Inc., Japan, Distributors : Newman-Howells Associates Ltd. and Analytical & Environmental Consultancy & Services, Bridgend, S.Wales. 13

Netzsch Annual 1: *Netzsch Annual for Science and Industry*, Vol.1, DSC on Polymeric Materials. Kaisersberger E and Moehler H, 1.4, Table 1. 2

Netzsch Annual 2: *Netzsch Annual for Science and Industry*, Vol.2, Thermal Analysis for Polymer Engineering. Kaisersberger E, Knappe S and Moehler H, Table 1.5. 2

Review 1: *Hydrocarbons In High- And Low-Boiling Mineral Oil Fractions*, Analytical & Environmental Consultancy & Services, Bridgend, S.Wales. 13

Richardson M J, Quantitative interpretation of DSC results. Plastics and Rubber: Materials and Applications, 1976, VI, 162-167. 11

Shell Chemicals data sheet: Shell Chemicals, Thermoplastic Rubbers Technical Manual; Data Sheet (a) TR 2.1.6.3 on Cariflex TR-1184F; (b) TR 2.1.3.2 on Cariflex TR-1107. 1

Shell Data Sheet 2

Tobin M C, *Laser Raman Spectroscopy*, Wiley-Interscience, 1971. 7

Williams D H and Fleming I, *Spectroscopic methods in organic chemistry*, 4th Edition, McGraw-Hill, 1989. 4

Wolever R D, Waters T H and Wan C C, Development of a Reproducible, Quantitative TLC/FID Method to Analyze Asphalts. *APACS*, 1992, 204, 1, 45-FUEL. 13

Chapter 3 CREEP IN 'ATACTIC POLYPROPYLENES' 1
3.1 Introduction 1
3.2 Experimental 1
3.3 Results & Discussion for Static Load TMA (Length *vs* Temperature) 2
3.3.1 Single 'Runs' 2
3.3.2 Repeated Runs 3
3.3.3 Minor Crystalline Components 3
3.3.4 More Repeated Runs 4
3.3.5 Linear Coefficient of Thermal Expansion 4
3.3.6 Check on Effect of Probe Tip 5
3.4 Results & Discussion for Static Load TMA (Length *vs* Time, i.e. Creep) 5
3.4.1 Effect of Increase in Temperature 5
3.4.2 Effect of Increase and Decrease in Load 6
3.5 Results & Discussion for Dynamic Load TMA (Lower Load Side of Curves) 8
3.5.1 Interpretation of Curves 8
3.5.2 Proposed Application of Deductions 9
3.6 Results & Discussion for Dynamic Load TMA (Depth of Pen Oscillations) 10
3.7 Summary of Conclusions 11
3.7.1 From Static Load TMA - Length *vs* Temperature 11
3.7.2 From Static Load TMA - Length *vs* Time 12
3.7.3 From Dynamic Load TMA – Effect of Lower Loading Limit 12
3.7.4 From Dynamic Load TMA – Effect of Load Oscillations 13
3.8 Tables 13
3.9 References 13

Chapter 3 CREEP IN 'ATACTIC POLYPROPYLENES'

3.1 Introduction

Question: An important consideration in the use of a bitumen-polymer blend system is the creep resistance. What is the relationship between content and performance?

No literature material could be found on this subject, so it was investigated 'from scratch.' The creep behaviour or deformation under load of the first four 'atactic polypropylenes' ('APPs') – **1C**, **MF80**, **32C**, and **43C** - was investigated by thermomechanical analysis (TMA), using the Mettler TMA-40, in the belief that understanding of the phenomenon in the 'APPs' would help towards understanding of the behaviour of commercial 'APP'/bitumen blends, which usually contain about 30% 'APP.' TMA measures the deformation of a sample under load during linear heating inside an insulated furnace (Section 2.5). Working with the tacky, black blends themselves was considered impractical – lower 'APP' blends would creep too much to be measured. Several different approaches were planned, using first Static Loads and then Dynamic Loads, using 'APP' samples taken from the interior of the supplied pellets.

3.2 Experimental

- Sections 3.3. With static loads, sample thickness/length (L) was monitored with increasing temperature (T) in order to measure: (a) changes in L and $\delta L/\delta T$ with T for different thickness samples, (b) normalised length change ($L'=\delta L/L$) for successive runs, to check reproducibility and effect of thermal history, and (c) linear coefficient of thermal expansion and compare it with literature, and hence judge the sensitivity and accuracy of the TMA-40. Repeat runs were cycles of controlled heating to 130°C, recorded at 5°C/min and 0.05 N load, with no disc under the probe, and then very slow cooling of the furnace.
- Section 3.4. Then, again with static loads, sample thickness/length was monitored with time, at constant temperature. This study of deformation or 'creep' was carried out at several different fixed temperatures, each higher than the previous one, on the same sample and on different fresh samples. Repeated runs were also made on one sample at a fixed temperature, with the load larger each time and then smaller.
- Section 3.5. Dynamic load TMA was also employed, to see whether this technique, with its rapidly repeated hammering effect, yielded information on long-term deterioration of

'APPs.' Several different combinations of thickness and load range were tried, and the deformation was compared from the lower-load side of the oscillating print-out.

- Section 3.6. It was reasoned that the depth of dynamic load oscillations was a measure of 'APP' compressibility. Conventionally Young's Modulus of Compressibility is measured by applying a range of loads at a fixed temperature, but measurements of oscillation depth taken at regular temperature intervals from charts recorded at different dynamic loads would give the same information. Therefore data were also analysed in this way.

3.3 Results & Discussion for Static Load TMA (Length *vs* Temperature)

3.3.1 Single 'Runs'

'APP' samples normally expanded as temperature rose, and reached a maximum thickness before compressing as they softened on approaching T_m at *c.*157°C (Fig.3.1). However very thin samples (2 mm or less) underwent a temporary deep compression before this maximum (Fig.3.2a). Charts for other *c.*2 mm and *c.*3 mm samples confirmed that the greater the load or the earlier the peak in expansion, the greater was the dip that followed in the derivative (Table 3.1). Use of a flat silica disc under the 1 mm^2 probe tip produced similar behaviour, so it was not due to tip penetration.

Table 3.1 TMA Data for Homopolymer 1C Samples of Similar Start Length

Start Length / mm	Load / N	Temperature of Endotherm Peak / °C	Depth of Dip in Derivative $\delta L/\delta T$ at 57°C / μm sec^{-1} (10^{-2})
2.13	0.03	43	-3.1
2.16	0.05	47	-2.0
2.21	0.05	43	-5.5

This compression could have been caused by one of three factors: (a) loss of volatiles from a separate surface layer, (b) compression of a less dense surface layer, or (c) crystallization caused by the load. However, (a) loss of material would be continuous with degradation, though slow till auto-oxidation (at about 400 h at 120°C in the dark - see section on Degradation), and (b) the compression was more marked with thinner samples.

Therefore load-induced crystallization was the most likely cause – a load would compress a thinner sample down to its rigid base, but just be cushioned by a thicker sample. However the

dynamic loads applied in this experiment were extremely small, with a maximum of only 0.05 N, spread over approx. 1 mm^2, *i.e.* $5(10^{-6})$ kbar. [1 bar = 10^5N per m^2, so 1 kilobar = 10^4N per mm^2]. These pressures are negligible compared with those needed to affect forces (in kilobars) between layers and thus cause load-induced crystallization downwards through the material, by compression against the rigid support surface. However, as a secondary process, the downward load may have produced a sideways stretch horizontally within a layer, creating a small nucleus of crystallization, which then spread out sideways. Thus the results indicated stress-induced crystallization, *i.e.* caused by the stretch or change in dimensions, whereby even extremely small loads (0.03 N) affected crystallinity in thin samples (2-3 mm) of the 'atactic' polymer.

3.3.2 Repeated Runs

When runs were repeated on *c.*2 mm samples of three of the 'APPs,' the 1st run peaked at *c.*40°C as before (Fig.3.2b,c), but the 2nd run did not peak early. Both plots for the 3rd run were the same as for the 2nd run. This was shown even better when the data were normalised and overlaid on the same scale axes for comparison (Fig.3.3). The 2nd and 3rd runs were identical but different from the 1st run, because the 'thermal history' of the sample was identical, but different from that of the original pellet. Therefore, for all later work, samples were to be given a standard heat treatment, so that they had a standard thermal history. Pellets would have cooled much faster in manufacture than here, and had some thermal shock of quenching, so they were more crystalline than here. When a glass is warmed up to above its T_g, renewed internal mobility can allow crystallization, known as cold crystallization. Perhaps the supplied 'APP' pellets, warmed under load, experienced this effect.

3.3.3 Minor Crystalline Components

All three runs for **1C** showed a small sharp positive peak in $\delta L/\delta T$ at about 100°C, clearer in the 2nd and 3rd runs (Fig.3.2). The other homopolymer **MF80** showed two such bumps while copolymers **43C** (Fig.3.4) and **32C** (Fig.3.5) showed none. Each peak corresponded to an expansion, probably due to release of constriction with melting of a minor crystalline component, an isotactic polypropylene (IPP), in the batch. Later DSC work at scan speed 10°C/min confirmed their presence in **1C** and **MF80**, with these approximate melting points (Table 3.2). Thus TMA and DSC plots can show up the crystalline components in an 'APP.'

The slight expansion occurred just before T_m of each minor crystalline component - the small difference in T probably arose because the TMA bump occurred at the T of fastest expansion, while the DSC peak was just past the point of fastest heat intake at T_m. The onset of melting of the lower melting (lower molecular weight) IPP must release other tightly-bound material, which can then expand to the same extent as the rest has already done. So this observation supported the theory that crystallizing sections of one material trap chains of another material, *i.e.* IPP crystallites trapped APP, just as IPP is known to trap isoprene.

Table 3.2 Correlation of Features in DSC and TMA Charts of Four 'APPs'

PP Blend	Supply Code	DSC Peak / °C	Bump in δL/δT for 2nd TMA Run / °C	T_m in 3rd TMA Run / °C
PP1	1C	107	100	155.5
PP2	MF80	107, 122	98, 112	-
PP3	32C	-	-	152.4
PP4	43C	-	-	153.5

3.3.4 More Repeated Runs

Another **1C** sample (1.8 mm) was heated to 130°C six times (at 10 K/min and 0.02N), and then cooled very slowly (after the 1st, 4th and 5th runs) or rapidly (after the 2nd and 3rd runs). The 1st and 2nd run plots behaved as before, but the 3rd was midway between the 1st and 2nd; the 4th resembled the 3rd, and the 5th and 6th were close to the 2nd. Thus the overlaid normalised plots (Fig.3.6) were always the same when the previous cooling had been standard with the furnace left closed. Plots were different if the furnace had been opened to speed up the previous cooling. Therefore results were reproducible when sample preparation was standardised by a previous run. It followed that samples did not need to be standardised by normal laboratory means, as was thought necessary, before TMA work.

3.3.5 Linear Coefficient of Thermal Expansion

Linear coefficient of thermal expansion was measured for the 2nd run of fresh samples of all four 'APPs' on the dilatometry scan mode, without the silica disc. Values were repeatable, constant till near the T_m, and very close to those quoted in literature (Table 3.3), so this technique was reliable. The plots were the same shape as those of the derivative δL/δT *vs* T, so they also showed the minor crystalline components.

3.3.6 Check on Effect of Probe Tip

When two samples of **32C**, one with and one without a silica disc under the 1 mm^2 probe, were subjected to three successive heating runs, each gave the same shape plots for linear coefficient of thermal expansion. So the results verified that the temporary early compressions seen earlier were not caused by the 1 mm^2 tip of the probe, when used without the disc. The coefficient was measured for the 2nd run in each case: average 24.8 (10^{-5}/K) for 40°-95°C with disc, and average 21.2 (10^{-5}/K) for 50°-90°C with no disc. Therefore the gradient of L *vs* T was slightly less steep by 15% with no disc, indicating that the probe tip did penetrate the surface very slightly more and more as temperature rose.

Table 3.3 Linear Coefficient of Expansion (10^{-5}/°C) of Four 'APPs'

'APP'	Supply Code	L / mm	2nd Run	3rd Run	Range / °C
PP2	MF80	2.29	22.1	-	50-85
PP3	32C	2.09	22.7	22.9	35-105
PP4	43C	2.17	21.4	21.6	35-115
PP4	43C	2.36	22.0	21.8	55-120

Literature values (10^{-5}/°C): 8-10 for copolymer (CRC Handbook, 1997-98, C-782?); 10 (20°-60°C), 15 (60°-100°C), 21 (100°-140°C) (Shell bulletin); 24 (Vestoplast Data Sheet)

3.4 Results & Discussion for Static Load TMA (Length *vs* Time, i.e. Creep)

3.4.1 Effect of Increase in Temperature

Curves for 'creep', or normalised deformation with time, under constant load and temperature, were plotted, for a series of temperatures, from print-outs that were isothermal scans of Length *vs* Time. Single runs on separate samples under the same load (0.2 N) were steeper at higher temperatures (Fig.3.7), showing that creep increased with mobility at higher temperatures, as was expected (Fig.3.8). For repeat runs on the same sample (2.25 mm **1C**, 0.2 N load), creep at 50°C was also greater than at 20°C (over 20-fold), but it decreased on the next run at 65°C, and decreased even more overnight at 65°C (Fig.3.9). The creep curves were plotted with correction for the change in start length for each run. The new resistance to compression was attributed to crystallization, induced by phase-separation on standing at a constant temperature, and possibly also induced by stress, caused by the load. Therefore, once again, tests showed that the 'APPs' could become more crystalline when kept hot under load. This behaviour was relevant to the

'APP'/bitumen blends - it illustrated again how blends with 'APP' as the main phase were very likely to become more crystalline, and therefore more subject to cracking. Therefore it would be better if 'APP' content did not exceed the inversion point value.

Only the first creep curve, run at 20°C, showed a very rapid compression over the first 5 min (Fig.3.10a), though most of the rapid change had probably happened in the 2 min settling time. This effect, not seen in later curves, was attributed to compression of a low-density surface layer. Polypropylenes are known to have a distinct surface layer, which makes them difficult to paint. Thus the TMA-40 was extremely sensitive, and could perhaps be used to study this surface layer.

3.4.2 Effect of Increase and Decrease in Load

It was expected that creep would increase as load or force was increased in steps at the same temperature (Fig.3.11). On repeat runs at 35°C on the same sample (1.86 mm **1C**), load was first 0.02 N and then 0.05 N. Creep was greater under 0.05 N, but larger loads (going up in equal increments of 0.03 N) caused creep to decrease (Fig.3.12a), indicating that stress-induced crystallization was occurring again. A plot of $\delta L/L$ *vs* load at any one time, *e.g.* $(\delta L/L)_{10}$ at 10 minutes (Fig.3.12b), showed the effect clearly. The reduction in compressibility observed overnight when Young's Modulus measurement was attempted was probably also due to heat- and stress-induced crystallization. The creep plot for the first load was steeper at the start than the others, which could be accounted for again by compression of a less-dense surface layer.

When a sample (2.45 mm **32C**) was run for 20 min after successive load increases in unequal steps, and the loads were then reduced in steps, the 'APP' expanded (Fig.3.13), showing that even when more crystalline it recovered slightly, illustrating the partly elastomeric (rubbery) nature of the APP/IPP combination.

For this sample and another sample (2.46 mm) subjected to loads increased in equal steps, all data points were changed for both samples from $(\delta L/L)_{10}$ (normalised length change after 10 min) to $(\delta L/L)_{10}$ per Newton. The plots were very similar (Fig.3.14) - stress per Newton produced by each load was large at first, and decreased rapidly with load, but the plots all became very much less steep from about 0.05 N load. The change in creep or compression under load was interpreted as marking the load at which the sample of given temperature and thickness began to undergo stress-induced crystallization. So perhaps creep measurements

could be used to obtain this information for a whole range of thicknesses and temperatures, but the procedure would be slow.

An idea for an alternative analysis of results of successive load increases and then decreases was followed up. Print-outs of sample length *vs* time were always optimised to fit the chart-paper width, so the width in mm after each 20 min scan was the same. Therefore, for direct comparison, data were measured off these charts, normalized and plotted on the same axes. If rates of compression on loading, and rates of expansion on removal of loads, were the same, then overlaid curves should have coincided. However they did not do so, so the variation was examined. Loads used in stepwise loading were 0.01, 0.03, 0.05, 0.08, 0.11, 0.15, 0.2, 0.3 and 0.4 N, which was left on overnight. Loads next day used in stepwise unloading were 0.5, 0.4, 0.3, 0.2, 0.1 and 0.02 N. A silica disc was not used beneath the probe tip.

Under stepwise addition of loads, curves matched exactly for the 3rd to 9th (last) scan, the 2nd load compressed slightly faster, and the 1st load compressed very much faster (Fig.3.15). Thus a 'steady state' was achieved after initial easier compression, presumably of the surface layer. Next day compression was more difficult, so stress-induced crystallization had probably occurred.

Under stepwise removal of loads, expansion was most rapid on removal of the 1st and largest load, and thereafter decreased steadily (Fig.3.16). Therefore the effect of removing each 0.1 N fell as load fell, as was to be expected for release of pressure on an elastic material – the 'APP' 'bounced back' more, the more it was squashed. So this treatment of data provided evidence for a less dense surface layer, for stress-induced crystallization, and for elasticity of the polymer.

The samples for this study were not standardised, *i.e.* given the same thermal history, as is normal for polymer samples before tests are run on them. To do this, they are annealed, *i.e.* kept just below the melting point for about an hour to attain the same crystallinity, and then quench-cooled. This could not be done at the time because the hot press, the vacuum oven, and the vacuum pump were out of action for several months. In retrospect, TMA heat treatment - one run up to 130°C and a slow cool in the instrument - would probably have been a better preliminary step anyway, able to achieve a closer degree of crystallinity than that obtainable even by a standard laboratory procedure.

3.5 Results & Discussion for Dynamic Load TMA (Lower Load Side of Curves)

3.5.1 Interpretation of Curves

On the charts, the pen position at the minimum load of 0.02 N showed that the depression of the surface increased with temperature and with dynamic load, *i.e.* that the 'APP' did not recover fully after each blow. However the curvature of the curves of the surface depression did not fit an obvious pattern related to the load, so the data were compared in detail later to find an explanation. Since the same probe, with area *c.*1 mm^2 was used, the terms 'pressure' or 'stress' could be used in place of 'load' or 'force.' In the following graphs (Figs.3.17-18 and Figs.3.20-24), the y-axis was L'/L (length change / start length), normalized depression or stress.

For dynamic load 0.06 N (charts 9 & 10): under the lightest 0.06 N hammering (and also under 0.1 N hammering) one sample showed a slight dip in the curve at about 80°C, one sample did not; so one was probably undergoing stress-induced crystallization, one was not (Fig.3.17). The dip corresponded to that seen in the earlier static TMA experiments.

For different lower loads (charts 10/11 & 7/12): plots for 10 and 11, and for 7 and 12 (Fig.3.18), showed that a higher value of lower load damped recovery more and therefore caused greater surface depression over the whole temperature range - as was to be expected.

For dynamic loads 0.40-0.12 N (charts 1-6): some evaluation charts showed a very large sudden increase in depression, followed by complete recovery (Fig.3.19). This bite out of the curve appeared on the on-line wrapped-round plot and on the corresponding evaluation plot, so was not due to the instrument. For the largest load of 0.5 N the smooth bite became a large jump. The larger the dynamic load, the sooner the on-line curve reached the lower edge of the chart-paper, and the lower the temperature of the wrap-round and of the 'bite.' Plots of the charts (Fig.3.20) showed the recovery from the 'bites' very well. These sudden compressions must have been caused by stress-induced crystallization under the hammering action. With continued rise in temperature the crystalline regions must have unlocked again, expanded, and then continued as before.

Samples were not standardized in thickness or thermal history, because this analysis was done some time after the measurements were made during investigation of the instrument. Even so, the overlaid plots for the charts showed that the larger the (range of) dynamic load,

the lower the temperature or the sooner the material was affected, and the deeper the 'bite', *i.e.* the greater the degree of induced crystallization. Plots 2 and 3, for samples thinner than the rest, went deeper and did not lie between 1 and 4 but overlapped 4, 5, and 6. This was attributed to greater induced crystallization and longer time (or higher temperature) for recovery, as to be expected for thinner samples, in which compression could be transmitted right through to the rigid base.

For dynamic loads 0.06-0.10 N (charts 7, 8 & 10): For dynamic loads of 0.1 N and less, no stress-induced crystallization was produced. The order for the next three lighter loads (Fig.3.21a) was also odd: by load it should have been 7, 8, 10, if thickness made no difference, but it was 8, 10, 7. The thinner 7 jumped the order and took longer to depress. But 8-7 = 5-4, therefore it was not just being thinner that made the difference but the actual thinness. It followed that the load affected the material down to a depth of about 2 mm, (*i.e.* between 1.86 and 2.31 mm) and then, at thinness less than that depth (the critical thickness) compression was harder to achieve, so the surface depression decreased considerably. This could be accounted for by an energy barrier to stress-induced crystallization - if this is exceeded, as in 1 to 6, sudden compression occurs, but if it is not exceeded then the 'APP' resists compression.

For dynamic loads 0.5-0.3 N (charts 0, 1 & 2): though incomplete, the curve for the greatest load supported the case for thickness mattering: curve 0 should have been below curve 1 (Fig.3.21b), so 0.5 N probably exceeded the critical load for that thickness.

3.5.2 Proposed Application of Deductions

A set of different loads on the same thickness samples would give the critical load for that thickness; repetition for a series of thicknesses would build up a profile of critical load against thickness. Alternatively, a set of different thickness samples under the same load would give the critical thickness affected by that load; repetition for a series of loads would build up a profile of critical thickness against load. As the TMA-40 was out of action after only about four months' use, these proposals, based on a small number of results, were not followed up.

Interpretation of Depression vs Temperature Data

Evaluation chart data would be re-scaled to all fit the same axes, for $T << T_m$, so the lines do not bend down (Fig.3.22 shows them as straight-lines). Depression of surface for several

different forces at just one T could be taken from this plot and re-plotted (Fig.3.23); the same could be done at several different T (Fig.3.24). For a sample of length L_A, this graph would give the combination of critical depth CD and temperature T for a particular applied dynamic force F_A, *e.g.* CD_{A1} the critical depth for F_A on L_A at T_1. The process would be repeated for other lengths L_B, L_C, etc., and the combined results plotted on a final graph (Fig.3.25). This graph would provide a profile of the behaviour of the polymer: for a given load and temperature, critical depth could be found; for a given thickness and temperature, critical dynamic force could be found.

As an alternative treatment of depression *vs* temperature data, all evaluation chart data would be re-scaled to fit the same axes (Fig.3.26). For one length L_A: for one depression D_1, a plot of T *vs* Force would give CF_A and CT_{A1}; repetition for depressions D_2, D_3, D_3, etc. would give a graph showing CT_1, CT_2, CT_3, etc. for D_1, D_2, D_3, etc. (Fig.3.27). The process would be repeated for other lengths L_B, L_C, etc., and the combined results plotted on a final graph (Fig.3.28). Fig.3.28 would be an alternative form of Fig.3.25.

Application of the Method

The suggested explanation could not be tested further by measurements with the same thickness or the same dynamic load, because the TMA-40 was out of action. If the deductions from this limited set of data were proved correct, possible practical applications might follow. Below the critical thickness, stress-induced crystallization would (a) render the polymer more brittle and susceptible to cracking, and (b) perhaps disturb the interface with any underlying or overlying material. So perhaps this technique could be useful to predict harmful loading and so (a) avoid brittleness and increase the lifetime of thin polymer layers and coatings under load, and (b) avoid disturbance and thus improve the adhesion of thin coatings of polypropylene or similar materials to other materials when under load.

3.6 Results & Discussion for Dynamic Load TMA (Depth of Pen Oscillations)

As outlined in section 2.5, Young's Modulus was determined from the plots of stress *vs* strain, for 'APP' 1C at 10°C intervals. Samples under the lighter dynamic loads reached their elastic limit at about 135°C. With heavier dynamic forces (>0.12 N), the plots developed progressively deeper 'bites,' attributed to stress-induced crystallization, where the

curves suddenly dipped, then recovered and carried on (Fig.3.20). Across the 'bite,' no pen oscillations readings could be taken.

The values for Modulus were then plotted *vs* Temperature (Fig.3.30), including the melting point (where Modulus is zero) at 149°C, to see whether part of the normal S curve of a polymer (Fig.1.5) was generated. The plot of Modulus *vs* Temperature was roughly as expected, *i.e.* part of the S-Curve, so the test was a success and this method of measuring T_g should work. At 75°C and 80°C the gradients should probably have been higher, and at 130°C there were not enough data points. This TMA method would be a new and simple way of determining T_g values, normally found by DSC. The Mettler TMA/DSC manual did not describe such an application, and no references to one were found.

The experiment should be repeated properly, using uniformly annealed samples, so that sample surfaces are smooth, and their crystallinity the same. The range and number of loads should be extended, and also the range of temperatures, with the aid of a cooling jacket round the furnace, to well below the expected T_g of about -30°C. Then $\log_{10}$(modulus) would be plotted *vs* temperature, and the T_g could be obtained from the point of change from brittle to leathery behaviour. A repeat experiment was planned on the heat-treated 'APP', extending the temperature range cold enough to obtain the S-curve and hence T_g. A cold jacket (Dewar flask) was made by the glass-blowing workshop but the experiment was not carried out because the TMA-40 broke down after only four months' use, and repair was prohibitively costly. It was found that a ribbon-cable had been crushed by the casing lid, perhaps since assembly during manufacture, and this may have caused the breakdown and subsequent problems with linked equipment, the DSC-30 and its processor. In any case, it was time to move on to other investigative techniques.

3.7 Summary of Conclusions

3.7.1 From Static Load TMA - Length *vs* Temperature

- As temperature was raised linearly, under loads of only 0.03-0.05 N, 2-3 mm samples underwent temporary compression before expanding again to their maximum length, prior to softening. This effect, deduced to be due to stress-induced crystallization, affected thicker samples less.

- Overlaid normalised plots were virtually identical for 2nd and successive plots provided that heating and cooling conditions, *i.e.* thermal histories, were identical.
- Linear coefficient of thermal expansion results were very close to literature values, so the instrument could be used in this mode with confidence in its reliability.
- TMA plots showed up the minor crystalline components in an 'APP.'

3.7.2 From Static Load TMA - Length *vs* Time

- For a *c.*2 mm sample under 0.2 N load, held at successively higher temperatures, there was an initial increase in creep, but then a resistance to compression, attributed to phase-separation crystallization and probably also stress-induced crystallization, due to the load.
- For only the first hold at 20°C there was initially a very rapid compression, which was seen as evidence for a distinct low-density surface layer - so perhaps TMA could provide a means of studying effects upon this layer.
- Reduction of load in steps allowed the 'APP' to expand, showing its partly rubbery nature.
- On stepwise addition of loads, at constant temperature, stress per Newton fell markedly at a certain load, indicating more resistance to compression, *i.e.* less creep, with onset of stress-induced crystallization.
- Overlaying of normalized plots for increase and then decrease in loads in equal steps provided evidence for a less dense surface layer, for stress-induced crystallization, and for elasticity of the polymer.

3.7.3 From Dynamic Load TMA – Effect of Lower Loading Limit

- *c.*2 mm samples underwent stress-induced crystallization even under only 0.06N dynamic load. As temperature rose linearly, under 0.40 to 0.12 N dynamic loads, samples suddenly compressed, then completely recovered/expanded and continued to compress gradually. This odd behaviour, attributed to stress-induced crystallization, happened at lower temperature and was more marked with higher dynamic load or for thinner sample.
- Overlaying of plots for surface compression *vs* temperature indicated that, at any temperature, there was a critical load/force (CF) for any thickness/depth (CD), and a critical thickness/depth for any load/force, at which stress-induced crystallization occurred. Similarly, for any thickness, there was a critical load/force (CF) for any temperature (T), and a critical temperature for any load/force. Such a polymer profile, built up from dynamic load TMA chart data, might be useful in prediction and avoidance of harmful loads.

3.7.4 From Dynamic Load TMA – Effect of Load Oscillations

It was deduced that the depth of the pen oscillations at one dynamic load over a range of temperatures gave the same information as would those at one temperature over a range of loads. So the TMA charts would allow determination of Young's Modulus of Compressibility at several temperatures, and hence the S-curve for the polymer and its T_g. A trial on data for pellets indicated that, with standardized samples and extension to lower temperatures, this new method of finding T_g, not previously reported, would work.

The above findings are relevant to 'APP'/bitumen blends with 'APP' at or above the inversion point value, which behave as if 'APP' is the main phase. Creep occurs in 'APPs' even at ambient temperatures, and is greater initially at higher temperatures. However, with time at higher temperatures, crystallization, induced by heating and load, inhibits creep. Thicker 'APP' layers need higher temperature or load to undergo stress-induced crystallization, so thicker blend layers would be more likely to creep and less likely to crack when walked on. For lower 'APP' content, behaviour would be more that of the bitumen. The influence of 'APP' content on the spreading out of a series of bitumen blends on heating was looked at separately (7.4.1).

3.8 Tables

Table 3.1 TMA Data for Homopolymer 1C Samples of Similar Start Length 1
Table 3.2 Linear Coefficient of Expansion (10^{-5}/°C) of Four 'APPs' 5
Table 3.3 Correlation of Features in DSC and TMA Charts of Four 'APPs' 5

3.9 References

8

CRC Handbook of Chemistry and Physics, Editor-in-Chief: Lide D R, CRC Press Inc., Boca Raton and New York, 78th Edition, 1997-98. 5

Shell Plastics Technical Bulletin, Shell Polypropylene - Structure and Performance, p.5. 5

Chapter 4 CRYSTALLINITY IN 'ATACTIC POLYPROPYLENES' 1
4.1 Introduction 1
4.2 Experimental 2
4.2.1 DSC Monitoring of Samples to Onset of Oxidation 2
4.2.2 DSC Monitoring of Samples to 600°C 2
4.2.3 Automatic Kinetic Data Analysis 2
4.3 Results and Discussion for Heating to Onset of Oxidation 3
4.3.1 Heat-Flow Diagrams for 20°-180°C 3
4.3.2 Crystallinity of Quenched Melts 4
4.3.3 Specific Heats 4
4.3.4 Phase-Separation Crystallization 5
4.3.5 Annealing and Crystallinity of 'Atactic' PP Copolymers 5
4.3.6 Annealing and Crystallinity of an 'Atactic' PP Homopolymer 7
4.3.7 Overlaid Heat Flow Diagrams for APP, IPP and EP up to 300°C 8
4.4 Results and Discussion for Heating to 600°C : Oxidation and Decomposition 9
4.4.1 For Scans Without Purge Gas 9
4.4.2 For Scans in Dry Air Purge Gas 10
4.4.3 For Scans in Nitrogen Purge Gas 11
4.5 Results and Discussion of Automatic Kinetic Data Analysis 11
4.6 Summary of Conclusions 13
4.7 Tables 14
4.8 References 14

Chapter 4 CRYSTALLINITY IN 'ATACTIC POLYPROPYLENES'

4.1 Introduction

FT-IR spectroscopy and solvent extraction had revealed that commercial 'atactic' polypropylenes ('APPs') were surprisingly highly crystalline. The crystallinity K of a sample is directly related to the measured ΔH, where ΔH_m = heat of fusion for 100% crystalline material (Eqn.4.1). A layer of polymer is more likely to crack when its crystallinity is high.

Eqn. 4.1 $$K = (\Delta H * 100\,\%) / \Delta H_m$$

'APP'/bitumen blends are subjected to very high application temperatures (about 200°C) and to prolonged high temperature in situ in summer. Several questions about 'APP' crystallinity required answers:

1. How crystalline were the commercial 'atactic' polypropylenes supplied?
2. Did the homopolymers have minor crystalline components, as deduced from TMA?
3. What effect would repeated heating and cooling have on crystallinity, on a daily or seasonal basis?
4. Was there a link between crystallinity and oxidation behaviour?
5. Why did 'APPs' ignite spontaneously at high temperatures (flashpoint 280°C)?

Study of these materials was to be undertaken by high temperature (above 20°C) differential scanning calorimetry (DSC), in order to obtain information on crystallinity and oxidation, and as preliminary experience of the instrument before low temperature work (below 20°C) on glass transitions (Chapter 5). In practice the value of ΔH is calculated and printed out automatically from the area under a melting endotherm in a DSC heat flow plot. Other workers have used DSC to measure polymer crystallinity (Gray, 1970; Blundell *et al*, 1981; Silberman *et al*, 1995). Incidentally specific heats were to be measured for comparison with literature. Four 'APPs' (homopolymers **1C** and **MF80**, and copolymers **32C** and **43C**), EP and IPP, were first to be scanned to onset of oxidation (about 180°C), just above melting point (about 160°C), for initial data on melting point (T_m), ΔH, onset of oxidation (T_{on}) and minor crystalline components (MCCs). The effect of very slow cooling on crystallinity was to be compared for the homo- and co-polymers. Then the effect of annealing and quenching

at one or at several different temperatures was to be investigated, to see whether MCCs made a difference. Onset and rate of oxidation were to be compared for the APP and IPP components of an 'APP.'

'APP'/bitumen blends probably reach much higher temperatures briefly when torched, so the study was to be extended to the upper limit of the DSC. Scans were to be made up to 600°C, to study oxidation in air and decomposition in nitrogen. To complete the picture, the kinetics of oxidation and decomposition were to be analysed automatically from the scan data.

4.2 Experimental

4.2.1 DSC Monitoring of Samples to Onset of Oxidation

The DSC-30 (section 2.6) was first used in the range from standby temperature to just above T_m. Charts were printed at 10°C/min from 20°C to 180°C or 200°C (just past the melting endotherm at *c.*160°C) for all four 'APPs' cut up into very tiny pieces. Pan lids were pierced as normal procedure; no purge gas was used; first runs acted as heat-treatment, as done on the TMA-40, to produce a standardized starting material. Samples were cooled down immediately to standby temperature (20°C) between runs either rapidly at RT out of the DSC, or medium-slowly in the DSC with a water-cooled block, or very slowly in the still-closed DSC.

4.2.2 DSC Monitoring of Samples to 600°C

Preliminary runs were made to give standardised heat-treatment, and to check reproducibility of the first set of data: 10 mg samples were pre-heated to 180°C and quenched at RT, all in sealed aluminium pans with one pin-hole to allow gaseous products to escape, and then they were scanned at 10°C/min to 600°C. Repeat runs were used to (a) deduce crystallinity of quenched 'APP' (as after application) and (b) demonstrate the effects on crystallinity of repeated heating and cooling (as after some time in situ). Scans were done with dry air purge gas, to study oxidation, and then with nitrogen purge gas, to study decomposition. In the first heating runs to 600°C no purge gas was used - it should have been. This important precaution was missed in the large Mettler operating manual, which ideally should have been read from cover to cover before starting, as some important points occurred in unexpected places.

4.2.3 Automatic Kinetic Data Analysis

Automatic kinetic evaluation, which requires the whole heat change peak, could be set up as part of the programming of the controller. The whole oxidation exotherm of 'APP' **32C** was

monitored in 200 ml/min of dry air and the whole decomposition endotherm of 'APP' **1C** was monitored in 200 ml/min of nitrogen.

4.3 Results and Discussion for Heating to Onset of Oxidation

4.3.1 Heat-Flow Diagrams for 20°-180°C

The cooling block saved considerable time between runs but caused water condensation, shown as a broad endotherm at 70°C (Fig.4.1), which would not occur if purge gas were used. **32C** and **43C** contained IPP of only one T_m and therefore one molecular mass range, while **1C** and **MF80** (Fig.4.2) contained one and two minor crystalline components (MCCs) of lower molecular mass range. The % composition of the homopolymers was deduced from the various data (Table 4.1) - the crystalline content from solvent extraction, the water content from manufacturers' information sheets. Subscripts 1,2,3 denote MCCs in descending order of T_m.

Table 4.1 Composition of 'APP' Homopolymers 1C and MF80

'APP'	Ratios from DSC Curves	Ratios from Solvent Extraction	Percentage Composition				
	IPP_3:IPP_2:IPP_1	IPP : APP	H_2O	IPP_3	IPP_2	IPP_1	APP
1C	7 : 93	43.7 : 54.3	2.0		3.1	40.6	54.3
MF80	3.4 : 3.3 : 93.3	43.5 : 54.5	2.0	1.5	1.4	40.6	54.5

Very slow cooling allowed gradual formation of extra crystalline material by phase separation, seen as a shoulder on the main melting endotherm of **1C** (Figs.4.1, 4.2). Onset of oxidation (at T_{on}) occurred only a few degrees above the end of the melting endotherm (at T_m), at most about 30°C above T_m, and repetition of the heating and cooling cycle made oxidation easier and faster: **MF80** at >190°, 168°, 164°C; **32C** at 173°, then 163°C; **43C** at 188°, then 173°C.

Prolonged heating of **MF80** at 120°C, *i.e.* annealing, enlarged the smaller endotherm there – its area went up from 1.2 to 2.1 J/g. Prolonged heating about 40°C above T_m (at 200°C) left material that was considerably softer and therefore much less crystalline. Its very broad endotherm indicated gradual softening all the way to T_m. The 2nd run, after slow cooling, gave the lowest T_m and T_{on}, and the broadest endotherm seen: the shoulder on the endotherm was now roughly the same size as the main endotherm, and curved gradually back to RT (Fig.4.3).

A likely explanation is that prolonged heating above T_m 'scrambled' the polymer chains up so much that they were no longer still close to their original neighbours when they cooled. Fewer

chains were aligned well enough to quickly reform their lamellar crystals, and more chains were left to crystallize more slowly by phase separation (*i.e.* move around and meet and align), which continued over the whole cooling range. Crystalline regions created at lower temperature were probably smaller and smaller, so the total % crystallinity was probably less than in non-heated polymer. It follows that even repeated heating at 10°C/min to 190°C in the DSC must have also caused a small amount of 'scrambling.' So the increasing ease and rate of oxidation on successive runs was probably associated with decreasing crystallinity.

4.3.2 Crystallinity of Quenched Melts

As mentioned earlier, the crystallinity K of a sample is directly related to the measured ΔH, where ΔH_m = heat of fusion for 100% crystalline material (Eqn.4.1). The measured ΔH for the quenched IPP was 115 J g^{-1}, so the crystallinity K of the commercial 'crystalline' PP was 55.6%. The literature value of ΔH_m for IPP is (i) 207 J g^{-1} (and (ii) 198 J g^{-1}) (Kaisersberger and Moehler, Table 1, p.4). For each 'APP,' ΔH of the main melting endotherm was evaluated and K was estimated from the ratio of ΔH to that of the IPP of known K. Hence, using the known % of IPP, K of the IPP in the 'APP' was found (Table 4.2).

Table 4.2 Crystallinity Data for Commercial IPP and Four 'APPs'

PP	T_m / °C	ΔH / J g^{-1}	(ΔH * 100) ÷ (ΔH of IPP)	av K / %	IPP content / %	K of IPP used / %
IPP	162	115.0	100.0	55.6	100.0	55.6
1C	157	25.4	22.1	12.3	43.7	28.1
MF80	157	24.3	21.1	11.7	43.5	27.0
32C	158	25.7	22.3	12.4	43.1	28.8
43C	157	25.4	22.1	12.3	39.7	30.9

Thus the crystallinity K of the APP/IPP blends was 12.2%(±0.5%), and that of the IPP used in those blends was 29% (±2%). Alternatively the % IPP content gave a predicted ΔH value; then K of the IPP in the 'APP' was obtained (Eqn.4.2) ..... the results were the same.

Eqn. 4.2 $K = (\text{measured } \Delta H / \text{predicted } \Delta H) * 55.6$

4.3.3 Specific Heats

The plots of specific heat C_p *vs* T were mirror images of the plots of Heat Flow *vs* T (Fig.4.4). All data were obtained after an initial heat-treatment run (melting and quenching), and were

corrected to allow for the pan (Table 4.3). Data were all slightly higher than the literature values (J/g*°C): 1.68 at 23°C and 2.10 at 100°C (Shell technical bulletin).

Table 4.3 Specific Heats of IPP, APP and EP

	Specific Heat (J/g*°C)			
Sample	60°C	100°C	120°C	
IPP from 'APP' 1C	2.18	2.63	2.63	uncorrected
IPP commercial	2.63	2.77	3.02	corrected
IPP from 'APP' 32C	2.65	2.83	2.96	..
APP from 'APP' 1C	2.55	2.57	2.60	..
EP	2.63	2.63	2.64	..

4.3.4 Phase-Separation Crystallization

The melting endotherms after slow cooling of the homo- and co-polymers looked different (Fig.4.5), so the ratio of the area under the shoulder to that under the main melting endotherm was found by cutting and weighing of each enlarged photocopy, and hence the proportion of crystals formed by phase-separation was estimated in each case: **1C** 35% and 36%, **MF80** 35% and 38%, **32C** 24%, **43C** 27%. Thus the homopolymers **1C** and **MF80** produced more extra crystals just below T_m than did the copolymers **32C** and **43C** when cooled very slowly. With commercial 56% crystalline IPP, the endotherm was very narrow for fast cooling, and broadened slightly for slow cooling, but without a shoulder.

4.3.5 Annealing and Crystallinity of 'Atactic' PP Copolymers

Results After Annealing and Quenching at One Temperature

As roofing felts are subjected to high temperatures for long periods, the effect on crystallinity of annealing quenched, molten **32C** was first followed isothermally. At 130°C the heat loss on crystallization was greatest over the first 5 min (plus the 2 min settling time) and then fell only very slightly over the next hour (Fig.4.6), so an hour was more than enough annealing time.

Heat Flow *vs* T of the annealed, quenched melt was recorded after 10 and 60 min at 130°C, and 60 min at 120°C. (Fig.4.7). Areas under melting endotherms of phase-separated and normal crystals were compared by cutting and weighing photo-enlarged copies of charts (Table 4.4). The optimum temperature for phase-separation crystallization of an 'APP' is about mid-way between T_g and T_m (Fig.1.4), so here was expected at about 65°C, mid-way between about -

30°C and about 160°C. **32C** results fitted this behaviour and also showed that 65% of the deposition in 60 min (+2 min) at 130°C occurred in the first 10 min (+2 min).

Results After Annealing and Quenching at Two Different Temperatures

To illustrate how repeated daily heating and cooling could affect the total crystallinity of the copolymers, one **32C** sample was kept at 100°C for an hour, quenched, kept at 70°C for an hour, quenched and then scanned as usual from 20°C (Fig.4.8). There were now two new broad endotherms corresponding to melting of the two sets of phase-separated crystals, with areas 8% (for 70°C) and 22% (for 100°C) compared with 70% for the 'normal' crystals. Thus at 100°C, annealed-peak:main-peak was 23.9%:76.1% (extending Table 4.4). The higher the annealing temperature, the larger was the delay in reaching the endotherm peak (Table 4.5).

Table 4.4 Areas Under the Melting Endotherms of Annealed 'APP' 32C

Annealing Temp T / °C	Time t / min	Annealed Peak Area / %	Main Peak Area / %
100	60	23.9	76.1
120	60	18.4	81.6
130	10	11.3	88.7
130	60	17.5	82.5

Table 4.5 Annealing Temperature and Endotherm Peaks for 'APP' 32C

T(anneal) / °C	T(endotherm) / °C	T(endotherm) -T(anneal) / °C
70	78.7	8.7
100	111.1	11.0
120	132.6	12.6
130	143.3	13.3

An 'APP' copolymer may behave in the same way but to a lesser degree when dispersed through bitumen. If so, if it were laid on a roof in mid-winter, each warmer day would re-melt the previous day's crystals but deposit a larger amount, until temperatures reached their maximum, say 60°C, *i.e.* not exceeding about 65°C, the optimum temperature for phase separation crystallization (Fig.4.9). Thereafter less and less would be deposited until mid-winter; crystallinity would increase very slightly but by less each year.

If the temperature reached 65°C before mid-summer, then from that time less would be deposited on successively hotter days until mid-summer (Fig.4.10). Then each cooler day would, without melting the previous day's deposit, add more crystals. The daily addition to the

total reached by 65°C after mid-summer would gradually decrease until mid-winter. Then each warmer day would melt a little but deposit more until reaching the maximum phase separation crystallization at about 65°C, when the total crystallinity would reach its maximum. From the 2nd mid-summer the cycle would repeat annually. Thus 'APPs' more susceptible to phase separation crystallization (*i.e.* **32C** and **43C**) would be more likely to crack in mid-winter and particularly in late spring frosts.

4.3.6 Annealing and Crystallinity of an 'Atactic' PP Homopolymer

Results After Annealing and Quenching at One Temperature

The areas under the melting endotherms for **MF80** were measured in the same way (Table 4.6). The thermal history of all samples was the same, *i.e.* they were melted and quenched rapidly at RT, then heated rapidly in the DSC to their annealing temperature; after annealing they were quenched rapidly likewise and then scanned at 10°C per min over 20°-180°C

Table 4.6 Areas Under Melting Endotherms of Annealed 'APP' MF80

Annealing Temp T / °C	Time, t / min	Annealed Peak Area / %	Main Peak Area / %
120	60	8.3	91.7
130	10	15.3	84.7
130	60	41.6	58.4

Only the new broad peak for IPP_1 was measured and not the small sharp peak for IPP_2 (the MCC) superimposed on it. After an hour at 130°C, the new % area was not slightly smaller than after an hour at 120°C, as expected, but about five times larger. This result suggested that much more IPP_1 became available at 130°C for phase separation crystallization because melting of IPP_2 at 122°C freed trapped chains of IPP_1. These odd results backed up the same explanation offered for the TMA derivative plots of **1C** and **MF80**. It followed that phase separation crystallization must have been more and more restricted below the T_m of each lower-melting MCC.

After an hour at 120°C, the new % area was less than half that for **32C**, so this result also showed that the IPP_2, still crystalline at 120°C, restricted phase separation crystallization. [Total IPP in **32C** and **MF80** differed by only 0.4%, and IPP_2 in **MF80** was only 3.3% of total IPP. So, if IPP_2 did not interfere, the new area should have been only about 3% less than for **32C**].

After an hour at 130°C, the new % area was about 2½ times that in the copolymer **32C**. Therefore, above T_m of the highest melting MCC, **MF80** underwent more phase separation crystallization than the copolymer **32C**, as already observed after very slow cooling of the melts - perhaps because **32C** was not entirely PP but had PE and EPR added.

Predictions for Annealing and Quenching Multiple Times

Below T_m of the lower-melting MCC of **MF80**, phase separation crystallization would be even more restricted, so total crystallinity over the year would be less than that for **32C** and **43C** (with no MCCs) (Fig.4.11a). Therefore **1C** and **MF80** would be less likely than **32C** and **43C** to crack in frosts. The temperatures reached on a flat, dark roof in midsummer can be extremely high, but not above 65°C, the optimum temperature for phase separation crystallization. Even so, for completeness, diagrams are given showing how crystallinity at higher temperatures would depend on the melting points of MCCs (Fig.4.11b,c,d).

At first the MCCs were assumed to be deliberate additives to **1C** and **MF80**, to restrict phase separation crystallization. However, later measurements on **32C** (4.4.3) showed that the 107°C component could be produced during the first heating run, *i.e.* though absent on the 1st scan, it was present on the 2nd scan. So perhaps the 107°C component in **1C**, and both the 107° and 122°C components in **MF80**, always present on the 1st scan, were formed during manufacture. The outcome was that below 107°C the copolymer **32C** (and **43C**) was subject to far more phase separation crystallization than the restricted homopolymer **MF80** (and **1C**), but to less phase separation crystallization than **MF80** (and **1C**) above 122°C.

4.3.7 Overlaid Heat Flow Diagrams for APP, IPP and EP up to 300°C

Data were measured in mW from the DSC heat flow charts and normalised to mW mg^{-1} for graphical comparison of the onset and ease of oxidation. IPP melted at a sharp T_m and then began to oxidise immediately afterwards, whereas APP and EP both only softened very gradually and reached T_{on} later, but then oxidised extremely rapidly (Fig.4.12). This difference of behaviour in the molten state indicated that the atactic polymers oxidised far more easily than the more regular isotactic polymer.

For **1C** and its constituent APP and IPP, again the IPP (residue from solvent extraction) began to oxidise sooner than the APP (extracted), but the rate of oxidation of the IPP was much lower than for the APP (Fig.4.13). Therefore the higher the tacticity, the lower the rate of oxidation.

The **1C** blend behaved like its IPP (with rate of oxidation very slightly lower), so the oxidation behaviour of the blend was governed by the presence of the IPP, *i.e.* by the isotactic content.

Commercial crystalline IPP was compared with IPP from **1C** and from **32C** (Fig.4.14). All T_{on} values were very close, but the commercial IPP oxidised much more slowly than the other two. Like **32C**, it had no MCCs. From ΔH data for the quenched melts, crystallinity of the commercial IPP was 56%, while that of the others was 28-29%. Crystallinity measured under the same conditions was a measure of the tacticity, so the rate of oxidation of the melt depended upon tacticity: the higher the tacticity, the lower the rate of oxidation.

4.4 Results and Discussion for Heating to 600°C : Oxidation and Decomposition

4.4.1 For Scans Without Purge Gas

Evaluation of peak positions required a straight base-line, as the exaggerated diagram shows (Fig.4.15). The presence of a melting endotherm in the scan of crystalline, isotactic PP - but not in that of non-crystalline, atactic PP (and APP/EP in **32C** and **43C**) (Fig.4.16) - clearly showed that solvent extraction had completely separated them. The IPP plot was similar to that of commercial IPP (Fig.4.17). The supplied ethylene-propylene (EP) copolymer was also non-crystalline (Fig.4.18).

There seemed to be two oxidation exotherms but this effect was attributed to restricted air supply. It seemed that the initial oxidation of the melt used up the meagre air supply, so decomposition without oxidation took over until there was enough air for oxidation of the rest. A Vestoplast Data Sheet for their polyolefins mentions that long periods of heating lead to decomposition even when oxygen is absent. According to the DSM Stamyroid Data Sheets, **32C** and **43C** have a flashpoint at 280°C, so decomposition was indeed probably occurring in two stages - an initial slow decomposition stage, for which the air supply was sufficient to fully oxidise the products, followed at about 280°C by a spontaneous extremely rapid decomposition, for which the air supply was insufficient to oxidise the products.

Above T_m the charts for **MF80**, **32C** and **43C** were very similar to that for **1C**. 200 Pen bitumen gave a broad low exotherm from about 250° to 450°C, and then a very large exotherm of onset about 500°C and peak 550°C (Fig.4.19), so the bitumen underwent slow oxidation at first, but ignited later. This high temperature work was not pursued further without purge gas

because the bitumen gave a few spikes on the chart, perhaps due to reaction of decomposition products with the pan. **MF80** gave one large single spike at about 370°C, not due to external power surges (because a power filter was used), so possibly this 'APP' contained an additive.

Specific heat plots, mirror-images of heat flow plots, naturally changed sign when the heat flow plot changed sign: C_p was +ve for endothermic, -ve for exothermic sections. So the intercepts of C_p with its zero line could be used to find the intercepts of heat flow whenever there was doubt about its zero line position. C_p values: 1.89-1.79 J/g*K for 200 Pen bitumen (over 60°-130°C), 2.36 J/g*K for **MF80** (over 30°-190°C).

4.4.2 For Scans in Dry Air Purge Gas

For **MF80** in 50 ml/min of dry air (using 1 pin-hole) there were no spikes, so purge gas helped; there were two dips in the large exotherm but no endotherm this time, so oxidation was better but still incomplete. The zero line position, and therefore also the area enclosed by peaks and zero line, could vary slightly with evaluation start temperature, so best position sometimes had to be judged by experience. For **MF80** in 100 ml/min of dry air (using 1 pin-hole) the degree of oxidation was about the same, so it was limited by the pinhole size. Spikes were present again, so this 'APP' was not run again.

For **32C** in 100 ml/min of dry air (using 1 pin-hole), the 1st heat-treatment scan showed the usual melting endotherm peak at about 160°C (Fig.4.20a), but the 2nd scan also showed an extra small melting endotherm peak at 107°C (Fig.4.20b), at exactly the same temperature as for a MCC in both **1C** and **MF80**! Therefore fragments of a particular T_m can break off during heating of these 'APPs,' and perhaps did so during the manufacture of **1C** and **MF80**. Oxidation was better but still incomplete (Fig.4.21), so needed even greater airflow.

For **32C** in 200 ml/min of dry air, using open reference and sample pans in the higher air flow provided almost enough oxygen for the oxidation to occur uninterrupted: there were two small exotherms after the main exotherm, presumably because air was used up (Fig.4.22). The Onset Evaluation mode was tried out: it gave temperatures of onset of melting and oxidation, and it gave temperatures at chosen heat flow thresholds (Fig.4.23). As the main rise in heat output was now smoothly exothermic, it was suitable for a trial of the Kinetic Analysis programme.

4.4.3 For Scans in Nitrogen Purge Gas

32C and **1C** were tested using one pin-hole in the pan lid. **32C** in 50 ml/min nitrogen flow underwent even, slow decomposition from T_m to about 360°C, then rapid decomposition (Fig.4.24), fitting well with the well-known melt instability and with the flash-point quoted in data sheets. In oxygen these two stages would produce slow oxidation, then auto-combustion or spontaneous ignition, fitting with the explanation for earlier partial oxidation curves. The instrument could be set to identify the temperature at onset of fast decomposition (Fig.4.25).

1C in 200 ml/min flow underwent slow decomposition till 351°C, marked by the evaluation auto-limits as the onset of the more rapid decomposition, which peaked at 457°C (Fig.4.26).

After the high temperature work, the DSC cell was cleaned by heating at 600°C for 45 min in 200 ml/min of dry air, as recommended in the manual, to ensure no contamination.

4.5 Results and Discussion of Automatic Kinetic Data Analysis

Automatic kinetic analysis was carried out on the full oxidation exotherm of **32C** and on the full decomposition endotherm of **1C**, to find the activation energy (Fig.4.27) and reaction order (section 2.6). For the **32C** exotherm, analysed from its start at 170°C to its end at 540°C (Fig.4.21), confidence limits on the Alpha *vs* Time plot (Fig.4.28) were all >10%, *i.e.* 31%, 29%, 43%. These values were rather high, probably because the exotherm was not smooth all the way. For the smooth endotherm of **1C** in 200 ml/min of nitrogen (Fig.4.25), from 351° to 500°C, confidence limits (Fig.4.29) were satisfactory, *i.e.* 13%, 5%, 6%. Ideally, for exact comparison both **1C** and **32C** should have been studied in both gases.

Reaction order (given on the print-out) in dry air was 2 to the nearest integer (2.33), so oxidation rate depended on 1 molecule of polymer reacting with 1 molecule of oxygen. Reaction order in nitrogen was 1 to the nearest integer (0.62), so decomposition rate depended on 1 molecule of polymer breaking up (as expected!).

Initial comparison of the plots at about the same temperature showed that oxidation of **32C** at 360°C was much faster than decomposition of **1C** at 370°C, so in unlimited air supply at this temperature oxidation would outstrip decomposition, and the material would auto-ignite, as well-documented for PP. The activation energy (E_a) required for oxidation (103 kJ mol^{-1}) was only half that required for decomposition (227 kJ mol^{-1}), so the former reaction would start at a

lower temperature, as found, *i.e.* about 200° rather than about 350°C. E_a, k and T (temperature) are linked by the Arrhenius equation, which also incorporates the Gas Constant R (8.31 J/mol*K), and a constant A (Eqn.4.3).

4.5 Eqn. 4.3 $k = A\ exp^{-E/RT}$

Taking natural logs, $\ln k = \ln A - E/RT$

Converting to base 10, $2.303 \log_{10}k = 2.303 \log_{10}A - E/RT$

Hence $\log_{10}k = \log_{10}A - E/2.303RT$

For a small rise in T (*e.g.* 350° to 360°C), the ratio of $\log_{10}k$ values should increase only very slightly (as in Table 4.7), but the ratio of k values should change much more (as in Table 4.8).

4.6 Table 4.7 Ln k and $Log_{10}k$ Values for Oxidation & Decomposition of 'APPs' 1C and 32C

T / °C	ln k_{ox} (32C)	ln k_d (1C)	$\log_{10}k_{ox}$ (32C)	$\log_{10}k_d$ (1C)	ln k_{ox}/ln k_d
350	-5.33	-11.38	-2.31	-4.94	0.468
360	-5.02	-10.69	-2.18	-4.64	0.470

4.7 Table 4.8 k and t Values for Oxidation & Decomposition of 'APPs' 1C and 32C

T / °C	k_{ox} (32C)	k_d (1C)	k_{ox}/k_d	t_{ox} / min	t_d / min	t_d/t_{ox}
350	$4.90(10^{-3})$	$1.15(10^{-5})$	427	53	2247	42
360	$6.61(10^{-3})$	$2.29(10^{-5})$	288	38.5	1125	29

At 350°C (the onset of decomposition), the rate constant for oxidation was about 400 times larger, and t for oxidation was about 40 times shorter, than for decomposition. These enormous differences accounted for the spontaneous ignition of PP as soon as it decomposed. By 360°C these ratios fell to about 300 and 30 respectively.

Was this comparison between homopolymer **1C** and copolymer **32C** valid? Later long-term degradation experiments at 120°C showed that they took different times to reach the rapid degradation stage - **1C** took 400 h, but **32C** took only 20 h. However their oxidation exotherms and decomposition endotherms at these extreme temperatures looked very similar, so reaction rates were probably similar, close enough for the general results to be valid. **1C** in dry air and **32C** in nitrogen were to have been compared too, but measurement of T_g values took priority.

No further very high temperature experiments were carried out on these 'APPs' in pans with pierced lids because the products were possibly the cause of the burn-out of the DSC-30

differential sensor, which had to be replaced. An industrial visitor commented that bitumen-like compounds are known to react with the aluminium pans. Even with only low-temperature work on the bitumens, polymers and their blends, from -80° to 180°C, using press-sealed pans, a very fine brown film built up on the underside of the instrument's lid over several months.

4.6 Summary of Conclusions

Data on T_m, ΔH and crystallinity were obtained for the four 'APPs,' on T_m for their minor crystalline components (MCCs), and on specific heats for IPP, APP and PE. Charts verified the separation of APP and IPP components by solvent extraction. Repeated heating cycles to 30°C above T_m (at about 160°C) made oxidation easier (*i.e.* lower temperature) and faster, probably by reducing crystallinity. Prolonged heating at 200°C reduced crystallinity considerably. On very slow cooling from T_m, extra crystals were produced by phase separation crystallization, more in the homo- than the co-polymers. The degree of phase separation crystallization at different annealing temperatures was consistent with the optimum temperature being about 65°C, midway between T_m and T_g. The effect of annealing a copolymer (without MCCs) at two different temperatures, 100° and then 70°C, led to predictions of the variation of the crystallinity of 'APP'/bitumens over the course of one year and successive years. The results for annealing a homopolymer (with MCCs) at different temperatures demonstrated how MCCs restricted phase separation crystallization, and hence could affect long-term crystallinity.

During its heat treatment scan to 180°C, prior to heating to 600°C, one copolymer without an MCC once developed one, with the same T_m as that in both homopolymers. 'APP' oxidation in a restricted air supply indicated two stages, one slow from about 200°C, one fast from about 280°C, the known flashpoint. This conclusion was verified using fast dry air purge gas flow (200 ml/min), which allowed almost completely smooth fast oxidation, and hence automatic kinetic analysis of the exothermic output. Heating in nitrogen showed a clear change from slow decomposition (from T_m) to very fast decomposition (at 351°C), which was analysed. Oxidation needed much less activation energy (about 100 kJ mol^{-1}) than decomposition (about 200 kJ mol^{-1}), which explained why it started sooner and was much faster (about 400 times at 350°C), so 'APP' ignited as soon as it decomposed.

Since amorphous PP oxidized at lower temperature and faster than crystalline PP, it was predicted that (a) the slightly more amorphous 'APPs,' **32C** and **43C**, would oxidize before **1C** and **MF80**, and (b) 'APP' oxidative degradation would involve loss of amorphous material. Therefore, during thermo-oxidative degradation, all 'APPs' should become more crystalline, aided by phase separation crystallization, and eventually % mass loss should level off. Degradation was studied in depth (Chapter 6), including any protection afforded by bitumen, and densities (related to crystallinity) before and afterwards (Chapter 7).

4.7 Tables

Table 4.1 Composition of 'APP' Homopolymers 1C and MF80 3
Table 4.2 Crystallinity Data for Commercial IPP and Four 'APPs' 4
Table 4.3 Specific Heats of IPP, APP and EP 5
Table 4.4 Areas Under the Melting Endotherms of Annealed 'APP' 32C 6
Table 4.5 Annealing Temperature and Endotherm Peaks for 'APP' 32C 6
Table 4.6 Areas Under Melting Endotherms of Annealed 'APP' MF80 7
Table 4.7 Ln k and $Log_{10}k$ Values for Oxidation & Decomposition of 'APPs' 1C and 32C 12
Table 4.8 k and t Values for Oxidation & Decomposition of 'APPs' 1C and 32C 12

4.8 References

8

Blundell D J , Beckett D R and Willcocks P H, Routine crystallinity measurements of polymers by d.s.c.. *Polymer*, 1981, 22, 704-707. 1

Gray A P, Polymer Crystallinity Determination by DSC. *Thermochim Acta*, 1970, 1, 563-579. 1

Kaisersberger E and Moehler H, Netzsch Annual for Science and Industry, Vol.1, *DSC on Polymeric Materials*, Year? 4

Shell Polypropylene - Structure and Performance. Shell Plastics Technical Manual, PP 2.1, 2nd Edition, p.5. 5

Silberman A, Raninson E, Dolgopolsky I and Kenig, S, The Effect of Pigments on the Crystallization and Properties of Polypropylene. *Polymers for Advanced Technologies*, 1995, 6, 643-652. 1

Chapter 5 GLASS TRANSITIONS IN BITUMENS, POLYMERS & THEIR BLENDS 1
5.1 Introduction 1
5.2 Preliminary Results and Discussion 1
5.2.1 Problems with Ice 1
5.2.2 Moisture in 'APPs' and Bitumens 2
5.2.3 Thermal History of an 'APP' From its DSC Plot 2
5.2.4 Cold Crystallization at a Pause in Quenching 3
5.2.5 Experiments to Demonstrate Phase Separation Crystallization in 'APPs' 4
5.3 Measurement of T_g by Single Scans 5
5.3.1 Preliminary Scans from –65°C and from –80°C 5
5.3.2 Variation of T_g and Crystallinity with 'APP' Content 6
5.3.3 Deductions on Miscibility and T_g 7
5.4 Experiments with Linked Methods 7
5.4.1 Investigation of the Best Cooling Rate for T_g Measurement 7
5.4.2 Investigation of Effect of Pause Time at 20°C During Quench of 'APP' 8
5.4.3 Investigation of Effect of Temperature at 10 min Pause in Quench of 'APP' 8
5.4.4 Conclusions on 'APP' Crystallization, from Linked Methods Experiments 9
5.4.5 Conclusions on 'APP' Crystallization, from Other DSC Results 10
5.4.6 Investigation of Effect of Crystallizing and Melting an 'APP' at Progressively Higher Temperatures 11
5.4.7 Investigation of Optimum Scan Speed for T_g Measurements 12
5.5 T_g Measurements by Linked Methods 12
5.5.1 Experimental 12
5.5.2 Results & Discussion for Series of 32C in 100 Pen Bitumen 13
5.5.3 Results & Discussion for Series of SBS in 200 Pen Bitumen 14
5.5.4 Polymer Additives: Conclusions on Proportions from T_g Measurements 14
5.5.5 Experiment to Find Inversion Point by Summing DSC Plots of T_gs 15
5.5.6 Results & Discussion for T_gs of Other Polymers & Polymer/Bitumen Blends 15
5.6 Summary of Conclusions 17
5.7 Tables 18
5.8 References 18

Chapter 5 GLASS TRANSITIONS IN BITUMENS, POLYMERS & THEIR BLENDS

5.1 Introduction

Glass transitions (T_gs) were discussed in Section 1.4.3. and literature T_gs of relevant polymers and copolymers were given in Table 2.5. The Mettler DSC-30 was described in Section 2.6. 'Atactic' polypropylenes ('APPs') were known to be able to reduce the T_g of bitumens to about –25°C, but the following points needed to be addressed:

1. How does glass transition (T_g) depend on composition in the APP/bitumen system?
2. Previous work suggested that the relationship between T_g and composition was not linear. No researched explanation was available.
3. A method was needed to find the optimum, most cost-effective, amount of additive.

T_gs could be measured by low temperature (below 20°C) differential scanning calorimetry (DSC) (Fig.2.11), so polymers, bitumens and polymer-modified bitumens were to be compared by this method. The T_gs of bitumen and 'APPs' were about 0°C and –30°C respectively. The fall in T_g with addition of 'APP' was known to be fast at first, but then slow down, so that further addition made much less difference, but the point at which this happened was not known. The behaviour was expected to mirror that of other physical properties such as cold break and hardness (Fig.1.7). Two series of blends – 'APP' **32C** in 100 pen bitumen and SBS in 200 pen bitumen - were to be examined, and some production line samples (Table 2.3), were also to be compared as a check on quality control. Heat flow scans would be started from at least 30°C below the expected T_g values of about –30°C.

5.2 Preliminary Results and Discussion

5.2.1 Problems with Ice

Before understandable, reproducible results could be obtained below ambient temperatures, a great deal of time went into preliminary testing under different conditions, in order to assess the effects of start temperature, scanning rate, purge gas type and flow rate, and whether holding the start temperature or subtracting a blank run was the better technique. All observations suggested that the DSC-30 was plotting not only the endotherm of a sample, but also the much larger endotherm of another effect - the melting of ice crystals - which began

from the start temperature and masked or distorted the true T_g. Evaluating and trying to overcome the problems due to icing-up used up a great deal of time until a thick cell lid (11 mm deep instead of only 2 mm) became available, not stored with the kit or mentioned in the manual. Naturally this lid improved results tremendously because it cut down the cell volume above the sample, and therefore the possible amount of moisture present. However, even then the measurement of T_gs was not straight-forward – several other chart features were present that had to be explained.

5.2.2 Moisture in 'APPs' and Bitumens

No matter how high the start temperature or how fast the purge gas flow rate, the small endotherm peak at about -3°C in most samples was not removed. Using reference and sample pans sealed under argon made no difference either, so the peak was due to water in the samples themselves. It was deduced that this peak, when close to the T_{g3} of a weak T_g inflexion at a slightly lower temperature, could be taken for the T_{g3} of that inflexion, and so change the apparent T_{g2}, the mid-point of the inflexion (Fig.5.1). It followed that, in general, two close T_g curves of not fully miscible materials would be marked by a change of gradient (Fig.5.2).

Using linked methods later, to compare T_g after cooling of the melt at different rates, it was found that the magnitude of the T_g was by far the largest after liquid nitrogen quenching, and its end (T_{g3}) became clearly distinguishable from the higher-temperature ice-melting endotherm (Fig.5.3). This observation confirmed that early plots were probably read wrongly, that T_{g3} was really lower than first thought, and that T_{g2} of 'APPs' was actually lower than the previously reported -30°C. The ice-melting endotherm could be very sharp, as for blend **98** immediately after liquid nitrogen quench of the melt (Fig.5.4).

With weathering, the bitumen in an 'APP'/bitumen would probably gradually take in a little more water, so the ice-melting endotherm would gradually dominate the close T_{g3} of the 'APP' so much that the apparent T_{g2} would rise to a maximum value (Fig.5.5a). For a polymer with lower T_{g2} than 'APP', which has its T_{g3} well before the ice-melting endotherm, the whole curve and hence T_{g2} would be less affected or even unaffected (Fig.5.5b).

5.2.3 Thermal History of an 'APP' From its DSC Plot

The very first DSC plots of 'APPs' above 20°C had a melting endotherm of onset about RT, large on the 1st run but small on a 2nd run, so it was not just the start-up deflection. Explanation

was not attempted at the time. However, low temperature scans from -60° or -80°C also showed such an endotherm for the 1st run of all 'APP' pellets. If, using linked methods, an 'APP' from a high temperature (80° or 180°C) was quenched to -60°C and re-scanned, that endotherm was absent (Fig.5.6), so it was due to melting of crystals deposited by phase separation crystallization when 'APPs' were stored at RT after rapid cooling after manufacture.

Melting endotherms with onset at RT were also seen for all supplied 'APP'/bitumens, showing that, with 'APP' content of 27% or 30%, they behaved like 'APP' itself. If, using linked methods, **96** was heated to 80°C, quenched, and heated to above 80°C, then a small melting endotherm was seen at onset 80°C. The same effect was seen for **97** stopped at 90°C (Fig.5.7). So even a momentary stop at any temperature allowed phase separation crystallization to occur, and this thermal history could be read on the next scan.

5.2.4 Cold Crystallization at a Pause in Quenching

(a) In 'APPs'

During fast cooling of an 'APP' from the melt at a steady rate, only normal hot crystallization occurred, so only the T_m endotherm was observed on the next heating scan. If cooling was paused at any intermediate temperature T_p, even momentarily, then on the next heating scan, a weak cold crystallization exotherm (of onset T_p) appeared, immediately followed by a weak melting endotherm for those new crystals, and then the normal strong T_m (Fig.5.8). Sometimes only the weak endotherm (of onset about T_p) was observed. So phase separation crystallization occurred at the pause, and further crystallization at T_p could be triggered off (if it had been incomplete at the pause), presumably by a crystal nucleus, on next warming; then all the new crystals immediately started to melt. Hot crystallization refers to an effect observed during cooling from hot, cold crystallization to an effect observed during warming from cold.

(b) In 'APP'/Bitumens

When quenched quickly down to below T_g, a molten 'APP' does not crystallize but becomes a glass, frozen in its amorphous state. On subsequent warming, cold crystallization can theoretically occur as soon as movement is possible, *i.e.* from the T_g, so a large exotherm can be observed, but there is normally a gap after the T_g (as in Fig.1.6). **96** underwent very rapid cold crystallization from the T_g on the 1st but not the 2nd scan (Fig.5.9). What triggered this behaviour? Presumably the same effect as in (a) above, *i.e.* the momentary halt in cooling

(isothermal arrest) at the T_g was sufficient for a crystal nucleus to form, which, on warming, triggered a large amount to crystallize at the same temperature. The 2nd scan showed three small melting endotherms for holds at RT (standby between runs), about 35°C (completion of melting unfinished in 1st scan), and 80°C (end of 1st scan). **97** and **98**, later samples from the same production run, did not show cold crystallization from T_g.

55 (but not **56**) showed cold crystallization from RT (storage temperature) and then melting, so it contained crystallizable material (Fig.5.10a). When scanned 10 days later, there was a very large cold crystallization exotherm starting at about -35°C, *i.e.* from T_g, and then the same melting endotherm (Fig.5.10b). **393** went exothermic after the T_g, while **392** went endothermic (and both showed the usual melting endotherm from almost 30°C). So successive production line samples, tested as supplied, could behave differently on first scans.

5.2.5 Experiments to Demonstrate Phase Separation Crystallization in 'APPs'

When an 'APP' or a blend was held at one temperature, phase separation occurred and crystalline regions grew by 'phase separation crystallization.'

43C was scanned from (a) -80° to 100°C (to erase its thermal history) and quenched to 20°C standby temperature. Then, using linked methods about 5 min later, it was (b) scanned from -80° to 180°C (to melt it) and immediately quenched with liquid nitrogen to -80°C, (c) scanned from -80° to 100°C and quenched to 20°C. Then, using linked methods about 10 min later (b) and (c) were repeated, and called (d) and (e). All scans, at 20°C/min in 500 ml/min of nitrogen purge gas, were evaluated against a blank; all took 2 min settling time before scanning began.

Scan (a) showed the normal ice-melting endotherm and the melting endotherm of onset about 20°C, common to all the supplied 'APP' pellets. Scans (b) and (d), following a hold at 20°C, had a melting endotherm starting there, larger for (d) (Fig.5.11d), which was held there for longer (about 12 min instead of about 7 min). Scans (c) and (e), after no hold at 20°C, did not have one (Fig.5.11e). Thus phase separation crystallization was fast, even well below the optimum temperature of about 65°C (Fig.1.4). Stopping the steady cooling nearer 65°C would produce larger melting endotherms.

1C and **32C** were annealed at 120°C, in open DSC pans in an oven, then press-sealed. Two scans were made on each, about an hour apart, from –60° to 200°C in 200 ml/min of dry air. On 1st scan, besides the main melting endotherm, both 'APPs' had endotherms for crystals formed

during manufacture and during annealing. On 1st scan, **32C** also had an ice-melting endotherm whereas **1C** showed cold crystallization from T_g, followed by immediate melting of those crystals, plus a sharp endotherm for the minor crystalline component (MCC) at 107°C. On 2nd scans thermal history was wiped out, leaving only peaks for ice, MCC and melting point.

5.3 Measurement of T_g by Single Scans

5.3.1 Preliminary Scans from –65°C and from –80°C

First results were obtained with single scans from –65°C to 100°C, using scan speed 20°C/min, *c.*10 mg samples, 300 ml/min N_2, the 2 mm cell lid, and auto-evaluation from -51.6°C. However this start temperature was not low enough for plots to be straight before the T_g inflexion started. Therefore the next scans were run from –80°C, with 300 ml/min dry air, and other conditions the same. The findings from –80°C (and a few at –65°C) for 'APP'/polymer blends are summarised:

Samples **96**, **97** and **98** were almost identical, as were **822** and **823**, **392** and **393**, **55** and **56**. **PFSD** naturally resembled **822** and **823**; **392** and **393** were drier than **96**, **97** and **98**. From –65°C, **96** showed cold crystallization from T_g (see Fig.5.9), and **55** showed cold crystallization from T_g, followed by immediate melting (Fig.5.10). **55** and **56**, containing oxidised bitumen, were different from all others. For **PFSD**, **SIS** and **SBS** the apparent T_{g1} for –80°C start was lower than for -65°C start, so the start needed to be lowered until T_{g1} did not change.

Samples containing **5, 10, 15, 20 and 30% 32C** were compared with **32C** and **100 Pen** bitumen. The -3°C ice-melting endotherm in all the plots made analysis extremely difficult, as it probably merged with T_{g3}. For <15% 'APP,' the 'run-in' to the plot was endothermic, for 15% 'APP' and above, exothermic. Probably by coincidence, this was the known value for optimum miscibility of the 'APP' and bitumen. For the series of **SBS in 200 Pen** bitumen, T_{g2} values were very similar if the -3°C peak for ice-melting, present in all samples and strongest in the bitumen, was mistaking for T_{g3}. In the bitumen itself, if the bend at 50°C was T_{g3}, then T_{g2} was about 0°C, which was close to the literature value (-5°C) for the cold break (Fig.1.7). The 1st scan of **43C** showed a clear melting endotherm, starting at its probable storage temperature but, after quenching from 180° to -80°C by linked methods, it was not in the 2nd scan.

With creation of a glass or frozen amorphous state, very rapid quenching maximised the amplitude of T_g, so that its end was clearly distinguishable below the -3°C ice peak (Fig.5.11e).

It was deduced that, in order to eliminate features due to cold crystallization or melting, and so distinguish T_g features, even a momentary pause in heating or cooling had to be avoided, so automatic linking of methods needed to be applied (5.4), and an even colder start (5.5).

5.3.2 Variation of T_g and Crystallinity with 'APP' Content

10 mg samples were scanned at 20°C/min from -90° to 180°C, and then from –120°C, in 200 ml/min N_2, and evaluated against a Blank scan recorded under identical conditions. Samples with different percentages of **32C** in **100 Pen** bitumen were studied. With clear separation of T_{g3} and the ice peak, the T_g of **32C** was clearly well below the literature value of -30°C. T_g of the bitumen fell with increasing **32C** content, but T_gs for 5% and 0 % **32C** were hard to estimate because of the -3°C ice peak. Nevertheless data for T_g (Table 5.1) were plotted (Fig.5.12) and roughly matched the shape of the known Cold Break Curve (Fig.1.7), confirming that addition of more than about 15 % **32C** caused little extra lowering of T_g, so this value was the optimum amount of additive for lowering T_g.

Content or % crystallinity was also obtained from the area under the melting endotherm (Fig.5.13) – it was printed out automatically if the ΔH for 100% crystalline IPP was entered at the start of the evaluation, together with required temperature limits. Content agreed well with that estimated from % **32C** × (content in 100% **32C**), better so at low %'s (perhaps because better mixed), so could be used to identify a blend, or deduce the 'APP' content (of known crystallinity) of a sample in a series.

Table 5.1 T_g and Crystalline Content of Series of 'APP' 32C in 100 Pen Bitumen, from Single DSC Scan of Quenched Melt from –120°C

% 32C	T_g / °C Eval'd	T_g / °C Estim'd	Crystalline Content from DSC / %	Crystalline Content Estimated / %	T_m / °C
100	-35.80	-42	8.7	-	154.7
30	-33.41	-35	2.2	2.6	147.8
20	-32.68	-33	2.0	1.75	147.3
15	-35.01	-32	1.7	1.3	146.2
10	-13.40	-24	0.9	0.9	146.0
5	-15.66	?	0.4	0.4	146.7
0	-17.69	-18	-	-	-

5.3.3 Deductions on Miscibility and T_g

While they remain miscible, *i.e.* while 'APP' is the minor dispersed phase, adding a low % of 'APP' (A) to bitumen (B) produces a new T_g for (A + B) between T_{gA} and T_{gB}. As the % of A rises, the T_g will fall and its magnitude will rise: both figures will reach their lowest and highest values respectively when maximum miscibility is reached. Thereafter, adding more A will produce a second weak T_g for A alone below that for (A + B), which will be hardly affected and will still be the predominant feature determining the cold break. Going beyond maximum miscibility, by adding more A, is pointless. Thus following variation of T_g with % of A is a way of finding optimum miscibility of an 'APP' and a bitumen. Comparison of different polymers, bitumens and blends would give the most economical combination for a required T_g.

Conversely, any method of finding optimum miscibility would indicate the optimum proportions for lowest T_g of a polymer-modified bitumen. [A melting method and a degradation method described elsewhere would do just that]. If optimum miscibility were already known, and also the T_{g1}, T_{g2} and T_{g3} values and corresponding ΔC_p of separate polymer and bitumen, then perhaps a computer programme to add curves would give a rough value of lowest likely T_g from any given combination. Then, based on performance and cost, further T_g tests could be carried out on a series of the best polymer/bitumen combinations.

5.4 Experiments with Linked Methods

In order to demonstrate the behaviour of samples more rigorously, totally linked methods were used in different ways on one 10.2 mg sample of **43C**, using the 11 mm cell lid. Linked methods involved repeated cycling between set temperatures at a set heating rate and a controlled or uncontrolled cooling rate (by liquid nitrogen), then a heat flow scan after each cycle. There were three purposes: (a) to cool the melt at different rates, to find the effect on T_g; (b) to pause the quench at the same hold temperature for different times, to confirm the effect on crystallization; (c) to pause the quench for the same hold time at different temperatures, to measure the heat change over 10 min each time, and to confirm the effect on crystallization.

5.4.1 Investigation of the Best Cooling Rate for T_g Measurement

Experimental

After 1st scan and liquid nitrogen quenching, the end of the T_g of an 'APP' was distinct from the ice-melting endotherm. To find out whether a fast controlled cooling rate would do the

same, the melt of copolymer **43C** was cooled at different rates. Linked runs were set up with uncontrolled cooling (>>50°C/min), and controlled cooling at 50, 40, 30, 20, and 10°C/min.

Results and Discussion

Plots showed that even up to 50°C/min the end of the T_g merged into the ice peak (Fig.5.14). Therefore, to obtain the best T_g results, melting and uncontrolled quenching were needed first, both to erase the thermal history and to give the largest possible T_g inflexion, so linked methods were needed. [As a side-line it was found that, during cooling stages, temperature oscillations masked features until the cooling rate was reduced to 10°C/min (Fig.5.15); then the onset of crystallization was 120°C, the same as the onset of melting found by heating at 20°C/min].

5.4.2 Investigation of Effect of Pause Time at 20°C During Quench of 'APP'

Experimental

The earlier rough cycled scanning (5.3.4) was repeated with exactly known time intervals, using totally linked methods to cycle the temperature (Fig.5.16). A sample of **32C** was repeatedly (a) scanned from -80° to 180°C, (b) quenched to 20°C, (c) held at 20°C for different times and (d) quenched to -80°C. On each cycle, the time at 20°C was increased, so the hold was for 1, 2, 4, 6 and 8 min plus 2 min settling time, and finally 20 h overnight (Fig.5.17).

Results and Discussion

3, 4 and 6 min pauses allowed more and more crystallization, and hence a larger melting endotherm, but there was no noticeable difference between 6, 8 and 10 min holds. The melting endotherm after 20 h was very much larger but not as large as for the starting state. So crystallization was very rapid for 4 and 6 min, but then was much slower. All isothermal plots on this day (Day 1) at the pauses were exothermic for 1-4 min, as expected for crystallization.

5.4.3 Investigation of Effect of Temperature at 10 min Pause in Quench of 'APP'

Experimental

On another day (Day 2), during successive cycles the quenching of **43C** was paused at 20°, 40°, 60°, 80° and 100°C for 10 min. The same cycle was repeated on another day (Day 3), with holds at -40°, -30°, -20°, -10°, 0°, 5°, 10°, 15°, 50°, 60° and 70°C all on one day, and a few more cycles were made on the next day (Day 4).

Results and Discussion

After a 10 min quench at each temperature, the next dynamic heat flow scan from -80°C showed a small new melting endotherm with onset at that same temperature (Fig.5.18), confirming earlier separate observations of this phenomenon; there was no new endotherm if the quench was not paused. During each pause the isothermal heat change (from 1 min adjustment time to 10 min) was endothermic this time (Day 2) for the whole set (Fig.5.19) and decreased as the hold temperature was raised. So a different crystallization process was occurring, depositing more crystals as the difference between hold and melt temperatures increased. When the same cycle was repeated throughout another day (Day 3), the heat changes were all exothermic again (Fig.5.20). A few extra measurements made the next day (Day 4) were endothermic again! All the exothermic and endothermic heat changes for those 10 min pauses were plotted against Hold temperature on the same graph (Fig.5.21).

5.4.4 Conclusions on 'APP' Crystallization, from Linked Methods Experiments

It was deduced that there were two ways for 'APP' **43C** to crystallize, involving either a very exothermic process, or an endothermic process, taking in more heat than the other put out. The first effect fitted with cold crystallization from T_g or above, as observed in some heat flow plots and attributed to the presence of a crystal nucleus acting as a trigger. This nucleus, acting like a seed, could be a region in which several polymer chains are closely aligned. The second effect fitted with phase separation crystallization, which must consume more energy to move polymer chains around than is evolved when they crystallize out. As to be expected by analogy with normal solutions, the lower the hold temperature below that of the melt, the greater the amount of crystallization and hence the heat change by either means.

In 5.4.2, isothermal plots at 20°C were all exothermic, and there was no change after 6 min, so the crystallization was initially the rapid 'seeded' type, while further slow changes continuing overnight were due to slow phase separation crystallization. Probably the exothermic process spread very rapidly through a certain distance because the large heat output allowed movement and alignment of nearby chains too.

In the combined plot (Fig.5.21) there was a step up in heat output for the exothermic process at the 0°C hold, probably because of the added effect of ice crystallizing too. If more data were obtained for the endothermic crystallization, there would probably be a corresponding step in

that plot too. If even colder hold temperatures were used, both exo- and endo-thermic plots would probably suddenly drop to zero at the T_g, the point at which translational motion ceases. Therefore such linked method scanning would be yet another method of obtaining the T_g of a sample, instead of or as well as DSC.

As all the results on any one day were either exo- or endo-thermic, crystallization kept occurring in whichever way it started the day. Therefore 'seeding' occurred either every time or not at all. Therefore the determining factor for exo- or endo-thermic crystallization was probably the crystalline state at the start of the day after phase separation crystallization overnight. Either sufficient chains were aligned conveniently for immediate exothermic crystallization or they were not, and the short heating at 180°C in each cycle did not scramble them enough to prevent this effect on successive cycles. So, if and when the degree of alignment reached some critical value, then a change-over in crystallization behaviour occurred, from endothermic to exothermic, an example of a catastrophic change.

This proposed change-over was later actually observed during the 1st isothermal scan of **43C** at 20°C, after quenching of the melt of a fresh sample (Fig.5.22). If the hold at 180°C were extended to longer times on **43C** that first crystallized exothermically, then eventually the heat flow at a 20°C hold would probably change from exo- to endo-thermic, not gradually but directly. With instruments out of action, there as no chance to verify this.

32C and **43C**, mixtures of IPP, APP, PE and EPR, acted partly like conventional saturated solutions of crystalline solutes in compatible solvents. In those, crystallization can occur instantly if triggered off by, for instance, just a single crystal or glass particle acting as a seed, or it can occur more slowly with standing, when all the molecules are in constant motion.

5.4.5 Conclusions on 'APP' Crystallization, from Other DSC Results

At whatever temperature there was a pause in steady cooling of the melt, crystals formed instantly, and these crystals melted next time the mixture was warmed to that same temperature. This imprinting effect was just like crystallization and melting ('de-crystallization') of 'normal' crystals, except that the two effects could occur at any one temperature, so the 'APPs' could also act like crystalline solids. On warming, further slight cold crystallization often, but not always, occurred at that temperature before the melting started. Whenever a quenched melt was warmed, and did not cold crystallize (from 'seeding'),

phase separation (*i.e.* unmixing) was going on all the time, best at midway between T_g and T_m. At whatever temperature warming was stopped, a crystal nucleus formed instantly and then, on next warming, melted at that temperature.

Therefore, as heat was put into the semi-crystalline mixtures, the crystals formed previously by phase separation crystallization (which were a different type from those which melt at T_m) were broken down again when the temperature reached that of their formation during cooling. This was the same principle as in 'normal' crystallization and melting. If phase separation crystallization were made to happen at two temperatures, then melting would occur at the same two temperatures, as demonstrated in 4.2.5.2.. Perhaps the cold crystallization sometimes triggered off first was easily precipitated because it was an exothermic process (with a very small energy barrier) that stabilized the system.

Homopolymers with similar crystalline content might behave in the same way as copolymer **43C** (and **32C**), but their MCCs might make a difference. With prolonged heating, **32C** could develop an MCC (Fig.4.20) and behave like **1C**. The 'APP'/bitumens containing 27% 'APP' or 30% **32C** behaved in the same way as the 'APPs,' just as they were expected to do with 'APP' as the main phase.

5.4.6 Investigation of Effect of Crystallizing and Melting an 'APP' at Progressively Higher Temperatures

It has been well shown that semi-crystalline 'APPs' undergo phase separation crystallization extremely easily, and that they have melting endotherms at whatever temperature it previously occurred. It was deduced that, if an 'APP' were heated from the same start temperature to a higher top temperature on each linked DSC cycle, then the top temperature of the 1st scan would be the onset of a melting endotherm in the 2nd scan, and so on. Then that endotherm would be absent from the 3rd scan, and so on. This demonstration was tried out with **43C**.

Experimental

After its heat treatment scan from –60°C to 180°C, and quench to –60°C (Fig.5.23), a sample of **43C** was warmed at 20°C/min to 7 different temperatures, higher each time, held there for 5 min and quenched to –60°C each time. Cycling was then repeated with no designated Hold at each top temperature, to see if the briefest possible pause had the same effect. Top temperatures were far enough apart for endotherms to be clear: 0°, 25°, 50°, 75°, 100°, 125° and 150°C. Hold

temperatures were actually 4°C below that programmed in, N_2 flow 200 ml/min, mass 10.0 mg, baseline 1 for no blank.

Results and Discussion

The predicted behaviour was confirmed (Fig.5.24). On repeat, with no Hold at each top temperature, but immediate turn-round into cooling, the same effect was still seen, just not quite so strongly. The possible consequences, for crystallinity of 'APP'/bitumen blends through the first and subsequent years, of this melting of crystals at one temperature and formation of others at a higher temperature were discussed earlier (4.2.5 and 4.2.6).

Suppose we have a sample of a semi-crystalline polymer with three adjacent melting endotherms of increasing onset temperatures T_1, T_2 and T_3 (Fig.5.25). On heating a 2nd sample from T_1 to T_2, the 1st melting will occur (endotherm same size) and extra crystals will also deposit at the stop at T_2 (exothermic process). If the next linked heating scan is from T_1 to T_3, the 1st endotherm will be absent, the 2nd melting will occur (endotherm now bigger) and extra crystals will deposit at the stop at T_3 (exothermic process). If the next linked heating scan is from T_1 to T_4 (end of 3rd endotherm) the 1st and 2nd endotherms will be absent, and the 3rd melting will occur (endotherm now bigger). [This experiment could easily be created]. This sort of behaviour was discussed in a study of IPP by C.Passingham and co-workers (Passingham *et al*, 1990), who suggested that there was an exothermic process between the endotherms.

5.4.7 Investigation of Optimum Scan Speed for T_g Measurements

Linked scans of **32C** from -120° to 180°C at 10, 15, 20 and 25°C/min showed 10°C/min was too noisy, 15°C/min was better but smoothed out features slightly, 20°C/min or more smoothed out features even more. Linked scans at 11, 12, 13, 14 °C/min showed 13°C/min to be best, so it was used for the whole set of samples.

5.5 T_g Measurements by Linked Methods

5.5.1 Experimental

All samples were first scanned to 180°C and quenched, and then scanned under the following conditions: scan rate 13°C/min, purge gas flow 200 ml/min of N_2, and scan range -130°C to 180°C (or -150°C to 200°C) with evaluation -120° to 175°C (or -140°C to 190°C) *vs* a Blank run under identical conditions. All samples produced a very small ice-melting endotherm at about

-2°C. The automatic dotted evaluation lines on the charts - and hence the values of ΔC_p, T_{g1}, T_{g2}, and T_{g3} - did not always make sense, because the instrument simply followed rules on where to put them. It was still sometimes a matter of judgement, built up from experience, to interpret the print-outs. Measurements were made on (a) the series of blends of **32C** in 100 Pen bitumen, (b) the series of blends of **SBS** in 200 Pen bitumen, (c) all the polymer additives – the other nine 'APPs,' plus SBS, SIS, LDPE and HDPE, and (d) some polymer/bitumen blends.

5.5.2 Results & Discussion for Series of 32C in 100 Pen Bitumen

Firstly the earlier scans (5.4.2) were repeated, with one sample re-used many times, and with a set of fresh samples. All samples contained about the same amount of moisture, causing an ice-melting endotherm with peak at -1° to -2°C, and ΔH 0.2 to 0.5 J/g. The more moisture, the higher were the temperature and ΔH.

For **100 Pen** Bitumen, ignoring the ice peak at -2°C, the plot showed three bends at -27°, -9° and 30°C, indicating two adjacent T_gs due to incomplete miscibility. Taking an average of the two, with a straight line from -27° (T_{g1}) to 30°C (T_{g3}), gave T_{g2} at the mid-point as +1.5°C, fitting with the expected value of just above 0°C. For **32C**, the amplitude of the T_g was large enough for the ice-melting peak to not interfere with evaluation of T_{g3}; so T_{g2} was -38°C, well below the literature value of -30°C (Fig.5.26). The bend at 30°C was reduced by **5% 32C** and absent with **10% 32C**, perhaps because the 'APP' improved miscibility of the bitumen components. Consequently there was now only the one lower T_g.

For added **15%, 20%, 30% 32C**, the bend at -9°C was removed (or became negligible) and the bend at -27°C was cancelled out by the T_{g3} of the 'APP.' At the same time the strong T_g of the 'APP' at -38°C became dominant, so T_g fell much further still. Addition of more than 15% **32C** to 100 Pen bitumen did not reduce T_g much further, so it is unnecessary. Also the amplitude ΔC_p between T_{g1} and T_{g3} increased to nearer that for **32C** itself, but amplitude probably did not matter provided it was still the largest step in the plot. Re-used and fresh samples gave very results (Table 5.2), so repeated melting and quenching had negligible effect over the short time involved (Fig.5.27).

The 'APP' content affected three factors, which could therefore all be used to identify a sample in a set or find the % 'APP' in an unknown sample (if crystallinity were known approximately): (a) T_m rose as 'APP' content rose (except for smallest peak for 5%); (b)

evaluated crystalline content matched calculated values (in brackets) well (as in Table 5.1) except for 15%; (c) amplitude ΔC_p rose with % 'APP.'

Table 5.2 T_g and T_m of Different Blends of 'APP' 32C in 100 Pen Bitumen, Using Re-used Samples and Separate Fresh Samples

	Re-used Samples				Separate Fresh Samples					
32C %	T_{g2} /°C	T_m /°C	Content	ΔC_p	T_{g1} /°C	T_{g2} /°C	T_{g3} /°C	T_m /°C	Content	ΔC_p
100	-36.48	156.5	8.9	0.27	-48.34	-37.99	-27.64	156.6	9.25	0.28
30	-35.16	149.8	2.4 (2.7)	0.15	-40.31	-34.49	-28.88	149.7	2.8 (2.8)	0.13
20	-36.20	148.3	2.1 (1.8)	0.12	-43.12	-35.78	-28.44	149.0	1.9 (1.9)	0.11
15	-35.58	148.2	1.9 (1.3)	0.08	-43.16	-36.25	-29.34	148.6	2.2 (1.4)	0.11
10	-25.5	147.4	1.0 (0.9)	--	-38.80	-27.78	-16.98	148.3	0.9 (0.9)	0.06
5	-15.38	147.9	0.4 (0.4)	0.14	-27.79	-19.15	-10.29	148.7	0.6 (0.5)	0.07
0	--	--	--		-27	+1.5	+30	--	--	--

5.5.3 Results & Discussion for Series of SBS in 200 Pen Bitumen

For **200 Pen** bitumen (Fig.5.28a), moisture content was higher than in 100 Pen, and T_{g1} was clearer. The plot showed three bends at -40°, -15° and 30°C, indicating two adjacent T_gs due to incomplete miscibility. The large ice-melting endotherm distorted automatic evaluation of T_g, but spanning the ice peak with a straight line from -40° to 30°C gave an estimated T_{g2} of -5°C.

For **SBS** (Fig.5.28b), the plot was the classic shape, with a very low T_g at –90.6°C and high ΔCp 0.387 J/g*K. Plots for **9% SBS** and **13% SBS** were almost the same, with a small ice peak, and a very long T_g inflexion from –110° to 30°C, with its centre at –40°C (Fig.5.28c). Therefore this material might be a more efficient additive than 'APP' to reduce the T_g of bitumens. The relative amplitudes of T_g for 13%:9% were 4:3 (2 mW to 1.5 mW for the same mass), so amplitude was roughly proportional to % SBS. 2nd Samples of each blend gave similar results. Lower start temperatures were not tried.

5.5.4 Polymer Additives: Conclusions on Proportions from T_g Measurements

It seemed that the action of an additive must depend upon creating a new 'step' in the heat flow plot that is sufficiently larger than that of the starting material to dominate it or extend it to

lower temperatures. So an additive with larger amplitude 'step' at lower temperature will be more efficient at reducing T_g. In the case of SBS in 200 Pen, 9% SBS was enough to do this, so adding more was probably unnecessary. Even less than 9% might be enough but no other samples were available to test. The more additive added, the larger the 'step', *i.e.* the higher the ΔC_p through the transition from brittle to rubbery state. How small an added 'step' in the plot is sufficient for the T_g to be affected in practice? This must depend upon the optimum miscibility – once again the point of inversion must indicate the best proportions.

5.5.5 Experiment to Find Inversion Point by Summing DSC Plots of T_gs

An Excel PC spreadsheet was used to sum the DSC plots of additive SBS (x% of all amplitudes) and 100 Pen bitumen (100-x% of all amplitudes) (Spreadsheets after Diagrams). It showed that high % SBS still resulted in two T_gs, but 9% SBS extended Tg_1 back to that of the additive. Thus, for very different pairs of curves, the approximate % at which the T_g of other additives would dominate or extend the T_g of a bitumen could be estimated by spreadsheet. This method would be yet another way, though only rough, of estimating the optimum composition or inversion point of a blend.

5.5.6 Results & Discussion for T_gs of Other Polymers & Polymer/Bitumen Blends

All the other polymer additives and blends were also studied (Table 5.3), though not all data were collected for every sample. Even on the same recording speed, temperatures could still vary slightly; subtraction of a blank made only a very small difference. **SIS** had two distinct T_gs, indicating poor miscibility; **SBS** and **SIS** should be the most efficient polymer additives for lowering T_g of bitumens because their T_gs were very low, with very high amplitudes; **95-X-06** had a very weak T_g, so would be a poor additive. **LDPE** began to soften from *c.*4°C, whereas **HDPE** had an endotherm 17.5°C higher, with 68% greater area and a shorter, steeper approach from 69°C. **C80**, **T1180, 95-X-06** and **V808** had two endotherms, one for PP and a lower one probably for LDPE. Long-term thermal degradation of **C80** and **T1180** also revealed two amorphous components, and hence crystalline components. Even **V891** and **MF500**, with negligible and no crystalline PE, might still contain amorphous PE. **95-X-06**, **V808** and **V891** showed a clear peak for moisture content, at –2.9, –2.7 and –2.0°C respectively. The 'APPs' had similar T_gs, below the literature value of –30°C: **V891** (-32°), **V808** (-34°C), **32C** and **95-X-06** (-38°), **MF500** (-40°), **C80** (*c.*-40°C) and **T1180** (*c.*-46°).

Table 5.3 DSC Data for Some 'APPs' and Other Polymer Additives

	T_g (°C)	Fig.	T_m (°C)	ΔH (J/g)	T_m (°C)	ΔH (J/g)
1C	*-30.4*	-	-	-	155.8	25.8
MF80	*-28.3*	-	-	-	155.6	24.1
32C	-36.48, -37.99, *-35.80, -38.2, -40.6*	-	-	-	156.5, 156.6, 156.7, 157.0	*18.0*, 18.4, *19.1*
43C	*[-44]*	-	-	-	*155.8*	*22.2*
MF500	-39.6	-	-	-	154.9	15.0
C80	[-40]	5.29f	91.7	94.71	151.6 (152.1)	7.03 (7.15)
T1180	[-46]	5.29g	95.2	2.3	145.4	5.8
95-X-06	-38.1 (-38.7)	5.29h	105.5	8.24	153.9	17.4
V808	-33.5 (-34.2)	5.29e	*102.0*, 100.4	*2.56*, 2.56	*157.6*, 158.3	*7.5*, 7.5
V891	-32.1, -32.3 (-32.9)	-	-	-	*159.0*, 158.0	*8.5*, 8.5
LDPE		5.29c	112.6, 112.8	131.7	-	-
HDPE		5.29d	132.0	221.0	-	-
100 Pen	+1.5	-	-	-	-	-
Ox.Bit.	*[-10]*	5.29a	-	-	-	-
SIS	-100, -59.7	5.29b	-	-	-	-
SBS	-90.6	5.28b	-	-	-	-
PFSD	[-40]	5.28d	-	-	-	-

Values were measured at 13K/min (and printed out automatically) except for those in italics, [ ] = estimated values, ( ) = values against a blank

Data for **96** and **392** closely matched those for 30% **32C** in 200 Pen bitumen with similar content (Table 5.4). **822**, with a long straight T_g section from -110° to 24°C, midpoint -43°C, was almost identical with 9% SBS in 200 Pen (the same content). For **PFSD** (6% IB in 100 Pen), the T_g was estimated as -40°, halfway between -110° and 30°C. **Oxidized bitumen** contained moisture and was different from straight bitumens: its T_{g3} was the most pronounced of all samples. In **55** only 2% SBS reduced its T_g from *c.*-10° to *c.*-30°C. All the SBS blends and PFSD could be scanned from lower temperatures to check that T_{g1} is not really even lower.

Table 5.4 DSC Data for Similar 'APP'/Bitumen Blends

Sample	Content	T_g (°C)	Crystallinity
96	27% 'APP' in 100 Pen	-39.7	3.0
	30% 32C in 200 Pen		
392	30% 43C in 200 Pen	-39.5	3.4

Experimental work ended when the TC-10A processor stopped working. Mettler-Toledo in Leicester had already repaired and returned the DSC-30 nitrogen heater and the TMA-40 free of charge. They also replaced the gas discharge tube in the processor but the board could not be repaired and needed to be replaced for *c.*£800. Vulcanite/Callenders asked if there was a method for measuring the actual temperature at which a sample cracks, to complement the standard fail/pass test at a fixed temperature. Apparatus designed by Dr Fawcett in Belfast, who has worked with Vulcanite, would have fitted the bill but would have taken over £700 and more time than there was available to construct it.

5.6 Summary of Conclusions

After initial problems, the low temperature DSC investigations using single scans provided a great deal of information, including the required variation of T_g of 'APP'/polymer blends with 'APP' content - it was found that below about 17% 'APP,' further addition made very little extra difference. This optimum, most cost-effective, amount of additive was also the amount at the inversion point of the 'APP'/bitumen system. Therefore any methods of finding the inversion point would also lead to the optimum amount of additive. Crystallinity of blends was also calculated automatically, from the area under the melting endotherm, and agreed well with estimated values, so the method could be used to deduce the 'APP' content of a related blend. The necessary investigations of other DSC features also led to a much wider understanding of the typical thermal behaviour of the 'APPs.' They underwent phase separation crystallization at even the briefest pause in cooling, and cold crystallization. Almost all the 'APPs,' bitumens and blends contained moisture, and the ice-melting endotherm could be misinterpreted as the end of the T_g and hence give a false value for its centre. To avoid icing-up of the cell, it was important to always use nitrogen purge gas and the thicker 11 mm cell lid for low temperature work.

All the observations were improved and proved more rigorously by use of linked methods. The T_g of 'APP' was –38°C, lower than the literature value of –30°C, and the optimum amount of 'APP' was 17%. The T_g of SBS was –90.6°C, and the optimum amount was probably less than 9%. With two linked scans, the first scans standardized the test samples, and pauses were avoided; with multiple scans, test cycles could be repeated with a change in only one factor each time. The effects of repeated cycles to different top temperatures were

discussed with reference to long-term crystallinity of blends in use on a roof-top, subject to daily and seasonal temperature cycles. Isothermal plots of heat change at pauses in cooling at different temperatures showed that 'APPs' either gained or lost heat at the pause, attributed to cold crystallization or to phase separation crystallization respectively on any one day. Extension of the experiment, with pauses in cooling at progressively lower temperatures should provide an alternative method of determining T_g – where there is no heat change at the pause. It was deduced that the optimum amount of a polymer additive was the lowest amount that gave not two T_gs but one large T_g with the T_{g1} of the polymer and the T_{g3} of the bitumen. Summation of T_g curves, in different proportions, for SBS and bitumen, by Excel spreadsheet, showed that the optimum amount could be predicted roughly in this way before tests on a whole series, at least for a combination with very different T_gs.

5.7 Tables

Table 5.1 T_g and Crystalline Content of Series of 'APP' 32C in 100 Pen Bitumen, from Single DSC Scan of Quenched Melt from –120°C 6

Table 5.2 T_g and T_m of Different Blends of 'APP' 32C in 100 Pen Bitumen, Using Re-used Samples and Separate Fresh Samples 15

Table 5.3 DSC Data for Some 'APPs' and Other Polymer Additives 15

Table 5.4 DSC Data for Similar 'APP'/Bitumen Blends 16

5.8 References

8

Passingham C, Hendra P J, Cudby M E A, Zichy V and Weller M, *Eur. Pol. J.*, 1990, Vol.26, No.6, pp.631-638: *The Re-evaluation of Multiple Peaks in the DSC Melting Endotherm of Isotactic Polypropylene* 12

Chapter 6 THERMO-OXIDATIVE DEGRADATION OF 'ATACTIC POLYPROPYLENES' 1
6.1 Introduction 1
6.1.1 Literature Information on Polypropylene Degradation 1
6.1.2 Literature Information on Protection Against Degradation 2
6.1.3 Literature Mechanism for Polyolefin Degradation 3
6.1.4 Main Question to Be Answered 4
6.2 Initial Degradation Experiments at 120°C 5
6.2.1 The Ovens 5
6.2.2 In Alternating Daylight & Darkness 5
6.2.3 In (Almost Complete) Darkness 6
6.2.4 In Winter Daylight 7
6.3 Long-Term Standardized Degradation at 120°C in 5 Lux 9
6.3.1 Experimental 9
6.3.2 Results and Discussion 10
6.4 Long-Term Standardized Degradation *en Masse* at 120°C in 4 Lux 11
6.4.1 Experimental 11
6.4.2 Results and Discussion 12
6.5 Long-Term Standardized Degradation at 120°C in Darkness 13
6.5.1 Dark Heating, with Exposure to About 4 Lux During Cooling 13
6.5.2 Dark Heating, with Exposure to <<1 Lux During Previous Cooling 14
6.5.3 Dark Degradation of 'APPs' After Cooling in Different Light Levels 15
6.5.4 Sealed Dark Heating, with No Light Exposure While Cooling 15
6.6 Long-Term Tests on Relationship Between Sample Preparation and Degradation 16
6.6.1 Background – Evidence for Thermal Shock 16
6.6.2 Experimental – Sample Preparation 17
6.6.3 Results and Discussion 18
6.7 Suggested Complementary Mechanism for Oxidative Degradation 20
6.7.1 Basic Outline 20
6.7.2 Suggested Other Factors Affecting Polymer Oxidation 21
6.7.3 Application of the Model to Features of % Mass Change Graphs 22
6.7.4 Spreadsheet Model of Thermal Degradation 23
6.8 Summary of Conclusions 25
6.9 Tables 26
6.10 References 27

Chapter 6 THERMO-OXIDATIVE DEGRADATION OF 'ATACTIC POLYPROPYLENES'

6.1 Introduction

6.1.1 Literature Information on Polypropylene Degradation

Some general literature information on thermal degradation of polypropylene was given in the Introduction (1.5). Several groups have also studied the degradation of PP by UV irradiation or photo-oxidation. The progress of oxidation has been followed from the growth of the 'carbonyl index,' from the IR of carbonyl groups (Subowo *et al*, 1986). The initial stage of photooxidation of PE was also monitored by uptake of oxygen (Bigger and Delatycki, 1987), and it was deduced that the initial rate of photooxidation was proportional to the concentration of polymer hydroperoxide present from processing, and that the rate was limited by the number of sites available to oxygen attack. Both approaches make use of the deduced mechanism, *i.e.* that 'carbon-centered radicals combine with atmospheric oxygen to form metastable peroxy radicals* and hydroperoxides*, which decompose to generate a variety of stable product groups such as hydroxyl, carbonyl and carboxylic groups' (Gengenbach *et al*, 1994). *[(R-O-O·) and (R-O-O-H)]. Auto-oxidation in organic materials in general is discussed by Sykes (Sykes, 1975, 11.5.2.2, 318-321).

Livanova investigated the induction stage in PP oxidation (Livanova, 1994) and deduced that its end was 'marked by the expansion of the oxidation reaction from the initiation sites and its propagation over the entire polymer.' Initially reaction is localized on randomly distributed initiation sites but is autoaccelerated into the bulk of the polymer by decomposition of hydroperoxides. Oxidation can also be termed autooxidation or spontaneous oxidation because of the rapid way it 'takes off,' and it can also be induced by load (Baumhardt-Neto and De Paoli, 1993; Baumhardt-Neto and De Paoli, 1993, 2).

For IPP-HDPE autooxidation, the shortest induction period was for 50:50 PP:PE (Shibryaeva and Popov, 1994), and data suggested 'that the initial oxidation rate of the PP-PE blends is controlled by oxidation of the PP component. The oxidation rate of the PP is lower, and that of the PE component is higher, as compared to the oxidation rate of the corresponding homopolymer.'

Polyolefin oxidation is accelerated in water and aqueous solutions of sodium salts or alkalis, by more for LDPE than for HDPE or PP (Henry *et al*; Ruaya *et al*), perhaps because these are more crystalline and less permeable. Neutral and basic aqueous media promote neucleophilic attack by peroxy anions on polymer hydroperoxides to give free radicals able to initiate further oxidation. Acidic solutions suppress oxidation by decomposing hydroperoxides to non-radical products. In roofing membranes, definitely in an aqueous environment, bitumen would protect polymer against neutral/basic attack and polymer would protect bitumen from acidic attack, for a long time. However, once degradation reached a certain stage, increased exposure of one or the other would lead to accelerated degradation by surface water. This is an argument for having sloping rather than flat roofs.

6.1.2 Literature Information on Protection Against Degradation

Commercial 'atactic' polypropylenes ('APPs'), like many polymers, are susceptible to oxygen/heat/UV/water, *i.e.* weathering (Hall, 1989). Photo-stabilization of the 'APPs' might help – by reducing rates of initiation or propagation of chains or by increasing rates of chain termination (Wayne and Wayne, 1996, Sykes, 1975, 11.5.1.4, 311-313). Subowo *et al* (*ibid*) showed by plots of carbonyl index *vs* time that carbonyl formation was slowed down slightly by a UV absorber, more by an excited-state quencher or antioxidant, and even more by a radical scavenger. Several classes of compounds can act as antioxidants, *e.g.* phenols, aromatic amines, organic hydroxylamines and thiophenols. Sterically hindered phenols have been studied as antioxidants (Shanina *et al*, 1995; Shanina *et al*, 1996), with conversion themselves to quinones, *e.g.* substituted 4,4'-HO-Ph-Ph-OH became substituted 4,4'-O=Ph=Ph=O. One monophenol (2,'6-di-*tert*-butyl-4-phenylphenol) rapidly increased the induction period for APP, but only above about 140°C (Shlyapnikov and Torsueva, 1995). At 140°C the remaining concentration of this antioxidant, plotted *vs* time, fell rapidly, then more slowly around 200 min, then rapidly again; at 160°C the slower oxidation period was around 50 min; at 180°C, there was no retardation. [Interestingly, this behaviour corresponded with observations in this work of slight mass gain between the slow mass loss and fast mass loss stages]. Other antioxidants, benzophenone-substituted xanthates, also inhibit photo-oxidation between the initial and later fast stages (Al-Malaika *et al*, 1984).

Zinc dialkyldithiocarbamates are very effective UV stabilisers in PP, their effectiveness increasing exponentially with their molar concentration, but their solubility is low

(Chakroborty *et al*, 1984). The nickel complex Cyasorb UV 1084 has an antioxidant action in PP, and was also found to decompose cumene hydroperoxide (a peroxidolytic effect) very efficiently at high temperatures, so this ability was deduced to be important to its action in PP (Allen *et al*, 1985).

Nitroso-*tert*-alkanes are highly active UV stabilizers in UV and at high temperatures in PP, to which they become partially attached and can form crosslinks (Chakroborty *et al*, 1985). Hindered amine stabilizers (HAS) produce hydroxylamine and nitroxyl radicals; ESR measurements have shown that 20% of the nitroxyl radicals are bonded to the polymer chain by =N-O-PP linkages (Hodgeman, 1981). With HAS, at above 100°C, there is no induction period, and degradation rate decreases with increasing HAS concentration, whereas phenolic antioxidants do have an induction period (Gugumus, 1994).

6.1.3 Literature Mechanism for Polyolefin Degradation

The higher the temperature the faster the degradation of PP, and it even degrades below 50°C (Gijssman *et al*, 1996). Iodometric investigation of peroxides formed in PP thermal degradation showed that there were two types, which decomposed slowly or quickly and were probably tertiary hydroperoxides and peracids respectively.

Gugumus wrote four papers on studies of polyolefin degradation in the solid state (Gugumus, 1996, 1; Gugumus, 1996, 2; Gugumus, 1996, 3; Gugumus, 1996, 4). In the third, on a heterogeneous oxidation model, thermal stability of PE and PP stabilized by phenolic antioxidant was best explained by treating these polymers as amorphous domains separated by crystallites. The amounts of free and associated hydroperoxides both go through a maximum, proportional to the sample thickness and to the amorphous content, and concentrations of both level off when they are the same in all domains, free sooner than associated. Peroxidation propagates very rapidly within an amorphous domain, and the low molecular mass products diffuse very rapidly to adjacent domains, initiating oxidation there. This continues until the whole sample is completely peroxidized. If, at the start, no domains are oxidized enough for oxidation to spread out from them, then an induction time is needed. Total hydroperoxide concentration would be the value for one domain times the number of domains peroxidized.

From the mathematical model for LDPE, curves calculated from equations for free hydroperoxide absorbance *vs* time fitted the data within experimental error. Interestingly, the

shapes of the plots with their induction periods were basically the same as those for % mass loss *vs* time for 'APPs' in this work. In the 4th paper the mathematical model also fitted the formation of associated hydroperoxides and of carbonyl groups in LDPE films.

In the same year, Bauer's group accounted for weight loss data for PP by using a multiple-step degradation mechanism (Bauer *et al*, 1996): reaction step (1) is 1st order with auto-catalysis, the consecutive reaction (2) is 2nd order and the parallel reaction (3) is of the 2-dimensional nucleation and growth type. The theoretical model agreed with the experimental data up to but not beyond 60% mass loss.

6.1.4 Main Question to Be Answered

- These materials are exposed to high levels of light and UV in use for very extended periods in air. Thus their oxidative deterioration is crucial. How does the deterioration rate depend on composition of the bitumen blends?

Earlier DSC work showed that the optimum amount of commercial 'atactic' polypropylene ('APP') additive for lowering T_g was that at the inversion point of about 17% 'APP.' Such a blend would be at the point of maximum miscibility, at the point of change from bitumen to 'APP' as main phase. It was expected that deterioration of a blend would depend upon the degradation of both components, and therefore it was considered important to understand the degradation behaviour of 'APPs,' and to compare a range of them on the commercial market. There was also the question of protection from degradation - whether bitumen protects 'APP,' 'APP' protects bitumen, or they protect each other.

DSC had shown that APP oxidized sooner and faster than IPP, so it was expected that (a) the slightly more amorphous 'APPs,' **32C** and **43C** would oxidize before **1C** and **MF80**, and (b) oxidation would involve loss of amorphous material. Therefore all the 'APPs' should become more crystalline, aided by phase separation crystallization, and % mass loss by oxidative degradation should level off eventually. Even if bitumen and 'APP' were mutually protective, this protection would decrease with time as loss of volatiles in bitumen reduced internal motion, and increase in crystallinity in 'APP' had the same effect.

The following experiments were considered essential to investigation of the phenomenon. A series of blends of 'APP' in bitumen was to be studied, in both light and in darkness. 'APP' degradation was to be monitored in darkness, to see whether it occurred to any measurable

extent, and also in light, because UV was known to speed it up. The main factor to be monitored was the percentage mass loss. Effects of changing variables such as temperature, UV level and sample size were considered useful. Maximum roof-top temperatures are probably about 60°C, but 120°C was to be used for most experiments, to speed things up in order to see long-term effects. Initially four 'APPs,' homopolymers **1C** (khaki) and **MF80** (dark grey), and copolymers **32C** (white) and **43C** (off-white) were to be tested.

6.2 Initial Degradation Experiments at 120°C

6.2.1 The Ovens

Oven 1: For the first test a vacuum oven (not under vacuum) was used, simply because it had just been repaired and was available. It was basically a cylinder on its side, with a 20-cm diameter round glass window in the front door, and a sample tray across the diameter, supporting a vertical thermometer through its centre. This oven was standing on a bench in a bright laboratory, not near a fume cupboard, but after the two initial tests (6.2.2 and 6.2.3), which produced a noticeable smell, it was moved to below the fume cupboard and gaseous products were vented into there by boxing-in around the oven door.

Oven 2: Another oven was used for dark degradation, but darkness was not absolutely total, because of a 75 mm round window in the back of the oven, which was near a glass partition to the next laboratory. This window was not noticed because of the angled position of the oven.

6.2.2 In Alternating Daylight & Darkness

6.2.2.1 Experimental

The four 'APPs' – homopolymers **1C** and **MF80**, and copolymers **32C** and **43C** - in four roughly equal size and mass pieces (totalling about 600 mg) on each of three thin glass slides, were heated at 118°C, for two 23 h periods initially, in light. Weighings of samples, before and after each heating period, in this and all subsequent experiments, were made on a balance accurate to 0.0001 g. 'In light' meant in normal daylight round the clock. Unexpectedly, the average % mass loss (Fig.6.1) of **32C** over the first two days was very much greater than measured before in the dark (2.5.1). To test whether this was due to UV light, even though glass was supposed to stop UV, heating was continued for seven days in the dark, one day in light, then six days in the dark. The experiment was discontinued because the products were unknown and the oven was not then ventable to a fume cupboard.

6.2.2.2 Results and Discussion

On the 1st lit day the order of % mass loss was the same as in the trial in the dark (2.5.1) - **32C<<43C<1C< MF80** - but on the 2nd lit day **32C** "took off" past the others. During the dark week, **43C** 'took off' and its mass loss passed that of **1C** and **MF80**. On the single lit day degradation of all samples accelerated, **32C** and **43C** by the most, and then resumed roughly the same dark rate afterwards. **32C** and **43C** broke down much more readily in the light than **1C** and **MF80**; **32C** was triggered off most easily, but **43C**, once started, went further faster. **32C** and **43C** had slightly lower % crystalline content than the other two, **43C** the lowest, so degradation seemed to be easier for the more amorphous polymers, as had been found earlier by DSC. Degradation happened in the dark but was greatly enhanced in daylight, even through glass. Samples went opaque and, once % mass loss began to rise rapidly, they became progressively more yellow, so colouration was deduced to be a result of the degradation.

6.2.3 In (Almost Complete) Darkness

6.2.3.1 Experimental

Fresh similar samples of the four 'APPs' were heated in darkness in Oven 2 at 120°C for about three weeks, until the first of them began to degrade. Heating was continued on each 'APP' only until each reached about 5% mass loss, because of the unknown nature of the escaping material.

6.2.3.2 Results and Discussion

As expected, degradation still occurred in the dark, just very much more slowly than in daylight (Fig.6.2). 'APPs' lost mass at first in the usual order **32C << 43C < 1C < MF80**, then more slowly, then steadily from about 100 h. **32C** pellets began to degrade faster after about 400 h, but to different extents: mass loss was 1.5% (still white), 4.7% (pale yellow), and 7.5% (strong yellow), so the greater the % mass loss, the more intense the yellow surface colouration, confirming that the colouration observed earlier was due to degradation. The three samples of each of the other three 'APPs,' as yet unaffected, varied very little in % mass loss. Raman spectra of **32C** pellets of different shades were compared. Even though the other three 'APPs' were followed up to 1500 h (in approx 1 or 2 day periods), % mass loss in the dark did <u>not</u> become rapid but stayed gradual, levelling off with **1C>MF80>43C**. The results confirmed that light had enhanced the lit degradation considerably. Enough daylight was still entering here

for **32C** to be affected, as if it had an extremely low light intensity threshold, which was eventually reached when winter daylight changed to stronger sunshine at the end of April.

6.2.4 In Winter Daylight

6.2.4.1 Experimental

Fresh samples of the first four 'APPs' (**1C**, **MF80**, **32C** and **43C**) were heated at 120°C in Oven 1 in a very gloomy lab, with winter daylight coming only from skylights, to follow long-term mass loss. Degradation was also followed at 90°C for 70 h and at 110°C for 800 h. Then, even though the material of the original oven window was unknown but probably soda glass, known to be impenetrable by UV, a double check was made on whether the UV component of daylight was responsible for the enhancement of degradation. Firstly, degradation of a fresh set of samples was followed with an extra sheet of 6-mm colourless soda glass was placed in front of the oven window. Secondly, degradation was resumed after a 14-week gap between weak spring daylight and the stronger daylight of mid-summer. Samples of four other polymers (SIS, SBS, LDPE and HDPE) and six other supplied 'APPs' (**MF500**, **C80**, **T1180**, **95-X-06**, **V808** and **V891**) were studied at 120°C, one as different size pieces, and two as melted and cooled discs. Lastly the UV spectrum of the sheet of soda glass was recorded.

6.2.4.2 Results At 120°C

After about a day **32C** began to degrade much faster than **1C** and **MF80**; **43C** started after 2 days but went faster; all % mass losses exceeded those in the dark (Fig.6.3a). Mass loss and colour intensity of 'APPs' depended upon position in the oven, so they were very sensitive to temperature. On further heating (Fig.6.3b), **MF80** was the most stable so it was possibly protected by its dark colour. From 72 h **32C** slowed down to resemble **1C**, while **43C** just kept going. UV exposure would be much greater on a roof-top, so understanding of the process was very relevant to the study. The fact that such dim light had such a huge effect in some cases was not previously reported.

6.2.4.3 Effect of Temperature

At 90°C (Fig.6.4), mass losses in light after 20 h were about half of those at 120°C in the light; mass losses in light after 60 h were about two-thirds of those at 120°C in the dark. At 110°C, fast degradation did occur eventually in the copolymers only: **43C** (at about 400 h) started after **32C** (at about 100 h), went faster, and began to level off later. So both 'took off' much later

than at 120°C, at which **43C** started at *c.*50 h and **32C** at *c.*25 h. The higher the temperature, the sooner fast degradation started, and the faster it went. By 800 h at 110°C degradation had reached *c.*24% (**32C**) and *c.*27% (**43C**), and looked as though it might level off at the % amorphous content. At this lower temperature, **43C** gained mass very slightly before the rapid degradation stage, a feature not found in literature.

The degree of thermal degradation would probably depend upon the degree of internal motion bringing fresh chains to the surface. Chain mobility would differ for **1C/MF80**, containing only PP chains (with methyl groups on), and for **32C/43C**, containing also EP chains (with fewer methyl groups) and PE chains (without methyl groups). In addition, TMA and DSC had shown the presence of minor crystalline components in **1C** (T_m 107°C) and **MF80** (T_m 107 and 122°C), whereas **32C** and **43C** did not, and that these could restrict motion. DSC plots of 'APPs' had illustrated how melting in polymers (*i.e.* increased motion) was not sudden but began gradually from well below T_m - for 'APPs' at least 40°C below T_m (about 160°C) - therefore differences in chain mobility could affect aerial oxidation down to 120°C.

6.2.4.4 Effect of Reducing or Increasing the UV Irradiation Level

When an extra sheet of 6-mm colourless soda glass was placed in front of the oven window, **32C** and **43C** 'took off' at 120°C after about 40 h and 75 h respectively (Fig.6.5), so they were slowed down considerably, so UV was the cause. [The UV absorption spectrum of soda glass was recorded later and showed a 'window' in the far UV (6.2.4.5)]. The 1st stage (slow degradation) of homo- and co-polymers was slowed down (Fig.6.6), and the start of the 2nd stage (rapid degradation) of the copolymers was delayed. Therefore it followed that the 2nd only started when the 1st had reached a certain point, and that if the 1st were prevented the 2nd would not start.

When the degradation was resumed 14 weeks later in the stronger daylight of mid-summer (Fig.6.5), **43C** was unaffected (presumably because so sensitive to the radiation), but the other three 'APPs' speeded up and tended towards higher limits of mass loss. The light level on samples (read by a light meter) was about 2 lux, instead of about 1 lux as before the time gap. When the weather turned to bright sunshine, all four 'APPs' speeded up further. Therefore the degree of thermal degradation depended upon the UV light level and upon susceptibility to it.

6.2.4.4 Effects of Other Variables

Several polymers (**MF500**, **C80**, **T1180** and **95-X-06**) degraded rapidly at 120°C in daylight (Fig.6.7a). An 'APP'-modified bitumen underwent only very slight degradation. Other polymers with very different DSC plots (with much lower T_{g1} and hence lower T_{g2}) gained mass (1% or less), so oxidized slightly but did not degrade (Fig.6.7b): these were SIS, **V808**, **V891**, LDPE, HDPE and oxidized bitumen. SBS was strongly oxidized (up to 7% mass gain) and peaked in mass gain, so it was deduced that all these materials would probably degrade eventually, once they had oxidized to a certain extent. Doubling the size of **95-X-06** samples slowed down the slow 1st stage slightly (Fig.6.8a), as expected for lower surface area per unit volume, and delayed the onset of the 2nd stage of degradation. **V808** and **V891**, which merely gained mass slightly in their supplied form, lost mass strongly in one test when the beads were melted and cooled to compare discs of different sizes (Fig.6.8b). Therefore an experiment was set up later (Section 6.6) to test how melting and cooling conditions affected the susceptibility to degradation and hence might affect the composition, crystallinity and properties.

6.2.4.5 UV Spectrum of Pyrex and Soda Glass

Soda glass was previously presumed to absorb all UV light, but an extra 6 mm sheet of it in front of the oven window had slowed down the slow stage and delayed the fast stage of degradation. So its UV spectrum (Fig.6.9a) was compared with that of Pyrex (Fig.6.9b). Though soda glass absorbed strongly below *c.*310 nm, it did allow light through below *c.*250 nm in the far UV region, therefore degradation of the polymers could be caused by UV light. Pyrex absorbed strongly only over two narrow regions, *c.*270-255 nm and *c.*210-195 nm.

6.3 Long-Term Standardized Degradation at 120°C in 5 Lux

6.3.1 Experimental

So far the experiments had yielded a great deal of information but conditions were not standardized – temperature of a sample varied with its position in an oven, and light level was known only roughly – so a set-up was devised to remedy this.

Adaptation of Oven 2: For a constant temperature of 120°C, Oven 2 was fitted with a fast fan to ensure that the temperature measured by a rigid thermocouple, inserted in the oven roof, was the same as that of the samples. A safety cage was made from ½" wire mesh to enclose the small external rotating blade on the motor. The powerful fan drew in colder outside air, so the

oven could no longer thermostat itself but, once every possible air entry point was blocked off, the temperature recovered fully after the fan was switched on. Then the thermostatting (6 min cycle) was better than without the fan, *i.e.* ±1.0°C rather than ±1.9°C.

Constant Known Light Level: A quartz-iodine lamp was rewired to provide a constant light level, and a safety cage was made from ½" wire mesh to enclose its very hot resistance unit. The light beam was focussed with a glass convex lens, fixed on a slider rod to the lamp housing. Light-meter readings of the focussed beam were measured along a metre rule in the dark room and were converted into lux (candle-power at 1 metre). Hence the closest distance was found (46 cm) with light output still on the top of the light-meter scale, at a reading of 5 lux, and the lamp was positioned so that the total light path was this distance. The horizontal light beam was directed vertically downwards onto samples with the aid of a ½" wire mesh frame supporting a mirror at 45° to the horizontal. The sample pellets of **1C**, **MF80**, **32C** and **43C**, close in size and mass (200 mg), were placed on pieces of microscope slide.

Depending on the weather, the background daytime light level measured from inside the oven varied between 1 and 2 lux, a large variation compared with the 5 lux lamp output, so the area around the lamp and the oven was boxed in with very thick cardboard sheets to stop daylight entering. Degradation of the original four 'APPs' was monitored to over 1000 h.

6.3.2 Results and Discussion

Only normal, slight mass loss was recorded for all the 'APPs' up to 40 h (Fig.6.10a). Then **32C** began to lose mass more rapidly and to change in appearance (at first only faintly yellow, dry and lined surface, no longer shiny), so even 40 h of 5 lux indoor lighting (focussed through a glass lens) was enough to degrade this copolymer. By 160 h **32C** had lost 21% mass, while the others had lost only 3.5 to 5.5% mass (Fig.6.10b). **43C** began to 'take off' after 225 h, following a brief mass gain, then degraded at the same rate as **32C**, while **1C** did so after 450 h and degraded more slowly. By 760 h mass losses of **1C**, **32C** and **43C** seemed likely to level off somewhere above 40%, and were expected to reach eventually the amorphous content - 56, 57, and 60% respectively - found by petroleum ether extraction. At each weighing the Raman spectrum of **32C** was recorded to confirm, in this controlled experiment, that crystallinity increased (Section 7.2), and to see whether progress could be monitored in that way. The 'APPs' shrank, lost 'tack', and went dark orange, and **32C** cracked lengthwise, showing how

they lost adhesion as they became more crystalline. Nearly-black **MF80** had degraded by only about 7 % by 760 h, when the others had reached about 35% mass loss, so it was protected, probably either by its colour or by restricted movement caused by its two minor crystalline components.

Going on till 1060 h showed that for copolymers the very rapid stage, almost a straight line plot, was actually followed by a much slower stage, also almost a straight line, going past 40% mass loss. These two sections indicated loss of two amorphous components, accounting for 34% loss and then 23% loss (=57%-34%). They could be APE and then APP, but **32C** also contained EPR (Table 2.1). Such a non-instrumental way of measuring total amorphous content and the ratio of amorphous components could be a useful, though slow, analytical method.

As only a few samples fitted in the light beam, standardized testing in 5 lux in this way was slow, so only this set of four 'APPs' was followed. [Degradation could be analysed this way at one temperature and different light levels, one light level and different temperatures, with and without extra soda glass, and also with a full UV filter, *e.g.* a tank of suitable liquid, in the light beam]. Several other polymers were supplied for testing: *i.e.* SBS and SIS, **MF500**, **C80**, **T1180**, **95-X-06**, **V808** and **V891**, and also EP, LDPE and HDPE. Therefore another method had to be used to accomplish this in the time available, running alongside this 5 lux test.

6.4 Long-Term Standardized Degradation *en Masse* at 120°C in 4 Lux

6.4.1 Experimental

In the meantime, samples of the supplied 'APPs' and 'APP'/bitumens, were degraded all together in Oven 1, this time with a constant, known light level. Very slight variation in temperature and lighting with position were ignored because (a) the layout of the samples on a grid was always the same, (b) it was more important to compare all the samples within a reasonable time period, and (c) it was essential to check whether bitumen provided full, partial or no UV protection to its 'APP' additive.

Adaptation of Oven 1: The calibrated 4 lux source, a Philip's 60 w "Floodline" light bulb (with an 80° angle of illumination) in an Anglepoise lamp, was placed inside an improvised cuboid tent of thick black polythene, constructed to enclose all the area in front of the oven, so that background variation in daylight had no affect. All the eight polymers were treated together in duplicate, using two slides of two 180-mg samples for each one. Other polymers (SBS, SIS,

PFSD), the 'APP'/bitumen series (0, 5, 10, 15, 20 and 30% **32C** in 100 Pen bitumen), the SBS/bitumen series (0, 9 and 13% SBS in 200 Pen bitumen), and different size pieces of two polymers (**T1180** and **95-X-06**) were compared too.

6.4.2 Results and Discussion

6.4.2.1 SBS Blends

Results for the SBS/bitumen series confirmed that SBS protected the 200 Pen bitumen from degradation (Fig.6.13): by 332h SBS (with 6% mass gain) changed its large mass loss (15%) to slight mass gain (0.4% for 9% SBS and 1% for 13% SBS). It would have been useful to have extra blends with less than 9% SBS. As predicted (6.2.4.4) from a preliminary test (Fig.6.7b), SBS itself started to degrade rapidly from *c.*500 h.

6.4.2.2 'APPs'

There was good agreement between the two sets of results for each 'APP.' All four 'APPs' degraded (Fig.6.14a) very much faster than at 5 lux in Oven 2, proving that the colourless glass convex lens used to focus the beam was absorbing the responsible radiation, which was therefore UV. [UV-induced oxidative degradation of PP and PE is well documented in literature]. **32C** and **43C** both gained mass slightly before 'taking off,' as seen for **43C** at 110°C (6.2.4.2).

Amongst the four other polymers (Fig.6.14b), **95-X-06** and was the only one with a slow stage, and, though later starting, it degraded much faster than the other seven 'APPs.' **MF500** coloured evenly like **1C**, **32C** and **43C**, so all these probably oxidized throughout the bulk of the material, not just at the surface, but **95-X-06** coloured strongest on sides facing the light. **C80** (brown) and **T1180** (black) degraded most rapidly, without even a slow stage, so their colouring was no protection. Division of 360 mg **95-X-05** into four, six and then eight equal-sized pieces, speeded up the slow stage and brought forward the onset of rapid oxidation (Fig.6.15a). Division of 250 mg **T1180** (with no slow stage) into three, six and then twelve equal-sized pieces brought forward the 2nd fast stage (Fig.6.15b). Thus use of finely divided material would speed up the monitoring of degradation. **95-X-06** (in eight pieces) and **T1180** (in twelve pieces) were followed for nearly 500 h, to see how far they would degrade (Fig.6.15): **95-X-06** reached c.35% mass loss and **T1180** reached c.27%, and neither was near to levelling off.

6.4.2.3 'APP' Blends

Monitoring of the series of **32C** in 100 Pen bitumen blends to 614 h showed that the bitumen and the 'APP' protected each other from degradation (Fig.6.16a,b) - separately they lost 7 % and 12 % mass respectively by 332 h, compared with only 3% for the 30 % **32C** blend.

The plot of % mass loss *vs* % **32C** (Fig.6.17a) comprised a fast section and then a much slower section, with an intersection of the gradients that became clearer as degradation progressed. By 332 h the intersection was clearly at about 17 % **32C**. So % mass loss by degradation was much reduced by addition of up to 17 % 'APP,' but not affected very much beyond that. In addition, 5% and 10% **32C** blends began to gain mass from 368 h, while those with 15% **32C** or more continued to lose mass slightly. Therefore addition of more than 17 % 'APP' would not be cost-effective, and this would be the optimum amount of 'APP' for longevity of the product. This value was also the optimum amount of additive for reduction of the T_g of the bitumen, found by DSC. The change in both properties - degradation and T_g - occurred at the inversion point of the blend, the composition at which it changed from polymer-in-bitumen to bitumen-in-polymer. It follows that monitoring of thermal degradation is a viable, alternative method for obtaining the inversion point and hence the optimum amount of additive for reduction of the T_g. This method is very simple and does not require expensive (DSC) equipment - just an oven with a window, a lamp, a sensitive balance, a fume cupboard - so it could be done on the manufacturing site. It could have been applied to the SBS/bitumen series if more samples with <9% SBS had been available. The test could be speeded up if samples were cut up into smaller pieces (as in 6.4.2) , and it could be backed up an even simpler, quicker melting method that was devised (7.4.1).

6.5 Long-Term Standardized Degradation at 120°C in Darkness

6.5.1 Dark Heating, with Exposure to About 4 Lux During Cooling

6.5.1.1 Experimental

Oven 3: Another windowless oven, located in a dark room, was used because Oven 2 had broken down and was too old to repair. Since most laboratory ovens do not have large windows in the front door (as in Oven 1), the experiment to find the optimum amount of 'APP' additive in the **32C**/bitumen series by degradation was repeated in the dark, to see whether such clear results could be obtained as in light. Samples cooled rapidly to RT in daylight (mainly about 4 lux) prior to weighing. All eight 'APPs' were also heated in

duplicate in total darkness for as long as possible, in order to test for slow loss, brief gain, then fast loss by oxidative degradation (Fig.6.19) – basically to see how degradation would differ.

6.5.1.2 Results and Discussion for 'APP' Blends

Naturally **32C**, the bitumen and the blends all degraded much less in the dark, but still showed mutual protection. **32C** had a very clear mass gain before 'taking off' (Fig.6.18a,b). The plot of % mass change *vs* % **32C** was not satisfactory – with smaller changes than in light, curves overlapped sometimes and the change of gradient was at about 8% **32C** (Fig.6.17b). Therefore observation of only partial oxidation and degradation gave a false value for the inversion point, and an oven window is necessary to do the test properly.

6.5.1.3 Results and Discussion for 'APPs'

Polymers with no slow stage (**C80**, **T1180**) or a very short slow stage (**MF500**) still degraded, but slightly more slowly, in the dark. Frequent early readings allowed recording of the brief mass gain stage for **32C** and **MF500**. Those with a long slow stage (**32C**, **43C**, **95-X-06**) took four or five times longer to reach the fast stage, which was also slower than in light. Therefore all the polymer additives would probably eventually degrade on their own, even in the dark. However it was suspected that the oxygen addition necessary for subsequent mass loss was occurring during the few minutes that samples were in daylight (about 4 lux) while not yet cooled to RT for weighing in daylight, so this was to be tested.

6.5.2 Dark Heating, with Exposure to <<1 Lux During Previous Cooling

6.5.2.1 Experimental

The whole series was repeated in duplicate with only a few seconds exposure to very dim light in a dark room (<< 1 lux) when hot, then cooling in the dark (Fig.6.20). Samples were heated in Oven 3, arranged in rows inside a rectangular tin, with the lid on but not tightly closed. After each heating session the lid was shut tight before the tin was removed from the oven and it was not removed (in the fume cupboard) until the samples had cooled down to RT for weighing in the darkroom.

6.5.2.2 Results and Discussion

Degradation was still about the same in 4 lux for **MF500**, **C80** and **T1180**, but negligible for **1C**, **MF80**, **32C**, **43C**, and **95-X-06**. It was deduced that, for high PE content, only extremely

brief and low light exposure of warm samples is needed for oxygen to add on, to then be driven off together with a polymer fragment on next dark heating.

6.5.3 Dark Degradation of 'APPs' After Cooling in Different Light Levels

6.5.3.1 Experimental

The effect of light on later degradation was checked further with two 'APPs' – **C80** (samples 1, 2, 3, 4) and **MF500** (sample 5) - that had no slow stage, to avoid complications of change of rate of mass loss. After the heating in the dark oven in the dark room the samples, each comprising two 200-mg pieces, were transferred (in only 1/7 lux) to a lightproof tin to cool. Samples 1/5 were cooled in the tin, and sample 4 in 4 lux, checked by light meter on a grey winter afternoon. Samples 2/3 were also cooled in the tin, and weighed, but were then heated 10/20 min in 4 lux before the next dark heating. Weighings were all done in the polymer laboratory dark room in 3 lux.

6.5.3.2 Results and Discussion

The plot of results (Fig.6.21) showed that 4 lux only while cooling rapidly led to almost as much mass loss on the next heating period as did 4 lux for 10 min at 120°C.

6.5.4 Sealed Dark Heating, with No Light Exposure While Cooling

6.5.4.1 Experimental

The degradation was also carried out in duplicate in a sealed lightproof tin that was only opened (in a fume cupboard) after it had cooled to RT. The tin, measuring 23.5 cm * 22.5 cm * 8.5 cm, was sealed with black PVC tape, so it was also airtight.

6.5.4.2 Results and Discussion

Even under these conditions **1C**, **32C** and **43C** had lost 2% and **MF80** had lost 4% mass by 600 h. Therefore bitumens should protect polymer additives from degradation – but perhaps only until loss of their volatile components, or phase separation, leaves the polymer as the main phase or exposes the polymer.

Oxidized bitumen was included from the start but left out by mistake from 103 h (Fig.6.22). A fresh sample was added at 262 h and had an unexpected effect on all the others. **95-X-06** was immediately triggered into its fast stage of degradation, which did not occur till 490 h in the dark in the lidded but unsealed tin. Whenever the oxidized bitumen gained or lost mass,

MF500, **V808** and **V891** always did the opposite (Fig.6.22a), whereas **1C**, **32C** and **C80** always did the same (Fig.6.22b). **MF80** and **43C** were unaffected, and **T1180** only slightly. The probable reason was competition for the limited air supply in the airtight tin. Oxidized bitumen suddenly removed a large amount of oxygen - it gained 7.8 mg (3.9%) over its first heating period - when **95-X-06** was well into its slow stage. The sudden air pressure drop triggered off loss of gaseous fragments from **95-X-06**, and to a very much lesser extent from **MF500**, **V808** and **V891**. However **1C**, **32C** and **C80** all still gained mass, so their gaseous products were harder to remove. **95-X-06** was exceptionally susceptible – so if partially oxidized in storage, it might easily auto-ignite near a fire that reduced its air pressure and heated it.

6.6 Long-Term Tests on Relationship Between Sample Preparation and Degradation

6.6.1 Background – Evidence for Thermal Shock

Earlier tests had showed that discs made from melted and cooled beads of **V808** and **V891** either both lost mass or both gained mass (Fig.6.8b). So trials were set up to find how preparation conditions affected subsequent oxidative degradation of all eight polymer additives.

DSC had shown that phase separation crystallization occurs during cooling only at a halt in the steady fall in temperature, *i.e.* with 'thermal shock.' Therefore it was expected that phase separation crystallization, and hence oxidative degradation, would depend upon the combination of phase separation and thermal shock to initiate the crystallization. Conditions for sample preparation were chosen with this in mind.

One sample of **43C** studied by linked DSC methods had behaved in an odd fashion when cycled between –80°C and 180°C with a hold at different temperatures during the quench (5.4.3 and Fig.5.21). On some days it crystallized with heat intake every time but on others it crystallized with heat release every time. A possible explanation is offered here, based on thermal shock. On some days initial phase separation must have been high and the short time at 180°C would not have dispersed the phases very much, so the thermal shock at the halt in cooling would have shunted chains together hard enough to initiate crystallization with its consequent energy release. On other days initial phase separation must have been low, so the same thermal shock wave was insufficient to overcome inter-chain repulsions. So the rapidly contracted material took in energy from its surroundings in order to expand back again to its

original state. No references have been found on this effect in polymers but only several papers on thermal shock effects in ceramics. There was no time to return to this phenomenon later to check on what action led to the difference at the start of each day.

6.6.2 Experimental – Sample Preparation

180-mg Samples were prepared by three different procedures: they were melted into 1-cm diameter discs and either (A) cooled rapidly to RT,

or (B) annealed for an hour at 130°C, then cooled rapidly to RT,

or (C) cooled very slowly to RT.

All pre-treatment was done in the fume cupboard. Half-inch metal grids were laid across the top of the two oilbaths, each with a thermometer stood in the centre, on two hotplates at 175-177°C and 130°C. The higher temperature was well above the T_m of the 'APPs' at about 160°C, and the oil depth of 1.5 cm was well above the level of molten 'APP.' Each sample of *c.*200 mg was cut up very small and placed in a glass specimen bottle, then these bottles were stood in the grids to keep them upright. After annealing for an hour at 175-177°C, Set B samples were transferred quickly to the other oilbath; to quench Sets A and B, samples were placed on the slab work surface in the fume cupboard; to cool Set C slowly with no thermal shock, the hotplate was just switched off. After pre-treatment, each specimen bottle, wrapped in a sheet of paper, was smashed carefully with a hammer, and the sample was placed on a weighed microscope slide and re-weighed.

All samples were degraded at 120°C, preliminary ones - **32C**, **C80**, **T1180** and **95-X-06** - in daylight in Oven 1. Sets A/B/C were heated at 120°C in 4 lux in Oven 1 and cooled in the fume cupboard. For these long tests the boxing-in was replaced with a rigid cabinet constructed from a metal trolley and thick cardboard panels. Data were plotted for **1C**, **MF80**, **32C** and **43C** (Fig.6.23), **MF500**, **C80**, **T1180** and **95-X-06** (Fig.6.24), and **V808** and **V891** (Fig.6.25a,b).

A second experiment was set up concurrently in which Sets A/B/C were heated in duplicate at 120°C in the dark - inside a metal tin (27 cm * 20 cm * 8 cm), with lid on top but not shut tight, in dark Oven 3. They were cooled with the lid on tight (so no light could get in) in the fume cupboard, and the lid was removed there for fumes to disperse. Samples were weighed in 3 lux in the darkroom (Fig.6.25c,d; Fig.6.26; Fig.6.27; Fig.6.28).

6.6.3 Results and Discussion

6.6.3.1 Preliminary

The preparation conditions were such that Set C had some phase separation but no thermal shock, so low phase separation crystallization; Set A had the same phase separation (or less) but with thermal shock, so medium phase separation crystallization; Set B had higher phase separation and similar shock to Set A, so high phase separation crystallization.

In an initial check on **32C** after only 22 h in daylight, the different shapes of the % mass loss plot did indicate that degradation varied greatly with preparation and hence crystallinity. However, samples had degraded in the order B>A>C, indicating that degradation was greater with greater crystallinity, which was the opposite of all other findings. Therefore the test was to be continued past the induction stage to a specific point – the onset of fast degradation.

6.6.3.2 Results and Discussion for Degradation in 4 Lux

Khaki-coloured **1C** began to degrade slowly, speeded up, and gradually levelled off at mass loss about 45 % - the approximate value of the atactic content of the 'APP.' Set C, which would have been much less crystalline than Sets A and B, degraded faster all the way.

Nearly-black **MF80** degraded very slowly up to about 550 h, by when it had lost only about 20 % of the **1C** loss. Set C again lost the most mass all the way. This 'APP' was protected from degradation, possibly by its colour, or by the minor crystalline components. From about 550 h, **MF80** degraded rapidly, with A > C > B.

32C gained mass slightly, and then degraded very fast, Set C fastest, as expected for the much less crystalline set; it was levelling off towards >32 % mass loss. Sets A and B showed two fast stages, probably for two amorphous components, one of 13%, one of 20% or more. This result fitted with the known presence of PE (and EP) as well as APP. So degradation curves could perhaps be used to show up two amorphous components, as was indicated earlier (6.3.2), and hence distinguish between copolymers from homopolymers.

43C degraded very fast from the start, Set C fastest, and levelled off at mass loss >36 %. For all four 'APPs' Set B degraded slightly less than Set A all the way. Thus Set B, with greater phase separation crystallization at 130°C than at 175°C, was slowest to degrade.

MF500, **C80**, **T1180** and **95-X-06** all showed no slow induction stage. For **MF500**, Set C was slightly faster, and amorphous loss changed at about 13%. For dark brown **C80**, Set A

soon emerged as fastest, while B and C were the same. For black **T1180**, crystallinity made little difference till about 300 h, then Sets A and C were equal and faster; there was a change of curve at about 15%, confirming that there were two amorphous components. For pale green **95-X-06**, Set B showed two fast loss stages, just like **32C**. **V808** and **V891** both gained mass before the fast stage, and Set C was fastest.

For all samples, Set B, the most crystalline, was always the slowest, and Set C, the least crystalline, was normally the fastest. The greatest % mass loss for A, B or C at the cut-off of the experiment (1130 h) gave a measure of stability of the polymers to long-term degradation in 4 lux at 120°C (Table 6.1). The two Vestoplast polymers **V808** and **V891** were by far the most stable, followed by the three coloured 'APPs' **C80** (brown), **T1180** (black) and **MF80** (black), even though **C80** and **T1180** had no slow stage.

Table 6.1 Maximum Observed % Mass Loss by 'APPs' at 120°C in 4 Lux for 1130 h

'APP'	1C	95-X	MF500	43C	32C	MF80	T1180	C80	V808	V891
%L	-41.6	-37.1	-35.6	-32.8	-31.4	-28.1	-26.2	-25.3	-17.1	-15.6

Key: %L = % mass loss in 4 lux

6.6.3.3 Results and Discussion for Degradation In the Dark

Lack of light caused several effects by slowing down the degradation process. **1C** extended its slow induction stage up to about 400 h. **32C** and **43C** both gained mass slightly before 'taking off.' **MF80** did not reach its fast stage. For **T1180**, the presence of two amorphous components, one of 15%, was much clearer. **C80** had two kinks in its curve at about 5% and 15%, so had three amorphous components. **V808** and **V891** had much longer mass gain periods, up to about 400 h, before they degraded rapidly. Most duplicate sets, except for **MF500** and **V891**, gave the same shape plots.

This time, in the dark, all the % mass losses (at 1159 h) were naturally reduced, and the same five 'APPs' were still the most stable. The reductions were noticeably larger for **C80** < **MF500** < **43C** < **1C** << **MF80** (Table 6.2), so **MF80** was now by far the best. In a blend with bitumen, protection from light might prevent some of them from reaching their fast stage, but they would probably still degrade slightly, and this order probably reflected their relative stabilities and therefore stabilizing effect upon the bitumens.

Table 6.2 Maximum Observed % Mass Loss by 'APPs' at 120°C in the Dark for 1159 h

'APP'	95-X	32C	MF500	1C	43C	T1180	C80	V808	V891	MF80
%D	-34.7	-30.4	-28.7	-27.5	-25.5	-25.4	-20.3	-15.1	-13.6	-4.2
%L-%D	2.4	1.0	6.9	14.1	7.3	0.8	5.0	2.0	2.0	23.9
100(%L-%D) ÷ %L	6.5	3.3	19.4	33.9	22.3	3.1	19.8	11.7	12.8	67.2

Key: D = % mass loss in dark, L = % mass loss in 5 lux

6.7 Suggested Complementary Mechanism for Oxidative Degradation

6.7.1 Basic Outline

One simple, overall, complementary scheme is proposed, not found elsewhere, which accounts for all the features observed in the oxidative degradation curves of all the 'APPs,' with and without PE: *i.e.* initial mass gain in some cases, slow mass loss stage, brief mass gain in some cases, rapid mass loss stage, slowing down. It also accounts for the different behaviour of samples prepared by different methods. According to this work and references, thermo-oxidation or photo-oxidation occur in the amorphous regions. In the very long heating experiments the levelling off seemed to be towards the % amorphous content. This simple statistical explanation was devised before Gugumus' much more complex mathematical model was read. Even though his model fitted experimental data for absorbance of hydroperoxides extremely well, these ideas are still proposed as possibly also involved. The sensitive mass loss curves showed up brief intermediate stages that his curves did not. [Antioxidant concentration curves of Shlyapnikov and Torsueva did have slow or stationary sections, which were not explained (Shlyapnikov and Torsueva, 1995)].

Oxidative degradation in all the 'APPs,' with and without PE, can be accounted for simply by one overall scheme if aerial oxidation involves an oxygen molecule link -O-O- between two adjacent C atoms on chains that are either crystalline (X) or amorphous (A). Chain-X bonds would be stronger than chain-A bonds, because of higher available electron density in connected adjacent chains. The melt has potentially all A-O-O-X links but as phase separation crystallization progresses the number of potential A-O-O-A links increases, so loss of fragments increases.

The initial short fast mass loss stage in some cases probably occurred because some phase separation crystallization and oxidation had occurred during storage since manufacture (seen in DSC), so brief degradation (seen in TMA) occurred till heating dispersed the zones. Next was a steady slow mass loss stage - with constant renewal of the surface by internal motion and phase separation crystallization slowly increasing again, a steady rate of mass loss occurred. With only phase separation crystallization, the total number of A-O-O-A and X-O-O-X links in all the zones would stay the same but the total number of A-O-O-X links would decrease with time as the number of zones falls and their sizes grow (see 6.8.6. and Excel spreadsheet).

With degradation going on too, A-O-O-A would be lost steadily and phase separation crystallization would slow down with time because mobility would fall as crystalline regions enlarged and amorphous material was lost. At low temperatures and light levels, only A-O-O-A links would break off but at high temperatures and light levels perhaps A-O-O-X links would break off too.

If all links were equally likely to form and to break, the mass loss plot would not have a slow induction stage and a fast stage. [An induction period may be due to deliberate addition of inhibitors to stored material, but the 'APPs' studied here were believed to be free of additives]. PP degradation is known to be faster than PE degradation. The brief mass gain seen in some cases just before the very rapid mass loss also indicated that some other factor(s), as well as statistics, mattered.

6.7.2 Suggested Other Factors Affecting Polymer Oxidation

Perhaps link formations are favoured sterically in the order A-O-O-A > A-O-O-X >> X-O-O-X, *i.e.* spacing in more compact crystalline regions is less suitable for incoming O-O molecules to bond in the first place. Perhaps the tighter spacing possible between PE chains, without CH_3 groups, also makes oxidation and hence degradation less likely than in PP. Perhaps link formations are also favoured energetically in the same order because X atoms, held more tightly in the crystalline structure, would be less reactive.

Hence A-O-O-A links would form much more easily than A-O-O-X links, and few or no X-O-O-X links would form. Thus mass loss would be slow to start with but would begin to rise rapidly once a certain crystallinity was reached and fewer Xs were involved. That is, once no. of A-O-O-A = no. of A-O-O-X, or even before, A-O-O-A formation would suddenly dominate

and temporarily cause a mass-gain build-up until these more easily lost species were driven off extremely fast - *i.e.* auto-oxidative degradation would take over. (In stronger UV or higher temperature there would be less build-up, as was found). Thus the timing of the fast stage, when auto-oxidation occurs, depends upon statistics, inter-chain distances and the degree of phase separation crystallization. [It was suggested early on in the DSC work that the fast stage could not happen till the slow stage was complete].

For some time there would be a steady fast stage of addition of –O-O- and immediate loss of fragments from the amorphous regions, while C_A-O-O-C_A outnumber C_A-O-O-C_X, until the size of those regions is so small and mobility so low (with increased crystallinity) that the –O-O- addition and fragment loss slows down as adjacent As get harder to find. Therefore, with time, mass loss would level off as available amorphous material decreased and mobility decreased with loss of amorphous 'lubricant,' and eventually % mass loss would approach the original % amorphous content.

6.7.3 Application of the Model to Features of % Mass Change Graphs

6.7.3.1 Initial Mass Gain Before the Slow Mass Loss

For a few 'APPs' (**32C**, **V808** and **V891**), there was small initial mass gain, up to 1.5% in 4 lux. In these the number of A-O-O-X links was probably high, and only the weaker-bonded end of the links were broken by UV/heat, so mass was initially gained by oxidation. As the number of A-O-O-A (plus X-O-O-X) links increased with phase separation crystallization - to rival the number of A-O-O-X links - both ends of this type of link were broken off by UV and heat, so mass loss outweighed mass gain. In **32C** and **43C**, the fast mass loss stage was slower than in **1C** and **MF80**, probably because APE slowed down the degradation of APP, as mentioned in several references.

6.7.3.2 Order of 'Take-off'

Samples held at 175°C for 20 min were (A) quenched, (B) held at 130°C for an hour and then quenched, (C) cooled very slowly. During long-term heating at 120°C (in 4 lux or in the dark) in general Set C, the least dense and therefore the least crystalline, 'took off' first, followed by set A, and then set B, the most dense and most crystalline. In Set C (not subjected to the thermal shock of quenching and therefore least crystalline set) phase separation would have been high and mobility highest, so the required ratio of A-O-O-A to A-O-O-X would have been

reached soonest. In Set B (annealed lower and then quenched, so the most crystalline set), amorphous regions would have been smallest and mobility least, so the required ratio would have been reached last. Set A (annealed higher and then quenched, so with medium crystallinity) lay between the other two in crystallinity and 'take-off' time.

Thus these data for sets A/B/C support the proposed ideas. However they also can be explained in the conventional way. Set C, the least crystalline, would allow propagation of oxidation through the bulk most easily, and B, the most crystalline, least easily.

6.7.3.3 No Slow Stage

For two 'APPs' (**C80** and **T1180**), only the fast degradation was observed, even when heated in the dark; for **T1180** the method of preparation made negligible difference. These were 'APPs' with very high PE content (deduced from DSC) but not necessarily low density. It was deduced that A-O-O-A content was high at the start and that non-methylated PE chains improved mobility, so little or no re-organising time was needed for A-O-O-A's to predominate. When **T1180** was heated in the dark, there were very clearly two components lost, the first by about 400 h, presumably APP and then APE. **C80** did the same, but less dramatically, losing the first at about 150-230 h. If these two 'APPs' were heated well below 120°C, a slow stage ought to be observed, as all stages would be slowed down. Indeed, when heated in the dark: **1C** did not 'take off' till 400 h; some **43C** showed initial mass gain before slow mass loss; **MF80** never reached its fast stage; **MF500** gained mass initially before the fast mass loss; **95-X-06** had a longer slow stage. However **32C** was hardly affected by light level – in light or dark it gained mass slightly at the start and reached about the same % mass losses.

6.7.4 Spreadsheet Model of Thermal Degradation

Under phase separation crystallization and degradation, the 'APP' surface is constantly renewed, and a snapshot could be taken at regular time intervals. This was tried in Excel (see 3rd spreadsheet after Chapter 8) in order to show that the suggested mechanism could produce a change from mainly A-O-O-X links (induction period) to mainly A-O-O-A links ('take-off' point, auto-oxidation), a steady level of A-O-O-A links (straight section on the % mass loss graphs) and a gradual fall in % A-O-O-A (slowing down of degradation).

Zones of IPP and APP were considered as two-dimensional squares of 20*20 sq units, increasing in size (under phase separation crystallization) by x units of length per unit of time,

where x was 0.8, 0.5 and 0.29. Firstly a table and graph were generated, showing how % A-O-O-X links fell with time, for the case of no degradation and all links equally probable. Then values of % A-A (short for A-O-O-A) were calculated, using those for % A-X, assuming % X-X to be constant. Tables were generated for each rate of phase separation crystallization, for three different rates of degradation – i.e. loss of 10, 12 and 15 A-A links per unit time. Figures showed that, with different rates of phase separation crystallization (falling A-X) and degradation (falling A-A), % A-A achieved a steady level for a while. At each phase separation crystallization rate, this steady state was lower, shorter and reached sooner with faster A-A loss (Fig.6.29); at each degradation rate, it was higher, shorter and reached sooner with faster phase separation crystallization. After the steady state, % A-A gradually fell.

Graphs were plotted of %A-A and %A-X Links against Time, to illustrate that, with degradation, % A-X links predominated early on, but % A-A soon took over (Fig.6.30). Taking this point to be that of auto-oxidation, fast degradation occurred sooner with higher phase separation crystallization rates - as observed in practice, as at higher temperatures. Figures were chosen such that, at the highest A-A loss rate and lowest phase separation crystallization rate, the % A-A plot did not cross the % A-X plot, to illustrate how in practice such a sample would not auto-oxidize but only continue to degrade slowly indefinitely. Thus any additive that restricted motion and hence phase separation crystallization enough could stabilize an 'APP' against degradation. Alternatively, any agent that suddenly reduced %A-X would bring the curve for %A-X to below that for %A-A, triggering auto-oxidation. This could explain what happened to one 'APP,' which had degraded only slowly for a long time in a sealed container, when oxidized bitumen was introduced (6.5.4), which rapidly removed oxygen, and probably A-X links too, and triggered 'APP' auto-oxidation.

Thus the spreadsheet model did show how the combined different rates of phase separation crystallization and degradation could produce A-O-O-X predominance (slow induction period), a transition to A-O-O-A predominance (auto-oxidation), a steady level of A-O-O-A links (fast degradation period), and then a fall in A-O-O-A (levelling off of % mass loss towards the value of the amorphous content). It also accounted for observations that a particular 'APP' could degrade only slowly, or with a long or short or zero induction period, depending on conditions.

6.8 Summary of Conclusions

From study of blends of 'APP' **32C** in 100 Pen bitumen at 120°C in 4 lux, it was found that the bitumen and the 'APP' protected each other from degradation: after 332 h they lost 7% and 12% mass respectively whereas the 30% **32C** blend lost only 3% mass. The graph of % mass loss *vs* % 'APP' showed a change of gradient, which became better as degradation progressed and was clear by 332 h. From that point at 17.5% 'APP' further addition of 'APP' had much less effect. This point was believed to correspond to the inversion point, at which 'APP' replaces bitumen as the main phase, also the point of maximum miscibility, and the point of optimum addition of polymer to reduce T_g (Chapter 4). Therefore thermal degradation could be a simple, standard method to obtain the inversion point and hence the optimum proportion of any polymer additive for any bitumen. By 332 h, 13% SBS, with 6% mass gain, had changed the 15% mass loss of 200 Pen bitumen to 1% mass gain, so it provided even better protection to bitumen than did 'APP.' As there were only two SBS blends available, the inversion point could not be assessed, but was found by T_g to be 9% or less.

Degradation of 'APP' pellets involved a slow induction stage and a fast auto-oxidation stage. The slow stage was slowed down, and the second stage was reached later, with larger samples, at lower temperatures or at lower light levels, as behind extra soda glass, which was shown to allow some far UV light through.

After preliminary experiments, conditions for the 'APP' pellets were standardized, still at 120°C, to compare results more quantitatively. Degradation with 4 lux was greater than with 5 lux through a glass lens. % Mass change followed a typical pattern: initial fast loss (of volatiles), slow loss, brief slight gain, long fast loss, levelling off towards the % amorphous content. Raising the temperature and/or light level light of any one 'APP' would first bypass the brief slight gain, then also the slow induction stage, until only fast loss would be observed. So the observed behaviour of any 'APP' would depend upon the conditions and upon its sensitivity to them. At 120°C and 4 lux, **32C**, **43C**, **MF500**, **C80** and **T1180** showed only fast mass loss, but **1C** and **MF80**, **95-X-06** showed the slow stage too, while SIS, **V808** and **V891** gained mass for a long time before fast loss. Straight bitumens lost mass rapidly but oxidized bitumen first gained mass for a long time.

Degradation in the dark was naturally slower, and depended upon exposure of the warm samples to light, even just while they cooled before being weighed ready for the next heating

session. If heated in a light-proof container, and cooled in << 1 lux, the 'APPs' still degraded – they did so more slowly, and reached the auto-oxidation much later than in 4 lux, so blending with bitumen would probably inhibit but not prevent auto-oxidation. If heated in an air-tight, light-proof container, and never lit while warm, **1C**, **MF80**, **32C**, **43C** and **MF500** had only gained mass slightly by 260 h, so they oxidized but did not degrade. Three 'APPs' still degraded: **T1180** >> **C80** >> **95-X-06**. Introduction then of fresh oxidized bitumen, which gained mass very rapidly by sudden removal of oxygen, triggered auto-oxidation in **95-X-06**, but only affected the others slightly, so this 'APP' was particularly unstable.

In an early test on melted and cooled material, degradation varied greatly with preparation method, so standardized samples were also tested at 120°C in 4 lux and in the dark. Three sets of 1-cm 180-mg discs were prepared by different combinations of annealing and cooling, so that they experienced different degrees of phase separation and thermal shock, and therefore had different crystallinities. The most crystalline set was usually slowest to reach auto-oxidation and the least crystalline set was usually fastest. By 1130+ h in 4 lux, the two Vestoplast polymers **V808** and **V891** were much more stable than the rest, followed by the three coloured 'APPs' **C80** (brown), **T1180** (black) and **MF80** (black), even though **C80** and **T1180** had no slow stage. In the dark, the same five 'APPs' were most stable, except that MF80 was by far the best. Kinks in the % mass loss plots revealed the presence of more than one amorphous component in a known copolymer, and other 'APPs,' which were therefore also copolymers.

A general mechanism was proposed for the thermo-oxidative degradation of 'APPs.' The ideas accounted for all the observed stages of the % mass loss behaviour. An Excel spreadsheet, based on the arguments, was used to produce a simple model of how auto-oxidation was reached rapidly or slowly or not all, depending on the balance between phase separation and mass loss.

6.9 Tables

Table 6.1 Maximum Observed % Mass Loss by 'APPs' at 120°C in 4 Lux for 1130 h 19
Table 6.2 Maximum Observed % Mass Loss by 'APPs' at 120°C in the Dark for 1159 h 20

6.10 References

8

Allen N S, Padron A J and Appleyard J H, The Decomposition of Cumene Hydroperoxide by Nickel (II) 2,2'-Thiobis(4-*tert*-octyl-phenolata)-*n*-butylamine (Cyasorb UV 1084) in *n*-Hexane Solution and its Possible Importance in the Photostabilisation of Polypropylene. *Eur Polym J*, 21, 2, 101-105. 1985 3

Al-Malaika S, Scott G and Huczkowski P, Mechanisms of Antioxidant Action: Effect of Benzophenone-Substituted Xanthates on the Stability of Polypropylene. *Poly Deg and Stab*, 1984, 7, 95-107. 2

Bauer M, Rembold M, Marti E, Schneider H A and Mülhaupt R, Modification of isotactic poly(propylene) by oxygen and helium plasma with reference to thermo-oxidative stability. *Macromol Chem Phys*, 1996, 197, 61-82. 4

Baumhardt R and De Paoli M-A, Photo-oxidation of polypropylene under load. *Poly Deg and Stab*, 1993, 40, 53-58. 1

Baumhardt-Neto and De Paoli M-A, Mechanical degradation of polypropylene: Effect of UV irradiation. *Poly Deg and Stab*, 1993, 40, 59-64 1

Bigger S W and Delatycki O, New Approach to the Measurement of Polymer Photooxidation. *J Poly Sci*: Part A: Poly Chem, 1987, 25, 3311-3323. 1

Chakroborty K B, Scott G and Poyner W R, Mechanisms of Antioxidant Action: Concentration Effects of Zinc Dialkyldithiocarbamates in the UV Stabilisation of Polypropylene. *Poly Deg and Stab*, 1984, 8, 1-11. 3

Chakroborty K B, Scott G and Yaghmour H, Mechanisms of Antioxidant Action: C-Nitroso Compounds as UV Stabilizers for Polypropylene. *J Appl Poly Sci*, 1985, 30, 189-203. 1985 3

Gengenbach T R,Vasic Z R, Chatelier R C and Griesser H J, A Multi-Technique Study of the Spontaneous Oxidation of *n*-Hexane Plasma Polymers. *J Poly Sci*: Part A: Poly Chem, 1994, 32, 1399-1414. 1

Gijssman P, Kroon M and van Oorschot M, The role of peroxides in the thermooxidative degradation of polypropylene, *Poly Deg and Stab*, 1996, 51, 3-13. 3

Gugumus F, Mechanisms of thermooxidative stabilisation with HAS. *Poly Deg and Stab*, 1994, 44, 299-322. 3

Gugumus F, Thermooxidative degradation of polyolefins in the solid state. Part 2: Homogeneous and heterogeneous aspects of thermal oxidation. *Poly Deg and Stab*, 1996, 52, 145-157. 3

Gugumus F, Thermooxidative degradation of polyolefins in the solid state. Part 3: Heterogeneous oxidation model. *Poly Deg and Stab*, 1996, 52, 159-170. 3

Gugumus F, Thermooxidative degradation of polyolefins in the solid state. Part 4: Heterogeneous oxidation kinetics. *Poly Deg and Stab*, 1996, 53, 161-187. 3

Gugumus F, Thermooxidative degradation of polyolefins in the solid state: Part 1. Experimental kinetics of functional group formation. *Poly Deg and Stab*, 1996, 52, 131-144. 3

Hall C, *Polymer Materials: An Introduction for Technologists and Scientists*, 2nd Edition, Macmillan Education, Basingstoke and London, 1989, Chap.5, 121-152. 2

Henry J L, Ruaya A L and Garton A, The Kinetics of Polyolefin Oxidation in Aqueous Media. Journal?, Year?, 1693-1703. 2

Hodgeman D K C, Formation of Polymer-Bonded Nitrosyl Radicals in the UV Stabilisation of Polypropylene by a Bifunctional Hindered Amine Light Stabilizer. *J Poly Sci*, Poly Chem, 1981, 19, 807-818. 3

Livanova N M, On the Nature of the Induction Stage in Polypropylene Oxidation. *Poly Sci*, Series A, 1994, 36, 1, 32-37. 1

Ruaya A, Shaw M T and Garton A, Oxidation of Elastomers in Aqueous Environments. *Rubber Chemistry and Technology*, 67, 775-785. 2

Shanina E L, Zaikov G E and Mukmeneva N A, Peculiarities of inhibiting the autooxidation of solid polypropylene with 4,4'-bis(2,6-di-*tert*-butylphenol). *Poly Grad and Stab*, 1996, 51, 51-56. 2

Shanina E L, Zaikov G E and Mukmeneva N A, Studies of the inhibition of autooxidation of polypropylene with 4,4'-bis(2,6-di-*tert*-butylphenol). *Can J Chem*, 1995, 73, 2011-2014. 2

Shibryaeva L S and Popov A A, Low-Temperature Autooxidation of Isotactic Polypropylene --High-Density Polyethylene Blends. *Poly Sci*, Series A, 1994, 36, 8, 1128-1136. 1

Shlyapnikov Y A and Torsueva E S, Oxidation of atactic polypropylene in the presence of 2,6-di-tert-butyl-4-phenylphenol, *Poly Deg and Stab*, 1995, 49,361-364. 2, 20

Subowo W, Barmawi M and Liang O B, Growth of Carbonyl Index in the Degradation of Polypropylene by UV Irradiation. *J of Poly Sci*: Part A: Poly Sci, 1986, 24, 1351-1362. 1

Sykes P, 1975, A guidebook to mechanism in organic chemistry, 4th edition, Longman, London, 1975. 1, 2

Wayne C E and Wayne R P, *Photochemistry*, Oxford Chemistry Primers, University Press, Oxford, 1996, 6.5, 80-83. 2

Chapter 7 EXTRA EXPERIMENTS ON 'ATACTIC POLYPROPYLENES,' BITUMENS & THEIR BLENDS 1

7.1 Introduction 1

7.2 FT-Raman Spectra 1

7.2.1 FT-Raman Spectra of 'APPs' Before and After Thermal Degradation 1

7.2.2 FT-Raman Spectrum of an 'APP' During Thermal Degradation 2

7.3 SARA Analysis of Bitumens By Thin-Layer Chromatography (TLC) With Flame Ionisation Detection (FID) 4

7.3.1 Experimental 4

7.3.2 Results & Discussion 4

7.4 Inversion Point of Polymer-Modified Bitumens 7

7.4.1 Melting Behaviour 7

7.4.2 Surface Crystallization 8

7.5 Density, Crystallinity and Degradation 8

7.5.1 Density Gradient Column : Experimental 9

7.5.2 Density Gradient Column : Results and Discussion 9

7.5.3 Alternative Density Method : Experimental 12

7.5.4 Alternative Density Method : Results and Discussion 12

7.6 Summary of Conclusions 14

7.6.1 FT-Raman Spectra During Degradation 14

7.6.2 SARA Analysis of Bitumens 14

7.6.3 Inversion Point of Polymer-Modified Bitumens 14

7.6.4 Density, Crystallinity and Degradation 15

7.7 Tables 16

7.8 References 16

Chapter 7 EXTRA EXPERIMENTS ON 'ATACTIC POLYPROPYLENES,' BITUMENS & THEIR BLENDS

7.1 Introduction

1. Since FT-Raman spectra of 'APPs' and IPP were different, it seemed logical to compare the spectra before and after thermal degradation, and also to monitor the changes throughout the degradation, in order to confirm that crystallinity increased and to see whether progress could be followed in that way instead of or as well as by % mass loss.
2. It is important that 'atactic' polypropylenes should be blended with compatible commercial bitumens, so that they do not phase separate too easily. The sponsor companies required SARA analysis of five bitumens, so the technique was investigated.
3. Since the T_g work proved that the optimum amount of 'APP' additive for lowering the T_g was the same as the amount at the inversion point, an idea on an alternative way of finding the inversion point from melting behaviour was pursued.
4. Density of 'APPs' increases with crystallinity, so the densities of 'APPs' annealed and heat-treated in three different ways were compared, before and after degradation, together with untreated 'APPs.' A density gradient column (special apparatus) and an alternative method (available in any laboratory) were used.

7.2 FT-Raman Spectra

7.2.1 FT-Raman Spectra of 'APPs' Before and After Thermal Degradation

Experimental

The basics of FT-Raman theory and instrumentation were given earlier (Section 2.4). FT-Raman spectra of homopolymer **1C** and copolymers **32C** (Fig.7.1) and **43C** were compared before and after heating for 16 days at 120°C in alternating darkness and light. All spectra used 100 scans at 4 cm^{-1} resolution, and 300 mW (before heating) or 200 mW laser power (after heating). FT-Raman spectra were also recorded (at 4 cm^{-1} resolution, 100 scans, and 200 mW power) for **32C** samples heated at 120°C totally in darkness and then selected by colour intensity (transluscent pellet, opaque white, pale yellow, medium yellow) rather than heating time, because colouration started with the change to rapid mass loss and intensified as degradation progressed.

Results & Discussion

After partial thermal degradation, several minor changes occurred, the first being greatest:

(i) 809, 842 cm^{-1} equal pair: the higher wavenumber peak height fell to 90% of lower wavenumber peak in **1C**, 80% in **32C**, 75% in **43C**;

(ii) 1153 cm^{-1} broad peak: in **1C** the shoulder height fell, in **32C** it fell to 57% of main peak and formed a step, in **43C** it resolved into a peak 60% of the main peak;

(iii) 1305, 1330, 1360 cm^{-1} triplet: in **1C** and **32C** the lower wavenumber side-band became weaker than the higher wavenumber side-band.

FT-Raman changes in three 'APPs' after degradation at 120°C in light and dark indicated a change towards IPP behaviour, *i.e.* an increase in crystallinity, which was expected as annealing causes phase-separation crystallisation. [Crystallinity could be found from the Content mode on the DSC-30, but this was not done]. All samples showed the same changes but to different degrees. Spectra showed that prolonged heating increased crystallinity and that the copolymers **32C** and **43C**, which degraded more, became much more crystalline than the homopolymer **1C**. Spectra of **32C**, heated in darkness and then selected by colour intensity, showed gradual changes from the start, the same as those seen before, but weaker, and fitting increasing crystallinity, so the same process was occurring, just more slowly without light.

7.2.2 FT-Raman Spectrum of an 'APP' During Thermal Degradation

Change in the Height of one Particular Peak

During the long heating at 120°C in 5 lux, the Raman spectrum of **32C** was recorded at most weighings up to 716 h - the initial and final spectra (Fig.7.2), run under identical conditions, were very different. The more crystalline a material is, the stronger and sharper are its peaks in the IR and Raman spectra, so the crystallinity rose considerably during degradation.

For **32C** the height and area of the strongest peak at 2884 nm were measured as it increased in size with heating time. Measurements were made on the one sample immediately after each heating, and instrument alignment could be slightly different each time, so figures were corrected according to the peak height of a $BaSO_4$ standard. Even then plotted points were scattered (Fig.7.3a,b). At any one measurement, peak heights could vary over the sample, so several should have always been made and the highest value plotted. When the highest points were joined up, the shape of these two graphs matched the shape of the corresponding graph of

% mass loss *vs* heating time (Fig.7.4), so crystallinity increased and levelled off as mass loss did so. The scatter illustrated the problem of measuring the absolute height of only one peak, but the method could still be used to follow the progress of degradation. A better alternative method might have been comparison of the ratio of two peaks that changes with crystallinity.

Change in the Ratio of Heights or Areas of a Pair of Peaks

The ratios of heights and areas of the 880-780 nm twin peaks had been observed to differ in the spectra of APP and IPP, so they were a measure of crystallinity in 'APPs.' The ratio of left:right twin peak heights and areas reflected the increase in crystallinity with oxidative degradation, values being approximately 1:1 for amorphous PP and 0.75:1 for crystalline PP. These ratios were compared (Table 7.1) in the spectra of **1C**, **32C** and **43C** before and after oxidative degradation at 120°C for 1060 h in 5 lux. [Coloured **MF80**, **C80** and **T1180** gave poor spectra so could not be compared in this way]. The area ratio for **1C** could not be compared with the rest because the minimum between the peaks moved. The other five ratios showed that crystallinity of the three 'APPs' rose with degradation by about the same degree.

Table 7.1 Ratios of FT-Raman Peak Heights and Areas at 880-780 nm for Three 'APPs'

'APP'	Code	Height Ratios			Area Ratios		
		Before	After	%Drop	Before	After	%Drop
PP1	**1C**	0.855	0.655	23	1.350	0.655	51
PP3	**32C**	0.991	0.756	23	1.278	1.025	20
PP4	**43C**	0.955	0.706	26	1.135	0.904	20

The order of the initial height ratios **32C>43C>1C** and area ratios **32C>43C** was the same as the order of ease of onset of rapid oxidation, *i.e.* the less crystalline the 'APP,' the sooner it degraded. This was a conclusion also reached in the DSC high temperature work. The 1600 nm region was also compared for evidence of oxidation: after degradation all three 'APPs' showed low broad bands for C=O, indicating oxidation, at 1600-1620 and 1715 nm. For **MF500** and **95-X-06**, initial ratios of heights or areas of the same twin peaks were also related to the ease of oxidation. Though more comparisons could be made to verify this, it seemed that these ratios could be used to predict the relative ease of degradation of 'APP' additives.

7.3 SARA Analysis of Bitumens By Thin-Layer Chromatography (TLC) With Flame Ionisation Detection (FID)

7.3.1 Experimental

The outline of the method and instrumentation were given earlier (Section 2.7). 2% Solutions of five bitumens (100 Pen, 200 Pen, 200E, 1X and 2X) were prepared in dichloromethane, in which they fully and readily dissolved. The same volume of each solution was applied to each of two Chromarods® in 1-5 μl portions with a 1 μl pipette. The rods were kept at 65% humidity for 10 min, suspended above the solvent(s) in each tank in turn for 10 min, and then developed in the solvent(s); after each tank they were dried in air at RT for 2 min; they were returned to the constant humidity tank in between each of the developing tanks.

The first trial used four decreasingly polar solvents to develop chromatograms of the bitumens, as recommended by Les Brown of Newman-Howells Associates Ltd. and AECS (Analytical & Environmental Consultancy & Services). 1 μl of each 2% solution (as in literature) was applied to each of two Chromarods®, developed at 21°C in tanks of:

(i) dichloromethane:methanol 66.5:3.5 for 1.5 cm (ii) toluene for 3.0 cm
(iii) cyclohexane for 6.0 cm (iv) n-hexane for 11 cm.

The second trial used three increasingly polar solvents, formerly the normal method. Only three tanks were used in ascending polarity, humidity tank time (not as important as development tank temperature) was cut to 5 min, and the distance in the first tank was reduced. 4 μl of each solution (*i.e.* four times more) was applied to each of two rods with a 1 μl pipette (Socorex pipette, made by Camlab), each 1 μl in five portions, and developed at 19°C in tanks:

(i) n-hexane for 9 cm (not 10 cm)

(ii) toluene:hexane 4:1 for 5 cm (iii) dichloromethane:methanol 95%:5% for 2.5 cm

7.3.2 Results & Discussion

In the first trial, spotting with a pipette with an angled end was unsatisfactory and noise-to-signal was very strong, so there was too little sample. All samples showed two strong peaks (1st for S and 3rd or R) (Fig.7.5a), some showed a small broad central 2nd peak and probably a 4th peak, so Aromatics were weak and Asphaltenes extremely weak in all five cases. The set needed repeating with a better pipette and stronger solutions (or more applications of the

same concentration). However a good separation was achieved of 0.30±0.02 min between the 1st and 3rd peak, and 0.35±0.02 min if the 4th peak was real.

In the second trial, signal:noise was better because the response was more than doubled, but not quadrupled (Fig.7.5b). For 200 Pen and 200E the 1st peak for S was split; for 200E only three peaks were obtained, because the 3rd and 4th were not separated; for other cases the 3rd and 4th peaks were slightly split, to different degrees in each pair of samples (Table 7.2). So resolution was not good enough to compare Asphaltene content. Separation of only 0.22±0.02 min between the first and last peak was achieved, so the first trial was over 50% better. Peaks were broader than in the first test: perhaps spotting with 1 µl of four-fold strength solutions would be better than 4 µl of original strength solution. Ratios of areas matched extremely well for pairs of 200 Pen and 200E samples, but not quite so well for the rest, probably because weak signals adjacent to main peaks slightly affected zero-line position and hence the peak areas. Stronger solutions (so stronger signals) and better resolution using four-step decreasing polarity again were expected to improve results. The ratio of % areas of peaks gave the approximate ratio of bitumen constituents.

Table 7.2 Ratio of Peak Areas for the Four Constituents of Five Bitumens

Bitumen	Ratio of Peak Areas on 1st Sample					Ratio of Peak Areas on 2nd Sample				
	S	A	R	A	R&A	S	A	R	A	R&A
100 Pen	47	29	12	12		32	44	14	10	
200 Pen	43+19	23	6	9		41+18	25	-	-	16
200E	44+20	23	-	-	12	45+20	24	-	-	11
X1	77	13	6	4		66	17	-	-	17
X2	74	16	7	3		61	21	-	-	18

Though results were obtained on the Iatroscan® Mark II in the Oceanography Department, they would have been much better if measured on the far more sensitive TH-10 Mark IV, which was sitting idle in the Chemistry Department, because the attached (now obsolete) Trivector processor was irreparable. So, for the mutual benefit of both departments, the Mark IV was moved to the Oceanography Department and connected to a PC with Turbochrom 3 data acquisition software. Four solvents of decreasing polarity had worked better so were to be used again. A different, specialised chromatographic tank was used, with a plunger to lower rods into the solvent without taking the lid off.

Use of 4 μl of 2 % solution in dichloromethane, as used with the Mark II, proved to be too much for the much more sensitive Mark IV. Peaks were broad and overlapped too much to distinguish the Asphaltenes in X1 and X2 (Fig.7.6). However 1 μl of 2 % solution gave a set with good separation into four peaks (Fig.7.7a,b,c,d,e), with good reproducibility, showing that X1 and X2 contained less than half the Asphaltenes in the other bitumens. Peak heights and % areas (Table 7.3) were compared in bar charts (Fig.7.9). The TH-10 responds differently to different types of compounds, so the peak height pattern did not match the % area pattern.

Table 7.3 SARA Analysis Data for Five Bitumens

	Average Peak Heights in mV				
	X2	X1	E200	200	100
Saturates	1946	2025	1358	1188	1116
Aromatics	898	684	832	900	899
Resins	946	909	1043	1104	1076
Asphaltenes	439	477	830	814	970
	Average Percentage Areas of Peaks				
	X2	X1	E200	200	100
Saturates	30.4	30.71	21.9	18.3	15.0
Aromatics	32.5	26.04	29.1	30.8	27.0
Resins	29.4	35.35	32.0	34.65	36.7
Asphaltenes	7.7	7.9	16.5	16.3	20.2

The figures gave an approximate, but not exact, composition of each sample because variation of response with dilution is slightly different for different bitumens. For exactness a set of standard solutions of compounds of each of the four types would be needed to calibrate the instrument (as done by Bharati *et al*, 1993).

Problems were met with developing the Chromarods® in the more volatile solvents in the very hot weather of midsummer. Another set of samples was developed without the use of a constant humidity tank stage between development in each solvent, as this was less important than the maintenance of cold conditions. The equilibration time in each tank was also cut down (to none in the most polar solvent), saving a great deal of time. The first rod gave sharper peaks (Fig.7.8) without splitting as before – the split was thought to be caused by the solvent vapour spreading out the origin spot into a band before development. However sensitivity was down on this plot and the rest of the set was wasted because the detector became clogged and gave negligible signal. The detector was cleaned satisfactorily but time had run out to continue work

on this investigation. It had achieved its purposes: the technique had been researched, mastered and improved, and the sponsors had the basic information that they sought.

7.4 Inversion Point of Polymer-Modified Bitumens

7.4.1 Melting Behaviour

The behaviour of 'APP'-modified bitumens in tests depends upon their compositions. They can behave as polymer-in-bitumen or bitumen-in-polymer, and the change from bitumen main phase to polymer main phase occurs at the 'inversion point.' This phenomenon shows up in simple tests on softening point and cold fracture, and was known to occur at around 20% 'APP.' When heated at 120°C, unmodified bitumens melted and spread out considerably, but 30 % **32C** in 100 Pen bitumen was hardly affected. Therefore an inversion point was expected in the melting behaviour and a test was set up on the **32C**/100 Pen series.

Experimental

Approximately equal mass (180 mg) and size samples (1 cm diameter discs) of each % composition were heated for 2 days in daylight at 120°C on glass slides - 2"×2" (for 0%, 5% and 10% 'APP') or 1"×3" (for 15, 20 and 30% 'APP'). The degree of melting and spreading was compared quantitatively - the slides were photocopied with 200 % enlargement, and the paper was cut out and weighed, correct to 0.1 mg (Fig.7.10, 71 % of original size). The melting test was repeated in the dark, to see whether the test would work so well, and to include an extra sample of unknown composition.

Results and Discussion

The data (Table 7.4) were plotted on a graph of melt area mass *vs* % 'APP' (Fig.7.11), which had a very clear inversion point at 17% 'APP.' This inversion point was the point of optimum miscibility, where neither component was the main phase. Interestingly, the shape of the graph matched that for DSC measurements of T_g *vs* % **32C** (Fig.5.27), so the most cost-effective amount of additive for lowering T_g was the same as that at the inversion point. This very simple method of measuring melt area over a couple of days could probably be applied to any combination of polymer and bitumen. It could provide a new, simple, quick, cheap standard method for finding the inversion point = optimum miscibility = optimum percentage additive for a new bitumen-polymer blend. It could be applied in the most basic laboratory and back up or even replace DSC measurements for this purpose, particularly since experience showed that

these were time-consuming and tricky to measure and interpret, particularly without computerized data handling. The graph for melt area mass *vs* % **32C** also matched that for % mass loss *vs* % **32C** (Fig.6.17a) for long-term degradation in 4 lux for 332 h (6.4.2). The latter showed that degradation can also provide the same information simply.

Table 7.4 Mass of Photo-enlarged Melt Area of 32C/100 Pen after 48 h at 120°C in 5 Lux

% **32C**	0	5	10	15	20	30
Mass / mg	360.6	249.2	141.9	38.8	21.8	17.8

The melting test in the dark confirmed the inversion point as about 18% 'APP.' The samples melted and spread out very little after 10 h, so longer heating was unnecessary. The unknown sample spread least, so 'APP,' if present, exceeded 30%. A graph of actual % mass loss *vs* % 'APP' showed the same relationship but the inversion point was less clear. The principle was correct but % mass loss by degradation needed much longer than two days in the dark to show differences properly.

7.4.2 Surface Crystallization

When the series of six **32C**/bitumen blends were heated in 4 lux at 120°C, samples with only 5% and 10% 'APP' developed a large amount of easily-visible colourless crystals on the surface by 232 hr; the same happened more slowly in the dark (Fig.7.12). The crystals could not be polymer because they did not turn yellow or degrade away, even when **32C** itself had begun rapid degradation. Also, tiny crystalline areas were seen in the bitumen itself, which also had cracked more and more as volatiles were lost. Only very slight crystallisation was observed by microscope on the 15%, 20% and 30% 'APP' samples. So it seemed that 'APP' below the inversion point composition caused a component of the bitumen to crystallize out, which might reduce adhesion. So this observation provided yet another reason for using no less than 17% 'APP.' After the same time 9% and 13% SBS/200 Pen blends and PFSD (6% SBS + SIS) showed much less surface crystallization.

7.5 Density, Crystallinity and Degradation

DSC of 'APPs' had shown that the less crystalline the sample, the more easily it underwent thermal oxidation. The long-term thermal degradation plots of mass loss also showed that degradation behaviour depended upon the method of preparation of the ten 'APPs,' and

hence upon the crystallinity at the start. The order of crystallinity for the three preparation methods also varied with the type of 'APP.' The higher the crystallinity, the higher the density of a polymer, so it was expected that the density would also depend upon the method of preparation, and that it would be the reverse of the order of ease of degradation.

7.5.1 Density Gradient Column : Experimental

The three methods of preparation (6.6.2) of all the 200-mg 1-cm sample discs involved melting of very small pieces at 175°C for 15 min, followed by:

(A) rapid quench to RT, (B) 50 min at 130°C, and then quench to RT, (C) slow cool to RT.

During thermal degradation at 120°C all the 'APPs' had shown large differences in the mass loss curves for sets A, B and C before they all slowed down and converged. Densities were measured for non-degraded and degraded 'APPs' with an ethanol-water density gradient column (Section 2.8). The first column had a density range of 0.86 to 0.94 g cm^{-3} at 22°C, the second 0.92 to 1.00 g cm^{-3} at 22°C, the third 0.82 to 0.93 g cm^{-3} at 30°C, the fourth 0.90 to 1.00 g cm^{-3} at 26°C. Densities were usually calculated at 2 min from placement on a column.

7.5.2 Density Gradient Column : Results and Discussion

Column 1 (Table 7.5)

Samples of untreated 'APP' pellets stayed where they settled on the column, with only negligible movement downwards. Polymers are normally only soluble in solvents, and vice versa, if the two have similar solubility parameters δ. Therefore interaction was not expected because the values for PP, PE and EP are 7.9, 8.0 and 11.0, and those for EtOH and water are 12.7 and 23.4 $cal^{½}$ $cm^{-3/2}$ respectively (Hall, 1989, Table 5.1, p.126).

Fresh A/B/C sets of six 'APPs' (one sample of each) were checked after 10 min on the column. For all except **43C**, the order of density was C < A < B or C ~ A < B (where A and C both floated); for **43C**, it was C < B < A. Therefore 'APPs' annealed at 130°C, and quenched, were generally most crystalline, as expected since the optimum temperature for phase separation crystallization is about 65°C, midway between T_g and T_m. Slow-cooled 'APPs' were least dense, least crystalline, so lack of thermal shock made a detectable difference. All 'APPs' showed a slight variation in density within a prepared 1-cm disc or a commercial pellet, so averages of three or more samples were taken thereafter.

Table 7.5 Densities (g cm^{-3}) of 'APPs' Before and After Partial Degradation at 120°C

	Supply Code	Pellet	Fresh A/B/C (Column 1 at RT)			Part-Degraded A/B/C (Column 1 at RT)		
'APP'			A	B	C	A	B	C
PP1	1C	0.874	0.876	0.878	0.875	0.910	0.912	0.909
PP2	MF80	0.876	<0.864	0.880	<0.864			
PP3	32C	0.917	0.870	0.878	<0.864	0.874	0.885	0.876
PP4	43C	0.866	0.876	0.870	<0.864			
PP5	MF500	0.864	0.868	0.878	<0.864			
PP6	C80	0.900	<0.864	<0.864	<0.864			
PP7	T1180	0.906	0.890	0.910	0.877			
PP8	95X	<0.864	<0.864	0.870	<0.864			
PP9	V808	0.868	0.872	-	-			
PP10	V809	0.870	0.872	-	-			

After partial degradation at 120°C in 4 lux for 215 h, **95-X-06** (six samples) and **1C** (six samples) were compared: **95-X-06** fell by 10 cm over 60 min on the column, so its density rose by up to 1.2%, much more than that of degraded **1C**, which rose 0.09% over 90 min. Therefore the particularly fast degradation of **95-X-06** was matched by its particularly fast interaction with solvent. Sets A, B and C of **1C** and **32C** (after 208 h) showed the reverse order in densities (both C < A < B) to that in mass loss (C > A = B or C > A > B). Therefore samples losing the most mass were still the least crystalline. The figures also showed that all sets A, B and C were more crystalline than before degradation. By 60 min the **32C** samples had gained an average of 2 % in density over the 5 min value, with falls of 17-32 cm. It seemed that once fast degradation had begun the surface was more reactive, both towards oxygen and towards solvent(s).

Column 2 (Table 7.6)

After long, dark degradation, sets A/B/C were expected to have high crystallinity, so they were tested on a higher range column, but many samples floated. Density order was C < B < A (for **C80**), C < A < B (for **T1180**) or C/A << B (for **95-X-06**), so again slow-cooled sets were least crystalline. Densities were well above those of original pellets or fresh A/B/C.

Column 3 (Table 7.6)

A third column was set up to monitor sets A/B/C after long, dark degradation. Unfortunately the density/height plot was linear to only about 50 cm, so only that height was useable. At

least two samples of each set A/B/C were mainly monitored for at least 30 min. 32C-B was denser than 32C-A, 95-X-06-A and MF80-A/B/C. From 12 min, MF80-C gained density faster than -A and -B, so the least crystalline form of **MF80** interacted most with the solvent. 43C-A floated for 60 min and MF500-A for 90 min (so had unexpectedly low density) before suddenly falling rapidly down the column and starting a (slower) steady descent.

Column 4 (Table 7.6)

After long, dark degradation all densities were very much higher than before degradation. Samples were also tracked down the column, to see whether descent rate reflected atactic content. The descents of samples were different and did not seem to fit any pattern. 95X-C dropped suddenly at about 30 min and 85 min. This behaviour rather resembled the large shrinkage transition observed in the swelling ratio for polymer gels at a certain concentration of acetone in water (Hall, 1989, Fig.5.2, p.125).

Table 7.6 Densities (g cm^{-3}) of 'APPs' After Long Degradation at 120°C

	Degraded A/B/C (Column 2 at 22°C)			Degraded A/B/C (Column 3 at 30°C)			Degraded A/B/C (Column 4 at 26°C)		
'APP'	A	B	C	A	B	C	A	B	C
1C	>0.981	>0.981	>0.981				>0.988	>0.988	>0.988
MF80	<0.925	<0.925	<0.925	0.888	0.890	0.887			
32C	<0.925	<0.925	<0.925	0.913	0.922				
43C	<0.925	<0.925	<0.925				<0.939	<0.939	<0.939
MF500	<0.925	<0.925	<0.925						
C80	>0.981	0.959	0.957				0.984	0.974	0.978
T1180	0.961	0.961	0.960				0.959	0.958	0.951
95X	<0.925	0.974	<0.925	0.909			-	0.963	0.941

Column temperatures varied slightly in the July heat-wave in spite of a thermostat and pump; there were problems with maintaining the fill rate of the column; there was a limit to the number of samples that could be put on a column together; many degraded samples did not settle but carried on sinking. Many samples floated or sank to the bottom, so were useless. In spite of difficulties, results did show that density, and hence crystallinity, was least for Set C (slow-cooled) samples and usually highest for Set B samples (quenched after annealing at 130°C). They also showed that degradation raised the density and hence crystallinity considerably.

In retrospect it would have been far more efficient to use just one column with a wider density range (about 0.8 to 1.1 g cm^{-3} = 0.3 g cm^{-3} range) than to use several columns, each with only 0.1 g cm^{-3} range. However at the start the magnitude of density differences between Sets A, B and C, and between 'APPs' before and after degradation, was not known.

7.5.3 Alternative Density Method : Experimental

For three reasons an alternative density method was devised, to see how it compared. (a) Several 'APPs' from the long thermal degradation in the dark probably had densities near or above 1.000 g cm^{-3}. (b) Since the densities of degraded 'APPs' did not stop changing in the EtOH/H_2O column, there was no point in leaving samples on the column to settle. (c) The column was not very efficient for bulk testing of samples, because it became difficult to distinguish them. The new method involved adding a tiny sample to a mixture of EtOH/CCl_4 (densities 0.79 and 1.59 g cm^{-3} respectively) in a 5-ml measuring cylinder, with a scale marked in 0.1 cm^3, so it could be read to 0.05 cm^3. Solvent volumes were adjusted drop-wise till the sample was just below the surface at 2 min (the same time as used in the column), when the density was that of the mixture. Several samples could be measured before the cylinder became too full; all samples were measured in triplicate and averages were taken.

7.5.4 Alternative Density Method : Results and Discussion

This method gave a large number of results (20 on pellets, 90 on degraded discs) much more quickly than by density column (Table 7.7). However orders of densities did not agree with those obtained on the density column, except for **MF500**. When the supplied 'APP' pellets that did not fall with time on the column were measured too (as the average of four, five or six measurements), the order did agree for **1C**, **32C** and **43C**, and all the polymers were denser after degradation (Table 7.8). It would have been useful to measure the densities of the freshly-prepared A/B/C sets before degradation, to confirm their deduced relative crystallinities/densities, and to compare orders before and after degradation. Comparison with a few measurements of crystallinity by DSC would have been useful too.

The solvent interaction with degraded 'APPs' (obvious in the EtOH/H_2O column) had only 2 min to work here (in EtOH/CCl_4), so the results were judged as reliable, and they were complete. There was a very strong correlation between the order in which the 'APPs' 'took off' on fast degradation and the orders of density for degraded 'APPs' (Table 7.9).

Table 7.7 Densities (g cm^{-3})of 'APPs' at the End of the Long Dark Degradation

'APP'	Code	A	B	C	Order
PP1	1C	1.075	1.036	1.045	B < C < A
PP2	MF80	0.942	0.966	0.966	A < C = B
PP3	32C	0.934	0.942	0.969	A < B < C
PP4	43C	0.856	0.888	0.871	A < C < B
PP5	MF500	0.851	0.910	0.887	A < C < B
PP6	C80	1.015	1.064	1.061	A < C < B
PP7	T1180	1.036	1.005	1.033	B < C < A
PP8	95X	1.044	0.983	0.946	C < B < A
PP9	V808	1.026	1.039	1.030	A < C < B
PP10	V891	0.995	1.025	1.029	A < B < C

Table 7.8 Changes in Density (g cm^{-3}) of 'APPs' With Long Degradation

'APP'	Code	Untreated	% Increase in Density		
		APP	A	B	C
PP1	1C	0.894	20.2	15.9	16.9
PP2	MF80	0.912	3.3	5.9	5.9
PP3	32C	0.909	2.8	3.6	6.6
PP4	43C	0.749	14.3	18.6	16.3

Table 7.9 'Take-Off' Order in Fast Oxidative Degradation of 'APPs,' and Ascending Density Order Afterwards

'APP'	1C	MF80	32C	43C	MF500	C80	T1180	95X06	V808	V891
Dark	CAB	CAB	CAB	CAB	CAB	ACB	CAB	CAB	CAB	CBA
	CAB	ACB	CAB	CAB	ACB	ACB	ACB	CAB	CBA	BAC
4 Lux	CAB	CAB	CAB	CAB	CAB	BAC	ABC	ACB	CBA	BAC
Density	BCA	ACB	ABC	ACB	ACB	ACB	BCA	CBA	ACB	ABC

Key: Dark = 'take off' order in duplicate sets, 4 Lux = 'take-off' order in single set, all at 120°C

Density = ascending density order, *i.e.* ACB means A<C<B

'Take off' order was usually the same in 4 lux (one set) and in the dark (two sets), and was in increasing order of density or crystallinity. In seven out of the ten cases, if samples A/B/C 'took off' in the order CAB, then the final order of density was A<C<B or A<B<C. This was logical since the sample (with lowest crystallinity) getting a head start on the others would increase its crystallinity relative to theirs, and so jump from 1st to 2nd or 3rd. Even when the 'take-off' order was different, this pattern still worked. In two out of the ten cases (**1C** and **V808**) C<A<B gave the final order B<C<A (for **1C**), and C<B<A gave

A<C<B (for **V808**) which fitted with the crystallinity of the 1st and 2nd least crystalline samples both increasing to above that of the 3rd. This very strong correlation between the two experiments suggested that the relative densities obtained by this alternative method were accurate. The method had the added advantage that it could be applied in any basic laboratory without the need for the special apparatus.

7.6 Summary of Conclusions

7.6.1 FT-Raman Spectra During Degradation

'APPs' were more crystalline after degradation, and the two copolymers crystallized more over 16 days than did a homopolymer. Crystallization progressed as the yellow colouration intensified. Graphs of the height and area of the 2884 nm peak throughout degradation were the same shape as that for % mass loss, provided that all the highest values were joined up, and the natural scatter was ignored. Thus such graphs could be used to follow degradation progress. The ratios of height and area of twin peaks at 880-780 nm twin peaks had already been seen to reflect degree of 'APP' crystallinity: the ratio of left:right was about 1:1 for APP and 0.75:1 for IPP. Comparison of this ratio before and after degradation for 1060 h in 5 lux showed that a higher value beforehand corresponded to earlier onset of auto-oxidation, so this ratio could be used to predict relative ease of degradation of 'APP' additives.

7.6.2 SARA Analysis of Bitumens

Several bitumens were analysed for SARA content (Saturates, Aromatics, Resins and Asphaltenes), with particular interest in the Asphaltenes, initially with an Iatroscan® TH-10 Mark II analyzer. The first trial, using four decreasingly polar solvents to develop the chromatograms, gave better spread and resolution of the components than the second trial, using three increasingly polar solvents. When the former solvents were used together with the much more sensitive TH-10 Mark IV, and techniques were adapted to allow for the greater sensitivity and the very hot weather, good resolution was achieved, and bitumens could be reliably classed as high or low in Asphaltenes.

7.6.3 Inversion Point of Polymer-Modified Bitumens

Samples of six different blends of an 'APP'/bitumen (0, 5, 10, 15, 20 and 30% **32C**) were heated for 2 days in daylight in an oven at 120°C in order to measure the melting behaviour. The degree of melting and spreading was compared quantitatively - the glass slides were

photocopied with 200 % enlargement, and the paper was cut out and weighed. A graph of area mass *vs* % 'APP' (Fig.7.12), gave a very clear inversion point at 17%, so this was the point of optimum miscibility. This simple method could be a standard method for finding the inversion point = optimum miscibility = optimum percentage additive for a new bitumen-polymer blend. During degradation of the **32C**/100 Pen series at 120°C in 4 lux, it was found that added 'APP' below the inversion point value caused a component of the bitumen to crystallize on the surface, so this effect gave an additional reason to use the inversion point amount of polymer.

7.6.4 Density, Crystallinity and Degradation

A density gradient column was set up according to standard methods, using ethanol and water. All untreated 'APPs' (densities 0.864-0.917) and all but three pre-treated 'APPs' hardly moved once they had settled. Pre-treatment involved annealing at 175°C, followed by (A) rapid quench to RT, (B) 50 min at 130°C, and then quench to RT, (C) slow cool to RT. For most fresh sets of A/B/C, the order of density was C<A<B or C~A<B (where A and C both floated); for **43C**, it was C<B<A. Therefore 'APPs' annealed at 130°C, and quenched, were generally most crystalline, as expected since the optimum temperature for phase separation crystallization is about 65°C, midway between T_g and T_m. Slow-cooled 'APPs' were least dense, least crystalline, so lack of thermal shock made a significant difference.

After partial degradation (at 120°C in 4 lux for 208 h) samples losing the most mass were still the least crystalline, and all sets A, B and C were more crystalline than before degradation. **32C** samples fell 17-32 cm down the column between 5 and 60 min, so increased in density by about 2 %. This 'APP' was always the first to reach auto-oxidation, so it seemed that the high degree of degradation left it vulnerable to interaction with solvent. Perhaps this was because solvent could infiltrate the sample better as phase separation increased and larger amorphous areas became exposed – just as oxidation was deduced to improve as larger amorphous areas became exposed (see theory in Section 6.7). Likewise the particularly fast degradation of **95-X-06** was matched by its particularly fast interaction with solvent. After degradation most 'APPs' did not settle but carried on sinking.

An alternative density method allowed fairly fast measurement in triplicate of all Sets A, B and C for all 10 'APPs' (90 samples) after the long, dark degradation. Results ranged from 0.851 to 1.075 g cm^{-3}. The new method, employing ethanol and chloroform, and just a 5-ml

measuring cylinder and two droppers, confirmed that all densities rose with degradation. For degraded 'APPs' the orders of densities were different to those from the columns. However the results tied in with the all the work on degradation behaviour of Sets A, B and C. The final order of density was that expected from the order of onset of auto-oxidation and the fact that least crystalline samples 'taking off' first would gain more in crystallinity.

7.7 Tables

Table 7.1 Ratios of FT-Raman Peak Heights and Areas at 880-780 nm for Three 'APPs' 3
Table 7.2 Ratio of Peak Areas for the Four Constituents of Five Bitumens 5
Table 7.3 SARA Analysis Data for Five Bitumens 6
Table 7.4 Mass of Photo-enlarged Melt Area of 32C/100 Pen after 48 h at 120°C in 5 Lux 8
Table 7.5 Densities (g cm^{-3}) of 'APPs' Before and After Partial Degradation at 120°C 10
Table 7.6 Densities (g cm^{-3}) of 'APPs' After Long Degradation at 120°C 11
Table 7.7 Densities (g cm^{-3})of 'APPs' at the End of the Long Dark Degradation 13
Table 7.8 Changes in Density (g cm^{-3}) of 'APPs' With Long Degradation 13
Table 7.9 'Take-Off' Order in Fast Oxidative Degradation of 'APPs,' and Ascending Density Order Afterwards 13

7.8 References

8

Bharati S, Rostum G and Loberg R, Calibration and standardization of Iatroscan (TLC-FID) using standards derived from crude oils. Advances in Organic Geochemistry, 1993. *Org Geochem*, 1994, 22,3-5, 835-862. 6

Hall C, *Polymer Materials: An Introduction for Technologists and Scientists*, 2nd Edition, Macmillan Education, Basingstoke and London, 1989, Chap.5, 121-152. 9, 11

Chapter 8 CONCLUSIONS

8.1 Outcome of Experiments

All techniques revealed useful information on the bitumens, 'atactic polypropylenes' ('APPs') and their blends and provided answers to the original questions about the materials. The investigations had not been previously reported in literature, except for the SARA analysis of bitumens, by TLC with FID, which was developed here to a point where good separation of the four main components of five bitumens was achieved. Several novel methods were introduced for demonstrating or investigating required or related phenomena.

T_gs of 'APPs,' bitumens and their blends were successfully measured by DSC. With linked scans and rapid quenching the T_g could be clearly separated from that of the moisture in the samples (at about –3°C), which otherwise interfered. Hence T_g of one 'APP' was –38°C, lower than –30°C in literature. The plot of blend T_g *vs* % 'APP' showed that T_g was reduced rapidly by added 'APP' until a certain value, beyond which it made much less difference. This value of 17% corresponded to that at the inversion point, the change from bitumen to 'APP' as main phase, already known approximately from other physical properties. This was also the point of maximum miscibility of the system. For SBS, which has a much lower T_g (-90.6°C), the value was only 9% or less.

On a DSC chart that point was reached when the T_g curve of the polymer joined on to the T_g curve of the bitumen in one smooth extended T_g curve. Therefore the digitization and summing of DSC plots of various proportions of bitumen and SBS were tried out on Microsoft Excel, to see whether this point could be found from comparison of plots. It was a subjective choice of which plot looked best but, even so, the method would give an approximate answer – here 9% or less. This point was also found for an 'APP' by another novel method – by melting behaviour of the same series of blends. Spreading out on melting was greatly reduced by added 'APP' until about 17%, beyond which it made much less difference. Long-term degradation of the series of 'APP' blends also provided the same value from a plot of % mass change *vs* % 'APP.' The thorough investigation of the effect of 'APP'content showed that the optimum amount of polymer could be found solely by DSC, partly by DSC and also by two alternative methods that required less expensive equipment. Inversion between 'APP'-in-

bitumen and bitumen-in-'APP' behaviour was the determining factor, so any method that found the inversion point would suffice.

Creep behaviour in 'APPs' was measured thoroughly by TMA. It could be high initially but was reduced by phase separation crystallization (induced by heating, and greatest at about 65°C) and stress-induced crystallization (induced indirectly by load). Therefore creep in an 'APP'/bitumen system would be less with high 'APP' content, so using no less than 17% would again be best. Creep would fall as crystallinity gradually increased with phase separation crystallization and thermo-oxidative degradation of the 'APP.'

DSC showed that atactic PP oxidized sooner and faster than isotactic PP, and that oxidation and decomposition were two-stage processes. It also provided evidence of phase separation crystallization, cold crystallization, and restriction of movement by minor crystalline components. Phase separation behaviour led to predictions on the long-term crystallinity of 'APPs' (in bitumens) experiencing daily and seasonal cycles of heating and cooling.

Degradation of 'APPs' was monitored satisfactorily by % mass change, which showed up features not reported before for conventional monitoring of degradation by its gaseous products. The typical plot of % mass change involved initial fast loss (of volatiles), slow induction stage, slight mass gain, fast loss stage, and levelling off towards the amorphous content. With higher temperature, higher UV level or greater sensitivity, degradation was faster, so the mass gain was missed out and then the slow stage, so only the fast stages were seen. Study of 'APP'/blends confirmed that bitumen protected 'APP' but also that 'APP' protected the bitumen. The long-term plot could distinguish a homopolymer (with one amorphous component) from a copolymer (with more than one). As mentioned above, a plot of % mass change *vs* % 'APP' showed that the optimum amount of polymer additive for reduction of degradation was 17%, as more than this had much less effect. The degradation of eight 'APPs' heat-treated in three different ways, so that they experienced different phase separation and thermal shock, proved that the least crystalline 'APPs' reached auto-oxidation first, and that the most crystalline 'APPs' reached it last.

FT-Raman was shown to be capable of monitoring the progress of degradation. One FT-Raman feature, which varies for APP and IPP, identified 'APPs' with higher amorphous content, so it could be used to distinguish those most likely to degrade more rapidly, before they are even tested. Commercial 'APPs' varied in their susceptibility to degradation – out of ten, three were

particularly stable, one particularly unstable – and still degraded at 120°C in the dark, if they had been warm in very dim light. If never lit while warm, most of them only oxidized at 120°C in the dark, but did not degrade. Therefore 'APPs' in a roofing felt, shielded from light by bitumen and mineral granules, would degrade only very slowly initially, but more so later as the protection deteriorated with weathering.

Use of a density gradient column proved that 'APPs' all became more dense and therefore more crystalline with degradation, and that the deduced relative crystallinities/densities of heat-treated 'APPs' were correct. After degradation 'APPs' interacted with the ethanol-water in the column, and sank at different rates; the 'APP' that was least stable to degradation also interacted most with solvent afterwards. For an alternative density method using ethanol-chloroform, there was very strong correlation between the order in which the 'APPs' 'took off' on fast degradation and the orders of density for those 'APPs' after degradation, so the method was considered reliable.

A theory on 'APPs' thermo-oxidative degradation was proposed that accounted for all the features of the % mass loss curves of the 'APPs.' The theory was supported by a Microsoft Excel spreadsheet that demonstrated how auto-oxidation could take a short or long time, or not happen at all, depending upon the balance between phase separation and degradation.

The project produced a great deal of information, answered the questions about the materials, showed that useful work could be done on the sticky black bitumen blends, and yielded several new techniques worth pursuing.

Fig. 8.1 Location of Details of New Techniques

New Technique	Section
T_g by Dynamic Load TMA	3.9
T_g by Summing of DSC Plots	5.6.5
Degradation of 'APPs' by % Mass Loss	6
Inversion Point by Thermal Degradation	6.4.2.3
Standardization of 'APPs' in 3 Ways	6.6.2
Monitoring of Degradation by FT-Raman	7.2.2.1
Inversion Point by Melting Behaviour	7.4
Alternative Density Method	7.5.4

8.2 Future Work

Two extra methods that were suggested for finding T_g could be developed as alternatives to conventional DSC, which was often tricky to interpret for the 'APPs.' The first method uses dynamic-load TMA results, involving calculation of Youngs Modulus at a range of temperatures and then a plot of the polymer S-curve, from which the T_g can be read. The second method uses linked DSC scans to find the temperature at which there is no heat change at a pause in cooling and therefore no crystallization because there is no translational motion. More blends in the SBS/bitumen series should be studied, in order to find the inversion point for the combination.

TMA of 'APPs' revealed the presence of a separate surface layer, so perhaps this technique might prove useful in its investigation. Dynamic load TMA data led to a proposed way of drawing up a profile of an 'APP', relating load, thickness and temperature at which stress-induced crystallization occurred. Even though, in time, phase separation crystallization would also affect the balance of these factors, this idea might be worth pursuing.

Now that the equipment works well, TLC with FID could perhaps be used to obtain molecular weight distributions of co- and homo-polymers. The chemical composition distributions of several styrene-ethyl methacrylate copolymer emulsions were investigated with an Iatroscan TH-10 several years earlier (Tacx and German, 1989). Isotactic polypropylene had been fractionated according to molecular weight and tacticity, by solvent extraction (Lehtinen and Paukkeri, 1994).

Whenever relative crystallinities/densities of a large number of samples is required, the new alternative density method could be applied fairly rapidly. Then a few samples could also be scanned by DSC, and a scale of density against crystallinity could be drawn up.

References

8

Lehtinen A and Paukkeri R, Fractionation of polypropylene according to molecular weight and tacticity. *Macromol Chem Phys*, 1994, 195, 1539-1556. 4

Tacx J C J F and German A L, Study on the Feasibility of TLC/FID to Reveal Chemical Composition Distributions of Copolymers by Emulsion Processes. *J Poly Sci*: Part A: Poly Sci, 1989, 27, 817-827. 4

Exploration of a Method of Determination of the Glass Transition (T_g) of APP by Dynamic Force TMA

During testing of the capabilities of the TMA instrument, several charts were recorded under different conditions.
2-3 mm samples were cut with a craft knife from the interior of supplied pellets.
Each fresh sample was subjected to a different dynamic load as it was heated at 10 K/min up to 130°C.
For all scans the lower limit of the dynamic load was 0.02 N and the probe tip area was 1 mm^2.
The melting point was known to be 149°C from Step Analysis of the static load TMA chart run at the same speed.
The depth of pen oscillations on the chartpaper were deduced to be a measure of the compressibility under those conditions.
Conventionally Young's Modulus of Compressibility is measured by applying a range of loads at a fixed temperature.
However measurements taken at regular temperature intervals from the charts gave the same information.
Although the experiment was not planned, data were plotted to obtain Young's Modulus of Compressibility at each temperature.
These results were then plotted, to see whether part of the normal S curve of a polymer was generated.
If so the experiment could be repeated using uniform annealed samples.
It could be extended, with the aid of a cooling jacket round the furnace, to temperatures below the expected T_g of about -30°C.
Then the T_g could be obtained from the point of change from brittle to leathery behaviour.
This method would be a new way of determining T_g values, requiring only a series of scans under different dynamic loads.
The manual did not describe such an application and no references to one were found.

Dynamic Loads

Chart No.	Minimum Load / N	Oscill'g Maximum Load / N	Start of Force F / N	EL/Bite / °C
18	0.2	0.08	0.06	135
19	0.2	0.08	0.06	135
16	0.2	0.10	0.08	135
20	0.2	0.12	0.10	135
21	0.2	0.14	0.12	130
22	0.2	0.16	0.14	108
23	0.2	0.18	0.16	96
28	0.2	0.26	0.24	113
29	0.2	0.32	0.30	97
25	0.2	0.42	0.40	71
26	0.2	0.52	0.50	68

Modulus of Compressibility = stress / strain = C = (F / A) / (c / L) = (force / area) / (length change / start length) where F in N, A in m^2, c in m, L in m.
So graph of c/L *vs* F gives C = (1 / A) * (1 / gradient) $A = 1\ mm^2 = 1(10^{-6})\ m^2$ Size of C approx $1*10^{-8}\ Nm^{-2}$
Samples under the lighter dynamic loads reached their elastic limit (EL) at about 135°C. Data: hardback notebook IA:p.35-51.
With heavier dynamic forces (>0.12 N), the plots developed progressively deeper 'bites.' Attributed to stress-induced crystallization.
The curves suddenly dipped, then recovered and carried on. Across the 'bite,' no readings could be taken.

Chart Measurements of Oscillation Depths

Values of compression measured off chart / mm

Chart No.	Start Lgth / mm	Load F / N	35°C	40°C	45°C	50°C	55°C	60°C	65°C	70°C	75°C	80°C	90°C	100°C	110°C	120°C	130°C
18	3.2082	0.06	8.0	10.0	19.0	22.0	25.0	25.0	27.0	27.0	28.0	28.0	28.0	29.0	30.0	30.0	
19	2.1448	0.06	6.5	9.0	12.0	13.5	15.0	17.0	19.5	21.0	23.0	24.0	26.0	28.0	28.0	29.0	33.0
16	2.3091	0.08	8.0	11.0	20.0	23.0	27.0	29.0	31.0	33.0	33.0	36.0	36.0		37.0	33.0	32.0
20	1.8559	0.10	11.0	12.0	15.0	16.0	18.0	20.0	22.5	23.0	25.0	26.0	25.0	28.0	31.0	35.0	45.0
21	2.3083	0.12	21.0	27.0	31.0	36.0	40.0	43.0	45.0	48.0	48.0	50.0	50.0	47.0	43.0		60.0
22	2.6472	0.14	19.0	23.0	29.0	33.5	38.0	43.0	45.0	50.0	53.0	57.0	64.0			58.0	
23	2.2090	0.16	24.0	29.0	35.0	38.0	40.0	45.0	47.0	54.0	55.0			72.0	77.0	82.0	
28	1.5440	0.24	24.0	28.0	33.0	34.5	37.0	38.0	38.0	38.0	37.0	38.0	44.0	52.0	64.0		
29	1.8476	0.30	41.0	47.0	49.0	50.5	54.0	55.0	55.0	55.0	54.0	54.0	62.0	71.0			
25	2.2003	0.40	44.0	57.0	65.0	68.0	75.0	80.0	85.0					124.0			

Values of actual compression converted to microns (chart measurement/1.1111)

Load F / N	35°C	40°C	45°C	50°C	55°C	60°C	65°C	70°C	75°C	80°C	90°C	100°C	110°C	120°C	130°C
0.06	7.2	9.0	17.1	19.8	22.5	22.5	24.3	24.3	25.2	25.2	25.2	26.1	27.0	27.0	

0.06	5.9	8.1	10.8	12.2	13.5	15.3	17.6	18.9	20.7	21.6	23.4	25.2	25.2	26.1	29.7
0.08	7.2	9.9	18.0	20.7	24.3	26.1	27.9	29.7	29.7	32.4	32.4		33.3	29.7	28.8
0.10	9.9	10.8	13.5	14.4	16.2	18.0	20.3	20.7	22.5	23.4	22.5	25.2	27.9	31.5	40.5
0.12	18.9	24.3	27.9	32.4	36.0	38.7	40.5	43.2	43.2	45.0	45.0	42.3	38.7		54.0
0.14	17.1	20.7	26.1	30.2	34.2	38.7	40.5	45.0	47.7	51.3	57.6			52.2	
0.16	21.6	26.1	31.5	34.2	36.0	40.5	42.3	48.6	49.5			64.8	69.3	73.8	
0.24	21.6	25.2	29.7	31.1	33.3	34.2	34.2	34.2	33.3	34.2	39.6	46.8	57.6		
0.30	36.9	42.3	44.1	45.5	48.6	49.5	49.5	49.5	48.6	48.6	55.8	63.9			
0.40	39.6	51.3	58.5	61.2	67.5	72.0	76.5					111.6			

Values of 10^{2}*c/L (compression/start length)

Load F / N	35°C	40°C	45°C	50°C	55°C	60°C	65°C	70°C	75°C	80°C	90°C	100°C	110°C	120°C	130°C
0.06	0.224	0.281	0.533	0.617	0.701	0.701	0.757	0.757	0.785	0.785	0.785	0.814	0.842	0.842	
0.06	0.273	0.378	0.504	0.566	0.629	0.713	0.818	0.881	0.965	1.007	1.091	1.175	1.175	1.217	1.385
0.08	0.312	0.429	0.780	0.896	1.052	1.130	1.208	1.286	1.286	1.403	1.403		1.442	1.286	1.247
0.10	0.533	0.582	0.727	0.776	0.873	0.970	1.091	1.115	1.212	1.261	1.212	1.358	1.503	1.697	2.182
0.12	0.819	1.053	1.209	1.404	1.560	1.677	1.755	1.872	1.872	1.950	1.950	1.833	1.677		2.339
0.14	0.646	0.782	0.986	1.139	1.292	1.462	1.530	1.700	1.802	1.938	2.176			1.972	
0.16	0.978	1.182	1.426	1.548	1.630	1.833	1.915	2.200	2.241			2.933	3.137	3.341	
0.24	1.399	1.632	1.924	2.011	2.157	2.215	2.215	2.215	2.157	2.215	2.565	3.031	3.731		
0.30	1.997	2.289	2.387	2.460	2.630	2.679	2.679	2.679	2.630	2.630	3.020	3.459			
0.40	1.800	2.332	2.659	2.781	3.068	3.272	3.477					5.072			

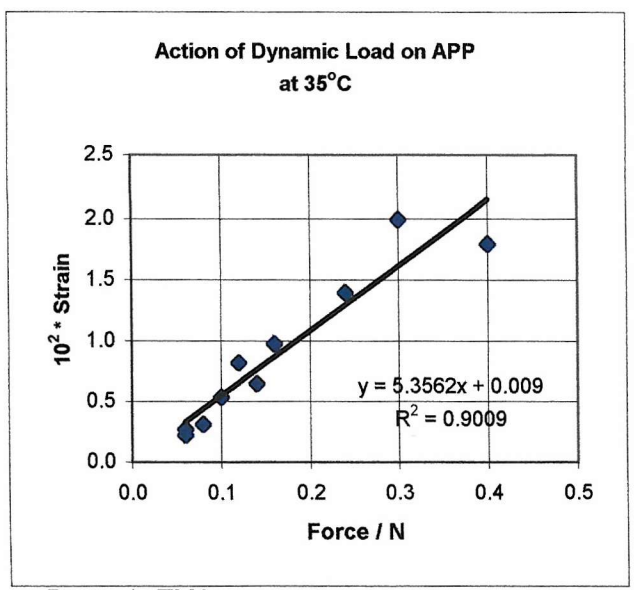

Dynamic TMA

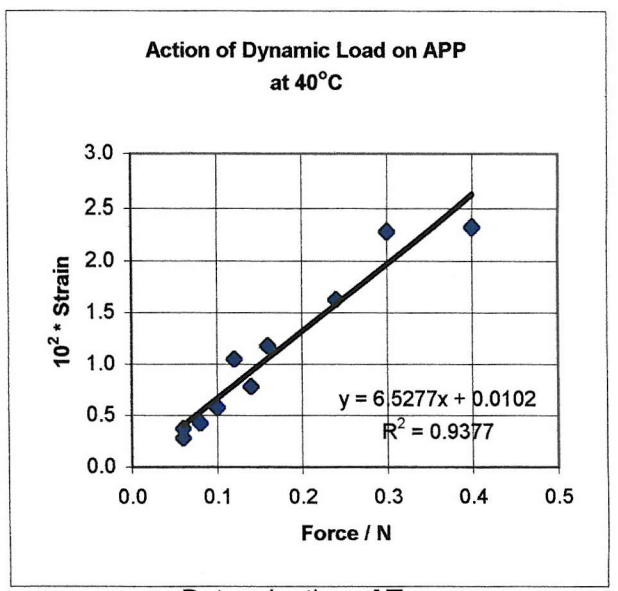

Determination of T_g

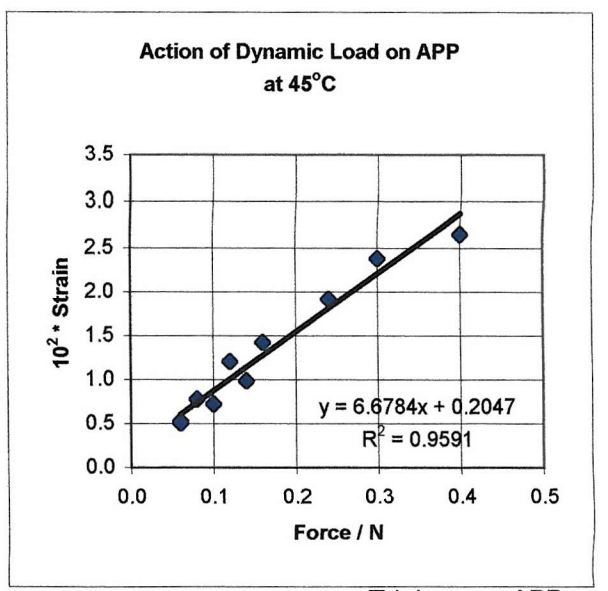

Trial on an APP

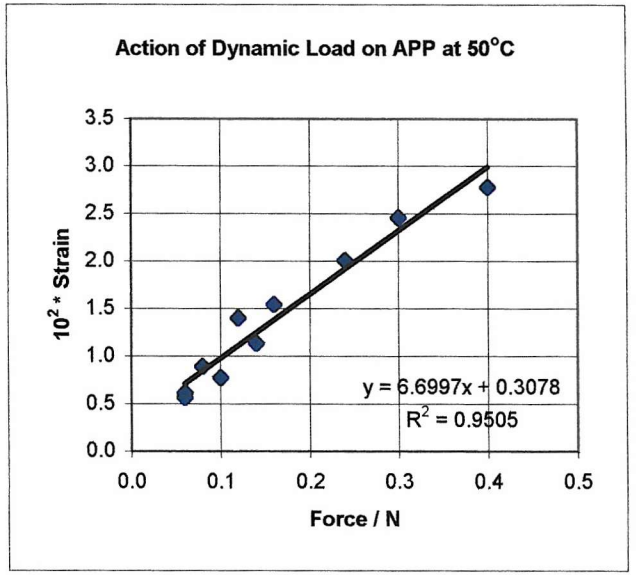

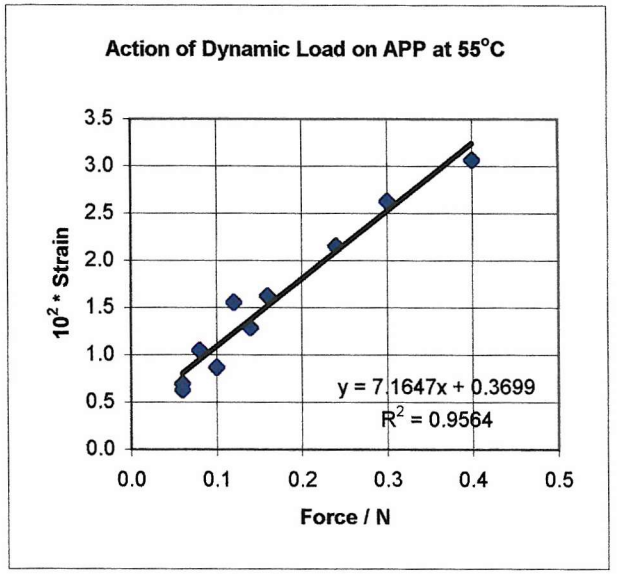

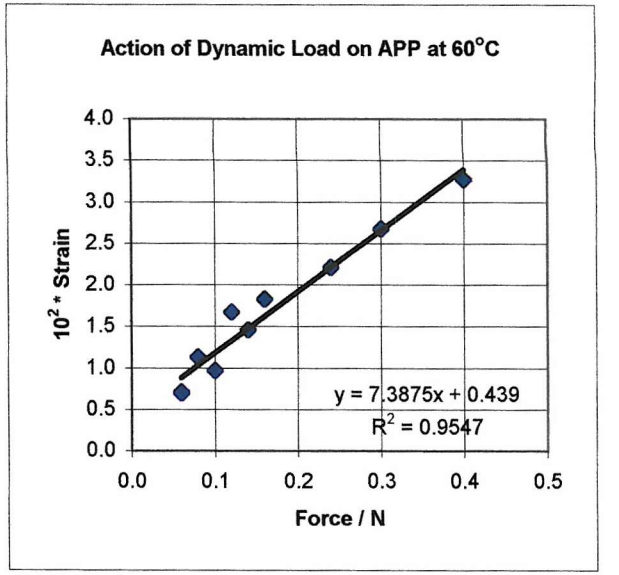

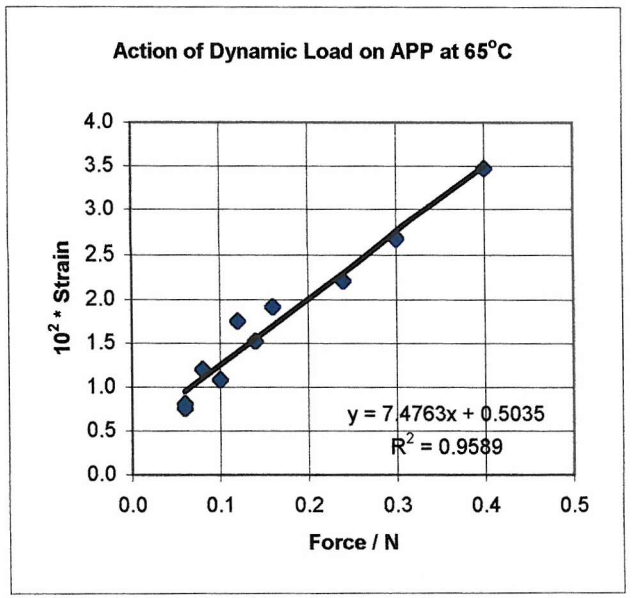

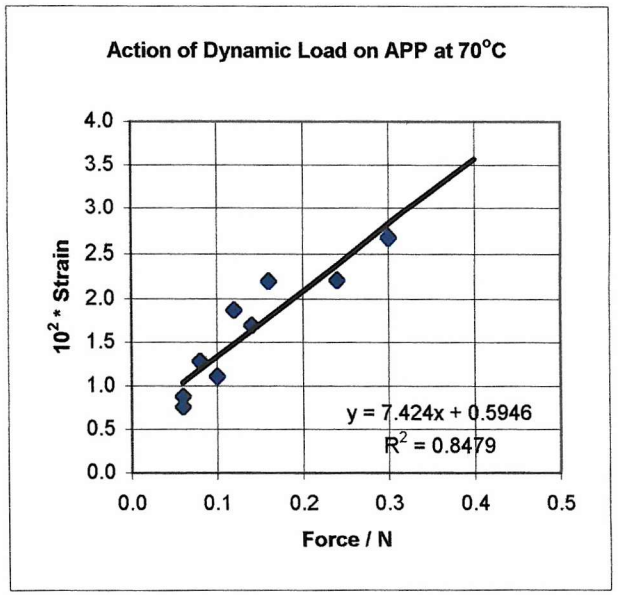

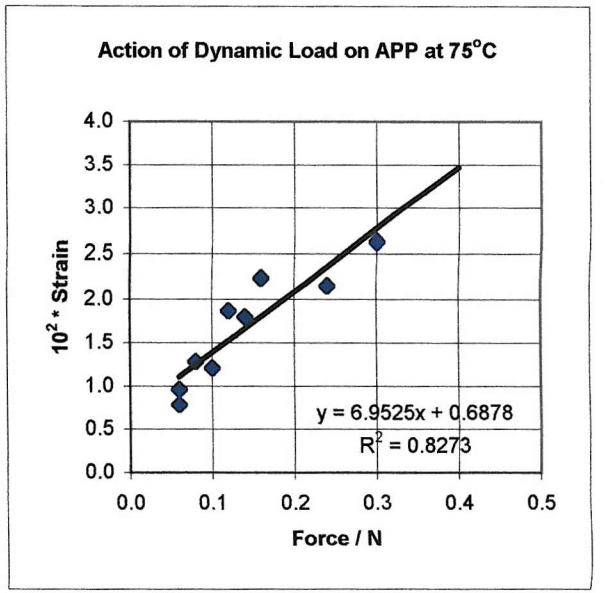

Dynamic TMA

Determination of T_g

Trial on an APP

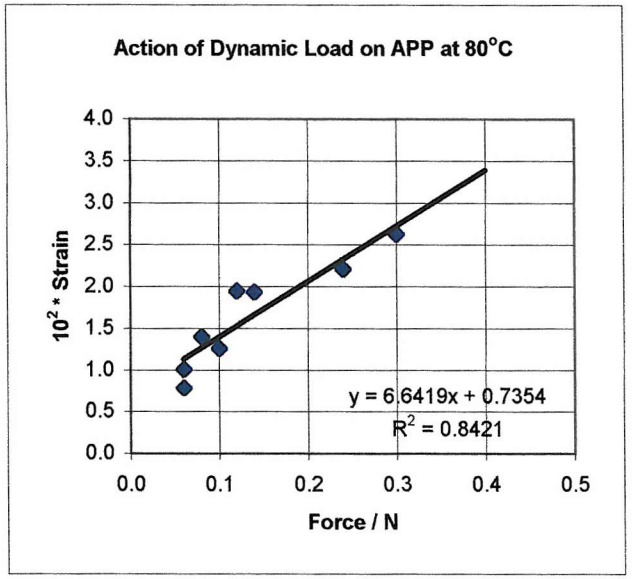

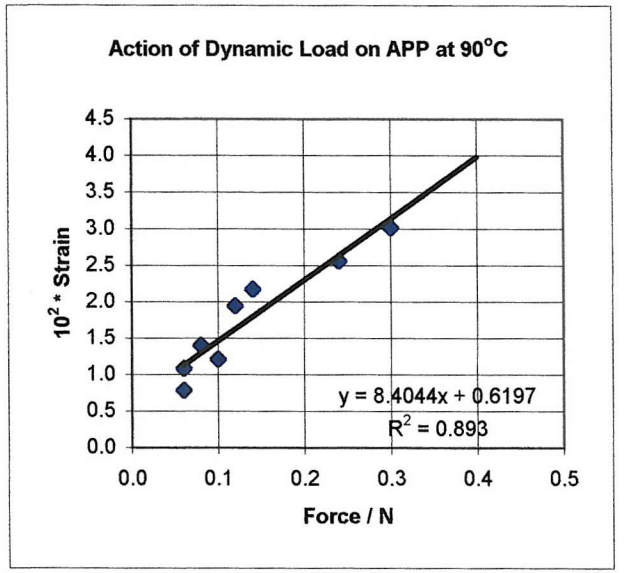

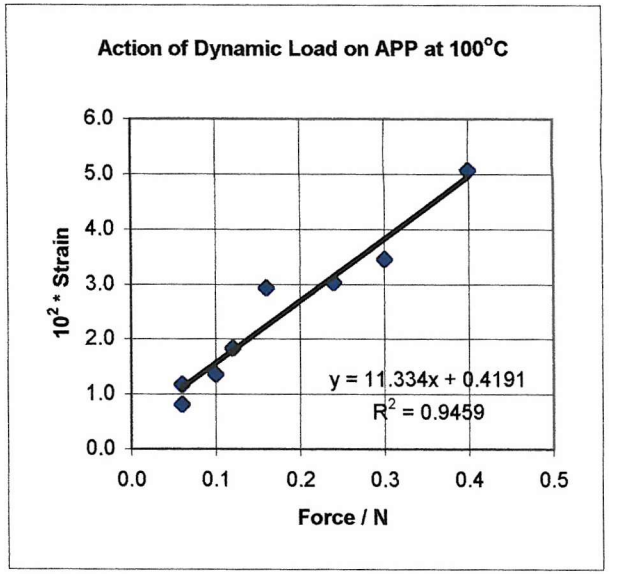

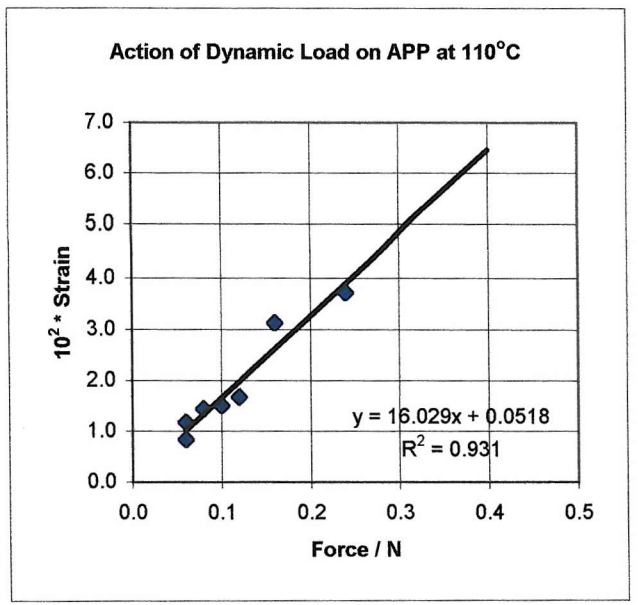

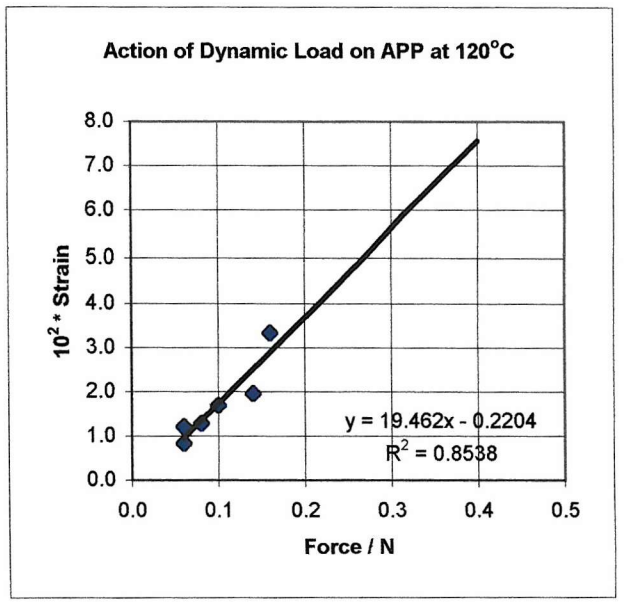

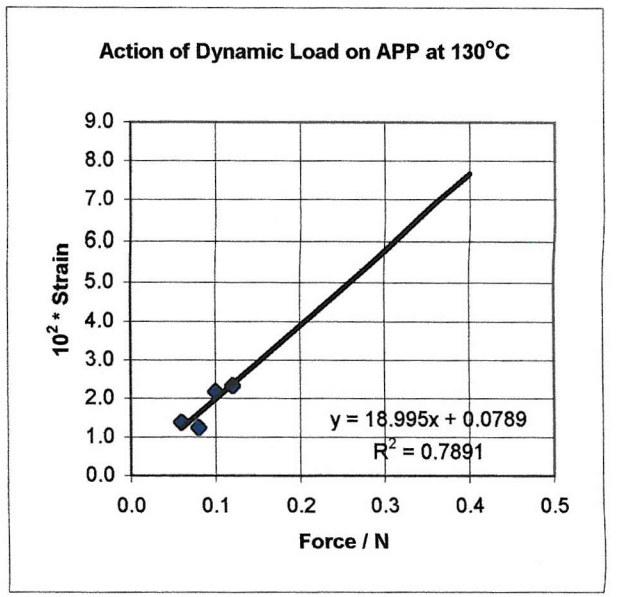

Dynamic TMA

Determination of T_g

Trial on an APP

Variation of Young's Modulus with Temperature - The S Curve for Polymers

Temp / °C	10^{-2} * Gradient =Strain/Stress	Y Mod
35	5.3562	1.8670
40	6.5277	1.5319
45	6.6784	1.4974
50	6.6997	1.4926
55	7.1647	1.3957
60	7.3875	1.3536
65	7.4763	1.3376
70	7.4240	1.3470
75	6.9525	1.4383
80	6.6419	1.5056
90	8.4044	1.1899
100	11.3340	0.8823
110	16.0290	0.6239
120	19.4620	0.5138
130	18.9950	0.5265
149		0.0000

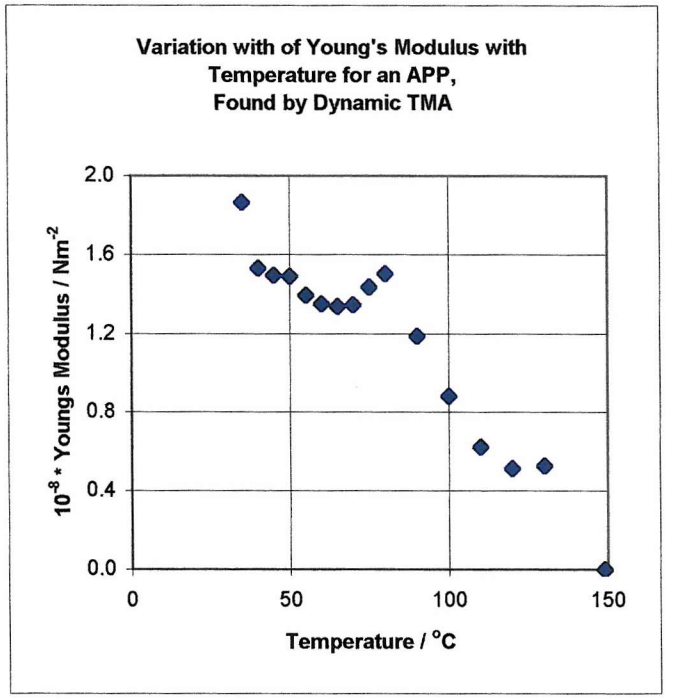

Conclusions

Shape of plot of Modulus vs Temperature was roughly as expected, i.e. part of the S Curve. Therefore the trial was a success.

At 75°C, 80°C - should gradient be higher?

At 130°C - not enough data points.

Conditions for Repeat Experiment

Samples should be annealed, so surface is smooth, and crystallinity is the same at the start.

Temperature range should be extended to 25°C.

More dynamic loads between 0.16 and 0.4 N should be used.

Cold jacket should be constructed to extend range down to below the T_g value of about -30°C.

Experiment was not refined because the TMA broke down and repair was too costly.

The method of meauring T_g should work.

With extension to lower T, plot $\log_{10}$modulus vs T.

Digitization and Addition of DSC Plots - Test on Determination of Tg of a Blend

SBS in 200 Pen Bitumen

Material	Scale	Start of Tg curve = Tg_1, end = Tg_3, midpoint = Tg_2.	
200 pen	1.0000 mW = 57.5 mm		
SBS	0.5000 mW = 46.5 mm	estimated from above -65°C	Tg = -90.6°C (auto)
9% SBS	1.0000 mW = 48.0 mm		

Tg of the bitumen was estimated from chart as -5°C (midway between Tg_1 at -40°C and Tg_3 at 30°C)
Actual position of zero line for heat flow was not necessary to summing the plots.

Chart Readings (in mm) from Left Hand Side

	Results for SBS		Results for 200P		Results for Blend		Sum of Plots for x % SBS		
Temp/°C	Rdg/mm	Rdg/mW SBS	Rdg/mm	Rdg/mW 200 Pen	Rdg/mm	Rdg/mW 9% SBS	Rdg/mW 50%	Rdg/mW 25%	Rdg/mW 9%
-120					103	2.146			
-115					115	2.396			
-110	114	1.226	115	2.000			3.226	1.806	1.930
-105	108	1.161	111	1.930			3.092	1.738	1.861
-100	102	1.097	107	1.861	105	2.188	2.958	1.670	1.792
-95	90	0.968	103	1.791			2.759	1.585	1.717
-92.5	80	0.860	101	1.757			2.617	1.532	1.676
-90	55	0.591	99	1.722	99	2.063	2.313	1.439	1.620
-87.5	32	0.344	98	1.704			2.048	1.364	1.582
-85	23	0.247	97	1.687			1.934	1.327	1.557
-80	13	0.140	95	1.652	92	1.917	1.792	1.274	1.516
-75	10	0.108	92.5	1.609			1.716	1.233	1.474
-70	8.5	0.091	90	1.565	86	1.792	1.657	1.197	1.433
-65	8	0.086	87.5	1.522			1.608	1.163	1.393
-60	7	0.075	85	1.478	82	1.708	1.554	1.128	1.352
-50	6	0.065	81	1.409	75	1.563	1.473	1.073	1.288
-45	5.5	0.059	79	1.374			1.433	1.045	1.256
-40	5	0.054	77	1.339	70	1.458	1.393	1.018	1.223
-35	4.5	0.048	70	1.217			1.266	0.925	1.112
-30	4	0.043	65	1.130	65	1.354	1.173	0.859	1.033
-25	3.5	0.038	60	1.043			1.081	0.792	0.953
-20	3	0.032	52	0.904	54	1.125	0.937	0.686	0.826
-15	2.5	0.027	45	0.783			0.809	0.594	0.715
-10	2	0.022	39	0.678	50	1.042	0.700	0.514	0.619
-5	1.5	0.016	33	0.574			0.590	0.434	0.524
-2	1.2	0.013	28	0.487	45	0.938	0.500	0.368	0.444
0	1	0.011	33	0.574	48	1.000	0.585	0.433	0.523
5			36	0.626			0.626	0.470	0.570
10			32	0.557			0.557	0.417	0.506
15			30	0.522			0.522	0.391	0.475
20			28	0.487	32	0.667	0.487	0.365	0.443
30			22	0.383			0.383	0.287	0.348
40			19	0.330	30	0.625	0.330	0.248	0.301
50			16	0.278			0.278	0.209	0.253
60			12.5	0.217	27.5	0.573	0.217	0.163	0.198
70			10	0.174			0.174	0.130	0.158
80			8	0.139	25	0.521	0.139	0.104	0.127
90			5	0.087			0.087	0.065	0.079

Conclusions

High %s of SBS still had 2 separate Tgs, so the Tg of the bitumen would still operate separately.
Addition of less SBS probably overcame Tg_1 of the bitumen and extended its straight part to the Tg_1 of the additive, giving new combined Tg at -40°C (midpoint of -110° and 30°C).
Only 9% SBS was enough to flatten Tg_1 of the bitumen and combine 2 plots to give 1 new Tg_2.
Estimated plot for 9% SBS was similar to the actual plot.
Actual plot for 13% SBS was almost the same as for 9% SBS, so no need to use >9% SBS.

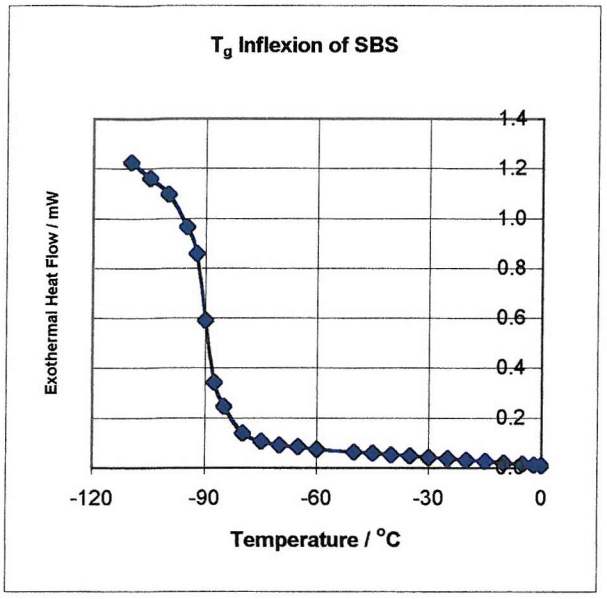

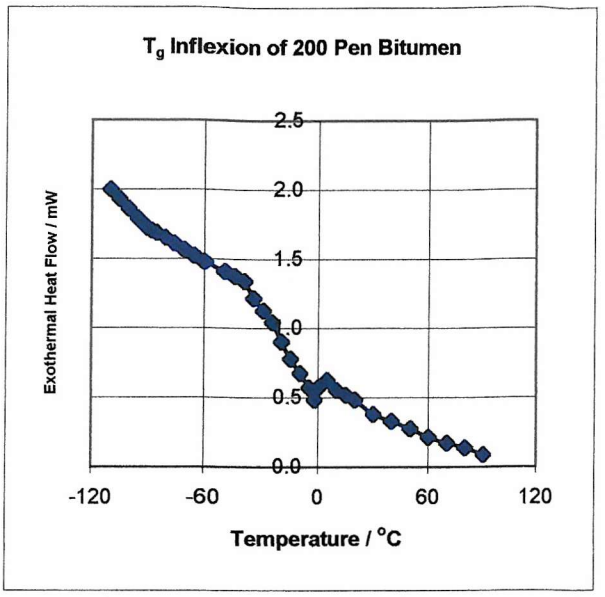

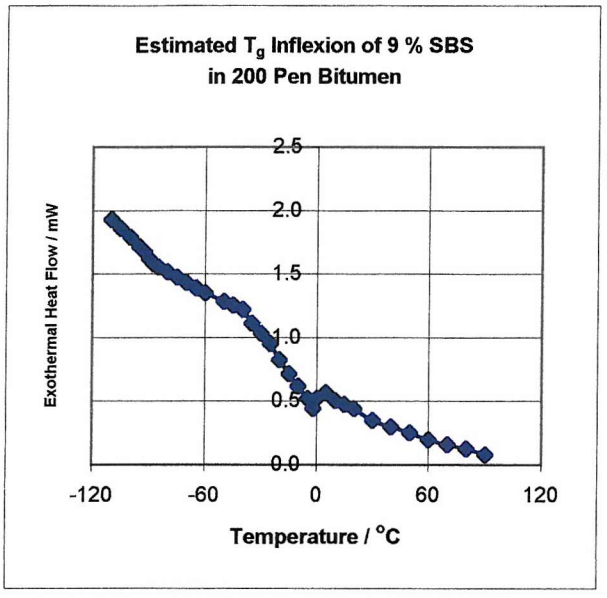

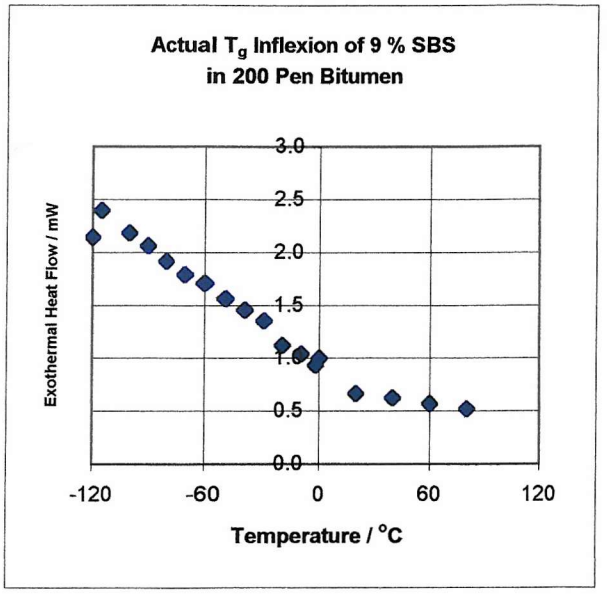

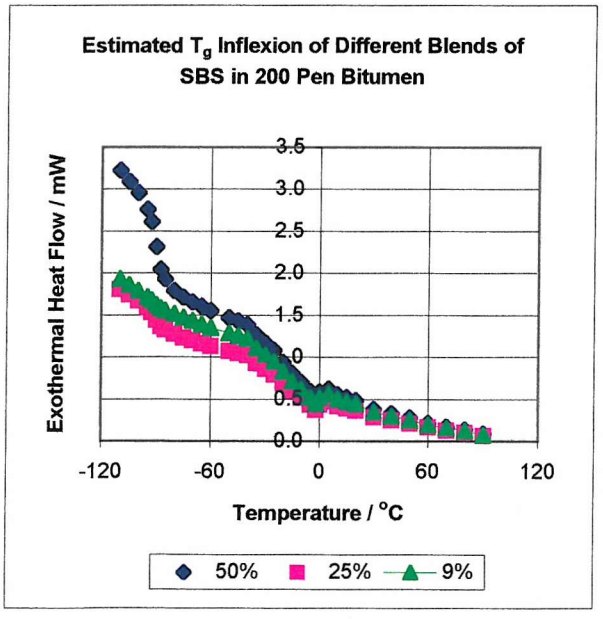

Graph for 50%, 25% and 9% SBS shows how 2 separate Tgs flatten off into one extended Tg when % of SBS is as low as 9%.
Perhaps even lower % SBS would work.

This method is approximate and depends on when, in practice rather than on paper, the 2 separate Tg curves merge into 1 extended Tg curve.

This method would show whether a large or small amount of additive would be required in a particular mix.
If the additive has a high amplitude inflexion (a high change in specific heat) less of it will be needed.

APP Degradation - Modelling of the Factors Producing the % Mass Loss Curve

Factors

size of amorphous zone
initial degree of crystallinity
(high if quenched)
rate of phase separation crystallization
temperature (fixed through run)
light level (fixed through run)
rate of addition of -O-O- (in excess)
rate of loss of fragments
time

Treatment

Assume degradation losses are from the constantly renewed surface.
Treat whole area and zone areas as squares on the surface.
Assume 50:50 APP:IPP
Assume each component has an area of 20*20 units = 400 sq units.
Let A stand for an link site in an amorphous zone,
and X for one in a crystalline zone.
Let A-A, A-X and X-X stand for A-O-O-A, A-O-O-X and X-O-O-X links
respectively, when an O2 molecule joins on.
No. of A-X = no. of inter-zone links per zone.
No. of zones falls as PSC progresses, so no.of A-X falls.
No. of A-A falls as PSC progresses because they are gradually lost.
Assume no. of X-X is constant, even with PSC, because they are not lost.
Without degradation, no. of A-A = no. of X-X (400 of each).
From 5 time units, calculate A-X per zone from formula; estimate earlier values.
From A-X per zone and no. of zones, calculate total A-X and % A-X (for graph).
For each rate of degradation, use same total A-X and total X-X and falling A-A.
Point where % A-A exceeds % A-X is probably the point of auto-oxidation.

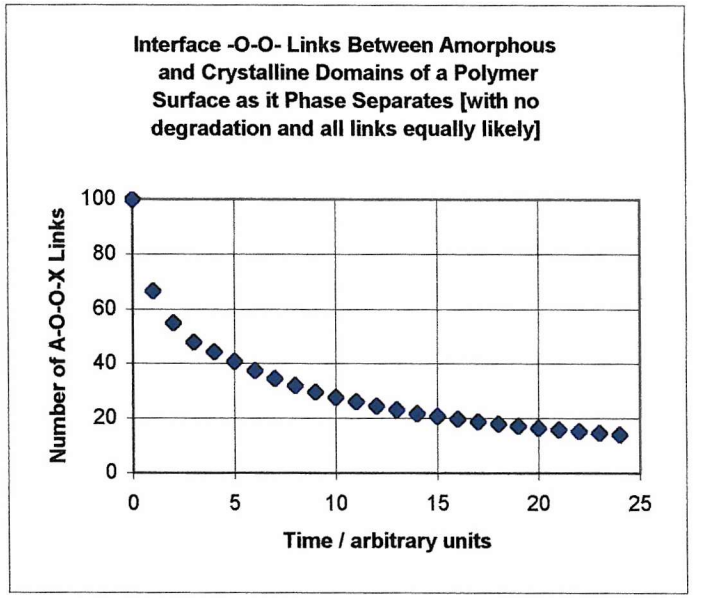

Graph for Set 1 with no degradation ($A40:$A74,$H40:$H74)

Set 1: Rate of PSC = zone growth by 0.5 unit per side per unit time

time	zone side	zone size	number of zones	Possible -O-O- links if no degradation, and all links are equally probable A-A	X-X	A-X per zone	A-X Total	%A-X	Possible -O-O- links with degradation with loss of 4 A-A per unit time A-A	A-X	Total Links	% A-A	% A-X
0	1.0	1.0	800.0	0	0	1	800	100	0	800	800	0	100
1	1.5	2.3	355.6	133	133	1.5	533	67	129	533	796	16	67
2	2.0	4.0	200.0	180	180	2.2	440	55	172	440	792	22	56
3	2.5	6.3	128.0	208	208	3	384	48	196	384	788	25	49
4	3.0	9.0	88.9	222	222	4	356	44	206	356	784	26	45
5	3.5	12.3	65.3	237	237	5	327	41	217	327	780	28	42
6	4.0	16.0	50.0	250	250	6	300	38	226	300	776	29	39
7	4.5	20.3	39.5	262	262	7	277	35	234	277	772	30	36
8	5.0	25.0	32.0	272	272	8	256	32	240	256	768	31	33

9	5.5	30.3	26.4	281	281	9	238	30	245	238	764	**32**	**31**
10	6.0	36.0	22.2	289	289	10	222	28	249	222	760	33	29
11	6.5	42.3	18.9	296	296	11	208	26	252	208	756	33	28
12	7.0	49.0	16.3	302	302	12	196	24	254	196	752	34	26
13	7.5	56.3	14.2	308	308	13	185	23	256	185	748	34	25
14	8.0	64.0	12.5	313	313	14	175	22	257	175	744	34	24
15	8.5	72.3	11.1	317	317	15	166	21	257	166	740	**35**	22
16	9.0	81.0	9.9	321	321	16	158	20	257	158	736	**35**	21
17	9.5	90.3	8.9	325	325	17	151	19	257	151	732	**35**	21
18	10.0	100.0	8.0	328	328	18	144	18	256	144	728	**35**	20
19	10.5	110.3	7.3	331	331	19	138	17	255	138	724	**35**	19
20	11.0	121.0	6.6	334	334	20	132	17	254	132	720	**35**	18
21	11.5	132.3	6.0	336	336	21	127	16	252	127	716	**35**	18
22	12.0	144.0	5.6	339	339	22	122	15	251	122	712	**35**	17
23	12.5	156.3	5.1	341	341	23	118	15	249	118	708	**35**	17
24	13.0	169.0	4.7	343	343	24	114	14	247	114	704	**35**	16
25	13.5	182.3	4.4	345	345	25	110	14	245	110	700	**35**	16
26	14.0	196.0	4.1	347	347	26	106	13	243	106	696	**35**	15
27	14.5	210.3	3.8	349	349	27	103	13	241	103	692	**35**	15
28	15.0	225.0	3.6	350	350	28	100	12	238	100	688	**35**	14
29	15.5	240.3	3.3	352	352	29	97	12	236	97	684	34	14
30	16.0	256.0	3.1	353	353	30	94	12	233	94	680	34	14
31	16.5	272.3	2.9	354	354	31	91	11	230	91	676	34	13
32	17.0	289.0	2.8	356	356	32	89	11	228	89	672	34	13
33	17.5	306.3	2.6	357	357	33	86	11	225	86	668	34	13
34	18.0	324.0	2.5	358	358	34	84	10	222	84	664	33	13

Set 2: Faster rate of PSC = zone growth by 0.8 unit per side per unit time

				Possible -O-O- links if no degradation, and all links are equally probable					**Possible -O-O- links with degradation with loss of 4 A-A per unit time (if X not involved)**				
time	zone side	zone size	number of zones	A-A	X-X	A-X per zone	A-X Total	%A-X	A-A	A-X	Total Links	% A-A Deg 4	% A-X
0	1.0	1.0	800.0	0	0	1.0	800	100	0	800	800	0	100
1	1.8	3.2	246.9	128	128	2.2	543	68	124	543	796	16	68
2	2.6	6.8	118.3	193	193	3.5	414	52	185	414	792	23	52
3	3.4	11.6	69.2	234	234	4.8	332	42	222	332	788	28	42
4	4.2	17.6	45.4	255	255	6.4	290	36	239	290	784	30	37

5	5.0	25.0	32.0	272	272	8.0	256	32	252	256	780	32	33
6	5.8	33.6	23.8	286	286	9.6	228	29	262	228	776	**34**	**29**
7	6.6	43.6	18.4	297	297	11.2	206	26	269	206	772	35	27
8	7.4	54.8	14.6	307	307	12.8	187	23	275	187	768	36	24
9	8.2	67.2	11.9	314	314	14.4	171	21	278	171	764	36	22
10	9.0	81.0	9.9	321	321	16.0	158	20	281	158	760	37	21
11	9.8	96.0	8.3	327	327	17.6	147	18	283	147	756	37	19
12	10.6	112.4	7.1	332	332	19.2	137	17	284	137	752	**38**	18
13	11.4	130.0	6.2	336	336	20.8	128	16	284	128	748	**38**	17
14	12.2	148.8	5.4	340	340	22.4	120	15	284	120	744	**38**	16
15	13.0	169.0	4.7	343	343	24.0	114	14	283	114	740	**38**	15
16	13.8	190.4	4.2	346	346	25.6	108	13	282	108	736	**38**	15
17	14.6	213.2	3.8	349	349	27.2	102	13	281	102	732	**38**	14
18	15.4	237.2	3.4	351	351	28.8	97	12	279	97	728	**38**	13
19	16.2	262.4	3.0	354	354	30.4	93	12	278	93	724	**38**	13
20	17.0	289.0	2.8	356	356	32.0	89	11	276	89	720	**38**	12
21	17.8	316.8	2.5	358	358	33.6	85	11	274	85	716	**38**	12
22	18.6	346.0	2.3	359	359	35.2	81	10	271	81	712	**38**	11
23	19.4	376.4	2.1	361	361	36.8	78	10	269	78	708	**38**	11
24	20.2	408.0	2.0	362	362	38.4	75	9	266	75	704	**38**	11
25	21.0	441.0	1.8	364	364	40.0	73	9	264	73	700	**38**	10
26	21.8	475.2	1.7	365	365	41.6	70	9	261	70	696	37	10
27	22.6	510.8	1.6	366	366	43.2	68	8	258	68	692	37	10
28	23.4	547.6	1.5	367	367	44.8	65	8	255	65	688	37	10
29	24.2	585.6	1.4	368	368	46.4	63	8	252	63	684	37	9
30	25.0	625.0	1.3	369	369	48.0	61	8	249	61	680	37	9
31	25.8	665.6	1.2	370	370	49.6	60	7	246	60	676	36	9
32	26.6	707.6	1.1	371	371	51.2	58	7	243	58	672	36	9
33	27.4	750.8	1.1	372	372	52.8	56	7	240	56	668	36	8
34	28.2	795.2	1.0	373	373	54.4	55	7	237	55	664	36	8

Set 3: Slower rate of PSC = zone growth by 0.28 unit per side per unit time

			Possible -O-O- links if no degradation, and all links are equally probable						**Possible -O-O- links with degradation with loss of 4 A-A per unit time (if X not involved)**				
time	zone side	zone size	number of zones	A-A	X-X	A-X per zone	A-X Total	%A-X		A-A	A-X	Total Links	% A-A	% A-X
0	1.00	1.0	800.0	0	0	1.0	800	100		0	800	800	0	100

1	1.28	1.6	488.3	58	58	1.4	684	85	54	684	796	7	86
2	1.56	2.4	328.7	104	104	1.8	592	74	96	592	792	12	75
3	1.84	3.4	236.3	140	140	2.2	520	65	128	520	788	16	66
4	2.12	4.5	178.0	169	169	2.6	463	58	153	463	784	19	59
5	2.40	5.8	138.9	192	192	3.0	417	52	172	417	780	22	53
6	2.68	7.2	111.4	205	205	3.5	390	49	181	390	776	23	50
7	2.96	8.8	91.3	221	221	3.9	358	45	193	358	772	25	46
8	3.24	10.5	76.2	229	229	4.5	341	43	197	341	768	26	44
9	3.52	12.4	64.6	237	237	5.0	325	41	201	325	764	26	43
10	3.80	14.4	55.4	245	245	5.6	310	39	205	310	760	27	41
11	4.08	16.6	48.1	252	252	6.2	296	37	208	296	756	28	39
12	4.36	19.0	42.1	259	259	6.7	283	35	211	283	752	28	38
13	4.64	21.5	37.2	265	265	7.3	271	34	213	271	748	28	36
14	4.92	24.2	33.0	270	270	7.8	259	32	214	259	744	29	35
15	5.20	27.0	29.6	276	276	8.4	249	31	216	249	740	29	34
16	5.48	30.0	26.6	281	281	9.0	239	30	217	239	736	29	32
17	5.76	33.2	24.1	285	285	9.5	230	29	217	230	732	**30**	31
18	6.04	36.5	21.9	289	289	10.1	221	28	217	221	728	**30**	**30**
19	6.32	39.9	20.0	293	293	10.6	213	27	217	213	724	**30**	29
20	6.60	43.6	18.4	297	297	11.2	206	26	217	206	720	**30**	29
21	6.88	47.3	16.9	301	301	11.8	199	25	217	199	716	**30**	28
22	7.16	51.3	15.6	304	304	12.3	192	24	216	192	712	**30**	27
23	7.44	55.4	14.5	307	307	12.9	186	23	215	186	708	**30**	26
24	7.72	59.6	13.4	310	310	13.4	180	23	214	180	704	**30**	26
25	8.00	64.0	12.5	313	313	14.0	175	22	213	175	700	**30**	25
26	8.28	68.6	11.7	315	315	14.6	170	21	211	170	696	**30**	24
27	8.56	73.3	10.9	317	317	15.1	165	21	209	165	692	**30**	24
28	8.84	78.1	10.2	320	320	15.7	161	20	208	161	688	**30**	23
29	9.12	83.2	9.6	322	322	16.2	156	20	206	156	684	**30**	23
30	9.40	88.4	9.1	324	324	16.8	152	19	204	152	680	**30**	22
31	9.68	93.7	8.5	326	326	17.4	148	19	202	148	676	**30**	22
32	9.96	99.2	8.1	328	328	17.9	145	18	200	145	672	**30**	22
33	10.24	104.9	7.6	330	330	18.5	141	18	198	141	668	**30**	21
34	10.52	110.7	7.2	331	331	19.0	138	17	195	138	664	29	21
35	10.80	116.6	6.9	333	333	19.6	134	17	193	134	660	29	20
36	11.08	122.8	6.5	334	334	20.2	131	16	190	131	656	29	20

Thermal Degradation

Oxidation Linkages

Modelling APP/IPP

Summary of Results: % A-A Links and Time of Steady State

Rate of Loss of A-A:	4			5			6		
Zone Growth Rate	Time to Auto-Ox	Maximum Value	Time Max Held	Time to Auto-Ox	Maximum Value	Time Max Held	Time to Auto-Ox	Maximum Value	Time Max Held
0.28	18.0	30	17-33	22.0	28	15-26	-	26	12-23
0.50	8.7	35	15-28	9.3	33/34	12-25	9.3	32	12-19
0.80	5.2	38	12-25	5.3	37	12-20	5.4	36	11-16

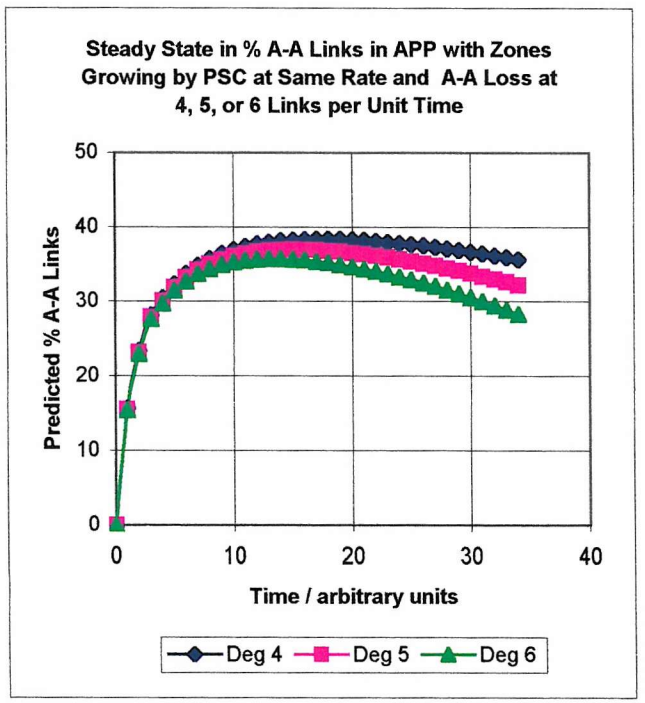

Number of A-X per zone was calculated from a formula, except for the earliest values, which were estimated from the graph.
Zone Growth Rate (in units per side per unit time rate of phase separation crystallization (PSC)
Rate of Loss of A-A (links per unit time) = rate of degradation

Conclusions

At each PSC rate: steady state of % A-A is lower, reached later and shorter with faster degradation

At each degradation rate: steady state of % A-A is higher, reached sooner and shorter with faster PSC

For 6 A-A loss per unit time and 0.28 PSC rate, % A-A did not reach % A-X.
When the 2 curves do not cross, there would be no auto-oxidation to fast stage mass loss, however long the degradation were continued.
Thus very slow PSC protects the APP from oxidative degradation.
Therefore anything restricting internal motion would act as a stabiliser.
With very fast PSC, as at high temperatures, % A-A would exceed % A-X very soon, and auto-oxidation would occur very soon -
so there might be no slow stage under those conditions.

The suggested mechanism did produce a change from predominantly A-X to predominantly A-A (i.e.A-O-O-X links to A-O-O-A links), corresponding to the change from slow degradation induction period to fast degradation.
Then there was a steady state in % A-A (corresponding to the straight section on % mass loss plot), and finally a gradual fall in % A-A (corresponding to the slowing down of degradation).
The figures also show how some combined rates of PSC and degradation would not allow fast degradation to occur.

Predicted Graphs of % A-A and A-X for an APP Degrading (at Rate 6 A-A per unit time) and under PSC with Different Growth Rates

(a) 0.8 unit per side per unit time

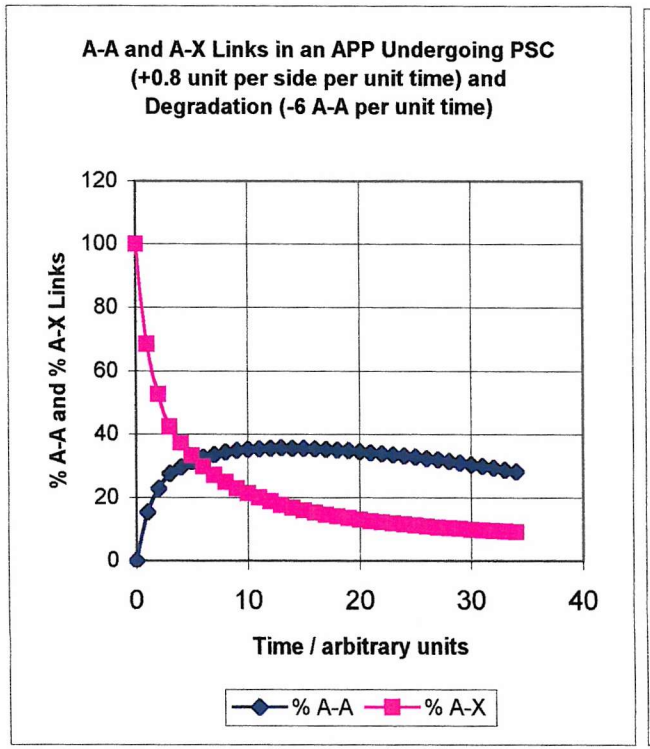

(b) 0.5 unit per side per unit time

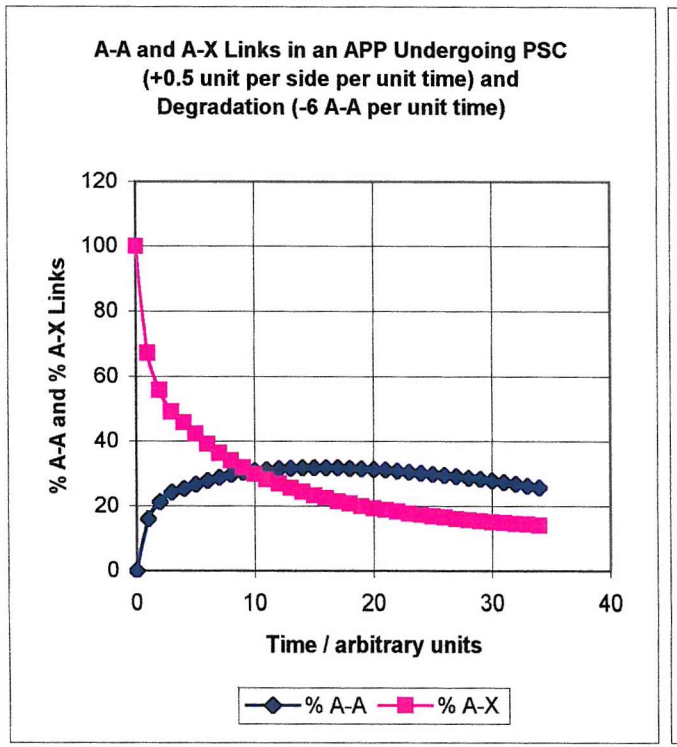

(c) 0.28 unit per side per unit time

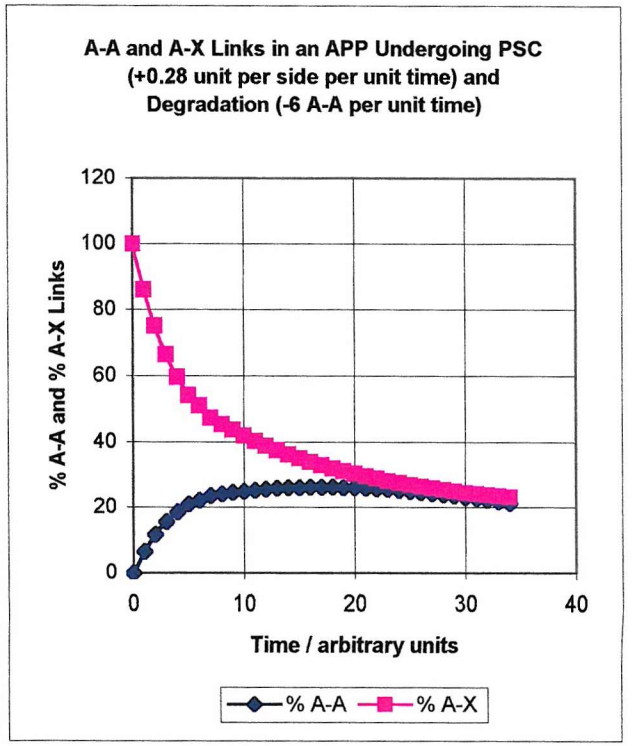

A-A predominates and therefore auto-oxidation occurs (a) by 6 time units, (b) by 10 time units and (c) possibly at 30 time units
If rate of A-A loss were less than 3 links per time unit, then the 2 curves would not touch, and there would be no auto-oxidation.
This treatment of the situation backs up the ideas proposed to account for the shape of the mass loss curves.

Set 1 Continued

Possible -O-O- links with degradation with loss of 5 A-A per unit time

A-A	A-X	Total Links	% A-A	% A-X
0	800	800	0	100
128	533	795	16	67
170	440	790	22	56
193	384	785	25	49
202	356	780	26	46
212	327	775	27	42
220	300	770	29	39
227	277	765	30	36
232	256	760	31	34

Thermal Degradation

Possible -O-O- links with degradation with loss of 6 A-A per unit time

A-A	A-X	Total Links	% A-A	% A-X
0	800	800	0	100
127	533	794	16	67
168	440	788	21	56
190	384	782	24	49
198	356	776	26	46
207	327	770	27	42
214	300	764	28	39
220	277	758	29	36
224	256	752	30	34

Oxidation Linkages

For graph - - -

% A-A	% A-X
0	100
16	67
21	56
24	49
26	46
27	42
28	39
29	36
30	34

Modelling APP/IPP

236	238	755	31	32
239	222	750	**32**	**30**
241	208	745	32	28
242	196	740	**33**	26
243	185	735	**33**	25
243	175	730	**33**	24
242	166	725	**33**	23
241	158	720	**33**	22
240	151	715	**34**	21
238	144	710	**34**	20
236	138	705	**33**	20
234	132	700	**33**	19
231	127	695	**33**	18
229	122	690	**33**	18
226	118	685	**33**	17
223	114	680	**33**	17
220	110	675	**33**	16
217	106	670	32	16
214	103	665	32	15
210	100	660	32	15
207	97	655	32	15
203	94	650	31	14
199	91	645	31	14
196	89	640	31	14
192	86	635	30	14
188	84	630	30	13

Set 2 Continued

Possible -O-O- links with degradation with loss of 5 A-A per unit time (if X not involved)

A-A	A-X	Total Links	% A-A Deg 5	% A-X
0	800	800	0	100
123	543	795	16	68
183	414	790	23	52
219	332	785	28	42
235	290	780	30	37

Thermal Degradation

227	238	746	30	32
229	222	740	**31**	**30**
230	208	734	31	28
230	196	728	**32**	27
230	185	722	**32**	26
229	175	716	**32**	24
227	166	710	**32**	23
225	158	704	**32**	22
223	151	698	**32**	22
220	144	692	**32**	21
217	138	686	**32**	20
214	132	680	31	19
210	127	674	31	19
207	122	668	31	18
203	118	662	31	18
199	114	656	30	17
195	110	650	30	17
191	106	644	30	16
187	103	638	29	16
182	100	632	29	16
178	97	626	28	15
173	94	620	28	15
168	91	614	27	15
164	89	608	27	15
159	86	602	26	14
154	84	596	26	14

Possible -O-O- links with degradation with loss of 6 A-A per unit time (if X not involved)

A-A	A-X	Total Links	% A-A Deg 6	% A-X
0	800	800	0	100
122	543	794	15	68
181	414	788	23	53
216	332	782	28	42
231	290	776	30	37

Oxidation Linkages

30	32
31	**30**
31	28
32	27
32	26
32	24
32	23
32	22
32	22
32	21
32	20
31	19
31	19
31	18
31	18
30	17
30	17
30	16
29	16
29	16
28	15
28	15
27	15
27	15
26	14
26	14

% A-A	% A-X
0	100
15	68
23	53
28	42
30	37

Modelling APP/IPP

247	256	775	32	33
256	228	770	**33**	**30**
262	206	765	34	27
267	187	760	35	25
269	171	755	36	23
271	158	750	36	21
272	147	745	36	20
272	137	740	**37**	18
271	128	735	**37**	17
270	120	730	**37**	16
268	114	725	**37**	16
266	108	720	**37**	15
264	102	715	**37**	14
261	97	710	**37**	14
259	93	705	**37**	13
256	89	700	**37**	13
253	85	695	36	12
249	81	690	36	12
246	78	685	36	11
242	75	680	36	11
239	73	675	35	11
235	70	670	35	10
231	68	665	35	10
227	65	660	34	10
223	63	655	34	10
219	61	650	34	9
215	60	645	33	9
211	58	640	33	9
207	56	635	33	9
203	55	630	32	9

Set 3 Continued

Possible -O-O- links with degradation with loss of 5 A-A per unit time (if X not involved)

A-A	A-X	Total Links	% A-A	% A-X
0	800	800	0	100

Thermal Degradation

242	256	770	31	33
250	228	764	**33**	**30**
255	206	758	34	27
259	187	752	34	25
260	171	746	35	23
261	158	740	35	21
261	147	734	**36**	20
260	137	728	**36**	19
258	128	722	**36**	18
256	120	716	**36**	17
253	114	710	**36**	16
250	108	704	**36**	15
247	102	698	35	15
243	97	692	35	14
240	93	686	35	14
236	89	680	35	13
232	85	674	34	13
227	81	668	34	12
223	78	662	34	12
218	75	656	33	11
214	73	650	33	11
209	70	644	32	11
204	68	638	32	11
199	65	632	32	10
194	63	626	31	10
189	61	620	31	10
184	60	614	30	10
179	58	608	29	10
174	56	602	29	9
169	55	596	28	9

Possible -O-O- links with degradation with loss of 6 A-A per unit time (if X not involved)

A-A	A-X	Total Links	% A-A	% A-X
0	800	800	0	100

Oxidation Linkages

31	33
33	**30**
34	27
34	25
35	23
35	21
36	20
36	19
36	18
36	17
36	16
36	15
35	15
35	14
35	14
35	13
34	13
34	12
34	12
33	11
33	11
32	11
32	11
32	10
31	10
31	10
30	10
29	10
29	9
28	9

% A-A	% A-X
0	100

Modelling APP/IPP

53	684	795	7	86
94	592	790	12	75
125	520	785	16	66
149	463	780	19	59
167	417	775	22	54
175	390	770	23	51
186	358	765	24	47
189	341	760	25	45
192	325	755	25	43
195	310	750	26	41
197	296	745	26	40
199	283	740	27	38
200	271	735	27	37
200	259	730	27	35
201	249	725	**28**	34
201	239	720	**28**	33
200	230	715	**28**	32
199	221	710	**28**	31
198	213	705	**28**	30
197	206	700	**28**	29
196	199	695	**28**	29
194	192	690	**28**	**28**
192	186	685	**28**	27
190	180	680	**28**	27
188	175	675	**28**	26
185	170	670	**28**	25
182	165	665	27	25
180	161	660	27	24
177	156	655	27	24
174	152	650	27	23
171	148	645	26	23
168	145	640	26	23
165	141	635	26	22
161	138	630	26	22
158	134	625	25	22
154	131	620	25	21

Thermal Degradation

52	684	794	7	86
92	592	788	12	75
122	520	782	16	66
145	463	776	19	60
162	417	770	21	54
169	390	764	22	51
179	358	758	24	47
181	341	752	24	45
183	325	746	25	44
185	310	740	25	42
186	296	734	25	40
187	283	728	**26**	39
187	271	722	**26**	37
186	259	716	**26**	36
186	249	710	**26**	35
185	239	704	**26**	34
183	230	698	**26**	33
181	221	692	**26**	32
179	213	686	**26**	31
177	206	680	**26**	30
175	199	674	**26**	29
172	192	668	**26**	29
169	186	662	**26**	28
166	180	656	25	28
163	175	650	25	27
159	170	644	25	26
155	165	638	24	26
152	161	632	24	25
148	156	626	24	25
144	152	620	**23**	**25**
140	148	614	23	24
136	145	608	**22**	**24**
132	141	602	22	23
127	138	596	21	23
123	134	590	21	23
118	131	584	20	22

Oxidation Linkages

7	86
12	75
16	66
19	60
21	54
22	51
24	47
24	45
25	44
25	42
25	40
26	39
26	37
26	36
26	35
26	34
26	33
26	32
26	31
26	30
26	29
26	29
26	28
25	28
25	27
25	26
24	26
24	25
24	25
23	25
23	24
22	24
22	23
21	23
21	23
20	22

Modelling APP/IPP

DIAGRAMS

Fig.1.1 Simplified Manufacture of Bitumen in a Refinery
(from Blanken and van Gooswilligen, Fig.1)

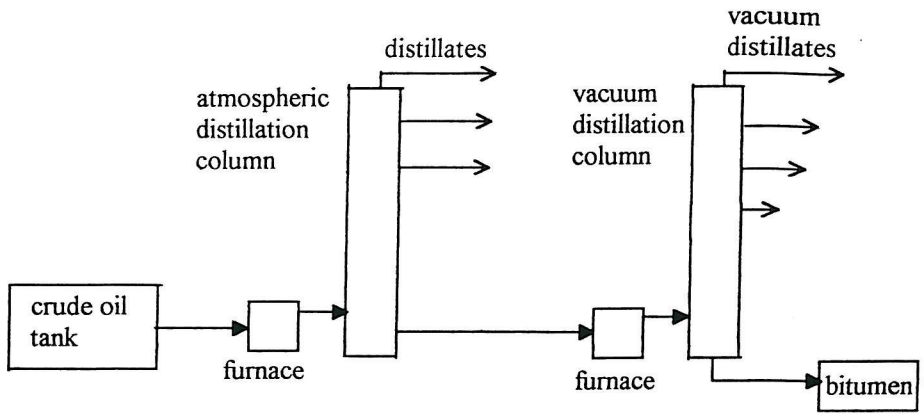

Fig.1.2. Industrial Uses of Bitumen [Blanken and van Gooswilligen, Fig.4]

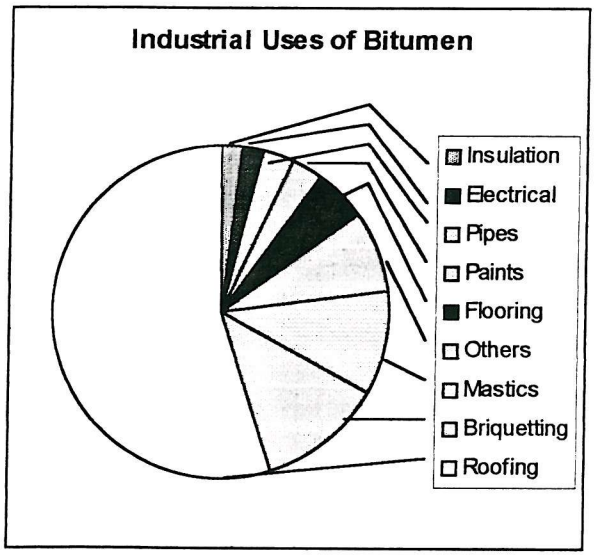

Fig.1.3. Computer-Controlled Bending System for Roofing Sheets [Fawcett and Lor]

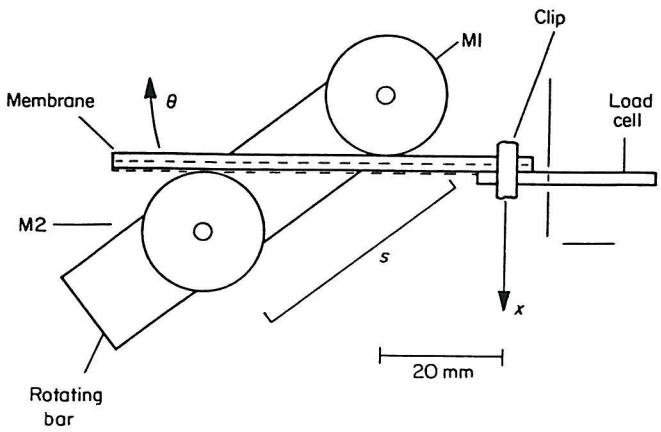

Cylinder M1 is fixed while cylinder M2, at the other end of a metal bar, rotates round M1 at 9^{o} min^{-1} and bends the roofing membrane sample around M1. The bending force is measured in the direction x by the load cell extension, attached to the membrane by a clip.

Fig.1.4. Relationship Between Rate of Crystallization, T_g and T_m of a Polymer

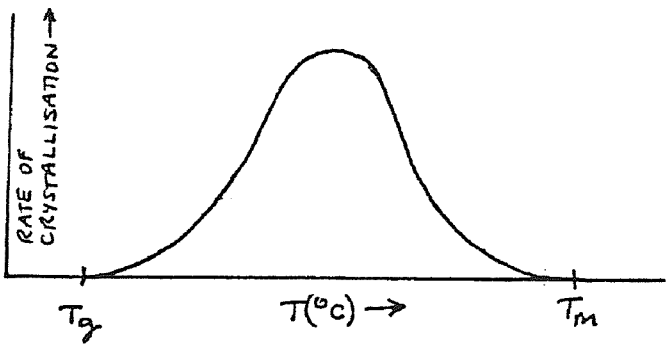

Fig.1.5. S-Curve of Polymers: Variation of Young's Modulus with Temperature

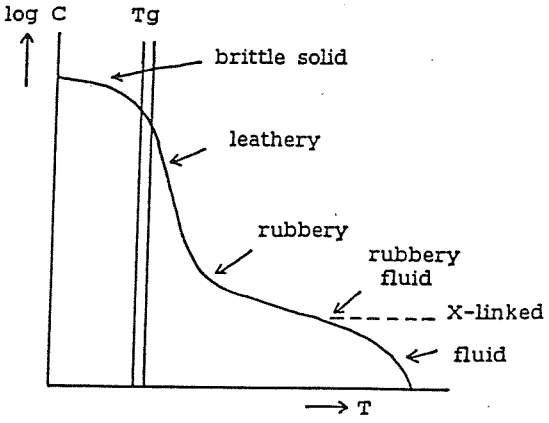

Fig.1.7. Phase Inversion in 'APP'/Bitumens

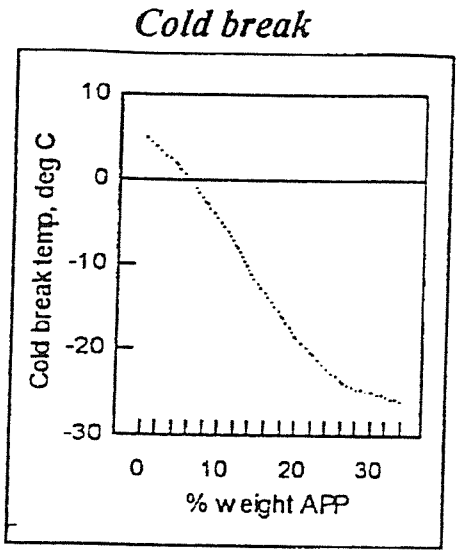

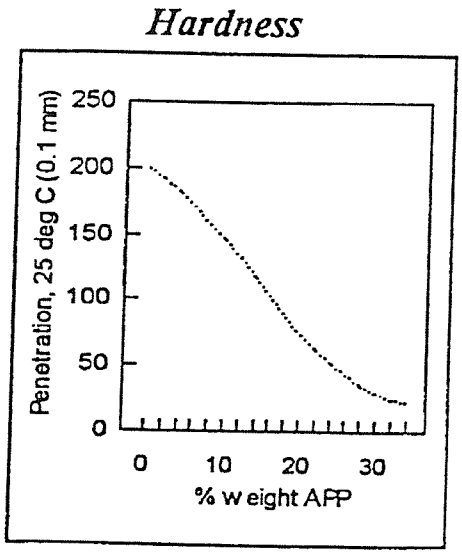

Fig.1.6. Features in a DSC Heat Flow Plot

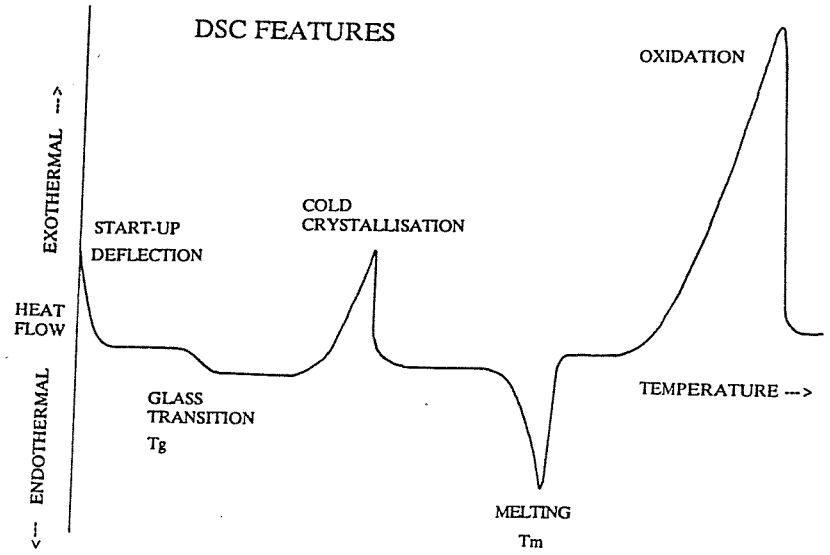

Fig.2.1. Mass Spectrum of 'APP' 1C, MF80 and Background Air

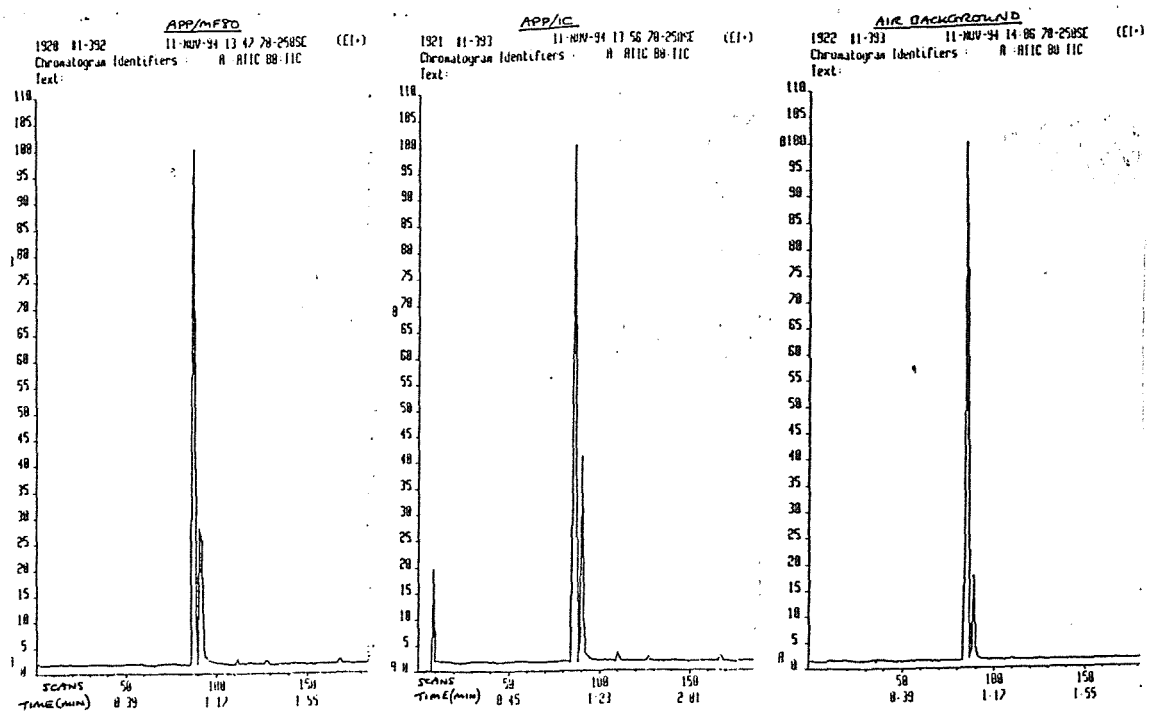

Fig.2.2. Reference FT-Raman Spectra of APP and IPP

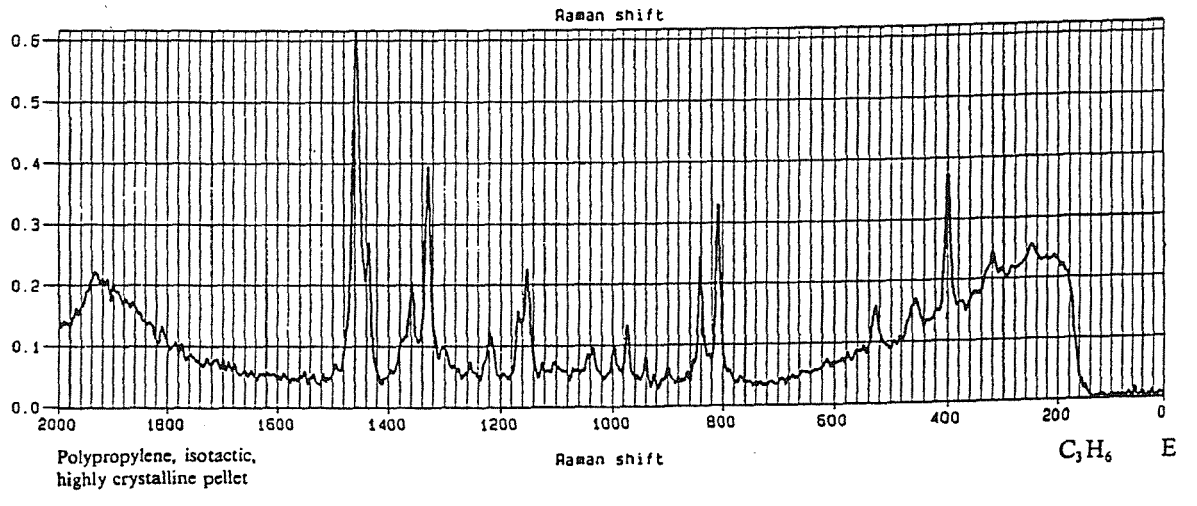

Polypropylene, isotactic, highly crystalline pellet

C_3H_6 E

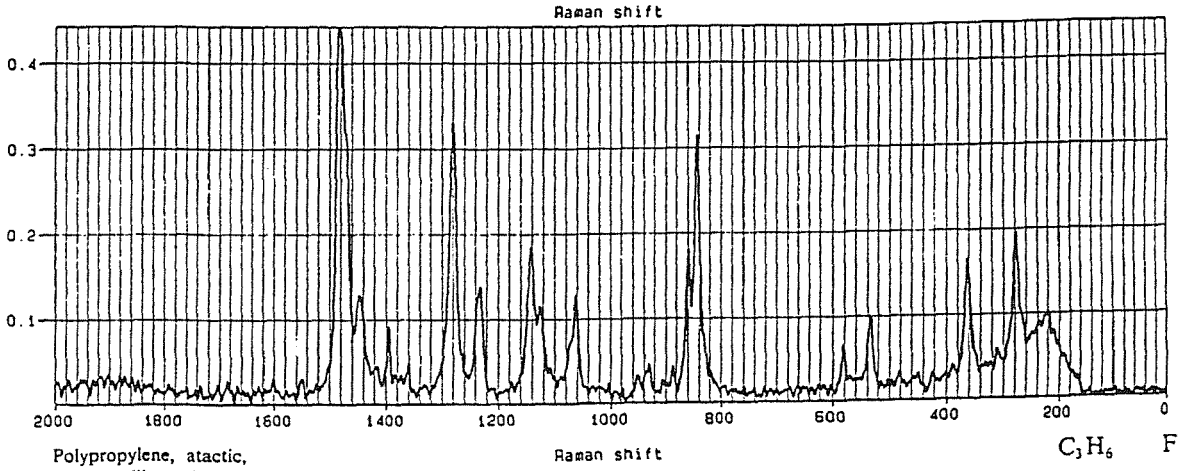

Polypropylene, atactic, noncrystalline pellet

C_3H_6 F

Fig.2.3. Overlaid FT-Raman and FT-IR Spectra of 'APP' 1C

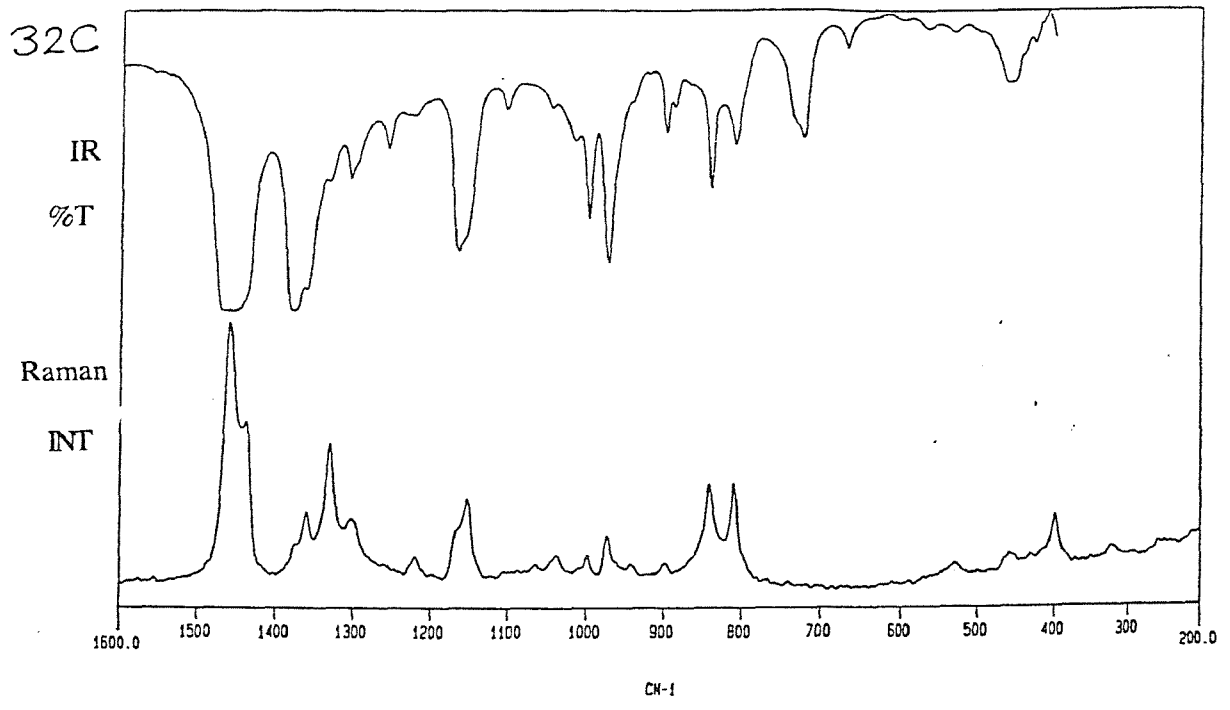

Fig.2.4. FT-Raman Spectra of 'APPs' 32C and 43C, and IPP

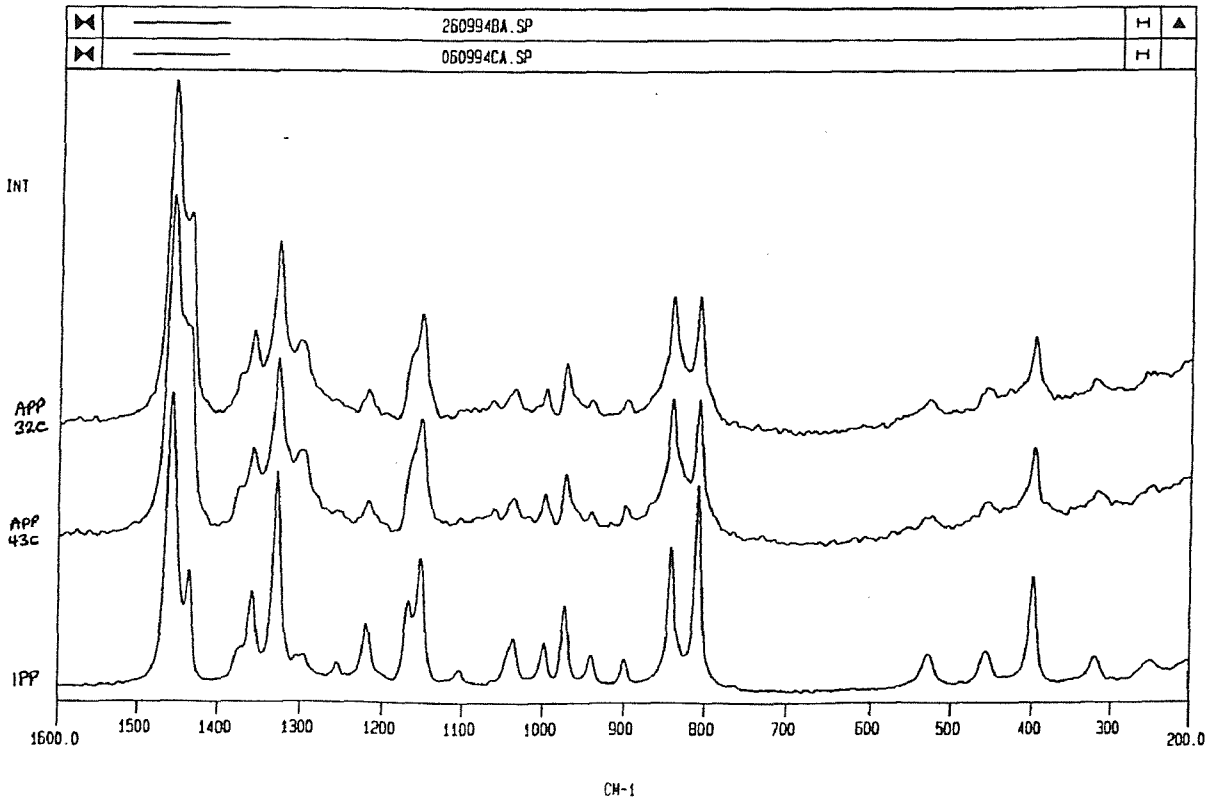

Fig.2.5. Potential Energy of a Molecular Vibration

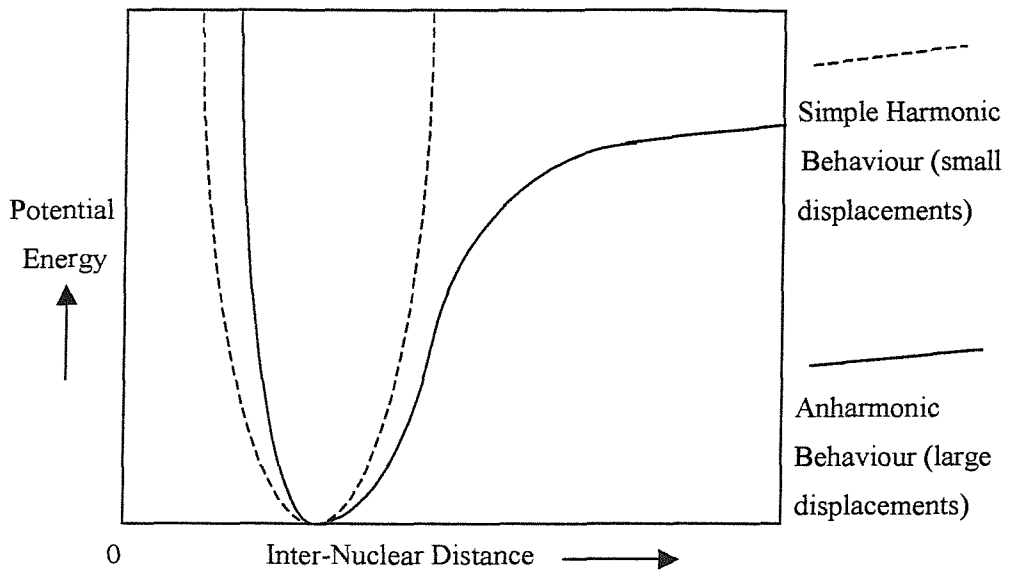

Fig.2.6. Vibrational Level Transitions Arising from Rayleigh, Stokes and Anti-Stokes Scattering

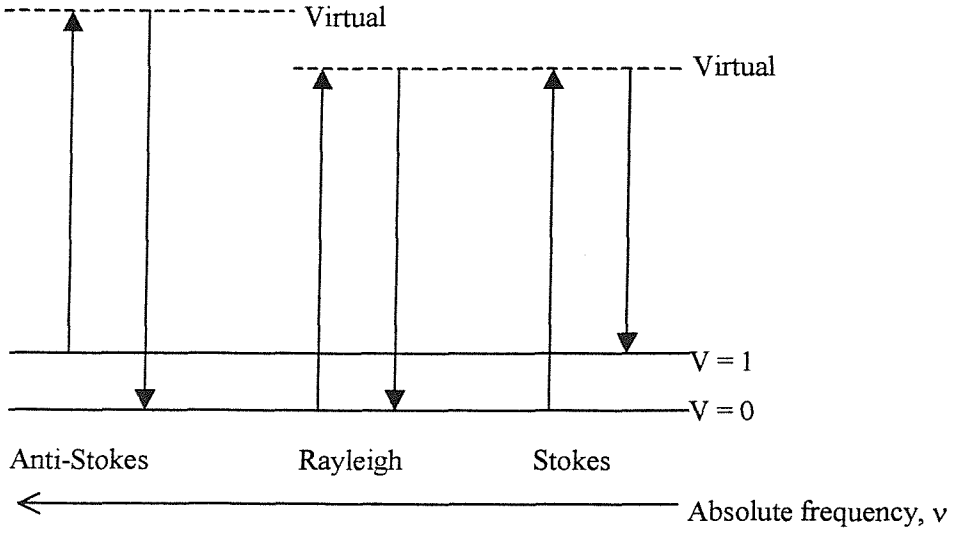

Fig.2.7. The Michelson Interferometer

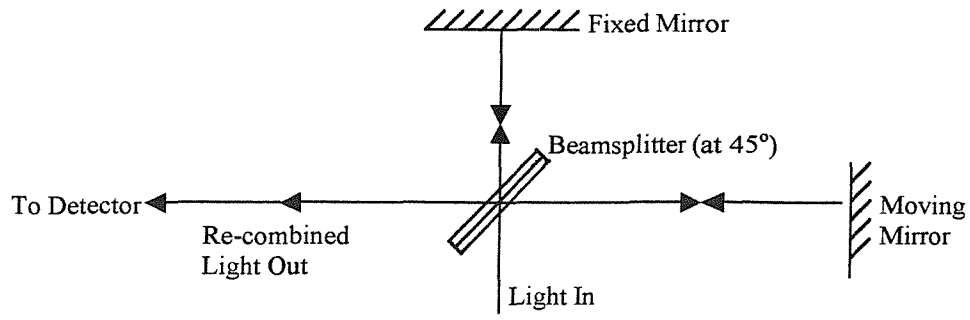

Fig.2.8. Basics of an FT-IR Spectrometer

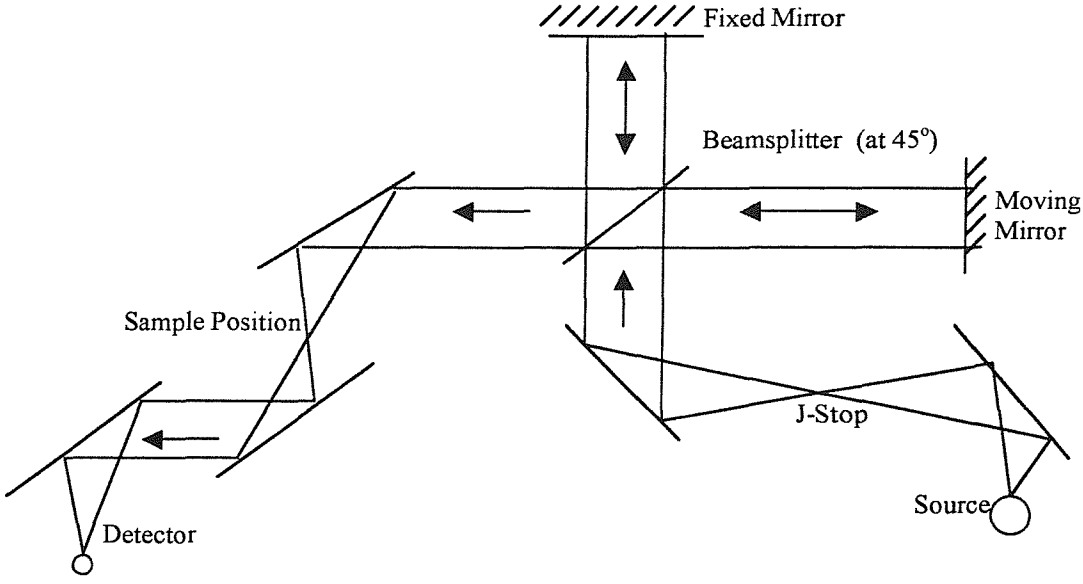

Fig.2.9. Basics of an FT-Raman Spectrometer

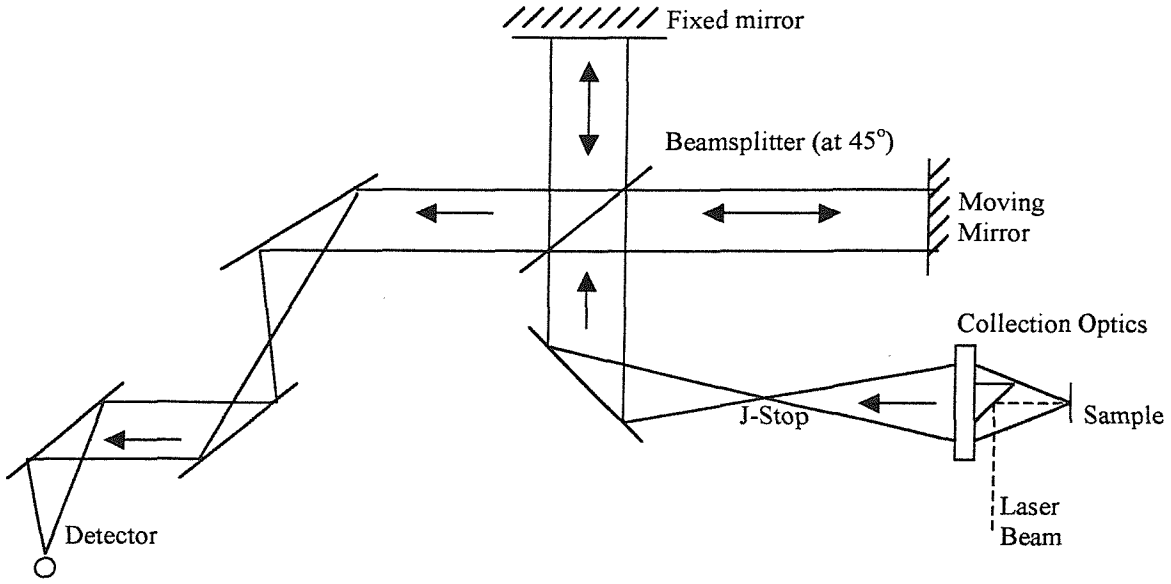

Fig.2.10. Thermomechanical Analysis (TMA)

Cross-section of Analyser

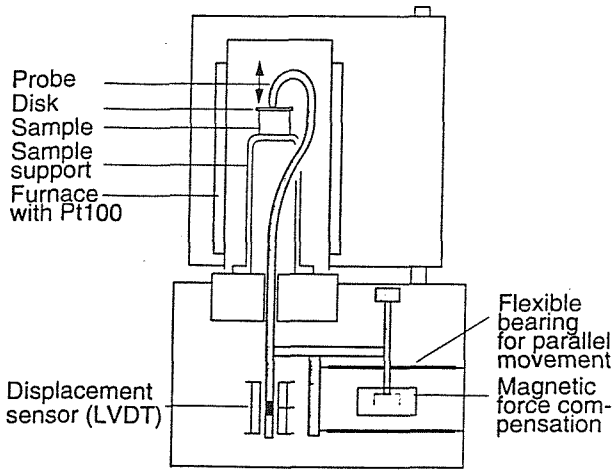

Typical TMA Curve

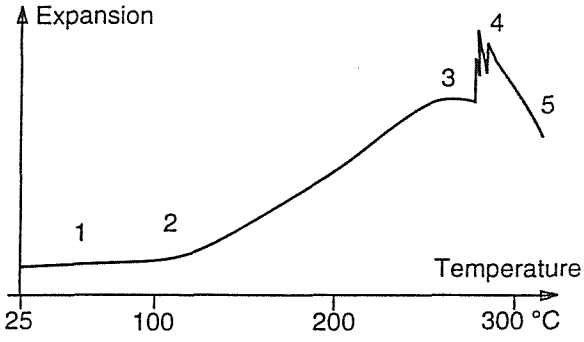

1 Thermal expansion (linear expansion coefficient)
2 Glass transition (change of expansion coefficient)
3 Softening, penetration
4 Foaming, delamination
5 Melting, viscous flowing

Oscillating Dynamic Load

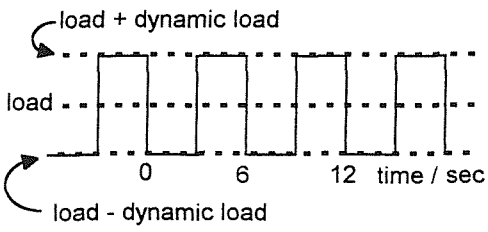

- In TMA the deformation of a sample under load is measured while the sample is heated linearly inside an insulated furnace. The change in length or thickness of a sample is converted into an electrical signal by a displacement sensor. Dimensional changes in films or fibres can be measured too by use of special probes. The sample (up to 20 mm thick) is positioned in a furnace and touched by a probe, made of fused silica, whose coefficient of thermal expansion is near zero. Electromagnetic force compensation allows application of a constant or regularly cycling load to the probe - techniques are then known as dilatometry or penetrometry respectively.
- TMA can measure linear expansion coefficient, glass transition, phase transitions, thermal stability, elastic behaviour and fibre shrinkage.

Fig.2.11. Differential Scanning Calorimetry (DSC)

- Sectional View of a Differential Scanning Calorimeter (Mettler-Toledo)

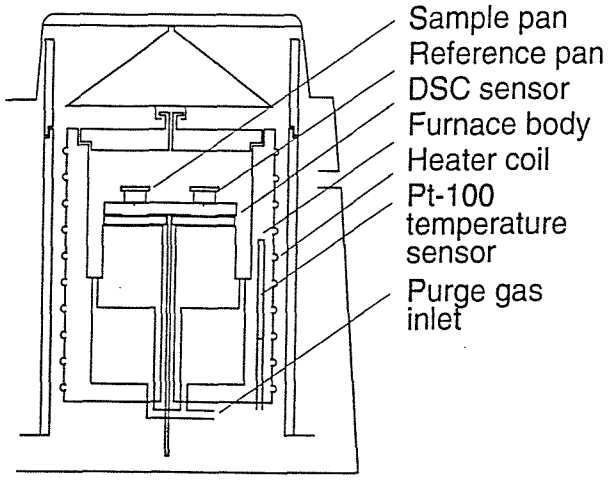

- Features in a Typical DSC Heat Flow Curve

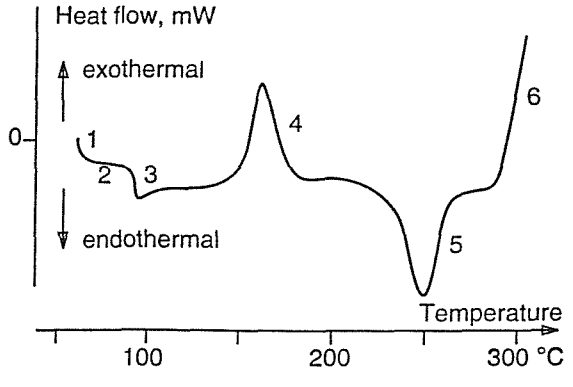

- The heat flux to a substance is measured as a function of temperature or time while it is subjected to a controlled temperature program. The sensor measures the heat flow/flux from the furnace to a few mg of material in the sample pan and to an empty reference pan - the difference is the DSC signal. There is always a start-up deflection proportional to the heat capacity of the sample. The reference temperature (T_r) lags behind the furnace temperature (T_c), and therefore reaches a lower maximum value than is preset, except when there is a final isothermal period, when it can catch up.
- DSC can measure the temperature of thermal effects, enthalpy changes, melting behaviour, crystallization, purity, polymorphism, glass transition, oxidative stability, chemical reactions, reaction kinetics and specific heat.
- The lid on the cell, excluding the lip, is 2 mm thick. For cold work below ambient temperatures, a 11-mm thick lid is used to reduce the amount of air and therefore the amount of moisture to a minimum.

1 Startup deflection (proportional to the heat capacity)
2 Heat flow signal depending on heat capacity and heating rate
3 Glass transition of the amorphous portion of the sample
4 Cold crystallization (devitrification)
5 Melting of the formed crystals
6 Oxidation (exothermal, chemical reaction)

Fig.2.12. The Iatroscan TH-10 Mark IV and Chromarod Development

(reproduced from Iatron Laboratories instruction manual)

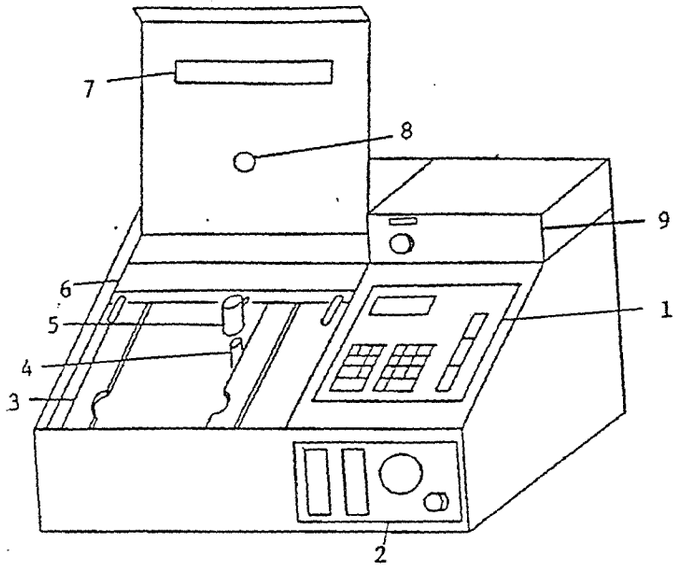

1. Keyboard
2. Hydrogen and air flow panel
3. Scanning frame
4. FID burner
5. FID collector electrode
6. Collector electrode mounting plate
7. Glass observation window
8. Exhaust stack
9. Amplifier

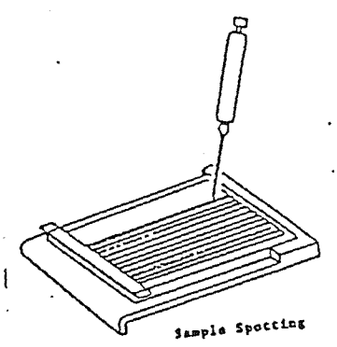

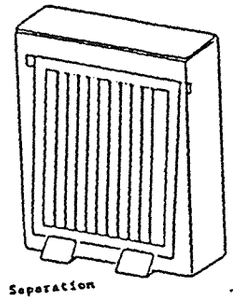

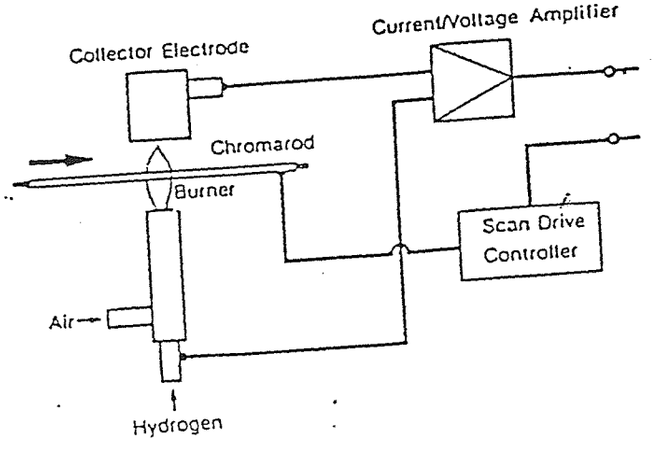

Fig.3.1. TMA Chart of L *vs* T, and δL/δT *vs* T, for 'APP' 1C (3.0 mm)

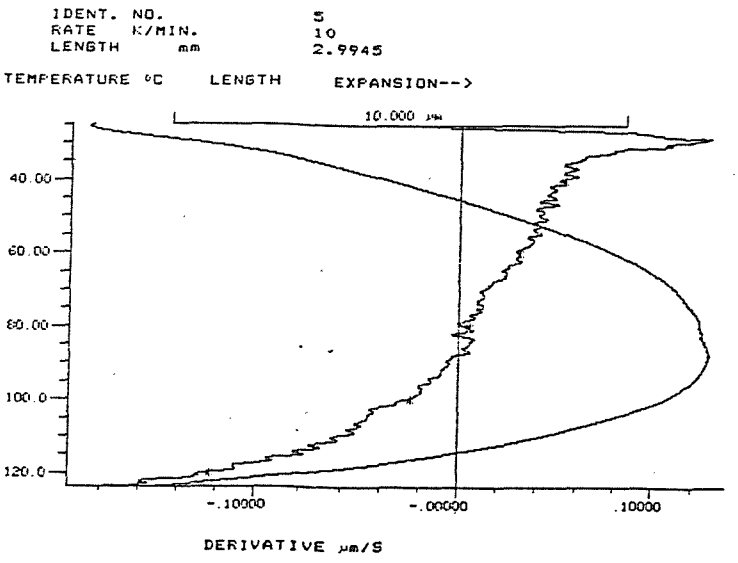

Fig.3.2. TMA Chart of L *vs* T, and δL/δT *vs* T, for (a) 1st Run, (b) 2nd Run and (c) 3rd Run of 'APP' 1C (2.1 mm) to 130°C

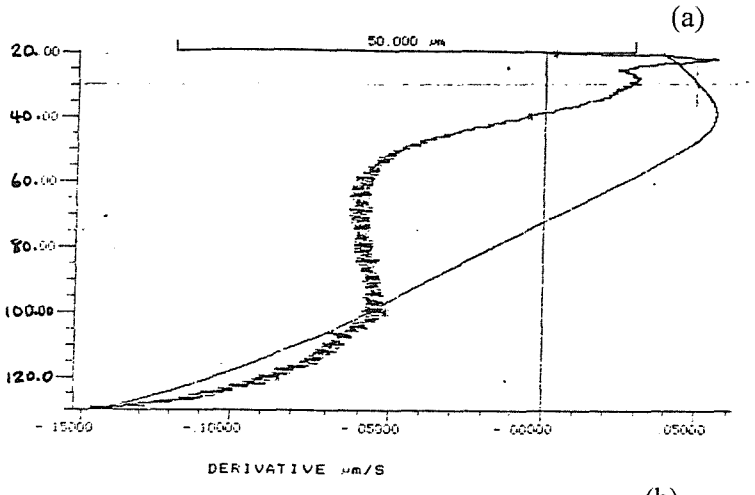

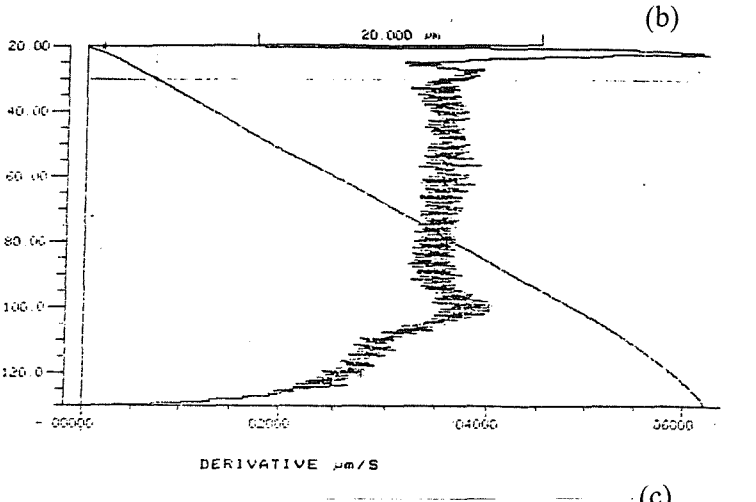

Fig.3.3. Overlaid Plots of Stress *vs* T for 1st, 2nd and 3rd Runs of 'APP' 1C (2.1 mm) to 130°C

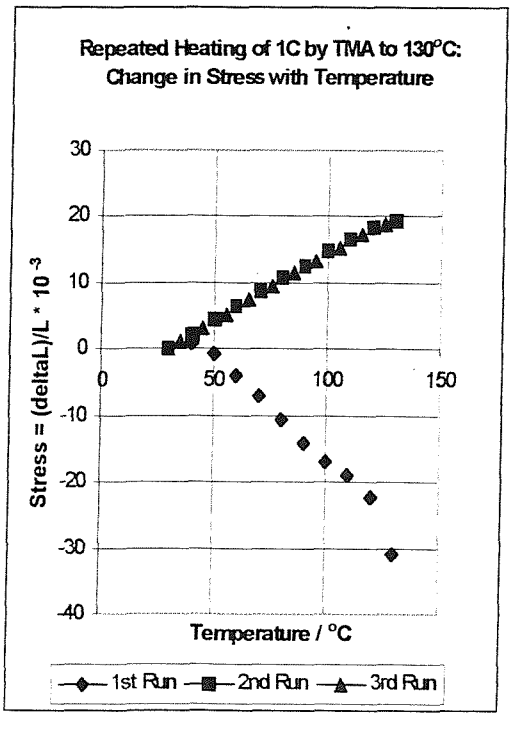

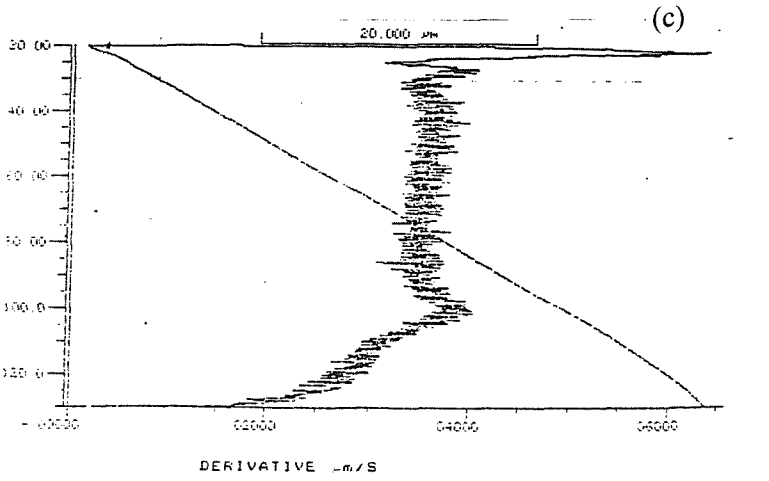

Fig.3.4. TMA Chart of L *vs* T, and δL/δT *vs* T, for (a) 1st Run, (b) 2nd Run of 'APP' 43C to 130°C

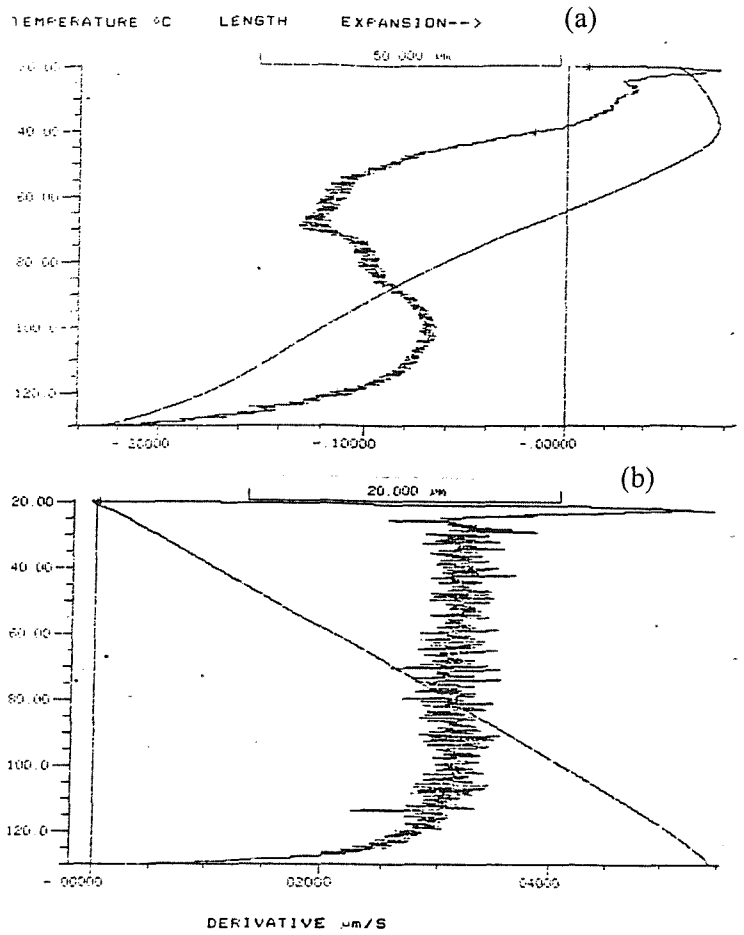

Fig.3.6. Overlaid Plots of Stress *vs* T for 6 Runs of 'APP' 1C to 130°C

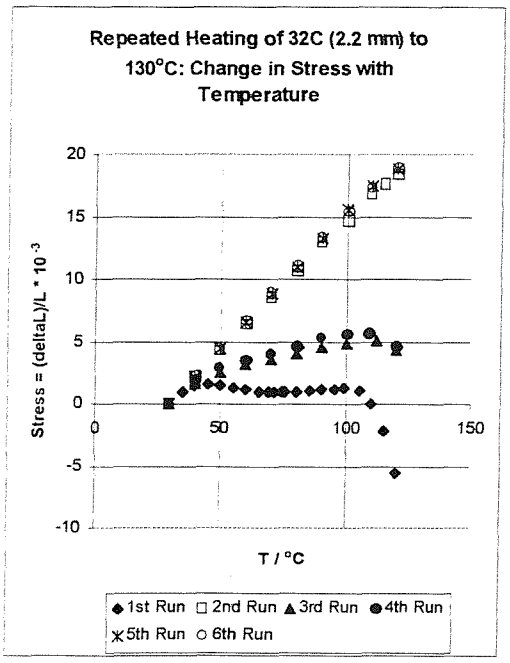

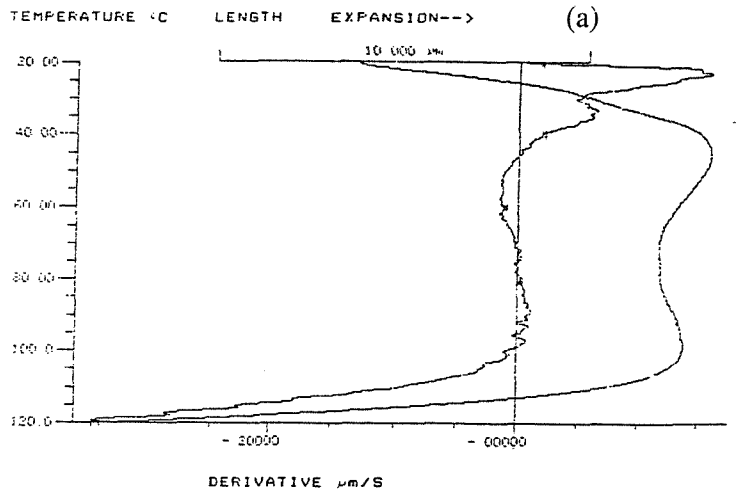

Fig.3.5. TMA Chart of L *vs* T, and δL/δT *vs* T, for (a) 1st Run, (b) 2nd Run of 'APP' 32C to 130°C

Fig.3.7. Creep Curves of Separate 'APP' 1C Samples Held for an Hour at Different Temperatures under 0.02 N Load

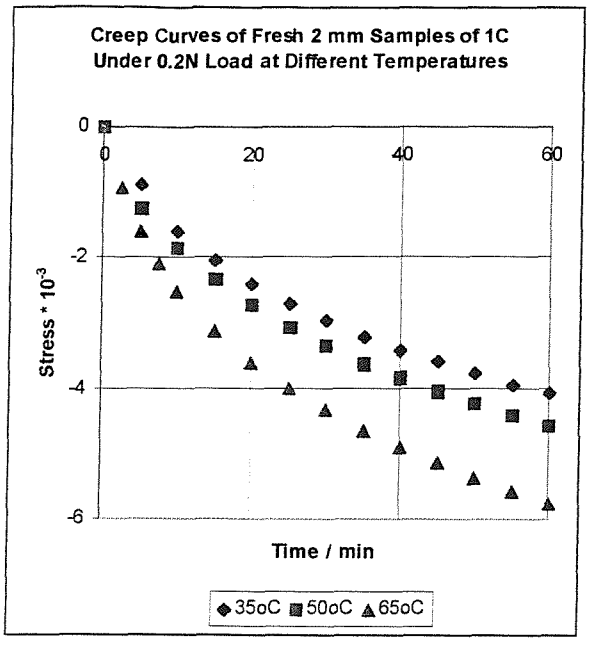

Fig.3.8. Expected Variation of Creep of Separate 'APP' Samples at Different Temperatures ($T_3 > T_2 > T_1$) under the Same Load

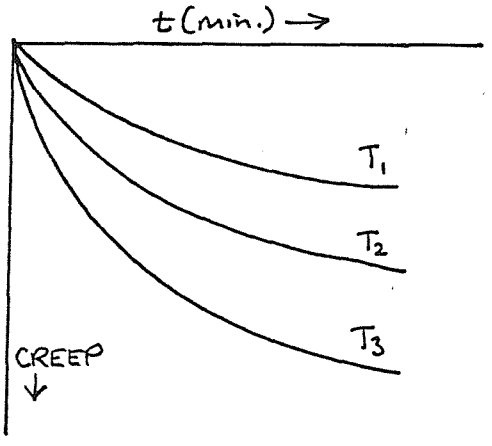

Fig.3.11. Expected Variation of Creep of Separate 'APP' Samples at the Same Temperature under Different Forces ($F_3 > F_2 > F_1$)

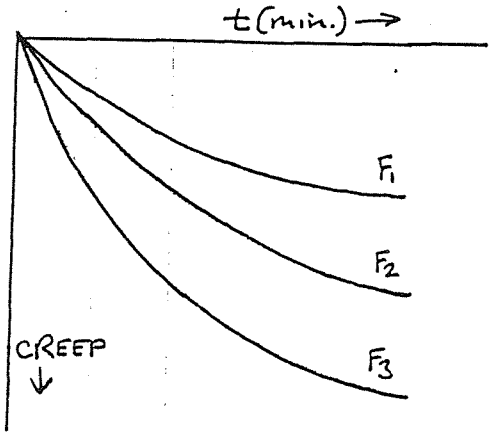

Fig.3.9. Observed Variation of Creep of One 'APP' Sample at Different Temperatures ($T_3 > T_2 > T_1$) under the Same Load (0.02 N)

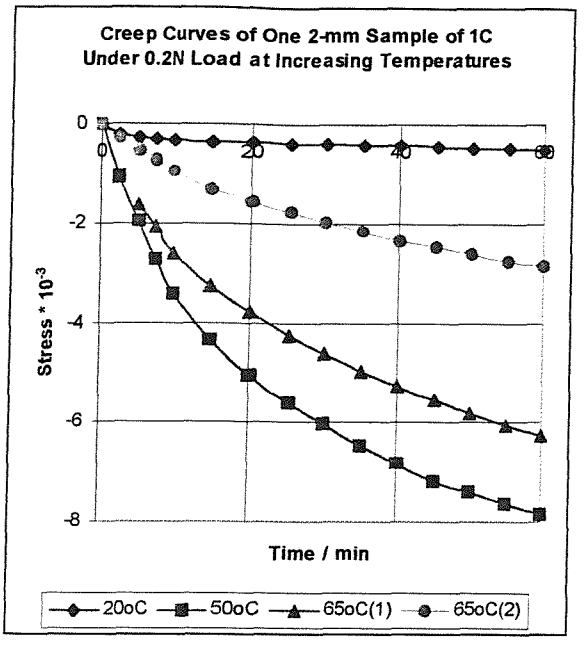

Fig.3.10. TMA Charts of L *vs* T for 'APP' 1C under 0.2N Load at (a) 20°C, (b) 50°C

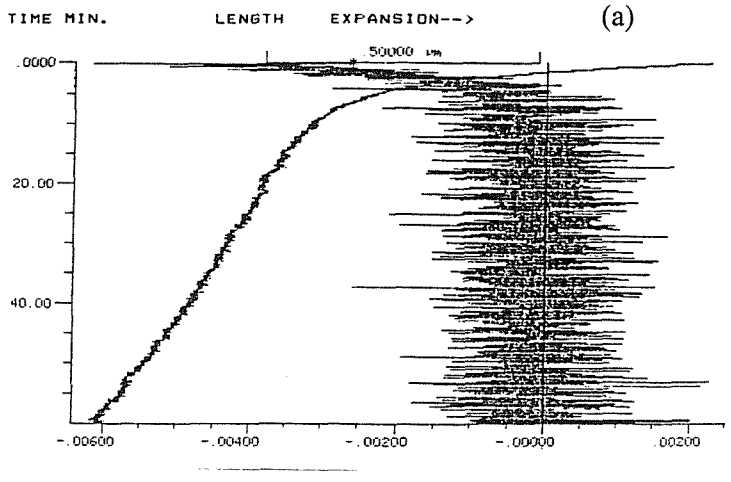

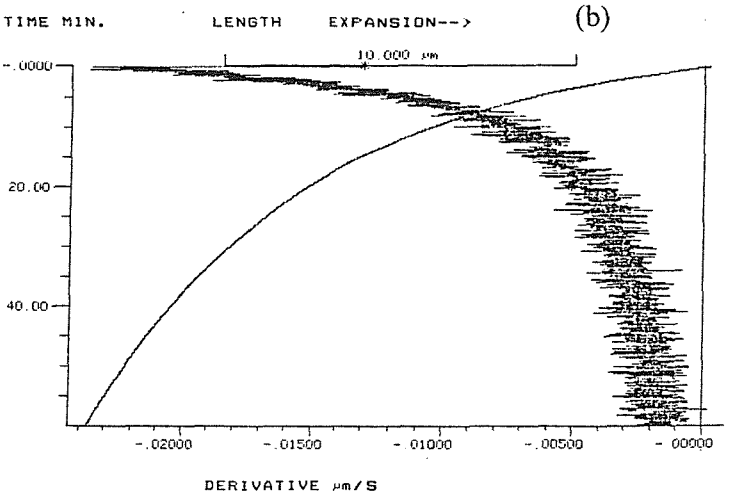

Fig.3.12. Creep Curve of 'APP' 1C Sample (a) under Increasing Loads, (b) after 10 and 20 min at Each Load

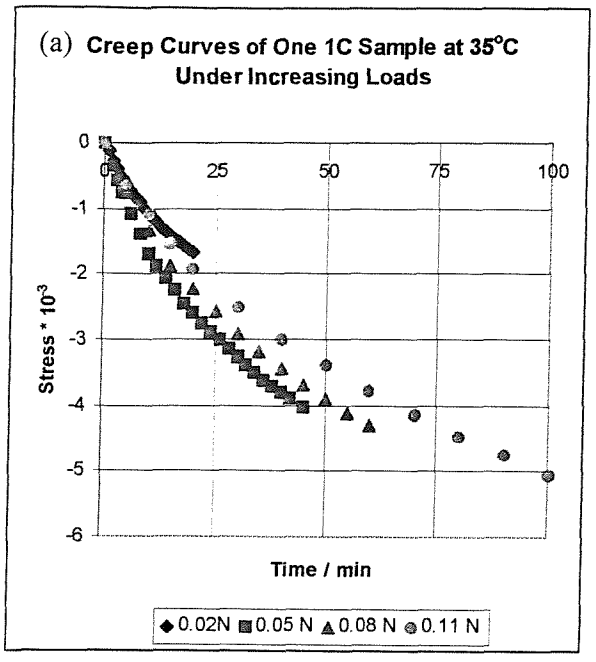

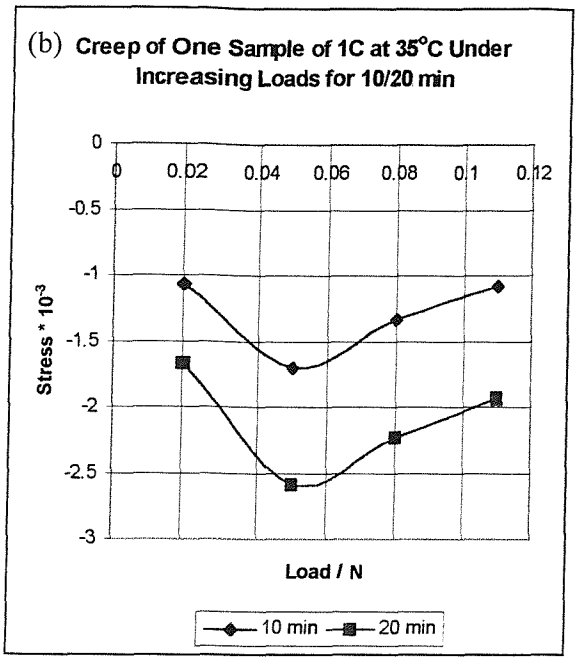

Fig.3.13. Creep Curve of 'APP' 32C Sample with Stepwise Increase and then Decrease in Load

Fig.3.14. Stress per Newton of Load *vs* Time for 'APP' 32C

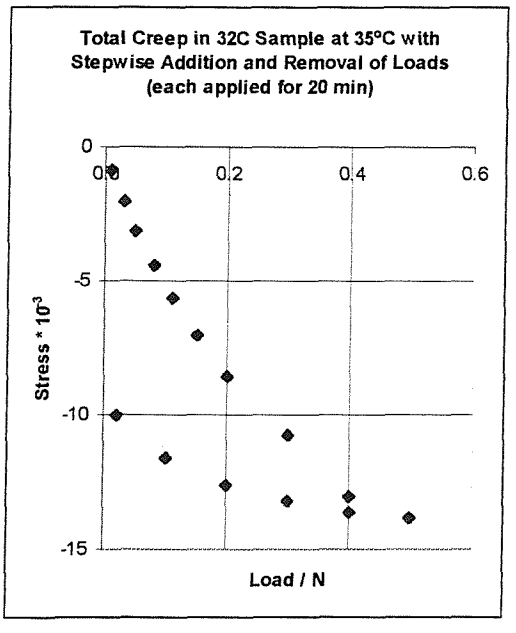

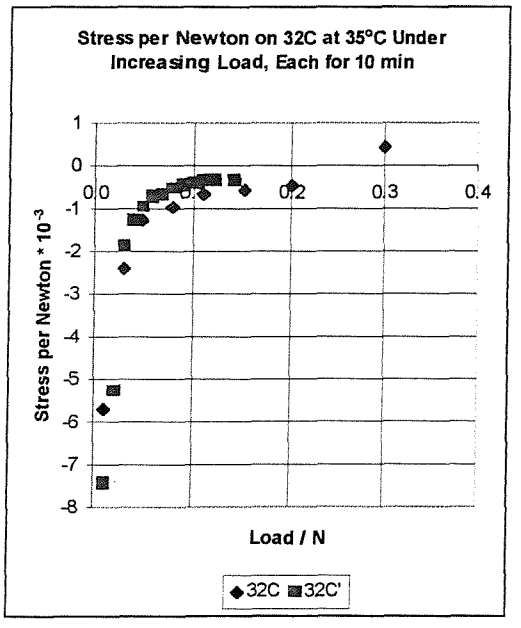

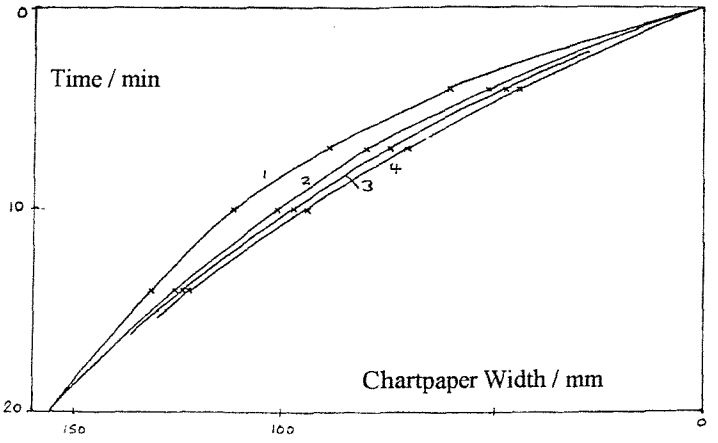

Fig.3.15. Effect of Stepping Up Loads on 'APP' 32C: Optimized Length *vs* Time

Loads: (1) 0.01N, (2) 0.03N, (3) 0.05-0.40N, (4) 0.50N (overnight)

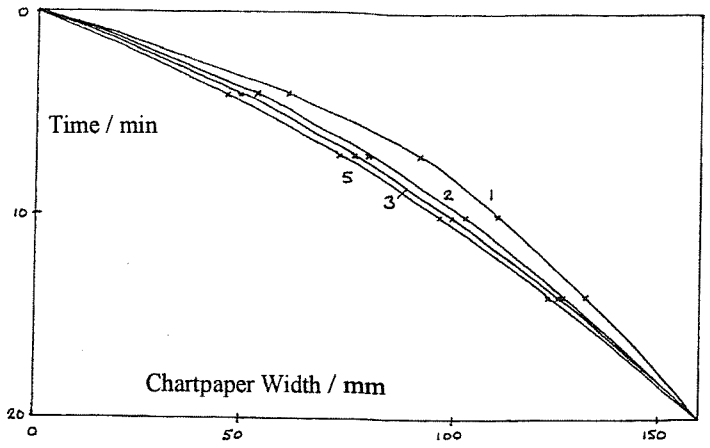

Fig.3.16. Effect of Stepping Down Loads on 'APP' 32C: Optimized Length *vs* Time

Loads: (1) 0.4N, (2) 0.3N, (3) 0.2N, [(4) 0.1N], (5) 0.02N

Fig.3.17. Surface Compression of 1C under Oscillating Load 0.06N (Samples 9 & 10)

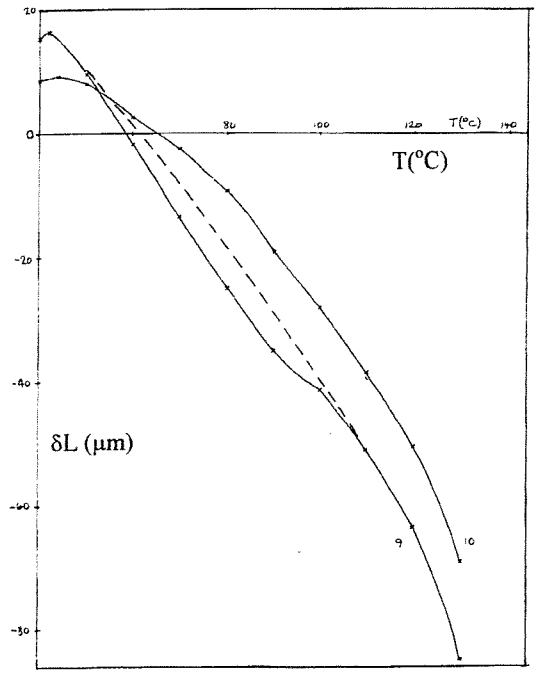

Fig.3.18. Surface Depression of 'APP' 1C under Oscillating Load 0.06N with Different Lower Loads (Samples 7, 10, 11, 12)

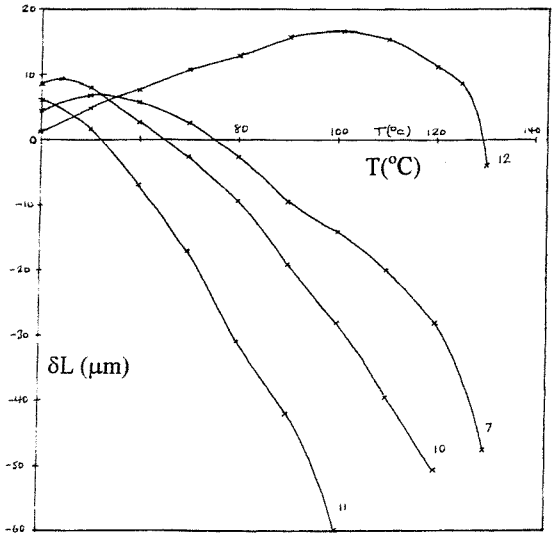

Fig.3.19. Typical On-line and Evaluation TMA Charts of 'APP' 1C under Dynamic Load

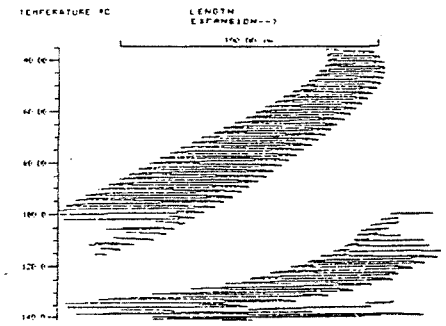

On-line Plot

Wrap-round

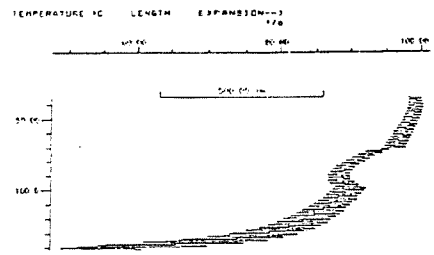

Evaluation Plot

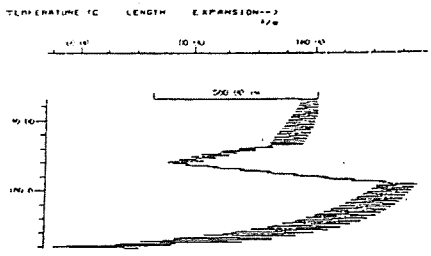

Evaluation Plot for 0.5N Dynamic Load

Fig.3.20. Surface Depression of 'APP' 1C under Oscillating Loads (a) (1) 0.40, (2) 0.30, (3) 0.24 N, and (4) 0.16, (5) 0.14 and (6) 0.12 N, Showing "Bites"

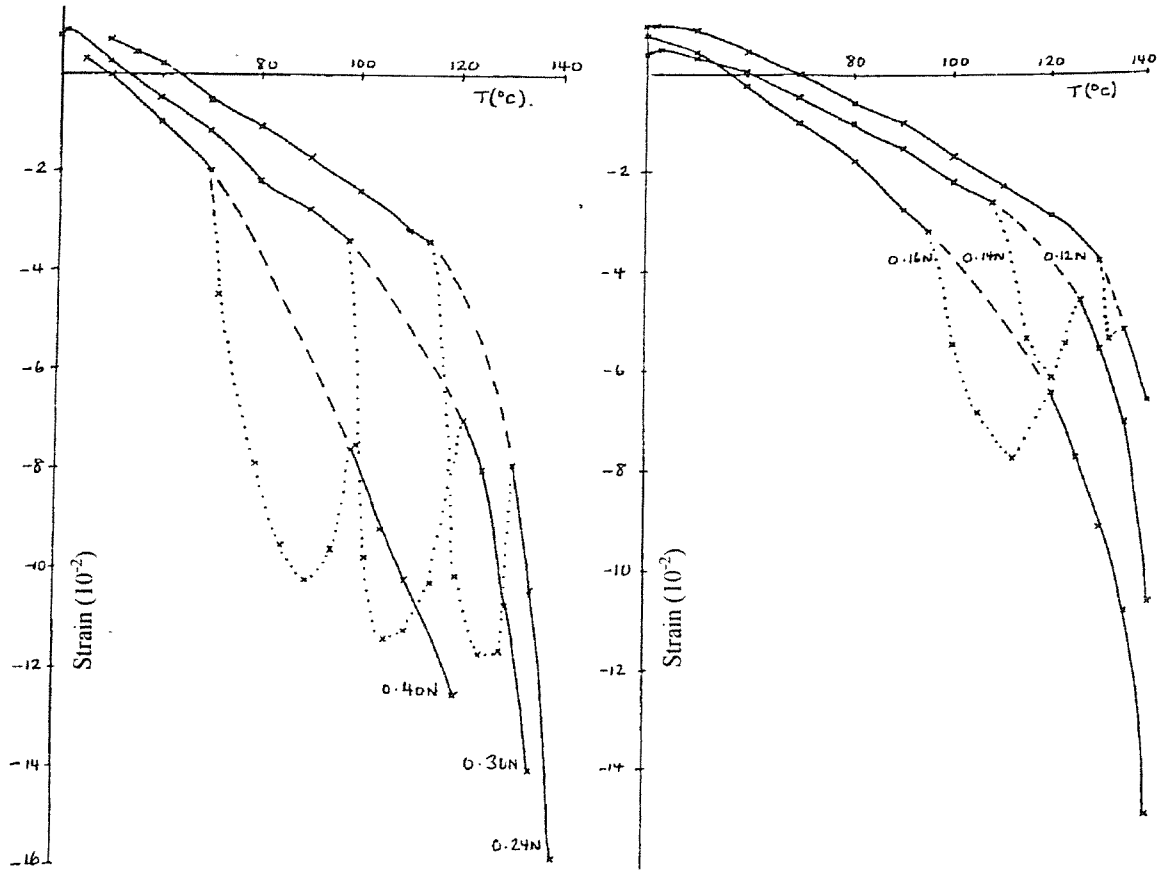

Fig.3.21. Surface Depression of 'APP' 1C under Oscillating Loads (a) (7) 0.10, (8) 0.08, (10) 0.06 N and (b) (0) 0.5, (1) 0.4, (2) 0.3 N

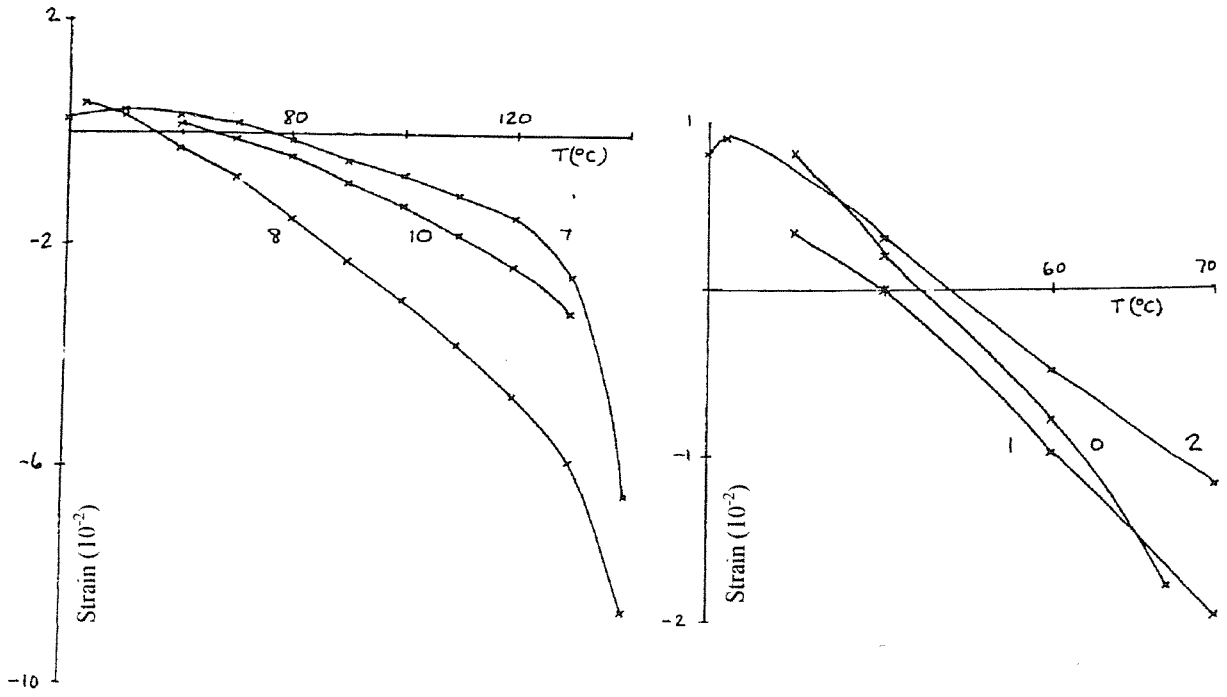

Fig.3.22. Surface Depression *vs* Temperature T for 'APP' Samples of Length L_A Subjected to Different Dynamic Forces F

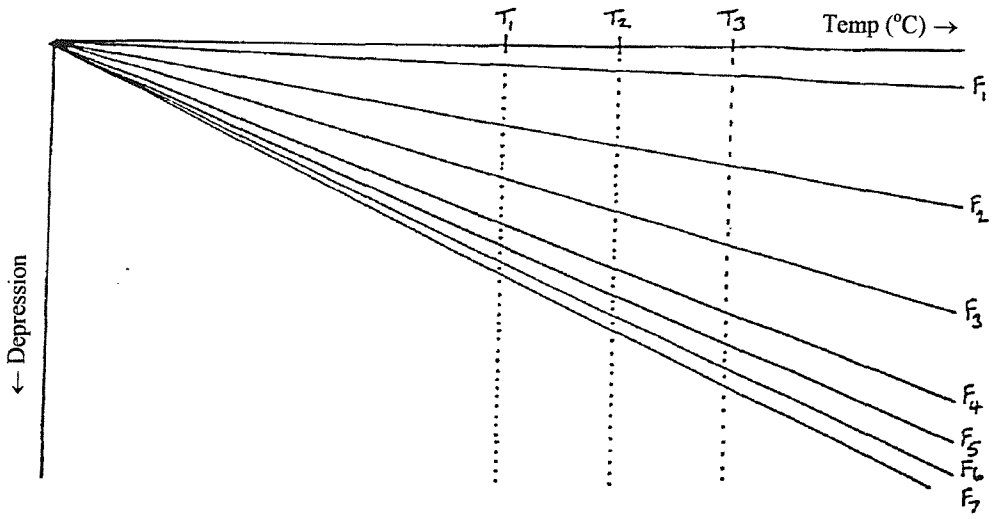

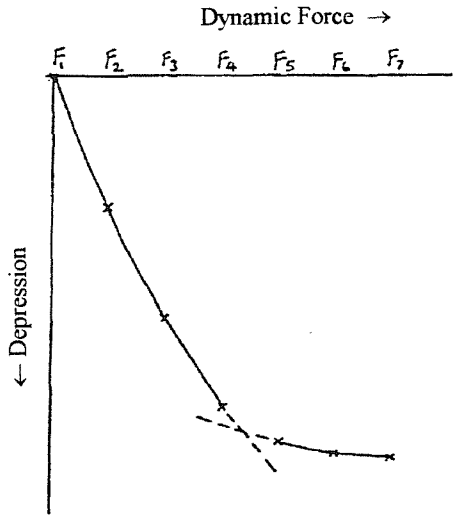

Fig.3.23. Surface Depression *vs* Dynamic Force for 'APP' Samples of Length L_A at Temperature T_1

Fig.3.24. Surface Depression *vs* Dynamic Force for 'APP' Samples of Length L_A at Different Temperatures ($T_3 > T_2 > T_1$)

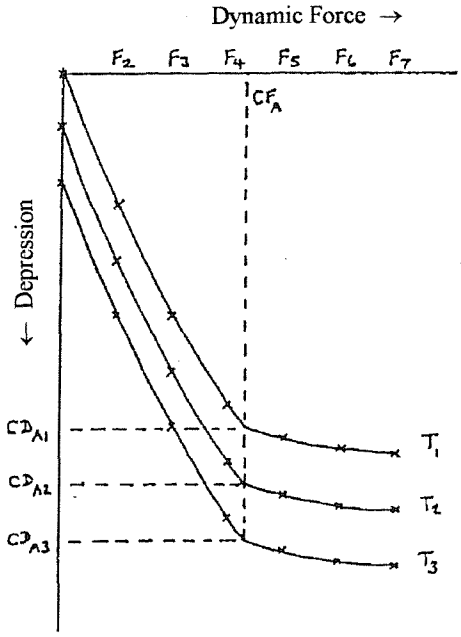

Fig.3.25. Relationship between Critical Dynamic Force and Critical Depth of an 'APP' at Different Temperatures ($T_3 > T_2 > T_1$)

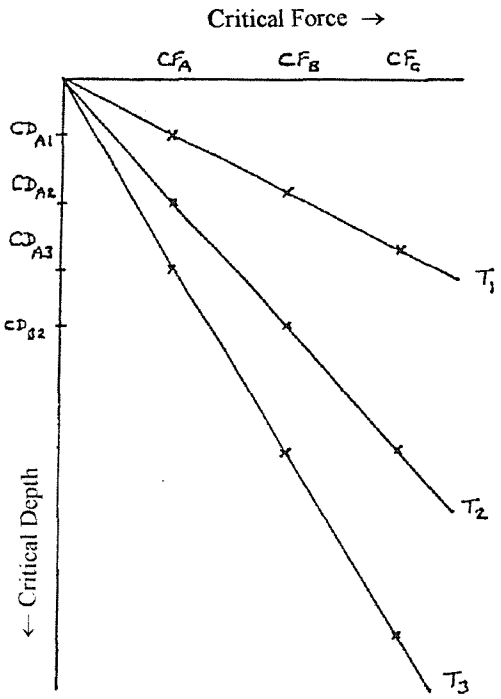

Fig.3.26. Surface Depression *vs* Temperature T for 'APP' Samples of Length L_A Under Different Dynamic Forces

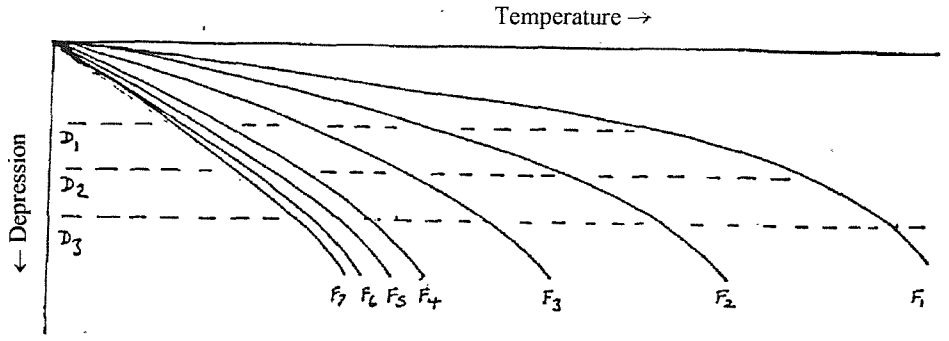

Fig.3.27. Temperature *vs* Dynamic Force for 'APP' Samples of Length L_A at Different Depressions ($D_3 > D_2 > D_1$)

Fig.3.28. Relationship between Critical Dynamic Force and Temperature of an 'APP' at Different Depressions ($D_3 > D_2 > D_1$)

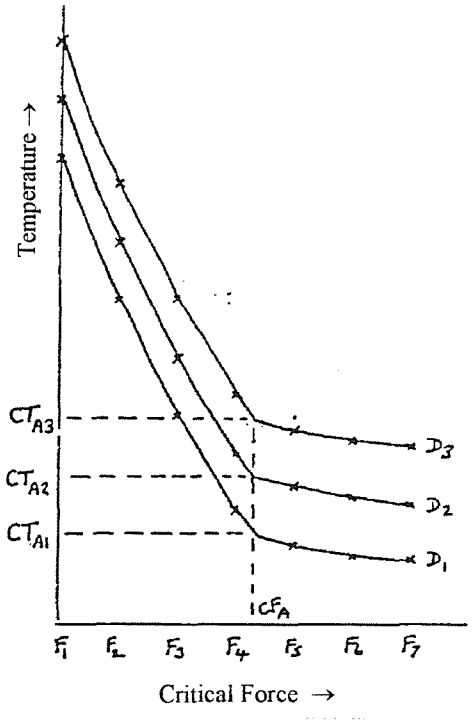

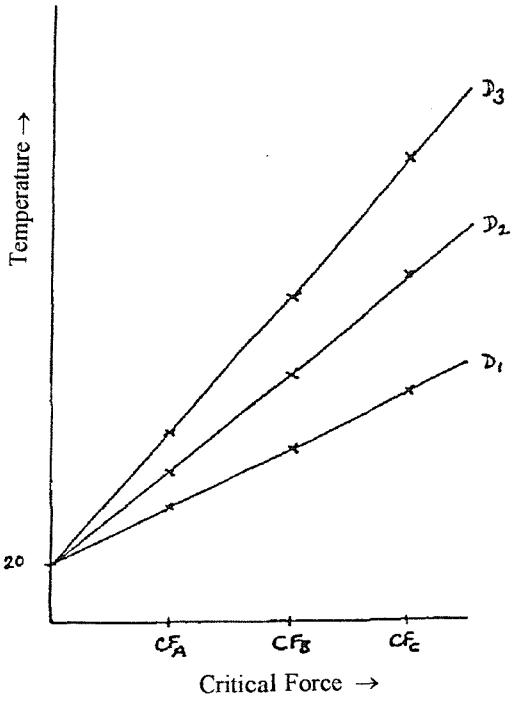

Fig.3.29. Action of Dynamic Load on 'APP' at 50°C

Fig.3.30. Variation of Young's Modulus with Temperature for an 'APP,' Found by Dynamic TMA

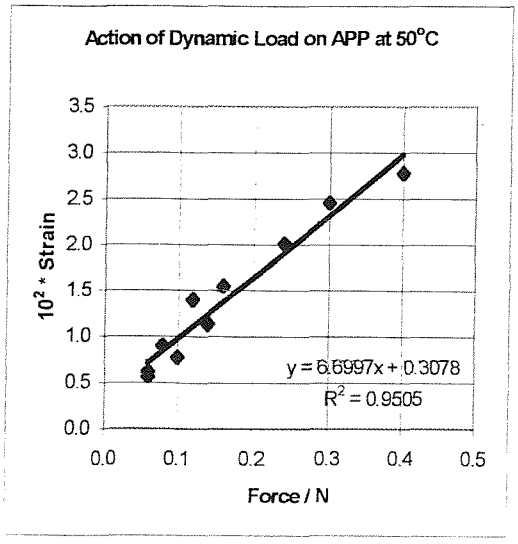

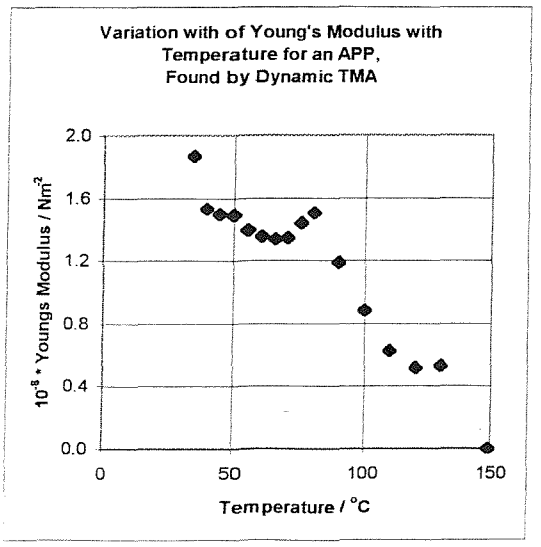

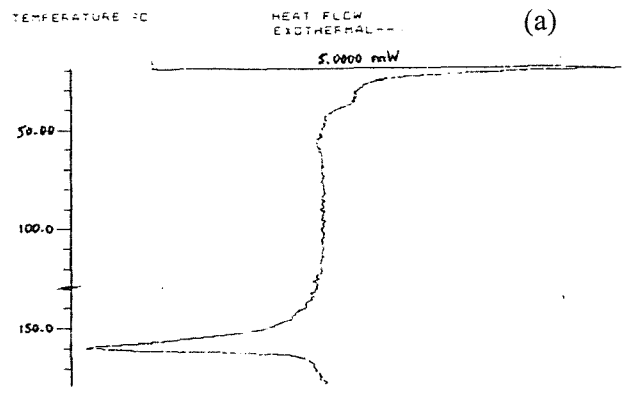

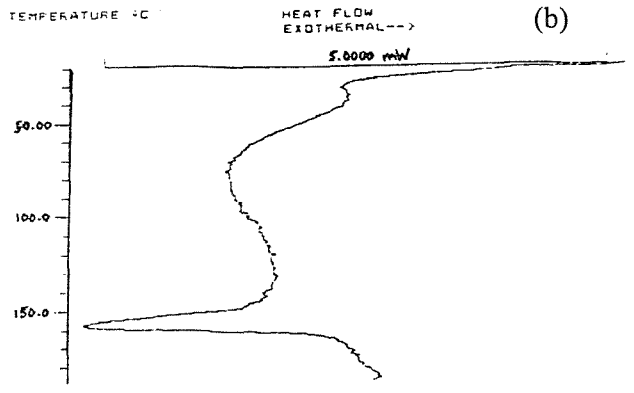

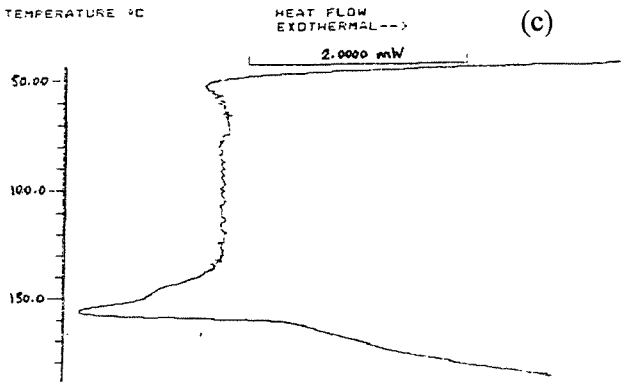

Fig.4.1. DSC Curve of 'APP' 32C on (a) 1st Run, (b) 2nd Run after Medium Cooling and (c) 4th Run after Slow Cooling

Fig.4.2. DSC Curve of 'APP' MF80 on (a) 1st Run, (b) 2nd Run after Slow Cooling

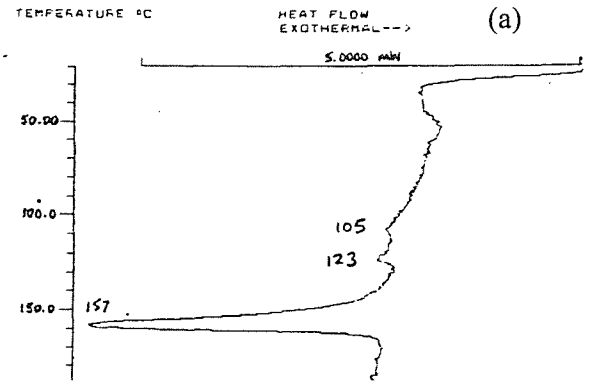

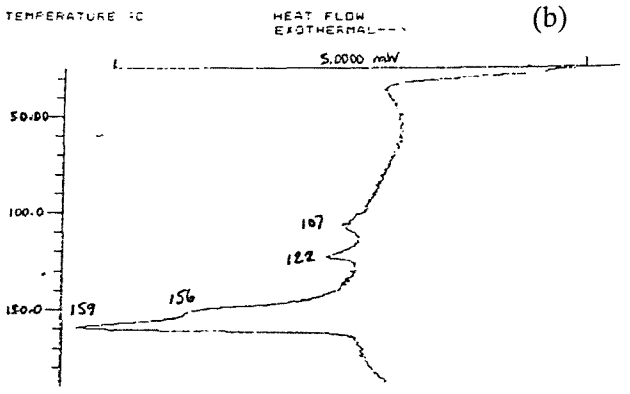

Fig.4.3. DSC Curve of 'APP' MF80 after 90 min at 200°C

Fig.4.5. Heat Flow after Slow Cooling of 'APP' 1C, Showing Shoulder for Crystals Deposited by Phase Separation

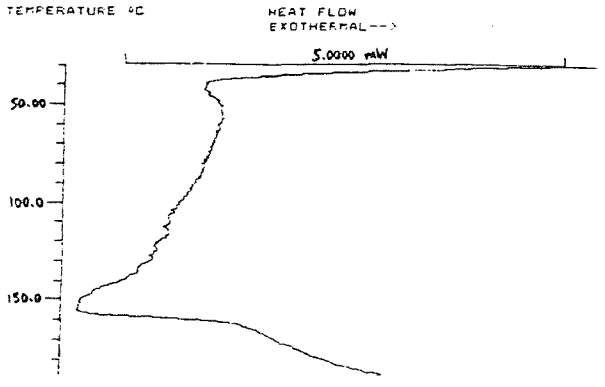

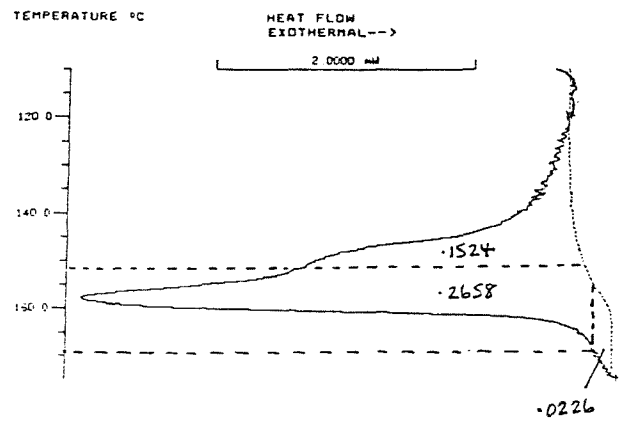

Fig.4.4. Specific Heat *vs* Temperature, and Heat Flow *vs* Temperature, for APP Extracted from 1C

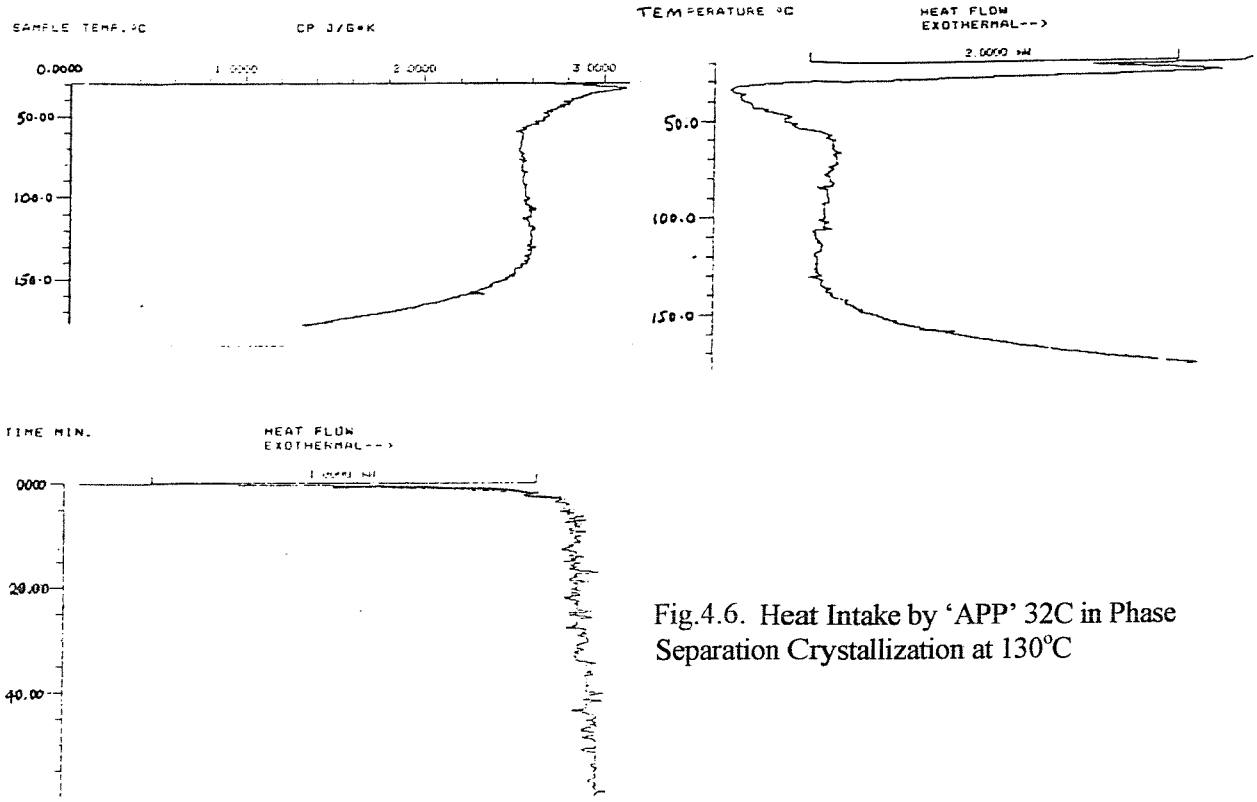

Fig.4.6. Heat Intake by 'APP' 32C in Phase Separation Crystallization at 130°C

Fig.4.7. Heat Flow in 'APP' 32C after (a) 60 min at 120°C and (b) 10 min at 130°C

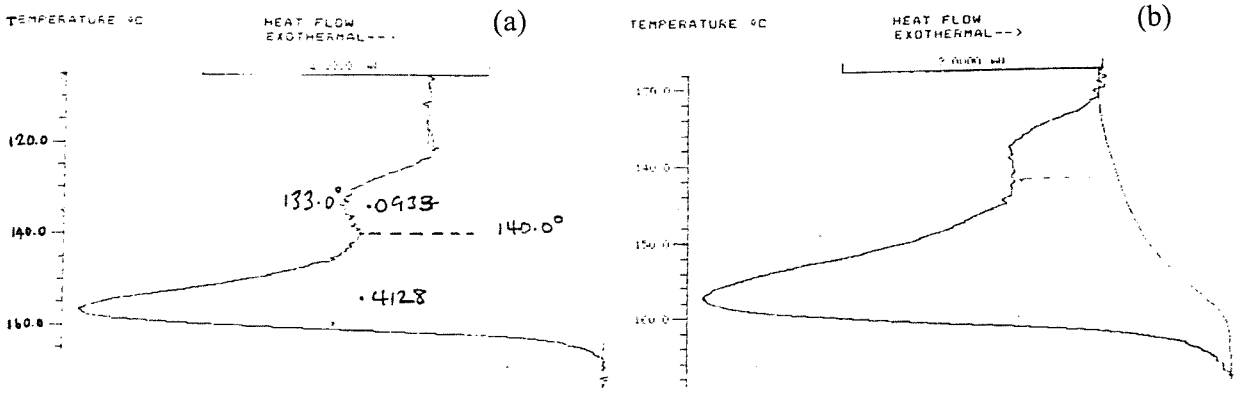

Fig.4.8. Heat Flow in 'APP' 32C after 60 min at 100°C and 60 min at 70°C

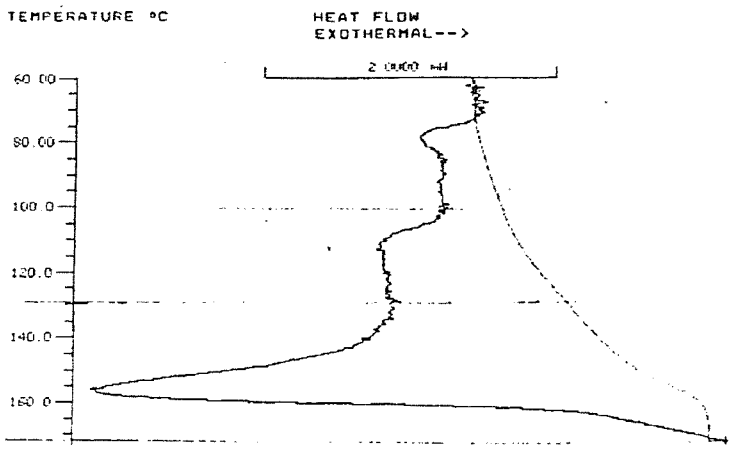

Fig.4.9. Predicted Crystallinity of 'APPs' 32C and 43C Over Several Years when Maximum Temperature <65°C

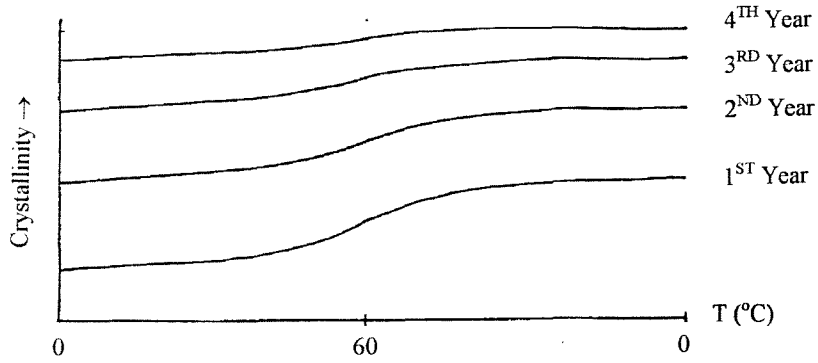

Fig.4.10. Predicted Crystallinity of 'APPs' 32C and 43C Over Several Years when Maximum Temperature >65°C

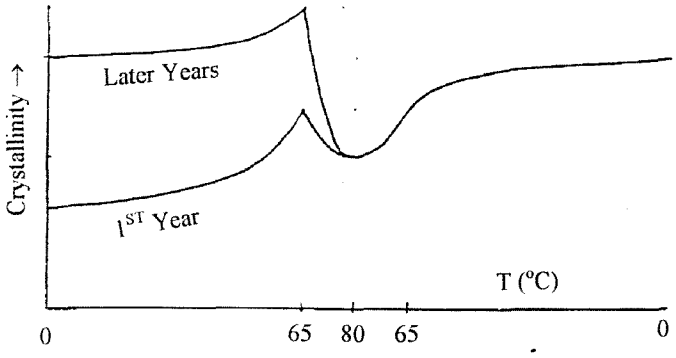

Fig.4.14. DSC Thermo-oxidation of IPP from Different Sources (without Air Flow)

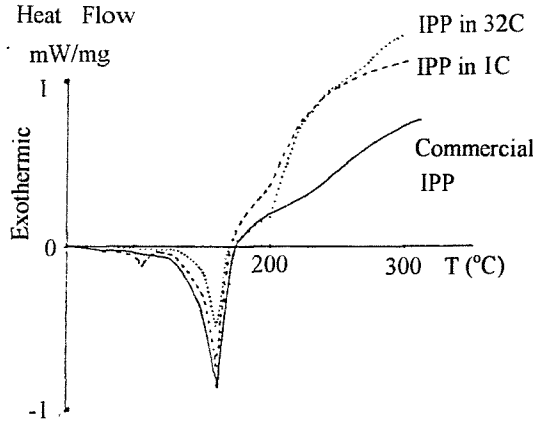

Fig.4.12. DSC Thermo-oxidation of Crystalline and Amorphous Polymers (without Air Flow)

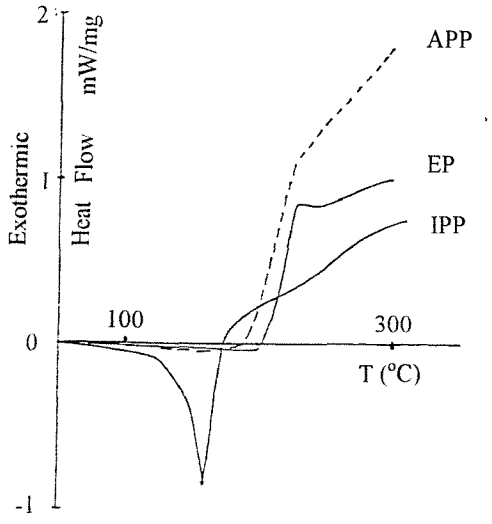

Fig.4.13. DSC Thermo-oxidation of 'APP' IC and its Constituent APP and IPP (without Air Flow)

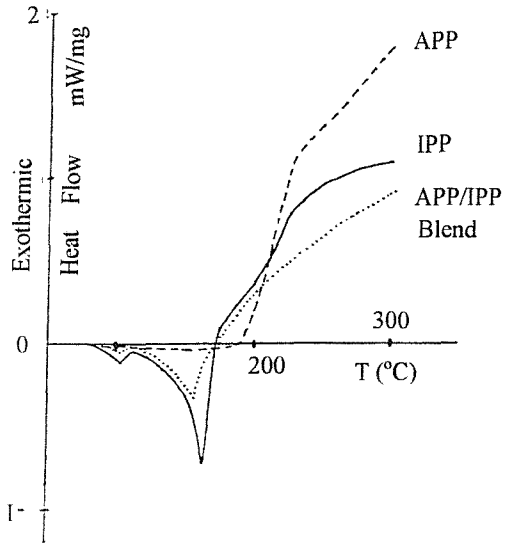

Fig.4.11a. Predicted Crystallinity of 'APPs' 1C, 32C, 43C, MF80 Over a Year when Maximum Temperature <65°C

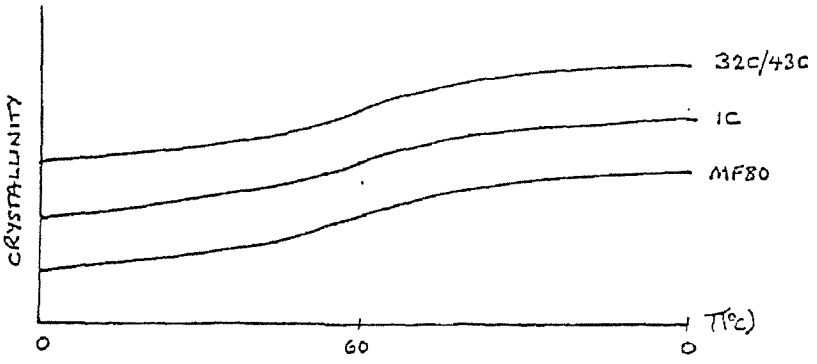

Fig.4.11b. Predicted Crystallinity of 'APPs' 1C, 32C, 43C and MF80 Over a Year when Maximum Temperature >65° but <107°C

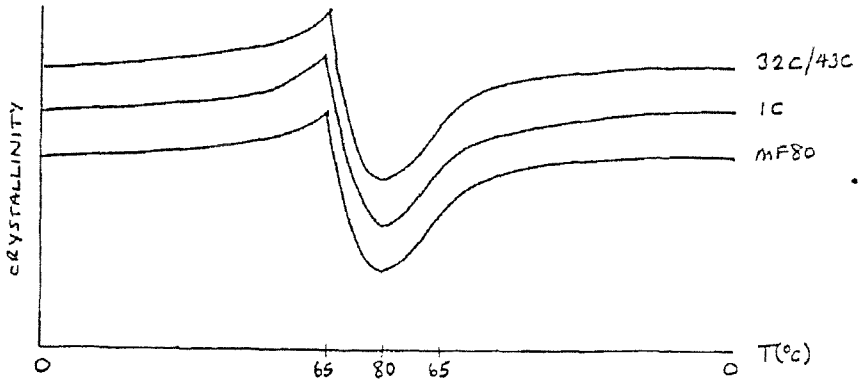

Fig.4.11c. Predicted Crystallinity of 'APPs' 1C, 32C, 43C and MF80 up to 120°C, when Maximum Temperature Exceeds T_m of Lowest Melting Component (107°C)

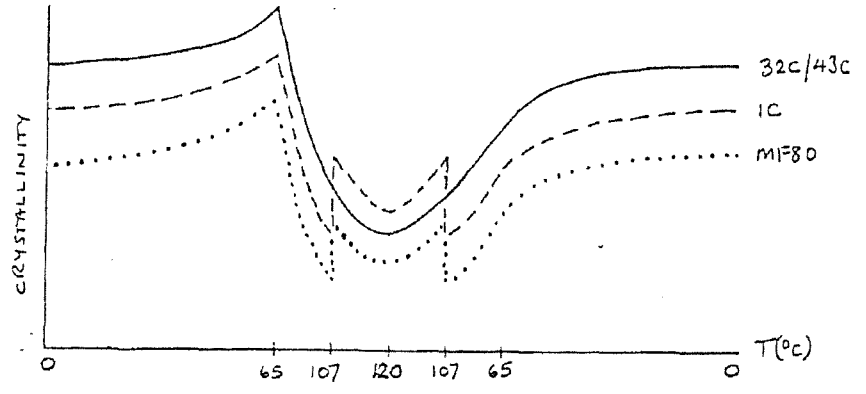

Fig.4.11d. Predicted Total Crystallinity of 'APPs' 1C, 32C, 43C and MF80 up to 130°C, when Maximum Temperature Exceeds T_m of Both Lower Melting Components (107°, 122°C)

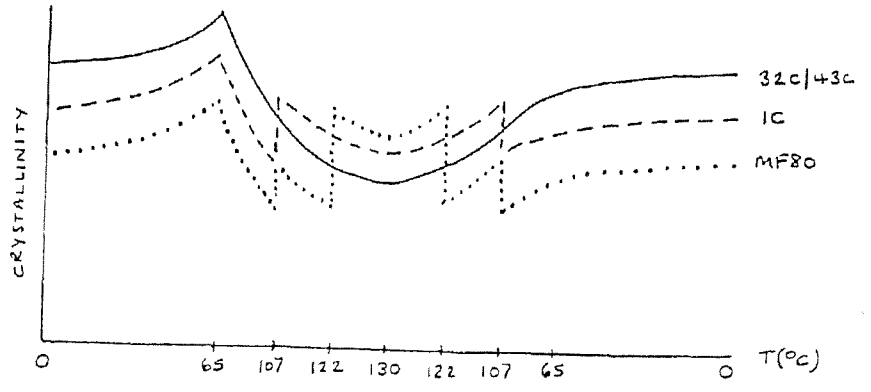

Fig.4.15. Use of Straight Base-Line to Evaluate DSC Peak Position for Decomposition

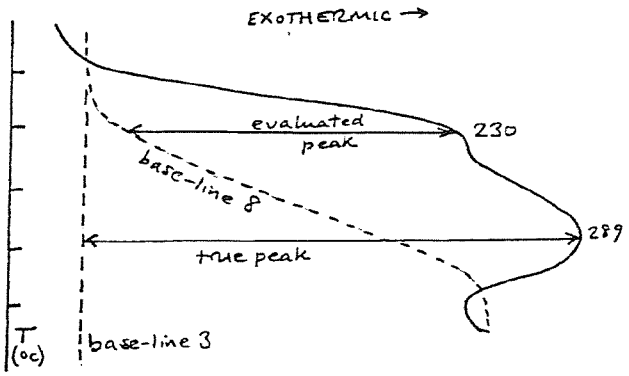

Fig.4.19. DSC Curve of 200 Pen Bitumen (without Air Flow)

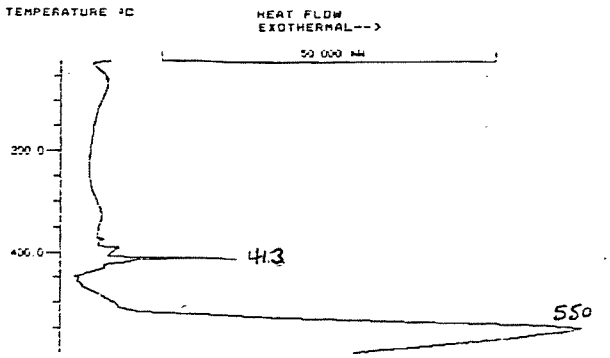

Fig.4.16. DSC Curves of (a) Atactic PP and (b) Isotactic PP in 1C (without Air Flow)

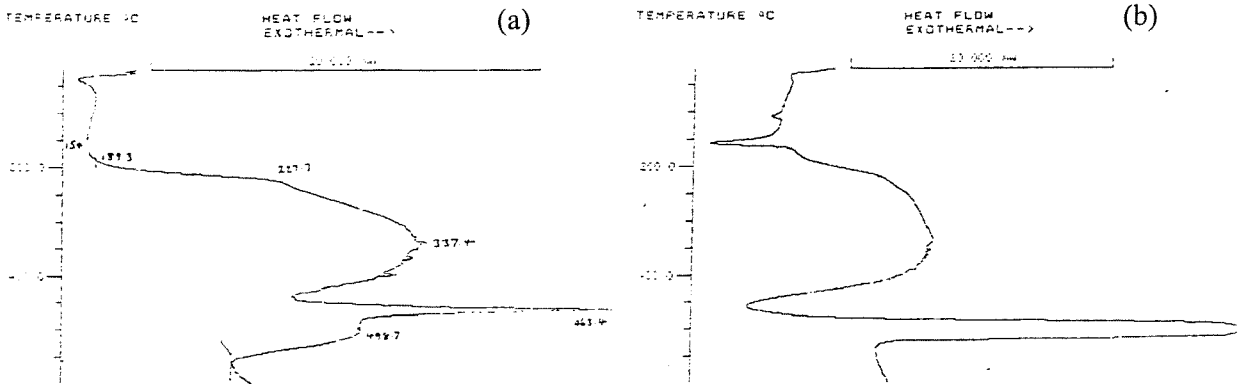

Fig.4.17. DSC Curve of Commercial Isotactic PP (without Air Flow)

Fig.4.18. DSC Curve of Ethylene-Propylene (EP) Copolymer (without Air Flow)

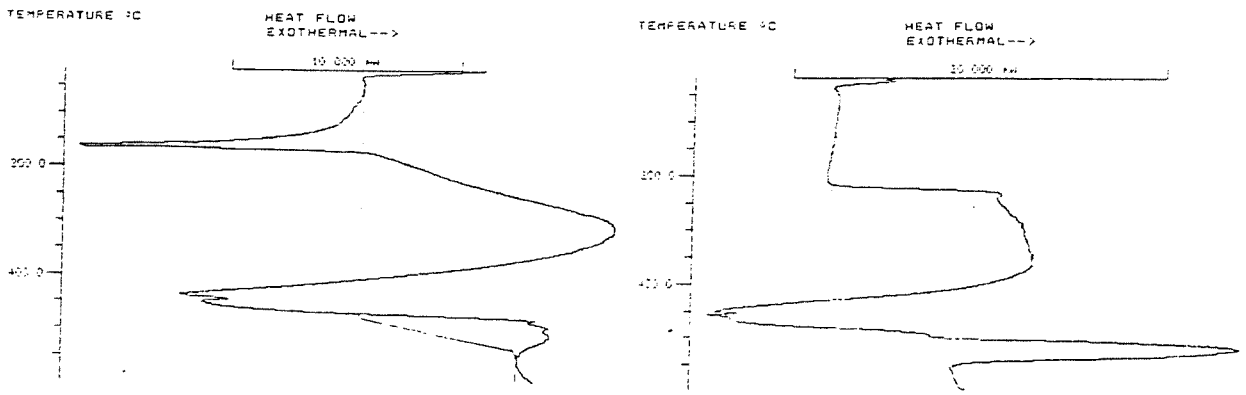

Fig.4.20. Melting Endotherms of 'APP' 32C on one 2nd Run to 210°C (without Air Flow), after 1st Run to 180°C

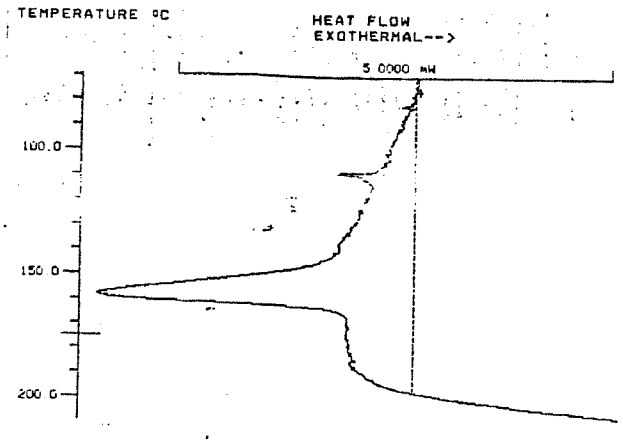

Fig.4.21. Heat Flow Curve of 'APP' 32C in Pierced Pan (in 100 ml/min of Dry Air)

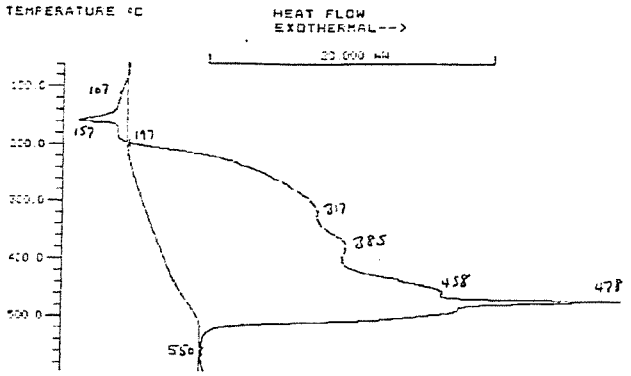

Fig.4.22. Heat Flow Curve of 'APP' 32C in Open Pan (in 200 ml/min of Dry Air)

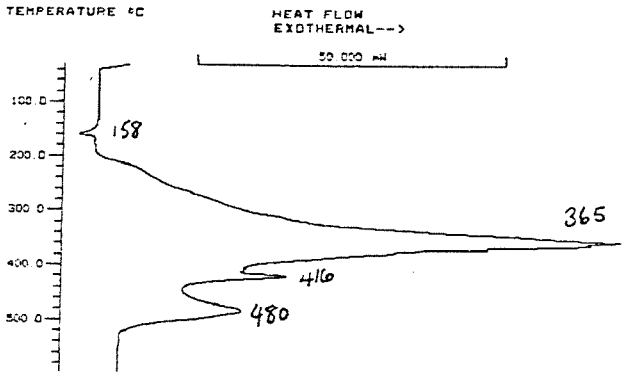

Fig.4.23. Temperatures at (a) Onset of Melting, and –1 mW Threshold, and (b) Onset of Oxidation, and +1 mW Threshold

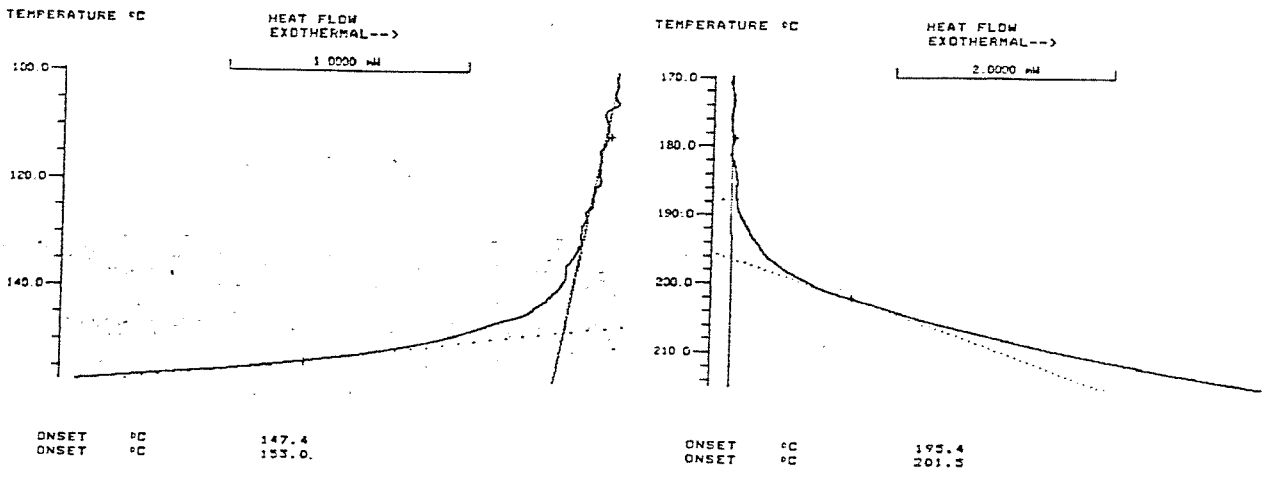

Fig.4.24. Heat Flow Curve of 'APP' 32C (in 50 ml/min of Nitrogen)

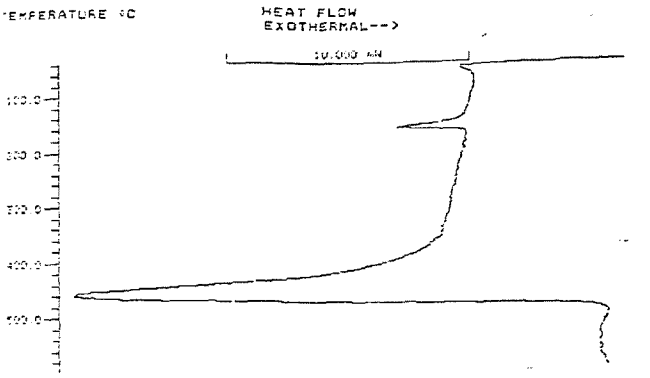

Fig.4.25. Automatic Marking of Onset of Rapid Oxidation of 'APP' 1C (in 200 ml/min of Nitrogen)

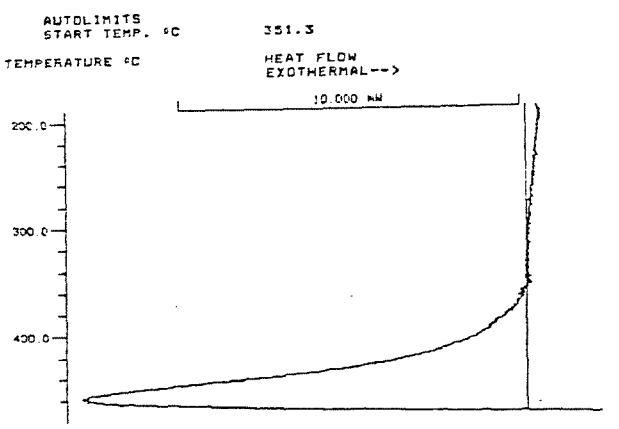

Fig.4.26. Decomposition Endotherm of 'APP' 1C (in 200 ml/min of Nitrogen)

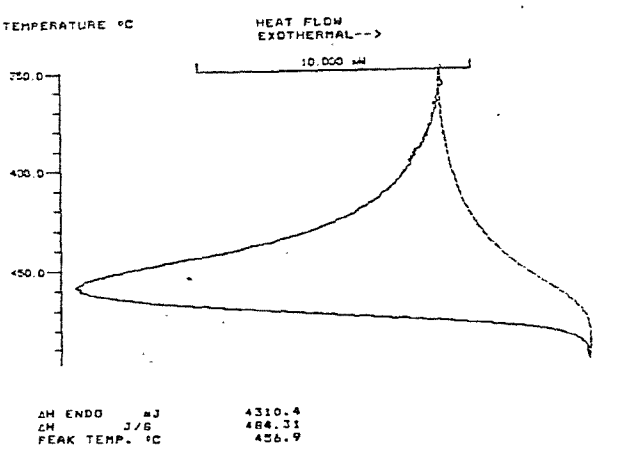

Fig.4.27. Energy Changes in (a) Exothermic and (b) Endothermic Reactions

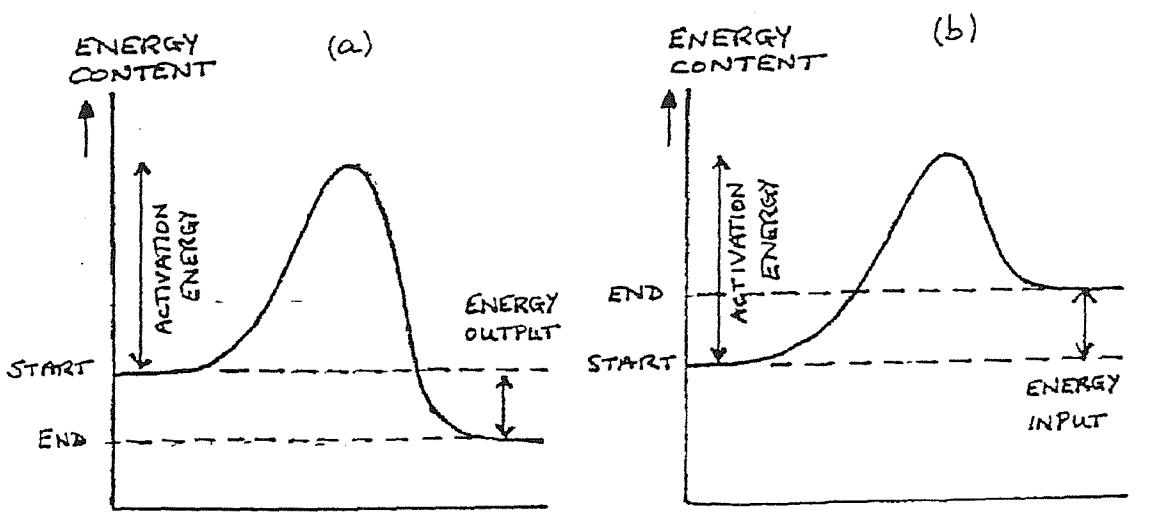

Fig.4.28. Kinetic Data and Alpha *vs* Time Plot for Oxidation of 'APP' 32C

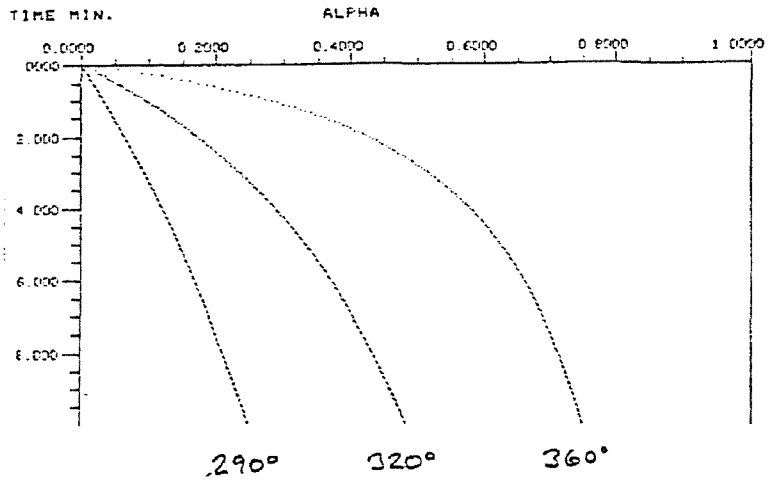

ΔH EXO	kJ	44298
ΔH	J/G	4451.7
PEAK TEMP.	°C	365.0
REACT. ORDER		2.33
CONF. LIMIT		0.74
E A	KJ/MOL	103.21
CONF. LIMIT		29.70
LN Ko		14.60
CONF. LIMIT		6.22

T °C	LN K	P W/KG	t MIN.
170.0	- 13.43	6.5	EEEEE
180.0	- 12.81	12.2	93130
190.0	- 12.22	22.0	51532
200.0	- 11.65	38.7	29227
210.0	- 11.11	66.6	16961
220.0	- 10.59	112.2	10083
230.0	- 10.09	185.1	6112.2
240.0	- 9.61	299.5	3778.2
250.0	- 9.14	475.7	2378.8
260.0	- 8.70	742.5	1523.9
270.0	- 8.27	1140.2	992.42
280.0	- 7.86	1723.9	656.39
290.0	- 7.46	2568.4	440.56
300.0	- 7.07	3773.8	299.84
310.0	- 6.70	5472.2	206.78
320.0	- 6.34	7836.2	144.40
330.0	- 6.00	EEEE.E	102.04
340.0	- 5.66	EEEE.E	72.924
350.0	- 5.33	EEEE.E	52.694
360.0	- 5.02	EEEE.E	38.463

Fig.4.29. Kinetic Data and Alpha *vs* Time Plot for Decomposition of 'APP' 1C

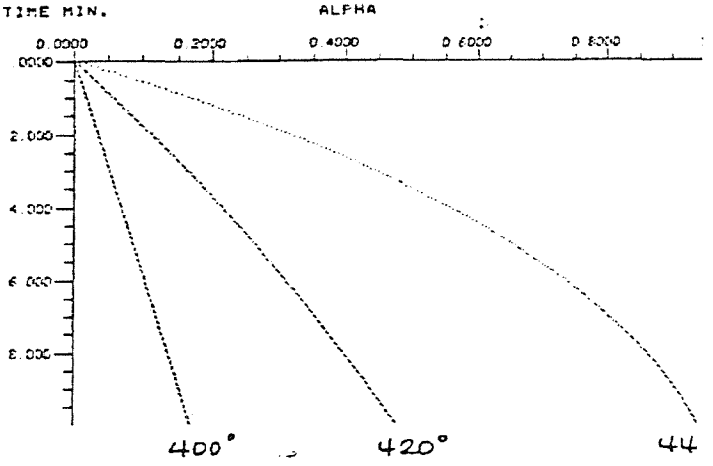

REACT. ORDER		0.62
CONF. LIMIT		0.08
E A	KJ/MOL	226.80
CONF. LIMIT		11.69
LN Ko		32.42
CONF. LIMIT		2.01

T °C	LN K	P W/KG	t MIN.
350.0	- 11.38	- 5.5	2247.2
360.0	- 10.69	- 11.0	1125.2
370.0	- 10.02	- 21.6	575.62
380.0	- 9.37	- 41.3	300.58
390.0	- 8.74	- 77.6	160.07
400.0	- 8.13	- 143.0	86.850
410.0	- 7.53	- 258.8	47.975
420.0	- 6.96	- 460.6	26.958
430.0	- 6.40	- 806.3	15.399
440.0	- 5.85	-1389.3	8.9355
450.0	- 5.32	-2358.9	5.2636
460.0	- 4.81	-3947.1	3.1456
470.0	- 4.31	-6513.8	1.9061
480.0	- 3.82	-EEEE.E	1.1705
490.0	- 3.35	-EEEE.E	.72803
500.0	- 2.88	-EEEE.E	.45841

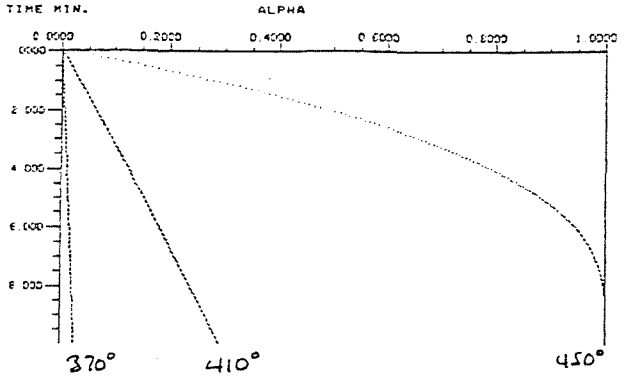

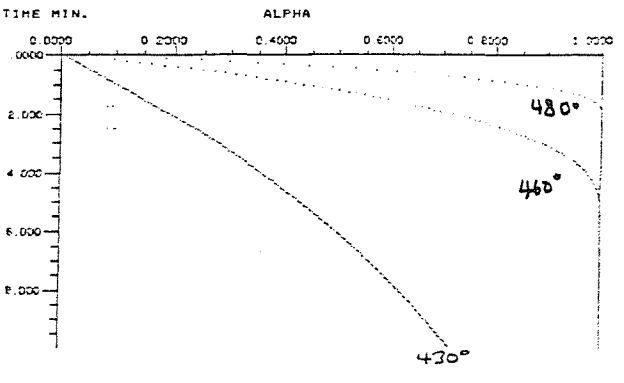

Fig.5.1. Distortion of Weak T_g Curve by Nearby Weak Melting Endotherm of Ice after Slow Cooling: (A) T_m of Ice, (B) T_g of APP, (C) Resultant of A + B

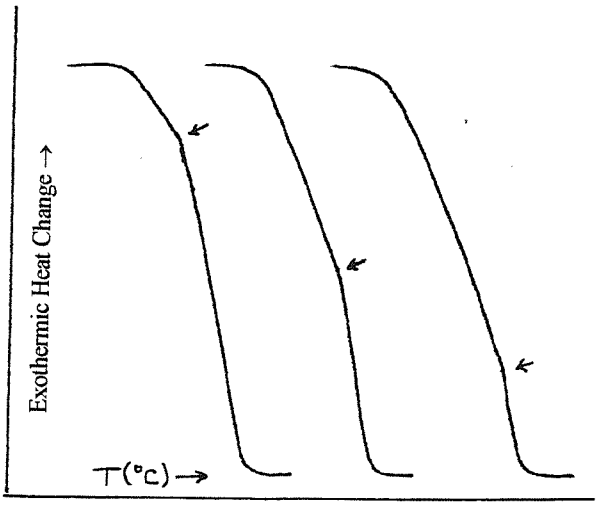

Fig.5.2. T_g Curves for 2 Materials Not Fully Miscible, Showing Bend Between Adjacent T_gs

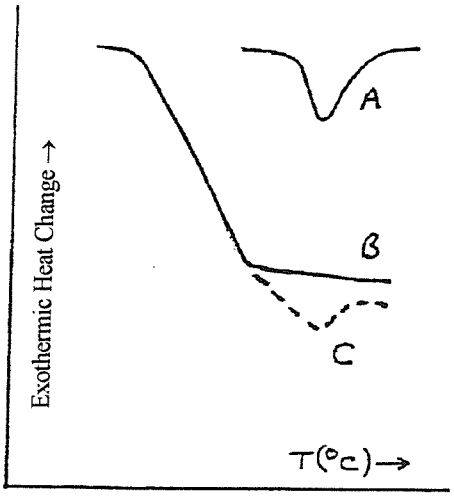

Fig.5.3. Clear Separation of Strong T_g Curve and Weak Melting Endotherm of Ice after Rapid Quenching: (A) T_m of Ice, (B) T_g of APP, (C) Resultant of A + B

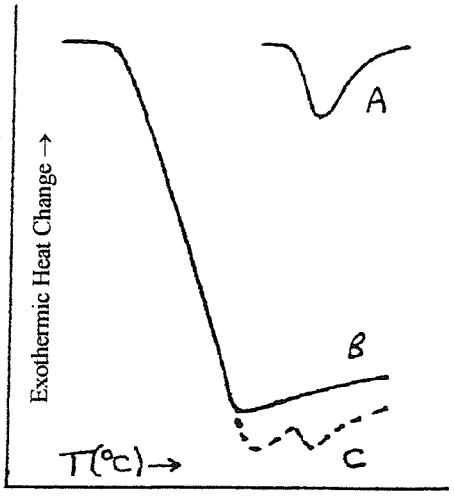

Fig.5.4. Sharp Ice-melting Endotherm in **98**

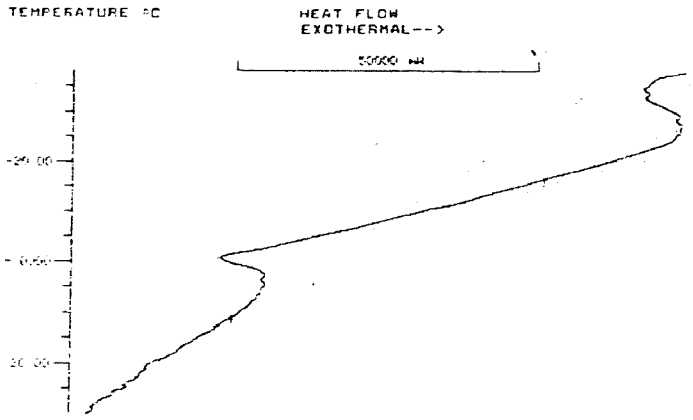

Fig.5.5. Predicted Effect of Water Intake on the T_g of Bitumen Modified with (a) APP, (b) a Polymer of Lower T_g than APP

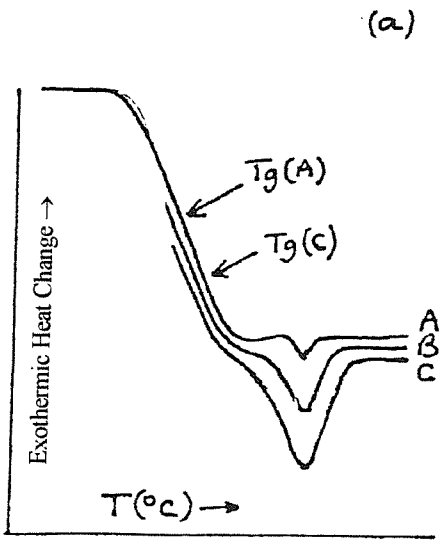

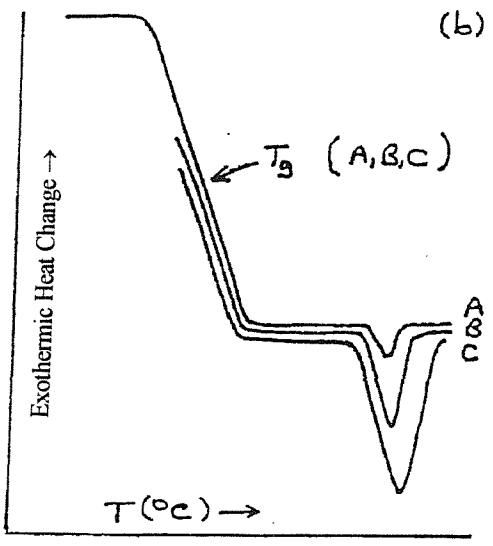

Fig.5.6. Small Melting Endotherm (Onset about RT) in 1st but not 2nd Heating Scan of Stored APP 32C

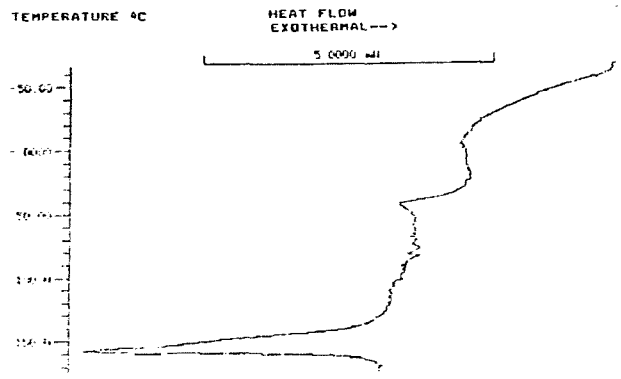

Fig.5.7. Small Melting Endotherms of Onset RT and 90°C for **97** after Reaching 90°C and then a Hold at 20°C

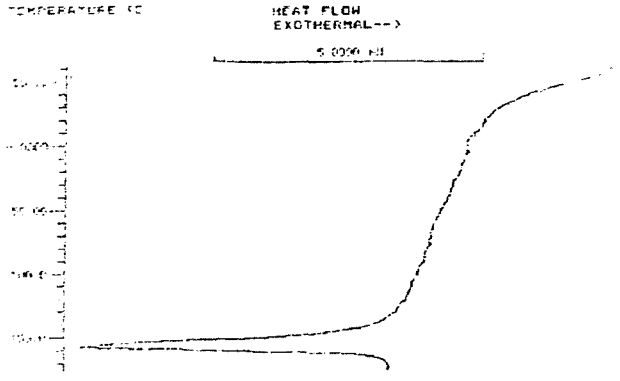

Fig.5.8. Cold Crystallization and Immediate Melting at Temperature of Pause (20°C) in Previous Quench of Blend **98**

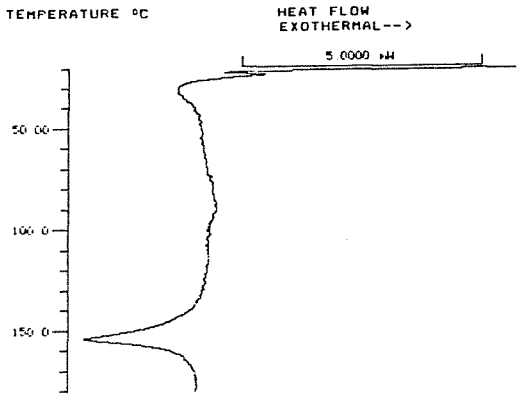

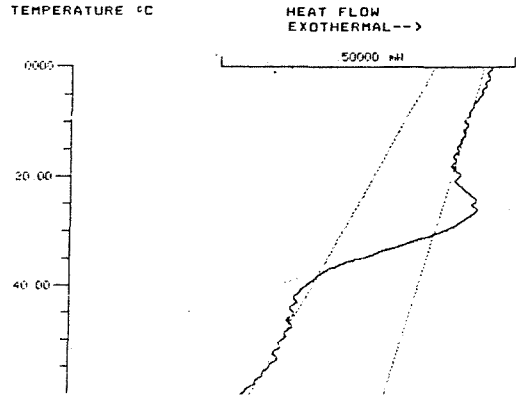

Fig.5.9. Heat Flow Plots of Blend **96**: (a) 1st Scan: Cold Crystallization, (b) 2nd Scan: No Cold Crystallization

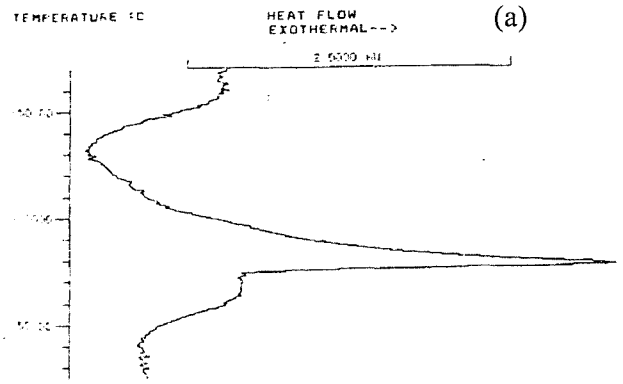

(a)

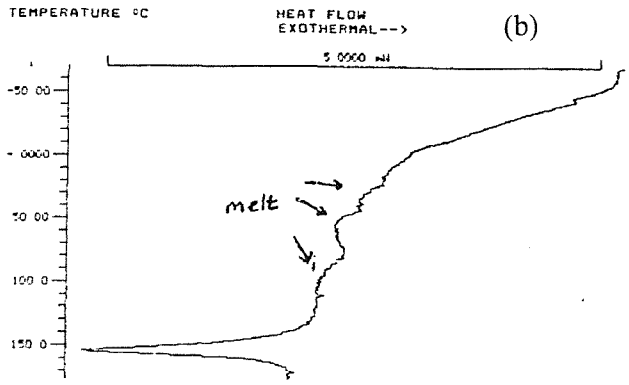

(b)

Fig.5.10. DSC Curve of SBS/Bitumen **55**: (a) 1st Scan, (b) later 2nd Scan

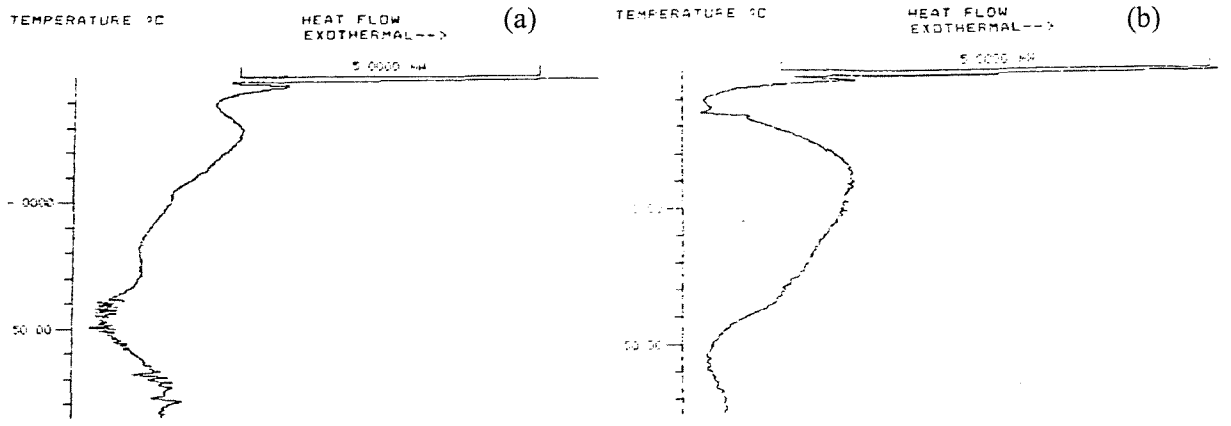

Fig.5.11. DSC Curve of APP 43C after Quench to –80°C, (d) with hold at 20°C, (e) with no hold at 20°C

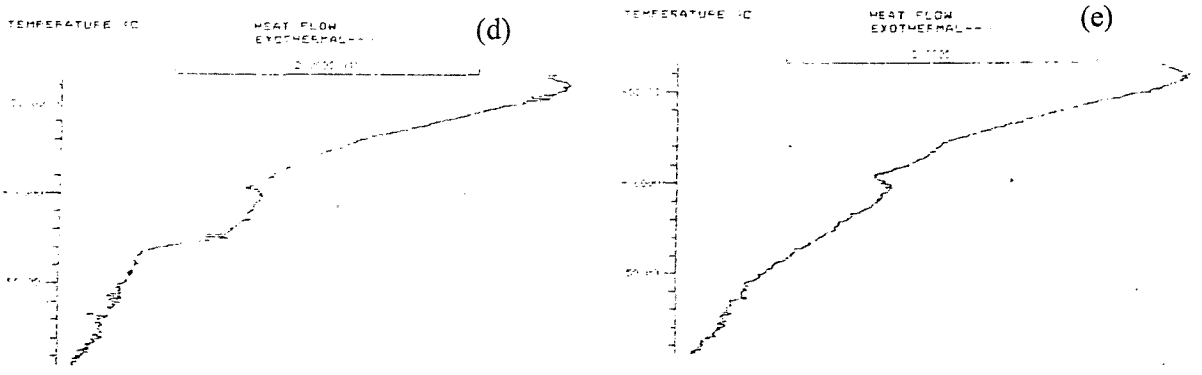

Fig.5.12. Variation of T_g with 32C Content in 100 Pen Bitumen

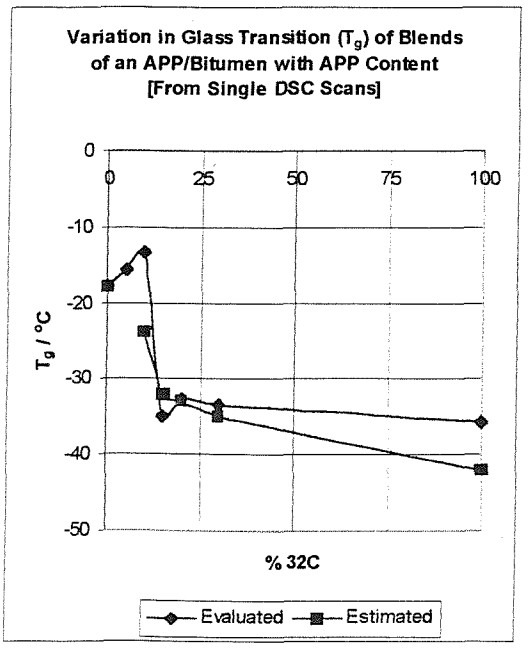

Fig.5.13. Crystallinity from Content Program on DSC Curve of 32C

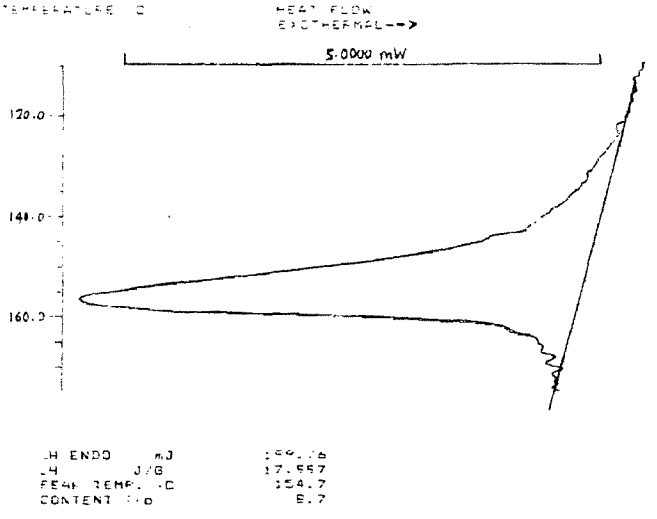

Fig.5.14. DSC Curve of 43C after Cooling of the Melt at Different Rates:
(a) Rapid Quench, (b) 50°C/min

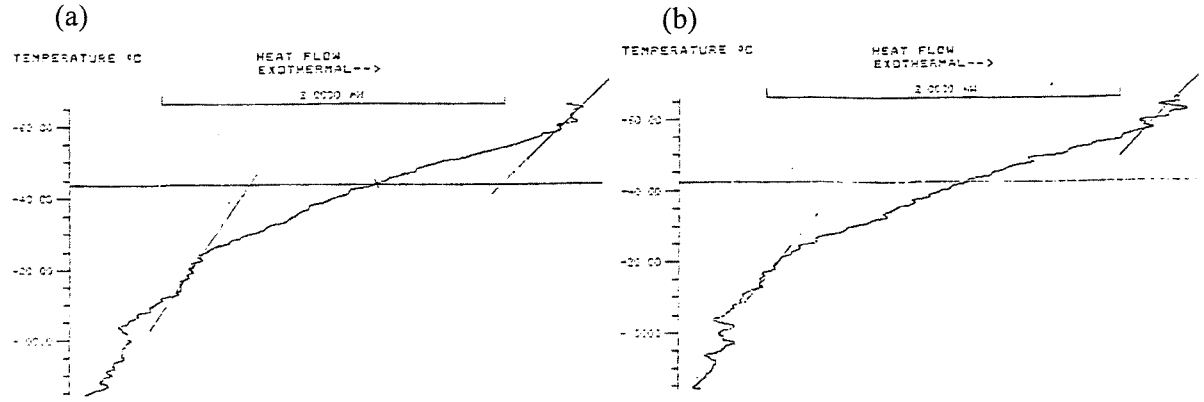

Fig.5.15. Decreasing Background Oscillations with Decreasing Cooling Rate:
(a) 50°C/min, (b) 40°C/min, (c) 30°C/min, (e) 10°C/min

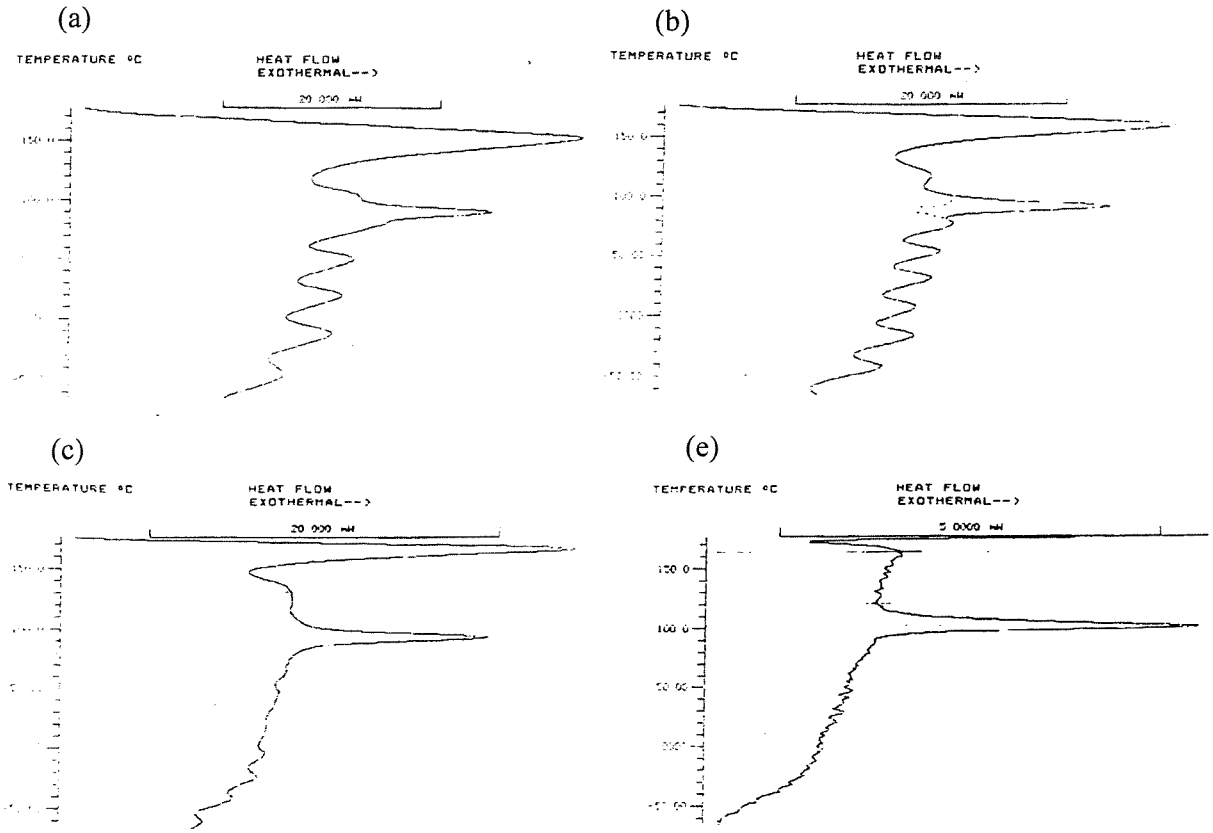

Fig.5.16. Heating and Cooling Cycles for Linked Method Experiments

(a) Cooling Melt at Different Rates

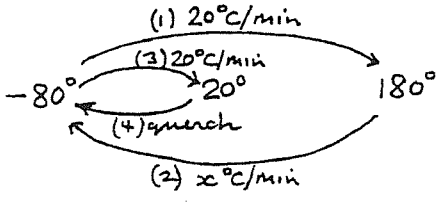

(b) Pause in Quench at 20ºC For Different Times

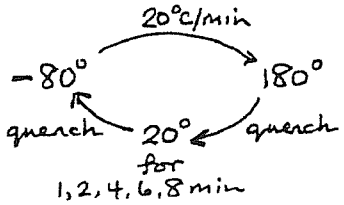

(c) Pause in Quench for 10 Min at Different Temperatures

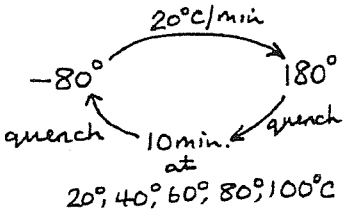

Fig.5.17. Heating Scans for 32C to 180°C after Quench to Timed Pause at 20°C:
(a) initial scan from storage, (b) 0 min, (c) 3 min, (d) 4 min, (e) 6 min,
(f) 8 min, (g) 10 min, (h) 20 h at 20°C

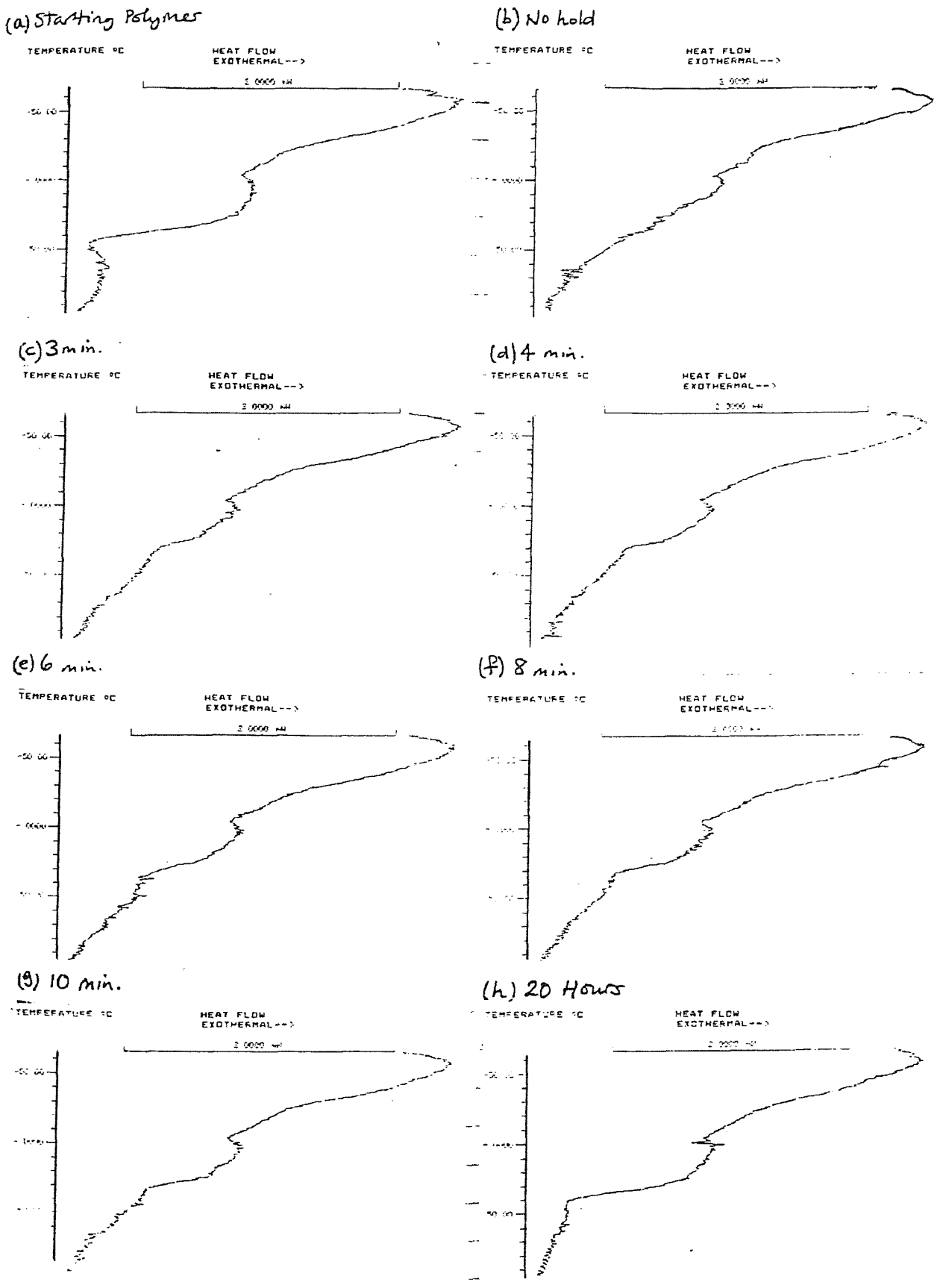

Fig.5.18. New Melting Endotherms in 43C with Onset at Temperature of the 10 min Hold During the Previous Quench

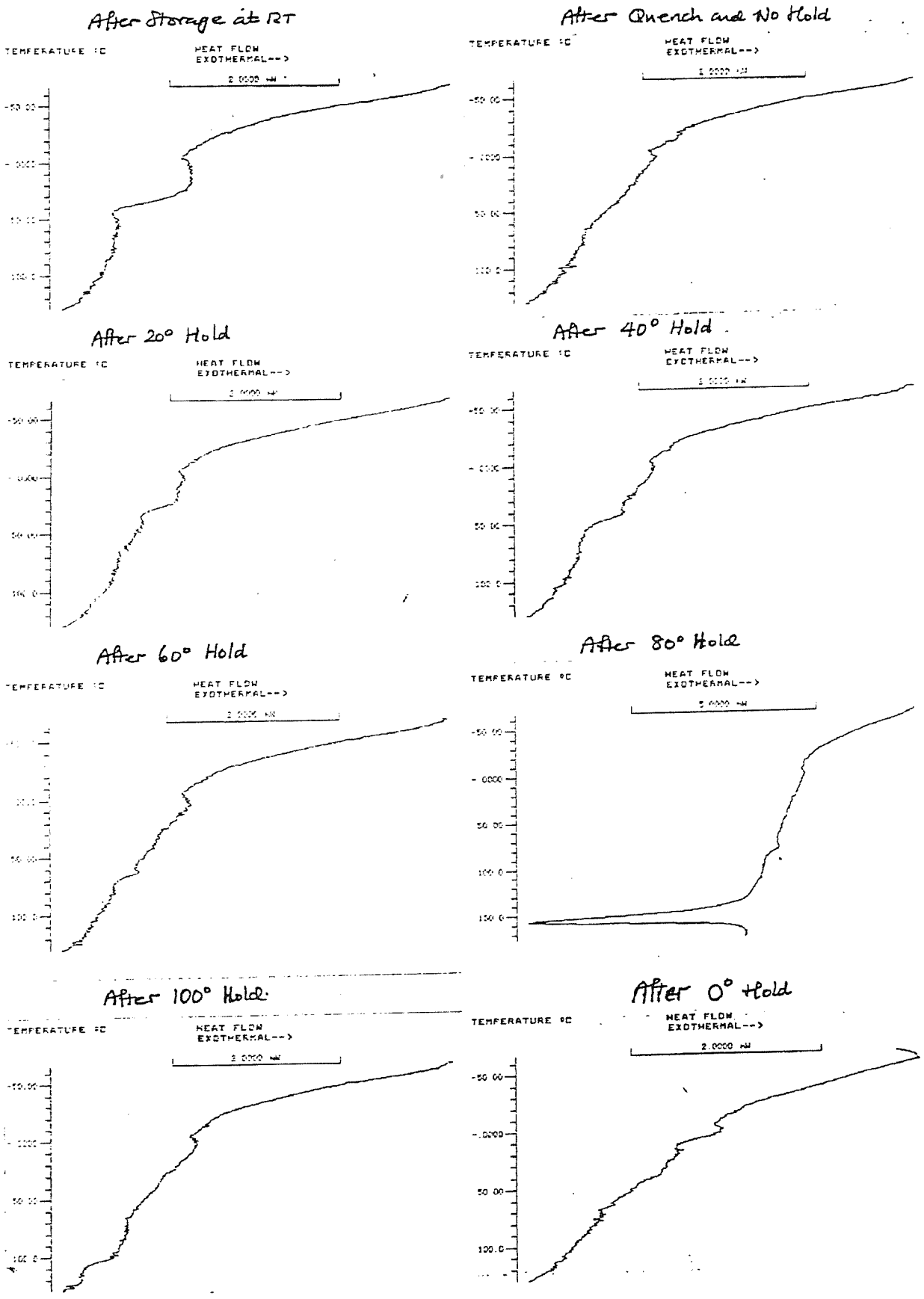

Fig.5.19. Chart of Heat Input to 43C in 10 min Hold at Different Temperatures During the Quench of the Melt (Day 2)

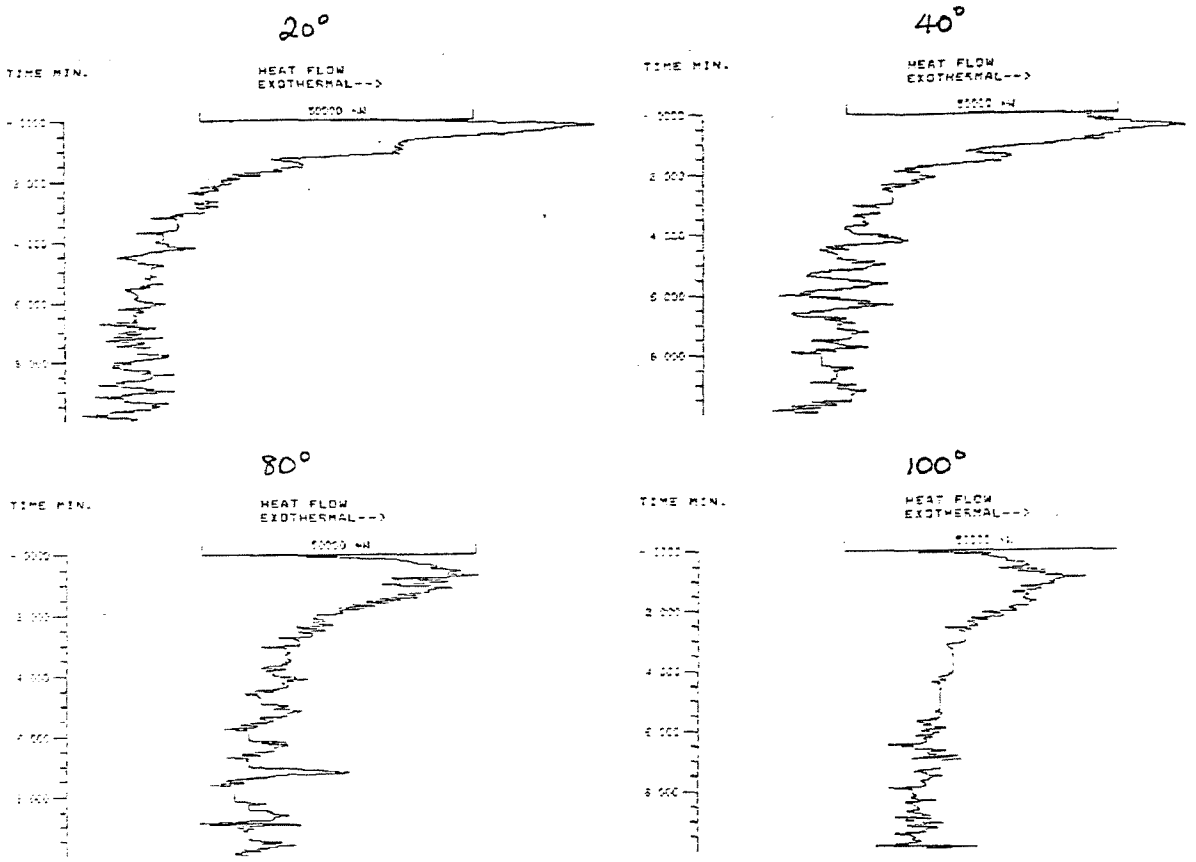

Fig.5.20. Chart of Heat Output from 43C in 10 min Hold at Different Temperatures During the Quench of the Melt (Day 3)

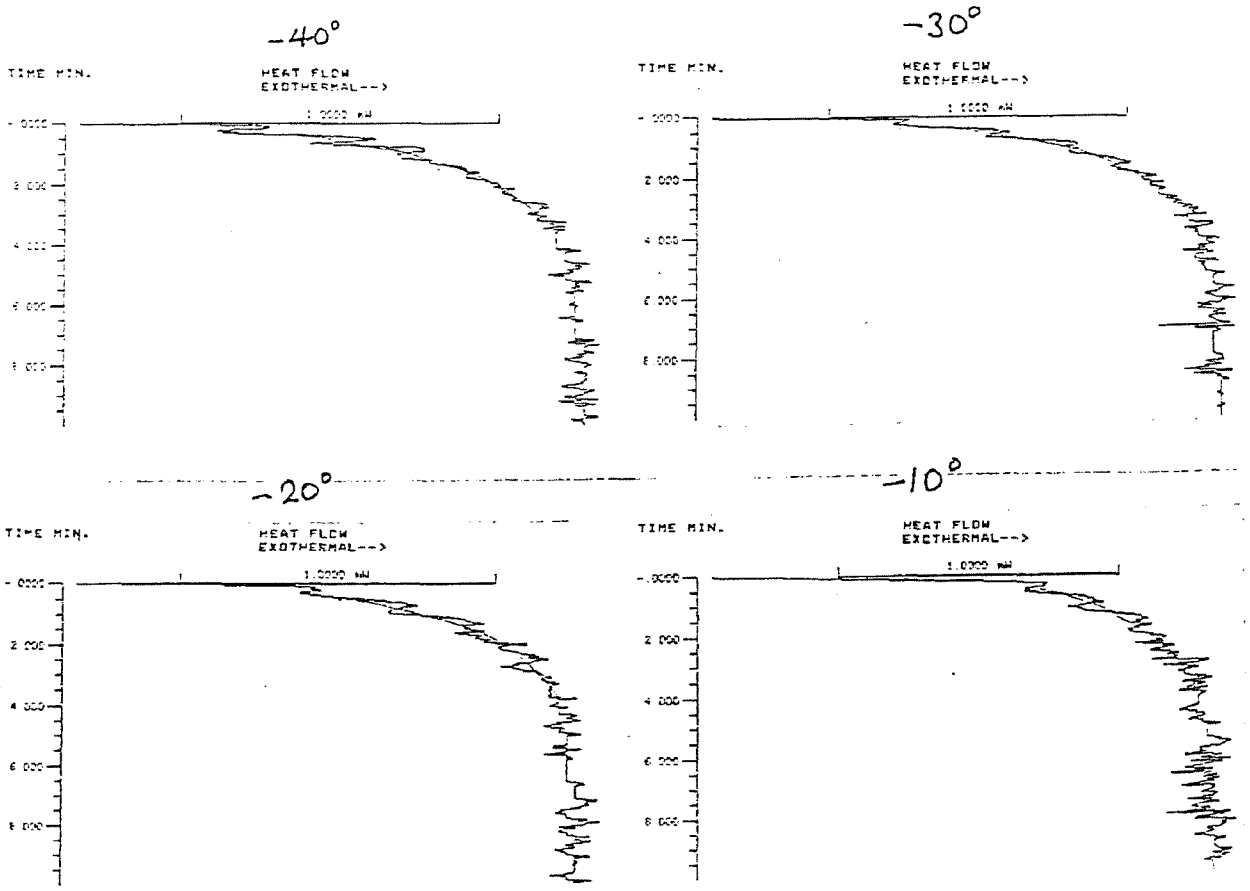

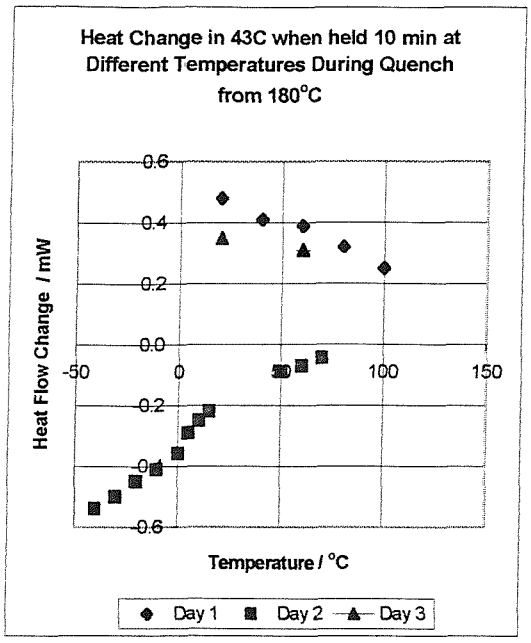

Fig.5.21. Graph of Heat Change in 43C in 10 min Hold at Different Temperatures During Quench from 180°C

Fig.5.22. Chart of Heat Change in 43C During a 10 min Hold in the Quench from 180°C: Change From Endothermic to Exothermic Crystallization

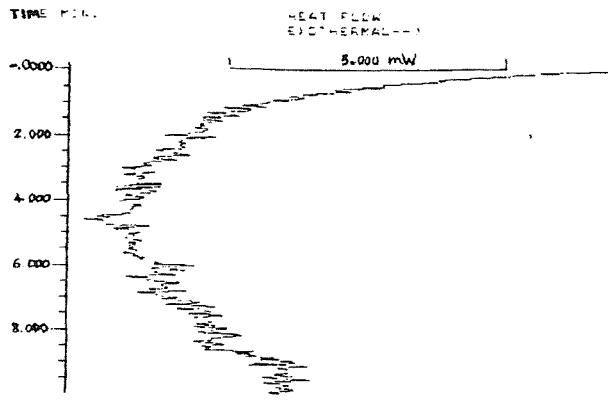

Fig.5.23. Scan Cycle for Crystallizing and Melting 43C at Progressively Higher Temperatures

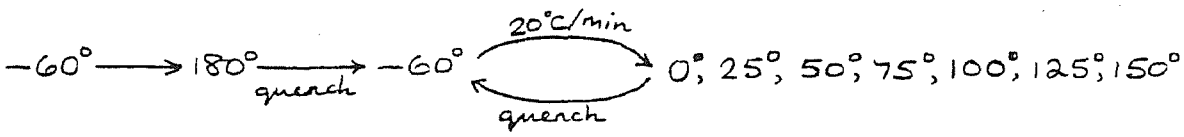

Fig.5.25. Predicted Removal of Successive Melting Endotherms in the DSC Chart of a Semi-Crystalline Polymer

(a) 1st sample full scan of 3 endotherms

(b) 2nd sample 1st scan, T_1 to T_2

(c) 2nd sample 2nd scan, T_1 to T_3

(d) 2nd sample 3rd scan, T_1 to T_4

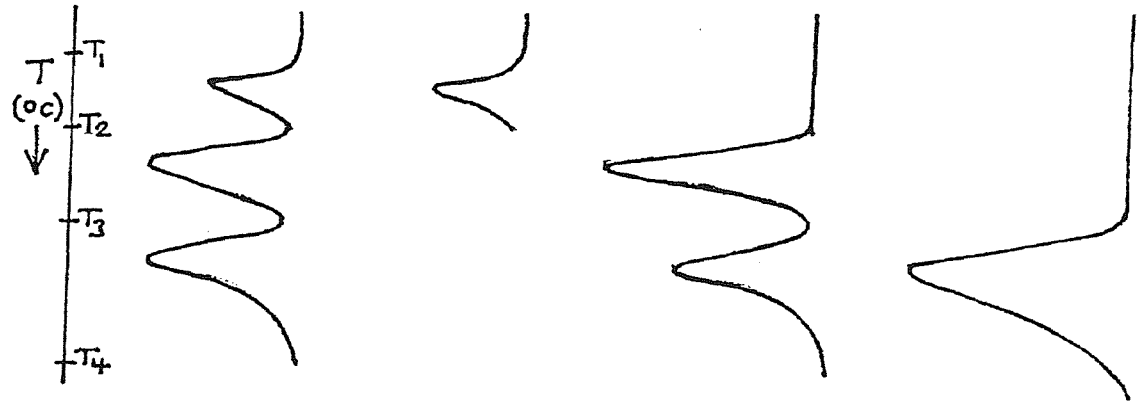

Fig.5.26. T_g of 32C from Linked Scans from –120° to 180°C

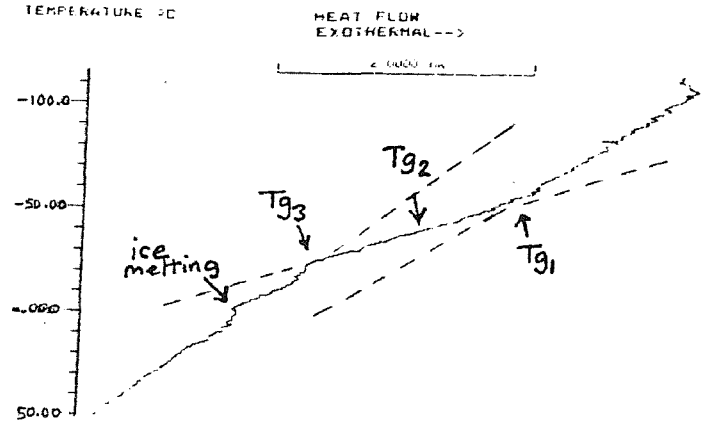

Fig.5.24. DSC Chart of 43C Heated on Successive Scans to (a) 0°C, (b) 25°C, (c) 50°C, (d) 75°C, (e) 100°C, (f) 125°C, (g) 150°C, and Held There for 5 min

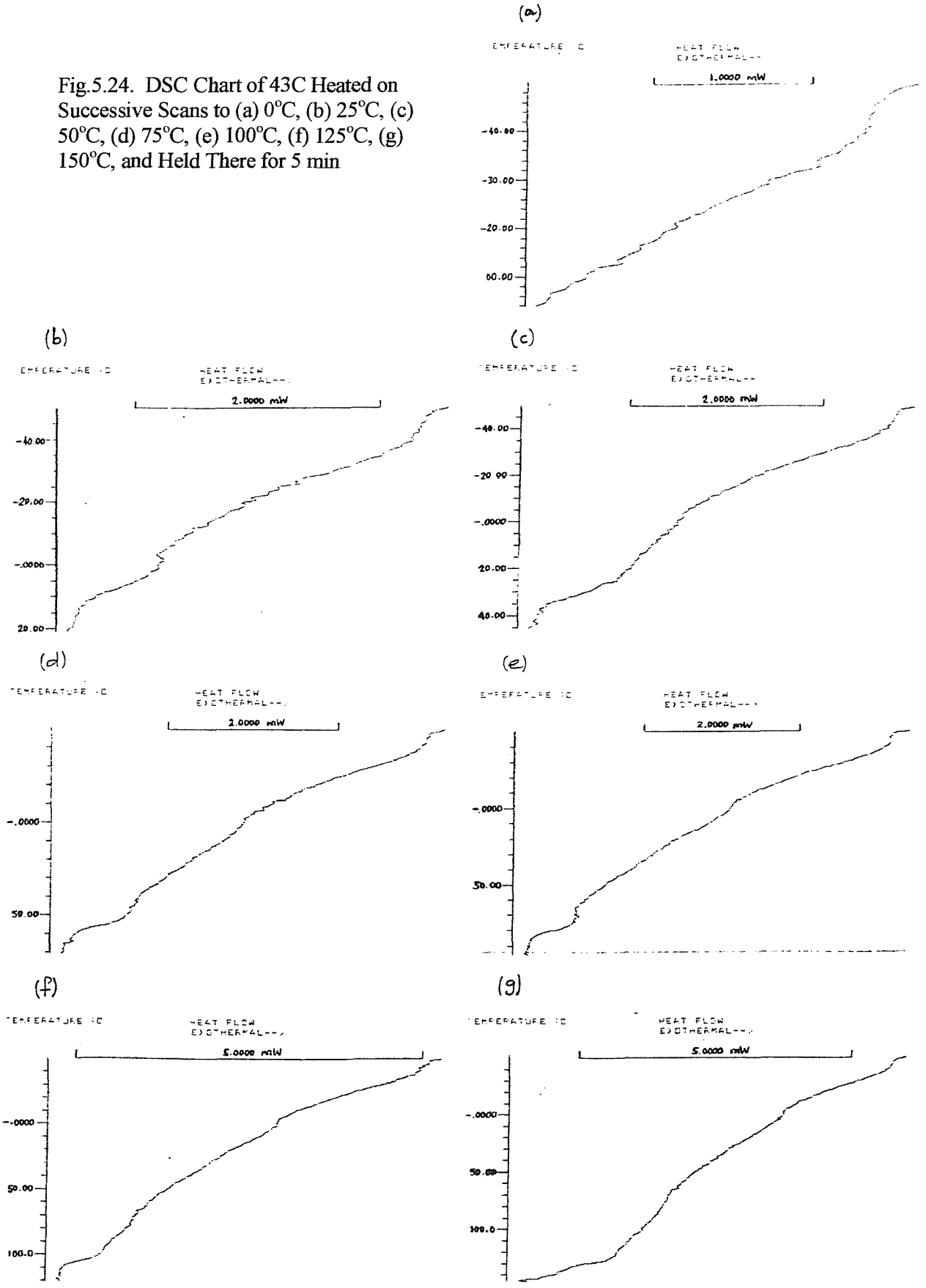

Fig.5.27. Graph of Variation in Glass Transition of Blends of an APP/Bitumen with APP Content

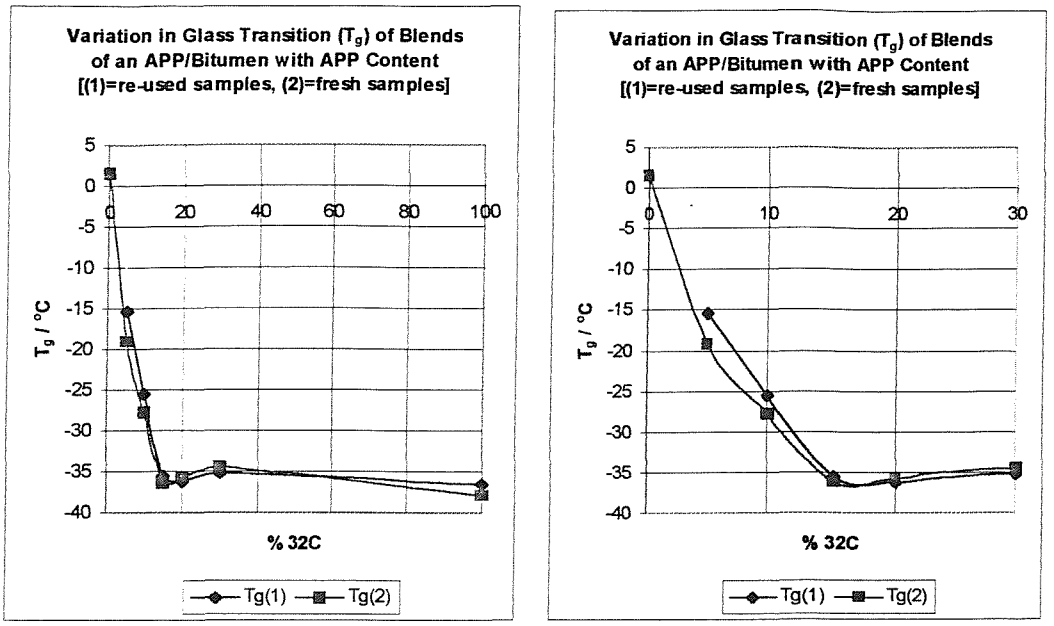

Fig.5.28. Glass Transitions (T_g)

(a) 200 Pen Bitumen

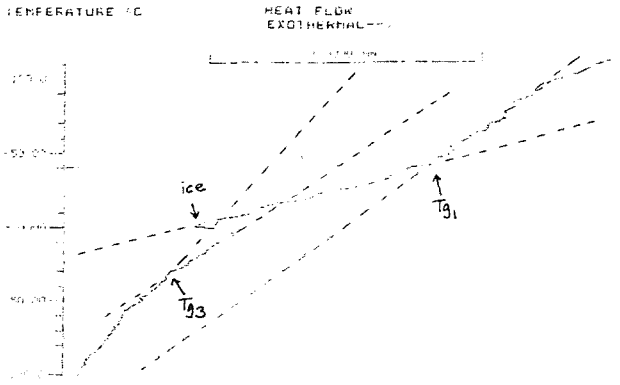

(b) SBS

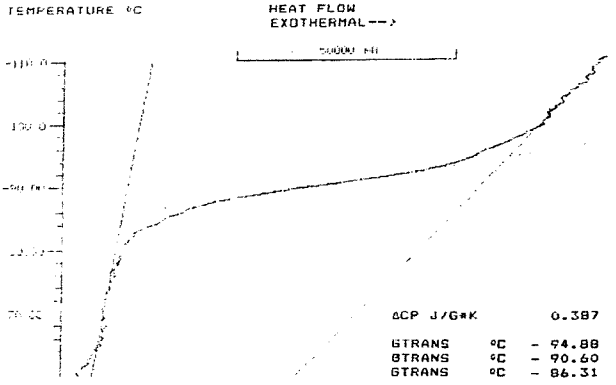

(c) 9% SBS in 200 Pen

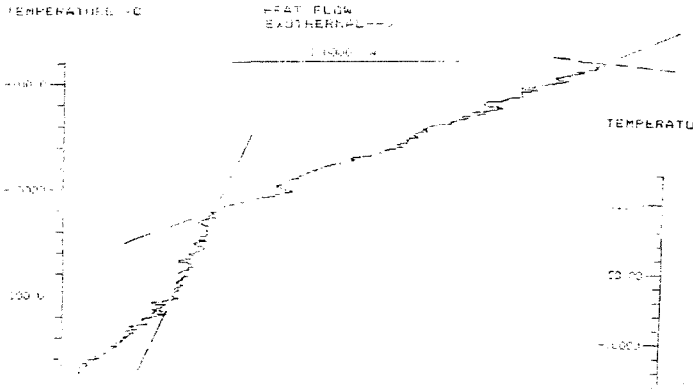

(d) PFSD (6% IB in 100 Pen)

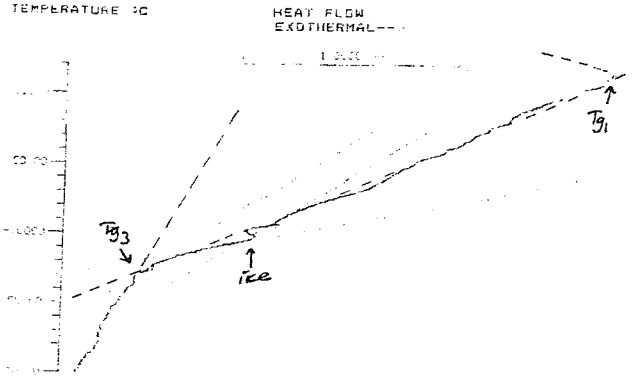

Fig.5.29. Glass Transitions (T_g)

(a) Oxidized Bitumen

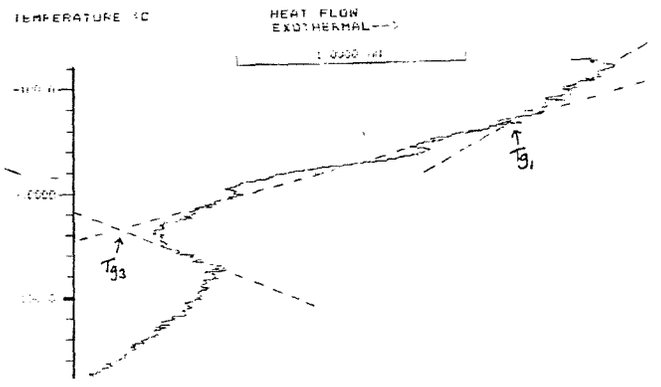

(b) SIS

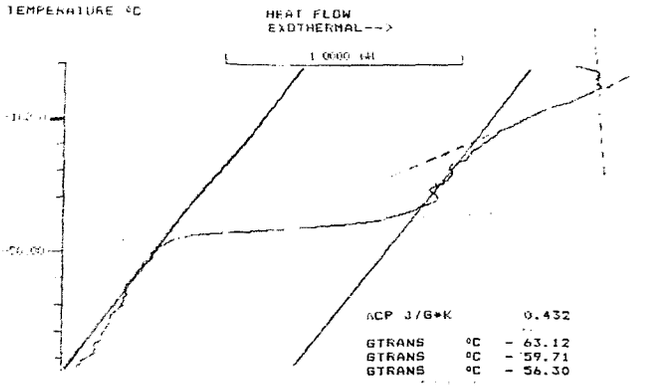

(c) LDPE

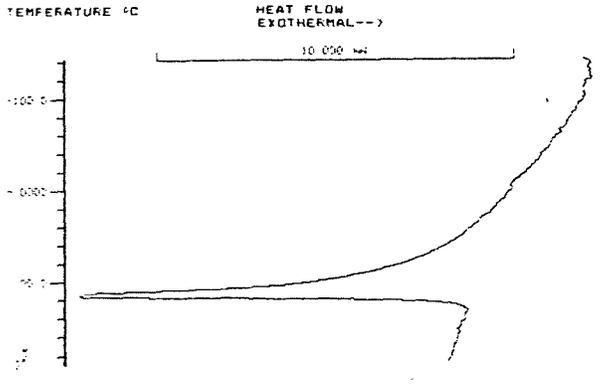

(d) HDPE

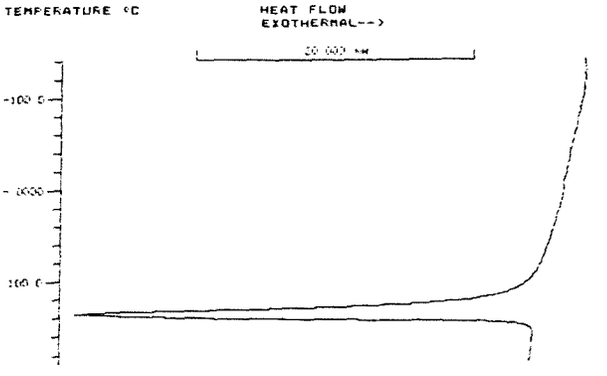

(e) V808

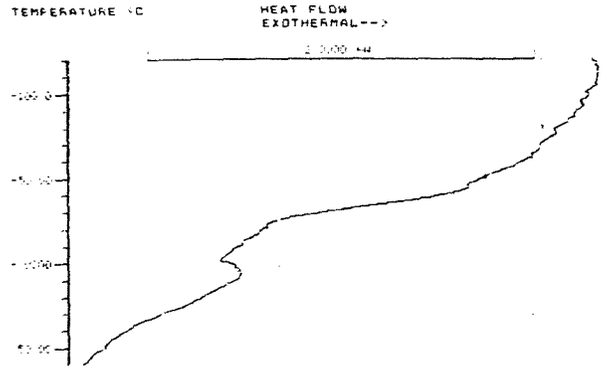

(f) C80

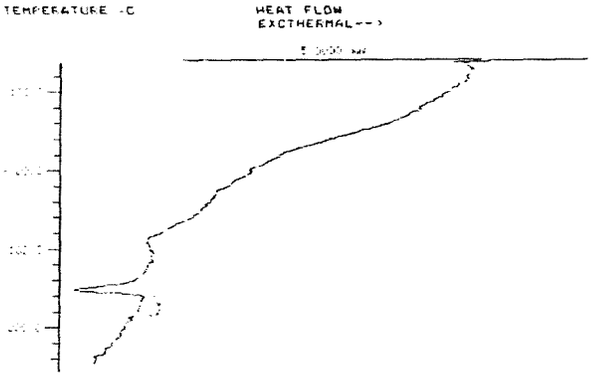

(g) T1180

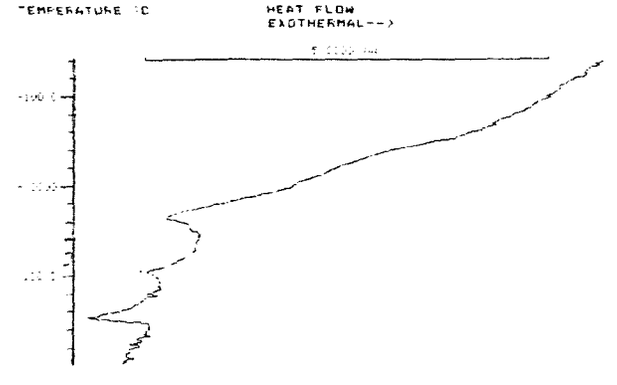

(h) 95-X-06

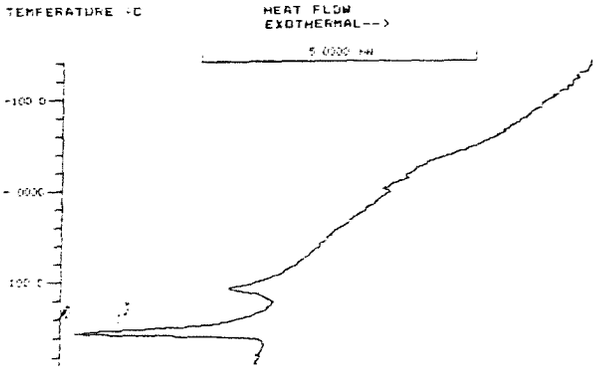

Fig.6.1. Degradation of 4 Pelleted APPs at *c.*120°C in Alternating Light and Dark Periods

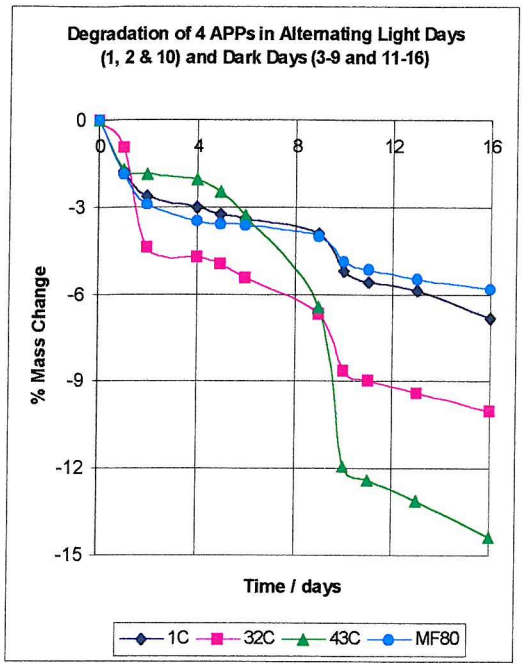

Fig.6.4. Degradation of 4 Pelleted APPs at 110°C in Daylight

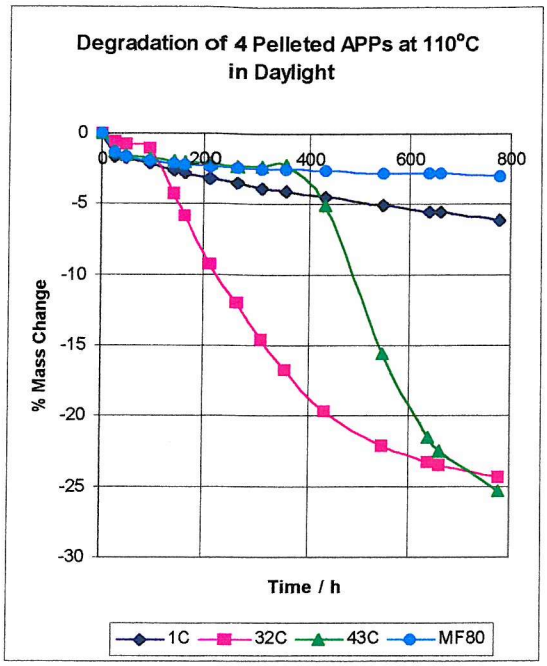

Fig.6.5. Degradation of 4 Pelleted APPs at 120°C in Daylight - Behind Extra Soda Glass - with 14 Week Gap in Measurements

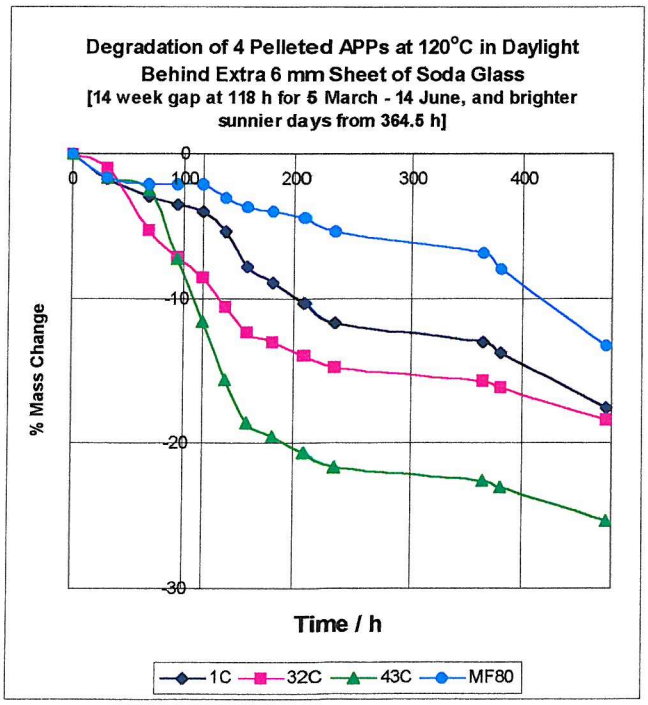

Fig.6.2. Degradation of 4 Pelleted APPs at *c.*120°C in Near Darkness
(a) to 100 h and (b) to 1500 h

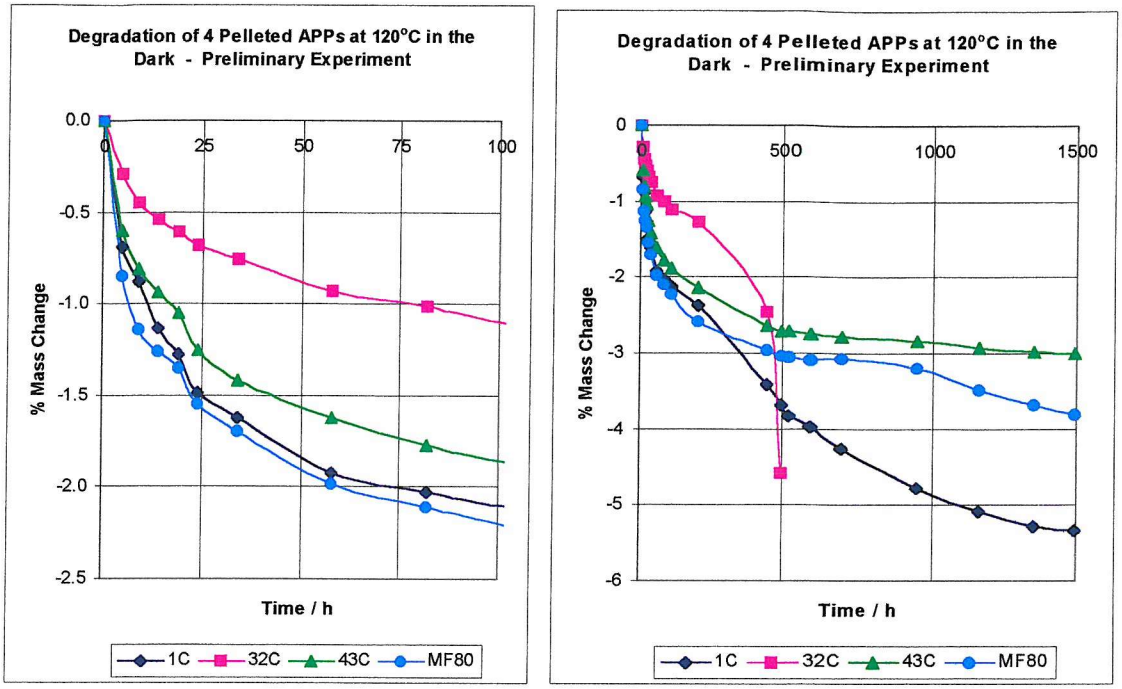

Fig.6.3. Degradation of 4 Pelleted APPs at *c.*120°C in Daylight
(a) to 100 h and (b) to 500 h

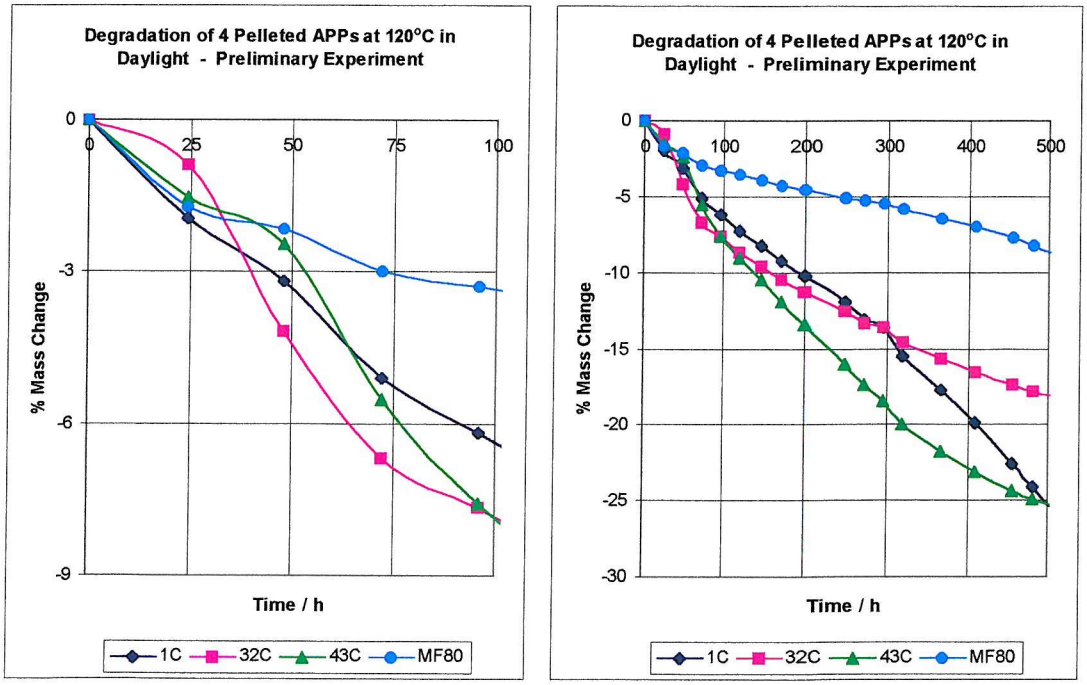

Fig.6.6. Comparison of Initial Degradation of 4 Pelleted APPs in Daylight Under Different Conditions: (a) 1C, (b) 32C, (c) 43C and (d) MF80

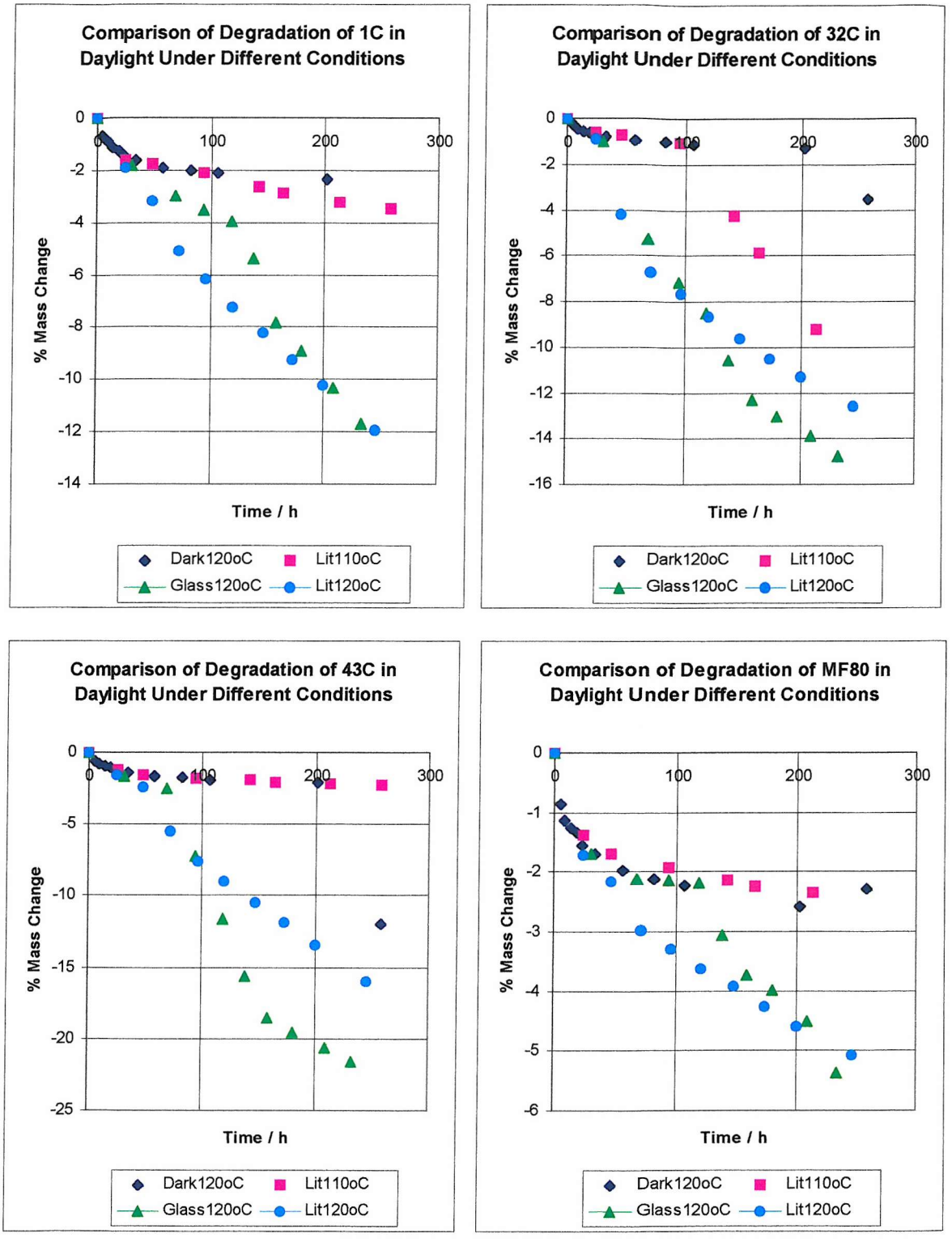

Fig.6.7. Degradation of (a) 4 APPs and a Bitumen Blend, and (b) 2 APPs, 4 Other Polymers and Oxidized Bitumen, at 120°C in Daylight

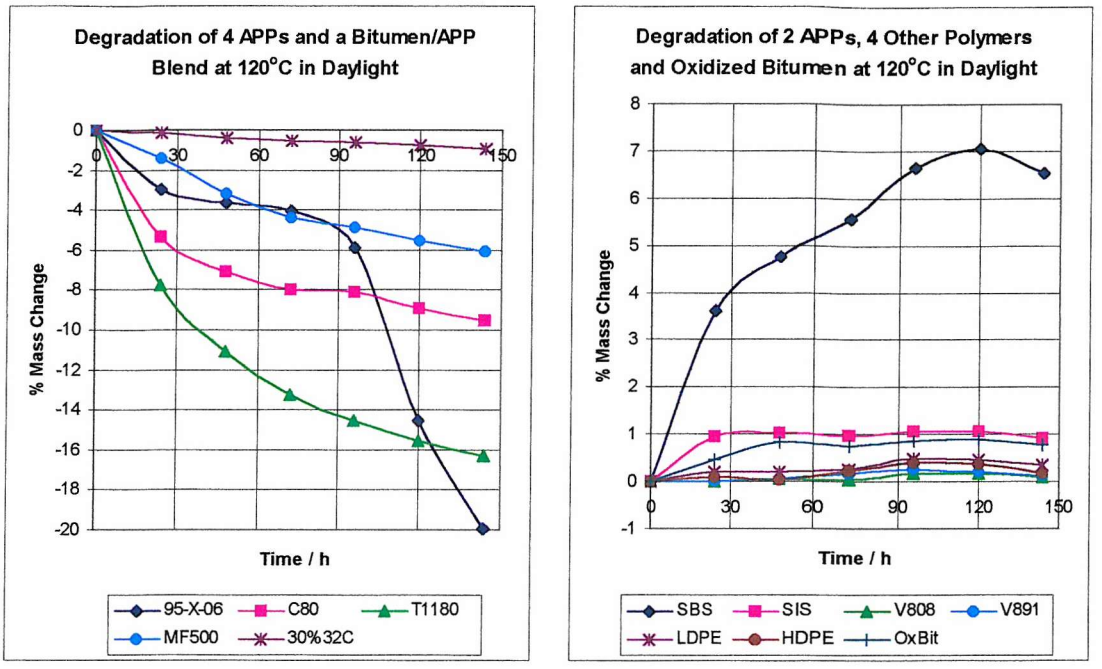

Fig.6.8. Degradation of APPs at 120°C in Daylight - Effect of Sample Size for (a) Supplied 95-X-06 and (b) Heat-treated V808 and V891

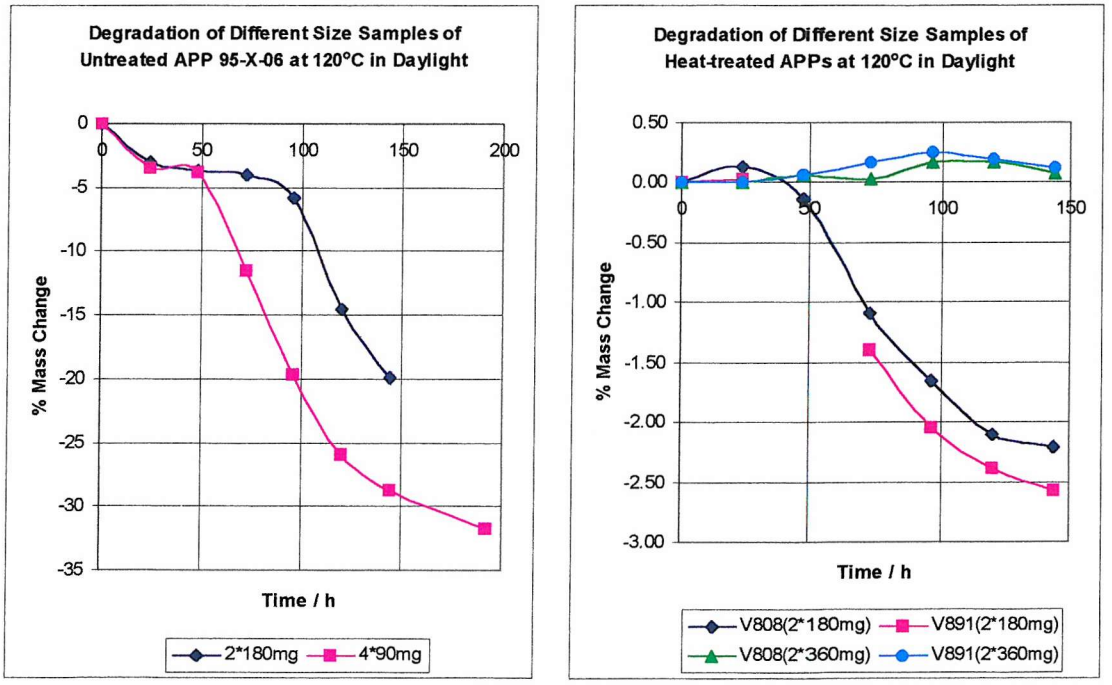

Fig.6.9. UV Spectra of (a) Soda Glass and (b) Pyrex

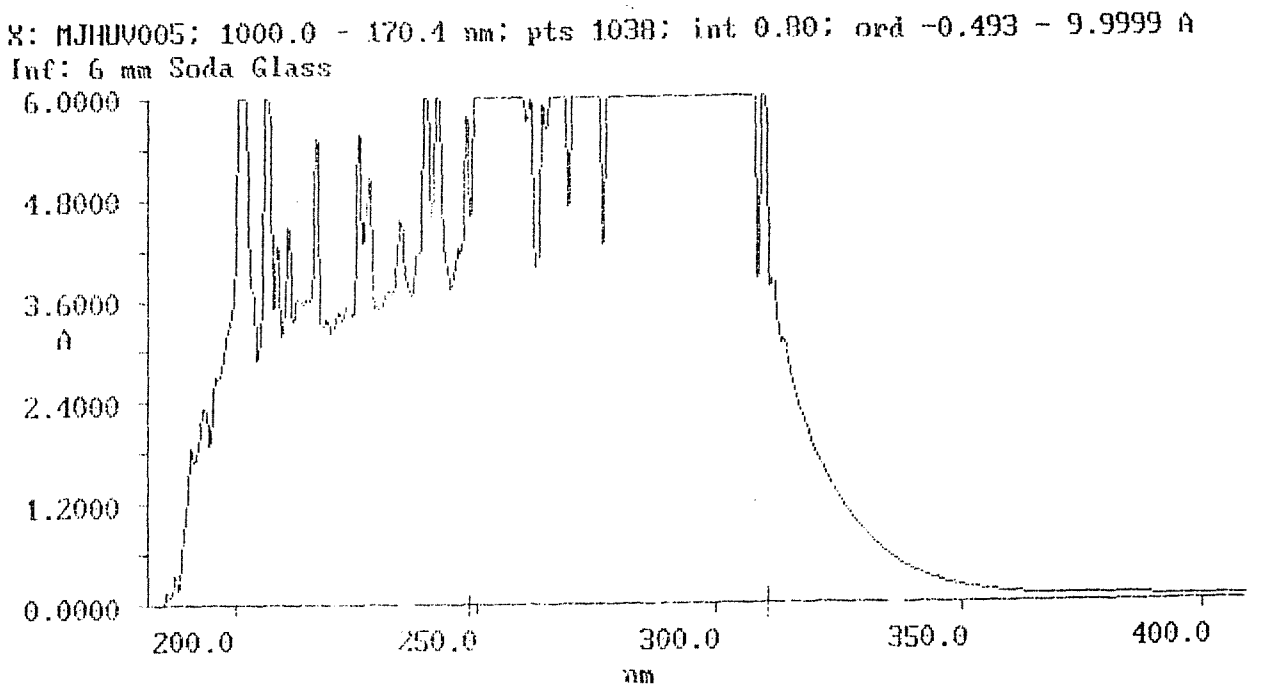

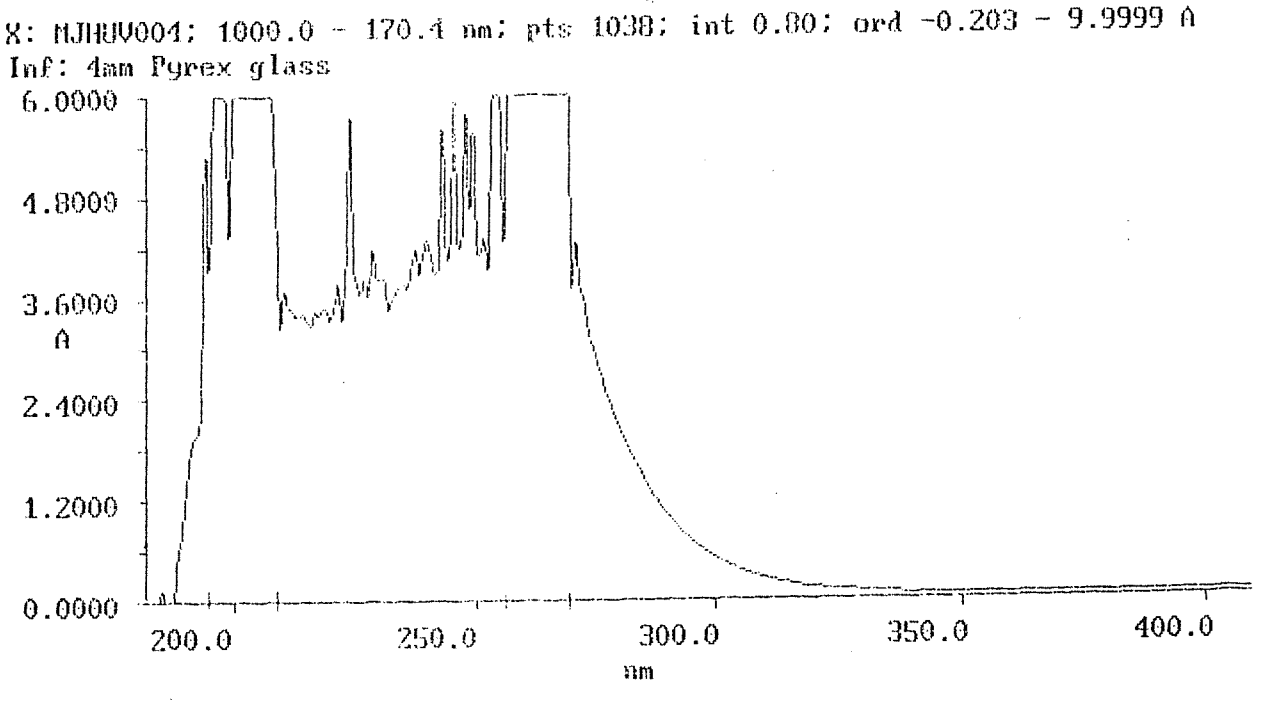

Fig.6.10. Degradation of 4 Pelleted 'APPs' at 120°C in 5 Lux (a) to 100 h and (b) to 716 h

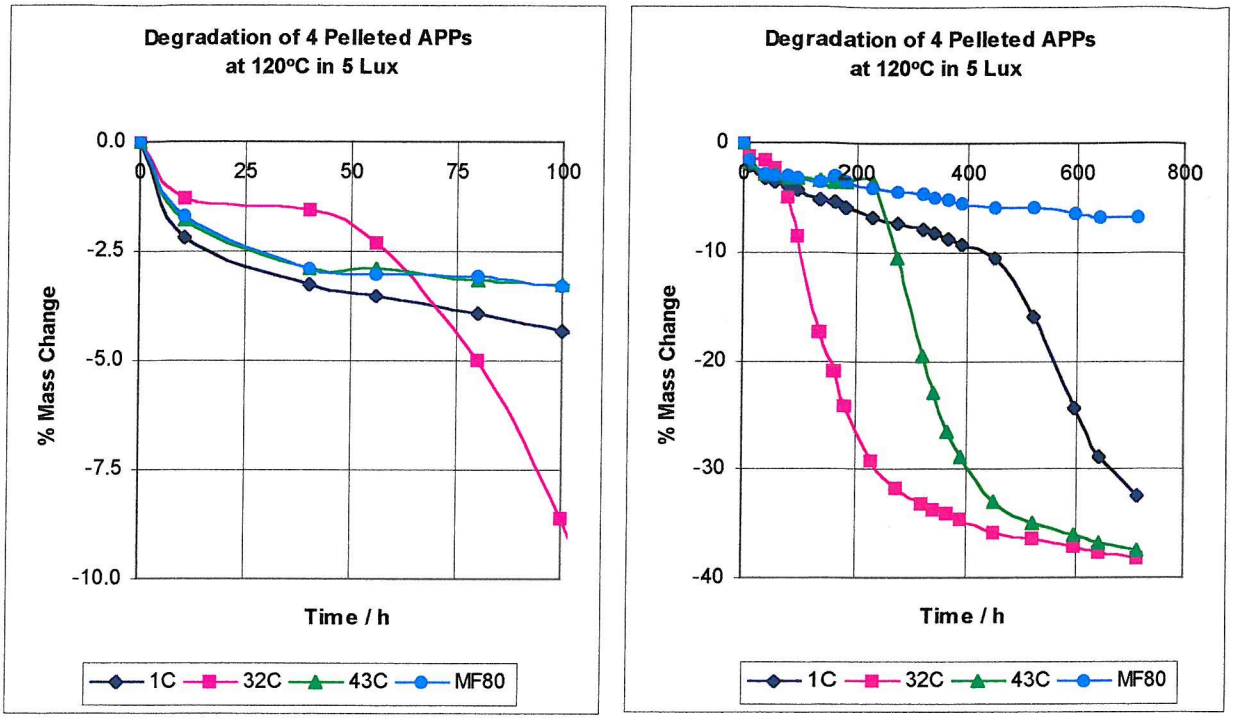

Fig.6.11. Degradation of SBS, SIS, PFSD, and SBS Blends in 200 Pen Bitumen at 120°C in 4 Lux

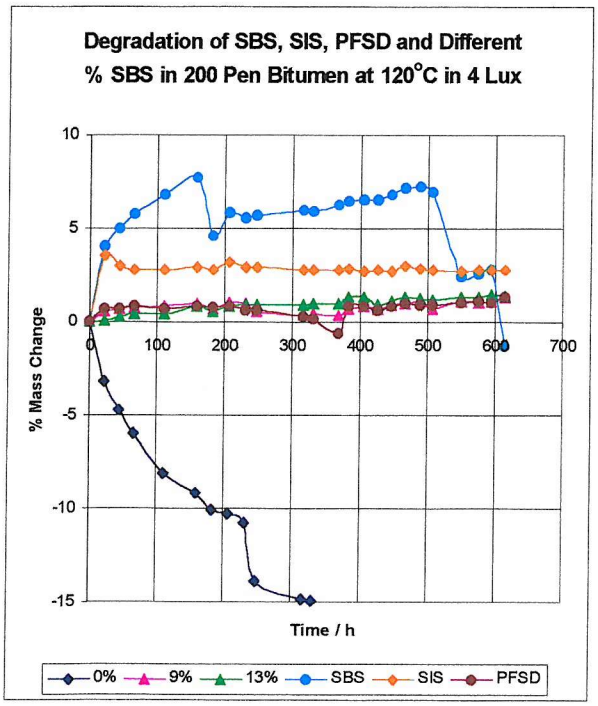

Fig.6.12. Degradation of 4 Pelleted 'APPs' - 1C, 32C, 43C and MF80 - at 120°C in 4 Lux

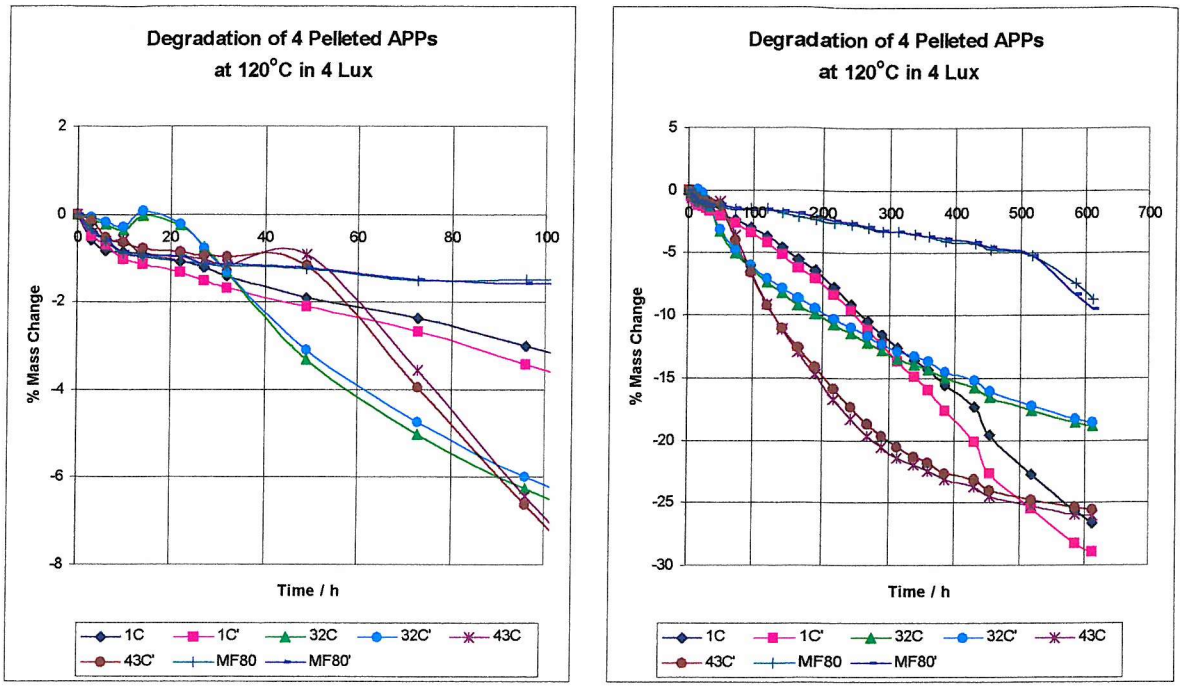

Fig.6.13. Degradation of 4 Pelleted 'APPs' - MF500, C80, T1180 and 95-X-06 - at 120°C in 4 Lux

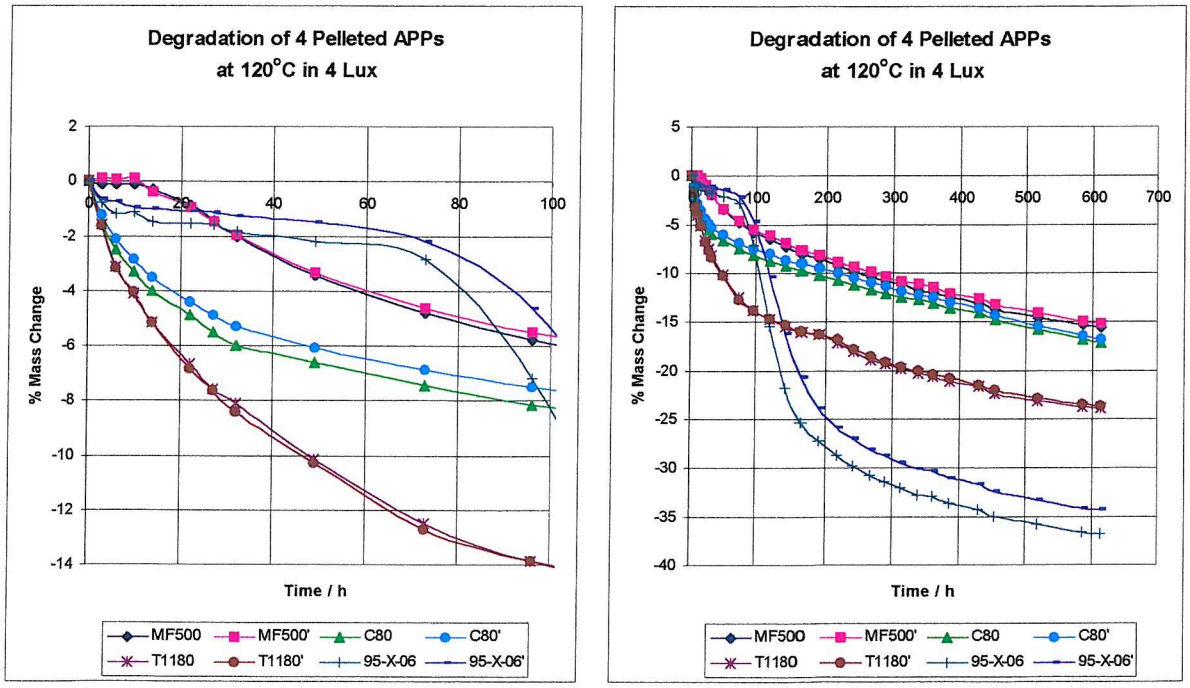

Fig.6.14a,b. Degradation of Different Size Samples of 2 'APPs' – (a) 95-X-06 and (b) T1180 – at 120°C in 4 Lux [Overlaid for most pieces in Fig.6.15, next to Fig.6.21]

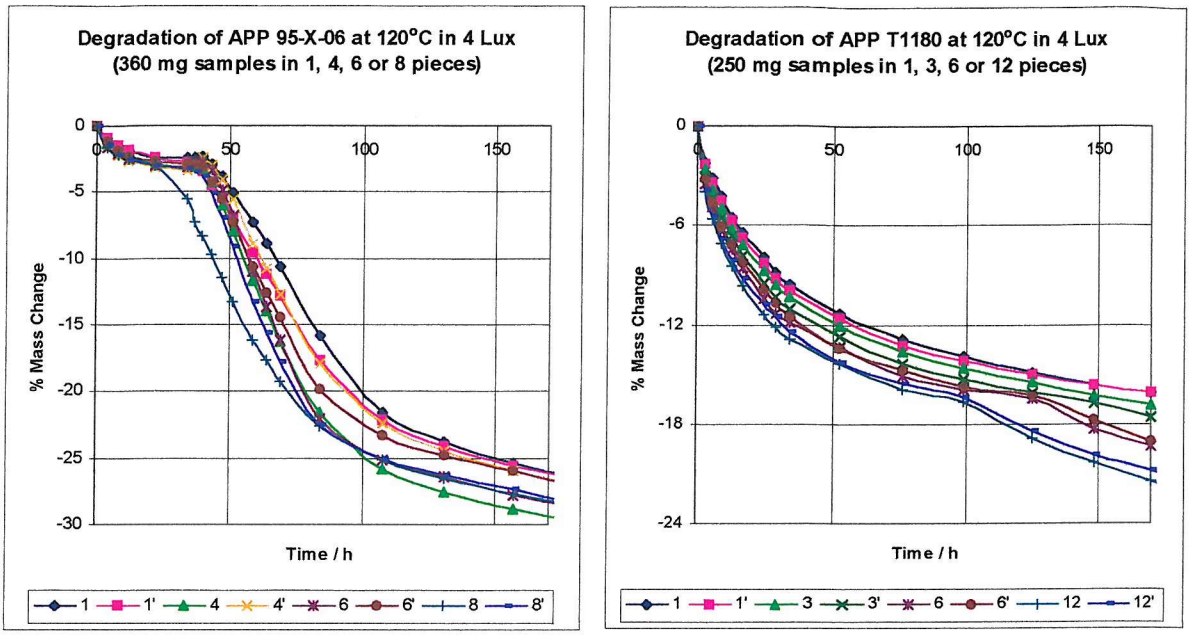

Fig.6.16. Degradation of Blends of 32C in 100 Pen Bitumen at 120°C in 4 Lux

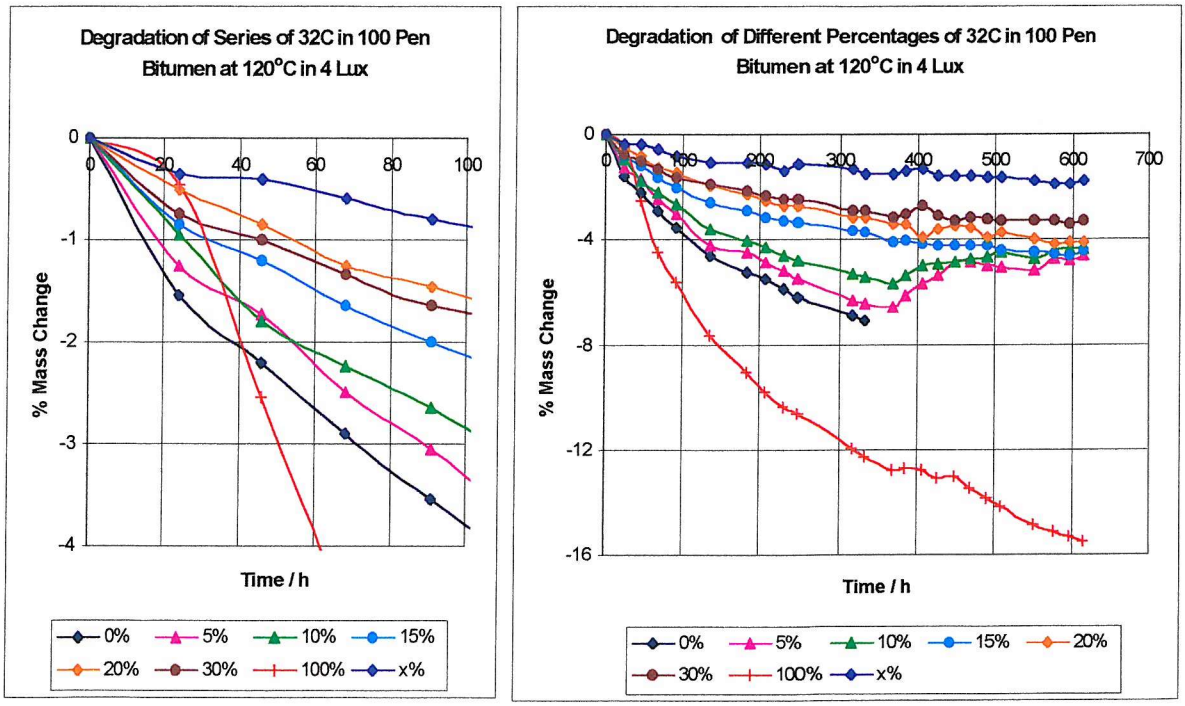

Fig.6.17. Variation of Degradation at 120°C with % 32C Content for Blends of 32C in 100 Pen Bitumen, after Different Times – (a) in 4 Lux, (b) in Darkness, with Exposure to about 4 Lux During Cooling

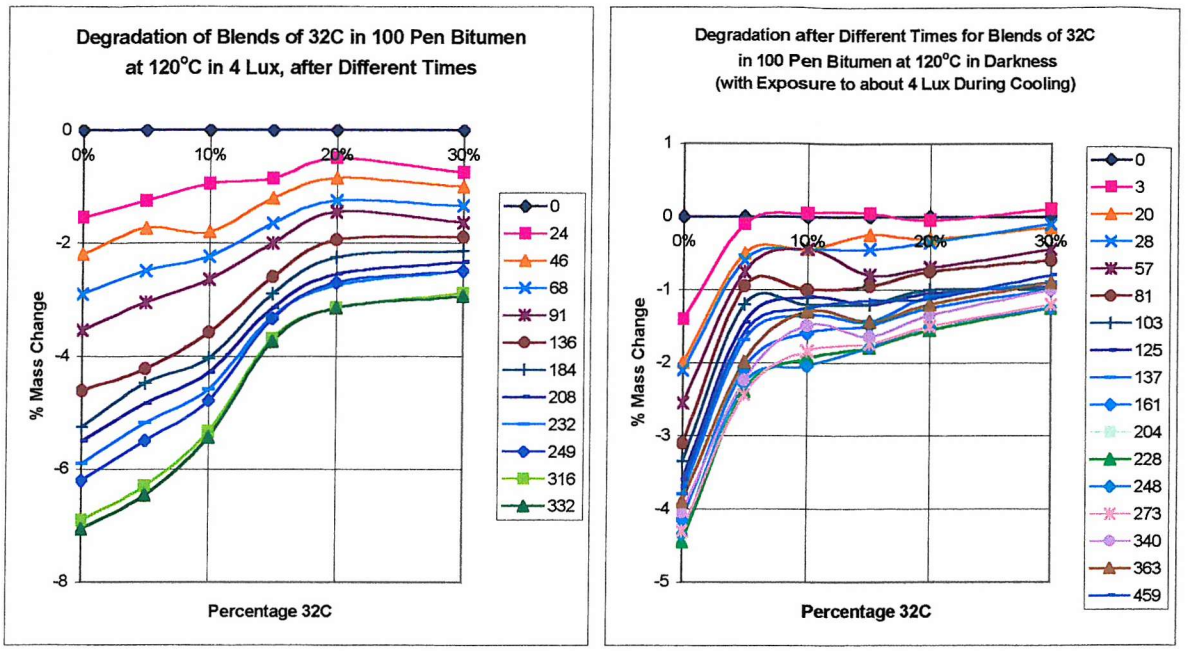

Fig.6.18. Degradation of Blends of 32C in 100 Pen Bitumen at 120°C in Darkness, with Exposure to about 4 Lux During Cooling

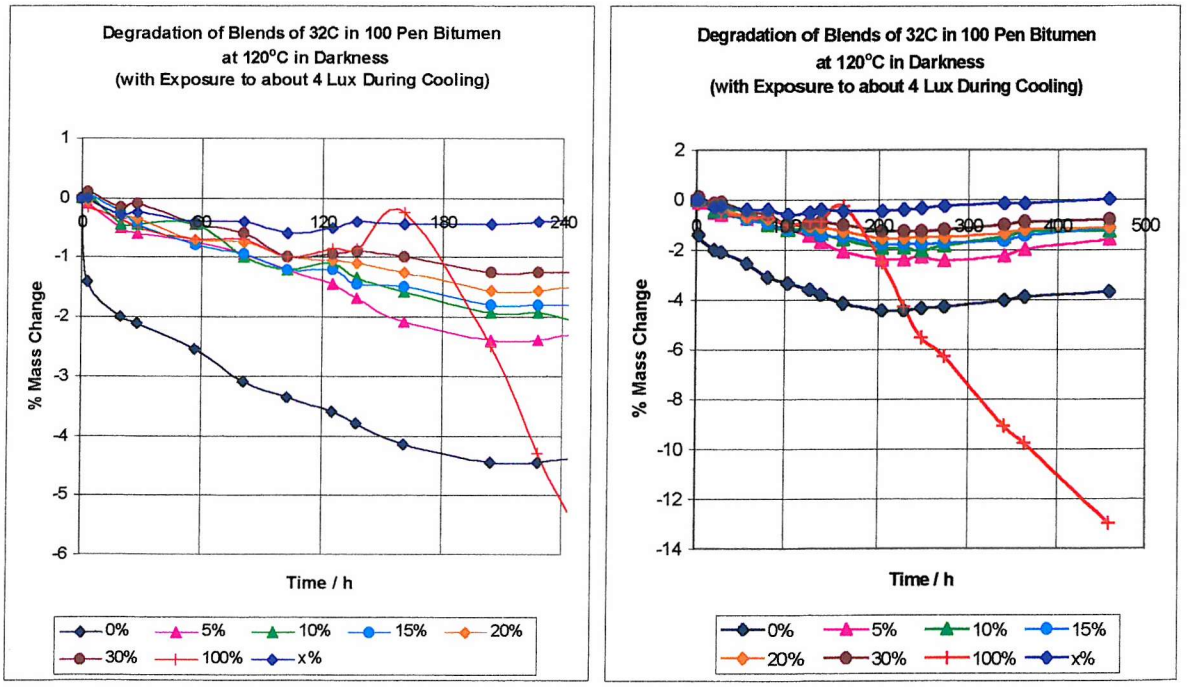

Fig.6.19. Degradation of 8 'APPs' in Duplicate at 120°C in Darkness, with Exposure to 4 Lux During Cooling: 1C, 32C, 43C, MF80, MF500, C80, T1180 and 95-X-06

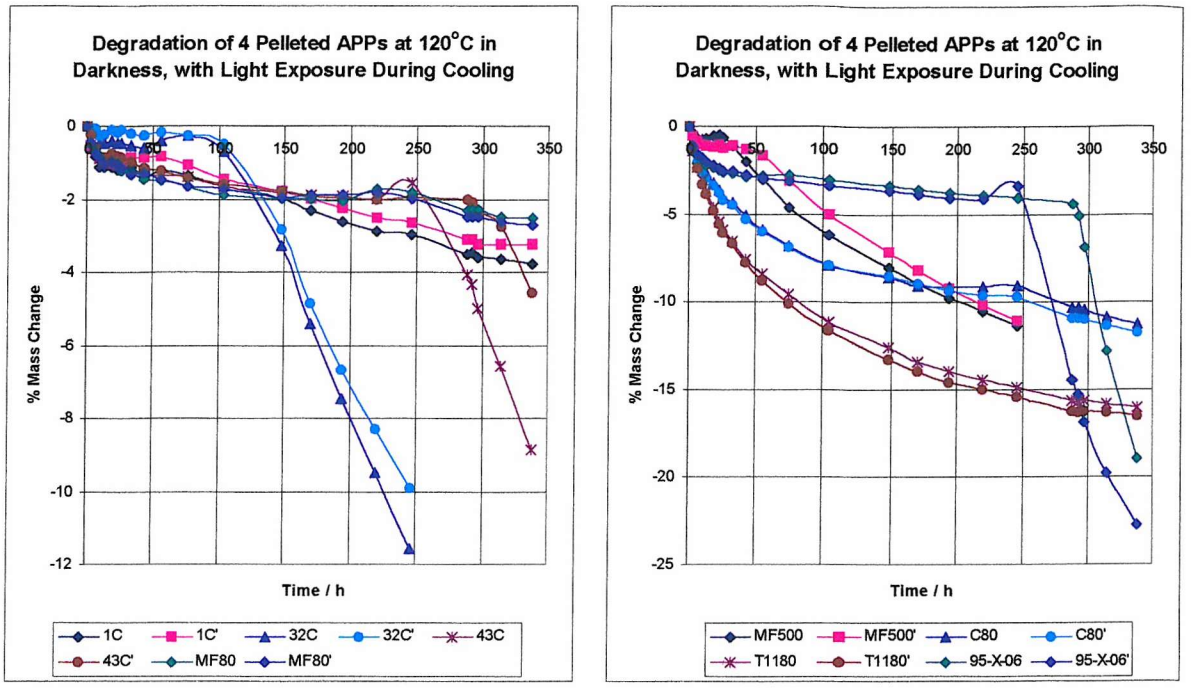

Fig.6.20. Degradation of 8 'APPs' in Duplicate at 120°C in Darkness, with Exposure to << 1 Lux During Cooling: 1C, 32C, 43C, MF80, MF500, C80, T1180 and 95-X-06

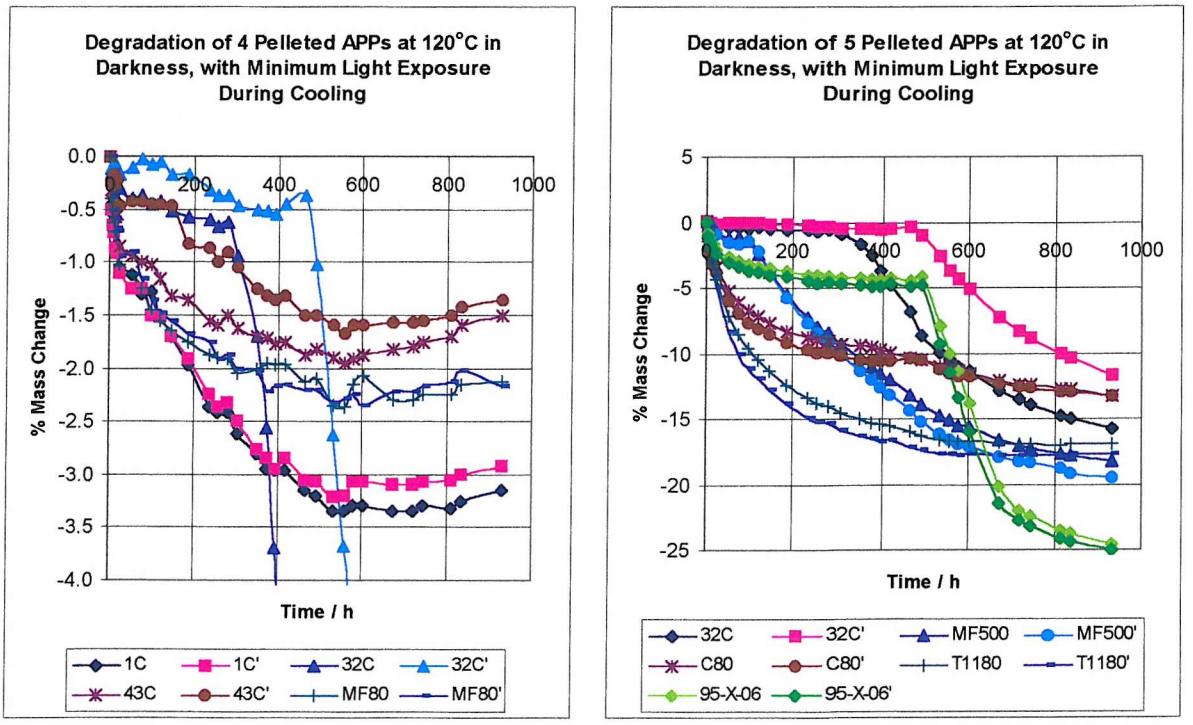

Fig.6.15. Degradation at 120°C in 4 Lux of 95-X-06 (360 mg in 8 Pieces) & T1180 (250 mg in 12 Pieces)

Fig.6.21. Dependance of APP Degradation at 120°C in Darkness upon Prior Light Exposure Conditions [1/5 cooled in tin, 4 cooled in 4 lux, 2/3 cooled in tin but heated in 4 lux at 120°C for 10/20 min before next heating]

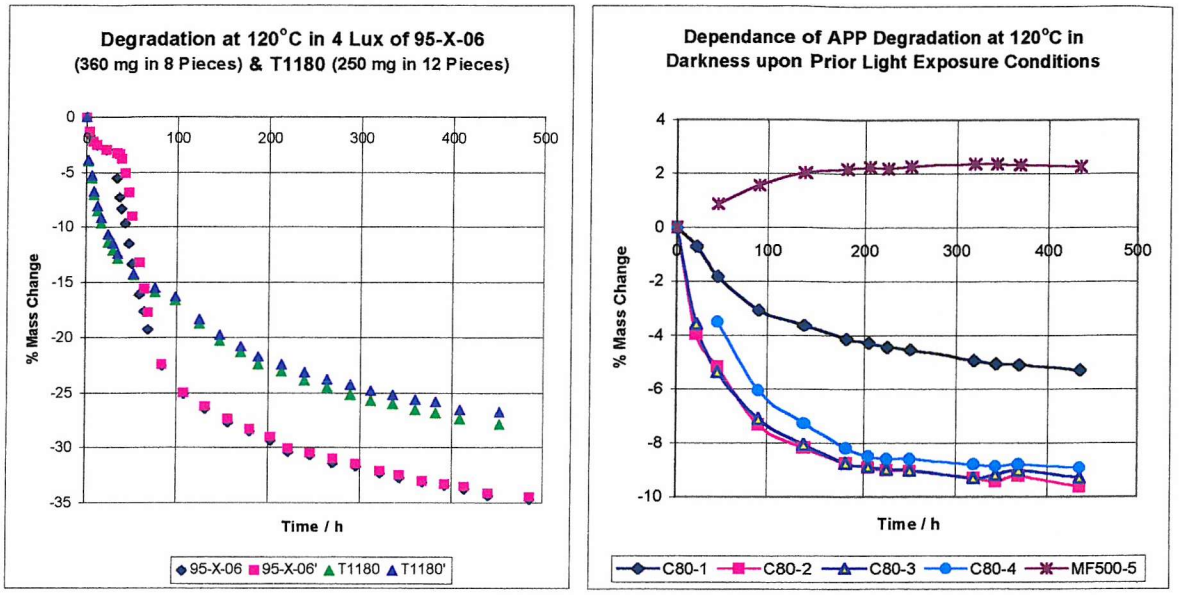

Fig.6.22. Degradation of 4 APPs at 120°C in a Sealed Tin – (a) APPs Affected in the Opposite Way to Oxidized Bitumen, (b) APPs Affected in the Same Way as Oxidized Bitumen

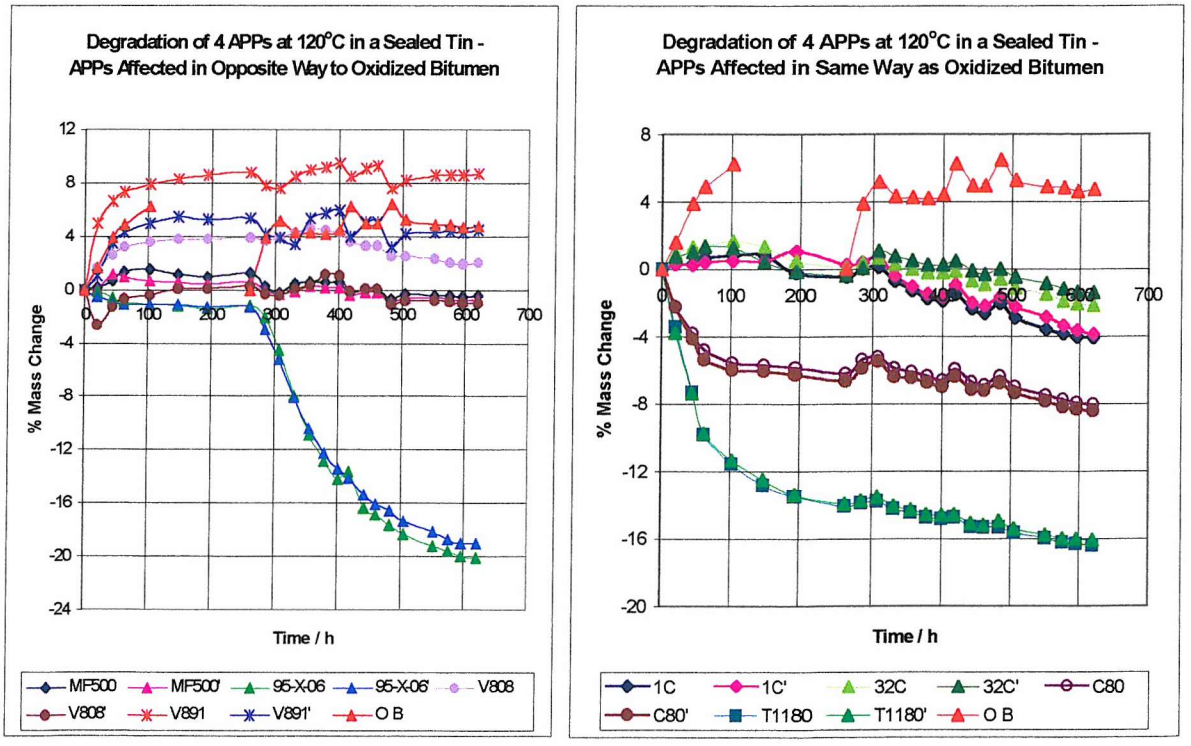

Fig.6.23. Degradation of 4 APPs – 1C, 32C, 43C and MF80 - at 120°C in 4 Lux after Preparations A, B and C

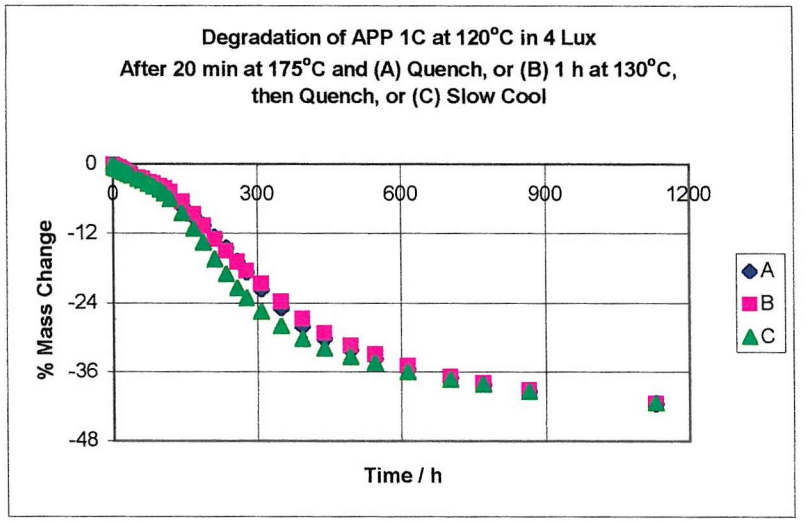

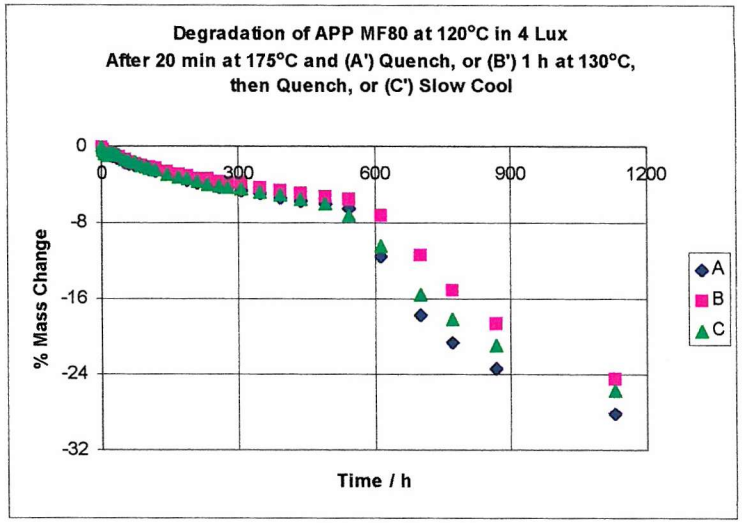

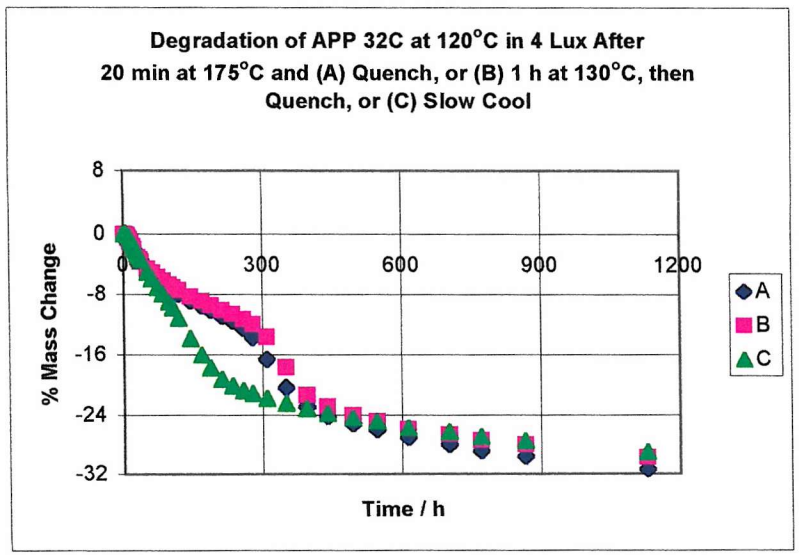

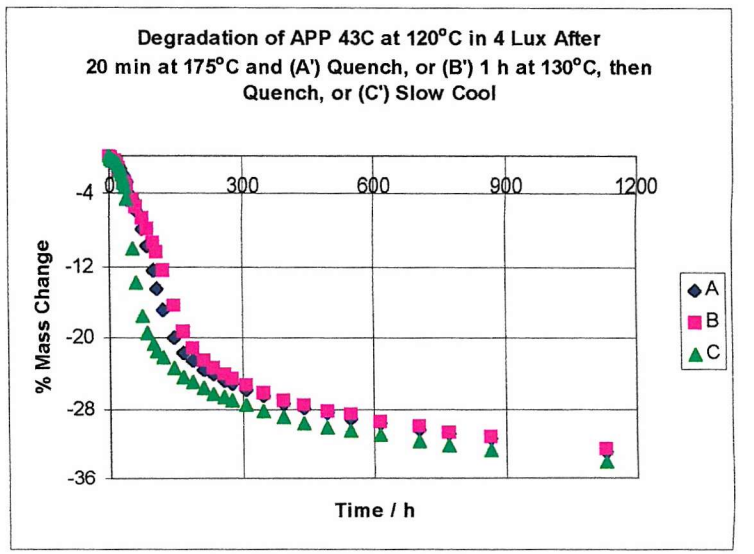

Fig.6.24. Degradation of 4 APPs – MF500, C80, T1180 and 95-X-06 - at 120°C in 4 Lux after Preparations A, B and C

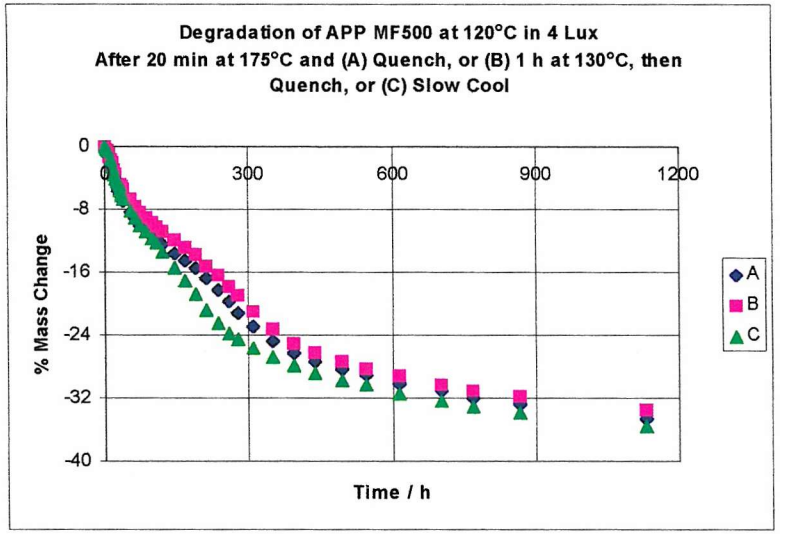

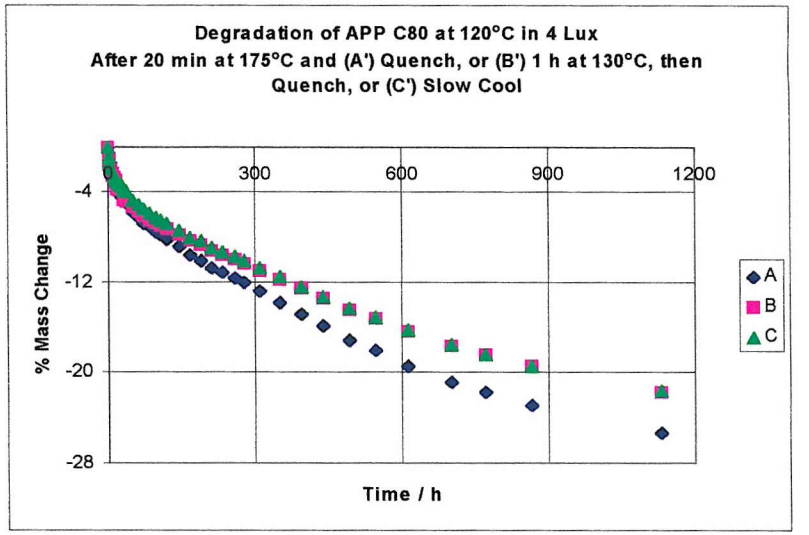

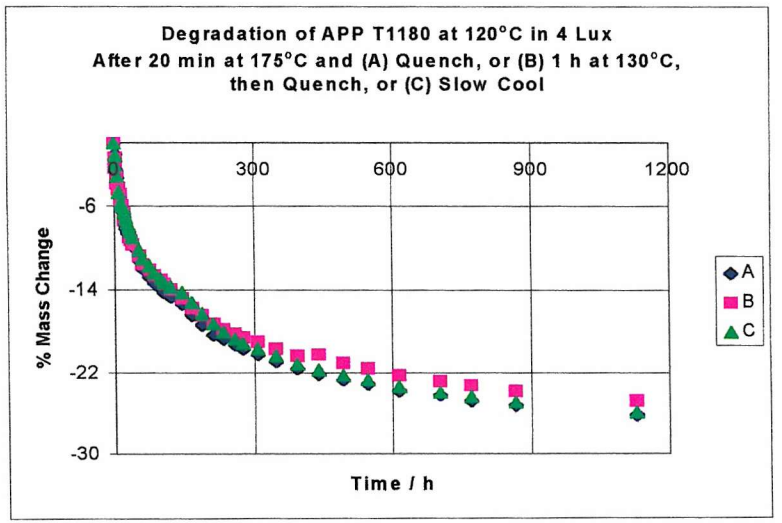

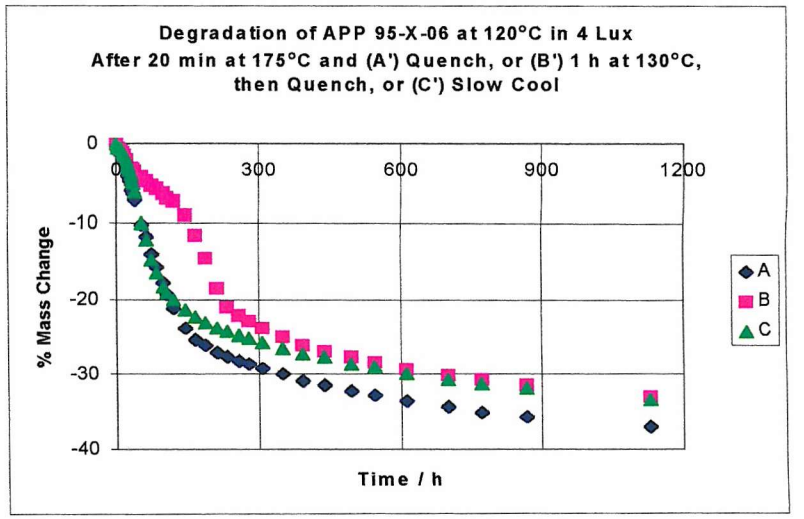

Fig.6.25. Degradation at 120°C of (a) V808 and (b)V891 in 4 Lux, and (c,d) 1C in Darkness, after Preparations A, B and C

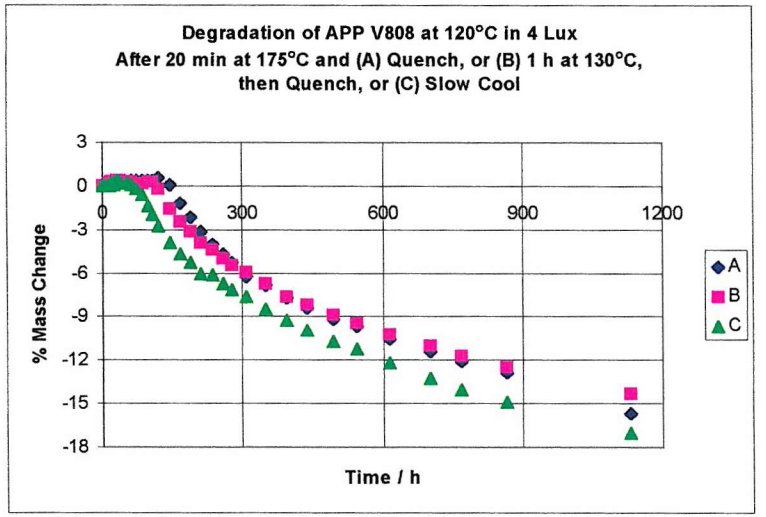

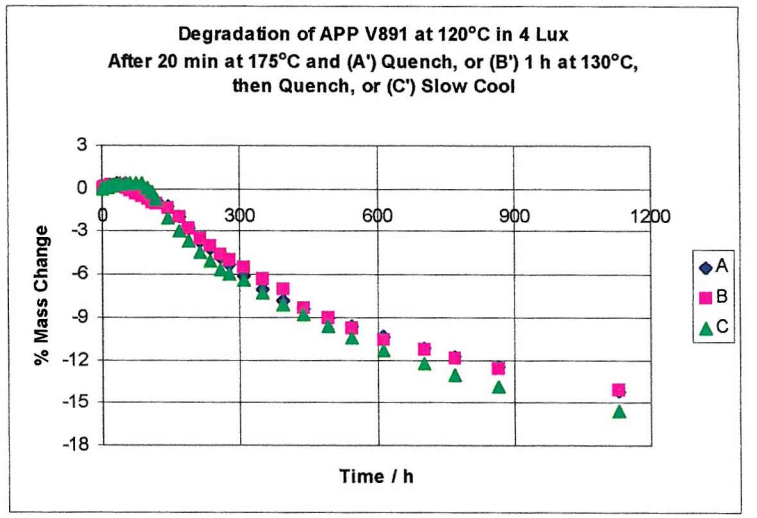

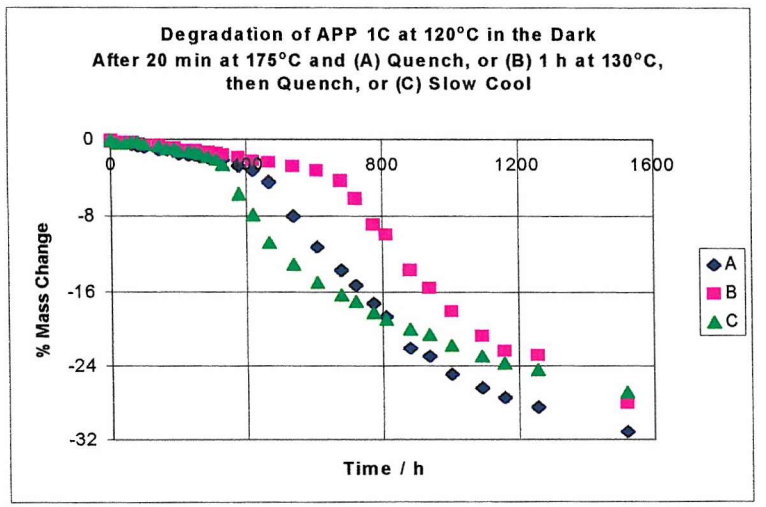

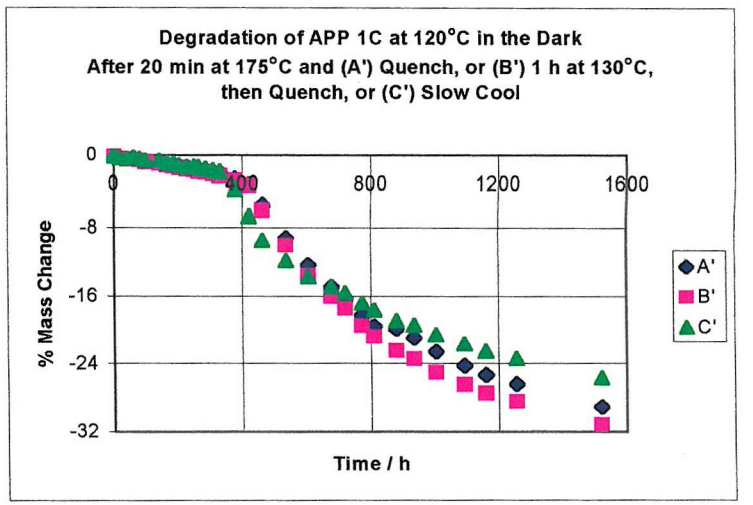

Fig.6.26. Degradation at 120°C of (a) 32C, (b) 43C, (c) MF80, (d) T1180 in Darkness, after Preparations A, B and C

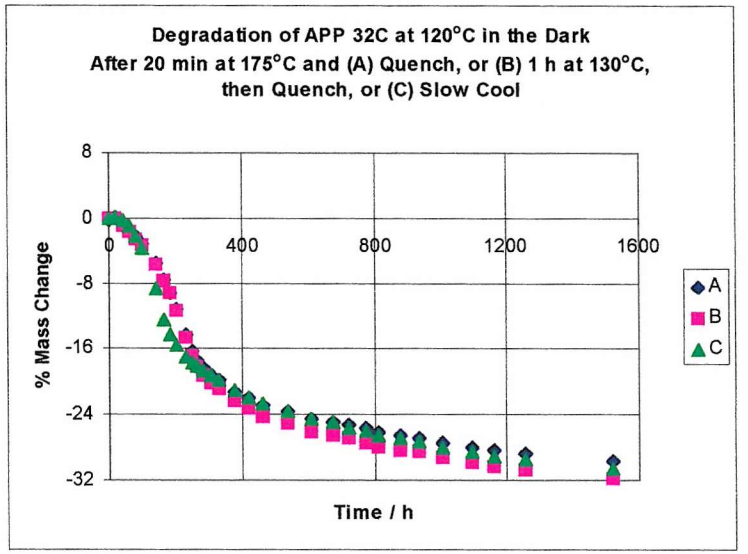

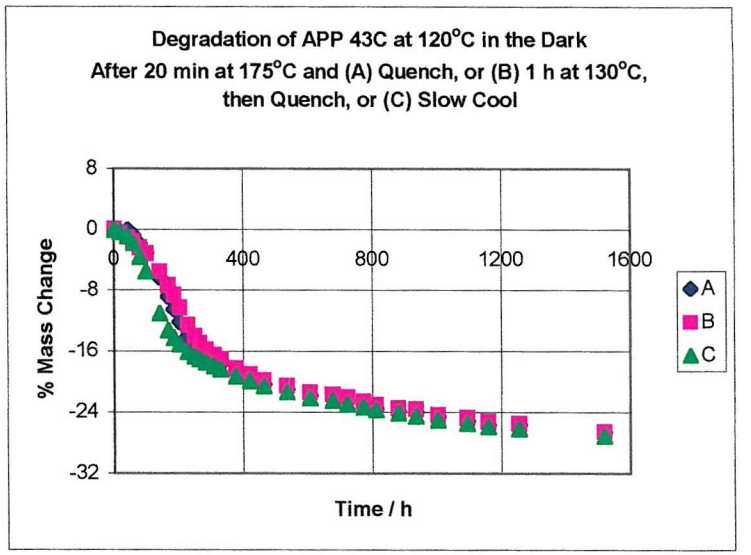

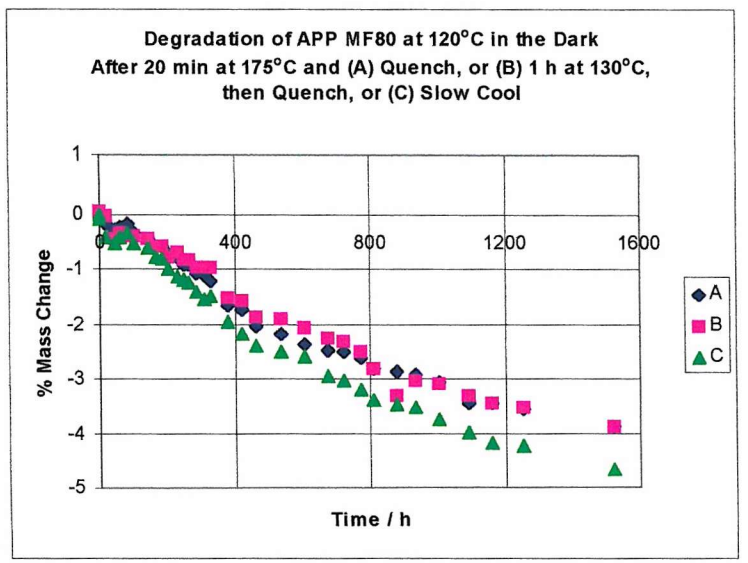

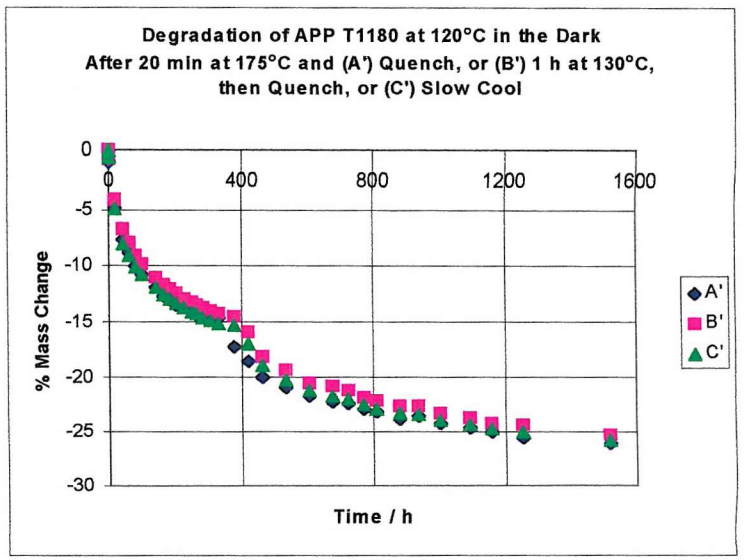

Fig.6.27. Degradation at 120°C of (a,b) MF500, (c,d) C80 in Darkness, after Preparations A, B and C

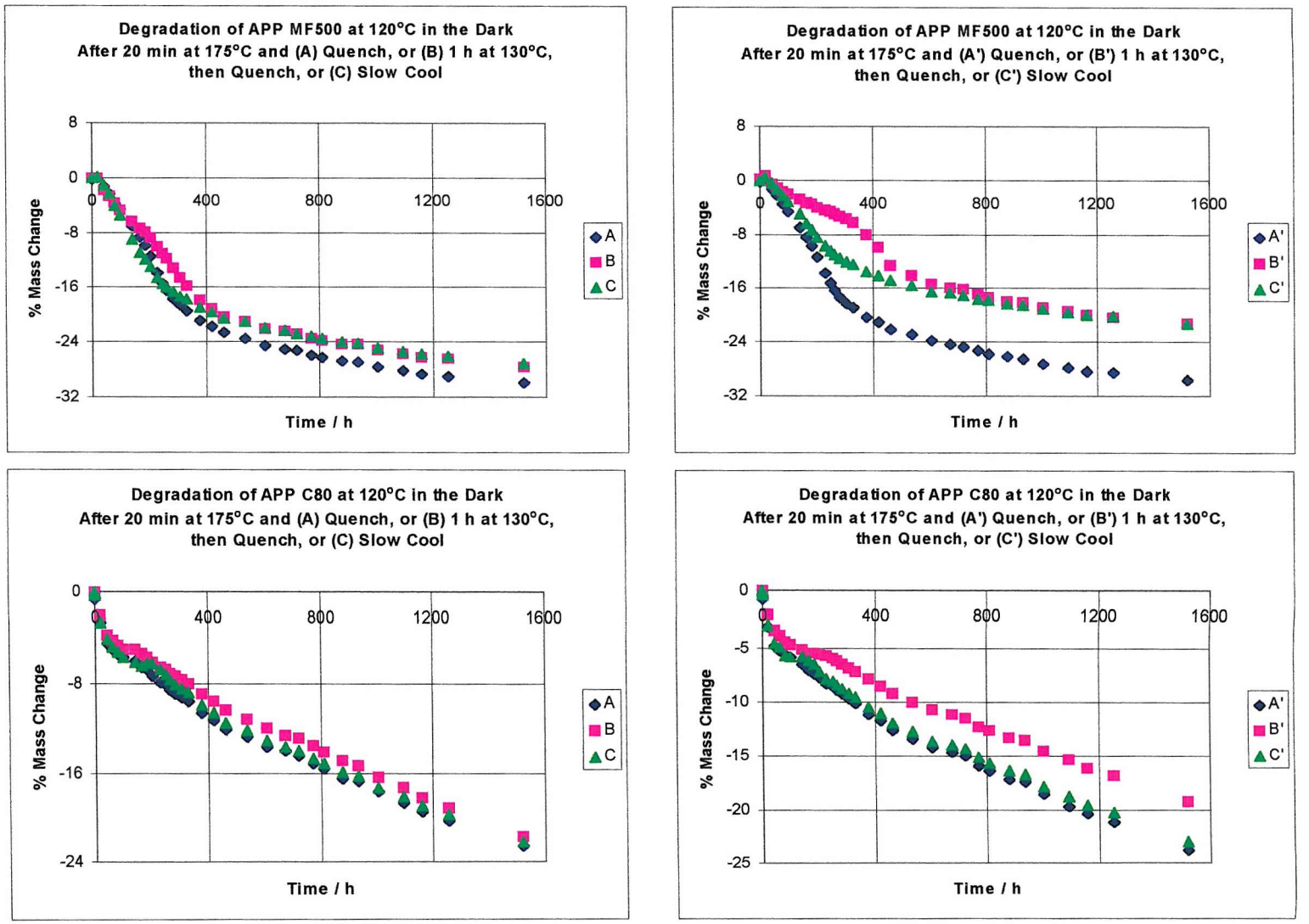

Fig.6.28. Degradation at 120°C of (a) 95-X-06, (b) V808, (c,d) V891 in Darkness, after Preparations A, B and C

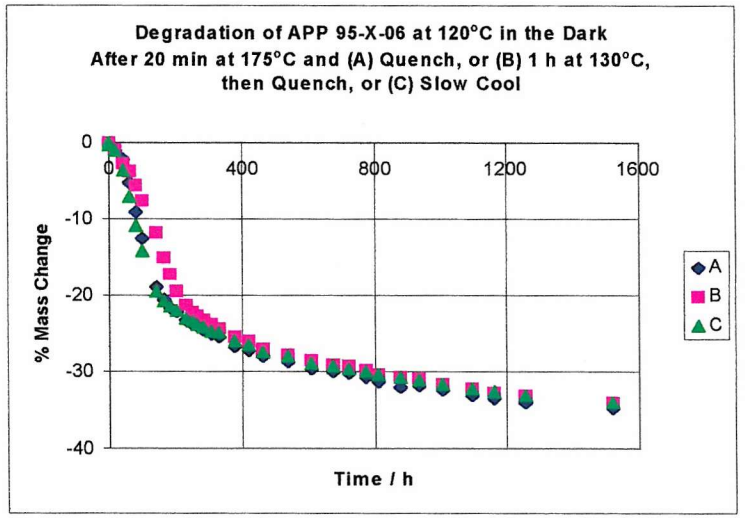

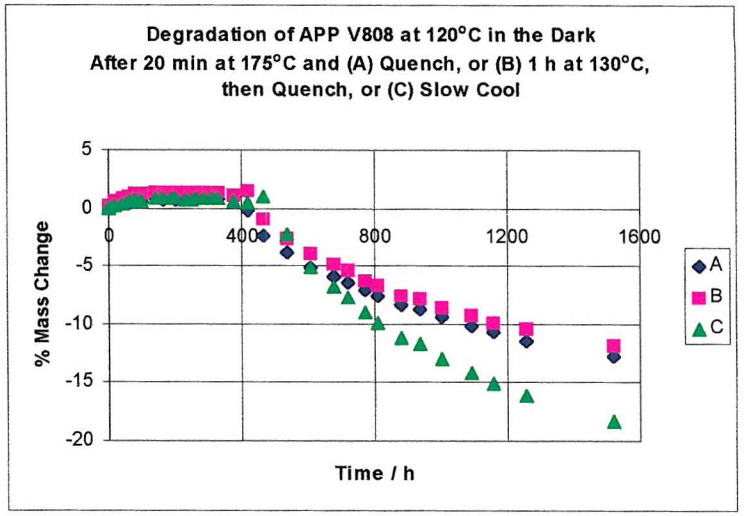

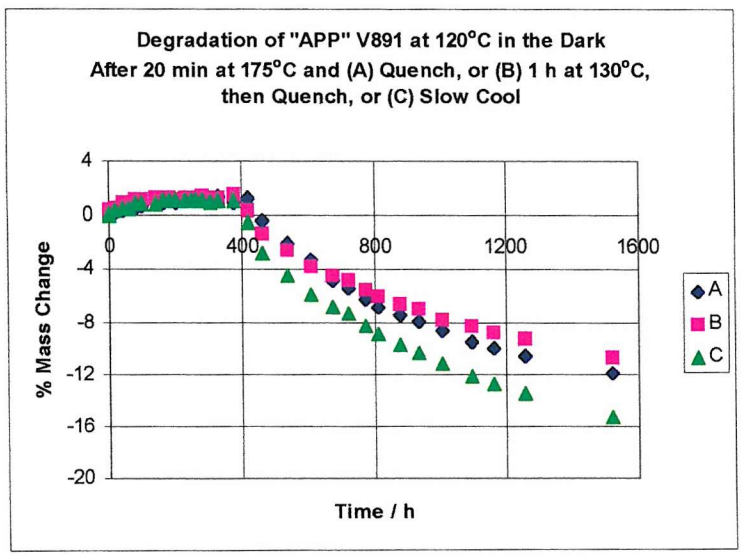

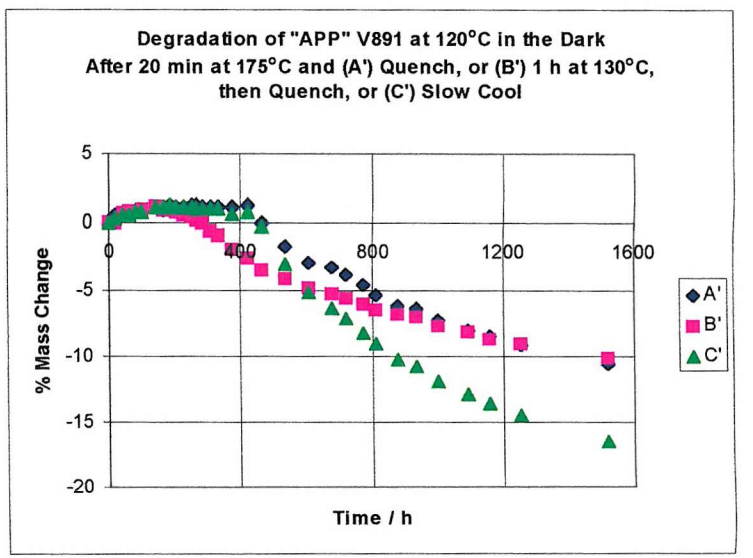

Fig.6.29. Predicted Attainment of Steady State in O_2 Links Between Amorphous APP Molecules During PSC/Degradation

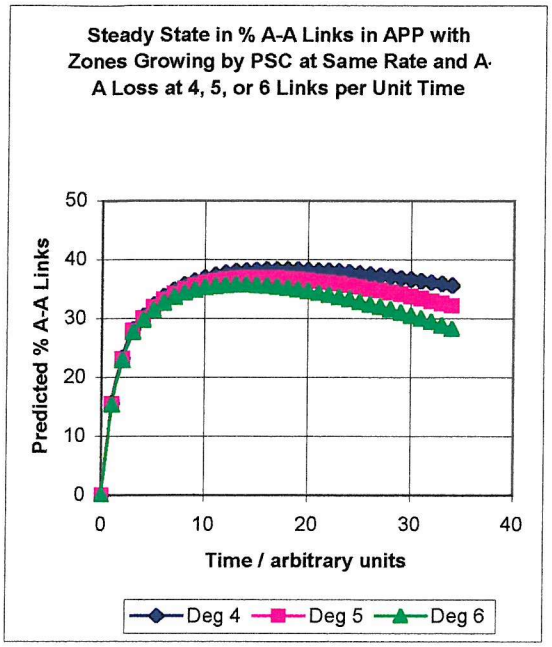

Fig.6.30a. Predicted Point of Change from Mainly A-O-O-X to Mainly A-O-O-A Links During Degradation of an APP Undergoing Fast PSC

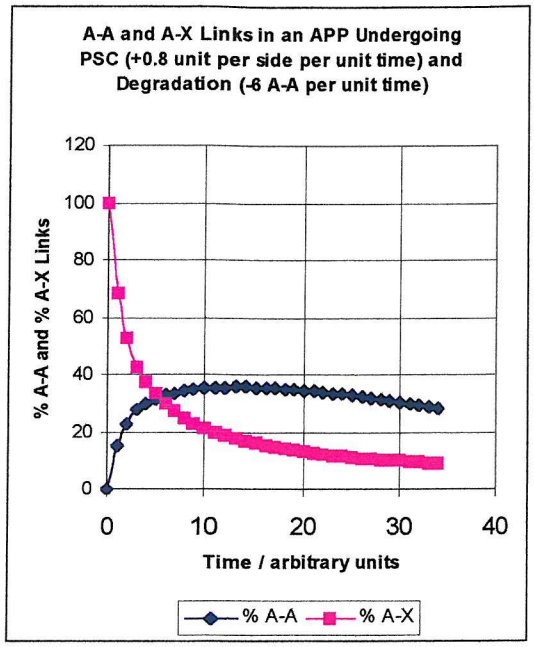

Fig.6.30b,c. Predicted Point of Change from Mainly A-O-O-X to Mainly A-O-O-A Links During Degradation of an APP undergoing (b) Medium PSC, and No Change-over for (c) Slow PSC

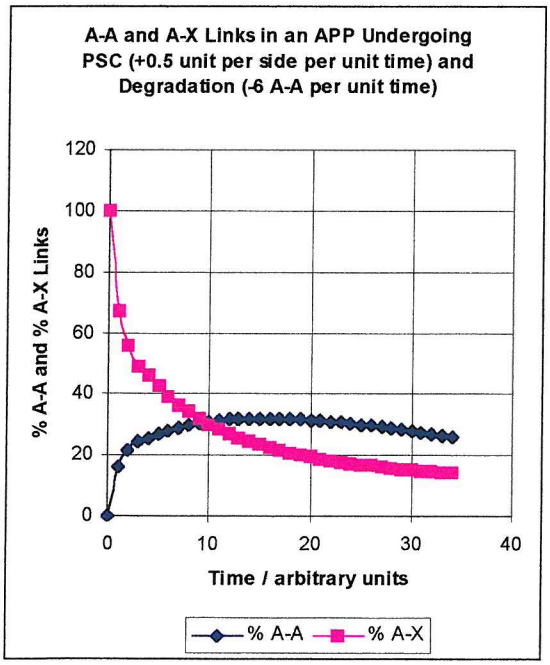

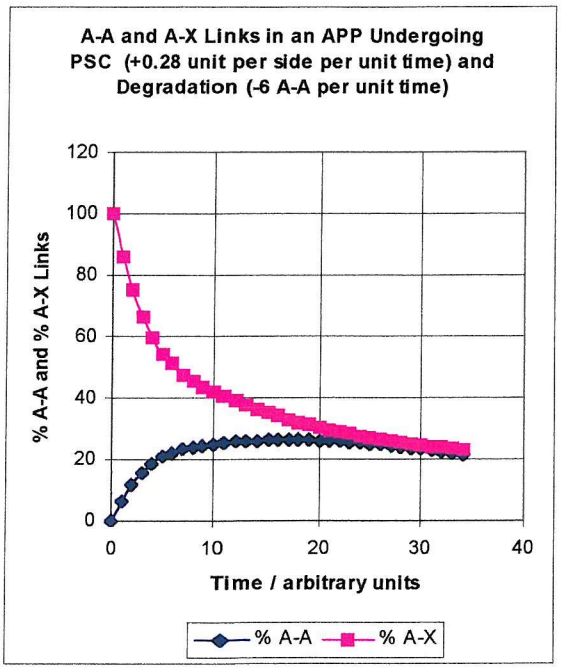

Fig.7.1. FT-Raman Spectra of 32C (A) Before and (E) After Heating at 120°C in Darkness and Daylight

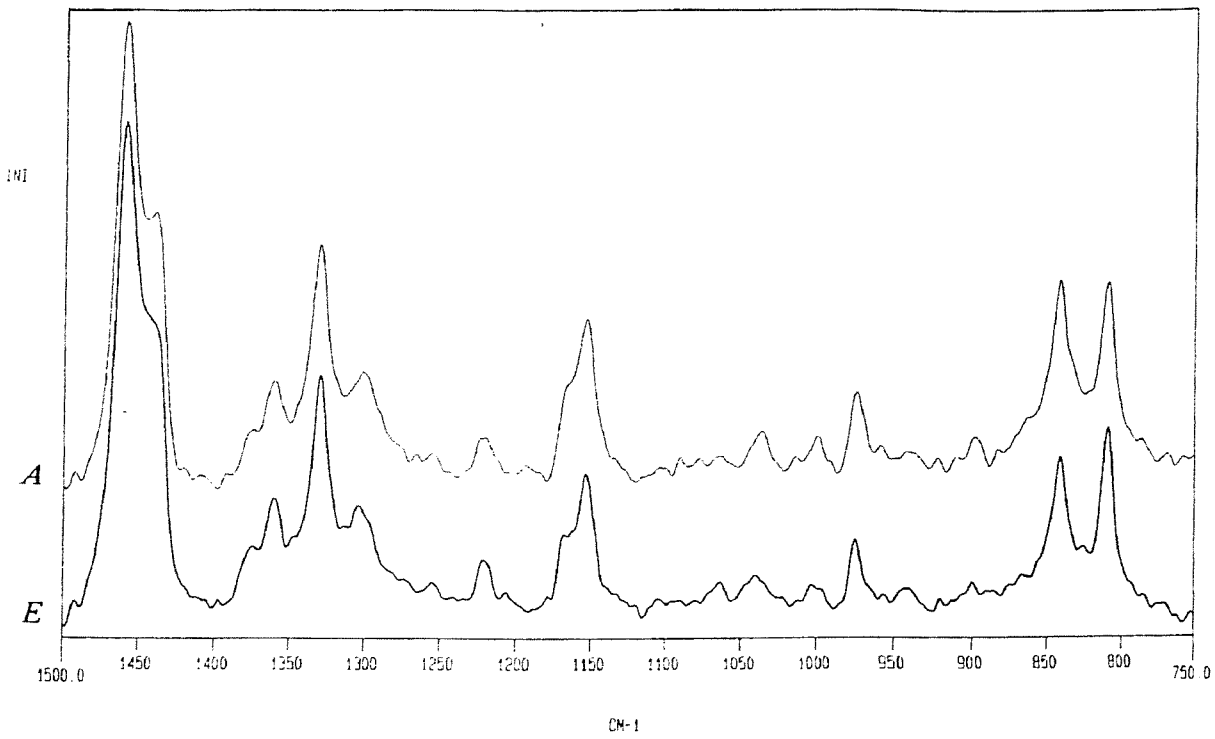

Fig.7.2. FT-Raman Spectra of Supplied 32C (B) Before and (A) After 716 h at 120°C in 5 Lux

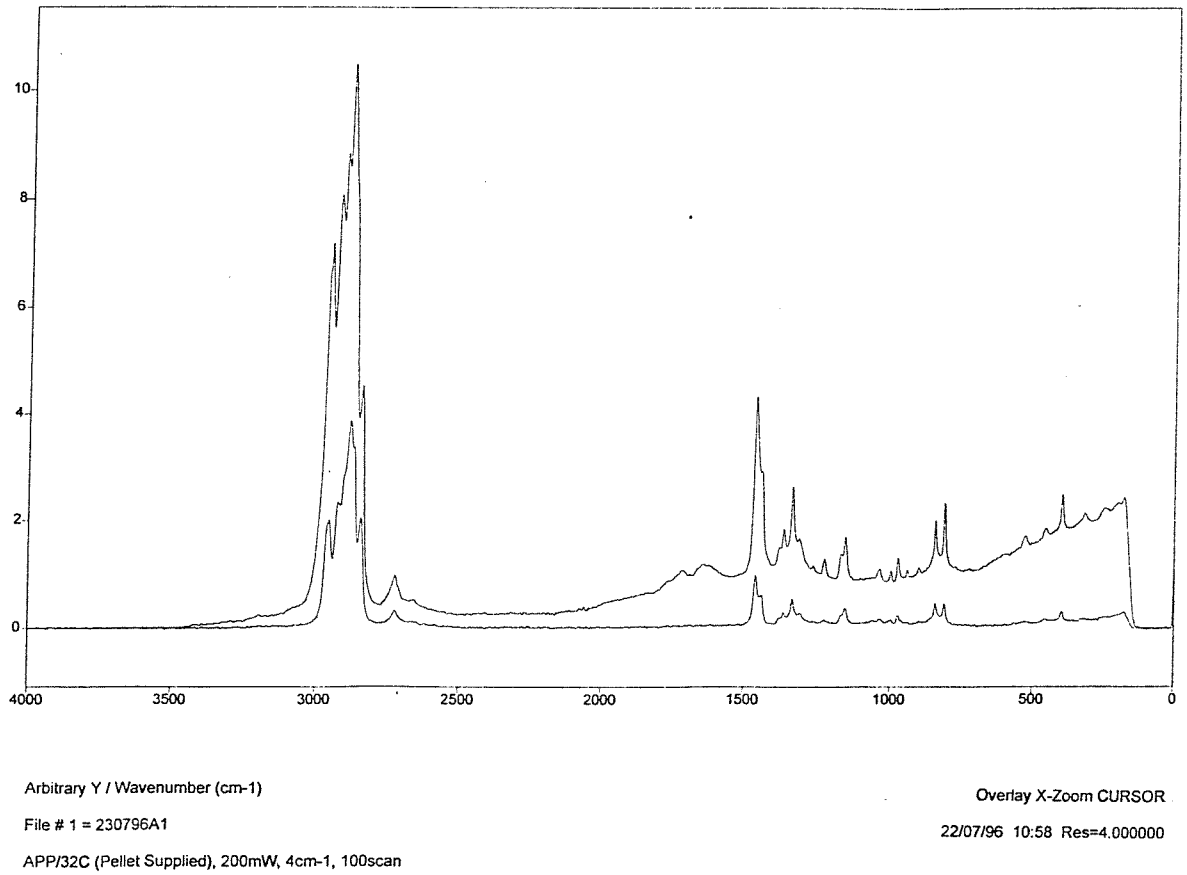

Fig.7.3. Monitoring of One FT-Raman Peak During Degradation of 'APP' 32C at 120°C in 5 Lux: (a) Peak Area and (b) Peak Height, with Maximum Values all Joined Up

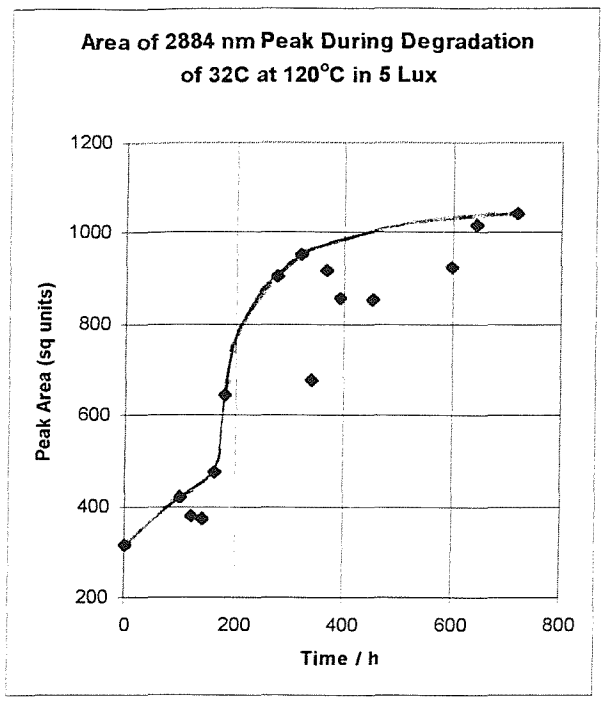

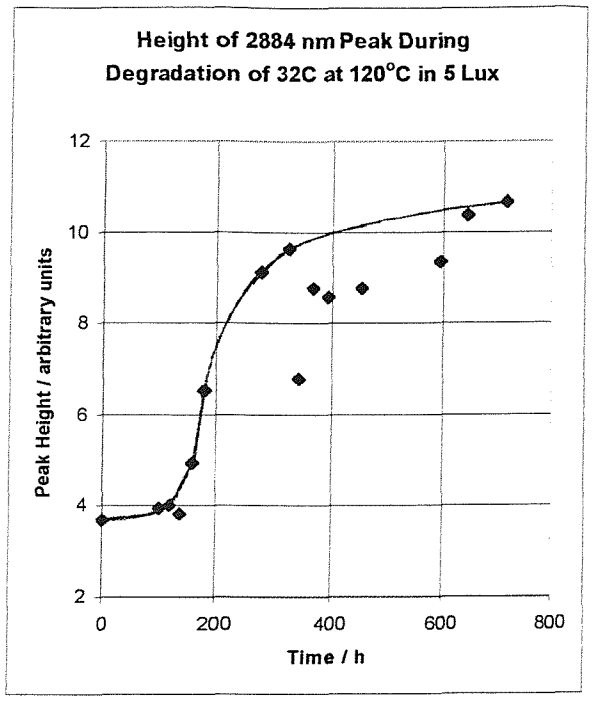

Fig.7.4. Monitoring of Degradation of 'APP' 32C at 120°C in 5 Lux: % Mass Loss Corresponding to Peak Area and Height Values (Fig.7.3)

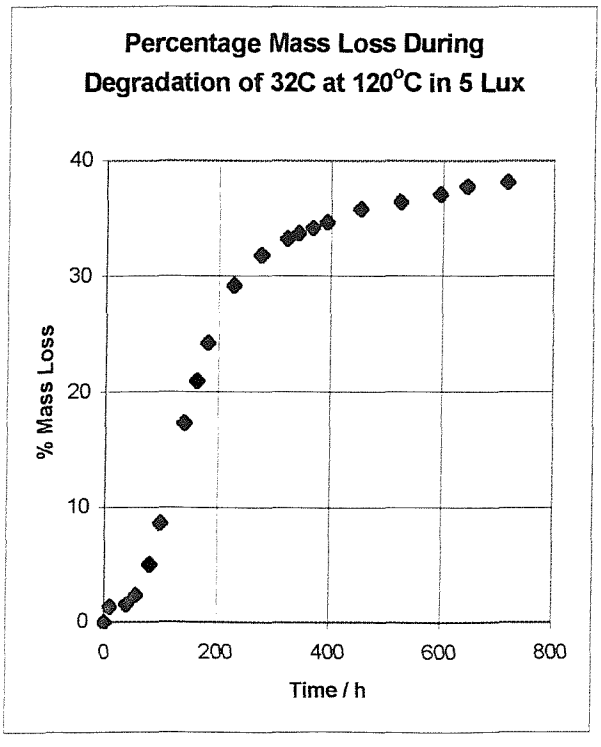

Fig.7.5a. Trial Chromatogram of Bitumen 200E on Iatroscan Mark II, after Development in Decreasing Polarity Solvents

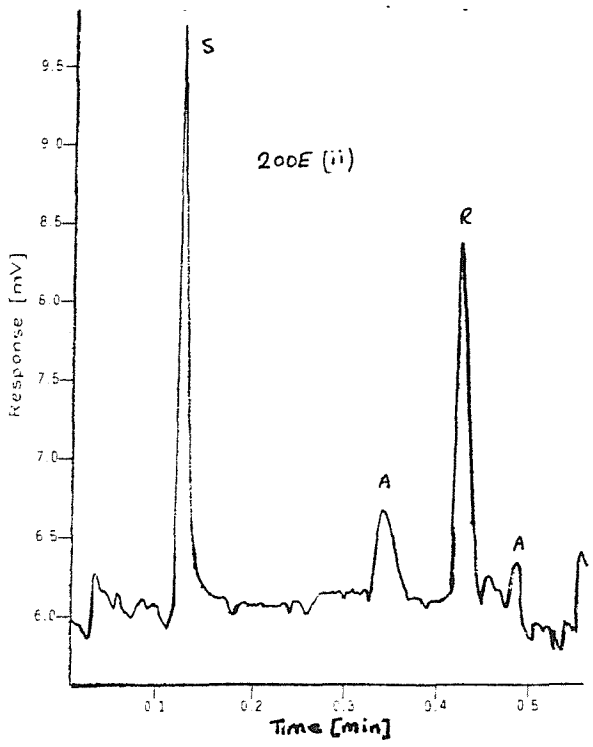

Fig.7.5b. Trial Chromatogram of Bitumen 200E on Iatroscan Mark II, after Development in Increasing Polarity Solvents

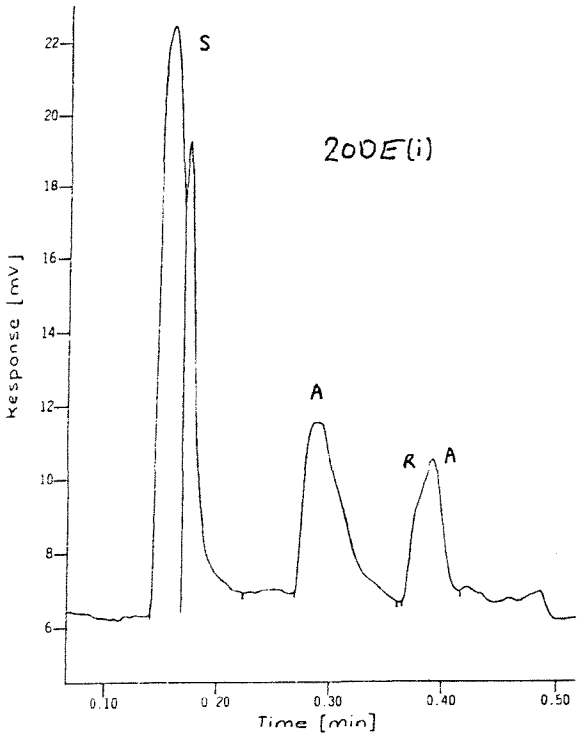

Fig.7.6. Trial Chromatogram of Bitumen X2 on Iatroscan Mark IV

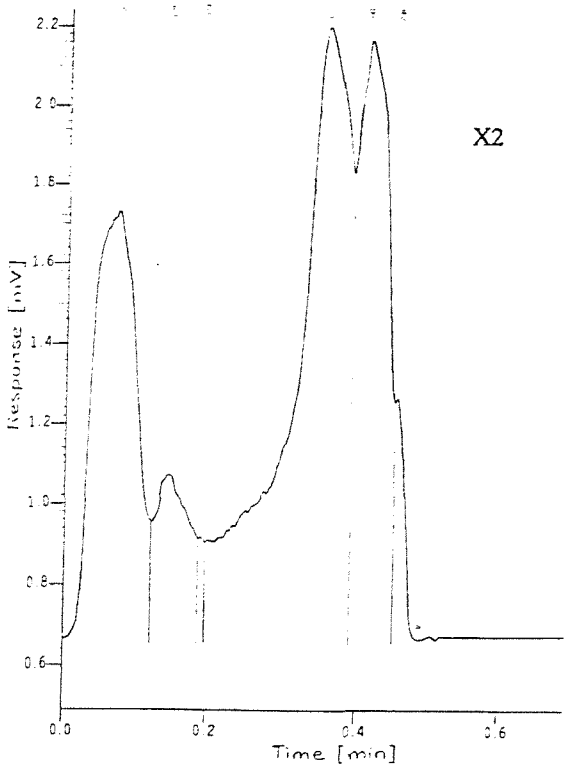

Fig.7.7a. Chromatogram of Bitumen X1 on Iatroscan Mark IV

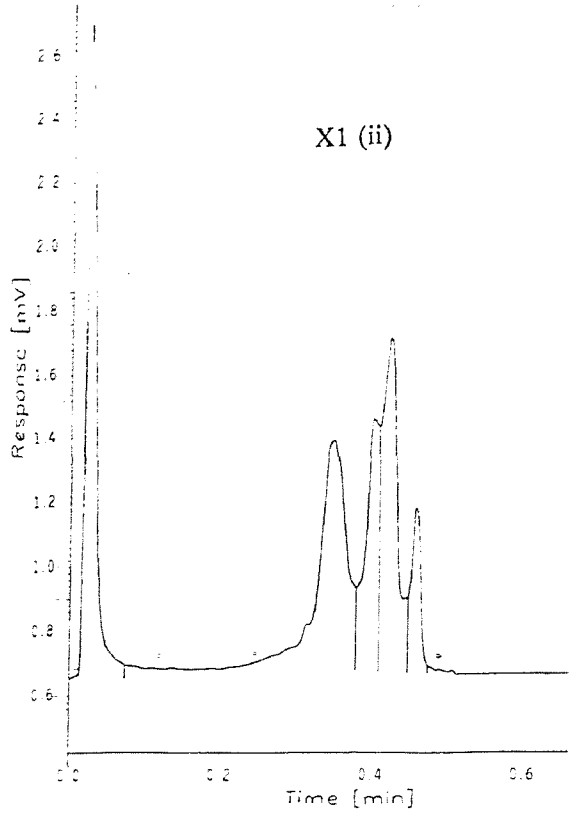

Fig.7.7b. Chromatogram of Bitumen 200 on Iatroscan Mark IV

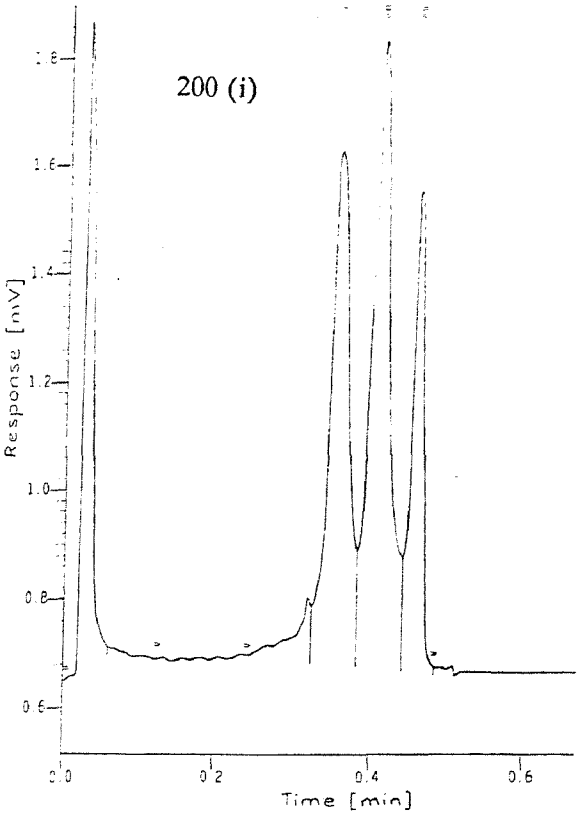

Fig.7.7c. Chromatogram of Bitumen 200E on Iatroscan Mark IV

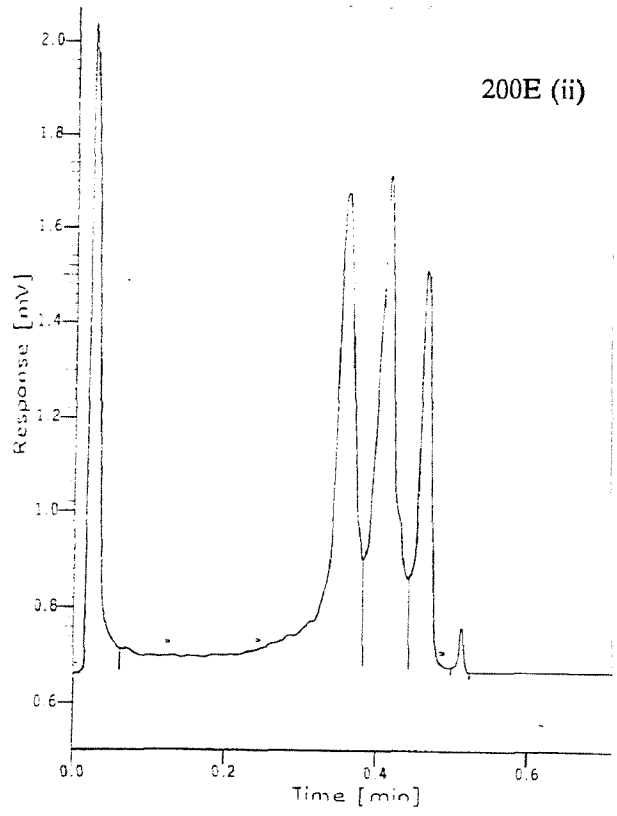

Fig.7.7d. Chromatogram of Bitumen X2 on Iatroscan Mark IV

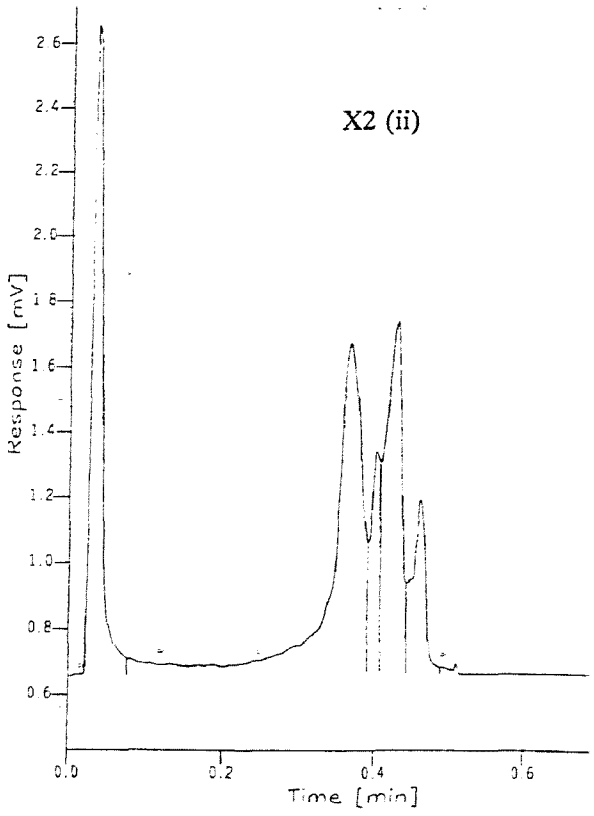

Fig.7.7e. Chromatogram of Bitumen 100 on Iatroscan Mark IV

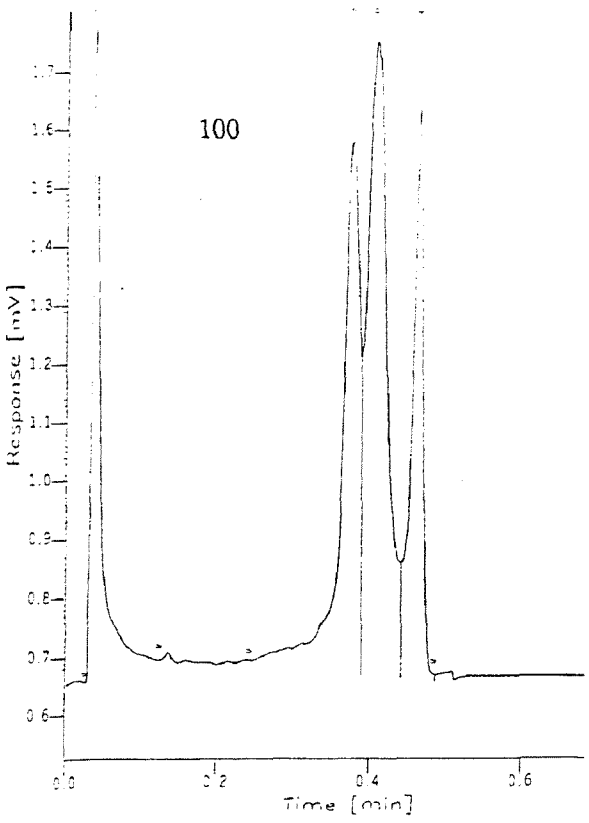

Fig.7.8. Chromatogram of Bitumen X2 in 2nd Analysis on Iatroscan Mark IV

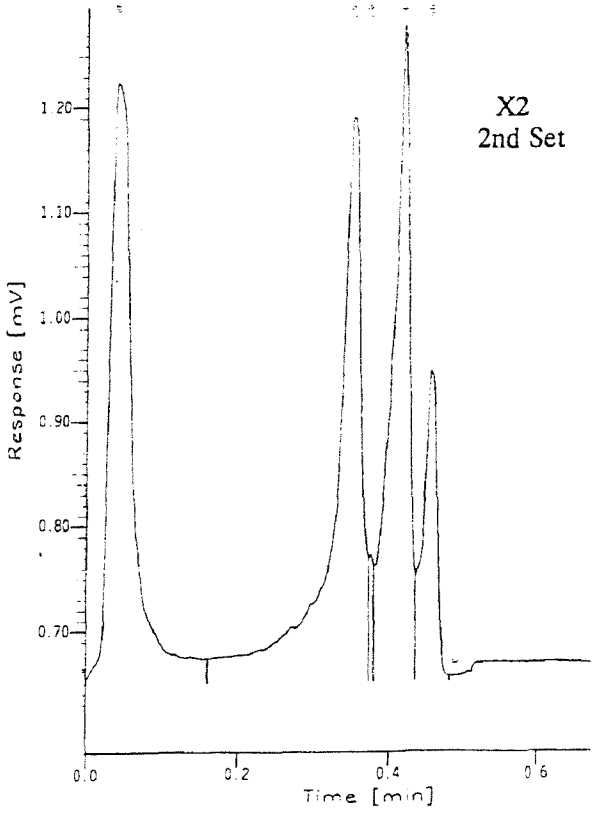

Fig.7.9. SARA Analysis of Bitumens: Saturates, Aromatics, Resins and Asphaltenes

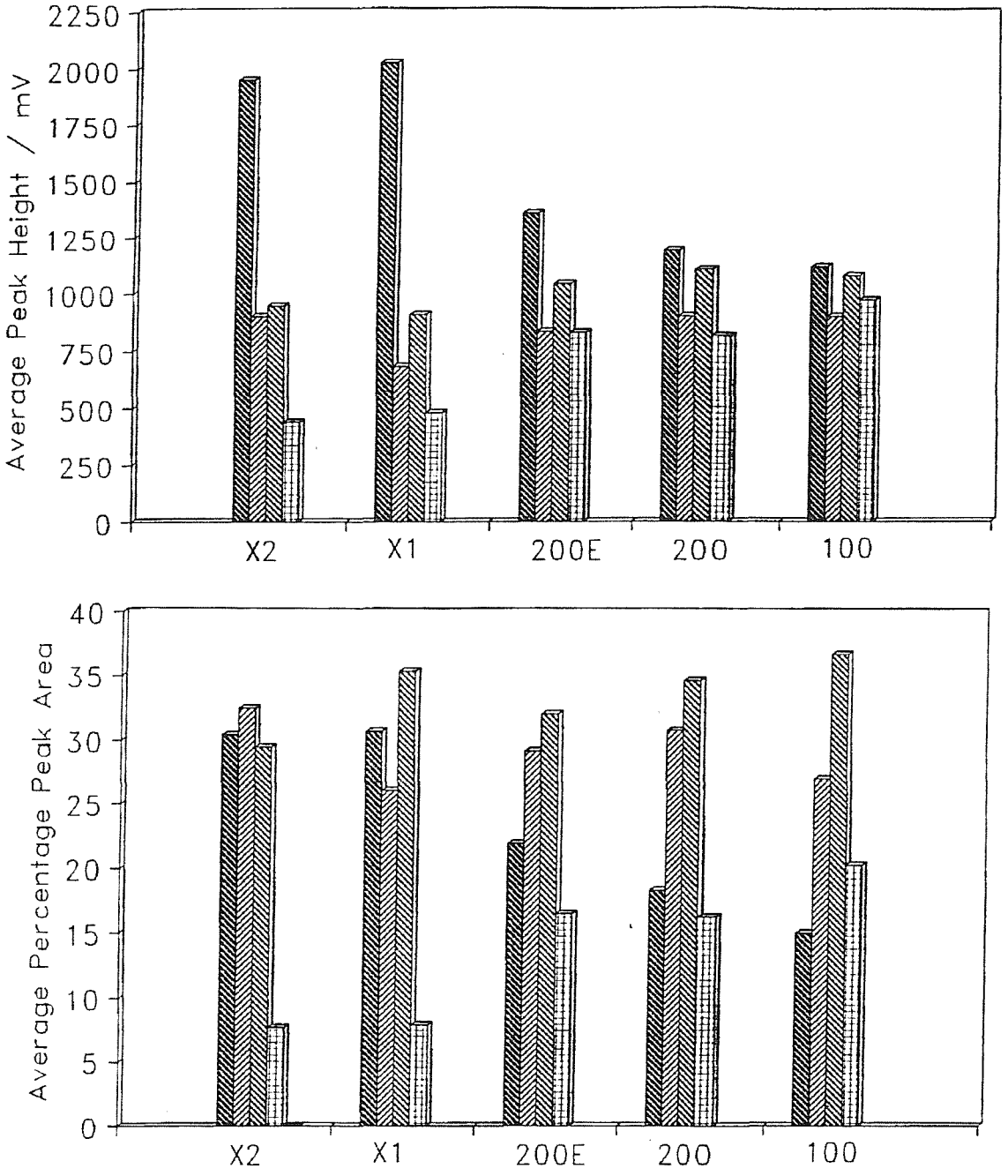

Fig.7.10. Photocopied Melts of Series of 32C in 100 Pen Bitumen (71% original size)

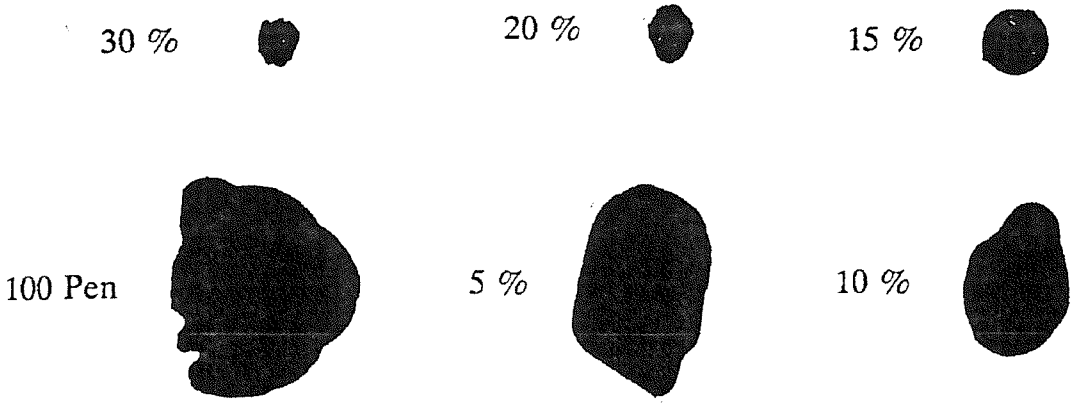

Fig.7.12. Crystals on the Surface of 5% 32C in 100 Pen Bitumen after Degradation at 120°C in the Dark for 125 h (with only a few seconds exposure to << 1 lux during cooling). Magnification × 9

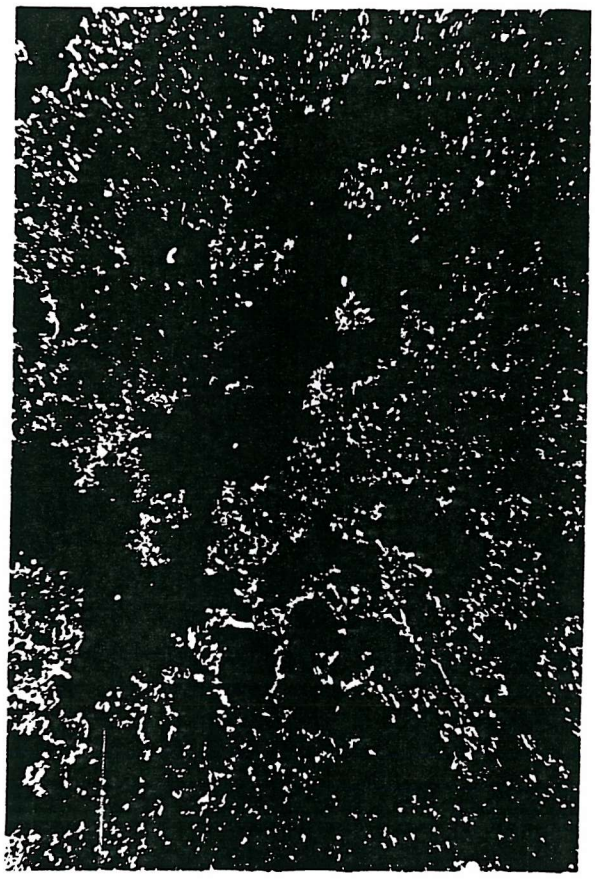

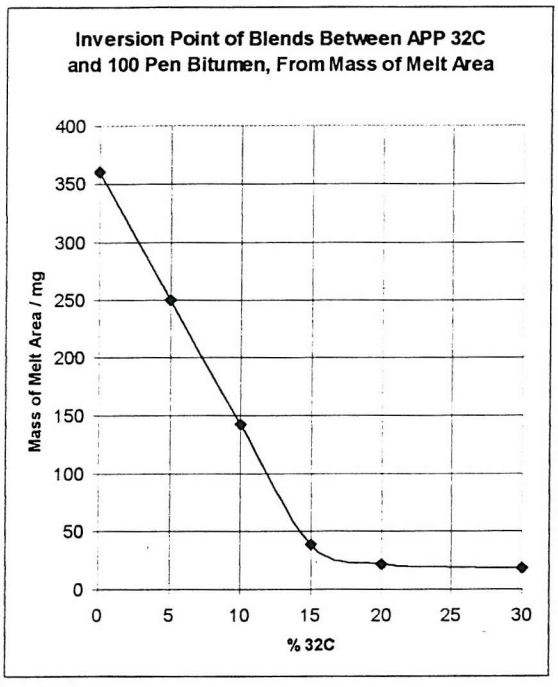

Fig.7.11. Inversion Point for Blends of APP 32C in 100 Pen Bitumen from Mass of Melt Area

APPENDIX

Degradation of 'APPs' and 'APP'-Modified Bitumens

Original 'APP' Pellets at 120°C in 4 Lux (9 pp)

8 'APPs' to 613 hours: 1C, 32C, 43C, MF80, MF500, C80, T1180, 95-X-06
Different Sizes of 95-X-06 and T1180
32C Set to 614 hours: 0, 5, 10, 15, 20, 30, 100% 32C in 100 Pen Bitumen
SBS Set to 614 hours (0, 9 and 13% SBS in 200 Pen Bitumen), SIS and PFSD
Preliminary Test on Effect of Sample Size and Preparation

Original 'APP' Pellets at 120°C in Darkness (7 pp)

8 'APPs' to 338 Hours:
(A) Some Light Exposure During Cooling Before Weigh-In
8 'APPs' to 930 Hours:
(B) Minimum Light Exposure During Cooling Before Weigh-In
Test of Dependence upon Prior Light Exposure Conditions
32C Set to 459 Hours: 0, 5, 10, 15, 20, 30, 100% 32C in 100 Pen Bitumen

Pre-Treated 'APPs' (Sets A, B and C) at 120°C in 4 Lux (10 pp)

Degradation up to 1130 hours:

1C and MF80	32C and 43C
MF500 and C80	T1180 and 95-X-06
V808 and V891	

Pre-Treated 'APPs' (Sets A, B and C) at 120°C in the Dark (12 pp)

Long-Term Degradation up to 1520 hours:
1C, 32C, 43C, MF80, MF500, C80, T1180, 95-X-06, V808 and V891

Degradation up to 620 Hours, Sealed in Airtight, Light-Tight Container:
1C, 32C, 43C, MF80, MF500, C80, T1180, 95-X-06, V808 and V891,
plus Oxidized Bitumen

Degradation of 8 Pelleted APPs at 120°C in 4 Lux

Controlled light level in vacuum oven below fume cupboard. Samples were supplied pellets, not heat-treated. Layout: COSSH 7:p.27
2 slides for each APP, with 2*180 mg per slide. So duplicates for verification, and high mass for accuracy. Set-up enclosed in black polythene.
Data: COSSH 6: 75-78 and 7: 13-14, 23, 27-28 Repeat of Expt. COSSH 6: 58-61, 74. Lit by Anglepoise lamp with Philip's 60w Floodline bulb.

Time / h	1C	1C'	32C	32C'	43C	43C'	MF80	MF80'	MF500	MF500'	C80	C80'	T1180	T1180'	95-X-06	95-X-06'
0.00	0.00	0.00	0.00	0.00	0.00	0.00	0.00	0.00	0.00	0.00	0.00	0.00	0.00	0.00	0.00	0.00
3.00	-0.58	-0.50	-0.11	-0.06	-0.28	-0.14	-0.33	-0.42	-0.11	0.08	-1.50	-1.23	-1.58	-1.64	-0.80	-0.66
6.00	-0.83	-0.69	-0.22	-0.17	-0.61	-0.53	-0.61	-0.58	-0.14	0.06	-2.49	-2.12	-3.11	-3.17	-1.19	-0.75
10.00	-0.86	-1.03	-0.36	-0.28	-0.58	-0.64	-0.89	-0.86	-0.14	0.08	-3.32	-2.87	-4.08	-4.06	-1.16	-0.94
14.00	-0.91	-1.14	-0.03	0.06	-0.89	-0.78	-0.97	-0.94	-0.28	-0.39	-4.01	-3.51	-5.18	-5.15	-1.47	-1.02
22.00	-1.08	-1.33	-0.25	-0.22	-0.97	-0.86	-1.08	-0.97	-0.89	-0.97	-4.90	-4.40	-6.68	-6.82	-1.52	-1.08
27.00	-1.22	-1.52	-0.75	-0.78	-1.03	-0.94	-1.14	-1.14	-1.45	-1.47	-5.51	-4.90	-7.57	-7.65	-1.60	-1.13
32.00	-1.42	-1.69	-1.33	-1.33	-1.17	-0.97	-1.20	-1.14	-2.00	-1.98	-5.98	-5.29	-8.10	-8.43	-1.83	-1.27
49.00	-1.92	-2.10	-3.33	-3.11	-0.92	-1.17	-1.25	-1.22	-3.42	-3.37	-6.64	-6.07	-10.15	-10.29	-2.21	-1.49
73.00	-2.39	-2.68	-5.02	-4.76	-3.56	-3.95	-1.53	-1.50	-4.81	-4.62	-7.48	-6.88	-12.48	-12.72	-2.85	-2.21
96.00	-3.00	-3.43	-6.26	-5.98	-6.44	-6.61	-1.50	-1.58	-5.79	-5.51	-8.17	-7.52	-13.86	-13.86	-7.19	-4.62
121.50	-3.72	-4.21	-7.37	-7.04	-9.08	-9.26	-1.50	-1.55	-6.59	-6.18	-8.72	-8.02	-14.75	-14.72	-15.44	-10.35
145.00	-4.61	-5.20	-8.29	-7.90	-11.17	-11.01	-1.86	-1.66	-7.32	-6.96	-9.27	-8.58	-15.50	-15.39	-21.78	-16.19
167.00	-5.55	-6.17	-9.20	-8.65	-13.03	-12.59	-2.17	-1.91	-8.01	-7.65	-9.80	-9.05	-16.05	-15.92	-25.35	-20.68
191.00	-6.44	-7.06	-9.87	-9.37	-14.75	-14.15	-2.36	-2.16	-8.57	-8.18	-10.27	-9.47	-16.33	-16.28	-27.28	-23.91
216.00	-7.72	-8.30	-10.73	-10.23	-16.72	-15.87	-2.61	-2.49	-9.27	-8.90	-10.71	-10.05	-17.13	-16.83	-28.75	-25.85
241.00	-9.08	-9.63	-11.47	-10.93	-18.31	-17.32	-2.75	-2.63	-9.82	-9.40	-11.18	-10.53	-18.08	-17.84	-29.86	-26.99
267.00	-10.44	-11.15	-12.25	-11.62	-19.61	-18.65	-3.06	-2.96	-10.41	-9.91	-11.71	-11.00	-18.88	-18.59	-30.77	-28.07
289.00	-11.52	-12.34	-12.80	-12.29	-20.50	-19.65	-3.28	-3.19	-10.85	-10.43	-12.10	-11.42	-19.35	-19.20	-31.49	-28.78
313.00	-12.55	-13.62	-13.47	-12.85	-21.36	-20.57	-3.36	-3.35	-11.13	-10.82	-12.43	-11.86	-19.77	-19.67	-32.07	-29.50
338.00	-13.55	-14.92	-13.97	-13.26	-21.97	-21.26	-3.53	-3.49	-11.91	-11.16	-12.74	-12.17	-20.29	-20.03	-32.76	-30.09
360.00	-14.38	-15.97	-14.30	-13.63	-22.44	-21.79	-3.72	-3.66	-11.96	-11.49	-13.10	-12.45	-20.63	-20.42	-32.98	-30.36
386.00	-15.55	-17.66	-14.99	-14.49	-23.14	-22.62	-4.06	-3.93	-12.49	-12.05	-13.59	-12.95	-21.15	-20.84	-33.65	-31.11
430.00	-17.32	-20.09	-15.77	-15.24	-23.67	-23.15	-4.31	-4.21	-13.05	-12.58	-14.12	-13.56	-21.68	-21.48	-34.28	-31.72
454.00	-19.57	-22.64	-16.55	-16.07	-24.47	-23.96	-4.72	-4.60	-13.72	-13.27	-14.87	-14.31	-22.35	-22.06	-35.00	-32.47
518.00	-22.77	-25.46	-17.60	-17.24	-25.31	-24.82	-5.26	-5.24	-14.55	-14.13	-15.86	-15.40	-23.15	-22.90	-35.83	-33.32
586.00	-25.63	-28.23	-18.60	-18.33	-25.92	-25.40	-7.45	-8.31	-15.33	-14.94	-16.81	-16.43	-23.81	-23.54	-36.64	-34.13
613.00	-26.57	-28.95	-18.85	-18.63	-26.08	-25.51	-8.73	-9.53	-15.53	-15.16	-17.22	-16.76	-23.90	-23.68	-36.83	-34.35

Thermal Degradation At 120°C in 4 Lux 8 Pelleted APPs

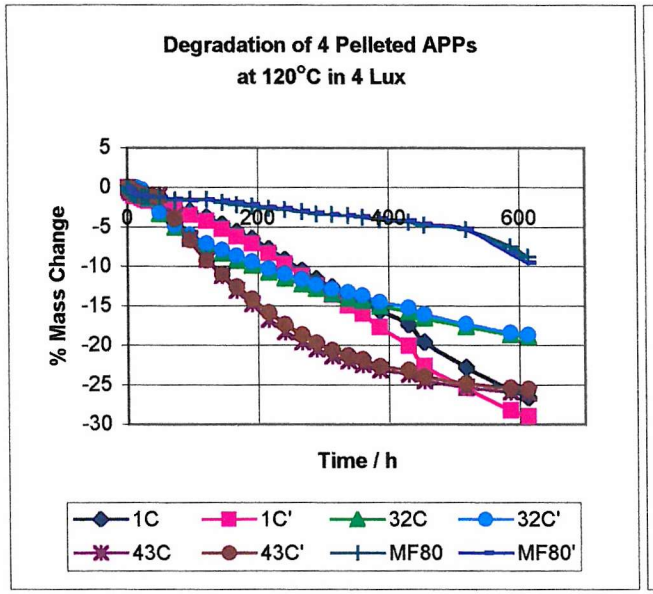

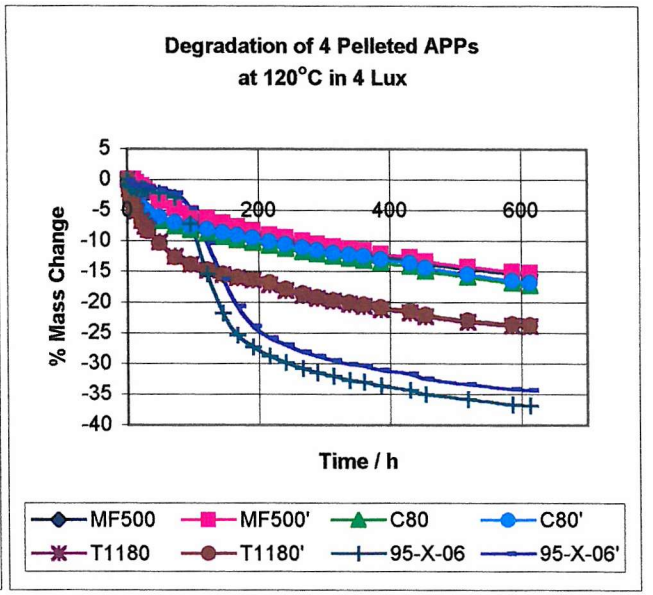

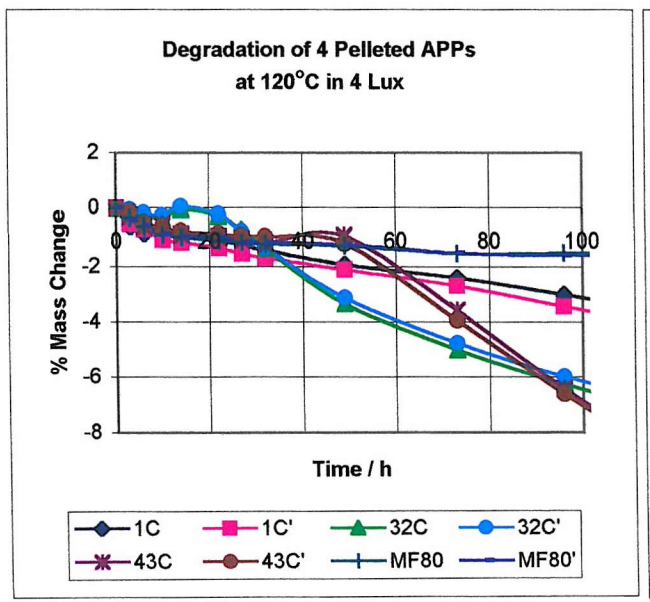

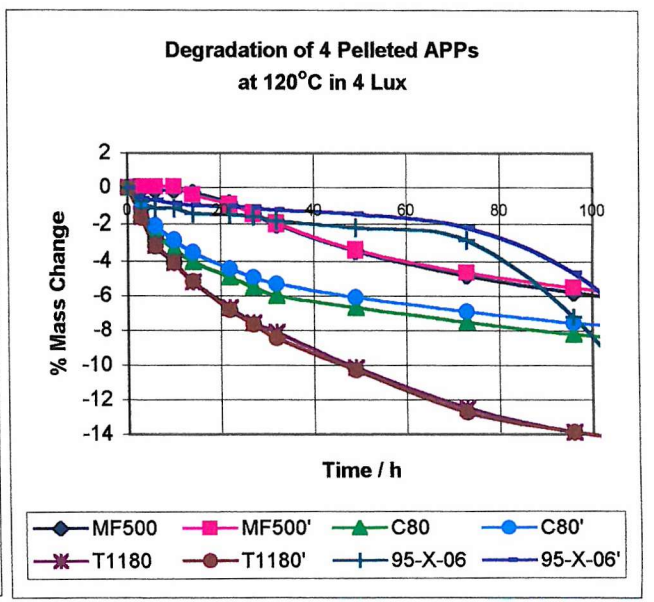

Thermal Degradation

At 120°C in 4 Lux

Good agreement between the 2 sets of results for each APP.

Homopolymers were affected less, MF80 least.

Copolymers 32C and 43C both gained mass slightly before 'taking off.'

MF80 was protected from fast degradation till 518 h.

One MF500 sample gained mass slightly before it 'took off.'

C80 and T1180 had no slow stage under these conditions.

95-X-06 degraded much faster than the other 7 APPs.

95-X-06 had slow stage to about 75 h.

8 Pelleted APPs

Degradation of Different Sizes of 'APPs' 95-X-06 and T1180 at 120°C in 4 Lux

Data for APP 95-X-06 (360 mg in 1, 4, 6 or 8 pieces)

Time / h	1	1'	4	4'	6	6'	8	8'
0.0	0.00	0.00	0.00	0.00	0.00	0.00	0.00	0.00
4.0	-0.91	-0.95	-1.29	-1.41	-1.57	-1.13	-1.62	-1.38
8.0	-1.52	-1.54	-2.09	-2.21	-2.07	-1.81	-2.23	-2.24
12.0	-1.90	-1.88	-2.50	-2.62	-2.51	-2.25	-2.59	-2.59
22.0	-2.45	-2.39	-3.02	-3.17	-3.00	-2.69	-2.95	-3.01
34.0	-2.42	-2.75	-3.13	-3.36	-3.06	-2.94	-5.59	-3.26
37.0	-2.37	-3.06	-3.13	-3.01	-2.81	-2.83	-7.30	-3.42
40.0	-2.34	-3.48	-3.27	-2.40	-2.76	-3.16	-8.29	-3.78
43.0	-2.89	-4.46	-4.32	-2.98	-3.34	-4.28	-9.69	-5.10
47.0	-3.86	-5.44	-5.96	-4.03	-4.88	-5.52	-11.48	-6.87
51.0	-5.02	-6.99	-7.97	-5.54	-6.84	-7.30	-13.30	-9.08
59.0	-7.22	-9.57	-11.65	-8.85	-10.92	-10.65	-16.16	-13.27
64.0	-8.87	-11.17	-13.94	-10.78	-13.64	-12.60	-17.70	-15.56
69.0	-10.61	-12.77	-16.25	-12.74	-16.21	-14.47	-19.30	-17.77
84.0	-15.84	-17.71	-21.58	-17.93	-22.02	-19.85	-22.58	-22.46
108.0	-21.55	-22.20	-25.87	-22.39	-25.14	-23.36	-25.17	-25.03
131.0	-23.78	-24.17	-27.54	-24.43	-26.46	-24.76	-26.49	-26.30
156.5	-25.41	-25.57	-28.89	-25.92	-27.78	-26.00	-27.70	-27.37
180.0	-26.40	-26.58	-29.74	-27.03	-28.67	-27.07	-28.52	-28.34
202.0	-27.20	-27.34	-30.59	-27.80	-29.49	-27.78	-29.35	-29.00
222.0							-30.34	-30.08
246.0							-30.67	-30.44
271.0							-31.36	-31.04
296.0							-31.75	-31.51
322.0							-32.32	-32.09
344.0							-32.74	-32.53
368.0							-33.12	-33.06
393.0							-33.43	-33.31
415.0							-33.78	-33.58

Combined Data for 95-X-06 (*8) and T1180 (*12)

Time / h	95-X-06	95-X-06'	T1180	T1180'
0.0	0.00	0.00	0.00	0.00
3.0			-3.98	-3.89
4.0	-1.62	-1.38		
6.0			-5.59	-5.38
8.0	-2.23	-2.24		
9.0			-7.04	-6.82
12.0	-2.59	-2.59		
13.0			-8.49	-8.11
17.0			-9.65	-9.15
22.0	-2.95	-3.01		
25.0			-11.38	-10.72
30.0			-12.15	-11.52
34.0	-5.59	-3.26		
35.0			-12.83	-12.44
37.0	-7.30	-3.42		
40.0	-8.29	-3.78		
43.0	-9.69	-5.10		
47.0	-11.48	-6.87		
51.0	-13.30	-9.08		
52.0			-14.36	-14.25
59.0	-16.16	-13.27		
64.0	-17.70	-15.56		
69.0	-19.30	-17.77		
76.0			-15.89	-15.54
84.0	-22.58	-22.46		
99.0			-16.65	-16.34
108.0	-25.17	-25.03		
124.5			-18.83	-18.35
131.0	-26.49	-26.30		

441.0							-34.39	-34.19
485.0							-34.69	-34.52
509.0							-35.32	-35.10
557.0							-35.46	-35.26
584.0							-35.77	-35.62

Data for APP T1180 (1, 3, 6 or 12 pieces)

Time / h	1	1'	3	3'	6	6'	12	12'
0.0	0.00	0.00	0.00	0.00	0.00	0.00	0.00	0.00
3.0	-2.24	-2.29	-2.56	-3.05	-3.47	-3.26	-3.98	-3.89
6.0	-3.12	-3.42	-3.85	-4.34	-4.83	-4.62	-5.59	-5.38
9.0	-4.20	-4.50	-4.93	-5.50	-6.19	-6.05	-7.04	-6.82
13.0	-5.52	-5.67	-6.25	-6.62	-7.42	-7.21	-8.49	-8.11
17.0	-6.48	-6.75	-7.17	-7.79	-8.58	-8.18	-9.65	-9.15
25.0	-7.88	-8.32	-8.69	-9.51	-10.38	-9.83	-11.38	-10.72
30.0	-8.80	-9.24	-9.54	-10.32	-11.29	-10.68	-12.15	-11.52
35.0	-9.56	-9.89	-10.34	-11.08	-11.85	-11.53	-12.83	-12.44
52.0	-11.32	-11.58	-12.06	-12.65	-13.32	-13.38	-14.36	-14.25
76.0	-12.89	-13.26	-13.62	-14.37	-15.04	-14.71	-15.89	-15.54
99.0	-13.89	-14.19	-14.62	-15.25	-15.92	-15.68	-16.65	-16.34
124.5	-14.93	-15.03	-15.46	-16.06	-16.48	-16.30	-18.83	-18.35
148.0	-15.65	-15.64	-16.27	-16.74	-18.28	-17.78	-20.31	-19.83
170.0	-16.05	-16.08	-16.87	-17.54	-19.35	-19.06	-21.40	-20.79
190.0							-22.49	-21.76
214.0							-23.09	-22.44
239.0							-23.89	-23.20
264.0							-24.58	-23.85
290.0							-25.22	-24.37
312.0							-25.74	-24.89
336.0							-26.03	-25.21
361.0							-26.55	-25.65
383.0							-26.87	-25.89
409.0							-27.39	-26.54
453.0							-27.92	-26.78

148.0			-20.31	-19.83
156.5	-27.70	-27.37		
170.0			-21.40	-20.79
180.0	-28.52	-28.34		
190.0			-22.49	-21.76
202.0	-29.35	-29.00		
214.0			-23.09	-22.44
222.0	-30.34	-30.08		
239.0			-23.89	-23.20
246.0	-30.67	-30.44		
264.0			-24.58	-23.85
271.0	-31.36	-31.04		
290.0			-25.22	-24.37
296.0	-31.75	-31.51		
312.0			-25.74	-24.89
322.0	-32.32	-32.09		
336.0			-26.03	-25.21
344.0	-32.74	-32.53		
361.0			-26.55	-25.65
368.0	-33.12	-33.06		
383.0			-26.87	-25.89
393.0	-33.43	-33.31		
409.0			-27.39	-26.54
415.0	-33.78	-33.58		
441.0	-34.39	-34.19		
453.0			-27.92	-26.78
485.0	-34.69	-34.52		
509.0	-35.32	-35.10		
557.0	-35.46	-35.26		
584.0	-35.77	-35.62		

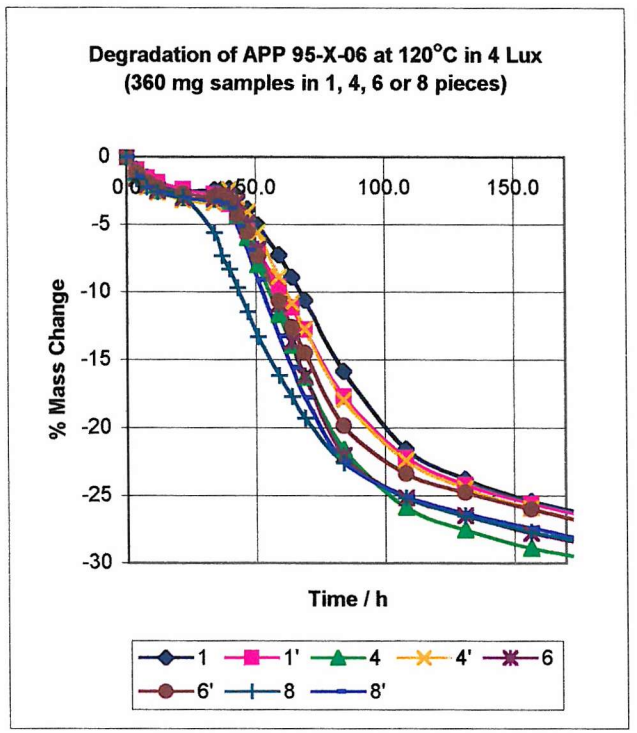

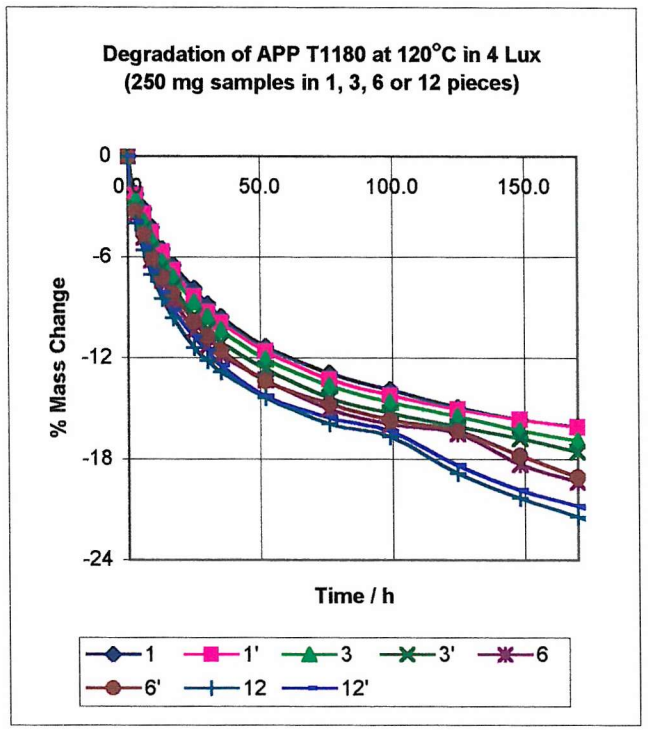

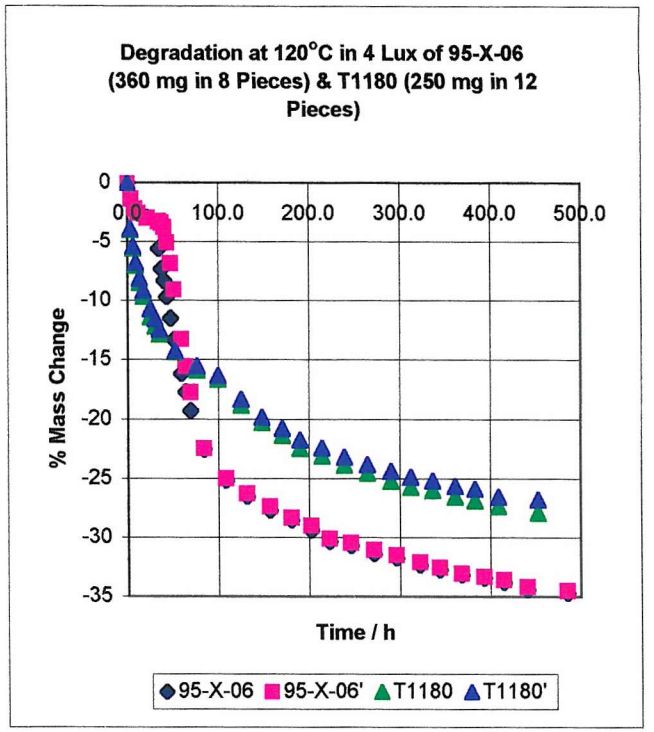

95-X-06

Data: 6: 62-63, 71, 94 7: 17-18, 51

In vacuum oven with window, lit by Anglepoise lamp on stool.
Area all enclosed in thick black polythene to keep out daylight.
Smallest pieces were followed as long as possible.
In duplicate, 2 slides of each, with
1*360 mg, 4*90 mg, 6*60 mg, or 8*45 mg.
Step from slow to fast degradation made comparison difficult.
I.e. curves crossed over each other and did not stay in order.
Should study an APP with no induction stage.

T1180

Data: 6: 69-70, 93 7: 17-18, 51

Total mass for each sample = 250 mg.
Divided into 3, 6 or 12 similar size pieces.
No induction stage.
2 components - 12 pieces lost the 1st one by 100 h.
6 pieces lost the 1st one by 125 h.
Curves stayed separate most of the way.
Showed degradation much faster with smaller pieces.

Combined Plot

Levelling off but still not near limit of mass loss.
T1180 contained 2 components, the 1st lost by 100 h.
Good reproducibility, even on supplied pellets.

Degradation of Series of 32C in 100 Pen Bitumen at 120°C in 4 Lux

One square 2"*2" slide for each blend with 0%, 5%, 10% and x% APP, because these would melt and spread out.
One normal microscope slide (1" * 3") for 15%, 20%, 30% and 100% APP. Each sample only 200 mg.
Samples heated in vacuum oven with 20 cm diameter window, lit by a lamp, placed on a stool.
Masses were checked approx daily to check (a) whether APP and bitumen protected each other
(b) whether there was an inversion point in the degree of degradation, as with other physical properties
Data: 7: 31-32, 71, 97 and 8 :21 Repeat of 7: 15-16

Time / h

	0%	5%	10%	15%	20%	30%	100%	x%
0	0.00	0.00	0.00	0.00	0.00	0.00	0.00	0.00
24	-1.55	-1.25	-0.95	-0.85	-0.50	-0.75	-0.45	-0.35
46	-2.20	-1.73	-1.80	-1.20	-0.85	-1.00	-2.55	-0.40
68	-2.90	-2.49	-2.24	-1.65	-1.25	-1.34	-4.50	-0.60
91	-3.55	-3.05	-2.64	-2.00	-1.45	-1.64	-5.64	-0.80
136	-4.61	-4.23	-3.59	-2.60	-1.95	-1.89	-7.64	-1.05
184	-5.26	-4.48	-4.04	-2.90	-2.25	-2.14	-9.04	-1.10
208	-5.51	-4.84	-4.29	-3.15	-2.55	-2.34	-9.79	-1.15
232	-5.91	-5.19	-4.59	-3.30	-2.75	-2.49	-10.34	-1.40
249	-6.21	-5.50	-4.79	-3.34	-2.70	-2.49	-10.64	-1.15
316	-6.91	-6.31	-5.34	-3.69	-3.15	-2.89	-11.94	-1.35
332	-7.06	-6.47	-5.44	-3.74	-3.15	-2.94	-12.29	-1.50
368		-6.57	-5.69	-4.09	-3.40	-3.14	-12.79	-1.50
383		-6.11	-5.39	-4.04	-3.40	-3.04	-12.74	-1.40
406		-5.70	-4.99	-4.19	-3.90	-2.74	-12.79	-1.35
425		-5.35	-4.94	-4.24	-3.60	-3.09	-13.09	-1.60
447		-4.84	-4.89	-4.24	-3.50	-3.29	-13.04	-1.60
467		-4.89	-4.74	-4.24	-3.55	-3.19	-13.49	-1.55
489		-4.99	-4.69	-4.24	-3.95	-3.24	-13.84	-1.65
507		-5.09	-4.49	-4.44	-3.75	-3.29	-14.19	-1.65
550		-5.19	-4.74	-4.49	-4.00	-3.29	-14.84	-1.75
575		-4.76	-4.44	-4.54	-4.20	-3.29	-15.13	-1.90
595		-4.79	-4.39	-4.59	-4.10	-3.39	-15.29	-1.90
614		-4.63	-4.39	-4.44	-4.10	-3.29	-15.48	-1.75

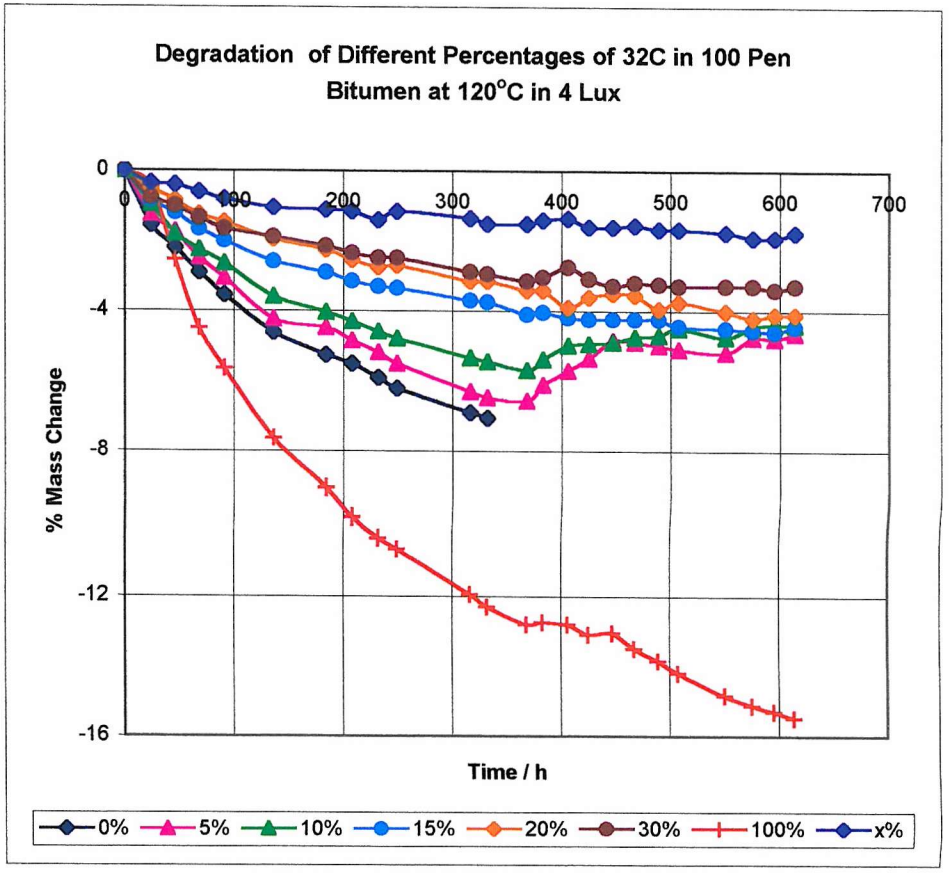

Thermal Degradation At 120°C in 4 Lux 32C in 100 Pen Series

Observations

100 pen bitumen dried out so much that it cracked and came unstuck by 332 h.
Therefore it was removed because conditions were not the same as for the rest.
32C and the bitumen protected each other from degradation..
Degree of protection of the bitumen increased with % 32C.
In light the slow stage of the APP was very short - only about 20 h.
No intermediate slight mass gain was seen.
In light everything was faster, so there was no build up before fast mass loss stage.

Alternative Analysis

At any one time a plot of % mass change vs % APP content shows the variation of physical property with composition.
The graph shows a change from steep to shallow gradient.
The point of change corresponds to the normal inversion point for physical properties of APP/bitumen blends.
Inversion point was at about 18% APP.
Much better comparison than that done in the dark.

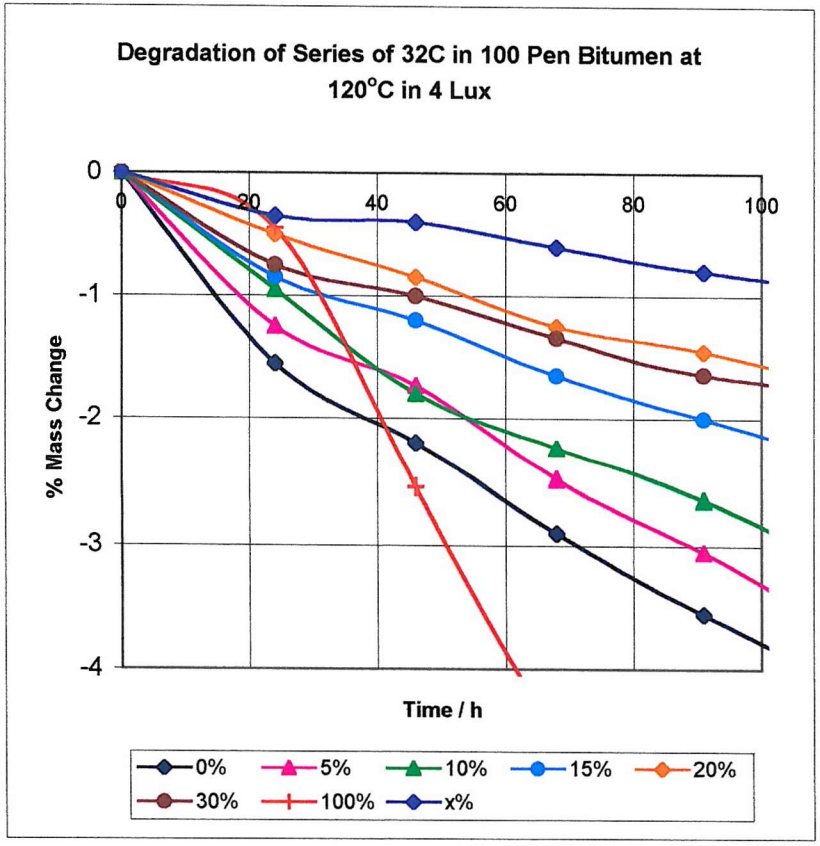

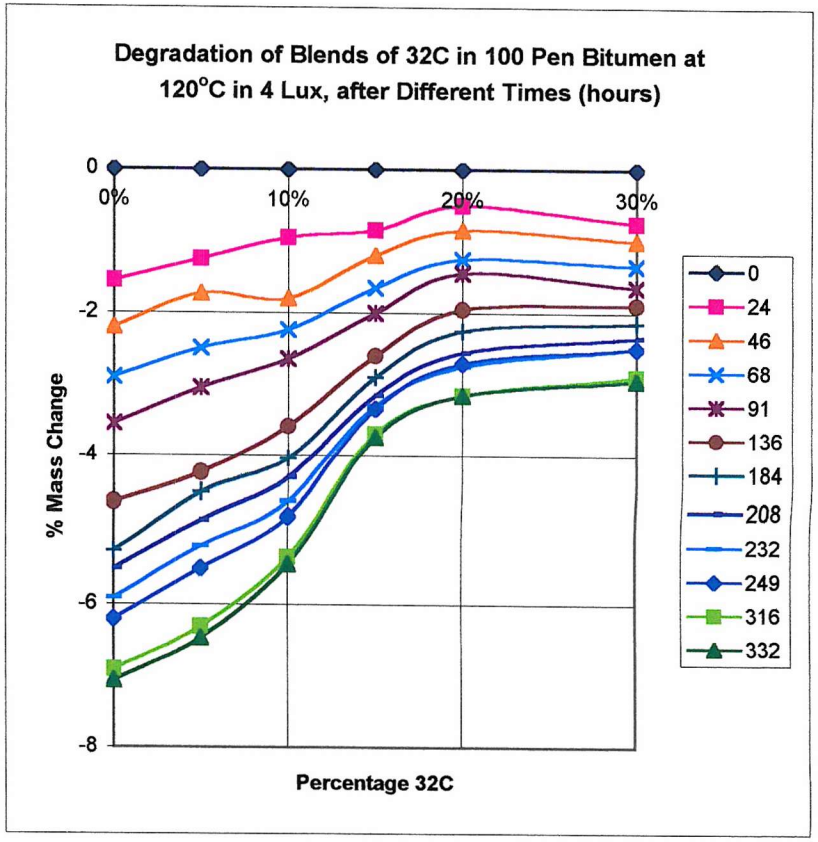

Thermal Degradation

At 120°C in 4 Lux

32C in 100 Pen Series

Degradation of SBS, SIS, PFSD and Different % SBS in 200 Pen Bitumen at 120°C in 4 Lux

Normal microscope slide (1" * 3") for one 200 mg sample of each polymer.
Samples heated in vacuum oven with 20 cm diameter window.
Area between lamp and oven enclosed by thick black polythene.
Mass checks done to see whether SBS and bitumen protected each other and whether SIS or the special blend PFSD (with 6% IB) degraded.
Data: 7: 33-34, 72, 97 and 8 :21
Time / h

	0%	9%	13%	SBS	SIS	PFSD
0	0.00	0.00	0.00	0.00	0.00	0.00
22	-3.20	0.55	0.05	4.00	3.51	0.70
44	-4.75	0.70	0.30	5.00	3.01	0.70
67	-6.00	0.75	0.45	5.79	2.81	0.85
112	-8.15	0.80	0.40	6.79	2.76	0.70
160	-9.15	0.99	0.80	7.69	2.91	0.85
184	-10.04	0.70	0.55	4.59	2.76	0.75
208	-10.29	1.04	0.80	5.84	3.21	0.85
232	-10.74	0.94	0.90	5.59	2.91	0.60
249	-13.89	0.55	0.90	5.69	2.91	0.60
316	-14.84	0.35	0.90	5.99	2.76	0.25
332	-14.94	0.40	0.95	5.89	2.76	0.15
368		0.35	0.95	6.24	2.76	-0.60
383		0.70	1.34	6.44	2.86	0.80
406		0.80	1.29	6.54	2.71	0.80
425		0.70	0.90	6.54	2.81	0.65
447		0.90	1.10	6.84	2.71	0.85
467		1.00	1.29	7.14	2.96	0.95
489		1.09	1.25	7.19	2.86	0.90
507		0.70	1.15	6.94	2.79	0.90
550		1.09	1.34	2.45	2.71	1.05
575		1.04	1.34	2.60	2.81	1.14
595		1.09	1.49	2.75	2.81	1.05
614		1.34	1.39	-1.35	2.81	1.29

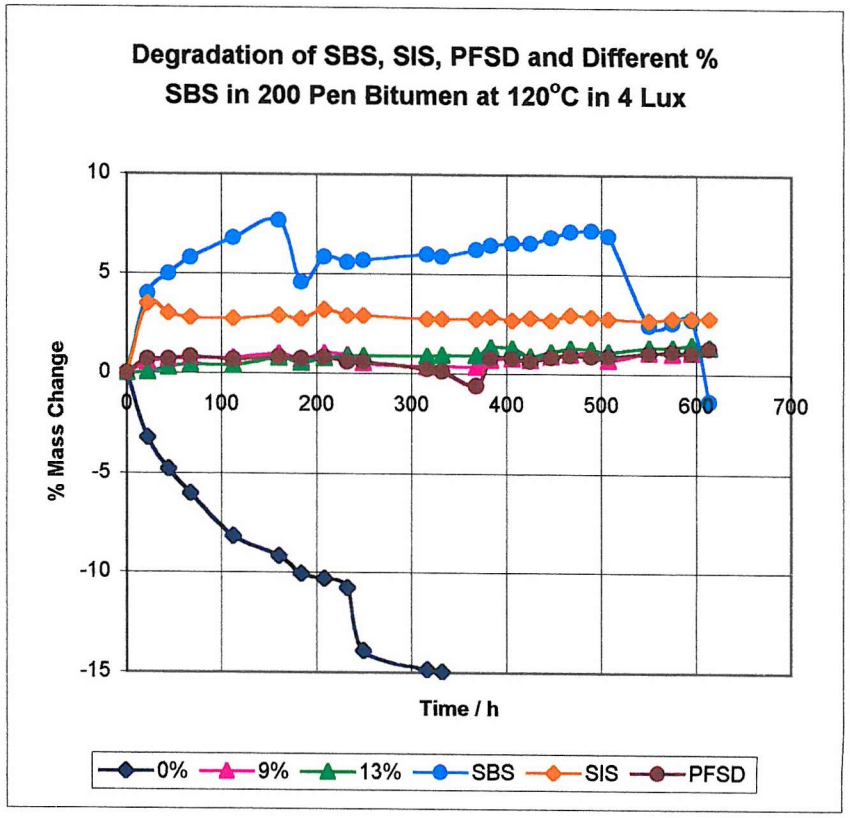

Observations

9% and 13% SBS, and PFSD protected the bitumen and did not degrade under the conditions and time used - they merely gained mass slightly.
SIS gained nearly 3% mass but still did not degrade - perhaps it needs higher temperature or light level to do so.
SBS itself gained >7% mass, and degraded rapidly from 490 h.
Perhaps all these polymers need to gain more mass (i.e. more oxygen) before they will degrade (i.e. lose oxidized fragments).

Degradation of APPs at 120°C in Daylight
- Effect of Sample Size and Preparation

Slides always placed in same relative positions on sample tray in vacuum oven.
Oven with 20-cm round glass window, plus extra 6 mm soda glass..
Daylight = normal daily winter cycle in lab.

APP 95-X-06 as Supplied

Data: hardback lab books IV: 143-145.
95-X-06 as 4 * 90 mg or 2 * 180 mg pieces.
Material as supplied, cut from large soft block.
APP known to have an early fast stage.

Time / h % Mass Changes

	2*180mg	4*90mg
0	0.00	0.00
24	-2.98	-3.44
48	-3.65	-3.85
72	-4.06	-11.56
96	-5.87	-19.64
120	-14.53	-25.96
144	-19.96	-28.74
192		-31.71

With smaller pieces, slow stage was faster and fast stage was reached sooner.
Therefore 1st stage probably had to be completed before 2nd stage could begin.

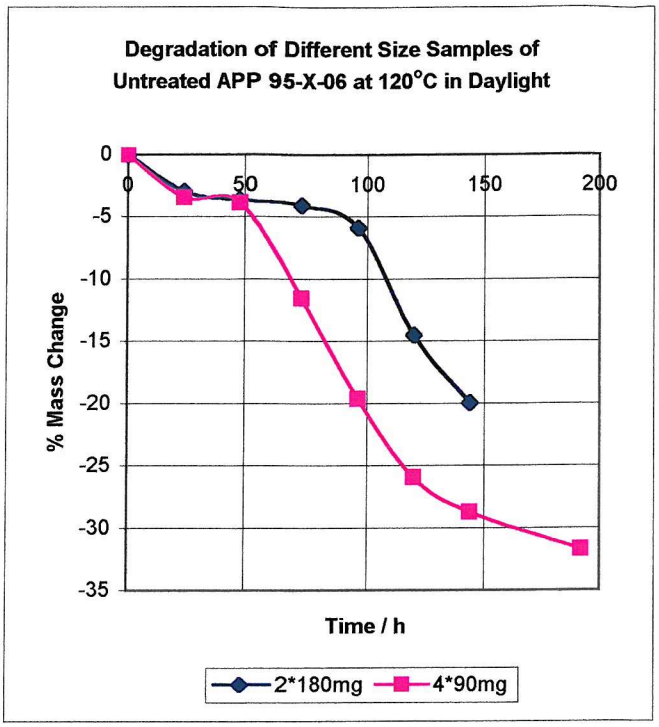

V808 and V891 as Prepared Discs

Data: hardback lab book IV: 129, 149-151.
Beads were melted in 1 cm diameter specimen bottles, made of very thin glass.
Melted in the dark in oven at approx 140°C for approx 15 min.
Then cooled to RT on the bench.
Then the glass was smashed and peeled off.

Time / h % Mass Changes

	V808(2*180mg)	V891(2*180mg)
0	0.00	0.00
24	0.14	0.03
48	-0.14	
72	-1.09	-1.4
96	-1.66	-2.04
120	-2.1	-2.39
144	-2.21	-2.57

Time / h % Mass Changes

	V808(2*360mg)	V891(2*360mg)
0	0	0
24	0	0
48	0.06	0.06
72	0.03	0.17
96	0.17	0.25
120	0.17	0.19
144	0.08	0.12

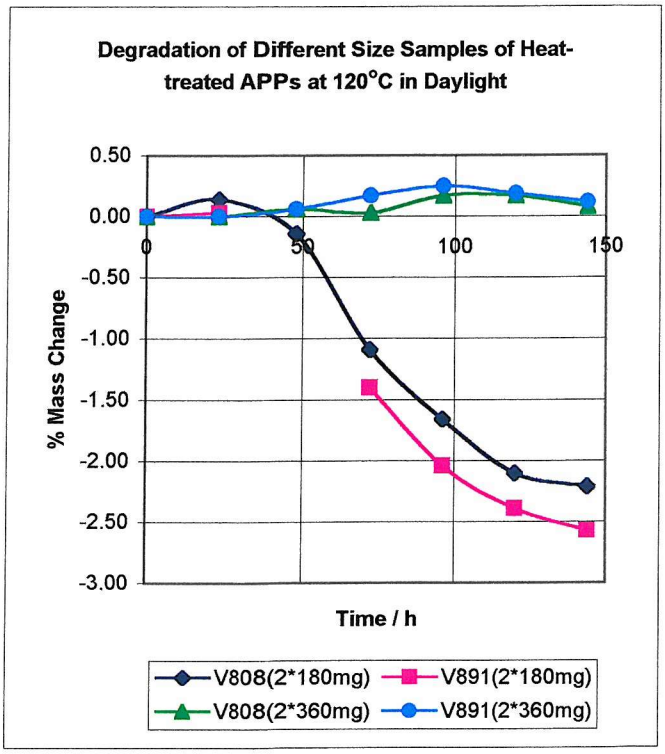

Very different behaviour!
Duplication verified that difference was real.
Results needed investigation.
Therefore test experiments were set up.

Degradation of 8 Pelleted APPs at 120°C in Darkness

(A) First Set with Some Light Exposure During Cooling

1st Set (1C, 32C, 43C, MF80): 6: 50-51, 67-68, 92
2nd Set (MF500, C80, T1180, 95-X-06): 6: 55-57, 72-73, 83

2 slides per APP, with 2*200 mg pieces.
Sample slides were arranged on a wire tray made to fit the oven.
Tray was exposed to light (4 lux) during cooling to RT

Time / h

	1C	1C'	32C	32C'	43C	43C'	MF80	MF80'	MF500	MF500'	C80	C80'	T1180	T1180'	95-X-06	95-X-06'
0	0.00	0.00	0.00	0.00	0.00	0.00	0.00	0.00	0.00	0.00	0.00	0.00	0.00	0.00	0.00	0.00
3	-0.61	-0.53	-0.08	-0.03	-0.36	-0.22	-0.48	-0.42	-0.36	-0.53	-1.12	-1.37	-1.4	-1.37	-1.12	-1.12
6	-0.81	-0.67	-0.14	-0.06	-0.59	-0.62	-0.7	-0.72	-0.67	-0.81	-1.82	-2.07	-2.32	-2.4	-1.62	-1.56
9	-1.12	-0.87	-0.47	-0.28	-0.89	-0.81	-0.87	-0.89								
10									-0.79	-1.06	-2.25	-2.52	-3.05	-3.3	-1.87	-1.81
13	-1.14	-0.87	-0.47	-0.22	-0.95	-0.87	-1.01	-1.03	-0.7	-1.09	-2.69	-2.94	-3.75	-3.88	-2.21	-2.01
18	-1.14	-1.01	-0.4	-0.11	-1.01	-0.76	-0.95	-1	-0.56	-1.17	-3.23	-3.38	-4.59	-4.81	-2.32	-2.2
23	-1.2	-1.07	-0.45	-0.17	-1.06	-0.81	-1.01	-1.06	-0.5	-1.01	-3.68	-3.78	-5.43	-5.56	-2.49	-2.43
26	-1.12	-1.07	-0.47	-0.11	-1.12	-0.87	-1.23	-1.17	-0.64	-1.23	-4.04	-4.17	-5.9	-6.04	-2.6	-2.57
33	-1.12	-0.87	-0.53	-0.2	-1.12	-0.95	-1.26	-1.31	-1.07	-1.12	-4.35	-4.45	-6.52	-6.71	-2.66	-2.57
43	-1.39	-0.87	-0.59	-0.28	-1.34	-1.15	-1.45	-1.28	-1.99	-1.31	-5.11	-5.29	-7.55	-7.77	-2.91	-2.76
56	-1.23	-0.81	-0.4	-0.17	-1.37	-1.23	-1.48	-1.45	-3	-1.62	-5.92	-5.96	-8.39	-8.8	-2.83	-2.93
76	-1.34	-1.07	-0.28	-0.25	-1.4	-1.43	-1.65	-1.64	-4.6	-3.07	-6.82	-6.88	-9.57	-10.11	-2.77	-3.07
104	-1.65	-1.46	-0.7	-0.5	-1.65	-1.6	-1.87	-1.73	-6.2	-5	-7.89	-7.92	-11.16	-11.65	-3.02	-3.4
148	-1.98	-1.77	-3.26	-2.85	-1.82	-1.79	-1.99	-1.95	-8.05	-7.18	-8.64	-8.53	-12.59	-13.27	-3.36	-3.63
170	-2.32	-1.99	-5.41	-4.85	-1.9	-1.93	-1.99	-1.89	-8.95	-8.19	-9.07	-8.92	-13.4	-13.97	-3.55	-3.88
194	-2.62	-2.24	-7.48	-6.67	-1.93	-1.96	-2.04	-1.89	-9.79	-9.22	-9.15	-9.34	-14.01	-14.61	-3.78	-4.04
220	-2.87	-2.5	-9.49	-8.31	-1.99	-2.02	-1.73	-1.81	-10.57	-10.2	-9.18	-9.62	-14.46	-15	-3.94	-4.1
246	-2.98	-2.64	-11.58	-9.93	-1.57	-1.96	-1.82	-1.98	-11.36	-11.06	-9.12	-9.71	-14.85	-15.4	-4.03	-3.35
288	-3.49	-3.11			-4.05	-2.02	-2.32	-2.48			-10.33	-10.97	-15.66	-16.23	-4.42	-14.45
292	-3.46	-3.11			-4.33	-2.07	-2.29	-2.48			-10.36	-10.94	-15.72	-16.29	-5.12	-15.31
297	-3.6	-3.23			-4.98	-2.3	-2.29	-2.48			-10.44	-11.05	-15.66	-16.26	-6.91	-16.85
314	-3.65	-3.23			-6.57	-2.75	-2.49	-2.62			-10.89	-11.38	-15.86	-16.35	-12.78	-19.78
338	-3.77	-3.25			-8.86	-4.57	-2.52	-2.7			-11.28	-11.78	-16.08	-16.51	-18.94	-22.76

Thermal Degradation At 120°C in Darkness 8 Pelleted APPs

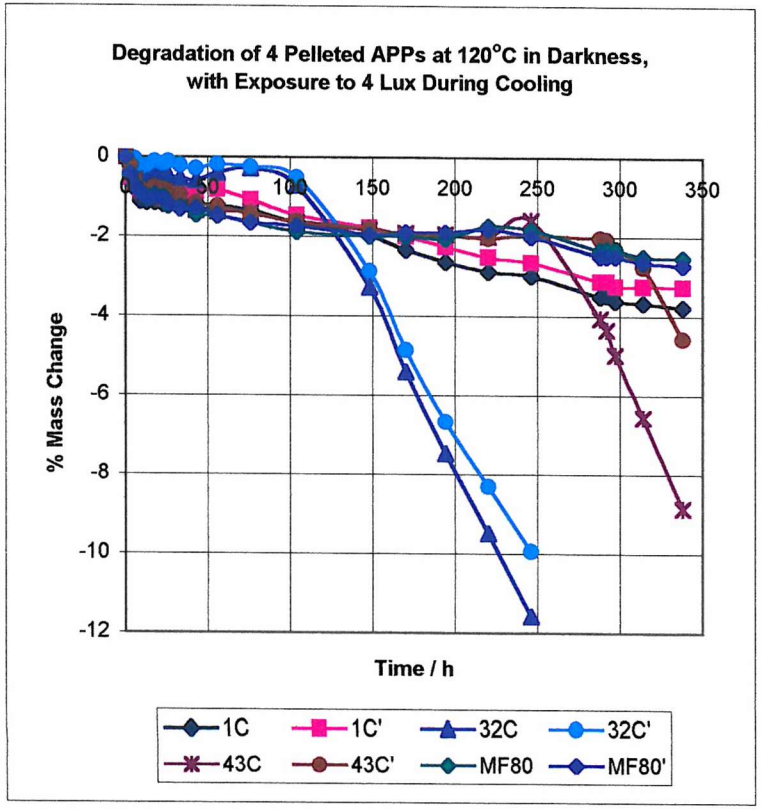

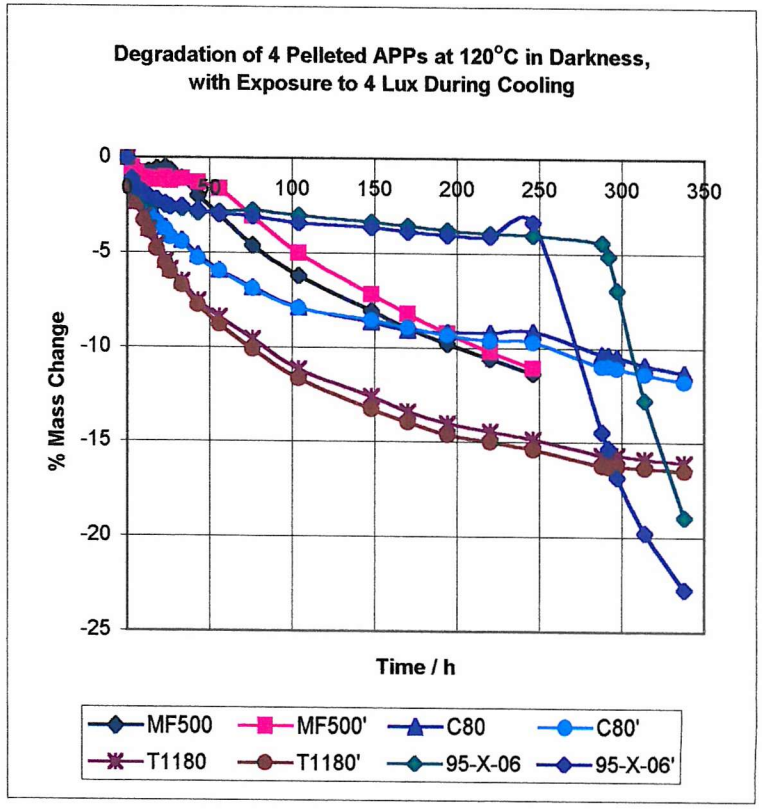

32C changed to fast stage at *c.* 80 h, 43C from *c.* 246/288 h
Very tiny mass gain between the 2 stages
Homopolymers 1C and MF80 hardly affected

95-X-06 changed to fast degradation from 246/288 h
In one case, small mass gain between stages
MF500 also gained mass very slightly
C80 probably had 2 components

APPs with slow stage took 4-5 times longer to take off, those with only slow stage were just slower.
Was degradation due to exposure to daylight during cooling?

Degradation of 8 Pelleted APPs at 120°C in Darkness

(B) Repeat with Minimum Light Exposure During Cooling

Repeated expt.: previous set did degrade even in the dark. Data: 7: 10-12, 24-26, 44-45. 2 slides per polymer, with 2*200 mg pieces.

Last time, those with slow stage took 4-5 times longer to take off; those with no slow stage were just slower.

Was the degradation due to exposure to daylight while the samples were cooling?

This time, base and sides of wire sample tray were enclosed in foil. Metal lid was put over the top as soon as oven door was opened.

Tray was immediately put into cardboard box till it had cooled to RT. The lid was taken off the box in the fume cupboard to vent the fumes.

Times:

	1C	1C'	32C	32C'	43C	43C'	MF80	MF80'	MF500	MF500'	C80	C80'	T1180	T1180'	95-X-06	95-X-06'
0.00	0.00	0.00	0.00	0.00	0.00	0.00	0.00	0.00	0.00	0.00	0.00	0.00	0.00	0.00	0.00	0.00
3.00	-0.45	-0.50	-0.12	-0.10	-0.32	-0.22	-0.40	-0.38	-0.30	-0.04	-1.02	-1.13	-0.95	-0.22	-0.80	-1.03
6.00	-0.55	-0.65	-0.17	-0.10	-0.42	-0.22	-0.50	-0.50	-0.35	-0.47	-1.52	-2.03	-1.64	-2.10	-1.15	-1.43
10.00	-0.70	-0.72	-0.15	-0.05	-0.45	-0.17	-0.62	-0.58	-0.50	-0.65	-1.87	-2.55	-2.22	-2.80	-1.40	-1.70
13.00	-0.85	-0.87	-0.17	-0.15	-0.57	-0.27	-0.70	-0.68	-0.65	-0.85	-2.35	-3.05	-2.89	-3.62	-1.60	-2.00
16.00	-0.87	-0.92	-0.12	-0.17	-0.55	-0.22	-0.72	-0.70	-0.60	-0.82	-2.60	-3.33	-3.21	-4.07	-1.68	-2.08
24.00	-1.05	-1.10	-0.30	-0.17	-0.85	-0.47	-1.02	-0.95	-0.70	-0.95	-3.37	-3.78	-4.36	-4.92	-2.10	-2.38
53.00	-1.12	-1.25	-0.40	-0.10	-0.95	-0.42	-1.12	-0.90	-1.25	-1.52	-5.25	-5.98	-7.17	-8.36	-2.60	-3.10
77.00	-1.30	-1.25	-0.37	-0.02	-1.00	-0.42	-1.25	-1.15	-1.15	-1.70	-6.10	-6.96	-8.57	-10.08	-2.94	-3.38
99.00	-1.27	-1.50	-0.45	-0.08	-1.02	-0.45	-1.45	-1.35	-1.40	-1.47	-6.77	-7.66	-9.62	-11.08	-3.15	-3.66
121.00	-1.50	-1.52	-0.42	-0.05	-1.15	-0.45	-1.55	-1.48	-2.37	-2.20	-7.19	-8.14	-10.49	-11.93	-3.35	-3.83
147.00	-1.70	-1.70	-0.52	-0.17	-1.32	-0.47	-1.65	-1.55	-3.77	-3.77	-7.69	-8.51	-11.31	-12.70	-3.53	-4.01
188.00	-1.97	-1.92	-0.57	-0.17	-1.35	-0.82	-1.75	-1.67	-5.54	-5.77	-8.29	-9.21	-12.41	-13.83	-3.70	-4.16
238.00	-2.37	-2.25	-0.60	-0.32	-1.55	-0.87	-1.87	-1.75	-7.21	-7.74	-8.74	-9.74	-13.38	-14.90	-3.98	-4.48
258.00	-2.42	-2.37	-0.67	-0.37	-1.60	-1.00	-1.90	-1.92	-7.98	-8.46	-9.02	-9.94	-13.85	-15.20	-4.05	-4.63
280.00	-2.42	-2.32	-0.62	-0.37	-1.50	-0.90	-1.92	-1.88	-8.46	-9.09	-9.09	-9.96	-14.05	-15.37	-4.10	-4.61
306.00	-2.62	-2.50	-0.95	-0.47	-1.62	-1.05	-2.05	-2.00	-9.33	-10.09	-9.34	-10.21	-14.52	-15.82	-4.23	-4.73
350.00	-2.80	-2.77	-1.70	-0.50	-1.70	-1.25	-2.00	-2.02	-10.40	-11.34	-9.37	-10.46	-14.97	-16.27	-4.28	-4.78
374.00	-2.95	-2.85	-2.57	-0.52	-1.72	-1.32	-1.95	-2.22	-11.00	-12.01	-9.49	-10.54	-15.30	-16.50	-4.38	-4.86
396.00	-2.97	-2.95	-3.70	-0.55	-1.77	-1.35	-1.97	-2.17	-11.58	-12.66	-9.77	-10.61	-15.47	-16.70	-4.40	-4.91
419.00	-2.97	-2.85	-4.77	-0.45	-1.75	-1.32	-1.97	-2.15	-12.00	-13.13	-9.99	-10.64	-15.57	-16.62	-4.25	-4.66
464.00	-3.15	-3.05	-6.84	-0.37	-1.87	-1.50	-2.12	-2.20	-13.12	-14.40	-10.39	-10.39	-15.99	-17.12	-4.48	-4.93
490.00	-3.20	-3.07	-8.62	-1.02	-1.82	-1.50	-2.10	-2.20	-13.97	-15.26	-10.47	-10.46	-16.27	-17.34	-4.10	-4.78
533.00	-3.35	-3.22	-9.92	-2.63	-1.90	-1.60	-2.35	-2.33	-14.82	-16.18	-10.97	-11.21	-16.62	-17.64	-7.93	-9.34
557.00	-3.35	-3.20	-10.52	-3.68	-1.95	-1.67	-2.37	-2.28	-15.12	-16.58	-11.17	-11.51	-16.69	-17.74	-10.01	-11.47

Thermal Degradation At 120°C in Darkness 8 Pelleted APPs

577.00	-3.30	-3.07	-11.07	-4.35	-1.92	-1.60	-2.15	-2.25	-15.52	-16.98	-11.39	-11.74	-16.72	-17.77	-11.36	-13.34
602.00	-3.30	-3.07	-11.37	-5.10	-1.87	-1.60	-2.07	-2.35	-15.69	-17.13	-11.52	-11.81	-16.74	-17.74	-13.83	-16.00
672.00	-3.35	-3.10	-12.84	-7.25	-1.82	-1.57	-2.30	-2.22	-16.59	-17.93	-12.07	-12.32	-16.84	-17.77	-20.21	-21.43
718.00	-3.35	-3.10	-13.51	-8.38	-1.80	-1.57	-2.30	-2.22	-17.02	-18.23	-12.37	-12.57	-16.92	-17.77	-21.96	-22.76
744.00	-3.30	-3.07	-13.89	-8.83	-1.75	-1.55	-2.25	-2.17	-17.22	-18.38	-12.44	-12.62	-16.94	-17.77	-22.46	-23.18
811.00	-3.32	-3.05	-14.74	-10.10	-1.70	-1.50	-2.25	-2.12	-17.74	-18.75	-12.74	-12.92	-16.99	-17.77	-23.51	-24.14
834.00	-3.25	-3.00	-14.96	-10.42	-1.60	-1.42	-2.15	-2.02	-17.81	-19.24	-12.79	-12.97	-16.97	-17.69	-23.74	-24.34
930.00	-3.15	-2.92	-15.76	-11.67	-1.50	-1.35	-2.12	-2.17	-18.21	-19.49	-13.29	-13.29	-16.97	-17.67	-24.56	-25.04

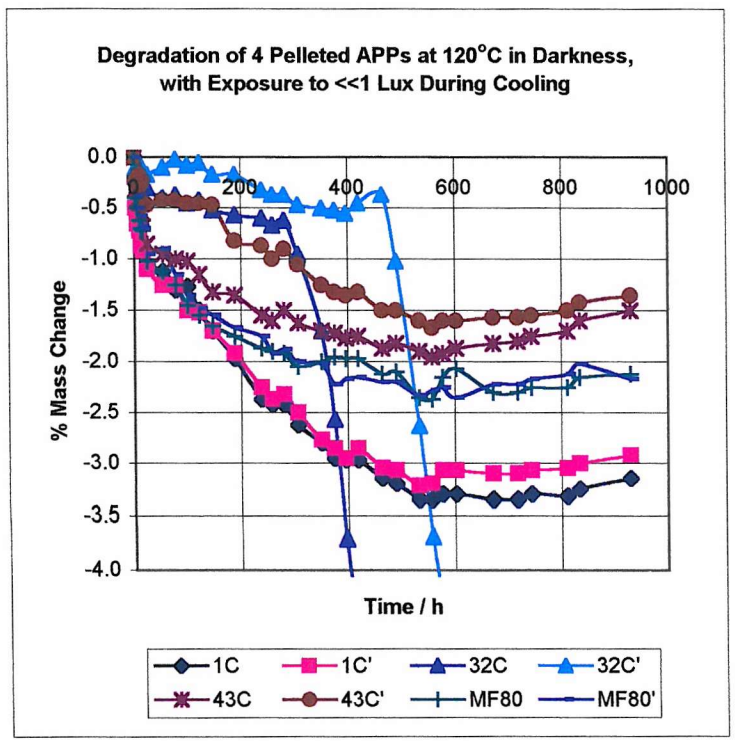

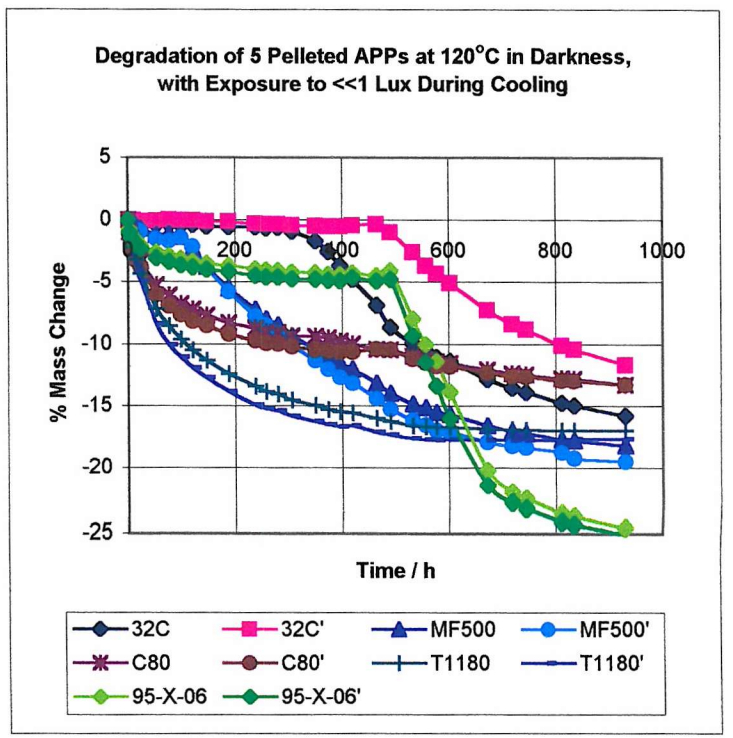

32C reached auto-oxidation at 280 and 464 h
Both preceded by slight mass gain, more marked at 464 h
Slow degrading APPs all gained mass v slightly from *c.* 530 h

MF500 reached auto-oxidation at 99 h, 95-X-06 at 490 h
No slow stage observed for C80 or T1180
C80 and T1180 probably contained 2 components

Dependence of APP Degradation of 2 APPs upon Prior Light Exposure Conditions

Purpose to check effect of light on later degradation, because MF500 and 32C had degraded even "in the dark"
Heating done in an open tin in the dark oven in the dark room.; lid on quickly afterwards.

Sample 1 C80 cooled in a lightproof tin
Sample 2 C80 cooled in a lightproof tin, but heated 10 min in 4 lux before next heating in the dark
Sample 3 C80 cooled in a lightproof tin, but heated 20 min in 4 lux before next heating in the dark
Sample 4 C80 cooled in daylight (4 lux) before weigh, and heat in dark
Sample 5 MF500 cooled in a lightproof tin

Sample no.4 was cooled in 4 lux, checked by light meter on grey winter afternoon.
Light level by oven in dark room was only 1/7 lux for transfer to sealed tin to cool.
Weighings were all done in the polymer lab dark room in 3 lux.
Data: 7: 35-37 All samples = 2*200 mg pieces per slide

% Mass Changes with Time (hours)

Time / h	Sample Numbers				
	C80-1	C80-2	C80-3	C80-4	MF500-5
0	0.00	0.00	0.00	0.00	0.00
22	-0.70	-3.97	-3.59		
45	-1.82	-5.19	-5.36	-3.50	0.87
90	-3.07	-7.32	-7.11	-6.05	1.57
138	-3.64	-8.19	-8.06	-7.27	2.04
181	-4.14	-8.76	-8.76	-8.20	2.17
205	-4.29	-8.91	-8.88	-8.50	2.24
225	-4.44	-9.01	-8.98	-8.60	2.19
250	-4.54	-9.04	-9.01	-8.60	2.27
320	-4.94	-9.31	-9.31	-8.80	2.37
344	-5.06	-9.44	-9.18	-8.87	2.37
369	-5.09	-9.24	-9.01	-8.80	2.32
436	-5.31	-9.64	-9.31	-8.92	2.27

Result: mass losses 2 = 3 > 4 >> 1
Heating in light caused greatest degradation; even exposure to light while cooling down increased the next degradation loss.
C80, heated and cooled inside the tin, still lost mass, but MF500 gained mass and did not reach mass loss stage.

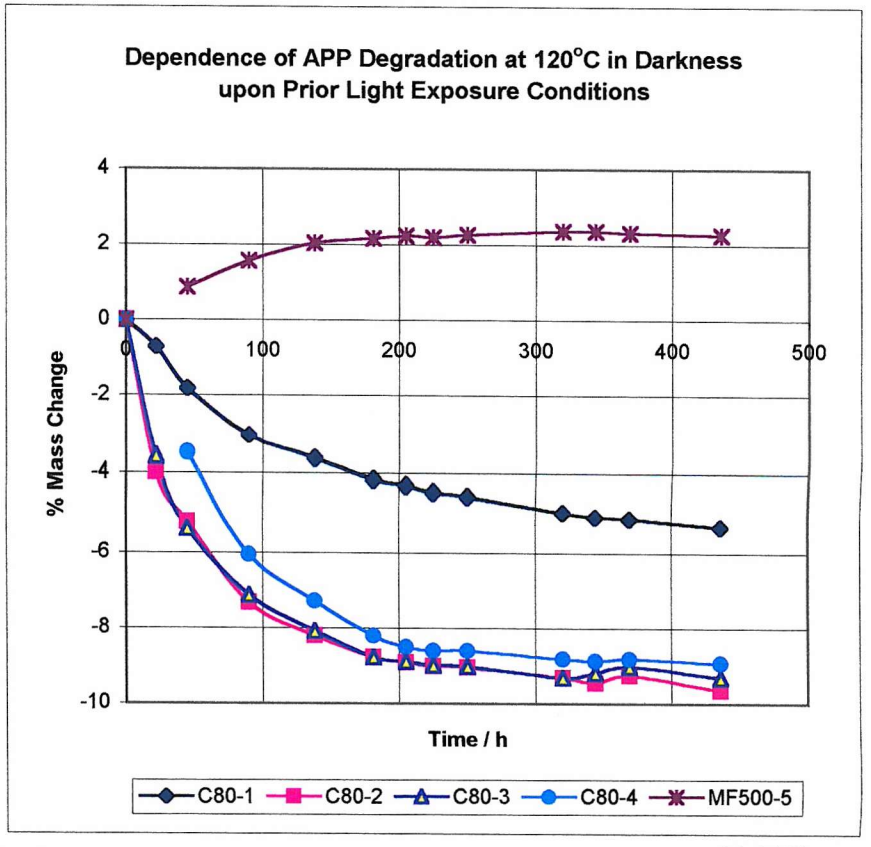

Thermal Degradation At 120°C in Darkness Light Exposure

Degradation of Series of 32C in 100 Pen Bitumen in Darkness

Repeat of 6: 78-81, 95 because it had to be left for 3 weeks.
Same details of samples: 200 mg of each APP on slides (1" * 3") or (2" * 2").
Heating in an oven without a window. Set at 248 h were used for photos (7: 39).
Samples were cooled in 4 lux daylight, so they were not kept totally dark.
Data: 7: 20-21, 39-40 Samples were weighed in dark room in 3 lux.

Time / h

	0%	5%	10%	15%	20%	30%	100%	x%
0	0.00	0.00	0.00	0.00	0.00	0.00	0.00	0.00
3	-1.40	-0.10	0.05	0.05	-0.05	0.10	-0.15	0.00
20	-2.00	-0.50	-0.45	-0.25	-0.30	-0.15	-0.35	-0.30
28	-2.10	-0.60	-0.45	-0.45	-0.35	-0.10	-0.50	-0.25
57	-2.55	-0.75	-0.45	-0.80	-0.70	-0.45	-0.70	-0.40
81	-3.10	-0.95	-1.00	-0.95	-0.75	-0.60	-0.70	-0.40
103	-3.35	-1.20	-1.20	-1.20	-1.00	-1.00	-1.00	-0.60
125	-3.60	-1.45	-1.10	-1.20	-1.05	-0.95	-0.85	-0.50
137	-3.80	-1.69	-1.35	-1.44	-1.10	-0.90	-0.85	-0.40
161	-4.15	-2.09	-1.59	-1.49	-1.25	-1.00	-0.25	-0.45
204	-4.45	-2.39	-1.94	-1.79	-1.55	-1.25	-2.50	-0.45
228	-4.45	-2.39	-1.94	-1.79	-1.55	-1.25	-4.29	-0.40
248	-4.35	-2.29	-2.04	-1.79	-1.50	-1.25	-5.54	-0.35
273	-4.30	-2.44	-1.84	-1.74	-1.50	-1.20	-6.29	-0.25
340	-4.05	-2.24	-1.49	-1.64	-1.35	-1.00	-9.08	-0.15
363	-3.90	-1.99	-1.30	-1.44	-1.20	-0.90	-9.78	-0.15
459	-3.70	-1.59	-1.25	-1.15	-1.12	-0.80	-12.97	0.02

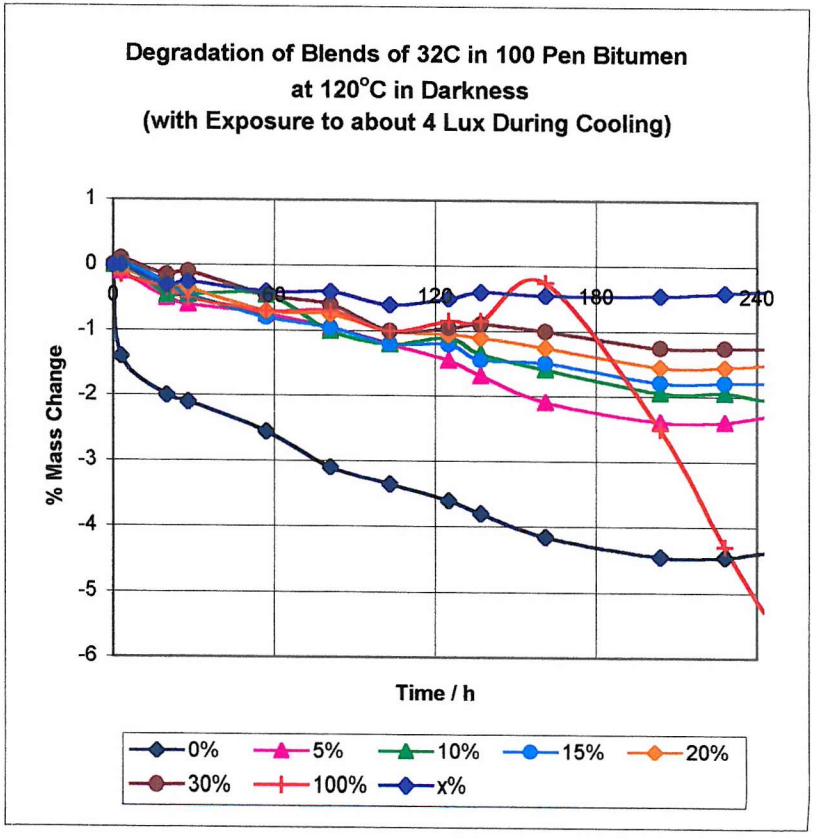

Observations

All mass losses were less than those in 4 lux.
From 200 h, masses stayed the same or rose slightly.
32C was so much slower that the intermediate slight mass gain was observed just before the fast oxidation stage.
32C was protected by bitumen, and bitumen was protected by 32C.
Degree of protection increased with increasing % 32C.
The unknown bitumen blend (x%) contained >30% APP, if it contained APP.
But probably not 32C, because position of plot indicates about 70% 32C!

Alternative Analysis

At any one time a plot of % mass change vs % APP content should show the variation of physical property with composition.
The graph shows change from steep to shallow gradient with first addition.
But in 4 lux the change was at about 19% 32C - this was the normal inversion point for physical properties of APP/bitumen blends.
Therefore this comparison does not work in the dark - it requires full mass gain and accompanying mass loss in each heating period.

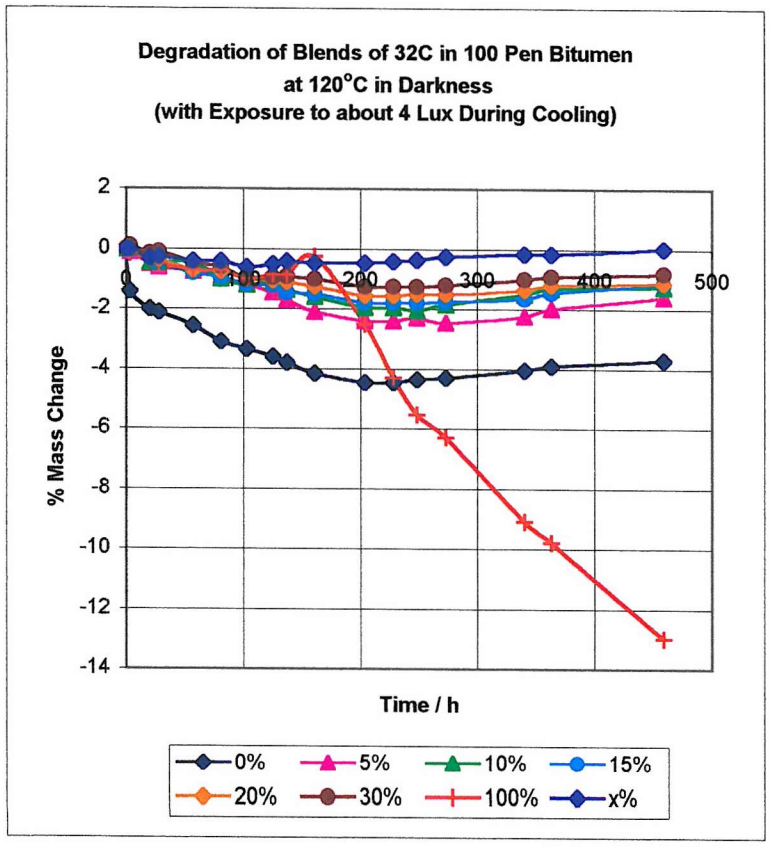

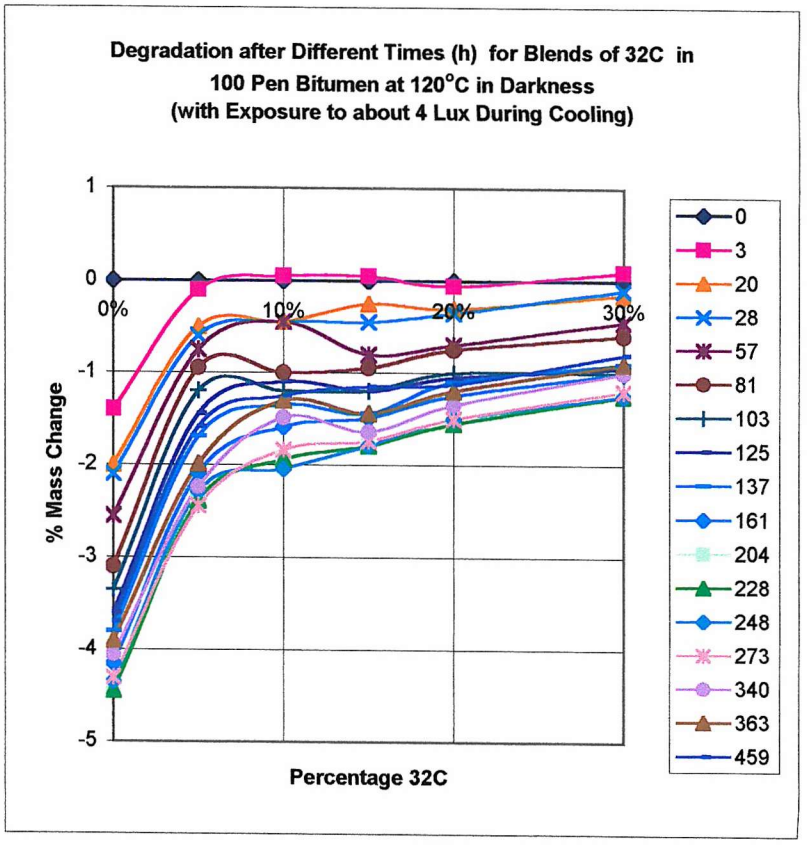

Thermal Degradation

At 120°C in Darkness

32C in 100 Pen Series

Long-Term Thermal Degradation of APPs 1C and MF80 at 120°C in 4 Lux

After 3 Different Sample Treatments A/B/C. **Graphs of % Mass Change vs Time.**

Time / h	% Mass Loss for 1C			% Mass Loss for MF80		
	A	B	C	A	B	C
0.0	0.00	0.00	0.00	0.00	0.00	0.00
2.0	-0.45		-0.50	-0.40		-0.36
2.5		-0.36			-0.33	
4.0	-0.65		-0.58	-0.55		-0.53
4.5		-0.46			-0.48	
6.0	-0.73			-0.65		
6.5		-0.56	-0.75		-0.60	-0.71
8.5	-0.85	-0.59		-0.73	-0.63	
10.5		-0.64			-0.73	
11.5			-0.91			-0.86
13.0		-0.66			-0.68	
13.5	-1.13			-0.95		
15.0		-0.84			-0.80	
15.5			-1.08			-0.81
17.0		-0.97			-0.85	
17.5	-1.23			-0.93		
18.0			-1.13			-0.76
20.0	-1.30	-1.02	-1.18	-0.88	-0.78	-0.61
22.0	-1.35		-1.33	-0.95		-0.86
22.5		-1.20			-0.80	
24.0	-1.50		-1.35	-1.00		-0.84
26.0	-1.53		-1.48	-0.98		-0.84
28.0	-1.65			-1.05		
28.5			-1.48			-0.76
30.5	-1.68		-1.58	-1.04		-0.89
32.0		-1.76			-1.00	
32.5	-1.86		-1.70	-1.15		-0.96
34.5	-1.86	-1.66	-1.75	-1.23	-1.05	-0.86
38.0	-1.98	-1.89	-2.00	-1.20	-1.13	-0.94
52.0	-2.51	-2.32	-2.50	-1.65	-1.46	-1.35
62.0	-2.78	-2.58	-2.85	-1.80	-1.63	-1.50
74.0	-3.26	-3.04	-3.35	-2.00	-1.88	-1.73

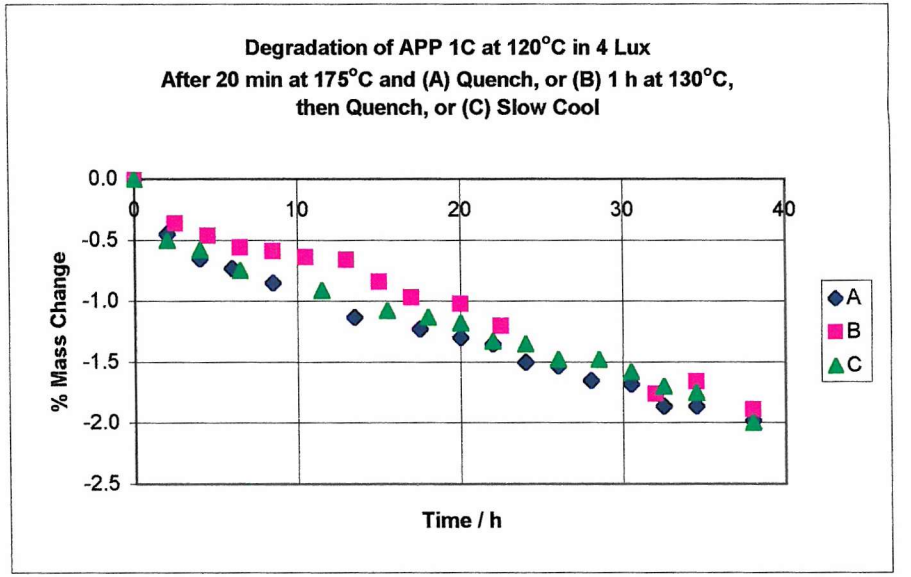

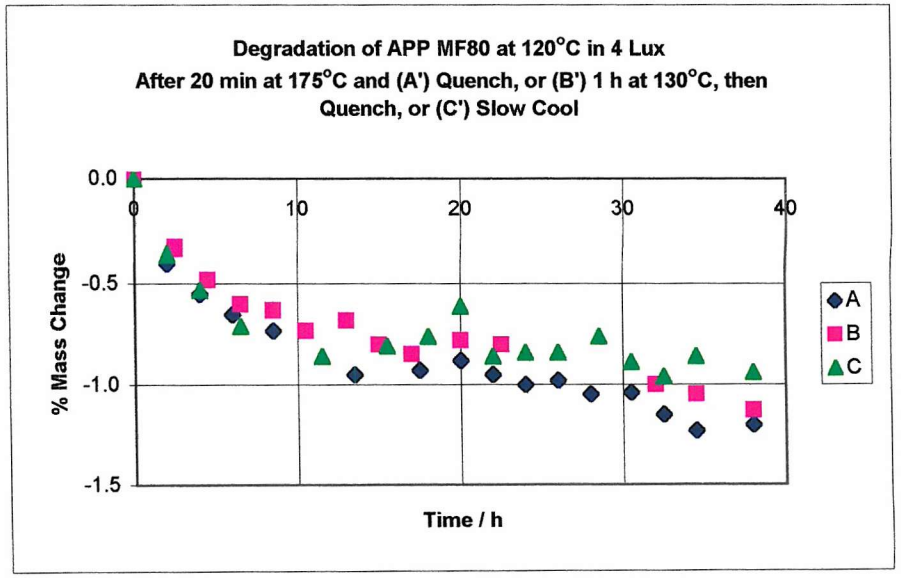

85.0	-3.63	-3.39	-3.83	-2.13	-1.98	-2.01
98.0	-4.14	-3.78	-4.48	-2.33	-2.08	-2.16
107.0	-4.69	-4.21	-5.11	-2.46	-2.16	-2.36
119.0	-5.39	-4.77	-6.03	-2.61	-2.31	-2.51
144.0	-7.17	-6.46	-8.48	-2.98	-2.59	-2.92
168.0	-8.97	-8.60	-11.16	-3.18	-2.86	-3.17
188.0	-10.55	-10.59	-13.54	-3.48	-3.06	-3.40
212.0	-12.56	-12.91	-16.42	-3.78	-3.31	-3.68
235.0	-14.41	-14.96	-18.97	-3.98	-3.44	-3.94
258.0	-16.75	-16.90	-21.37	-4.26	-3.64	-4.14
278.0	-18.68	-18.45	-23.17	-4.38	-3.77	-4.27
308.0	-21.61	-20.70	-25.50	-4.64	-3.92	-4.47
349.0	-24.87	-23.74	-28.00	-4.99	-4.29	-4.80
394.0	-28.00	-26.80	-30.23	-5.36	-4.64	-5.15
439.0	-30.26	-29.20	-31.91	-5.66	-4.87	-5.49
494.0	-32.24	-31.42	-33.36	-6.01	-5.20	-5.97
545.0	-33.62	-32.98	-34.48	-6.44	-5.52	-7.19
613.0	-35.37	-34.89	-36.01	-11.53	-7.18	-10.44
702.0	-37.05	-36.80	-37.39	-17.64	-11.40	-15.49
770.0	-38.21	-37.95	-38.16	-20.57	-15.09	-18.16
866.0	-39.28	-39.15	-39.36	-23.38	-18.55	-20.90
1130.0	-41.56	-41.45	-41.39	-28.14	-24.40	-25.70

Observations

1C, off-white, began to degrade slowly at first, then speeded up.
It gradually levelled off at mass loss about 45 %.
This was approx the value of the atactic content of the APP.
Set C, the slow cooled set, degraded faster all the way.
Set C would have been much less crystalline than Sets A and B
because annealed and subjected to thermal shock.
MF80, nearly black, degraded very slowly up to about 550 h.
By that point it had lost only about 20 % of the loss by 1C.
Set C, the slow cooled set, lost the most mass all the way.
This APP seemed to be protected from degradation ..... by its colour?
(C80, dark brown, was not protected from degradation by its colour).
However from about 550 h, it degraded rapidly, with A > C > B.
It seemed that the mass loss was levelling off to > 35 %.

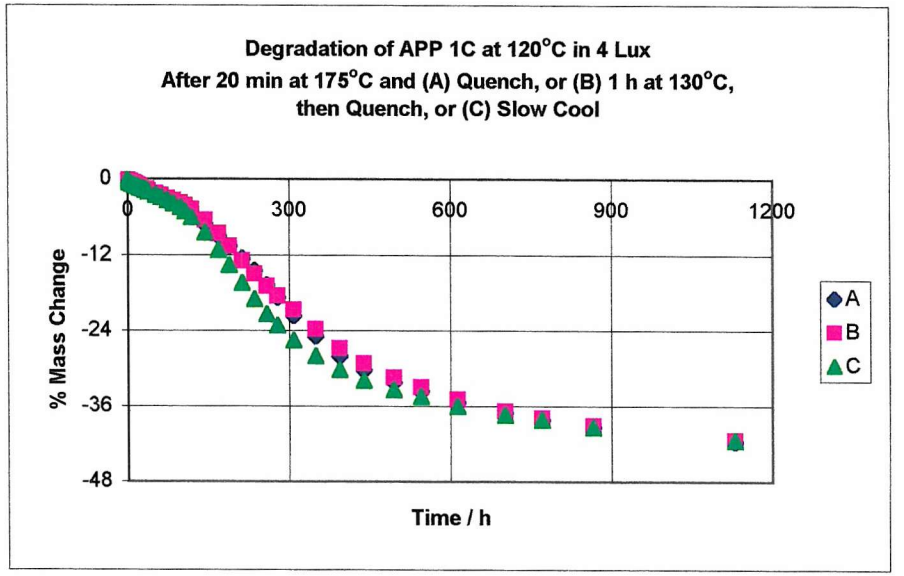

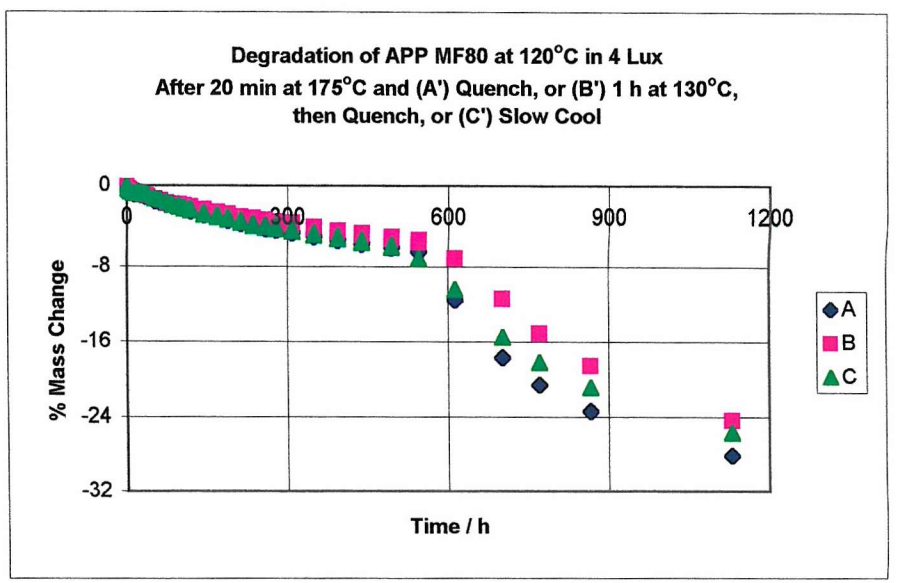

Thermal Degradation At 120°C in 4 Lux 1C and MF80

Long-Term Thermal Degradation of APPs 32C and 43C at 120°C in 4 Lux.

After 3 Different Sample Treatments A/B/C. **Graphs of % Mass Change vs Time.**

Time / h	% Mass Loss for 32C			% Mass Loss for 43C		
	A	B	C	A	B	C
0.0	0.00	0.00	0.00	0.00	0.00	0.00
2.0	0.02		0.05	-0.33		-0.15
2.5		0.00			-0.25	
4.0	0.12		0.05	-0.33		-0.35
4.5		0.00			-0.40	
6.0	0.05			-0.56		
6.5		-0.08	-0.02		-0.53	-0.48
8.5	-0.20	-0.15		-0.74	-0.55	
10.5		-0.50			-0.58	
11.5			-0.30			-0.48
13.0		-0.70			-0.58	
13.5	-0.82			-0.79		
15.0		-0.98			-0.78	
15.5			-0.80			-0.58
17.0		-1.28			-0.93	
17.5	-1.27			-1.04		
18.0			-1.03			-0.63
20.0	-1.55	-1.63	-1.23	-1.04	-1.30	-0.86
22.0	-1.80		-1.50	-1.14		-1.06
22.5		-2.00			-1.61	
24.0	-2.10		-1.68	-1.42		-1.26
26.0	-2.27		-1.98	-1.52		-1.57
28.0	-2.55			-1.90		
28.5			-2.22			-1.85
30.5	-2.65		-2.53	-2.03		-2.33
32.0		-3.08			-2.71	
32.5	-2.90		-2.78	-2.31		-2.83
34.5	-3.12	-3.42	-3.03	-2.56	-2.86	-3.29
38.0	-3.45	-3.65	-3.48	-2.84	-3.26	-4.43
52.0	-4.50	-4.58	-5.08	-4.54	-4.67	-9.91
62.0	-5.09	-5.15	-5.93	-5.76	-5.34	-13.81
74.0	-5.89	-5.70	-7.06	-7.71	-6.62	-17.63
85.0	-6.44	-6.18	-7.91	-9.59	-7.75	-19.42

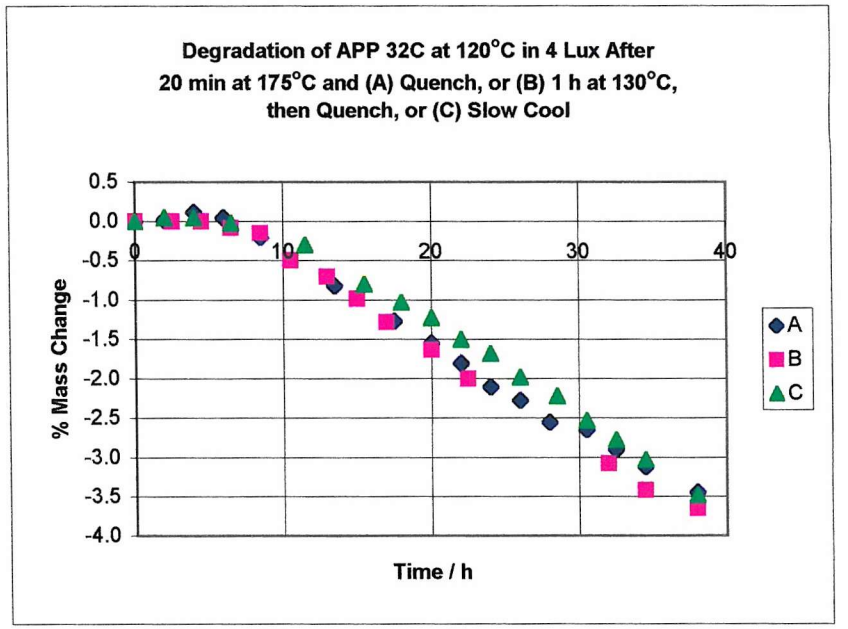

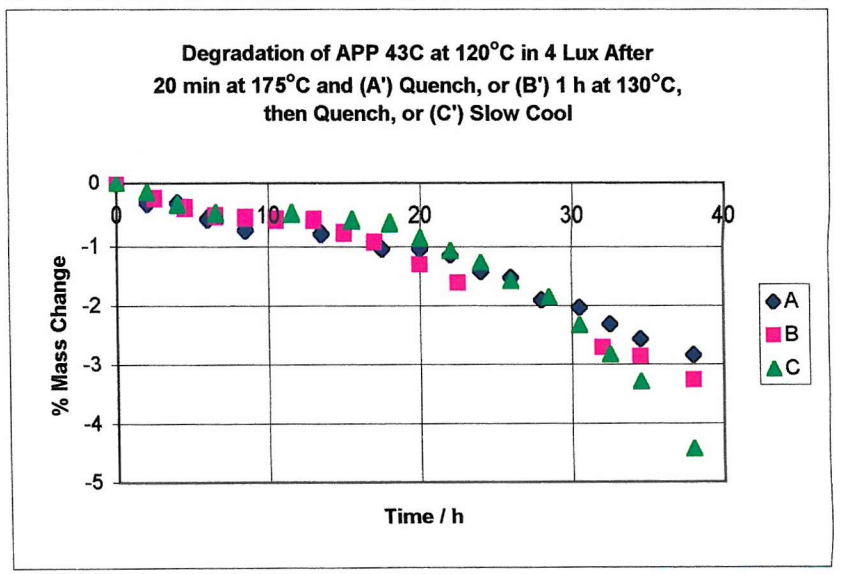

Thermal Degradation At 120°C in 4 Lux 32C and 43C

98.0	-6.99	-6.68	-9.01	-12.40	-9.28	-20.71
107.0	-7.42	-7.05	-9.79	-14.48	-10.39	-21.47
119.0	-7.94	-7.45	-11.16	-16.84	-12.32	-22.26
144.0	-8.84	-8.30	-13.84	-20.04	-16.31	-23.50
168.0	-9.52	-8.90	-15.97	-21.76	-19.32	-24.41
188.0	-10.09	-9.43	-17.75	-22.60	-21.20	-24.99
212.0	-10.89	-10.10	-19.22	-23.56	-22.60	-25.75
235.0	-11.54	-10.60	-20.10	-24.19	-23.48	-26.28
258.0	-12.46	-11.30	-20.75	-24.78	-24.16	-26.76
278.0	-13.66	-11.98	-21.15	-25.16	-24.59	-27.04
308.0	-16.61	-13.63	-21.75	-25.79	-25.29	-27.57
349.0	-20.33	-17.67	-22.45	-26.50	-26.19	-28.28
394.0	-22.85	-21.32	-23.10	-27.34	-26.97	-28.98
439.0	-24.15	-22.87	-23.78	-27.87	-27.62	-29.56
494.0	-25.25	-24.02	-24.43	-28.46	-28.25	-30.15
545.0	-26.02	-24.80	-24.88	-29.09	-28.63	-30.42
613.0	-27.12	-25.85	-25.71	-29.60	-29.40	-31.08
702.0	-28.05	-26.70	-26.31	-30.28	-29.95	-31.61
770.0	-28.87	-27.43	-26.98	-30.84	-30.58	-32.25
866.0	-29.60	-28.07	-27.53	-31.42	-31.13	-32.75
1130.0	-31.37	-29.75	-29.01	-32.82	-32.49	-34.09

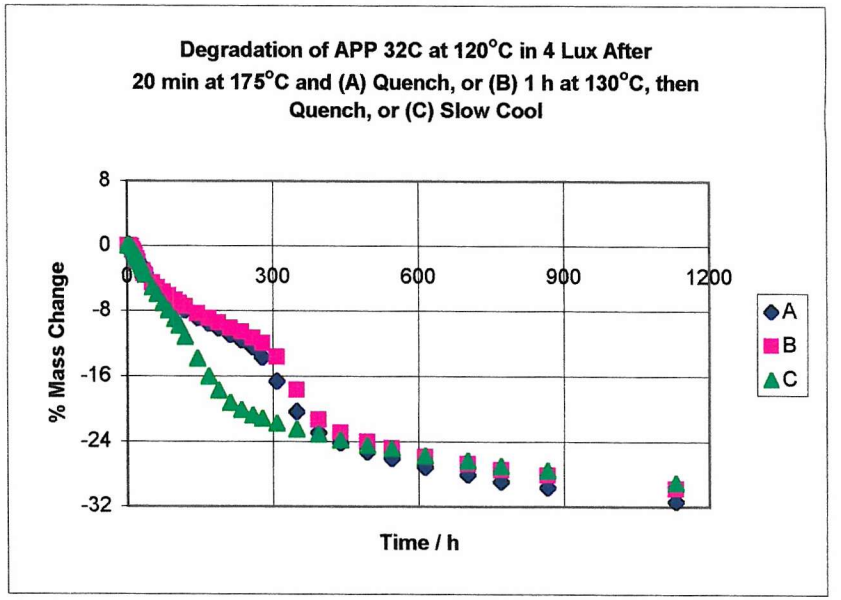

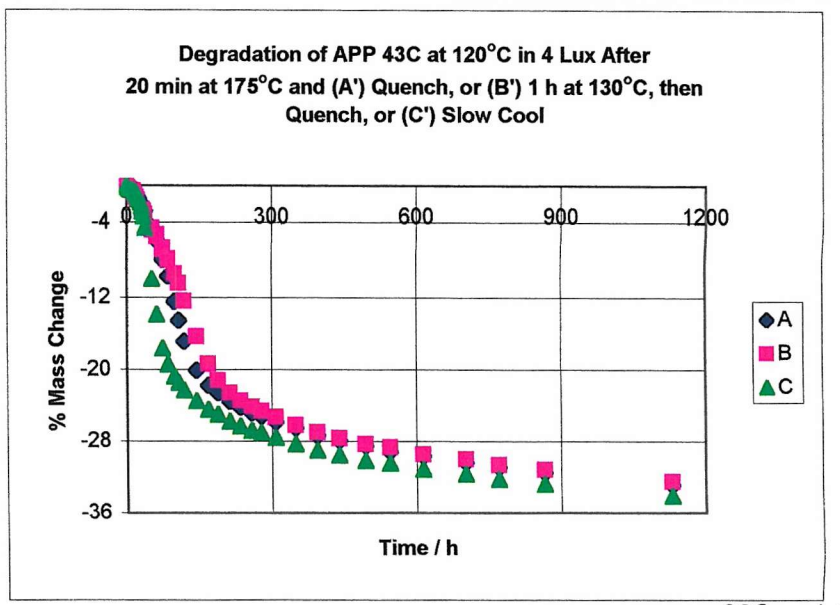

Observations

32C gained mass slightly, and then degraded very fast.
Slow-cooled set C degraded much faster than sets A and B,
as expected for the much less crystalline set.
It levelled off smoothly towards mass loss of at least 32 %.
Both more crystalline quenched sets, A and B, degraded in two sections.
So there were two atactic components, one of 13%, one of at least 20%.
This result fitted with the known atactic content of PE plus APP.
Therefore degradation curves can be used to find out number of atactic components.
43C also degraded very fast from the start, and levelled off at mass loss > 36 %.
Again the slow-cooled set C degraded most all the way.
Again set B degraded slightly less than set A all the way.
This fitted with greater phase separation crystallization at 130°C than at 175°C
... the more crystalline set B was slowest to degrade.

Long-Term Thermal Degradation of APPs MF500 and C80 at 120°C in 4 Lux.

After 3 Different Sample Treatments A/B/C. **Graphs of % Mass Change vs Time.**

Time / h	% Mass Loss for MF500			% Mass Loss for C80		
	A	B	C	A	B	C
0.0	0.00	0.00	0.00	0.00	0.00	0.00
2.0	-0.20		-0.23	-1.70		-0.88
2.5		-0.30			-0.97	
4.0	-0.20		-0.28	-1.75		-1.38
4.5		-0.35			-1.50	
6.0	-0.38			-2.27		
6.5		-0.58	-0.60		-1.94	-1.98
8.5	-0.91	-0.89		-2.76	-2.27	
10.5		-1.37			-2.54	
11.5			-1.64			-2.57
13.0		-1.67			-2.70	
13.5	-1.77			-3.40		
15.0		-2.10			-2.98	
15.5			-2.59			-2.81
17.0		-2.51			-3.16	
17.5	-2.70			-3.71		
18.0			-3.22			-2.94
20.0	-3.79	-3.04	-3.62	-3.84	-3.72	-3.04
22.0	-4.04		-4.05	-4.00		-3.22
22.5		-3.49			-3.82	
24.0	-4.52		-4.38	-4.17		-3.30
26.0	-4.80		-4.38	-4.22		-3.38
28.0	-5.51			-4.48		
28.5			-4.73			-3.46
30.5	-5.71		-5.11	-4.51		-3.66
32.0		-4.93			-4.77	
32.5	-6.09		-5.49	-4.71		-3.87
34.5	-6.31	-5.06	-6.14	-4.89	-4.74	-3.85
38.0	-6.85	-5.47	-6.70	-5.02	-4.87	-3.98
52.0	-8.31	-6.78	-8.26	-5.79	-5.38	-4.73
62.0	-9.04	-7.59	-9.16	-6.21	-5.74	-5.12
74.0	-9.98	-8.40	-10.09	-6.75	-6.12	-5.56
85.0	-10.63	-9.06	-10.85	-7.08	-6.47	-5.93

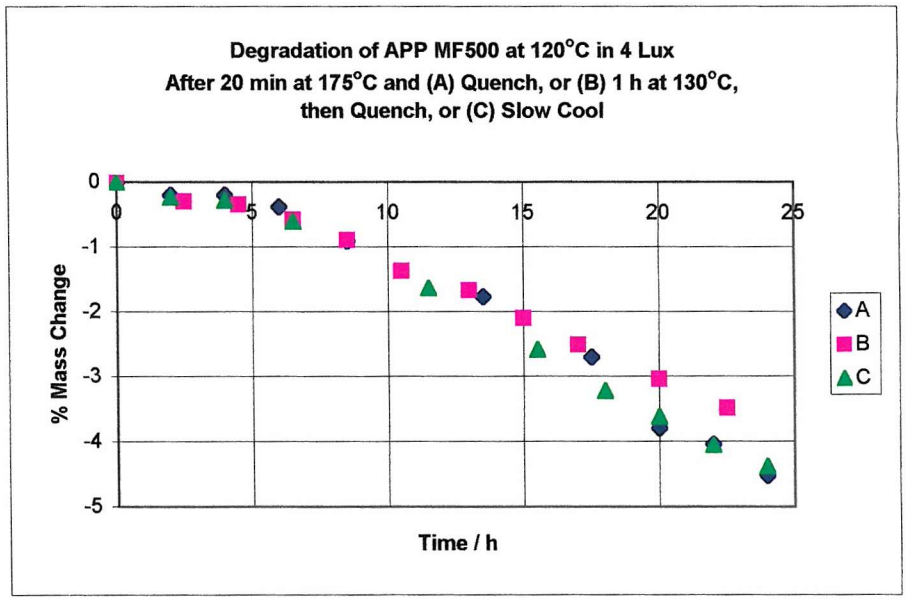

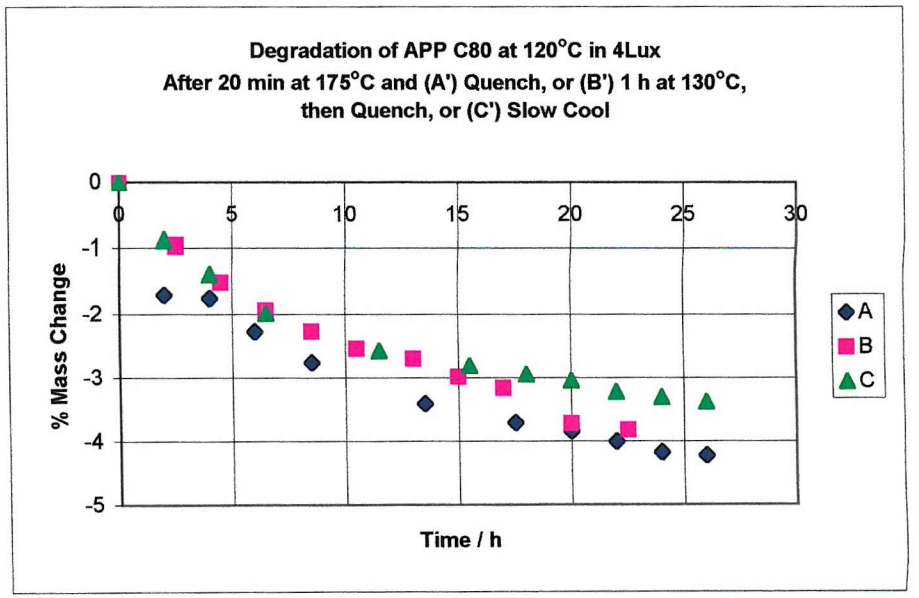

Thermal Degradation At 120°C in 4 Lux MF500 and C80

98.0	-11.44	-9.74	-11.68	-7.52	-6.73	-6.31
107.0	-11.87	-10.20	-12.33	-7.80	-7.01	-6.50
119.0	-12.50	-10.80	-13.34	-8.19	-7.26	-6.78
144.0	-13.59	-11.89	-15.35	-8.88	-7.80	-7.43
168.0	-14.45	-12.88	-17.17	-9.53	-8.28	-8.00
188.0	-15.38	-13.84	-18.85	-10.04	-8.64	-8.37
212.0	-16.77	-15.18	-20.82	-10.71	-9.15	-8.91
235.0	-18.16	-16.37	-22.43	-11.18	-9.56	-9.33
258.0	-19.75	-17.81	-23.76	-11.67	-10.02	-9.77
278.0	-21.19	-19.05	-24.62	-12.08	-10.40	-10.14
308.0	-22.96	-20.98	-25.67	-12.77	-10.94	-10.68
349.0	-24.73	-23.30	-26.78	-13.75	-11.73	-11.51
394.0	-26.24	-25.18	-27.94	-14.83	-12.59	-12.45
439.0	-27.28	-26.27	-28.90	-15.89	-13.41	-13.36
494.0	-28.24	-27.35	-29.68	-17.07	-14.40	-14.35
545.0	-29.00	-28.19	-30.41	-18.00	-15.24	-15.10
613.0	-30.18	-29.20	-31.39	-19.37	-16.34	-16.29
702.0	-31.14	-30.24	-32.34	-20.78	-17.59	-17.57
770.0	-31.93	-31.05	-33.12	-21.79	-18.46	-18.45
866.0	-32.81	-31.78	-33.80	-22.94	-19.47	-19.44
1130.0	-34.60	-33.45	-35.59	-25.34	-21.69	-21.65

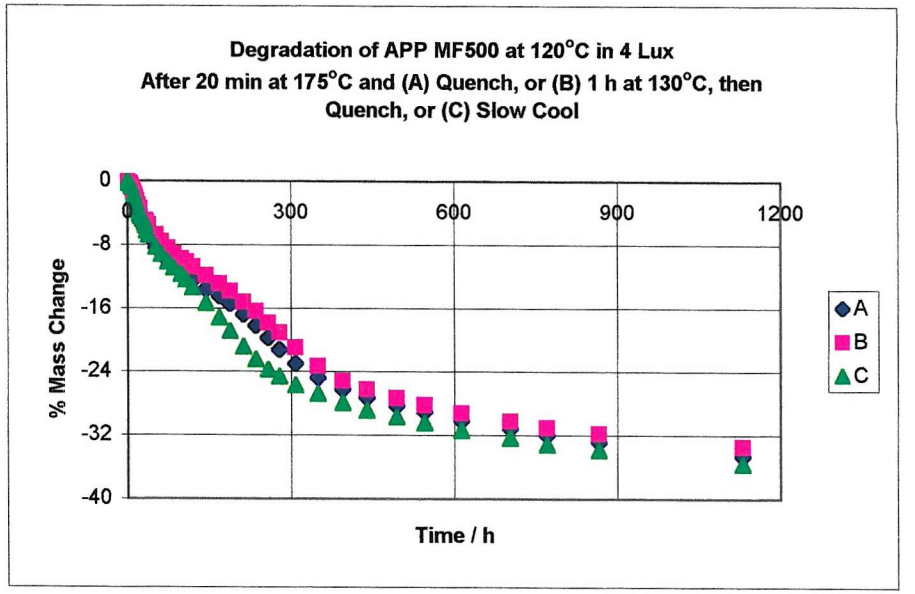

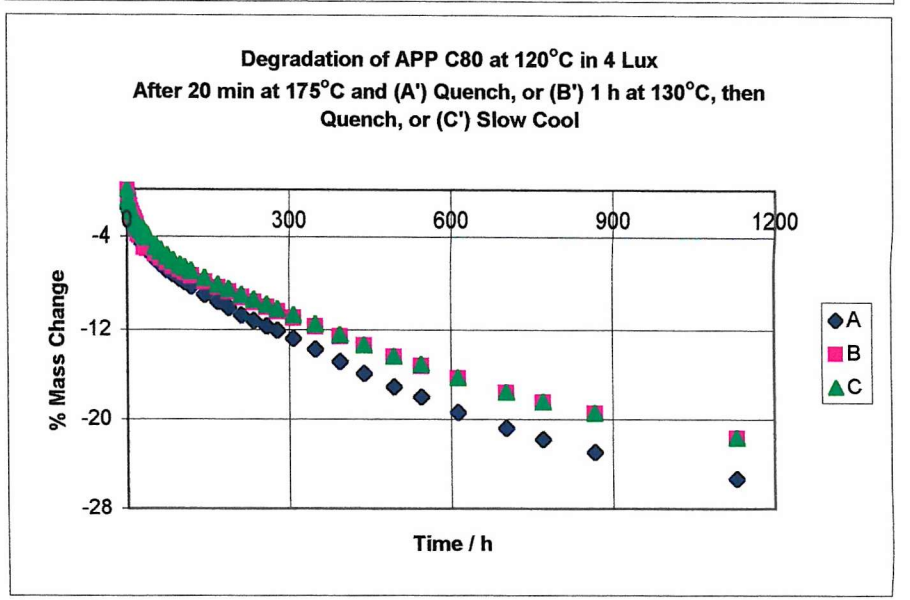

Observations

MF500, a white "APP," degraded very rapidly from the start.

Mass loss began to slow down but speeded up again from 15% loss.

After steady fast loss till about 25% loss, it began to slow down again.

The curve seemed to be levelling off towards about 40% loss.

So MF500 contained two atactic components, comprising 15% and 25% of the total.

Slow-cooled set C, the least crystalline, degraded fastest all the way.

Set A, quenched from 175°C, was next, and set B, quenched from 130°C, was slowest.

Therefore set B was the most crystalline -

this was to be expected since the optimum temperature

for phase separation crystallization of PP is about 65°C.

C80 was not protected from degradation by its dark brown colour.

Sets B and C gave virtually identical mass loss curves.

Set A degraded much faster than B and C, so must have been the least crystalline.

So even slow cooling caused as much crystallization as annealing at 130°C.

Thermal Degradation At 120°C in 4 Lux MF500 and C80

Long-Term Thermal Degradation of APPs T1180 and 95-X-06 at 120°C in 4 Lux

After 3 Different Sample Treatments A/B/C. **Graphs of % Mass Change vs Time.**

Time / h	% Mass Loss for T1180			% Mass Loss for 95-X-06		
	A	B	C	A	B	C
0.0	0.00	0.00	0.00	0.00	0.00	0.00
2.0	-1.13		-1.23	-0.74		-0.43
2.5		-1.53			-0.55	
4.0	-2.56		-2.21	-0.91		-0.48
4.5		-2.43			-0.65	
6.0	-3.48			-0.94		
6.5		-3.24	-3.27		-0.70	-0.53
8.5	-4.43	-3.91		-1.19	-0.77	
10.5		-4.56			-1.00	
11.5			-4.76			-0.76
13.0		-5.08			-1.15	
13.5	-5.79			-1.86		
15.0		-5.65			-1.35	
15.5			-5.74			-1.21
17.0		-6.01			-1.52	
17.5	-6.50			-2.52		
18.0			-5.94			-1.57
20.0	-7.04	-6.71	-6.22	-3.00	-2.07	-2.00
22.0	-7.35		-6.62	-3.46		-2.45
22.5		-7.23			-2.20	
24.0	-7.81		-6.95	-3.99		-2.81
26.0	-8.12		-7.17	-4.45		-3.23
28.0	-8.45			-4.98		
28.5			-7.50			-3.56
30.5	-8.70		-7.78	-5.39		-4.22
32.0		-8.94			-3.25	
32.5	-8.96		-8.08	-6.02		-4.73
34.5	-9.37	-9.12	-8.41	-6.48	-3.32	-5.21
38.0	-9.70	-9.58	-8.86	-7.24	-3.60	-6.24
52.0	-11.11	-10.75	-10.14	-10.29	-4.35	-10.01
62.0	-11.88	-11.45	-10.90	-11.84	-4.85	-12.16
74.0	-12.70	-12.10	-11.70	-13.95	-5.50	-14.71
85.0	-13.31	-12.56	-12.28	-15.76	-5.92	-16.58

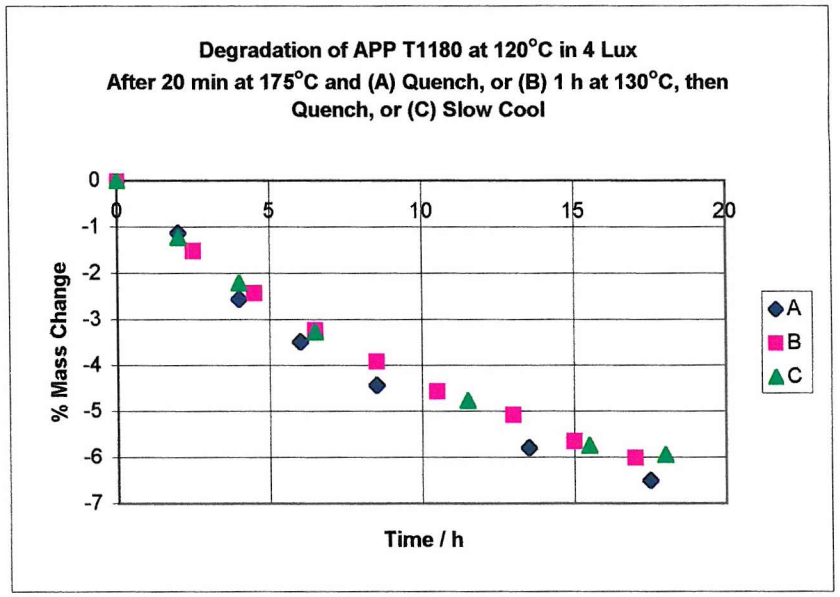

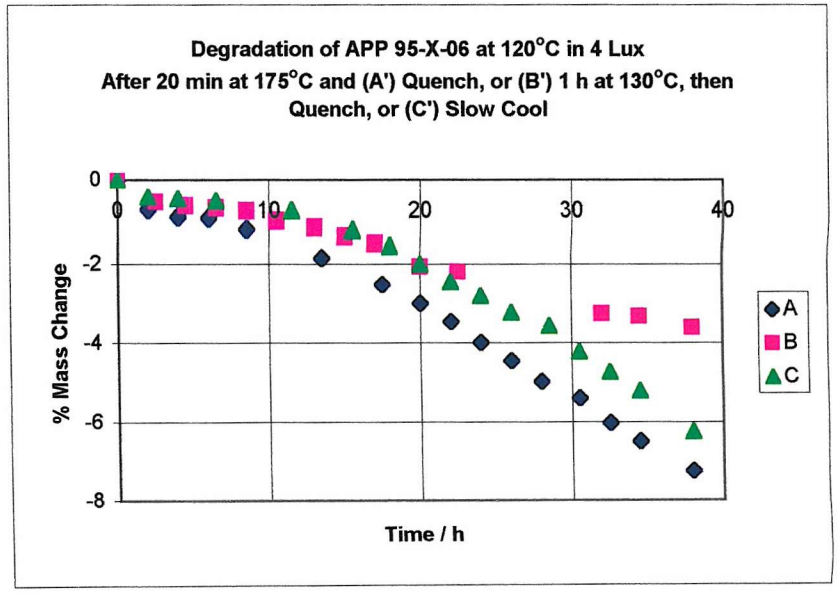

98.0	-13.85	-13.00	-12.84	-17.84	-6.47	-18.32
107.0	-14.26	-13.39	-13.26	-19.36	-6.94	-19.23
119.0	-14.64	-13.93	-13.67	-21.19	-7.44	-20.09
144.0	-15.31	-14.81	-14.20	-23.91	-9.14	-21.41
168.0	-16.49	-15.77	-15.18	-25.31	-11.54	-22.39
188.0	-17.38	-16.49	-16.26	-26.20	-14.59	-23.07
212.0	-18.31	-17.28	-17.32	-27.12	-18.59	-23.83
235.0	-18.82	-17.74	-18.02	-27.70	-21.03	-24.31
258.0	-19.38	-18.26	-18.73	-28.28	-22.23	-24.84
278.0	-19.76	-18.60	-19.13	-28.67	-23.03	-25.20
308.0	-20.28	-19.06	-19.76	-29.28	-23.96	-25.70
349.0	-20.92	-19.76	-20.44	-30.04	-25.11	-26.48
394.0	-21.61	-20.41	-21.22	-30.85	-26.11	-27.24
439.0	-22.15	-20.33	-21.82	-31.51	-26.93	-27.77
494.0	-22.71	-21.13	-22.28	-32.27	-27.75	-28.56
545.0	-23.12	-21.68	-22.78	-32.78	-28.40	-29.06
613.0	-23.78	-22.30	-23.48	-33.60	-29.30	-29.92
702.0	-24.30	-22.87	-24.01	-34.31	-30.08	-30.63
770.0	-24.76	-23.31	-24.44	-35.02	-30.80	-31.29
866.0	-25.24	-23.78	-24.89	-35.60	-31.38	-31.84
1130.0	-26.22	-24.84	-25.87	-37.05	-32.90	-33.36

Observations

T1180 degraded rapidly from the start with no initial slow stage.
The kink at 14% in the degradation curve indicated 2 atactic components.
The curve was levelling off towards possibly 32% mass loss.
Set B, quenched from annealing at 130°C was slowest, so most crystalline.
Therefore quench or slow cool from 175°C made little difference, therefore supplied material was not very crystalline and not subject to thermal shock.

95-X-06 began to degrade slowly but smoothly speeded up.
Set A was very fast all the way, so supplied material was not highly crystalline.
Set B was took 144 h getting to the fast stage; after that stage it matched set B.
Set C was very close to set A till 120 h but then slowed down more than did set A.
In the short term (300 h), speed of cooling from 175°C made little difference - crystallinity was so low that thermal shock had no effect.
In the long term (>300 h), slow cool or annealing at 130°C produced similar crystallinity.

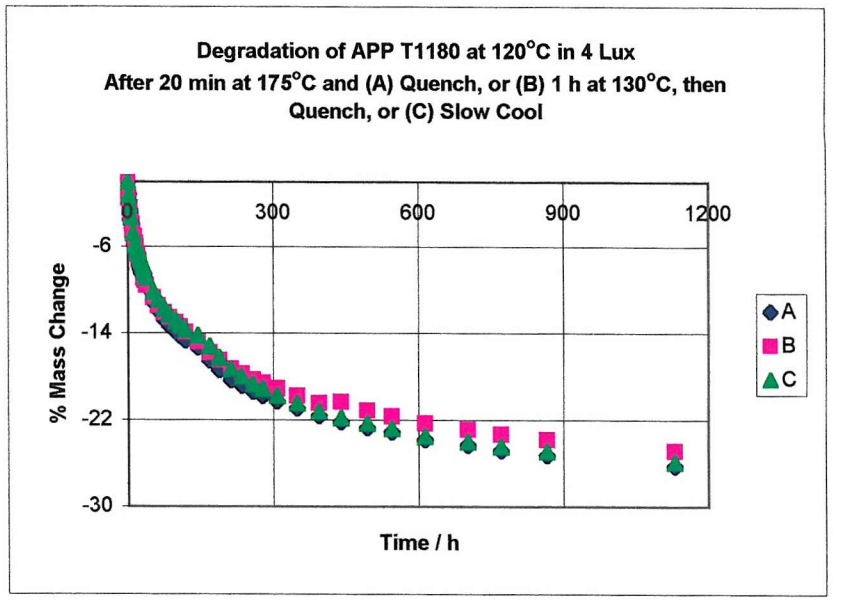

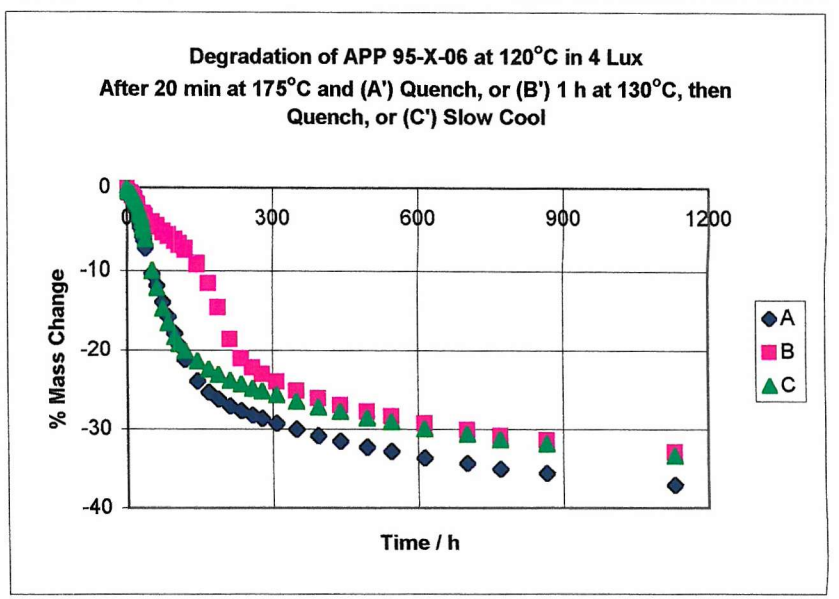

Long-Term Thermal Degradation of APPs V808 and V891 at 120°C in 4 Lux.

After 3 Different Sample Treatments A/B/C. **Graphs of % Mass Change vs Time.**

Time / h	% Mass Loss for V808			% Mass Loss for V891		
	A	B	C	A	B	C
0.0	0.00	0.00	0.00	0.00	0.00	0.00
2.0	0.02		0.00	0.00		0.10
2.5		-0.05			0.10	
4.0	0.02		0.02	0.10		0.07
4.5		-0.02			0.10	
6.0	0.10			0.10		
6.5		0.00	0.00		0.15	0.07
8.5	0.02	-0.02		0.10	0.20	
10.5		0.02			0.13	
11.5			0.02			0.12
13.0		0.12			0.22	
13.5	0.20			0.20		
15.0		0.20			0.22	
15.5			0.02			0.19
17.0		0.10			0.22	
17.5	0.13			0.23		
18.0			0.15			0.27
20.0	0.20	0.30	0.17	0.28	0.30	0.27
22.0	0.23		0.10	0.03		0.22
22.5		0.30			0.20	
24.0	0.18		0.10	0.23		0.27
26.0	0.18		0.22	0.28		0.27
28.0	0.23			0.23		
28.5			0.27			0.31
30.5	0.33		0.32	0.33		0.27
32.0		0.37			0.18	
32.5	0.35		0.25	0.25		0.24
34.5	0.38	0.40	0.40	0.25	0.25	0.29
38.0	0.33	0.35	0.32	0.25	0.20	0.36
52.0	0.28	0.25	0.17	0.33	0.05	0.39
62.0	0.33	0.27	0.10	0.18	-0.15	0.39
74.0	0.33	0.20	-0.25	0.10	-0.38	0.34
85.0	0.38	0.22	-0.62	-0.10	-0.58	0.34

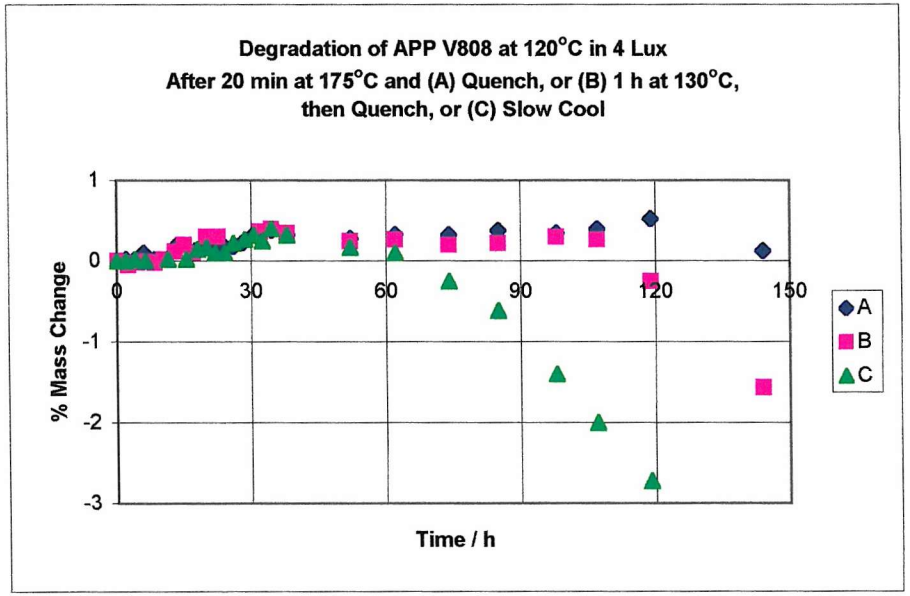

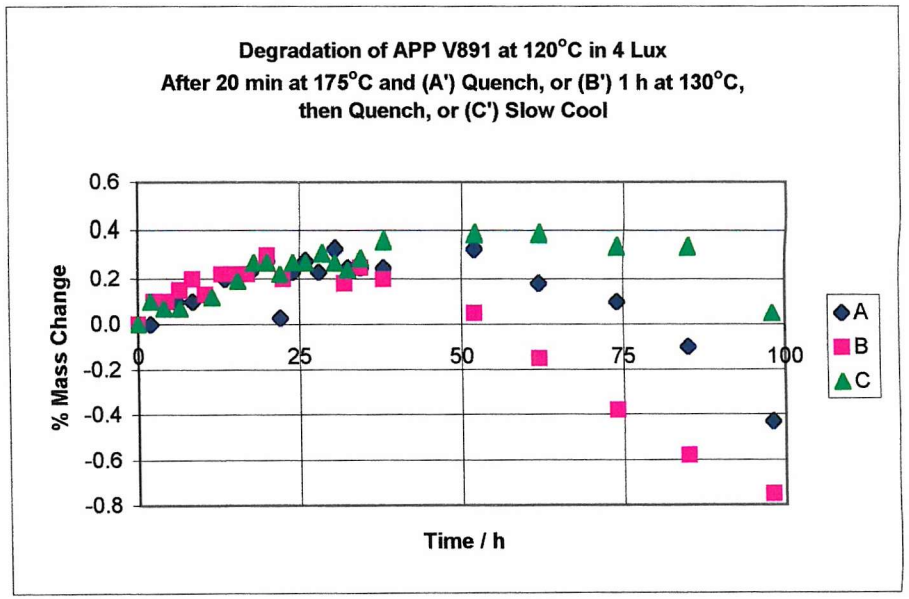

98.0	0.35	0.30	-1.40	-0.43	-0.75	0.05
107.0	0.40	0.27	-2.00	-0.60	-0.90	-0.19
119.0	0.53	-0.25	-2.72	-0.88	-1.05	-0.72
144.0	0.13	-1.57	-3.90	-1.28	-1.35	-2.00
168.0	-1.19	-2.49	-4.72	-1.93	-1.98	-2.99
188.0	-2.12	-3.14	-5.25	-2.71	-2.71	-3.71
212.0	-3.08	-3.87	-6.02	-3.62	-3.43	-4.48
235.0	-4.04	-4.39	-6.15	-4.19	-3.96	-5.06
258.0	-4.72	-4.96	-6.72	-4.75	-4.54	-5.64
278.0	-5.25	-5.44	-7.15	-5.28	-4.96	-6.00
308.0	-6.28	-5.91	-7.62	-6.05	-5.49	-6.34
349.0	-6.79	-6.71	-8.45	-6.98	-6.24	-7.25
394.0	-7.65	-7.58	-9.27	-7.84	-6.99	-8.10
439.0	-8.35	-8.18	-9.90	-8.39	-8.27	-8.82
494.0	-9.11	-8.88	-10.67	-9.04	-8.97	-9.59
545.0	-9.67	-9.48	-11.22	-9.62	-9.77	-10.39
613.0	-10.50	-10.18	-12.17	-10.37	-10.55	-11.30
702.0	-11.38	-11.00	-13.22	-11.18	-11.28	-12.24
770.0	-12.06	-11.67	-13.97	-11.78	-11.88	-13.02
866.0	-12.85	-12.45	-14.87	-12.48	-12.53	-13.83
1130.0	-15.70	-14.34	-17.07	-14.14	-14.11	-15.59

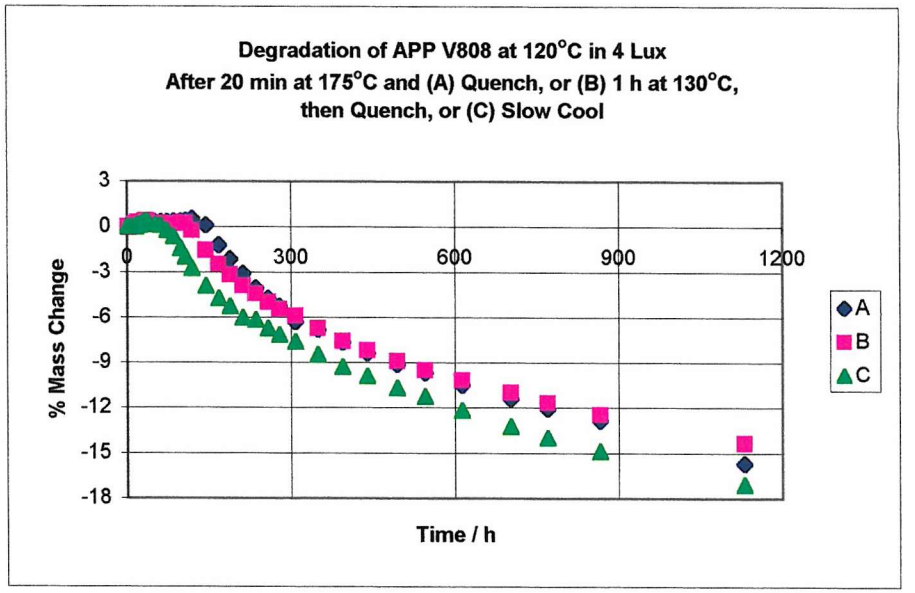

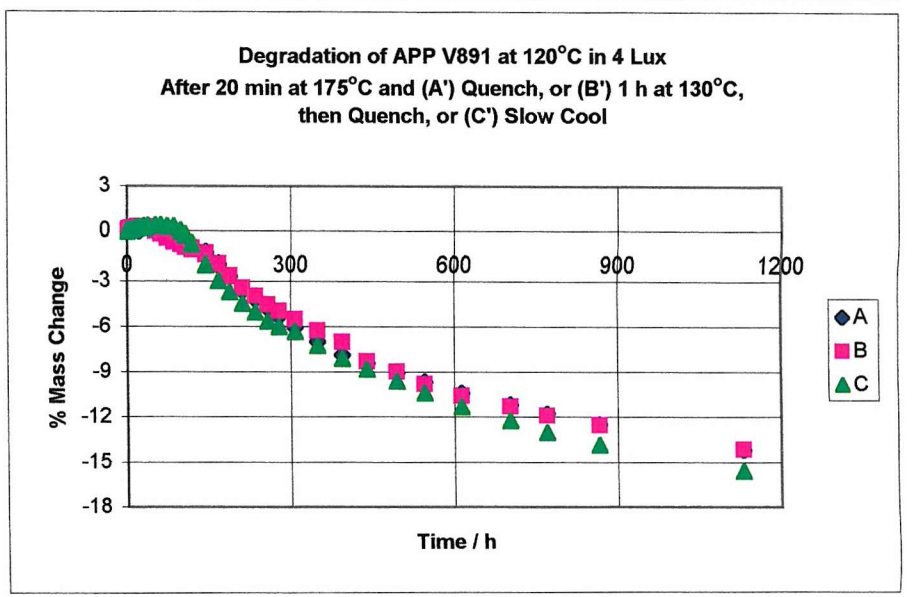

Observations

V808 samples all gained mass to start with, but varied widely in 'take off' time.
Set C gained 0.4 % before degrading earliest, from 34.5 h, and always fastest.
Set B gained 0.27 % before degrading from 107 h.
Set A gained 0.53 % before degrading from 119 h (so plot close to B).
Deduction: high temperature annealing created
less crystallinity than the very slow cooling.

V891 behaved differently early on, and C was closer to A and B than for V808.
Set C gained 0.39 % before being last to begin degradation from 85 h -
once started it was the fastest.
Set B gained 0.3 % before starting to degrade first from 32.5 h.
Set A gained 0.33 % before degrading from 52 h.

Deductions: V891 had slightly higher crystallinity - it gained the required mass for degradation sooner, and preparation had less effect.
V891 was very similar to V808 from about 300 h, so they had similar tacticity.

Long-Term Thermal Degradation of APP 1C at 120°C in the Dark

After 3 Different Sample Treatments A/B/C. **Graphs of % Mass Change vs Time.**

1st Set=A/B/C, 2nd Set=A'/B'/C'

Time/h	% Mass Losses					
	A	B	C	A'	B'	C'
0	0.00	0.00	0.00	0.00	0.00	0.00
2	-0.24	-0.25	-0.15	-0.20	-0.10	-0.15
20	-0.49	-0.44	-0.49	-0.29	-0.39	-0.35
44	-0.49	-0.34	-0.39	-0.39	-0.58	-0.40
62	-0.63	-0.34	-0.34	-0.29	-0.49	-0.25
81	-0.73	-0.39	-0.34	-0.49	-0.63	-0.40
100	-0.87	-0.54	-0.59	-0.74	-0.83	-0.60
142	-1.12	-0.59	-0.78	-0.88	-1.02	-0.65
167	-1.21	-0.89	-0.98	-1.03	-1.22	-0.90
186	-1.36	-0.94	-0.98	-1.13	-1.31	-0.94
204	-1.55	-1.13	-1.28	-1.23	-1.46	-1.19
229	-1.80	-1.23	-1.37	-1.37	-1.66	-1.34
250	-1.70	-1.23	-1.52	-1.52	-1.70	-1.29
264	-1.90	-1.33	-1.62	-1.62	-1.90	-1.44
285	-2.09	-1.38	-1.91	-1.77	-1.95	-1.59
309	-2.24	-1.53	-2.21	-1.91	-2.14	-1.79
330	-2.28	-1.57	-2.84	-2.06	-2.39	-1.89
377	-2.96	-1.92	-5.74	-2.70	-2.92	-3.73
421	-3.40	-2.31	-7.75	-3.34	-3.41	-6.71
464	-4.52	-2.56	-10.79	-5.50	-6.09	-9.50
536	-7.92	-2.90	-13.14	-9.18	-10.08	-11.83
607	-11.27	-3.44	-15.06	-12.32	-13.58	-13.67
677	-13.75	-4.43	-16.33	-14.87	-16.07	-14.92
722	-15.35	-6.25	-17.17	-16.34	-17.43	-15.61
773	-17.25	-8.81	-18.34	-18.25	-19.47	-16.81
811	-18.66	-9.94	-18.98	-19.53	-20.74	-17.65
880	-22.16	-13.78	-20.11	-19.87	-22.44	-18.95
935	-23.03	-15.60	-20.65	-20.90	-23.42	-19.44
1004	-24.88	-18.11	-21.82	-22.57	-25.02	-20.59
1093	-26.34	-20.72	-22.95	-24.19	-26.44	-21.68
1159	-27.41	-22.39	-23.69	-25.32	-27.46	-22.48
1255	-28.52	-22.79	-24.52	-26.35	-28.43	-23.37
1520	-31.10	-27.95	-26.78	-29.05	-31.16	-25.61

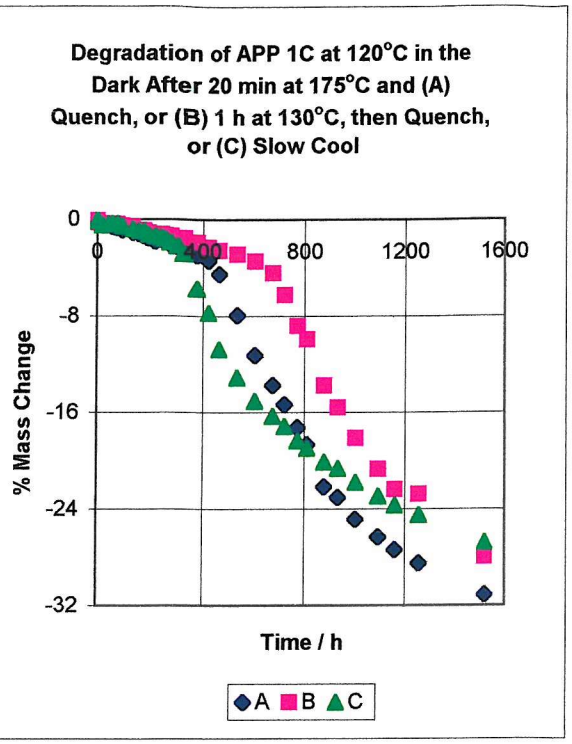

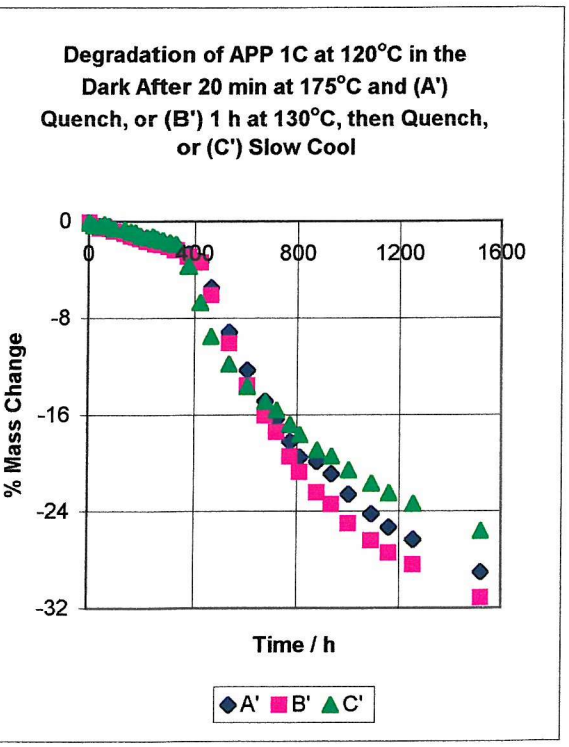

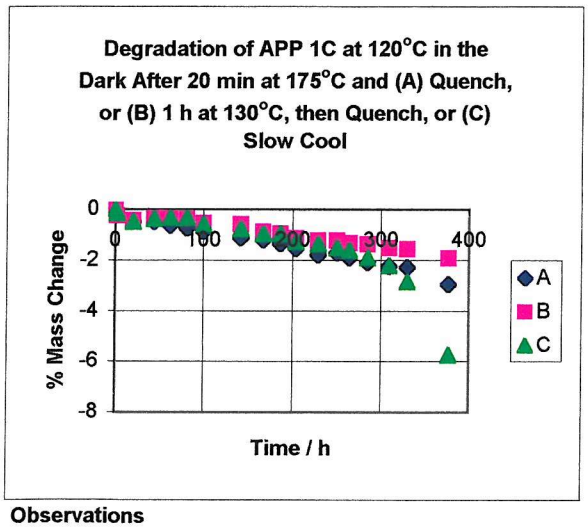

Observations

All 3 sets started off with slow mass loss, a small mass gain from about 20 h, and then continued slow mass gain.
Onset of fast stage was in order C, A, B - from about 300 h, 420 h and 650 h respectively.
Rapid mass loss gradients were all the same initially, but C began to level off much sooner than the others.
All 3 sets looked likely to level off in mass loss, in the order C, A, B.
Same pattern was observed in the 2nd set of 32C samples treated in same way except for position inside tin.
Eventual final mass loss would probably have been about 40 % - approx the same as the atactic content.
Samples came unstuck from their slides as they degraded and lost 'tack' -
A, A' and C' at 264 h, C at 285 h, B' at 309 h, B at 607 h.

Long-Term Thermal Degradation of APP 32C at 120°C in the Dark

After 3 Different Sample Treatments A/B/C. **Graphs of % Mass Change vs Time.**

1st Set=A/B/C, 2nd Set=A'/B'/C'

Time/h	% Mass Losses					
	A	B	C	A'	B'	C'
0	0.00	0.00	0.00	0.00	0.00	0.00
2	-0.15	0.05	-0.05	-0.19	0.05	0.15
20	0.10	-0.10	0.15	0.29	0.15	0.38
44	-0.63	-0.98	-0.29	-0.72	-0.88	0.05
62	-1.41	-1.71	-0.98	-1.53	-1.51	-0.24
81	-2.24	-2.60	-2.20	-2.59	-2.53	-1.57
100	-3.11	-3.33	-3.62	-3.64	-3.21	-2.76
142	-5.54	-5.78	-8.62	-6.47	-4.97	-6.67
167	-7.48	-7.74	-12.54	-8.38	-6.82	-10.19
186	-9.14	-9.16	-14.30	-9.91	-8.13	-12.19
204	-11.22	-11.27	-15.52	-11.88	-10.18	-13.95
229	-14.33	-14.60	-16.99	-15.18	-13.29	-15.76
250	-16.33	-16.85	-17.68	-17.05	-15.68	-16.48
264	-17.40	-18.13	-18.12	-18.06	-16.89	-16.90
285	-18.32	-19.26	-18.66	-19.01	-17.92	-17.67
309	-19.14	-20.09	-19.29	-19.78	-18.84	-18.10
330	-19.83	-20.87	-19.78	-20.45	-19.57	-18.67
377	-21.14	-22.39	-21.01	-21.65	-20.93	-19.76
421	-21.87	-23.22	-21.89	-22.41	-21.76	-20.67
464	-22.84	-24.30	-22.67	-23.47	-22.64	-21.57
536	-23.57	-24.99	-23.51	-24.23	-23.32	-22.52
607	-24.54	-26.11	-24.53	-25.14	-24.25	-23.29
677	-24.88	-26.56	-24.83	-25.43	-24.78	-23.86
722	-25.17	-26.95	-25.56	-25.86	-24.98	-24.24
773	-25.61	-27.44	-25.95	-26.34	-25.46	-24.18
811	-26.19	-27.93	-26.49	-26.82	-25.85	-25.29
880	-26.58	-28.37	-26.93	-27.16	-26.39	-25.67
935	-26.82	-28.61	-27.28	-27.35	-26.58	-26.10
1004	-27.45	-29.30	-27.96	-27.97	-27.22	-26.90
1093	-28.04	-29.84	-28.50	-28.50	-27.75	-27.33
1159	-28.43	-30.43	-29.04	-28.98	-28.19	-27.86
1255	-28.67	-30.72	-29.38	-29.26	-28.53	-28.24
1520	-29.59	-31.90	-30.51	-30.27	-29.55	-29.33

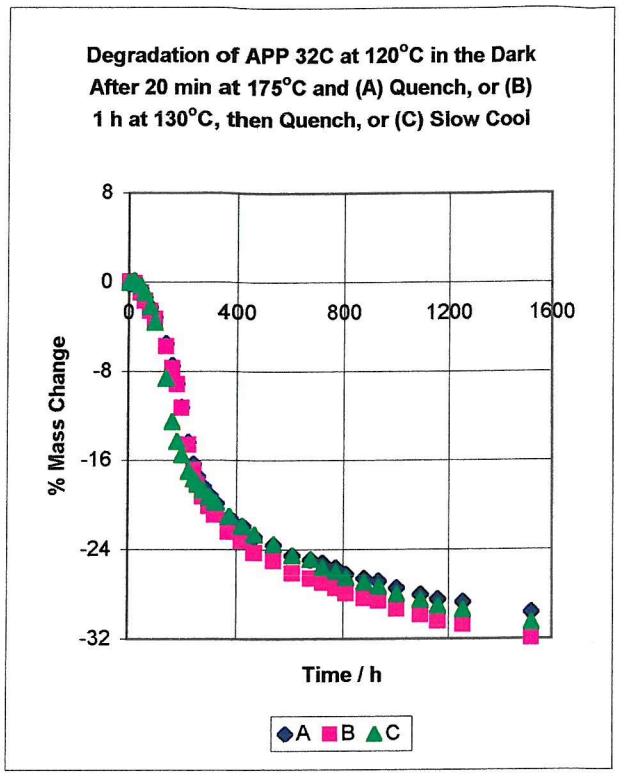

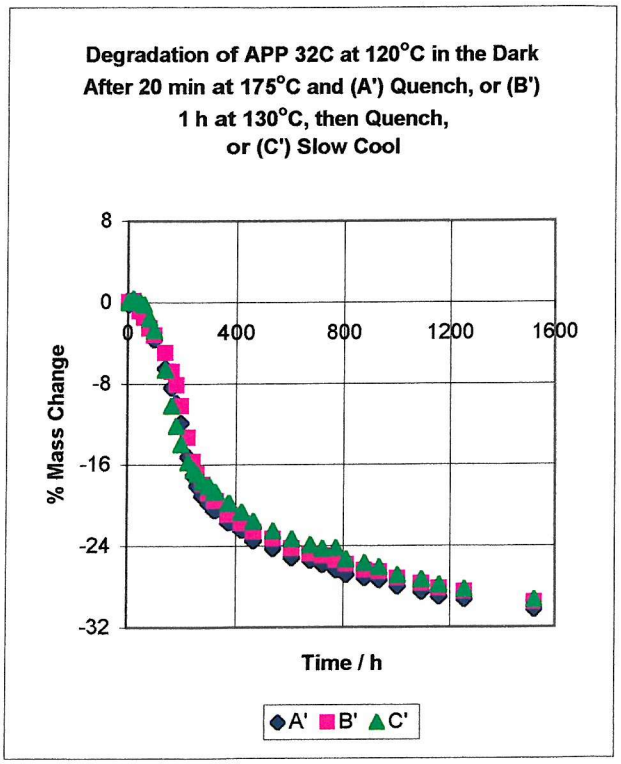

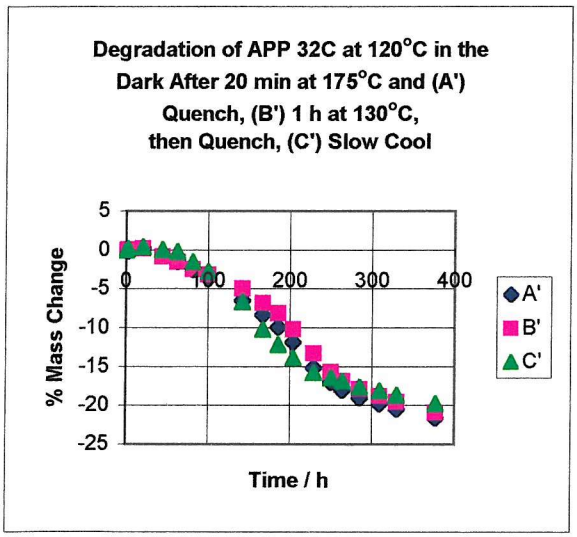

Observations

All 3 sets gained mass very slightly initially, and then lost mass slowly for only a very short time.
They all changed to fast mass loss, first C (from about 80 h), later A and B almost together (from about 130 h).
The fast mass loss gradients were the same, with a spread of the graph of about 50 h.
C began to level off sooner (at about 200 h) than A and B (about 260 h).
Eventual final mass losses for A, B and C would probably have been 35-40 %.
The same pattern was oberved for the repeat set of samples, treated identically except for position in oven.
The order for fast "take-off" was C, then A, then B, with a spread of the graph was only 23 h.
Degree of yellowing by 100 h = C > A = B.

Long-Term Thermal Degradation of APP 43C at 120°C in the Dark.

After 3 Different Sample Treatments A/B/C.

Graphs of % Mass Change vs Time.

1st Set=A/B/C, 2nd Set=A'/B'/C'

Time/h	% Mass Losses					
	A	B	C	A'	B'	C'
0	0.00	0.00	0.00	0.00	0.00	0.00
2	-0.15	0.10	-0.10	-0.10	0.15	0.00
20	-0.35	-0.45	-0.35	-0.15	-0.45	-0.35
44	-0.10	-1.04	-0.94	-0.84	-0.74	-0.75
62	-0.76	-1.54	-1.78	-1.14	-1.42	-1.55
81	-1.92	-2.43	-3.60	-2.18	-2.21	-3.15
100	-3.09	-3.18	-5.57	-3.12	-3.00	-4.95
142	-6.33	-5.56	-11.05	-5.45	-5.11	-9.85
167	-8.81	-7.34	-13.27	-7.39	-6.88	-12.54
186	-10.53	-8.64	-14.26	-8.73	-8.01	-13.64
204	-12.15	-10.27	-15.10	-10.21	-9.58	-14.49
229	-14.02	-12.61	-16.13	-12.35	-11.59	-15.54
250	-15.03	-14.04	-16.72	-13.68	-12.92	-16.09
264	-15.54	-14.94	-17.02	-14.53	-13.80	-16.44
285	-16.30	-15.78	-17.46	-15.52	-14.73	-16.89
309	-16.95	-16.48	-17.96	-16.26	-15.52	-17.34
330	-17.51	-17.07	-18.35	-16.86	-16.01	-17.74
377	-18.57	-18.31	-19.24	-18.10	-17.19	-18.79
421	-19.38	-19.06	-19.88	-18.84	-17.88	-19.24
464	-20.24	-19.85	-20.62	-19.68	-18.76	-20.04
536	-20.95	-20.55	-21.36	-20.33	-19.45	-20.74
607	-21.76	-21.34	-22.10	-21.27	-20.24	-21.54
677	-22.06	-21.64	-22.50	-21.52	-20.68	-21.89
722	-22.42	-21.99	-22.94	-21.81	-20.87	-22.29
773	-22.87	-22.63	-23.33	-22.31	-21.41	-22.74
811	-23.43	-23.03	-23.68	-22.81	-21.86	-23.04
880	-23.79	-23.42	-24.07	-23.20	-22.30	-23.39
935	-23.94	-23.57	-24.47	-23.40	-22.50	-23.49
1004	-24.49	-24.32	-24.96	-24.10	-23.18	-24.24
1093	-25.05	-24.71	-25.46	-24.54	-23.58	-24.84
1159	-25.51	-25.21	-25.90	-24.94	-23.97	-25.14
1255	-25.56	-25.46	-26.15	-25.19	-24.26	-25.54
1520	-26.57	-26.50	-27.08	-26.13	-25.25	-26.49

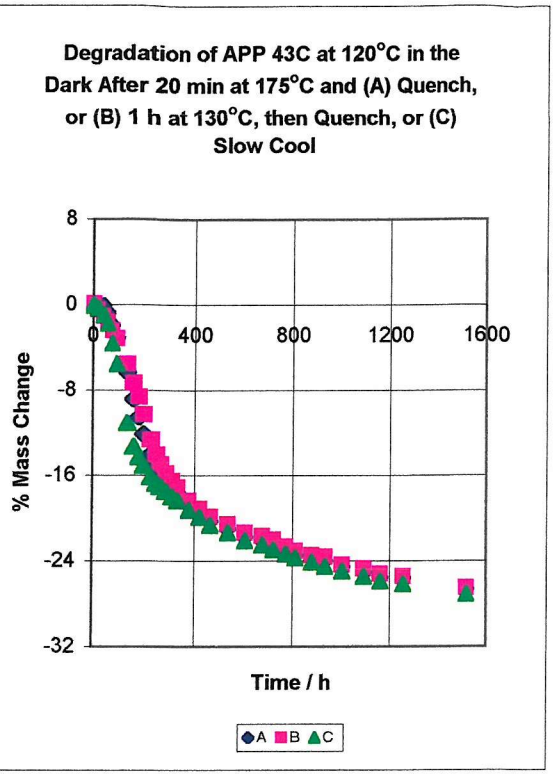

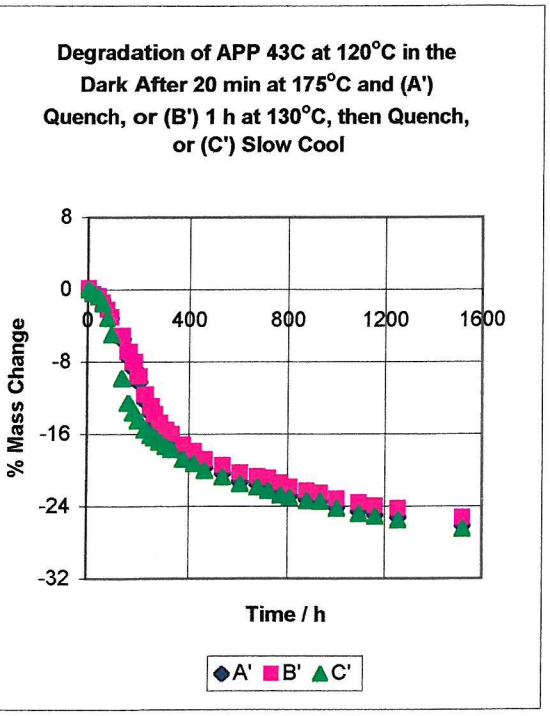

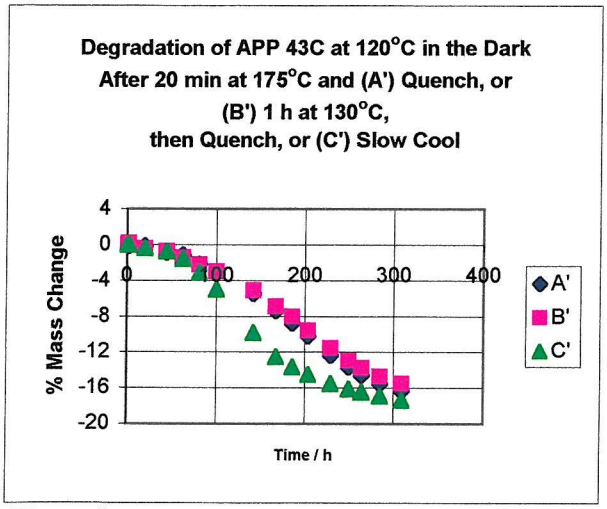

Observations

Only C showed no initial mass gain before the mass loss.

All 3 sets moved smoothly from slow to fast mass loss, with no sharp change of gradient.

The fast gradients were all the same and the spread of the graph at its widest point was about 70 h.

Onset of fast stage was in order C, A, B; C began to level off much sooner than A and B.

The order C, A and B was maintained even in the levelling off stage.

All 3 sets looked likely to level off at the same mass loss of about 40 %.

Same pattern was observed in 2nd set of 43C samples, treated exactly alike except for position inside the tin.

In the 2nd set, the horizontal spread of the graph was about 80 h, and A was much closer to B.

43C samples had begun to turn yellow at 100 h, at about 3.1 % mass loss, with intensity C > B > A.

Long-Term Thermal Degradation of APP MF80 at 120°C in the Dark

After 3 Different Sample Treatments A/B/C.

Time/h	% Mass Losses.					
	A	B	C	A'	B'	C'
0	0.00	0.00	0.00	0.00	0.00	0.00
2	0.00	0.05	-0.10	-0.39	0.00	-0.10
20	-0.19	-0.05	-0.43	-0.29	-0.20	-0.39
44	-0.29	-0.44	-0.53	-0.44	-0.59	-0.34
62	-0.24	-0.34	-0.43	-0.24	-0.49	-0.34
81	-0.19	-0.39	-0.34	-0.39	-0.34	-0.29
100	-0.34	-0.39	-0.53	-0.34	-0.44	-0.29
142	-0.44	-0.44	-0.63	-0.44	-0.15	-0.29
167	-0.58	-0.58	-0.77	-0.68	-0.44	-0.49
186	-0.58	-0.59	-0.82	-0.63	-0.39	-0.44
204	-0.73	-0.79	-1.01	-0.77	-0.59	-0.64
229	-0.78	-0.69	-1.15	-0.87	-0.59	-0.69
250	-0.92	-0.83	-1.20	-0.97	-0.64	-0.88
264	-0.92	-0.83	-1.25	-1.07	-0.64	-0.83
285	-1.07	-0.98	-1.40	-1.16	-0.79	-0.93
309	-1.11	-0.98	-1.54	-1.36	-0.83	-1.08
330	-1.21	-0.98	-1.49	-1.36	-0.83	-1.13
377	-1.65	-1.52	-1.97	-1.89	-1.18	-1.57
421	-1.75	-1.57	-2.17	-2.08	-1.42	-1.67
464	-2.04	-1.87	-2.41	-2.32	-1.62	-1.86
536	-2.18	-1.91	-2.50	-2.47	-1.77	-2.06
607	-2.38	-2.06	-2.60	-2.71	-2.06	-2.31
677	-2.47	-2.26	-2.94	-2.81	-2.06	-2.40
722	-2.52	-2.31	-3.03	-2.81	-2.16	-2.45
773	-2.62	-2.50	-3.18	-2.95	-2.31	-2.65
811	-2.81	-2.80	-3.37	-3.05	-2.51	-2.65
880	-2.86	-3.29	-3.46	-3.15	-3.00	-2.89
935	-2.91	-3.04	-3.51	-3.15	-2.75	-2.80
1004	-3.05	-3.09	-3.75	-3.34	-2.95	-3.09
1093	-3.44	-3.29	-3.99	-3.54	-3.19	-3.33
1159	-3.44	-3.44	-4.19	-3.68	-3.29	-3.53
1255	-3.54	-3.53	-4.23	-3.73	-3.39	-3.63
1520	-3.88	-3.88	-4.67	-4.18	-3.68	-3.92

Graphs of % Mass Change vs Time.
1st Set=A/B/C, 2nd Set=A'/B'/C'.

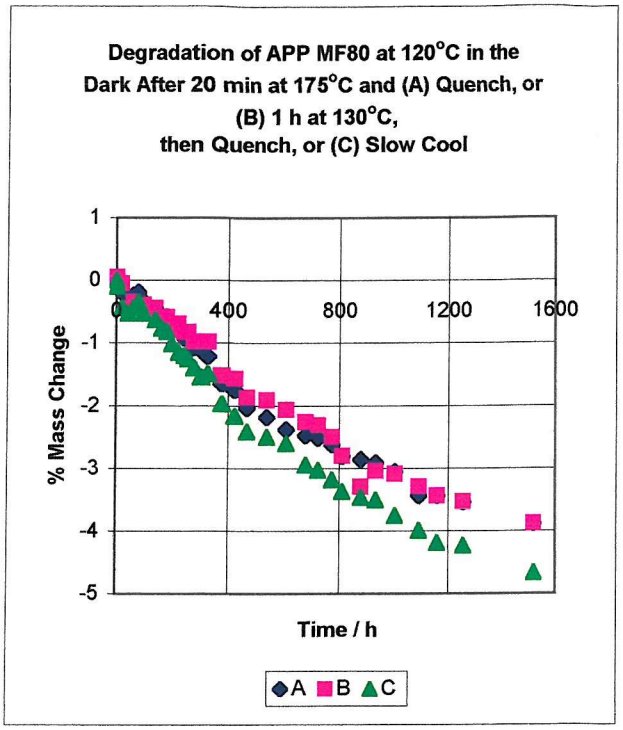

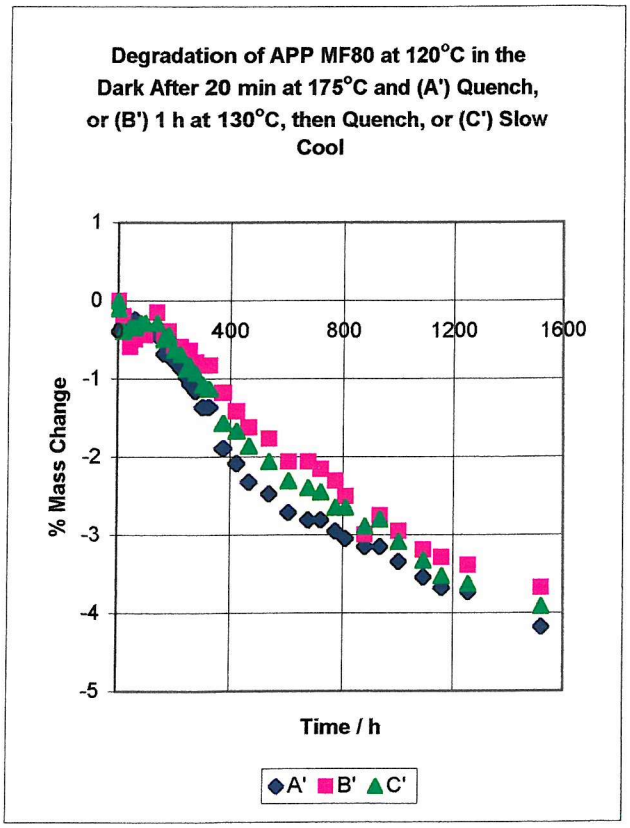

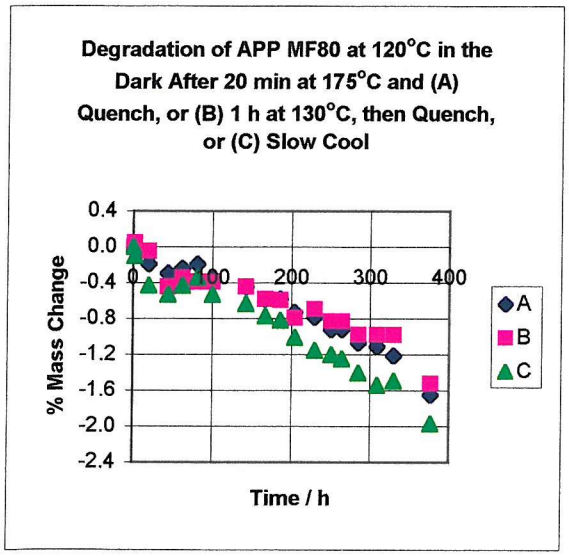

Observations

Only B showed initial mass gain before the initial mass loss.
All samples gained a little mass from 44 to 81 h.
Mass losses were all very slow, but order of onset and steepness of plot was C, A, B.
Fast mass loss was never reached.
The pattern was repeated in the 2nd set of samples.

Long-Term Thermal Degradation of APP MF500 at 120°C in the Dark

After 3 Different Sample Treatments A/B/C.

Graphs of % Mass Change vs Time.

1st Set=A/B/C, 2nd Set=A'/B'/C'

Time/h	% Mass Losses					
	A	B	C	A'	B'	C'
0	0.00	0.00	0.00	0.00	0.00	0.00
2	-0.19	0.05	-0.10	-0.19	0.15	0.00
20	0.00	-0.05	0.19	-0.05	0.64	0.54
44	-1.31	-1.82	-1.17	-1.28	-0.59	-0.35
62	-2.33	-2.71	-2.38	-2.14	-1.13	-1.33
81	-3.73	-3.74	-4.03	-3.47	-1.77	-2.22
100	-4.61	-4.67	-5.44	-4.52	-2.06	-3.06
142	-7.03	-6.39	-8.89	-6.95	-2.85	-5.03
167	-8.63	-7.38	-10.83	-8.47	-3.39	-6.52
186	-9.80	-7.92	-11.85	-9.66	-3.58	-7.31
204	-11.40	-8.80	-13.02	-11.27	-3.97	-8.39
229	-13.92	-9.99	-14.57	-13.70	-4.42	-9.67
250	-15.32	-10.97	-15.49	-15.22	-4.66	-10.41
264	-16.44	-11.76	-15.93	-16.27	-4.91	-10.96
285	-17.60	-13.08	-16.61	-17.32	-5.30	-11.50
309	-18.53	-14.56	-17.29	-18.22	-5.74	-12.09
330	-19.35	-15.79	-17.73	-18.93	-6.28	-12.49
377	-20.85	-17.90	-18.84	-20.31	-8.05	-13.57
421	-21.63	-19.13	-19.52	-21.12	-9.96	-14.17
464	-22.65	-20.22	-20.40	-22.07	-12.61	-14.91
536	-23.52	-21.00	-21.08	-22.93	-14.13	-15.55
607	-24.49	-22.04	-21.95	-23.83	-15.41	-16.39
677	-24.98	-22.48	-22.24	-24.36	-16.00	-16.68
722	-25.17	-22.73	-22.68	-24.64	-16.19	-17.03
773	-25.80	-23.36	-23.07	-25.31	-16.88	-17.52
811	-26.29	-23.86	-23.46	-25.83	-17.42	-17.82
880	-26.72	-24.25	-23.94	-26.12	-17.96	-18.26
935	-26.87	-24.40	-24.14	-26.50	-18.11	-18.56
1004	-27.59	-25.18	-24.82	-27.16	-18.79	-19.10
1093	-28.08	-25.63	-25.40	-27.74	-19.38	-19.60
1159	-28.66	-26.22	-25.74	-28.26	-19.92	-19.99
1255	-29.00	-26.46	-25.98	-28.59	-20.26	-20.19
1520	-29.97	-27.59	-27.10	-29.64	-21.25	-21.27

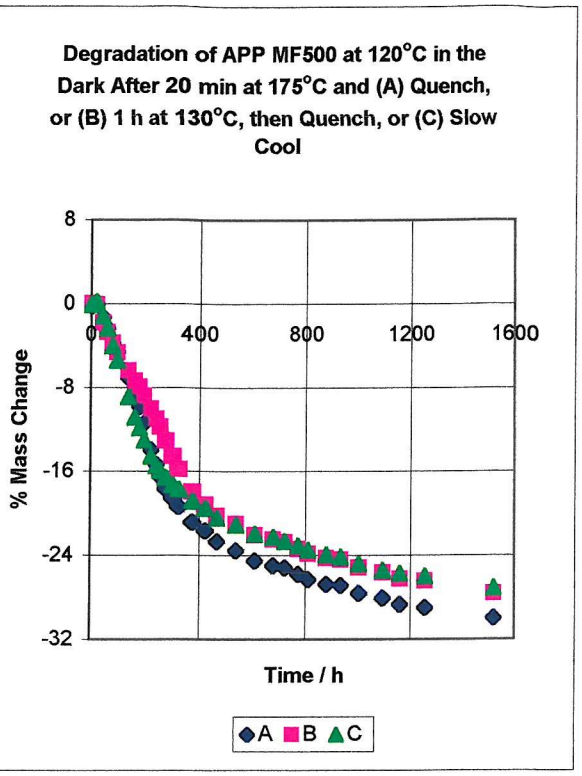

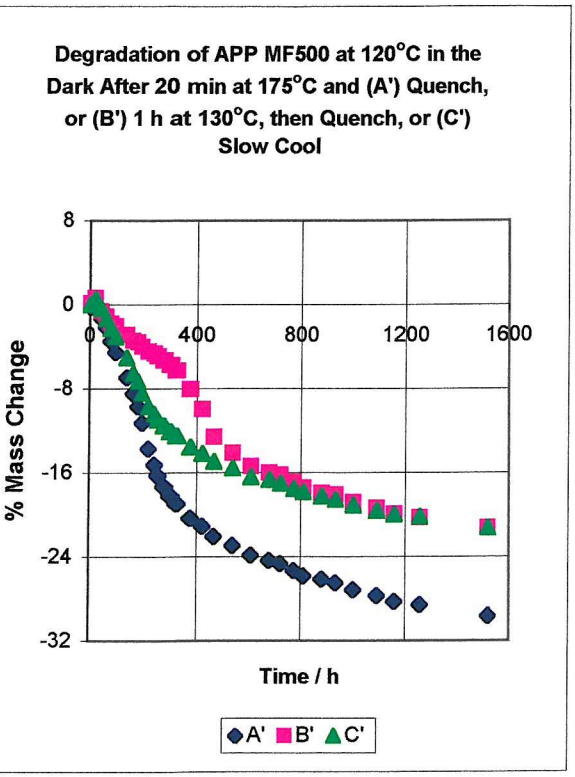

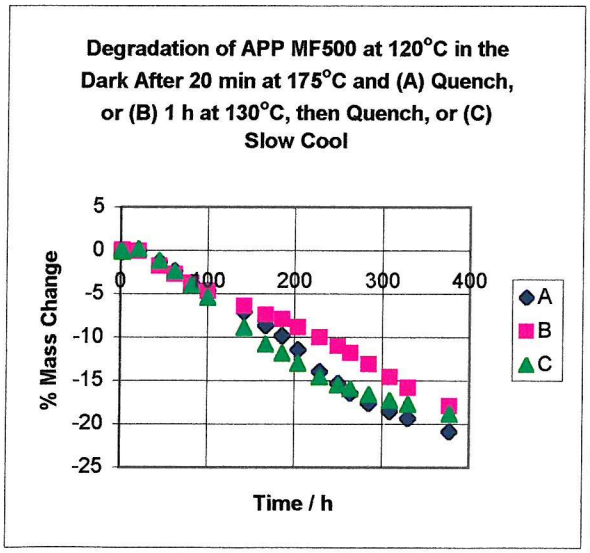

Observations

All 3 sets gained mass very slightly initially, and then lost mass slowly for only a very short time.

Onset of degradation was in the order C, A, B.

The fast mass loss gradients were the same, with a large spread to the graph of about 77 h.

Plot for C began to level off sooner (from about 260 h) and almost matched B from 536 l So A was the odd one out.

Eventual final mass losses for A, B and C would probably have been 35-40 %.

The plots were much better separated for the repeat set of samples, treated identically except for position in oven.

The order for fast 'take-off' was C, then A, then B, after approx 20, 186 and 330 h respectively.

Samples had began to turn yellow at 100 h, after about 4.5 % mass loss, with intensity C > B > A.

Long-Term Thermal Degradation of APP C80 at 120°C in the Dark

After 3 Different Sample Treatments A/B/C.

Graphs of % Mass Change vs Time

1st set=A/B/C, 2nd Set=A'/B'/C'

Time/h	% Mass Losses					
	A	B	C	A'	B'	C'
0	0.00	0.00	0.00	0.00	0.00	0.00
2	-0.56	-0.30	-0.26	-0.67	-0.35	-0.35
20	-2.50	-1.89	-2.45	-3.09	-2.03	-2.95
44	-4.29	-3.64	-4.01	-4.78	-3.46	-4.59
62	-4.85	-4.09	-4.63	-5.20	-3.81	-4.89
81	-5.31	-4.59	-5.15	-5.61	-4.45	-5.64
100	-5.56	-4.84	-5.57	-5.81	-4.70	-5.84
142	-5.87	-4.84	-6.04	-6.48	-5.10	-5.84
167	-6.43	-5.23	-6.35	-7.10	-5.44	-6.09
186	-6.74	-5.53	-6.19	-7.36	-5.49	-6.44
204	-7.25	-5.98	-6.19	-7.77	-5.59	-7.14
229	-7.81	-6.43	-6.66	-8.33	-5.64	-7.79
250	-8.07	-6.68	-7.18	-8.49	-5.89	-8.04
264	-8.52	-7.03	-7.60	-8.90	-6.19	-8.39
285	-8.88	-7.33	-8.07	-9.26	-6.53	-8.79
309	-9.19	-7.63	-8.43	-9.67	-6.83	-9.24
330	-9.60	-7.98	-8.80	-10.08	-7.13	-9.59
377	-10.57	-8.87	-9.89	-11.11	-7.87	-10.43
421	-11.23	-9.52	-10.57	-11.73	-8.56	-11.03
464	-12.05	-10.37	-11.45	-12.65	-9.25	-11.93
536	-12.71	-11.17	-12.18	-13.37	-9.95	-12.68
607	-13.63	-11.96	-13.12	-14.25	-10.69	-13.63
677	-13.99	-12.66	-13.69	-14.71	-11.18	-13.98
722	-14.45	-12.81	-13.95	-15.02	-11.43	-14.33
773	-15.16	-13.56	-14.63	-15.90	-12.27	-15.08
811	-15.62	-14.11	-15.15	-16.36	-12.67	-15.68
880	-16.49	-14.91	-15.93	-17.13	-13.31	-16.38
935	-16.74	-15.30	-16.24	-17.44	-13.56	-16.67
1004	-17.61	-16.35	-17.28	-18.57	-14.50	-17.87
1093	-18.68	-17.30	-18.12	-19.65	-15.39	-18.77
1159	-19.40	-18.20	-18.90	-20.32	-16.13	-19.57
1255	-20.27	-19.09	-19.63	-21.14	-16.82	-20.22
1520	-22.56	-21.68	-22.23	-23.71	-19.20	-22.97

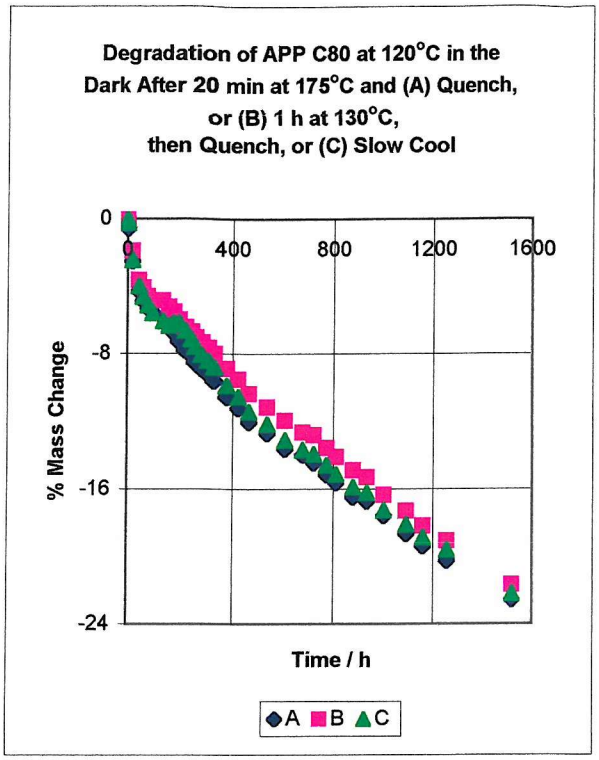

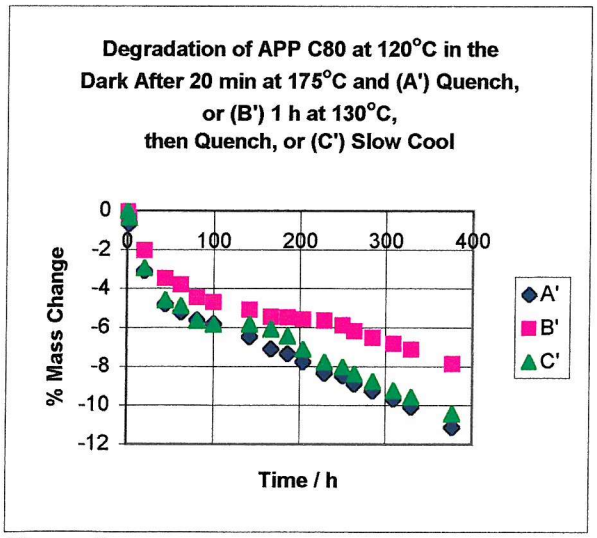

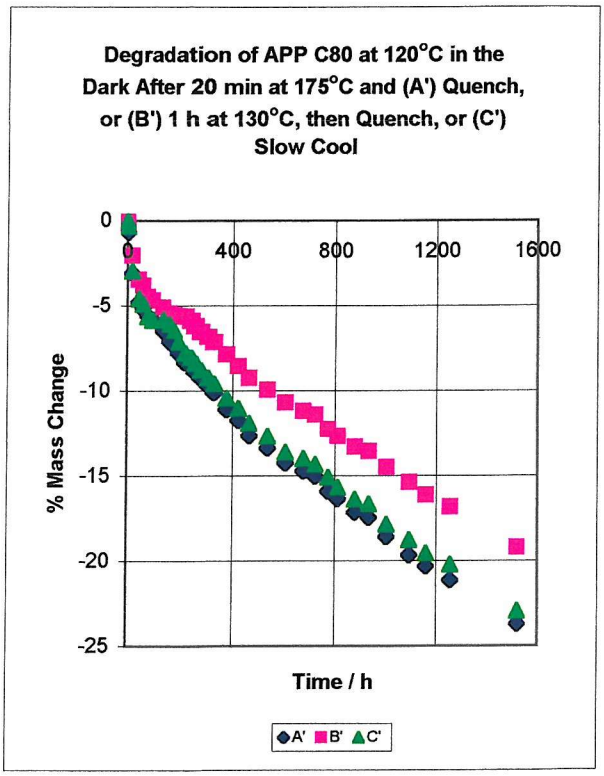

Observations

C80 did not gain mass at the start, but began to lose mass rapidly, even though it was dark brown.
All gained mass slightly or at least slowed their loss, A and B at 100-142 h, C at 167-204 h.
The fast mass loss gradients were approx the same, with a spread of the graph of about 70 h.
From 200-1520 h, order of mass loss was A > C > B, with C nearer to A tha Diferent from most of the other APPs.
None of the plots showed sign of levelling off, so eventual final mass losses for A, B and C could not be estimated.
The same pattern was oberved for the repeat set of samples, treated identically except for position in oven.
except that the difference between A/C and B was much more marked.

Long-Term Thermal Degradation of APP T1180 at 120°C in the Dark

After 3 Different Sample Treatments A/B/C. **Graphs of % Mass Change vs Time.**

Time/h **% Mass Losses** **1st set=A/B/C, 2nd Set=A'/B'/C'**

	A	B	C	A'	B'	C'
0	0.00	0.00	0.00	0.00	0.00	0.00
2	-0.95	-0.69	-0.66	-0.91	-0.65	-0.50
20	-4.22	-3.82	-4.14	-4.78	-4.00	-4.89
44	-6.98	-6.65	-6.66	-7.60	-6.65	-7.99
62	-8.19	-7.79	-7.87	-8.80	-7.89	-9.04
81	-9.19	-8.34	-8.78	-9.91	-8.99	-10.08
100	-10.15	-9.48	-9.74	-10.76	-9.80	-10.73
142	-11.50	-11.02	-11.31	-11.92	-11.01	-11.93
167	-12.31	-11.61	-12.22	-12.65	-11.66	-12.58
186	-12.56	-12.06	-12.42	-12.98	-12.01	-12.93
204	-13.01	-12.46	-12.87	-13.48	-12.46	-13.38
229	-13.36	-13.00	-13.23	-13.68	-12.91	-13.78
250	-13.81	-13.25	-13.63	-14.03	-13.22	-14.18
264	-14.21	-13.50	-13.73	-14.44	-13.47	-14.33
285	-14.52	-13.85	-14.08	-14.69	-13.82	-14.68
309	-14.82	-14.34	-14.39	-14.79	-14.07	-14.98
330	-15.02	-14.39	-14.49	-14.64	-14.32	-15.23
377	-15.32	-15.24	-15.19	-17.25	-14.52	-15.32
421	-17.28	-15.38	-14.94	-18.61	-15.98	-17.02
464	-19.19	-17.67	-17.52	-20.02	-18.19	-18.97
536	-20.59	-18.86	-19.13	-20.98	-19.45	-20.27
607	-21.70	-19.80	-20.39	-21.78	-20.55	-21.22
677	-22.10	-20.45	-21.05	-22.23	-20.85	-21.77
722	-22.50	-20.60	-21.30	-22.38	-21.16	-22.07
773	-23.05	-21.29	-21.91	-22.94	-21.86	-22.52
811	-23.36	-21.59	-22.21	-23.19	-22.16	-22.87
880	-24.21	-22.08	-22.72	-23.79	-22.61	-23.27
935	-23.91	-22.28	-22.97	-23.64	-22.71	-23.51
1004	-24.46	-22.83	-23.47	-24.30	-23.32	-23.91
1093	-24.96	-23.28	-23.93	-24.65	-23.77	-24.41
1159	-25.36	-23.72	-24.28	-25.00	-24.22	-24.71
1255	-25.72	-24.02	-24.58	-25.50	-24.42	-25.01
1520	-26.47	-24.86	-25.44	-26.06	-25.23	-25.81

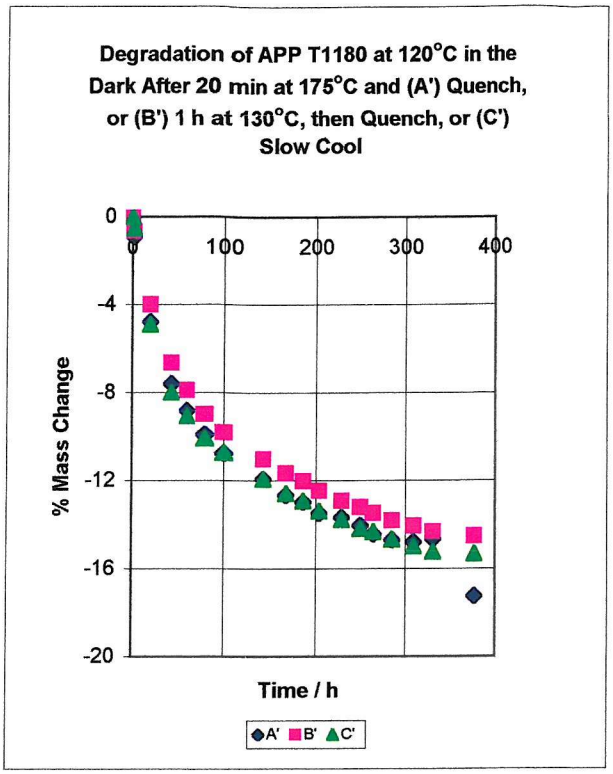

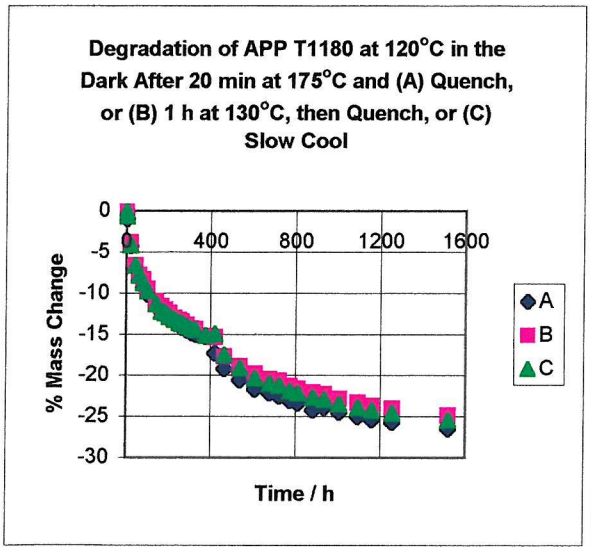

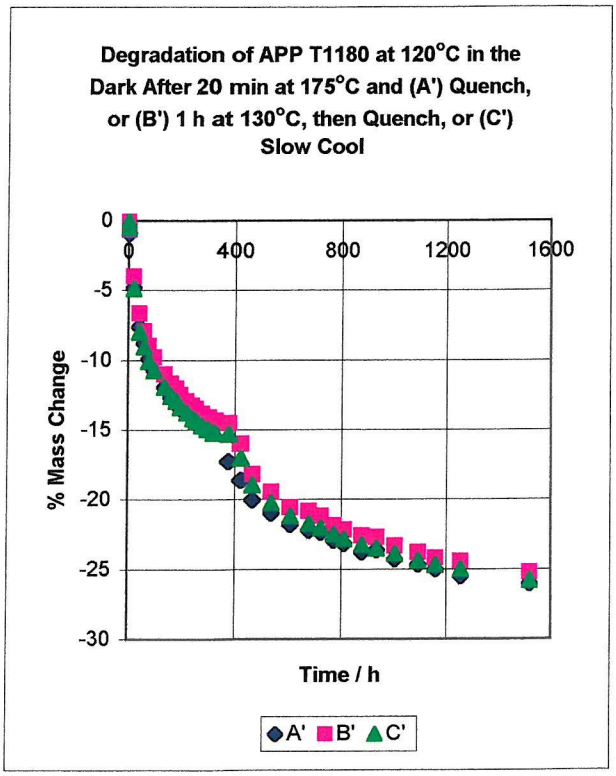

Observations

T1180 did not gain mass at the start, but began to lose mass rapidly, even though it was dark grey.

Smooth mass loss till almost 400 h, in order A, C, B, but all very close.

Plots looked likely to level off, but mass loss became faster, as though another component started to degrade.

From 400-1520 h, order of mass loss was A > C > B, with levelling off towards about 30 %.

The same pattern was observed for the repeat set of samples (treated identically except for position in oven), except that A and C were closer together, but was not observed for other APPs.

T1180 was monitored together with 7 other APPs, so this behaviour was not due to monitoring conditions.

Long-Term Thermal Degradation of APP 95-X-06 at 120°C in the Dark

After 3 Different Sample Treatments A/B/C.

Time/h	% Mass Losses					
	A	B	C	A'	B'	C'
0	0.00	0.00	0.00	0.00	0.00	0.00
2	-0.20	-0.25	-0.35	-0.79	-0.82	-0.60
20	-1.05	-0.99	-1.08	-1.68	-1.46	-1.40
44	-2.15	-2.66	-3.65	-3.87	-3.20	-3.11
62	-5.26	-3.74	-7.00	-7.10	-4.42	-7.31
81	-9.11	-5.71	-10.94	-11.28	-6.60	-12.47
100	-12.52	-7.59	-14.24	-14.56	-8.59	-16.38
142	-18.98	-11.87	-19.41	-20.67	-12.66	-20.49
167	-20.58	-15.07	-20.79	-22.26	-16.98	-21.69
186	-21.58	-17.24	-21.38	-23.00	-19.07	-22.34
204	-22.23	-19.46	-22.07	-23.23	-21.28	-23.00
229	-23.23	-21.28	-23.00	-24.69	-22.37	-23.95
250	-23.74	-22.12	-23.50	-25.19	-22.95	-24.40
264	-24.04	-22.66	-23.74	-25.53	-23.48	-24.60
285	-24.49	-23.25	-24.14	-25.93	-24.07	-25.10
309	-25.04	-23.74	-24.68	-26.48	-24.60	-25.60
330	-25.49	-24.33	-24.98	-26.88	-25.08	-25.90
377	-26.69	-25.37	-26.06	-27.92	-26.15	-26.75
421	-27.29	-26.06	-26.60	-28.61	-26.98	-27.61
464	-28.09	-27.04	-27.39	-29.46	-27.75	-28.51
536	-28.79	-27.73	-28.03	-29.96	-28.53	-29.49
607	-29.64	-28.62	-28.92	-30.85	-29.45	-29.71
677	-29.94	-29.06	-29.26	-31.30	-29.94	-30.01
722	-30.25	-29.26	-29.66	-31.45	-30.23	-30.51
773	-30.80	-29.90	-30.05	-31.94	-30.86	-30.81
811	-31.20	-30.34	-30.39	-32.39	-31.44	-31.26
880	-32.03	-30.74	-30.79	-32.89	-31.93	-31.71
935	-31.80	-30.94	-31.13	-33.13	-32.17	-32.01
1004	-32.45	-31.72	-31.72	-33.53	-32.80	-32.62
1093	-33.00	-32.22	-32.17	-34.13	-33.43	-33.07
1159	-33.50	-32.76	-32.56	-34.72	-33.92	-33.42
1255	-34.05	-33.05	-33.00	-35.22	-34.26	-33.82
1520	-34.75	-34.09	-34.04	-36.02	-35.32	-34.87

Graphs of % Mass Change vs Time.
1st Set=A/B/C, 2nd Set=A'/B'/C'

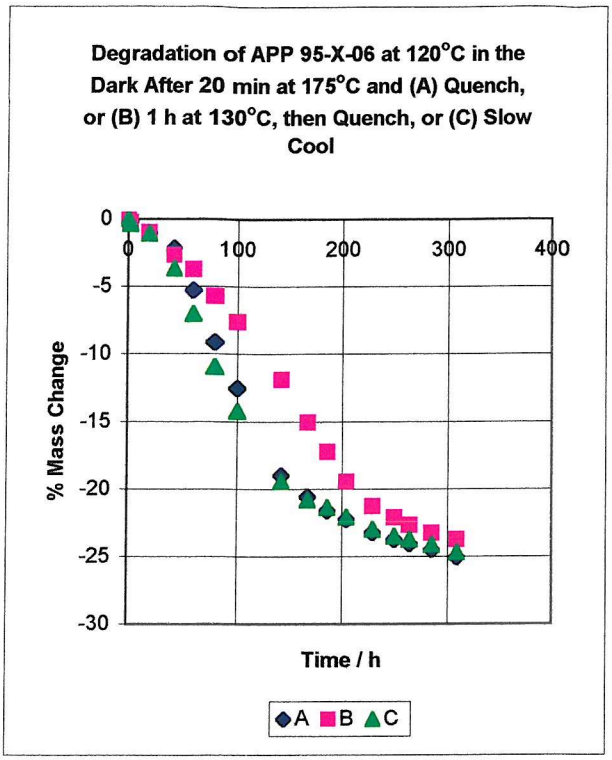

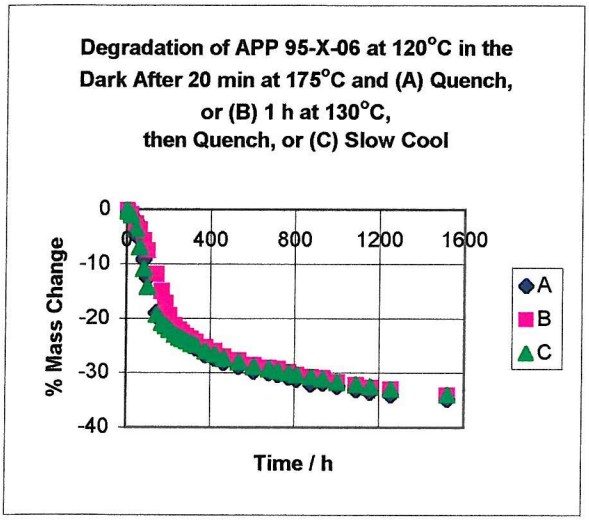

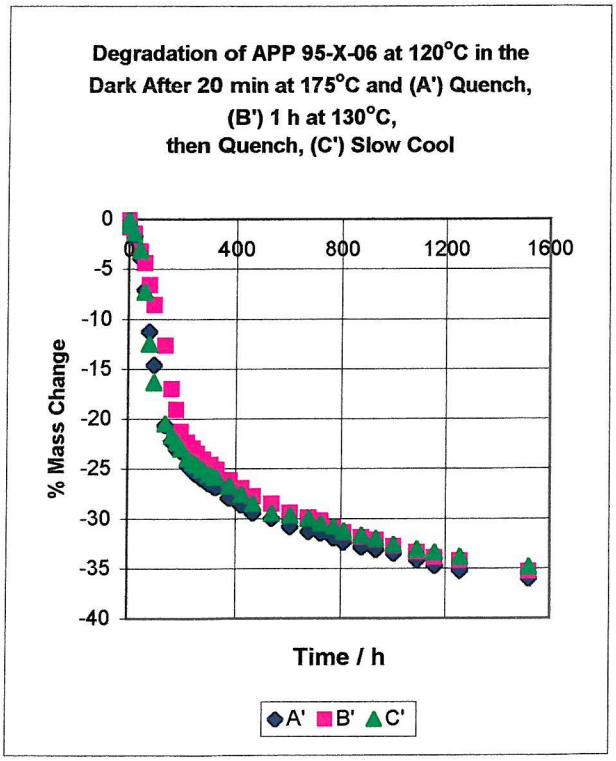

Observations

This polymer was very pale green and soft to cut; by 100 h, yellowing was C > B > A
Smooth change from slow loss to fast loss at 30-40 h; no mass gains.
Fast mass loss in order C, A, B (C and A very close) over fastest section, with spread of 60 h.
All levelled off towards about 40 %; C levelled off sooner, so order became A > C > B.
The same pattern was oberved for the repeat set of samples, treated identically except for position in oven.

Long-Term Thermal Degradation of APP V808 at 120°C in the Dark

After 3 Different Sample Treatments A/B/C.
Time/h % Mass Losses.

	A	B	C	A'	B'	C'
0	0.00	0.00	0.00	0.00	0.00	0.00
2	0.05	0.20	0.05	0.10	-0.10	0.15
20	0.19	0.61	0.20	0.33	0.25	0.20
44	0.33	0.87	0.35	0.43	0.89	0.35
62	0.42	1.02	0.55	0.62	0.89	0.44
81	0.61	1.27	0.79	0.57	0.94	0.54
100	0.65	1.22	0.65	0.71	0.94	0.69
142	0.89	1.43	0.84	0.81	1.08	0.39
167	0.75	1.33	0.89	0.81	1.08	-0.15
186	0.84	1.38	0.89	0.71	1.18	-0.44
204	0.79	1.33	0.84	0.62	1.03	-0.79
229	0.75	1.38	0.79	0.52	1.13	-1.23
250	0.84	1.33	0.79	0.47	1.13	-1.38
264	0.89	1.38	0.84	0.38	1.08	-1.48
285	0.89	1.33	0.89	0.05	1.08	-1.63
309	0.84	1.22	0.89	-0.47	0.98	-1.87
330	0.89	1.33	0.89	-1.38	1.08	-1.92
377	0.98	1.07	0.60	-2.32	0.94	-2.51
421	-0.23	1.48	0.50	-3.18	-0.59	-2.71
464	-2.34	-0.97	0.94	-4.13	-2.36	-3.06
536	-3.78	-2.65	-2.23	-4.84	-3.64	-3.40
607	-5.04	-3.98	-5.06	-5.55	-4.68	-3.84
677	-5.89	-4.90	-6.75	-5.98	-5.51	-4.19
722	-6.35	-5.41	-7.65	-6.21	-5.81	-4.34
773	-7.10	-6.27	-9.04	-6.78	-6.65	-4.88
811	-7.61	-6.68	-9.88	-7.12	-6.99	-5.13
880	-8.36	-7.55	-11.17	-7.64	-7.68	-5.67
935	-8.69	-7.85	-11.72	-7.87	-7.98	-5.86
1004	-9.43	-8.57	-13.06	-8.44	-8.71	-6.55
1093	-10.14	-9.23	-14.20	-8.97	-9.40	-7.10
1159	-10.70	-9.84	-15.09	-9.49	-9.75	-7.69
1255	-11.44	-10.40	-16.09	-9.96	-10.44	-8.13
1520	-12.80	-11.83	-18.37	-11.20	-11.87	-9.41

Graphs of % Mass Change vs Time.
1st Set=A/B/C, 2nd Set=A'/B'/C'.

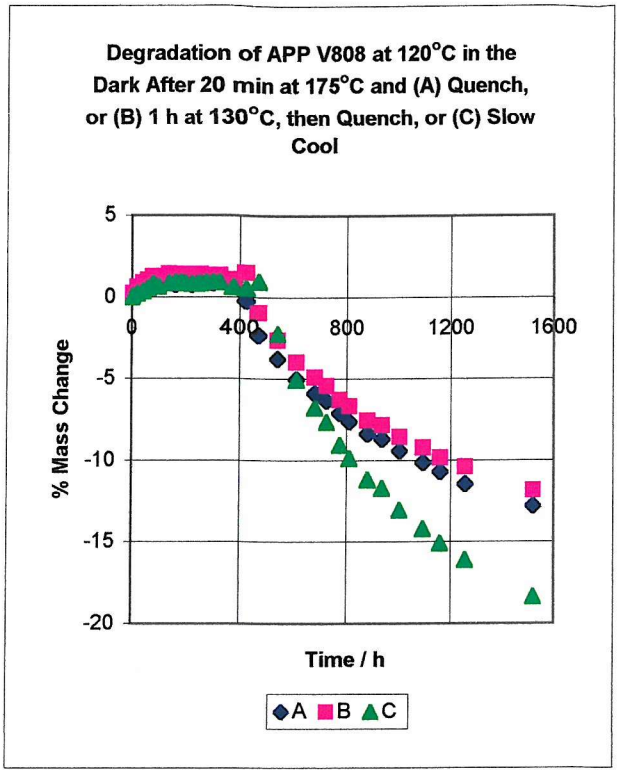

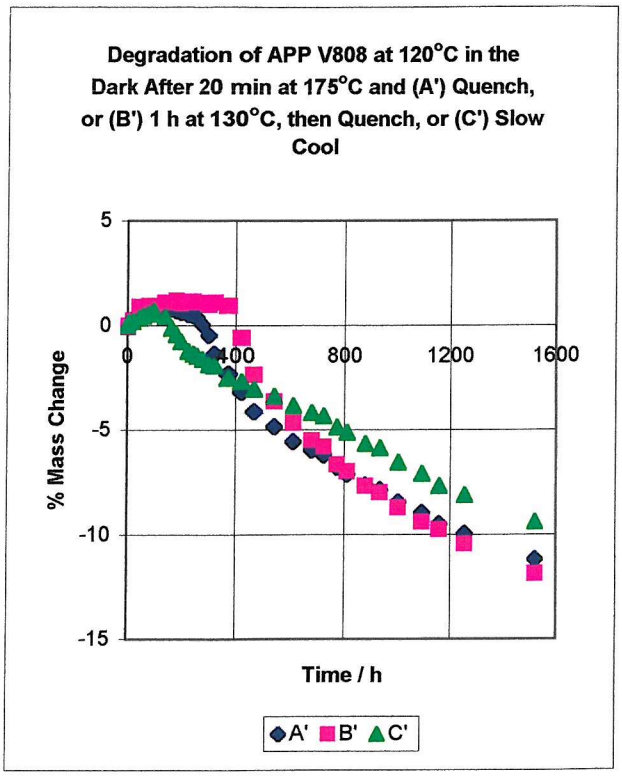

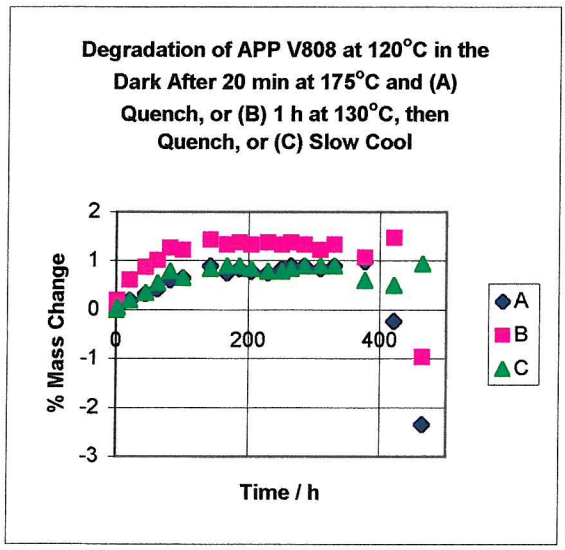

Observations

C' went yellow at 167 h, A' at 377 h, A at 421 h - when mass change became -ve instead of +ve.

All samples gained mass initially, much more than any other APPs : B > B' > A = C > A' > C'

(1.43%, 1.18 %, 0.89 %, 0.81%, 0.69 %). Fast mass loss began eventually, all roughly together at *c.* 400 h.

In the 2nd set, in the order C, A, B (from 100 h, 170 h, 380 h).

Steep plot at first, changing to a less steep plot.

In 2nd set, change occurred in the order C, A, B (from 230 h, 465 h, 465 h).

The same pattern was oberved for the repeat set of samples, treated identically except for position in oven.

Therefore this Vestoplast polymer will be less degradable for a long time, but will eventually succomb.

Long-Term Thermal Degradation of APP V891 at 120°C in the Dark

After 3 Different Sample Treatments A/B/C.

Graphs of % Mass Change vs Time.

1st set=A/B/C, 2nd Set=A'/B'/C'.

Time/h	% Mass Losses					
	A	B	C	A'	B'	C'
0	0.00	0.00	0.00	0.00	0.00	0.00
2	0.18	0.39	0.19	0.14	0.00	0.00
20	0.32	0.54	0.39	0.51	0.02	0.34
44	0.36	0.83	0.53	0.55	0.63	0.54
62	0.73	0.88	0.53	0.83	0.77	0.54
81	0.68	1.07	0.87	0.78	0.77	0.78
100	0.73	1.07	0.82	0.83	0.87	0.83
142	0.95	1.27	0.92	1.10	1.07	1.07
167	1.00	1.27	1.06	0.92	0.92	1.07
186	1.09	1.27	1.06	1.20	0.87	1.22
204	0.95	1.12	1.11	1.06	0.82	1.12
229	1.09	1.22	1.06	1.10	0.58	1.12
250	1.14	1.22	1.06	1.24	0.39	1.07
264	1.09	1.27	1.06	1.24	0.24	1.02
285	1.09	1.32	1.06	1.15	0.00	1.02
309	1.00	1.22	1.01	1.10	-0.58	1.02
330	1.36	1.27	1.11	1.15	-0.92	1.02
377	1.00	1.41	1.16	1.10	-1.84	0.68
421	1.18	0.44	-0.48	1.24	-2.52	0.73
464	-0.32	-1.32	-2.75	0.00	-3.39	-0.19
536	-2.04	-2.54	-4.39	-1.66	-4.07	-3.02
607	-3.27	-3.66	-5.89	-2.90	-4.79	-5.11
677	-4.86	-4.39	-6.81	-3.18	-5.18	-6.28
722	-5.45	-4.83	-7.38	-3.82	-5.52	-7.15
773	-6.27	-5.56	-8.35	-4.51	-6.00	-8.27
811	-6.86	-6.05	-8.88	-5.34	-6.39	-9.05
880	-7.49	-6.63	-9.75	-6.12	-6.83	-10.17
935	-7.90	-7.02	-10.33	-6.31	-6.97	-10.80
1004	-8.72	-7.80	-11.20	-7.18	-7.65	-11.92
1093	-9.45	-8.34	-12.11	-7.97	-8.14	-12.90
1159	-9.99	-8.78	-12.79	-8.47	-8.67	-13.58
1255	-10.54	-9.27	-13.51	-9.07	-8.96	-14.45
1520	-11.94	-10.68	-15.35	-10.59	-10.07	-16.45

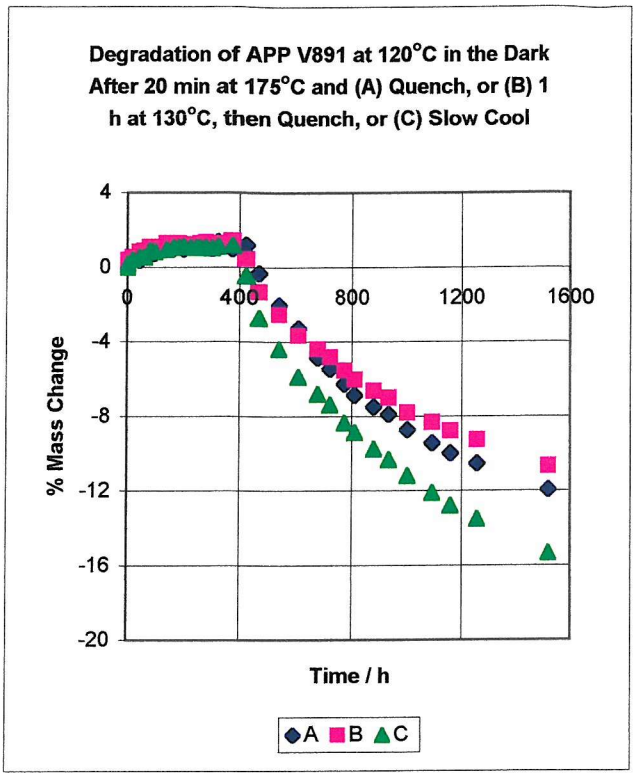

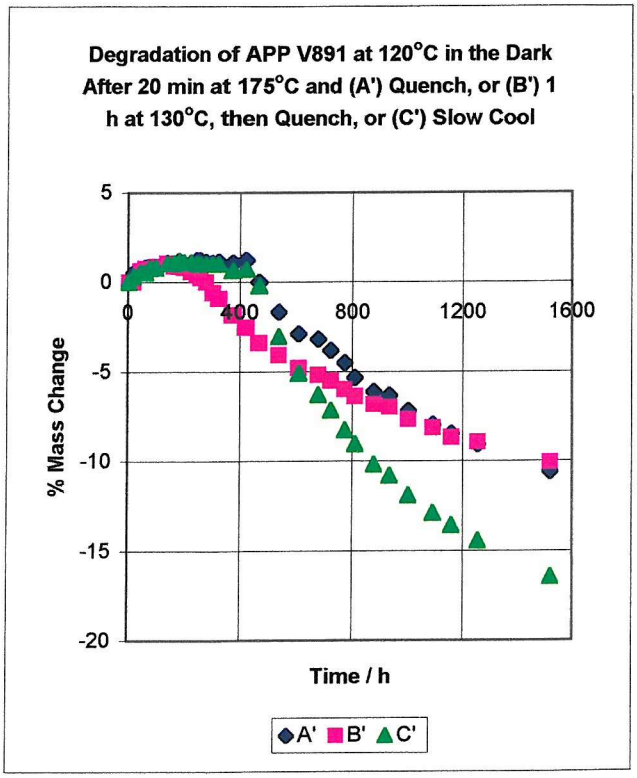

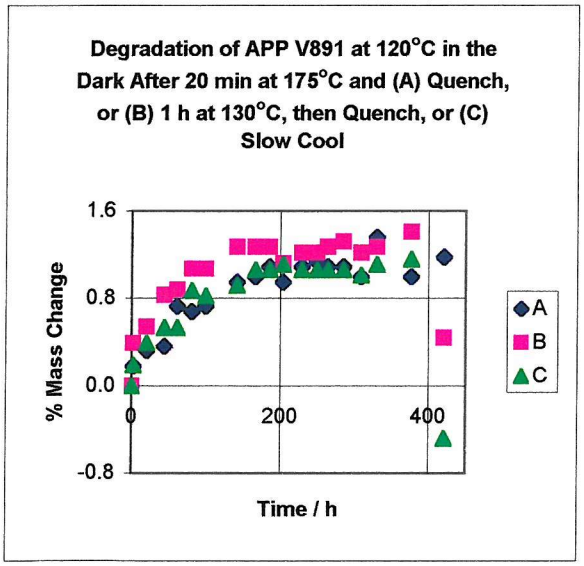

Observations

Samples turned yellow when mass change became -ve instead of +ve.

All samples gained mass initially, much more than non-Vestoplast APPs, with B > A = C, and stayed level till *c.* 400 h.

Eventually fast mass loss did begin, all roughly together at ab Smooth change from steep to less steep plot all the way.

The same pattern was oberved for the repeat set of samples, treated identically except for position in oven.

So this polymer will be less degradable than non-Vestoplast polymers for a long time, but will eventually succomb.

In 2nd set, fast loss started in order C, A, B (from 142 h, 330 h, 420 h) and carried on for longer in C than in A & B.

Degradation of Ten Pelleted APPs and Oxidized Bitumen at 120°C, Sealed in Total Darkness

2 slides for each APP, with 2*200 mg samples cut from pellets.
V808/V891 were small beads, 95-X-06 was cut from a slab.
Samples were sealed in a square biscuit tin, which was only opened each time in the fume cupboard after it had reached room temperature.
Therefore the samples were never exposed to light while warm.

Tin = 23.5 cm * 22.5 cm * 8.5 cm, sealed with black PVC tape.
Therefore volume = 4494 cm^3 or 273 in^3
Tin was both lightproof and airtight.
Fresh limited air supply after each weighing.
Data: 7: 46-48, 63-64, 88, 95 and 8: 14

Time/h	Percentage Mass Changes																				
	1C	1C'	32C	32C'	43C	43C'	MF80	MF80'	MF500	MF500'	C80	C80'	T1180	T1180'	95-X-06	95-X-06'	V808	V808'	V891	V891'	OB
0.0	0.00	0.00	0.00	0.00	0.00	0.00	0.00	0.00	0.00	0.00	0.00	0.00	0.00	0.00	0.00	0.00	0.00	0.00	0.00	0.00	0.00
20.0	0.28	0.27	0.92	0.72	0.45	0.07	-0.07	-0.08	0.12	0.02	-2.22	-2.22	-3.45	-3.77	-0.12	-0.55	1.65	-2.66	4.94	1.00	1.59
45.0	0.33	0.25	1.30	1.00	0.55	0.35	0.30	0.43	0.70	1.10	-3.82	-4.12	-7.28	-7.37	-0.65	-0.90	2.65	-1.35	6.62	3.47	3.88
62.5	0.65	0.40	1.35	1.32	0.70	0.45	0.58	0.63	1.32	0.97	-4.79	-5.35	-9.79	-9.75	-0.95	-1.10	3.19	-0.75	7.31	4.32	4.88
103.0	0.80	0.52	1.67	1.27	0.82	0.65	1.08	1.15	1.50	0.70	-5.54	-5.97	-11.54	-11.32	-1.07	-1.08	3.59	-0.38	7.86	4.94	6.22
149.0	0.85	0.45	1.32	0.42	0.80	0.65	1.35	1.45	1.15	0.55	-5.67	-6.02	-12.83	-12.52	-1.22	-1.10	3.77	0.03	8.26	5.49	
195.0	-0.25	1.05	0.45	-0.15	0.82	1.20	1.13	1.55	0.97	0.47	-5.84	-6.27	-13.48	-13.40	-1.44	-1.28	3.77	0.03	8.56	5.29	
262.0	-0.45	0.25	0.10	-0.37	0.82	0.32	0.65	0.75	1.20	0.57	-6.19	-6.65	-14.08	-13.95	-1.24	-1.35	3.92	0.23	8.76	5.39	0.00
285.0	0.02	0.42	0.42	0.07	0.65	0.30	0.18	0.28	0.27	-0.02	-5.39	-5.87	-13.88	-13.75	-2.09	-2.98	3.69	-0.35	7.84	4.14	3.87
308.0	0.15	0.72	0.65	1.07	0.50	0.25	-0.08	0.05	-0.25	-0.35	-5.22	-5.47	-13.78	-13.52	-4.58	-5.19	3.89	-0.45	7.64	3.92	5.16
331.0	-0.70	-0.42	0.27	0.75	0.32	0.05	-0.03	0.13	0.45	-0.10	-5.86	-6.37	-14.25	-14.05	-7.94	-8.05	4.32	0.05	8.51	3.42	4.32
356.0	-1.25	-1.05	0.00	0.52	0.10	-0.07	-0.10	0.08	0.55	0.22	-6.11	-6.47	-14.45	-14.30	-10.93	-10.45	4.54	0.38	8.94	5.32	4.27
379.0	-1.75	-1.50	-0.20	0.25	-0.12	-0.30	-0.15	0.00	0.52	0.20	-6.36	-6.72	-14.73	-14.55	-12.85	-12.23	4.44	1.10	9.16	5.77	4.17
401.0	-1.88	-1.70	-0.20	0.25	-0.32	-0.45	-0.20	-0.20	0.55	0.12	-6.59	-6.97	-14.83	-14.62	-14.26	-13.43	4.27	1.05	9.44	5.92	4.42
419.0	-1.50	-0.95	-0.12	0.50	-0.45	-0.47	-0.75	-0.63	-0.25	-0.47	-5.94	-6.37	-14.73	-14.60	-13.64	-14.14	3.54	-0.15	8.49	4.02	6.26
443.0	-2.33	-2.00	-0.70	-0.10	-0.65	-0.72	-0.90	-0.68	0.05	-0.25	-6.71	-7.17	-15.28	-15.07	-16.36	-15.39	3.29	0.03	9.09	5.02	4.97
462.0	-2.63	-2.17	-0.90	-0.32	-0.92	-0.92	-0.93	-0.78	0.07	-0.27	-6.89	-7.22	-15.33	-15.20	-16.90	-16.04	3.27	0.03	9.26	5.02	4.97
484.0	-2.03	-1.67	-0.62	0.00	-1.00	-0.92	-1.30	-1.18	-0.67	-0.90	-6.36	-6.75	-15.33	-14.97	-17.65	-16.54	2.52	-1.13	7.56	3.20	6.46
506.0	-2.90	-2.25	-1.12	-0.47	-1.27	-1.15	-1.40	-1.20	-0.37	-0.65	-6.99	-7.37	-15.65	-15.42	-18.32	-17.32	2.55	-0.85	8.21	4.14	5.26
551.0	-3.58	-2.85	-1.50	-0.87	-1.57	-1.42	-1.83	-1.40	-0.40	-0.65	-7.49	-7.87	-15.97	-15.77	-19.19	-18.12	2.27	-0.85	8.61	4.29	4.87
576.0	-3.85	-3.35	-1.92	-1.17	-1.87	-1.67	-2.05	-1.53	-0.47	-0.70	-7.76	-8.17	-16.22	-16.00	-19.64	-18.67	2.07	-0.93	8.56	4.37	4.82
596.0	-4.03	-3.65	-2.07	-1.37	-2.05	-1.84	-2.20	-1.68	-0.52	-0.77	-7.94	-8.32	-16.32	-16.05	-19.97	-18.97	1.97	-0.98	8.54	4.32	4.62
620.0	-4.05	-3.87	-2.14	-1.40	-1.97	-1.79	-2.28	-1.70	-0.40	-0.75	-8.01	-8.42	-16.42	-16.10	-20.06	-19.05	2.05	-1.00	8.69	4.42	4.72

Thermal Degradation At 120°C in Total Darkness Sealed Pelleted APPs and Oxidized Bitumen

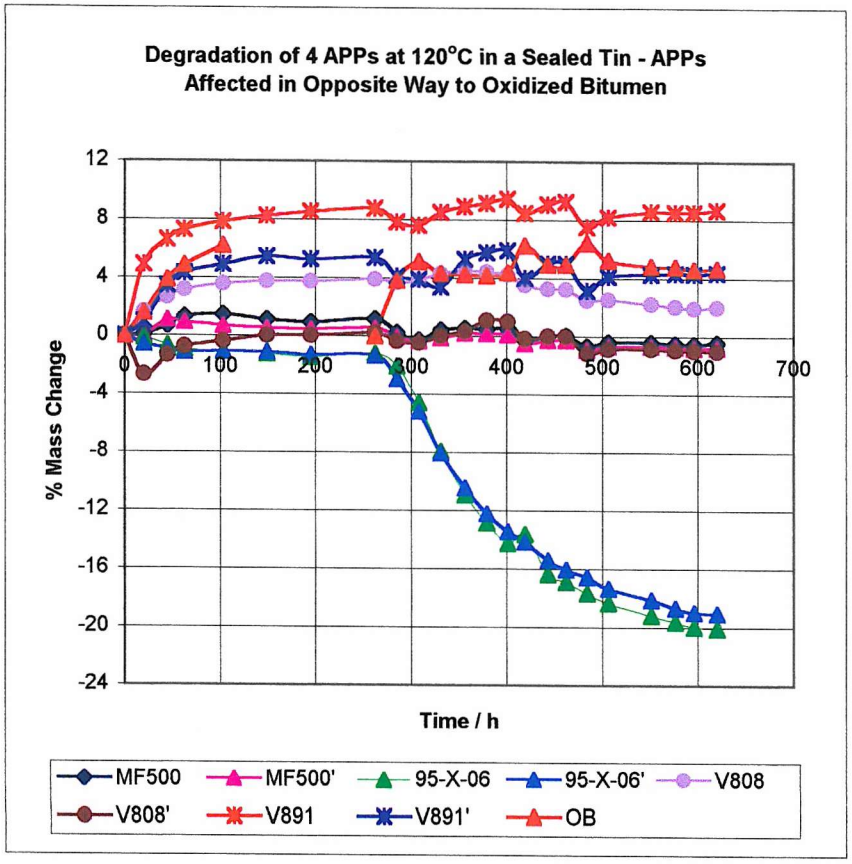

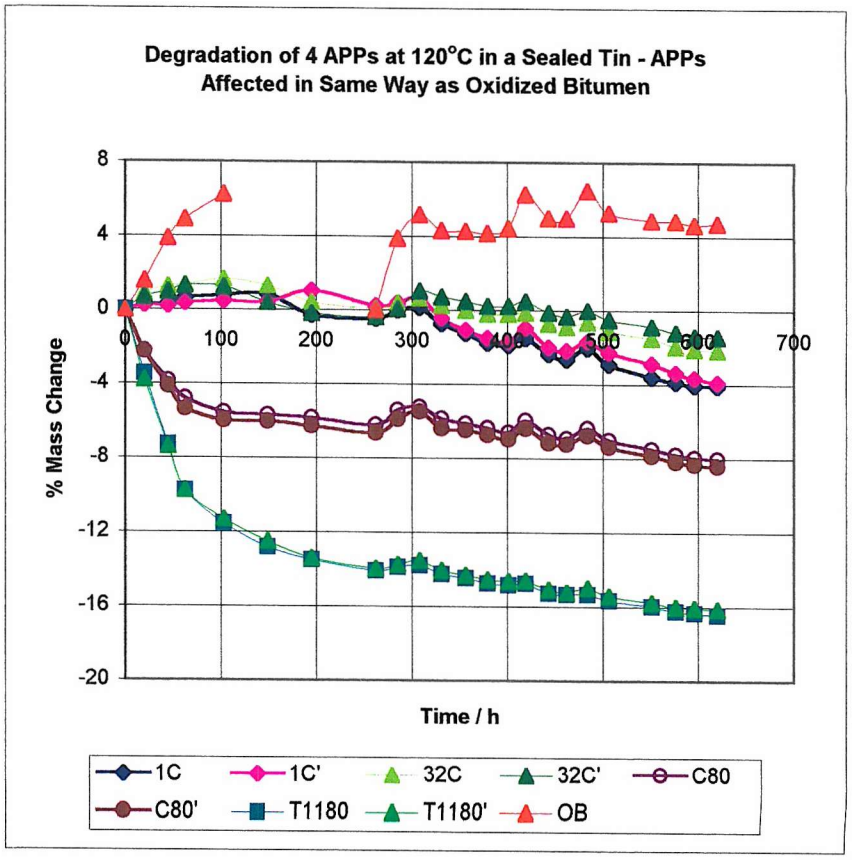

When fresh Oxidized Bitumen (OB) was introduced after 262 h it affected all the other samples, mainly only slightly.
However 95-X-06 was immediately triggered into its fast stage of degradation, which did not occur till 490 h in the dark in unsealed tin.
1C, 32C, C80 and T1180 always gained or lost mass v slightly when OB did so. 43C and MF80 were unaffected, T1180 only slightly.
However 95-X-06, MF500, V808 and V891 always went the opposite way to OB.
Probable reas competition for the limited air supply in the tin sealed with black PVC tape.
OB suddenly removed large amount of oxygen when 95-X-06 was well into its slow stage. OB gained 7.8 mg (3.87%) over its first heating period.
Sudden air pressure drop triggered off loss of gaseous fragments from 95-X-06, and to a very much lesser extent from MF500, V808 and V891.
1C, 32C, C80 and T1180 always gained mass with OB - i.e. it was harder to remove gaseous oxidation products from these 4 APPs.

Thermal Degradation At 120°C in Total Darkness Sealed Pelleted APPs and Oxidized Bitumen